Development of a 3D Geological Mapping and Database Interface to Support Interconnected Groundwater and Surface Water Management

Activity
National Water Commission
Raising National Water Standards Project
Groundwater Project

Inclusions
Final Completion and Project Reports

Authors
B. Kelly[1,2,3], B. Giambastiani[1,3], M. Andersen[1,2,3], A. McCallum[1,3], A. Greve[1,2,3] and I. Acworth[1,2,3]
[1]Connected Waters Initiative, UNSW
[2]National Centre for Groundwater Research and Training
[3]Cotton Catchment Communities CRC

April 2010

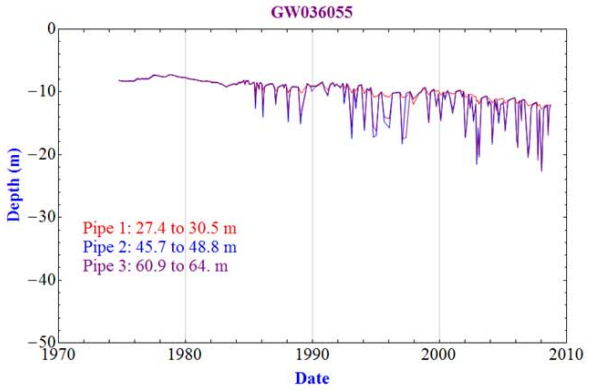

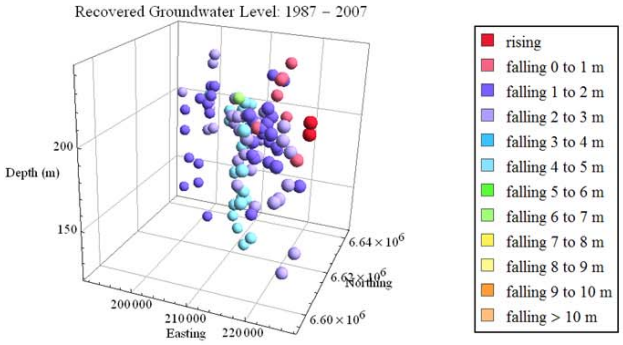

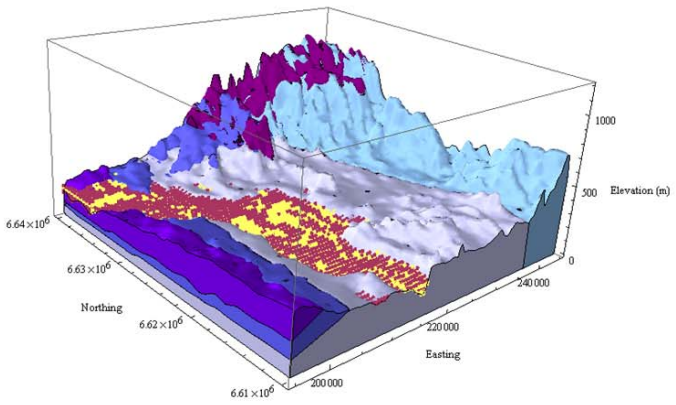

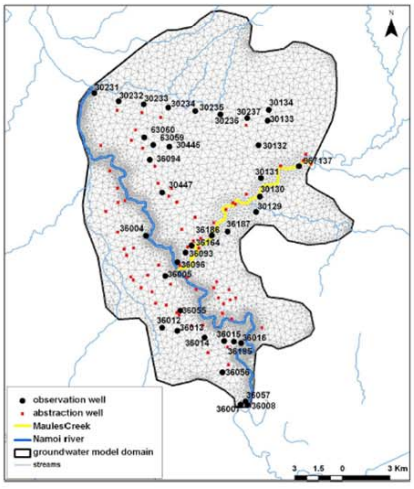

Australian Government
National Water Commission

Namoi CMA CATCHMENT MANAGEMENT AUTHORITY

Cotton Catchment Communities CRC

UNSW THE UNIVERSITY OF NEW SOUTH WALES SYDNEY • AUSTRALIA

Development of a 3D Geological Mapping and Database Interface to Support Interconnected Groundwater and Surface Water Management

Activity
National Water Commission
Raising National Water Standards Project
Groundwater Project

Status
Final Report

Authors
B. Kelly[1,2,3], B. Giambastiani[1,3], M. Andersen[1,2,3], A. McCallum[1,3], A. Greve[1,2,3] and I. Acworth[1,2,3]
[1]Connected Waters Initiative, UNSW
[2]National Centre for Groundwater Research and Training
[3]Cotton Catchment Communities CRC

April 2010

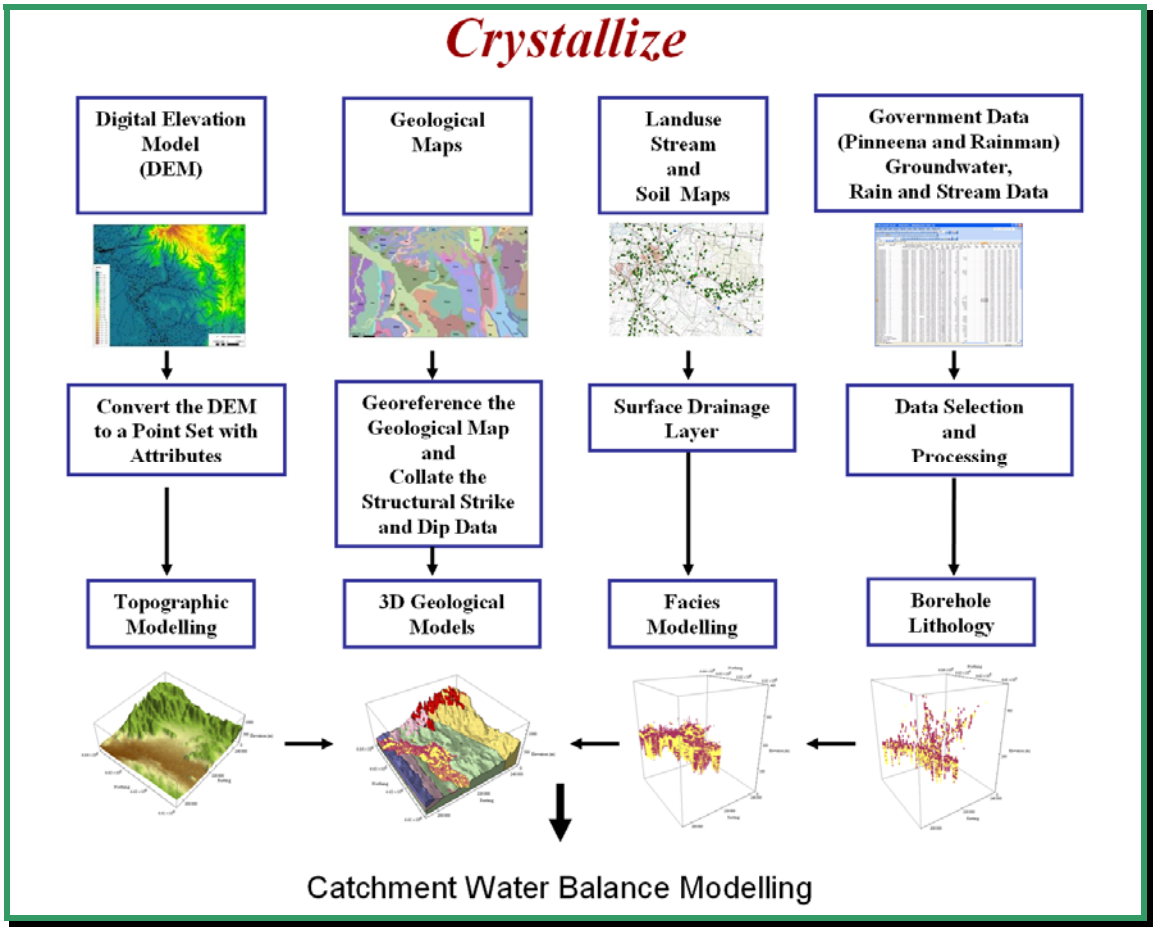

Australian Government
National Water Commission
Namoi CMA Catchment Management Authority
Cotton Catchment Communities CRC
UNSW The University of New South Wales Sydney • Australia

Contents

Development of a 3D Geological Mapping and Database Interface to Support Interconnected Groundwater and Surface Water Management

1 Introduction

This project demonstrates one approach to coordinating and analysing hydrogeological data to help with the evaluation of catchment water management issues. The methodologies presented in this report are not intended to replace existing approaches to coordinating hydrogeological data being used by NSW state government water management departments. Rather the applications presented complement.

Four software programs are used for this project: MS Access, ArcGIS, *Mathematica* and FEFLOW.

MS Access (http://office.microsoft.com/en-au/default.aspx) is used to coordinate the data from the NSW Water Information Pinneena Groundwater Works CD, which is the primary data set for the bore construction details and the standing water level measurements. This information is combined with other continuously recorded climatic data from the Bureau of Meteorology and the Pinneena Continuous Flow CD into a single MS Access database.

ArcGIS (http://www.esri.com/software/arcgis/index.html) is used to coordinate all the 2D spatial information. Important information in this database includes the digital elevation model (DEM), geological maps, soil maps, landuse maps and the stream network.

Mathematica (Wolfram Research, Inc., 2008, http://www.wolfram.com/) is used for the plotting and analysis of the hydrograph data, for constructing the 3D conceptual site model of the catchment hydrogeology, populating the FEFLOW (www.dhigroup.com) mesh, and the post processing of the modelled groundwater hydrographs. The *Mathematica* notebooks developed for this project have been coordinated under the name ***Crystallize***. These notebooks are to be placed in the public domain. To use the *Mathematica* notebooks requires the purchasing of a *Mathematica* license. The hydrograph analysis applications described in this report could all be used on the web by running the applications using Wolfram web*Mathematica*3 (http://www.wolfram.com/).This would make the information on the Pinneena CDs accessible to anyone in a visual format.

Only a few representative data analysis applications are presented, because there are numerous aspects to coordinating the data for a catchment, and approaches to analysing the data are open ended. The components that are presented demonstrate working with the databases, the workflow for key aspects of constructing a conceptual 3D geological model of a catchment, and pre and post processing information when using FEFLOW for the catchment water balance modelling.

A copy of the MS Access database, ArcGIS database, all the ***Crystallize*** notebooks (*Mathematica* .nb files), supporting Excel files and a MS Word document version of the notebooks are located on the accompanying USB memory stick. Below, the contents of the USB memory stick are described in more detail.

1.1 Comments on the Choice of MS Access

Three database systems dominate the commercial world: MS Access/SQL server, mySQL and Oracle (http://www.mysql.com/why-mysql/marketshare/). This project used MS Access because MS Access is used in most government water management organisations, making adoption easier.

Another advantage in using MS Access for a demonstration project is that the database can easily be transferred between offices and computers. Each of the other major database programs is tied to a server.

The database is designed with the expectation that it will need to be migrated to another platform at some stage. This is because MS Access is only meant to be a small scale database application. The MS Access database developed for this project can be migrated to any of the market leading database systems.

For details on the migration of MS access refer to:
- MS Access to MS SQL server (http://support.microsoft.com/kb/237980)
- MS Acess to mySQL (http://www.mysql.com/why-mysql/migration/)
- MS Access to Oracle (http://www.oracle.com/technology/tech/migration/focusareas/access.html)

Further details about the information in the MS database are provided in Appendix 1 and the database is located in the folder Appendix1_Databases.

1.2 Comments on the Choice of ArcGIS

The decision to use ArcGIS for the 2D database was driven by a number of factors:

- Both the NSW Office of Water and the Namoi CMA already have people skilled in the use of ArcGIS;
- Many of the 2D data sets obtained from the various government agencies were already in an ArcGIS compatible format;
- *Mathematica* has functions that link directly to ArcGIS; and
- There is considerable interest in the use of ArcHydro for managing catchment data by various government departments.

Further details about the information in the ArcGIS database are provided in Appendix 1 and the database is located in the folder Appendix1_Databases.

1.3 Comments on the Choice of Mathematica

Mathematica was originally developed as a system for doing mathematical computations. It has evolved into a powerful environment for interacting with databases, spreadsheets and text files. It has a comprehensive library for visualising data in traditional graphs and as 3D objects. The flexible programming and visualisation environment has enabled the development of a new 3D geological modelling environment which costs a fraction of the market leading products (a copy of *Mathematica* is required, but the ***Crystallize*** notebooks are free). This was not the original goal of the project, but is a major outcome.

The *Mathematica* programs are run from inside notebooks. These notebooks are live documents; they contain the text, the programs, and the graphical outputs of the calculations. All the images that are created in the notebooks are interactive. The *Mathematica* notebooks associated with this project are to be placed in the public domain and marketed under the name ***Crystallize***. The ***Crystallize*** notebooks are at the core of the workflow (Figure 1).

Eight examples of the application of ***Crystallize*** are presented:

- Appendix 3 (and folder Appendix3_Crystallize3DGeology) demonstrates how to build 3D geological models, which are used to provide the framework for the groundwater flow model;
- Appendix 4 (and folder Appendix4_CrystallizeFEFLOWmesh) shows how to populate a FEFLOW mesh;
- Appendix 6 (and folder Appendix6_CrystallizeFEFLOWHydrographs) gives an example of the post processing of the FEFLOW outputs, comparing the field measured versus the modelled groundwater hydrographs. Two methods are presented. In the first example continuous approximate functions are fitted to the measured and modelled hydrograph data sets and then the statistics are determined using the functions. In the second example the statistical comparisons are done on the field measured data points, and the estimated data points from the model;
- Appendix 7 (and folder Appendix7_CrystallizeHydrographs) illustrates how *Mathematica* links to the MS Access database and can be used to plot a single hydrograph set for a selected groundwater works number, or plot every hydrograph set in the database, saving the plots as individual images that can be loaded into other applications; and
- Appendix 8 (and folder Appendix8_Crystallize3DGroundwater) demonstrates the value of analysing the hydrograph data in 3D. The first example examines the long term trend in the recovered standing groundwater level. And the second example shows how the seasonal impact of groundwater pumping can be used to characterise aquifer connectivity, in particular, showing where to position a boundary between the unconfined and semi-confined aquifers from which the irrigation groundwater is extracted.

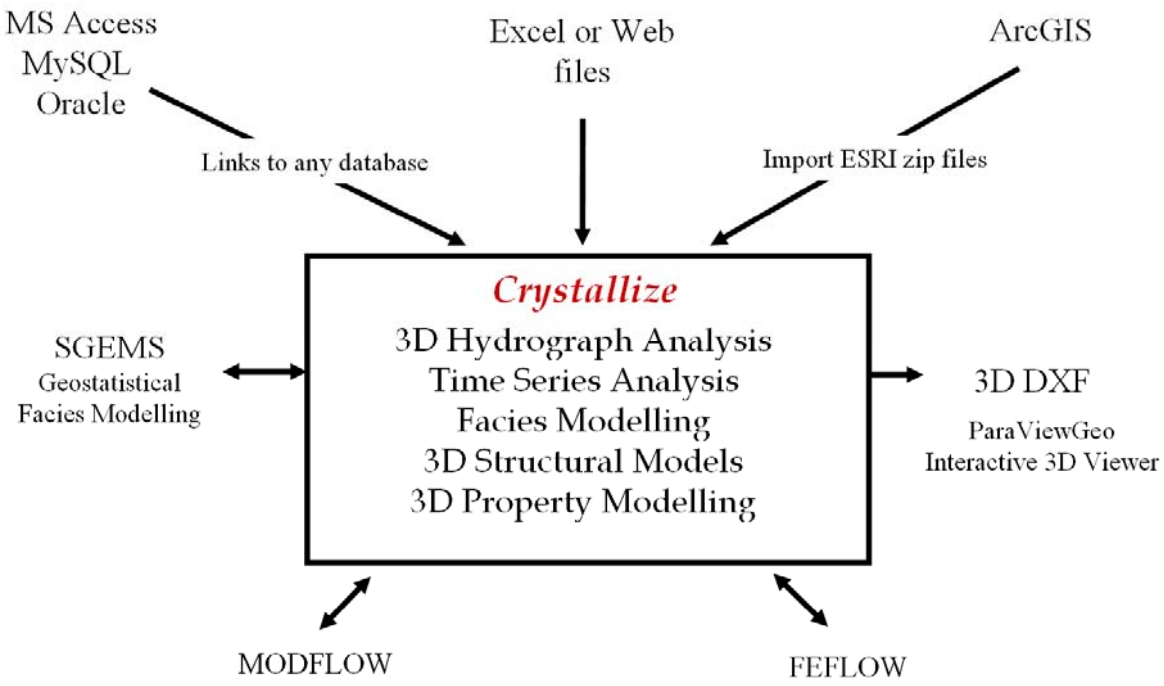

Figure 1. Schematic of the role of ***Crystallize*** in the analysis of catchment water data.

1.4 Comments on the Choice of FEFLOW

To date most catchment scale water balance models throughout the Murray-Darling Basin have used MODFLOW (http://water.usgs.gov/nrp/gwsoftware/modflow.html). The MODFLOW models consist of 1 to 3 layers which aim to capture the majority of the behaviour observed in the bore hydrographs (often an unconfined layer overlying one or two semi-confined layers). This is appropriate when the purpose of the catchment water balance model is to provide a feel for the sustainable use of groundwater. However, these MODFLOW models do not account correctly for the local point scale residence time of the water moving through the complex aquifer system, nor do they honour the sediment distribution in any detail and they cannot be used to investigate the migration of different water quality zones.

FEFLOW provides a framework that allows more geological complexity to be incorporated into the groundwater flow model. This project demonstrates how to incorporate a complex facies model into the groundwater modelling framework. Comprehensive details on FEFLOW modelling are presented in Appendices 4, 5 and 6 (and folders: Appendix4_CrystallizeFEFLOWmesh; Appendix5_FEFLOWmodel; Appendix6_FEFLOWhydrographs).

2 The Need for 3D Conceptual Geological Models of Catchments

There is growing awareness that managers need comprehensive 3D geological models of valley-fill aquifers if they are to manage these aquifers sustainably (Faunt et al., 2009). In particular, the accessible groundwater is in the sand and gravel rich palaeochannels. To understand the flow of groundwater through the aquifer system the palaeochannels need to be mapped and correctly incorporated into the groundwater flow models. This has clearly been demonstrated by the research and application of flow modelling in the petroleum industry, where most of the developments in facies modelling have been driven by the need for better production forecasts (Vargas-Guzman, 2009). Keogh et al. (2007) recently reviewed the development of fluvial stochastic modelling focusing on the petroleum sector. Many of the methods described by Keogh et al. (2007) have potential application in unconsolidated and consolidated sedimentary aquifers.

Constructing 3D geological models from multiple data sets (for example geological maps, well logs, geophysical surveys and digital elevation models), is a relatively mature process and there are now many advanced geological modelling packages available, including 3D GeoModeler (www.geomodeller.com), 3D and 4D Move (www.mve.com), EarthVision (www.dgi.com), EVS-MVS (www.ctech.com), Gocad (www.gocad.org), Jewel Suite (www.jewelsuite.com), Roxar (www.roxar.com), Petrel (www.slb.com) and Vulcan3D (www.maptek.com). These software packages have been used in many commercial and university research projects, however, they are costly and not widely used for teaching large classes, and have limited use in economically disadvantaged countries, and the groundwater sector. The procedure for constructing similar structural framework and parameter models using *Mathematica* was created for this project to address the concern about cost of the presently available 3D geological modelling environments.

To guide the visualisation of all aspects of the geometry and the distribution of parameters (porosity and hydraulic conductivity) of an aquifer, it has become common practice to build 3D geological models by collating the hydrogeological data from various sources (Jones et al. 2002, Artimo et al. 2003, Herzog et al. 2003, Lemon and Jones 2003, Pantea and Cole 2004, Robins et al. 2005, Ross et al. 2005, Bonomi 2009, Gallerini and De Donatis 2009, Wycisk et al. 2009). The visual coordination of data and the interpolation of sparse data sets throughout the domain of interest can

now be achieved using *Mathematica*. The procedure for constructing 3D geological models in *Mathematica* is demonstrated for the Maules Creek catchment in the ***Crystallize*** notebook Crystallize_3D_Geological_Model.nb located in the folder Appendix3_Crystallize3DGeology.

2.1 Mathematica as a Geological Modelling Environment

Mathematica is a comprehensive programming environment which has an extensive library of mathematical and graphics functions that can be integrated into small scripts to solve many numerical and spatial visualisation problems.

Previous applications of *Mathematica* in the field of geology include: the reconstruction of complex folded surfaces (Johnson and Moore 1993; Moore and Johnson 2001), simulation of hanging wall deformation (Perez 2000), displaying animated 3D structures of the Earth's interior (Sato et al. 2003), strain analysis of folds (Bobillo-Ares et al. 2004) and the mapping of tortuosity and porosity of porous media (Nakashima and Yamaguchi 2004). There are also numerous examples relating to the earth sciences in Haneberg (2004).

3D geological framework models are constructed by modelling geological features as surfaces, which intersect according to rules that allow the visual representation of the geological features of interest (Mayoraz et al. 1992, Mallet 1997, de Kemp 1998, de Kemp 1999, Jones et al. 2002, Mallet 2002, Lemon and Jones 2003 and Galera et al. 2003). These surfaces may represent continuous depositional surfaces, the tops of lenses, or intrusions. The surfaces may also be faulted and folded. The model thus consists of a sequence of volume elements, bounded on the top, bottom and sides by continuous functions across the modelling domain. Each volume element can then be populated with a geological parameter (for example hydraulic conductivity).

2.2 An Overview of Constructing a 3D Catchment Scale Geological Model

The major steps in the workflow for building a 3D geological structural and facies model are presented in Figure 2. There are three primary data sets used for building the 3D geological structural and facies model; the geological mapping details of the catchment, the DEM, and the driller bore lithology logs (Figures 2, 3 and 4).

For the unconsolidated sedimentary aquifer system the lower boundary is usually taken as the palaeovalley erosion surface. This is defined by the outcropping rock and the basement picks from the driller bore lithology logs (Figures 2 and 3). In areas of steep terrain the DEM can be sorted into sediment and rock data sets on the basis of the gradient. This process is described in detail in Haneberg (2004). A description of the DEM sorting calculations using the gradient method and a tutorial data set is located in the folder Appendix2_DEMSorting. An alternative approach to sorting the DEM based on elevation of the ground surface is presented in the ***Crystallize*** notebook Crystallize_3D_Geological_Model.nb located in the folder Appendix3_Crystallize3DGeology. The sorted DEM used for the Maules Creek catchment model is presented in Figure 4. The continuous blue patches are the inferred rock zones from the DEM and the points are the bedrock picks from the bores. The combined outcropping rock and the bore bedrock pick data are gridded to form a single surface, which forms the base of the model.

The next step is to fill the unconsolidated sediment volume with the facies model. The driller logs throughout the catchment are divided into two classes: low (clay) and high (sand and gravel) hydraulic conductivity. The space between the boreholes is then filled using k-nearest neighbour

(KNN). It has been demonstrated that KNN is a good classification interpolator of categorical data (Dubois et al. 2007, Tartakovsky et al. 2007). The facies model is then combined with the structural model to give the complete conceptual 3D geological model of the catchment (Figure 5). The workflow for constructing 3D geological structural and facies models is described in more detail in the ***Crystallize*** notebook Crystallize_3D_Geological_Model.nb, located in the folder Appendix3_Crystallize3DGeology.

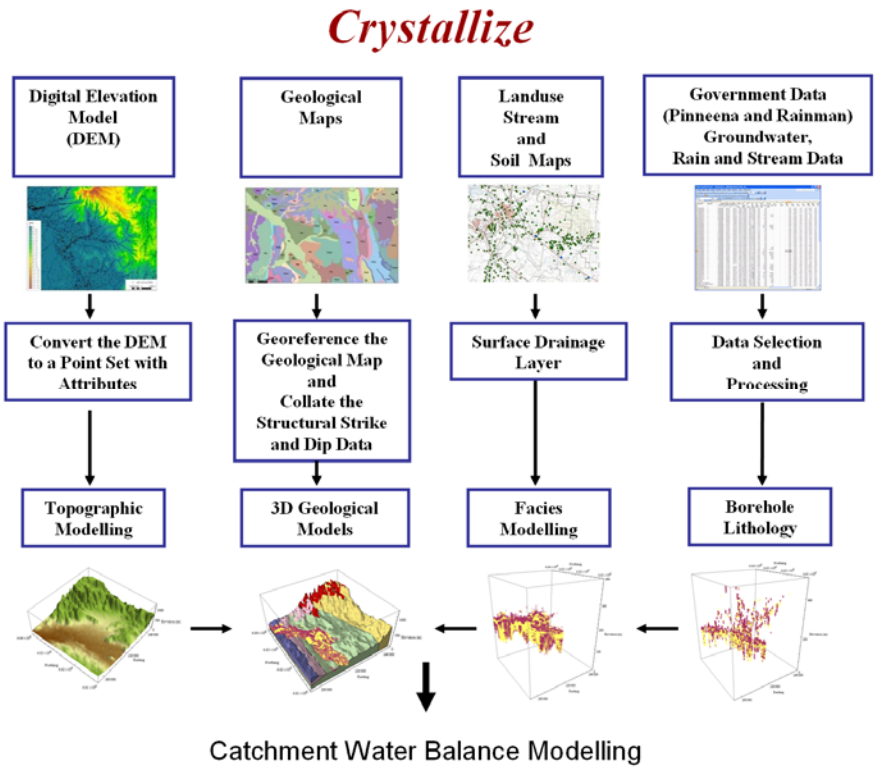

Figure 2. A schematic of the workflow for constructing a 3D geological structural and facies model, also called a conceptual site model.

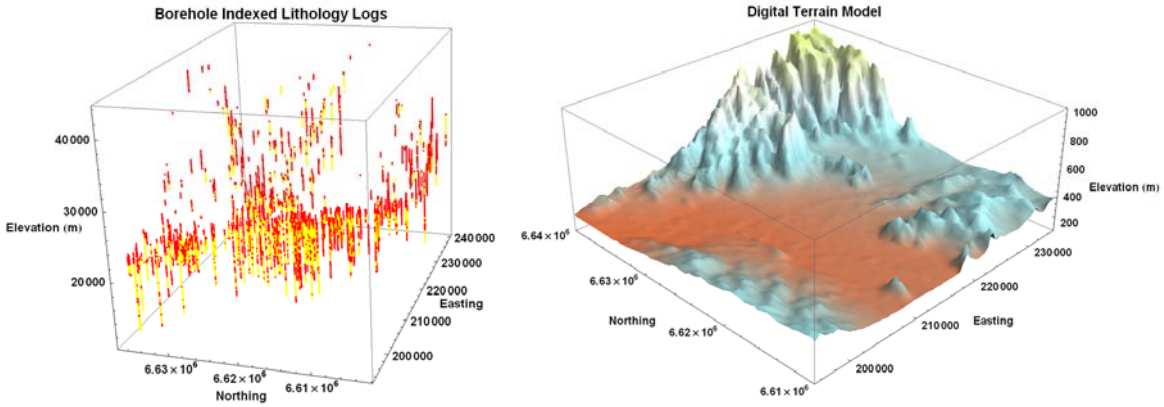

Figure 3. Data used to construct the 3D geological model; left the indexed borehole lithology logs (yellow - high hydraulic conductivity, red - low hydraulic conductivity sediments), and the DEM (Universal Transverse Mercator coordinate system zone 56, units metres).

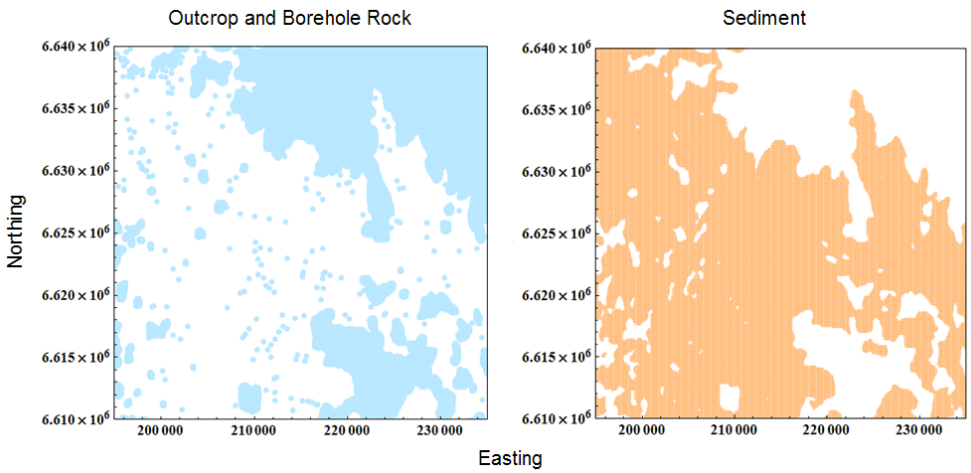

Figure 4. The aquifer bottom data is defined by the bedrock picks in the boreholes and the high gradient zones (rock outcrop) in the DEM (left), and the aquifer top is defined by the low gradient zones (sediments) in the DEM (right).

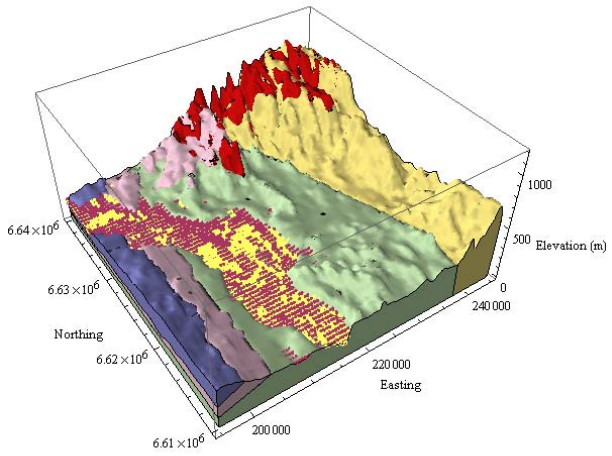

Figure 5: The Maules Creek 3D geological structural and facies model built using *Mathematica*. Each geological period is represented as a solid colour. The colour key used below is: Tertiary basalt (red), Jurassic (blue), Triassic (pink), Permian (green), and Carboniferous (yellow). In the unconsolidated sediment zone the purple is clay, and the yellow sand and gravel.

3 Groundwater Hydrographs

Throughout the Murray-Darling Basin in the unconsolidated sedimentary aquifers used for irrigation, numerous monitoring bores have been installed. The standing water level has been measured in these bores four or more times per year since installation (the majority were installed in the 1970s and 1980s). The hydrographs from these bores provide insights into how the aquifer system is responding to groundwater recharge events and irrigation extractions. Four representative ***Crystallize*** notebooks for hydrograph presentation and analysis are located in Appendices 7 and 8 (and folders: Appendix7_CrystallizeHydrographs and Append8_Crystallize3DGroundwater).

An example of the 3D bubble chart and 2D plot generated using the ***Crystallize*** notebook Crystallize_3DGroundwaterHeadTrends.nb is presented in Figure 6. The ***Crystallize*** notebooks in

Appendix 7 (folder Appendix7_CrystallizeHydrographs) are for the plotting of one or more hydrograph sets for a selected groundwater works number, while the notebooks in the Appendix 8 (folder Appendix8_Crystallize3DGroundwater) provide examples of the 3D analysis of the long term trend in the standing water level recorded in the bores, and the extent of the fluctuation in the groundwater level within a year. In regions where there are large groundwater extractions, mapping zones of high and low standing water level fluctuation provides a method for mapping aquifer connectivity in 3D. This can help with the construction of the catchment conceptual site model used for the catchment water balance modelling.

The results from the collation of the climatic, streamflow, groundwater usage, the conceptual 3D geological model and the 3D hydrograph analyses are presented in a time-lapse video (located in folder Appendix9_MaulesCreekTimeLapseVideo). This video gives a visual interpretation of the connection between rainfall, streamflow, groundwater usage and the recovered bore standing groundwater level (referred to as the head in the video).

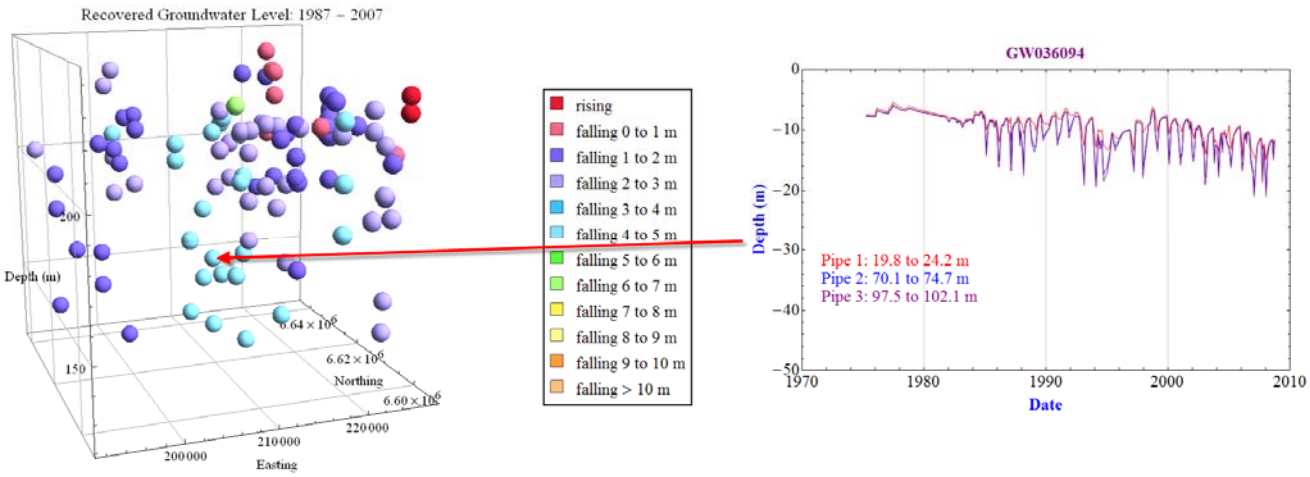

Figure 6. An example of the ***Crystallize*** 3D bore hydrograph analysis. Shown on the right hand side of the figure is an example of the groundwater works number hydrograph set that is automatically plotted when you click on a point in the 3D plot.

4 Groundwater Chemistry

In catchments throughout Australia there has been little consistency in the collection and analysis of groundwater chemistry data. In Appendix 10 there are four papers (Andersen and Acworth, 2007; Andersen et al., 2008; Patterson et al., 2008; Andersen and Acworth 2009) about the groundwater chemistry in the Maules Creek Catchment and adjacent reach of the Namoi River. These papers make use of the water chemistry data stored in the Maules Creek MS Access database. They demonstrate that analysing surface and sub-surface water chemistry is critical for understanding aquifer connectivity and the impact of irrigation extractions on groundwater movement, deep drainage and stream aquifer interactions.

The surface and sub-surface water chemistry clearly shows that there are distinct pathways of movement. In some intervals of the aquifer system there is recharge from young water (rainfall deep drainage, irrigation deep drainage, and stream recharge). In other portions of the aquifer old water, which is not mixing with the newer water, occurs. This work clearly demonstrates the need for incorporating water chemistry as part of assessing the sustainable use of groundwater.

5 References

Andersen M.S., Meredith K., Timms W. & Acworth R.I. (2008): Investigation of δ18O and δ2H in the Namoi River catchment – elucidating recharge sources and the extent of surface water/groundwater interaction. *XXXVI IAH Congress Toyama, Japan 26th of October - 1st of November 2008.*

Andersen, M.S., and Acworth, I.R. (2009) Stream-aquifer interactions in the Maules Creek catchment, Namoi Valley, New South Wales, Australia Hydrogeology Journal, 17: 2005 - 2021. doi:10.1007/s10040-009-0500-9

Andersen M.S. & Acworth R.I. (2007): Hydrochemical investigations of surface water groundwater interactions in a sub-catchment in the Namoi Valley, NSW, Australia. *Proceedings of the XXXV IAH Congress "Groundwater and Ecosystems", Lisbon. September, 2007.*

Artimo A, Makinen J, Berg RC, Abert CC, Salonen V-P, 2003, Three-dimensional geologic modelling and visualization of the Virttaankangas aquifer, southwestern Finland. *Hydrogeology Journal,* 11(3): 378-386.

Bobillo-Ares NC, Toimil NC, Aller J, Bastida F, 2004, FoldModeler: a tool for the geometrical and kinematical analysis of folds. Computers & Geosciences, 30(2):147-159.

Bonomi T, 2009, Database development and 3D modelling of textural variations in heterogeneous, unconsolidated aquifer media: Application to the Milan plain. *Computers & Geosciences,* 35(1): 134-145.

de Kemp EA, 1998, Three-dimensional projection of curvilinear geological features through direction cosine interpolation of structural field observations. *Computers & Geosciences,* 24(3): 269-284.

de Kemp EA, 1999, Visualization of complex geological structures using 3-D Bézier construction tools. *Computers & Geosciences,* 25(5):581-597.

Dubois MK, Bohling GC, Chakrabarti S, 2007, Comparison of four approaches to a rock facies classification problem. Computers & Geosciences, 33(5): 599-617.

Faunt, C.C., Belitz, K., Hanson, R.T., 2009, Development of a three-dimensional model of sedimentary texture in valley-fill deposits of Central Valley, California, USA. Hydrogeology Journal, Published online: 29 October 2009, DOI 10.1007/s10040-009-0539-7.

Galera C, Bennis C, Moretti I, Mallet JL, 2003, Construction of coherent 3D geological blocks. *Computers & Geosciences,* 29(8): 971-984.

Gallerini G, De Donatis M, 2009, 3D modelling using geognostic data: The case of the low valley of Foglia river (Italy). Computers & Geosciences, 35(1):146-164.

Haneberg, WC, 2004, *Computational geosciences with Mathematica*, Springer-Verlag Berlin Heidelberg.

Herzog BL, Larson DR, Abert CC, Wilson SD, Roadcap GS, 2003, Hydrostratigraphic modelling of a complex, glacial-drift aquifer system for importation into MODFLOW. *Ground Water*, 41(1): 57-65.

Johnson SE, Moore RR, 1993, Surface reconstruction from parallel serial sections using the program *Mathematica*; example and source code. Computers & Geosciences, 19(7): 1023-1032.

Jones NL, Budge TJ, Lemon AM, Zundel AK, 2002, Generating MODFLOW grids from boundary representation solid models. *Ground Water*, 40(2):194-200.

Keogh, K.J., Martinius, A.W., Osland, R., 2007, The development of fluvial stochastic modelling in the Norwegian oil industry: A historical review, subsurface implementation and future directions. Sedimentary Geology, 202:249-268.

Lemon AM, Jones NL, 2003, Building solid models from boreholes and user-defined cross-sections. *Computers & Geosciences,* 29(5): 547-555.

Mallet J-L, 1997, Discrete modelling for natural objects. *Mathematical Geology,* 29(2):199-219.

Mallet J-L, 2002, *Geomodelling*. Oxford University Press, Inc., New York, USA.

Mayoraz R, Mann CE, Parriauz A, 1992, Three-dimensional modelling of complex geological structures: New development tools for creating 3-D volumes. In: Hamilton DE and Jones TA, (eds) *Computer modelling of geological surfaces and volumes*, Computer Applications in Geology, No 1: 261-271.

Moore RR, Johnson SE, 2001, Three-dimensional reconstruction and modelling of complexly folded surfaces using *Mathematica*. *Computers & Geosciences,* 27(4): 401-418.

Nakashima Y, Yamaguchi T, 2004, DMAP.m: A *Mathematica* program for three-dimensional mapping of tortuosity and porosity of porous media. *Bulletin of the Geological Survey of Japan*, 55(3/4): 93-103.

Patterson J., Andersen M.S. & Acworth R.I. (2008): Development of an integrated conceptual model of a connected surface water-groundwater system using a hydrochemical approach at Maules Creek, NSW, Australia. *XXXVI IAH Congress Toyama, Japan 26th of October - 1st of November 2008.*

Pantea MP, Cole JC, 2004, *Three-dimensional geologic framework modelling of faulted hydrostratigraphic units within the Edwards aquifer, northern Bexar County, Texas.* US Department of the Interior, USGS Scientific Investigations Report 2004-5226, pp. 10.

Perez S, 2000, Computer simulation of hangingwall deformation. Paper presented at GeoComputation 2000, Proceedings of the 5th International Conference on GeoComputation, University of Greenwich, United Kingdom, 23-25 August 2000.

Robins NS, Rutter HK, Dumpleton S, Peach DW, 2005, The role of 3D visualisation as an analytical tool preparatory to numerical modelling. *Journal of Hydrology* 301(1-4): 287-295.

Ross M, Parent M, Lefebvre R, 2005, 3D geologic framework models for regional hydrogeology and land-use management; a case study from a Quaternary basin of southwestern Quebec, Canada. *Hydrogeology Journal,* 13(5-6):690-707.

Sato H, Muro K, Hasegawa A, and Zhao D, 2003, *Mathematica* as a powerful and practical tool for displaying animated three-dimensional structures of the Earth's interior. *Geochemistry Geophysics Geosystems G*^{3}, 4(4): pp. 8.

Tartakovsky DM, Wohlberg B, Guadagninni A, 2007, Nearest-neighbor classification for facies delineation. *Water Resources Research,* 43(W07201), pp. 5.

Wolfram Research, Inc., 2008, *Mathematica edition: version 7.0,* Wolfram Research, Inc., Champaign, Illinois. Available from www.wolfram.com

Wycisk P, Hubert T, Gossel W, Neumann C, 2009, High-resolution 3D spatial modelling of complex geological structures for an environmental risk assessment of abundant mining and industrial megasites. *Computers & Geosciences,* 35(1):165-182.

Appendix 1a

Development of a 3D Geological Mapping and Database Interface to Support Interconnected Groundwater and Surface Water Management

Project Databases

Authors
B. Giambastiani and B. Kelly

A1a.1 Microsoft Office Access Database

The groundwater data are sourced from the New South Wales Government - NSW Water Information "Historic Data CD Pinneena for Groundwater Works" 2007 version 2.1 (http://waterinfo.nsw.gov.au/pinneena/gw.shtmll).

The Pinneena for Groundwater Works CD includes:

- The location of approximately 107.000 groundwater works.
- Construction details of approximately 96000 groundwater works.
- Groundwater levels for approximately 11000 monitoring groundwater works.
- Drillers logs for approximately 79000 groundwater works.
- Geologists logs for approximately 900 groundwater works.
- Water bearing zone for approximately 69000 groundwater works.
- Great Artesian bores (various data including pressure) approximately 9000 bores.
- Purpose and use information for approximately 100000 groundwater works.
- Maps including: locations of groundwater works, groundwater management areas and local government areas.

A subset of the information from 2007 Pinneena groundwater works CD was extracted for the Maules Creek catchment considering the following geographic limits:

Geographic Coordinates		**Cartesian Coordinates**	
Minimum Longitude	149.8	Minimum Easting	191903.64
Maximum Longitude	150.5	Maximum Easting	260523.67
Minimum Latitude	30.25	Minimum Northing	6593669.78
Maximum Latitude	30.75	Maximum Northing	6650838.18

Extensive checks on the quality of the data needed to be undertaken, and this has been one of the more time consuming tasks. This quality control is particularly important because the data have been collected over several decades, using different coordinate systems, and much of the information has been manually entered.

The main issues associated with the groundwater database have been:

- differences between the Pinneena Groundwater 2005 and 2007 CDs, especially for the coordinates; after manually checking many of the bore details a decision was made to use the 2007 Pinneena Groundwater CD details;
- insufficient and poor geological descriptions (some units and depths are repeated, some descriptions are missing or there is a lack of clear or proper geological descriptions);
- the surface elevations are not given for all bores; and
- the slotted interval depths are not provided for all bores and in some cases are confusing and not consistent each other.

Data have been checked and cleaned based on the project's purposes and integrated with field data (GPS surveys) collected during several field campaigns in 2007-2009.

Daily streamflow and river heights from the NSW Office of Water in the Department of Environment, Climate Change and Water (http://www.water.nsw.gov.au/) are available for the period 1913 to 2008 for 3 gauging stations within Maules Creek Catchment: Boggabri (DNR code: 419012), Turrawan at Wallah (DNR code: 419023) and Maules Creek at Avoca East (DNR code:419051). Duplicate records have been cleaned and a single database table has been created for each parameter.

Climate data was obtained from SILO (http://www.nrm.qld.gov.au/silo) for the period January 1889 to December 2009 for 5 weather stations in the region: Narrabri West Post Office (53030), Barraba-Mount Lindsay (54021), Boggabri Post Office (55007), Turrawan - Wallah (55058); Boggabri - Kanownda (55076).

Finally, surface water and groundwater chemistry data collected during 4 different campaigns by the UNSW Connected Waters Initiative have been included in the database. Surface water data include monitoring points along the Namoi River and the main streams in Maules Creek Catchment (Middle Creek, Horsearn Creek, Ti Tree Creek, and Black Mountain Creek). Groundwater data include groundwater samples collected in the NSW State Government monitoring bores.

Tables and fields in the database have been assigned brief descriptions which can be seen in the 'Properties' table and in the 'Design View' window.

Note: Throughout this report and in the database DWE stands for the NSW Department of Water and Energy. This department has now been incorporated into the NSW Office of Water, in the Department of Environment, Climate Change and Water.

A1a.1.1 Maules Creek MS Access Database Files

TABLE NAME	NOTES
Casing Elevation	Elevation of well casings Bore name Pipe Elevation Data source (EV=values back interpolated on the DEM using EarthVision software, DWE = data from DWE database, GPS_wrl = from GPS surveys in the field)
Chemistry Data Groundwater	From the WRL team, field trips between 2006-2008: Bore name Pipe Date of sampling Elevation of sampling Water level Flow cell parameters (temperature, electrical conductivity, pH, reduction potential, oxygen) Cations (Fe(II), B, Ca, K, Mg, Mn, Na, Si, Sr, NH_4) Alkalinity Anions (Cl, NO_3,SO_4, F, NO_2, Br, PO_4) H_2S DOC (Dissolved Organic Carbon) Trace elements (Al, As, Ba, Cd, Co, Cr, Cu, Ga, Li, Mo, Ni, Pb, Rb, Se, Ti, Zn, Zr)
Chemistry Data Surface Water	From the WRL team, field trips between 2006-2008: Bore name Pipe Date of sampling Elevation of sampling Water level Flow cell parameters (temperature, electrical conductivity, pH, reduction potential, oxygen) Cations (Fe(II), B, Ca, K, Mg, Mn, Na, Si, Sr, NH_4) Alkalinity Anions (Cl, NO_3,SO_4, F, NO_2, Br, PO_4) H_2S DOC (Dissolved Organic Carbon) Trace elements (Al, As, Ba, Cd, Co, Cr, Cu, Ga, Li, Mo, Ni, Pb, Rb, Se, Ti, Zn, Zr)
Construction Details General	DWE construction details table (information about the slotted intervals is sometimes confusing) Bore name; Type of work; Information relating to hole, casing components and opening screen (number of holes and pipes) Top and bottom depth of each screens (m from ground level)
Daily Climate Data	From SILO (Jan 1889-Dec 2009)

TABLE NAME	NOTES
	Weather station code Dates Tmax (ºC) Tmin (ºC) Rain (mm) Evaporation (mm) Daily solar radiation ((MJ/m^2) Pressure (hPa) Relative humidity at maximum and minimum temperatures (%) FAO56 (Potential evapotranspiration calculating using FAO Penman-Monteith formula, see http://www.fao.org/docrep/X0490E/X0490E00.htm) (mm) Morton evaporation and evapotranspiration (calculated using Morton's method, see Morton, 1983) (mm) Comparison between pan evaporation and synthetic pan evaporation (mm) Data sources and quality control
Daily River Heights	From DWE (1913-nov 2009) Gauging station code Date Mean height (m from station benchmark at the gauging station)
Daily Streamflow Data	From DWE (1913-2008) Gauging station code Date Streamflow (ML/day)
Drillers Description General	Original table from DWE database (duplicate data, inconsistent geological descriptions, many unknown records) List of geological core logs Bore name Depths of different strata which were drilled (from-to depths) (m from ground level) Drillers description Rock type code
Drillers Description Modified	An interpreted lithological description from driller_description_general table (no duplicate points, number of rock type codes have been reduced). Bore name Depths of different strata which were drilled (from-to depths) (m from ground level) Drillers description Rock type code This file can be updated or changed and used to create input file for geological modelling.
EARTHVISION Geology	Description of geology used in the EarthVision and *Crystallize* 3D geological models Bore name Location Depth of the geological records (metres from ground level) Assigned geological code (0 topsoil; 1 clay; 2 silt-loam; 3 sand-gravel; 4 rock)

TABLE NAME	NOTES
	Elevation of the geological record (mAHD) Depth of the drilling (mAHD)
FEFLOW Abstraction Wells	A list of abstraction wells within the groundwater model domain and used in FEFLOW groundwater model. Bore name location Top, bottom and middle depth of each screens (m from ground level)
FEFLOW Observation Wells	A list of observation wells within the groundwater model domain and used to calibrate FEFLOW groundwater model Bore name Pipe number Top, bottom and middle elevation of screen (mAHD) Actual elevation used in FEFLOW (necessary adaptation to the 3D layer configuration of the groundwater model) FEFLOW slice number on which the observation well has been set
Geology Description	A list of geological codes and driller descriptions used in table 'driller description general' and 'driller description modified'.
GW Continuous WL Data	Groundwater level continuous data Bore name Pipe Measurement date Standing water level (SWL) (m from top of casing)
GW Level	Groundwater levels updated until 2008 Bore name Pipe number Location Measurement date Standing water level (SWL) (m from top of casing) Casing elevation Water level (WL) (mAHD)
License Description	Bore name; License Purpose description
Slotted Intervals	Slotted interval depths (interpreted from DWE database) Top, bottom and middle depth of each screen (m from ground level)
Usage Data 1996-2008 Maules Creek	Groundwater usage data provided by the DWE (1996-2008):values are in ML/year
Well and Pipe Coordinates	A list of all boreholes in Maules Creek Coordinates (LAT and LONG in AMG from DWE database; EASTING and NORTHING in MGA94 zone56 converted in ArcGIS); Data sources (GPS_wrl code for data which are from GPS surveys in the field and DWE code for data from DWE database)
Work Details General	General details for all wells in Maules Creek (from DWE database, not modified)

TABLE NAME	NOTES
	Bore name Location information Type of bores; Date of construction; Owner type; Method of construction; County information; Elevation and depth of bore Salinity at the time of construction

A1a.1.2 Using the MS Access Database

Users can extract data from the database using MS Access Queries via *Mathematica* in the Crystallize notebooks.

All of the following discussions on querying the database are valid if the operator works with Microsoft® Access 2003. The latest version of Microsoft Access (2007) has a different graphic interface and the follow operations could be slightly different.

Queries

'Sorting Climate Data'

> The 'Sorting Climate Data' query extracts climate data based on date and weather station ID. Click on the 'Queries' and open the 'Design View' window; in the fields 'Year' and 'Month' select the required interval of time, then select the required fields (i.e. 'Rain' and 'FAO56') and the operation to be performed on the data (i.e. monthly sum, average).

'Sorting River Heights'

> The 'Sorting River Heights' query extracts the river water level data based on the date and gauging station ID.
>
> Click on the 'Queries' and open 'Design View' window; in field the 'ID' select the gauging station for which data are required, in fields 'Year' and 'Month' select the required interval of time, in field the 'river height' select which operation needs to be performed on the data (i.e. average over the selected period of time, etc.).

'Sorting Streamflow'

> The 'Sorting Streamflow' query extracts streamflow data based on the date and gauging station ID.
>
> Click on the 'Queries' and open the 'Design View' window; in field the 'ID' select the gauging station for which data are required, for the fields 'Year' and 'Month' select the required interval of time, and for the field 'Streamflow' select which operation needs to be performed on the data (i.e. sum, average, etc.).

'Top Rock Elevation'

> The 'Top Rock Elevation' query sorts the top bedrock elevation from all geological core logs in Maules Creek Catchment. The output of this file has been used in EarthVision and the *Crystallize* 3D geological models.

‘Update GW Level’

The ‘Update GW Level’ query updates the groundwater level using data from future Pinneena releases.

Click on the ‘Queries’ and open the ‘Design View’ window; replace ‘example table’ with the table of data to be uploaded and follow the queries designed to append new data to the “GW level’ table in the database.

‘Usage data sorting’

The ‘Usage Data Sorting’ query extracts usage data for a specific interval of time in the Maules Creek Catchment.

Tables

‘Construction Details General’

The ‘Construction details general’ Table includes the original records from DWE database of slotted intervals and their depths. This table is a bit confusing, with duplicate data or missing data for some boreholes. If information about slotted intervals of specific wells is required, it is necessary to go through this table manually, searching the well of interest and checking the depths one by one. Due to the inconsistency of data in this table, it is not possible create queries to automatically sort data.

‘Driller Description General’

The ‘Driller description general’ Table contains the original records from DWE database and has duplicate data, inconsistent geological descriptions and many unknown records. This table has been simplified, cleaned and the result recorded in the ‘Driller description modified’ table.

‘EARTHVISION Geology’

The ‘EarthVision Geology Table’ includes the geological data as they have been used to build the 3D geological models of Maules Creek. Geological records from ‘Driller description general’ Table have been cleaned and simplified in 5 classes. A code has been assigned to each class: 0 topsoil; 1 clay; 2 silt-loam; 3 sand-gravel and 4 rock.

‘FEFLOW Abstraction Wells’ and ‘FEFLOW Observation Wells’

These tables store data used in the FEFLOW groundwater model. They do not include all abstractions and observation bores in Maules Creek Catchment.

'GW Level'

The 'GW Level' table includes all groundwater level data until 2008 (last update received from DWE). Any future groundwater level data need to be appended to this table using the instructions above. The table format is the one required by Python scripts used in the early stages of the project to create hydrographs of all bores in the Maules Creek Catchment.

'Work Details General'

The 'Work Details General' Table contains duplicate records for each WORK_NO. This is a potential issue as each 'WORK_NO' has coordinates associated with it, and the 'WORK_NO' is referenced by other tables, e.g. each borehole is identified by a 'WORK_NO'. This is the original table from the DWE database. Careful needs to be taken when making queries since it can result into duplicate values.

For further information about how to import/export tables and create queries refer to the Microsoft Office Access Help or Microsoft® Office Online.

Importing Tables

Data tables can be imported by right-clicking on the main window, selecting import and the file to import.

Exporting Queries and Tables

MS Access Queries and Tables can be exported to .xls, .dbf, .txt, .csv and ASCII format by right-clicking on the table, selecting export, and specifying the file name.

A1a.2 ArcGIS DATABASE

ArcGIS® 9.2 has been used to manage the large quantities of 2D spatial data and produce different thematic maps. In ArcGIS® the data have been stored and managed in several formats: vector (shapefile, geodatabase tables), raster (.tiff, .ecw, .jpeg) and DEM (Digital Elevation Model). ArcGIS® has also been used to create input data to upload into FEFLOW groundwater model.

GDA/MGA94 has been chosen as the unique coordinate system for the research project. However the data are from several sources and have different coordinate systems. By associating a spatial reference (.prj file) to each dataset, it is possible to integrate data with different coordinate systems and overlay them in a single project.

GIS files in the database have various associated documents (metadata, WebPages, .pdf files, etc.) that describe the content, quality, condition, origin and other characteristics of the data.

Data sources are listed below:

- Bureau of Meteorology (BOM)
- NSW Department of Primary Industries (DPI)
- Geoscience Australia
- NSW Office of Water (previously known as the Department of Water and Energy DWE)
- Namoi Catchment Management Authority (Namoi CMA)
- Land and Property Management Authority (LPI)
- Department of Information Technology and Management (LPI)

A1a.2.1 Maules Creek ArcGIS Database Files

	NAME FILE AND FORMAT	COORDINATE SYSTEM	NOTES AND DATA SOURCE
DPI data			
Faults in Maules Creek area	Faults.shp	GDA_1994_NSW_Lambert_State	
Coal bores	Coal_bores.shp	GDA_1994_NSW_Lambert_State	List of coal bores in Maules Creek area Bore ID Location Company Work construction details
Geological Boundaries	Geol_boundaries.shp	GDA_1994_NSW_Lambert_State	Geological boundaries in Maules Creek area
Gravity	Gravity.img	GCS_GDA_1994	Georeferenced images
Isostatic Gravity	Isostatic_Gravity.img	GCS_GDA_1994	Georeferenced images
	P_Narrabri_1VD_TMI_RTP_GDA94.ecw	D_GDA94	
Maules Creek Geology, Primarily the Hard Rock Geology	Rock_geologic_units.shp	GDA_1994_NSW_Lambert_State	All geological units and strata names in Maules Creek area.
Total Magnetic Intensity	TMI.img	D_GDA94	Georeferenced images
New South Wales Mineral Exploration 'Geoscience Data Package version 2'			This database contains a synthesis of exploration-related digital geological dataset for New South Wales from NSW Department of Primary Industries. It includes: • Mineral Exploration Bore Holes • Industrial Mineral Occurrences • Metallic Mineral Occurrences • Geophysical Imagery, Magnetics, Gravity, Radiometric Digital Terrain and LANDSAT • NSW 1: 250000 and 1:1000000 scale geology • Georeferenced Geological and Metallogenic Maps • NSW Petrographic Samples • NSW Isotopic Age Dates • topographic, basic hydrographic information and infrastructure.
EVAPOTRANSPIRATION AND PRECIPITATION			
Average Rainfall	Rainann.shp Rainjan.shp	Australian_Lambert_Conformal_Conic Geographic Coordinate System:	Average annual and monthly rainfall distribution across Australia based on 30 years (1961-1990)

	NAME FILE AND FORMAT	COORDINATE SYSTEM	NOTES AND DATA SOURCE
	Rainfeb.shp Rainapr.shp Rainmar.shp Rainmay.shp Rainjun.shp Rainjul.shp Rainaug.shp Rainsep.shp Rainoct.shp Rainnov.shp Rainoct.shp Rainnov.shp Raindec.shp	GCS_Australian	http://www.bom.gov.au/jsp/ncc/climate_averages/rainfall/index.jsp
Average Actual Evapotranspiration	aaann.shp aajan.shp aafeb.shp aaapr.shp aamar.shp aamay.shp aajun.shp aajul.shp aaaug.shp aasep.shp aaoct.shp aanov.shp aaoct.shp aanov.shp aadec.shp		Average annual and monthly evapotranspiration distribution across Australia based on 30 years (1961-1990) http://www.bom.gov.au/jsp/ncc/climate_averages/evapotranspiration/index.jsp
GEOLOGY DATASET			
Australian Geological Provinces	Geolprov.shp	GCS_WGS84	Provinces (Name, subprovinces, type, age, description, area) , (note: dataset not complete for the whole of Australia) . From Geoscience Australia http://www.ga.gov.au
Geological Region	Greglndd.shp Gregplddd.shp	GCS_WGS84	Geological regional boundaries (name, age, area, type, landforms, stratigraphy, mineral deposits) from Geoscience Australia http://www.ga.gov.au
Geology	Geolpldd.shp Geollndd.shp	Unknown	Geological boundaries; Major rock types and geological groups;

	NAME FILE AND FORMAT	COORDINATE SYSTEM	NOTES AND DATA SOURCE
			Age; Time/space plot of geological units from Geoscience Australia http://www.ga.gov.au
Sedimentary basins_basement relief	Sedbasdd.shp	GCS_WGS84	Sedimentary basin name and type. From Geoscience Australia http://www.ga.gov.au
Surface Geology	Geolpldd.shp Geollndd.shp nsw_geol_line.lyr nsw_geol_poly.lyr	GCS_WGS84	Surface geology of Australia 1:1,000,000 scale (rock unit; name; formation; member; age; lithology group and description. From Geoscience Australia http://www.ga.gov.au
	Geo_MaulesCreek_points.shp Geo_MaulesCreek_zone56	GCS_GDA_1994 GDA_1994_MGA_Zone_56	Maules Creek geology. Geological polygons have been exported into point data file for building 3D geological models in EarthVision and Crystallize.
EarthVision Files	ALLUVIUM_sorted.shp FAKE_ROCK_sorted.shp ROCK_sorted.shp	GDA_1994_MGA_Zone_56	Point data files obtained by sorting the DEM into alluvium and rock domains based on the topographic gradient.
	LowerNamoi_alluvium_zone55.shp	GDA_1994_MGA_Zone_55	From Namoi CMA modified boundary of Lower Namoi alluvium aquifer
Namoi Geology	Namoi_geology.shp	GCS_GDA_1994	Namoi geology (rock unit; name; formation; member; lithologic group, age; lithology group and description)
Maules Creek Geology	Rock_geologic_units.shp	GDA_1994_NSW_Lambert_State	From DPI (all geological units and strata names of Maules Creek area)
GRAVITY AND MAGNETIC			
Gravity Anomaly Images of the Australian Region	Gravcl800md.ecw	GCS_WGS84	grid cell size = 0.5 minutes of arc (~800 m) Scale 1:1,000,000. From Geoscience Australia http://www.ga.gov.au
Magnetic Anomaly Images of the Australian Region	Magcl1000md.ecw	GCS_WGS84	grid cell size = 0.01 degree (~1km) Scale 1:1,000,000. From Geoscience Australia http://www.ga.gov.au
HYDRO-HYDROGEOLOGY			
Australian Surface Water Management Areas	Swma_geom_nat_point.shp Swma_geom_nat_chain.shp Swma_geom_nat_polygon.shp	GDA/MGA1994	Boundaries and names of surface water management areas (SWMA), river basins, drainage divisions used by each State and Territory for the management of surface water (basin name, area, perimeter, State). From Geoscience Australia http://www.ga.gov.au

	NAME FILE AND FORMAT	COORDINATE SYSTEM	NOTES AND DATA SOURCE
Hydrogeological Division	Hydgeodd.shp	GCS_WGS84	Hydrogeological unit; Type; Characteristic of the aquifer from Geoscience Australia http://www.ga.gov.au
Rivers	Stream_nambas_amgz56.shp	AGD/AMG1984	Rivers in Namoi Catchment
	Stream_GDA_ZONE55.shp	GDA_1994_MGA_Zone_55	Data transformed in ArcGIS using 'Project and Transformation' tool. Original data 'streams_nambas_amgz56'
	Stream_GDA94_ZONE56.shp	GDA_1994_MGA_Zone_56	Data transformed in ArcGIS using 'Project and Transformation' tool. Original data 'streams_nambas_amgz56'
Rivers & Sub-Catchments	Namoi_RAUs_v2.shp	GDA_1994_MGA_Zone_55	Information about river style, sub-catchments, regions and channel name.
Groundwater Management Areas	GMA.shp Namoi_GMA.shp GMAs selection.lyr GMAs for Namoi catchment.lyr	GCS_GDA_1994	Groundwater management areas.
Namoi Catchment	Namoi_catchment_bdy.shp	GCS_GDA_1994	Namoi Catchment (from Namoi CMA)
Drainage	ba_drainage_grid.shp + many polyline shapefiles of drainage	GCS_Australian_1966	Drainage system of a portion of NSW (Namoi Catchment and surroundings). Canals and watercourses.
Water Body	Many polyline shapefiles of water bodies	GCS_Australian_1966	Water bodies of a portion of NSW (Namoi Catchment and surroundings). Lakes, swamps, land subject to inundation and watercourses.
NAMOI CMA DATA			
Namoi Catchment Data	Namcma_towns_GDA.shp Namcma_rivers_GDA.shp Namcma_roads_GDA.shp Namcma_bdy_GDA.shp NaCMA_SoilLandscape_060908_GDA94.shp NaCMA_landuse.shp NaCMA_LandManagementUnits_190908_GDA94.shp NaCMA_LandSoilCapability_080908_GDA94.shp Acidity.shp Sodicity.shp Erosion.shp	GCS_GDA_1994	Information about: towns, rivers, roads, water bodies, soil map, land use map, land soil capability, acidity, sodicity, and erosion. All the data are from Namoi CMA
NSW_GROUNDWATER ARCHIVE 2007 (Pinneena CD)			

	NAME FILE AND FORMAT	COORDINATE SYSTEM	NOTES AND DATA SOURCE
NSW Local Government Area Boundaries	LGA_.shp	GDA/MGA1994	
Ground Water Management Area Boundaries	Macro plans.shp	GDA/MGA1994	GMA (number, name, type); Provinces;
Town NSW	Nswtowns_point.shp	GDA/MGA1994	Town; population and State
Murray	MRY.shp	GDA/MGA1994	Bore name; License; Location; Owner type; Date of construction; Depth; Water level; Salinity at the time of construction (description)
South coast	South.shp	GDA/MGA1994	See above
Hunter	Hunter.shp	GDA/MGA1994	See above
Murrumbidgee	Murrumbidgee.shp	GDA/MGA1994	See above
North coast	North.shp	GDA/MGA1994	See above
Macquarie	Macquarie.shp	GDA/MGA1994	See above
Lower Murray	Lmurray.shp	GDA/MGA1994	See above
Lachlan	Lachlan.shp	GDA/MGA1994	See above
Barwon	Barwon.shp	GDA/MGA1994	See above
TOPOGRAPHY			
Bathymetry and topography			
Australian Bathymetry and Topography Images	Bathcl500md.ecw	GCS_WGS84	Grid cell size = 0.01 degree (~1km) Scale 1:1,000,000 From Geoscience Australia http://www.ga.gov.au
DEM (Digital Elevation Model)			
SRTM_3arcsec	Australia (ARC GRID) My area2 (ARC GRID)	GCS_WGS84	3 arc seconds (about 90 m resolution) (downloaded from CGIAR-CSI http://srtm.csi.cgiar.org/) see associated DEM_read document
	MaulesCreek.shp	GCS_WGS_1984	Point shapefile extrapolated from SRTM_3arcsec DEM using ArcGIS tool x,y, elevation
DEM 30 s	dem_aus30s (ARC GRID)	GDA/MGA1994	Australia 30 arc seconds DEM (about 1 km resolution, for regional and continental scale topographic data) from Geoscience Australia

	NAME FILE AND FORMAT	COORDINATE SYSTEM	NOTES AND DATA SOURCE
			http://www.ga.gov.au
DEM 9s	dem_aus9s (ARC GRID)	GDA/MGA1994	Australia 9 arc seconds DEM (about 250 m, for application requiring data at a scale of 1:250000 and smaller) from Geoscience Australia http://www.ga.gov.au
	LowerNamoi_dem_9arcsec_points_zone55.shp	GDA_1994_MGA_Zone_55	Point shapefile extrapolated from dem_aus9s DEM using ArcGIS tool x,y, elevation
CONTOUR LINES			
Topographic contour lines	Many polygon shapefiles	GCS_Australian_1966	10 m contour lines for Namoi Catchment and surroundings From LPI – Department of Information Technology and Management
SATELLITE IMAGES (FROM Namoi CMA)			
Angledool	Angledool.ecw	GDA_1994_MGA_Zone_55	
Dorrigo	Dorrigo.ecw	GDA_1994_MGA_Zone_56	
Gilgandra	Gilgandra.ecw	GDA_1994_MGA_Zone_55	
Hastings	Hastings.ecw	GDA_1994_MGA_Zone_56	
Manilla	Manilla.ecw	GDA_1994_MGA_Zone_56	
Moree	Moree.ecw	GDA_1994_MGA_Zone_55	
Narrabri	Narrabri.ecw	GDA_1994_MGA_Zone_55	
Tamworth	Tamworth.ecw	GDA_1994_MGA_Zone_56	
Walgett	Walgett.ecw	GDA_1994_MGA_Zone_55	
TOPOGRAPHIC MAPS			
Topography map of NSW	currentTOPOgeo50.ecw	GDA/MGA1994	Georeferenced topographic map, 1:10000 This database also contains all topographic maps 1:25000 and 1:50000 for New South Wales from Land and Property Management Authority (LPI) From LPI
Moree, Narrabri, Tamworth	H5508.ecw H5512.ecw H5613.ecw + Shapefiles geodatabase	GDA/MGA1994	Map Cartography; Elevation; Framework; Habitation; Hydrography; Infrastructure, Terrain Transport;

	NAME FILE AND FORMAT	COORDINATE SYSTEM	NOTES AND DATA SOURCE
			Utility; Vegetation (from Geoscience Australia http://www.ga.gov.au)
USAGE DATA			
Usage Data Maules Creek 1996-2008	Usage_data_MaulesCreek.shp Usage_00_01.shp Usage_01_02.shp Usage_02_03.shp Usage_03_04.shp Usage_04_05.shp Usage_05_06.shp Usage_06_07.shp Usage_07_08.shp Usage_96_97.shp Usage_97_98.shp Usage_98_99.shp Usage_99_00.shp	GDA_1994_MGA_Zone_56	Groundwater usage data on an annual basis (from 1996 to 2008) provided by DWE.
PROCESSED DATA			
GENERAL DATA			
Boreholes	All_wells_Namoi.shp	GDA/MGA1994 zone 56	All boreholes in the Namoi Catchment (DWE database)
	LowerNamoi_monitoring_wells		Monitoring Bores in Lower Namoi sub-catchment
	Namoi_monitoring_wells.shp		Monitoring Bores in the Namoi Catchment
	Observation_wells_MaulesCreek.shp		list of monitoring wells in Maules Creek info of screen depths
Namoi Catchment	Namoi catchment study area.shp	GDA/MGA1994 zone 56	Digitised Namoi catchment boundary
Weather Stations	Rainfall_stations_MaulesCreek.shp		List of all weather stations in Maules Creek (from BOM)
Study Area	Study area_MaulesCreek.shp	GDA/MGA1994 zone 56	Boundary of the study area (Maules Creek) used for the geological modelling.
GROUNDWATER MODEL DATA			
Land Use	1E.shp 2E.shp 3E.shp Landuse_GWmodel.shp Landuse_mesh_transient_model.shp Maules_C_hills_landuse.shp Maules_C_plain_landuse.shp S1.shp S2.shp	GDA/MGA1994 zone 56	Land use of the Maules Creek surface water catchment used to calculate diffuse recharge and fluxes for the groundwater model

	NAME FILE AND FORMAT	COORDINATE SYSTEM	NOTES AND DATA SOURCE
	S3.shp S4.shp W1.shp W2.shp W3shp		
Abstraction Well and Usage Data	Abstraction_wells.shp	GDA/MGA1994 zone 56	From the DWE database modified list of abstraction wells in FEFLOW groundwater model domain and info about slotted intervals
	Usage_data_GW_model.shp		Usage data within groundwater model domain
Boundary conditions	BC_north_boundary.shp	GDA/MGA1994 zone 56	Boundary conditions used in FEFLOW groundwater model .
	BC_river_line.shp		
	BC_river_points.shp		
	BCs.shp		
Rivers	Creek_points_catchment.shp	GDA/MGA1994 zone 56	Created using the “Feature to Points” tool from river polyline shape.
	MaulesCreek.shp Namoi_river.shp		
Cross Sections	Cross_section_GWmodel.shp	GDA/MGA1994 zone 56	
FEFLOW Mesh	FEFLOW_mesh_GWmodel.shp	GDA/MGA1994 zone 56	FEFLOW mesh (distribution of triangles and nodes)
Gauging Stations	Gauging_station.shp	GDA/MGA1994 zone 56	List of gauging stations used in FEFLOW groundwater model
Study Area	GW_boundary.shp GW_catchment.shp GW_sub_catchment.shp Maules_C_hills.shp Maules_C_plain.shp	GDA/MGA1994 zone 56	Groundwater model domain boundary Catchment boundary
Monitoring Bore	Observation_wells.shp	GDA/MGA1994 zone 56	From DWE database modified The shape also includes info about depth and FEFLOW slice number where the observation bores have been applied in the groundwater model

A1a.2.2 Using the ArcGIS Database

Importing

Data can be imported into an ArcGIS project by clicking on the 'Add Data' icon, navigating to the project folder on the computer and selecting the desired file.

Exporting

Property tables of shapefiles can be exported from ArcGIS into ASCII, .dbf and .txt formats and imported and used in other software.

Export a Shapefile to the dbf, .txt Format

Select and open the shapefile attribute table by right-clicking on the shapefile, select the 'Option' button and then 'Export Data'. Finally set the location and name for the .dbf or .txt file and all fields present in the attribute table will be exported.

Export a Shapefile to ASCII Format

From the 'ArcToolbox' menu select 'Spatial Statistics Tools > Utilities > Export Feature Attribute to ASCII'

In the 'Export Feature Attribute' to ASCII window the following steps are required:

1) specify the input feature class (shapefile needed to be exported);
2) choose the attribute value to export;
3) choose 'Space' as the delimiter option; and
4) set the location and name for the ASCII file.

Export a Polygon Shapefile to a Point Data File

From the 'ArcToolbox' menu select 'Data Management Tools > Features > Feature Vertices To Points'
In the 'Feature Vertices To Points' window specify input and output features (.ASC or .txt format)

An example of the need for this operation is exporting a geological unit boundary to point data.

Export a Polygon Shapefile to a CAD Format File

From the 'ArcToolbox' menu select 'Conversion Tools > to CAD > Export to CAD'
In the 'Export to CAD' window the following steps are required:

1) specify the input feature class (shapefile needed to be exported);
2) choose the output type required (.dwg, .dxf, etc.); and

3) set the location and name for the ASCII file.

Export a Raster File to an ASCII format

From the ‘ArcToolbox’ menu select ‘Conversion Tools > From Raster > Raster to ASCII’.
In the ‘Raster to ASCII’ window specify input (raster file) and output features (.ASC or .txt format).

An example would be exporting a DEM to a point data set for use in a geological model.

A1a.2.3 Additional Help about Using ArcGIS

For further information about how to import, export and convert ArcGIS file please refer to the ArcGIS® Desktop Help.

In Appendix 2 there is a tutorial with detailed instructions and example files about exporting, importing and separating a digital elevation model (DEM). Sorting the DEM is required as part of preparing the data for constructing a 3D geological model.

Appendix 1b

Connecting to the MS Access Database

A1b.1 Introduction

Before the database can be used on a new computer a link needs to be established between the MS Access database and *Mathematica*. You do not have to have MS Access installed on the computer that is being used to access the database using *Mathematica*.

Below is a subset from the *Mathematica* help library.

A1b.2 Setting Up the Connection

You need to use the ODBC control panel to register the data source. This is typically found in the **Administrative Tools** folder of the Windows **Control Panel**. When it is opened it looks something like the following.

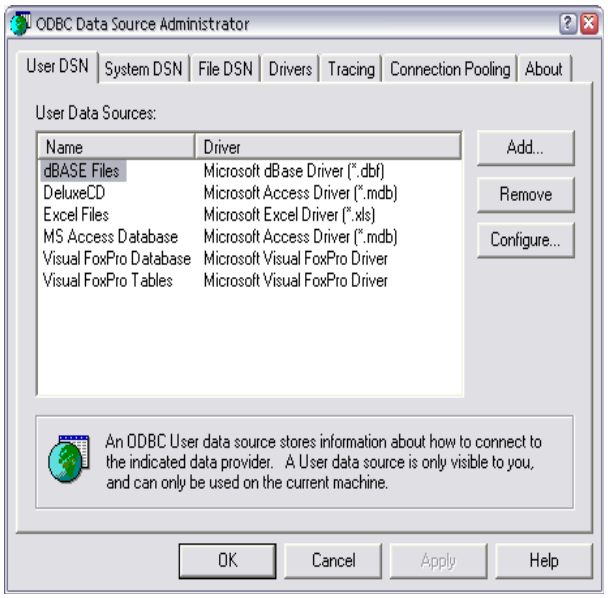

Click the **Add** button, this will bring up the **Create New Data Source** window.

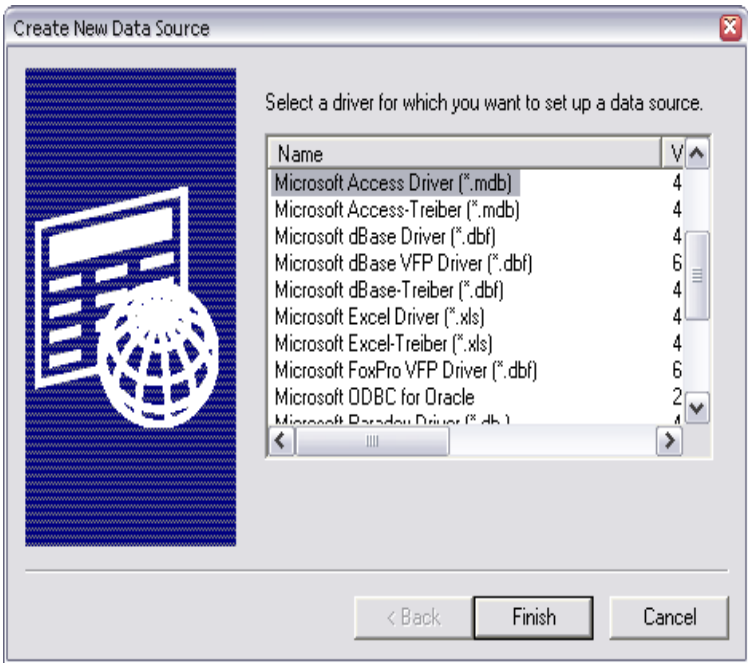

Select **Microsoft Access Driver** and then click **Finish**. This will bring up an **ODBC Microsoft Access Setup** window.

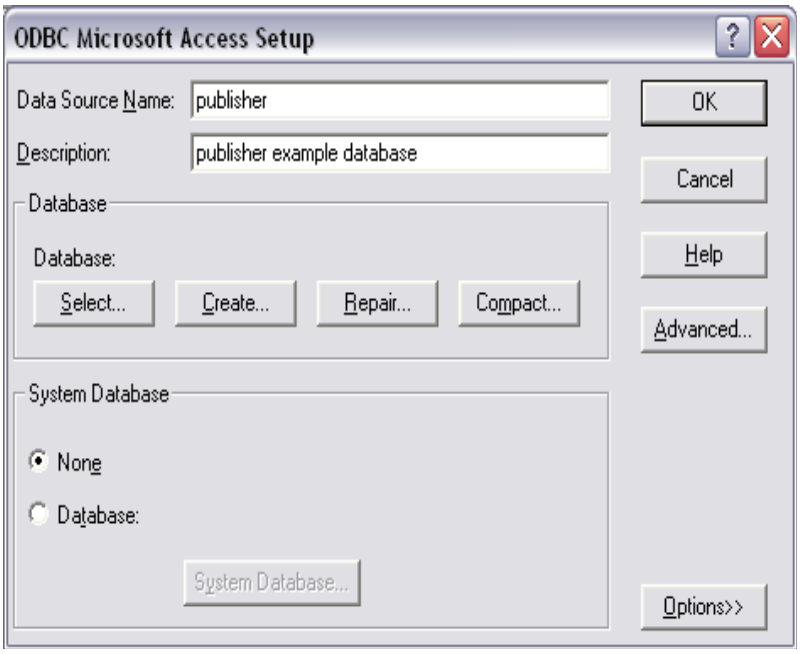

You should fill in the **Data Source Name** text field, using the name "publisher" (this is the name that ODBC will use). Then, click the **Select** button, which allows you to find and select the `publisher.mdb` file.

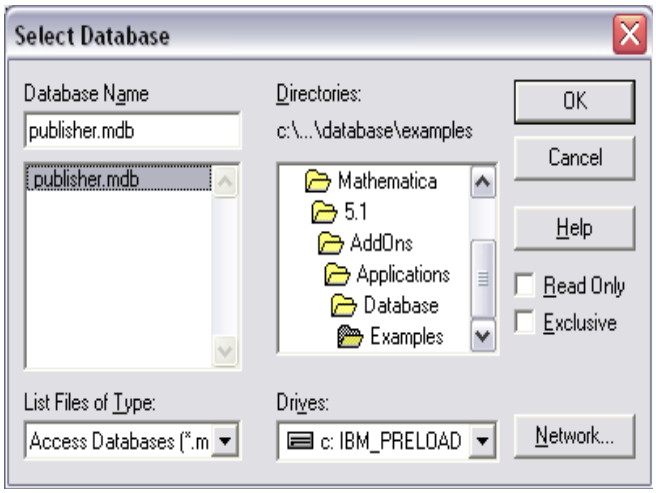

Click **OK** in each successive window until the control panel has been closed. Note that publisher and its driver now appear in the list of available files in the **ODBC Data Source Administrator** window.

Appendix 2

Importing and Separating a Digital Elevation Model (DEM) for Near Surface Geological Models

Authors
B.Giambastiani and B. Kelly

A2.1 Introduction

The top surface of 3D Geological Models that represent the near surface geology in catchments is the surface topography. Data that define the topographic surface can be obtained from many sources including satellite, land-based and airborne geophysical surveys, geological field mapping and borehole logging. The most common form of topographic data used in spatial data analysis are the freely available Digital Elevation Models (DEMs).

Often sediment filled valleys are surrounded by mountains with exposed rock outcrops. In this situation the DEM defines the top of the rock surface and the top of the sediments. When building a 3D *EarthVision* geological model of a catchment the DEM needs to be separated into the two domains. This manual details how this can be achieved in *EarthVision*.

If the DEM data are in a GIS raster format then the data need to be preprocessed in a GIS package before being imported into *EarthVision*. For this manual the DEM is firstly imported into *ArcGIS*, cleaned, trimmed and then exported into a format compatible for *EarthVision*.

The data used for this example are from the Maules Creek catchment located in the state of New South Wales, in Australia. The methodology developed for this case study can be successfully applied on any area of steep rocky mountains surrounded by flat alluvial plains. In these locations the gradient of the DEM data is sufficient for sorting the data into regions of rock outcrop and alluvial plains. High gradient (the rock outcrop) are sorted from the flat areas (the alluvial sediments) by calculating the partial differential in X and Y directions.

In *EarthVision* there is a Slope Grid program. Using this program to separate low gradient alluvial areas from step rocky areas may be appropriate in some catchments. The process detailed below although based on examining the slope of the surface, has some subtle variations compared to using the Slope Grid program and yields a slightly different degree of separation. The major differences are adding the X and Y partial differential grids and then filtering this output.

A2.2 Method Overview

Frequently data coming from diverse sources are in different formats which require conversion to a suitable format before being imported into the software that is being used. A DEM is a digital representation of ground-surface topography commonly built using remote sensing techniques and land surveys. Commonly the DEM is represented as a raster that is a matrix of cells where each cell contains an attribute value and location coordinates. The accuracy of a DEM is determined primarily by the resolution (the size of the cells). In this example SRTM (Shuttle Radar Topography Mission) 90 m Digital Elevation Data of Australia has been used as the initial DEM. The SRTM 90 m DEM's have a resolution of 90 m at the equator and are provided in a mosaic of cells of size 5 x 5 degrees and they are available in *ArcInfo ASCII* and *GeoTiff* formats from the CGIAR Consortium for Spatial Information website (CSI-CGIAR).

The steps outlined below are those required to convert a raster DEM into an X, Y and Z ASCII data point file, required for data transfer to the coordinate transformation program and then into *EarthVision*. Then once the data are in *EarthVision* they are further sorted into two classes (rock and alluvium). The major steps in the two software packages are:

1) *ArcGIS Data Preparation*

- Import the DEM into *ArcGIS*
- Clip the DEM to the study area
- Convert the raster DEM to a point data shapefile
- Add X and Y coordinates
- Export from *ArcGIS* as latitude, longitude and elevation (X, Y and Z) ASCII data
- Convert the data from latitude and longitude to Eastings and Northings

2) *EarthVision Data Sorting*

- Import the point data file into *EarthVision*,
- Using 2D Minimum Tension Gridding calculate a 2D grid of the DEM,
- In the Formula Processor determine the X and Y direction partial differentials,
- Filter the data using the Grid Filtering program, and
- Sort in the Formula Processor into the alluvial horizon data and rock outcrop horizon data.

After all the above steps are completed the data will be ready for incorporating into a 3D Geological Model built using either the Geologic Structure Builder or the WorkFlow Manager.

EarthVision supports DEM in ASCII format where data (X, Y and Z) are stored as columns of Easting, Northing and elevation. Sometimes it is possible to download a DEM in a format suitable for *EarthVision* (such as all Digital Elevation Models distributed by the United States Geological Survey (USGS)). If this applies to you, go directly to Section 4 EarthVision Data Sorting. Follow the instructions below if the DEM for your area is in a raster format, or other format not compatible with *EarthVision.*

A2.3 ArcGIS Data Preparation

Import the DEM into *ArcGIS*

Add the DEM of Australia to your project: click on the *Add Data* icon (Figure 1), navigate to the project folder on your computer, select australia.aux and click *Add* (Figure 2; Australia requires the australia.aux file and the associated folder called "australia").

(Note: If your dataset is larger than 1024 by 1024 cells, a dialog box will be displayed asking you to select the building pyramids option. Click NO if you do not wish to build pyramids and reduce the spatial resolution of your dataset).

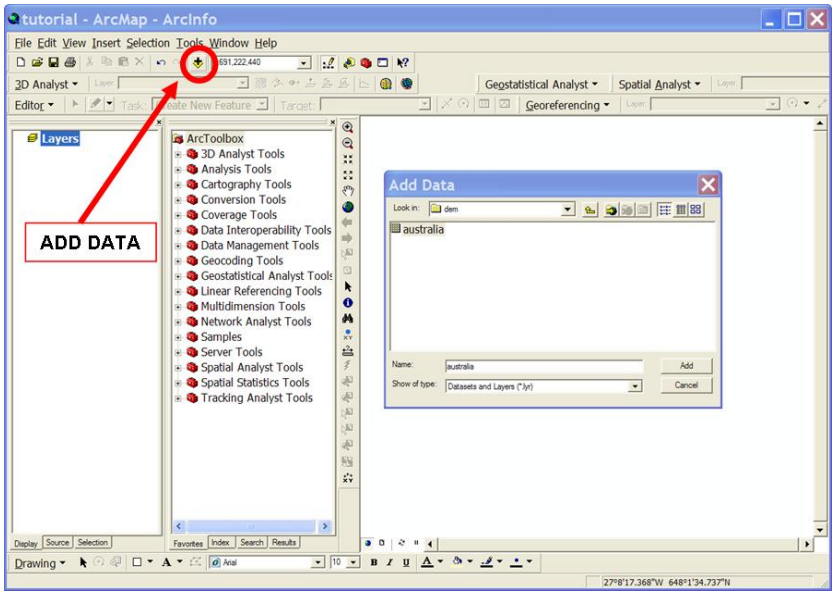

Figure 1: The Add Data push-button.

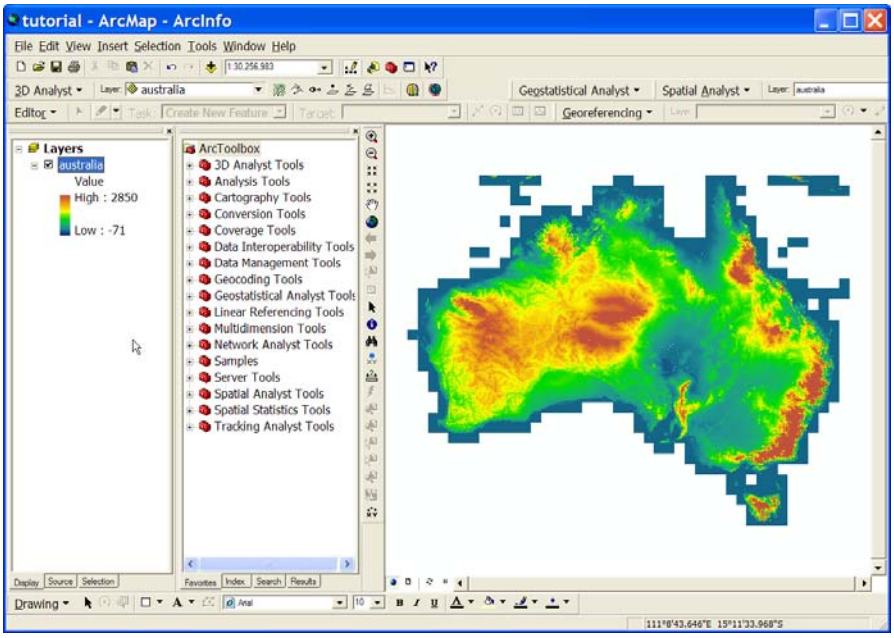

Figure 2: Australia DEM example (SRTM).

Clip DEM to the study area

From the *ArcToolbox* menu select the tool to *Clip* the DEM based on the coordinates of the boundary of your study area: *Data Management Tools* > *Raster* > *Clip* (Figure 3).

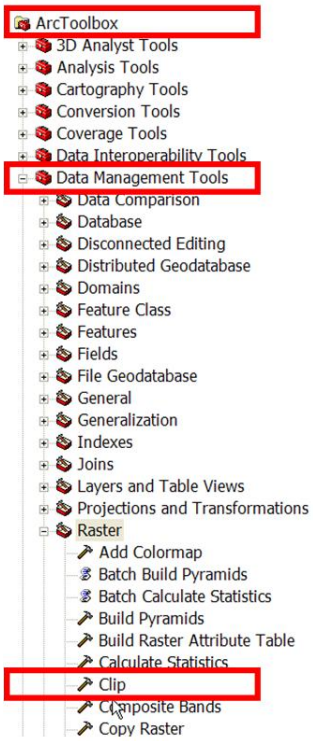

Figure 3: *ArcToolBox* menu path to the *Raster* > *Clip* tool.

In the Clip window you need to specify the input raster (the DEM you want to cut) and the clipped rectangular area specifying the minimum and maximum X and Y coordinates based on the coordinate system of your project (Figure 4). Choose a folder and name for the output raster dataset and select OK (Figure 4). After clipping you will have a subset of the original data (Figure 5).

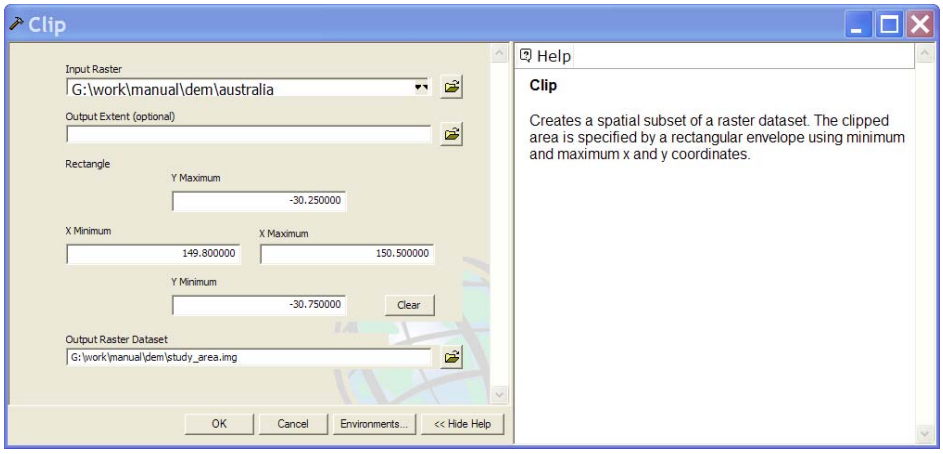

Figure 4: Raster Clip window.

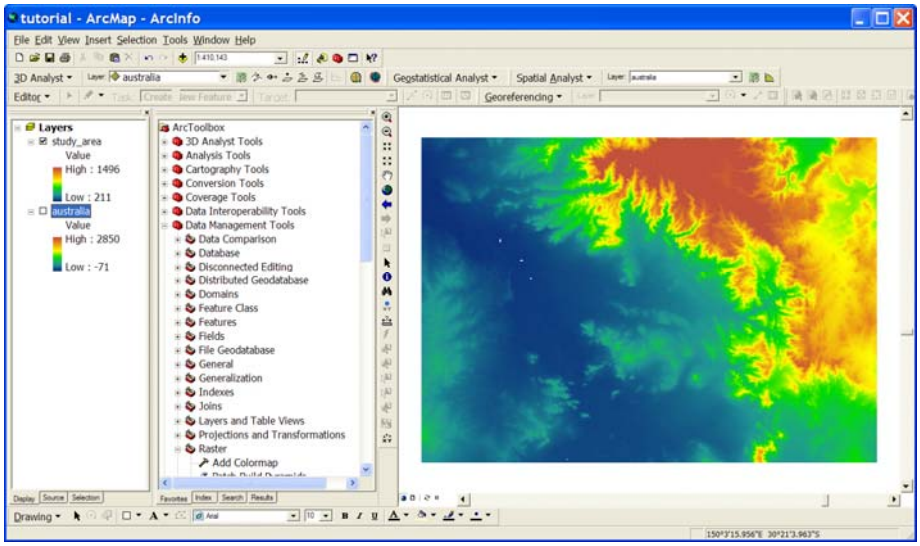

Figure 5: DEM of the study area after clip operation.

Convert raster DEM to a point data shapefile

From the *ArcToolbox* menu select the tool to convert the raster dataset of the study area to point features: *Conversion Tools* > *From Raster* > *Raster to Point* (Figure 6).

In the Raster to Point window you need to specify the input raster dataset (your study area), select the folder and name of the output feature class (shapefile) that will contain the converted points and select OK (Figure 7).

(Note: in the Field window, click the dropdown arrow and select which column in the raster dataset will become an attribute in the output point file. In the following example the column selected is Value because it contains DEM elevation values. Check the attributes table of the DEM you are working on and be sure you are selecting the right column)

After this operation you will get a point shapefile where the elevation values of the DEM cells become the column *Grid_code* in the attribute table of the point feature class generated. For each cell of the input DEM a point is created and positioned at the centre of cells they represent (Figure 8).

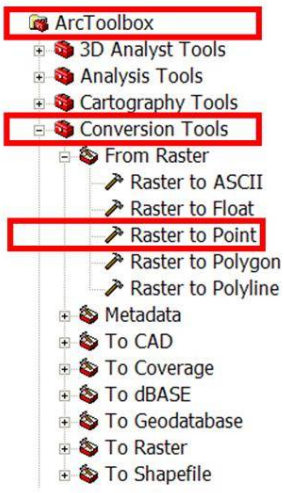

Figure 6: ArcToolBox menu path for Conversion Raster to Point.

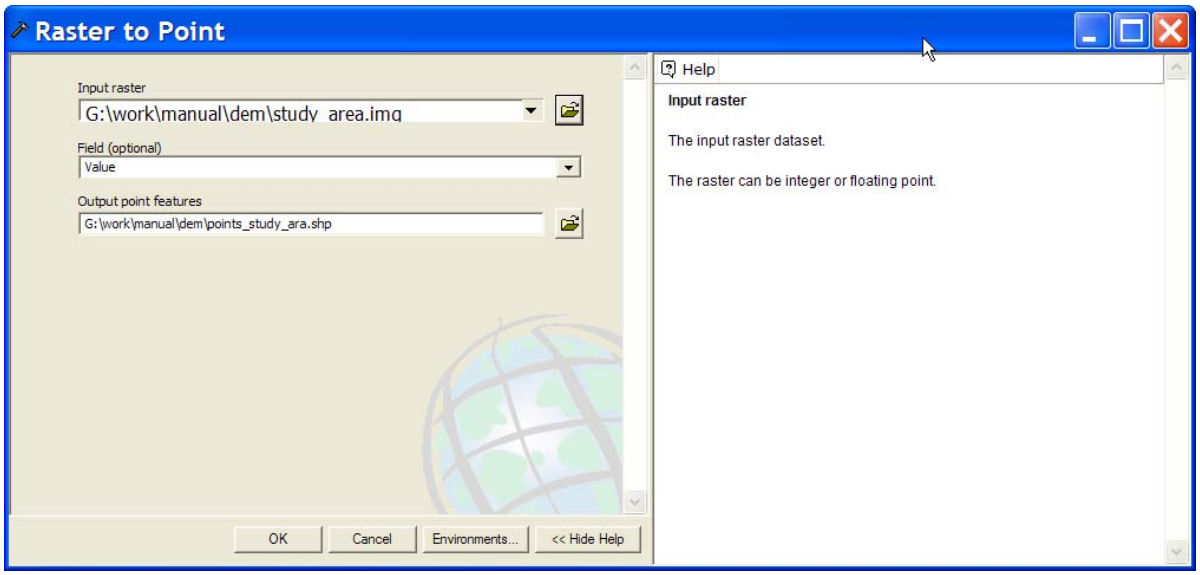

Figure 7: Raster to Point window.

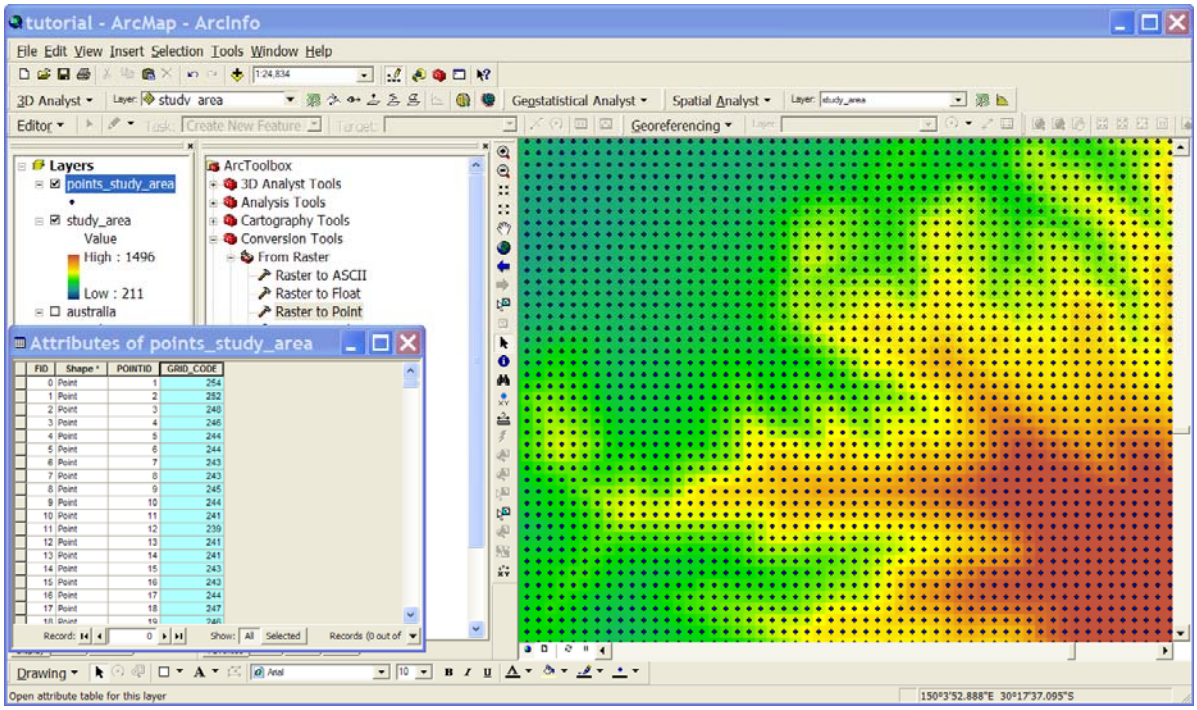

Figure 8: Point feature class generated by the DEM raster conversion (Note: in the attribute table the *GRID_CODE* column contains elevation data).

Add XY Coordinates

From the *ArcToolbox* menu select the tool to add XY coordinates to the point data file in order to get an attribute table with X,Y and Z columns suitable to be exported as an ASCII file and imported into *EarthVision*: *Data Management Tools* > *Features* > *Add XY Coordinates* (Figure 9).

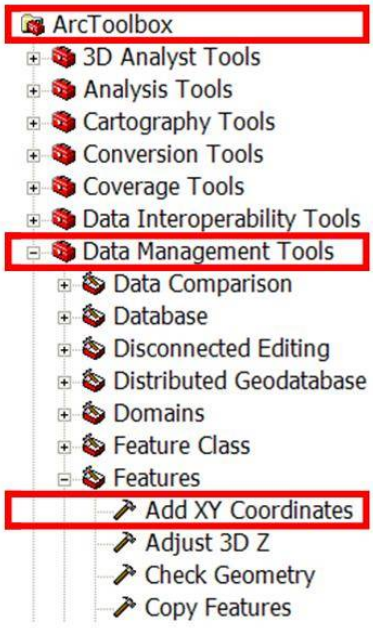

Figure 9: *ArcToolbox* menu path for *Add XY Coordinates*.

In the Add XY Coodinates window you need to select the point shapefile saved in the steps above as input features (Figure 10).

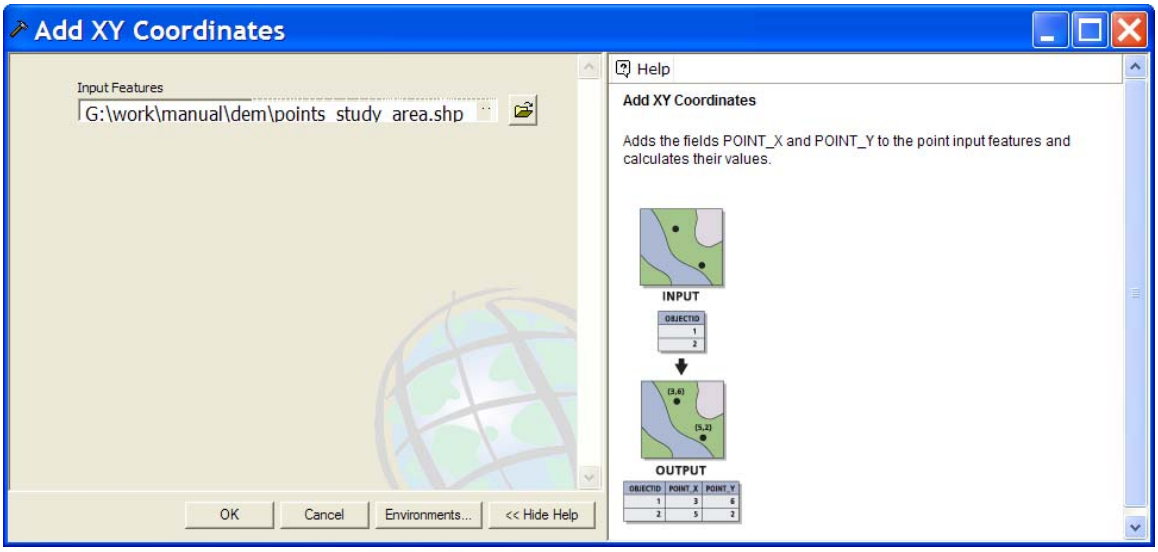

Figure 10: Add XY Coordinates window.

This operation will add fields to your attribute table containing geographic location information based on the coordinate system of your project (GCS_GDA_1994 for the Australian example). At this stage your point shape file is ready to be exported as point data in an ASCII file (Figure 11).

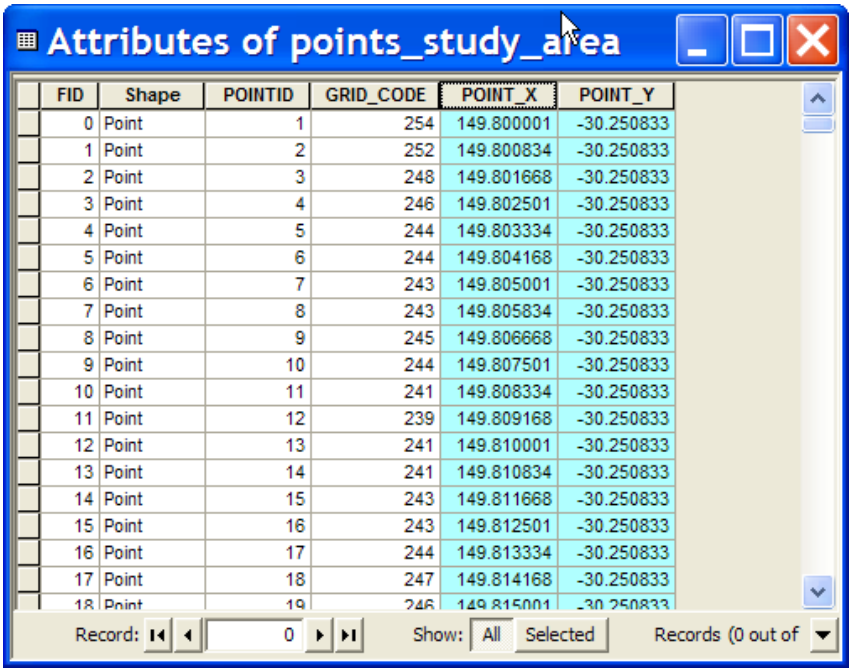

Figure 11: The appearance of the attribute table of the point data after the calculation of XY coordinates.

Export file from *ArcGIS*

From the *ArcToolbox* menu select *Spatial Statistics Tools* > *Export Feature Attribute to ASCII* (Figure 12).

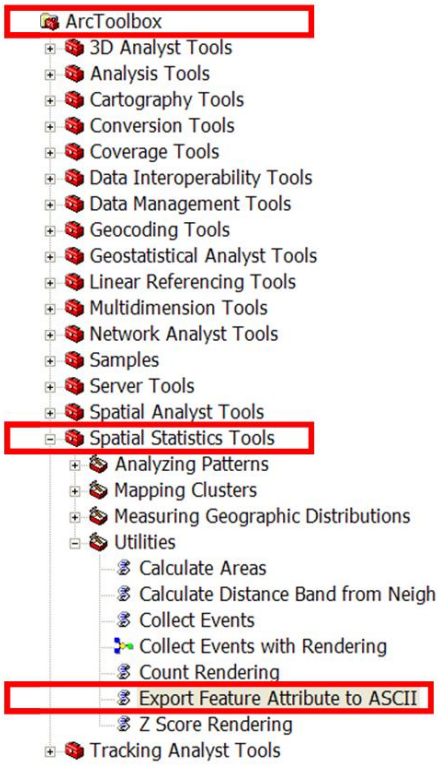

Figure 12: *ArcToolBox* menu path for *Export Feature Attribute to ASCII*.

In the Export Feature Attribute to ASCII window (Figure 13) the following steps are required:

1) specify the input feature class (your point shapefile created in the steps above);

2) select the dropdown arrow and chose the attribute value you want to export along with X and Y coordinates (in the example the field to export is *GRID_CODE* but the name could be different. Check your file and select the field which contains Z (elevation) information);

3) choose the *Space* option as the delimiter;

4) set location and name for the ASCII file you are creating (save the file as a text file) and select OK;

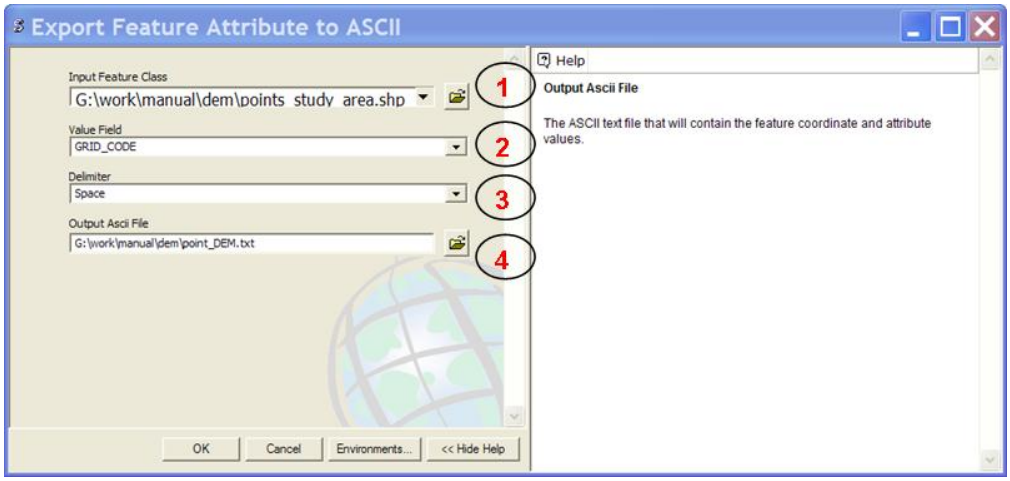

Figure 13: Export Feature Attribute to ASCII window.

The DEM raster has now been converted to a point file and the text output should look like Figure 14, with X, Y and Z space delimitated columns.

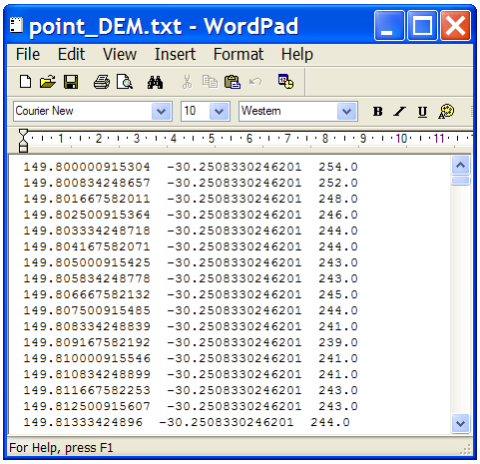

Figure. 14: Point data file text file appearance after being exported from *ArcGIS*.

EarthVision requires that the data be in rectangular units. For this example the Geographic coordinates have been converted into Cartesian coordinates (GDA/MGA, zone 56) using GEOD V03.42 (Geodetic Transformation software, NSW Department of Lands). The output after converting the coordinate units is shown in Figure 15.

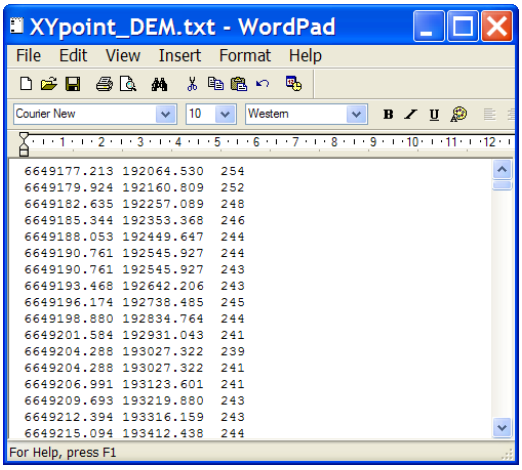

Figure 15: Point data text file appearance after the transformation from Geographic to Cartesian coordinates.

A2.4 EarthVision DEM Data Sorting

Import the point data file into *EarthVision*

Once you have started *EarthVision* and selected the directory that has data files listed, the first operations to perform are:

1) open the List Files window from the *File* pull-down menu in the menu bar: *File* > *List files…* (Step 1, Figure 16).

2) change the file extension from *.txt* (text file suffix) to *.dat* (scattered data file suffix) by selecting the desired file (in this case *XYpoint_DEM.txt*) and then the *Rename* push-button (Step 2, Figure 16).

3) create the header information for the new file (in this case the renamed file *XYpoint_DEM.dat*) by selecting the *Header* push-button to produce the Edit Header window (Step 3, Figure 16).

4) The Edit Header window (Figure 17) contains a box for entering a file description, a row of edit function buttons, a scrolling window for entering a field name and column or position information, and an area for specifying the projection system. Enter an appropriate description for the file by typing it in the *Description* text box (Step 4, Figure 17).

5) Set names, field positions and units from the scrolling windows based on the fields in your file. X and Y fields can not have their units changed and they refer to the file's projection. It is recommended that the units of measurement be specified whenever possible (Step 5, Figure 17).

6) In the Projection window (accessed via the Projection button) specify the file's projection and X,Y units using the scrolling bars. In the example the data have *Local Rectangular Projection* and the X,Y units are meters (Figure 18).

7) Save the file header and exit the Edit Header window: select *File* > *Save* and then *File* > *Exit* (Figure 19).

The DEM is now ready for use in *EarthVision* and you should be able to see the data in 3D by highlighting the file XYpoint.dat in the Files window and selecting the *3D Viewer* push-button or by opening 3D Viewer and then loading the file (Figures 16, 20 and 21).

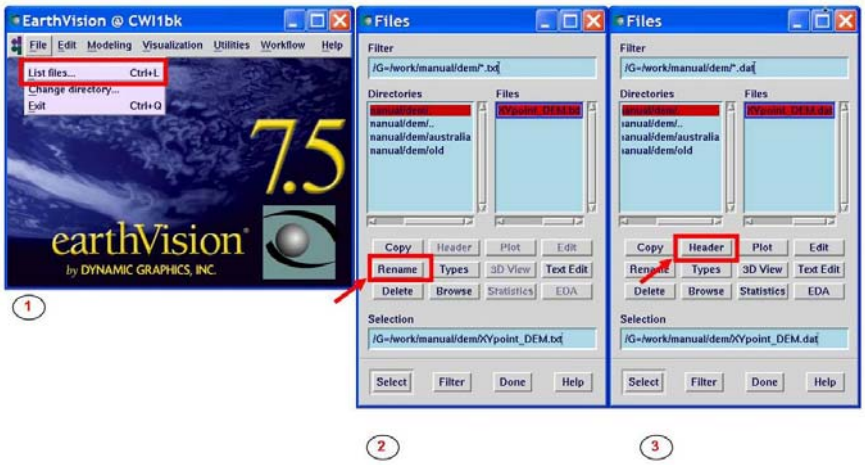

Figure 16: Steps 1-3 for importing a point data file into *EarthVision*.

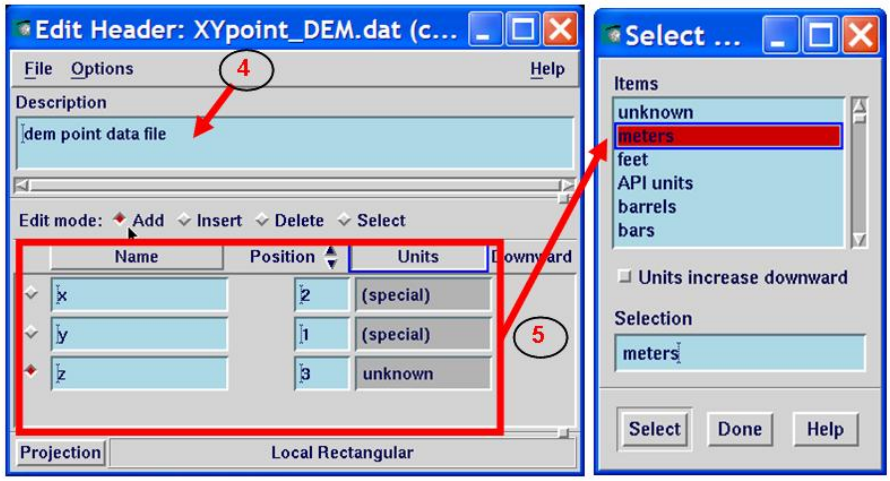

Figure 17: Steps 4 and 5 for creating the header information.

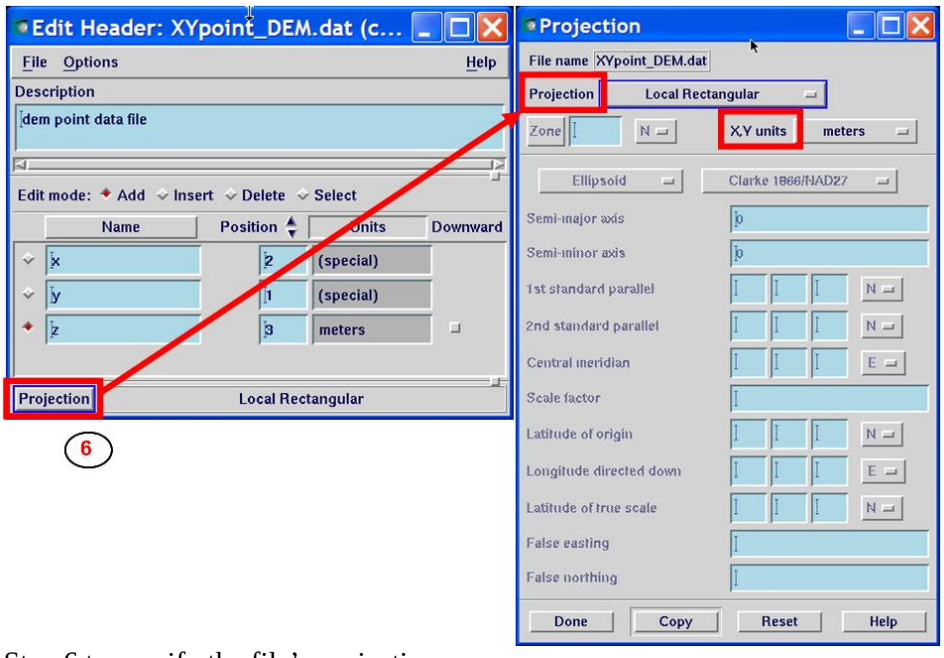

Figure 18: Step 6 to specify the file's projection.

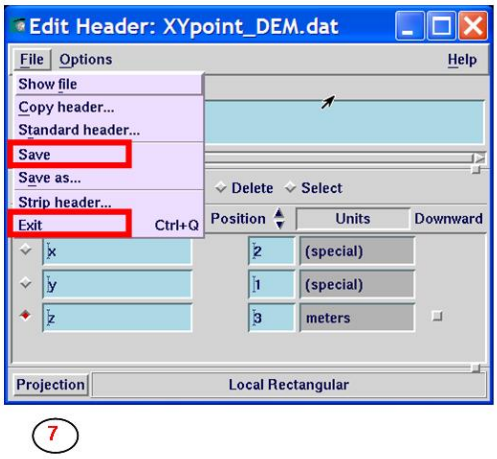

Figure 19: Step 7 save the header information and exit.

Figure 20: Opening the 3D Viewer.

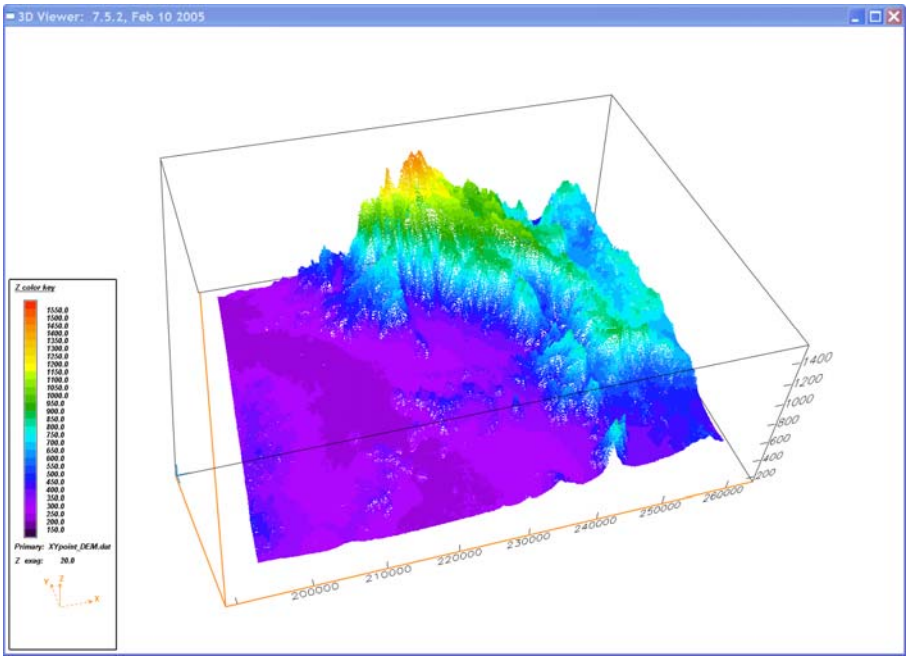

Figure 21: The DEM point file data displayed in the *EarthVision* 3D Viewer.

2D DEM Minimum Tension Grid Calculation

The next step is to calculate a two-dimensional minimum tension grid for the elevation data. The sorting process applied in this manual is based on partial derivative functions in the X and Y directions and this process requires a 2D grid. The 2D Minimum Tension Gridding program is accessed from the *Modeling* pull-down menu on the menu bar: *Modeling > 2D Minimum Tension Gridding* (Figure 22).

Figure 22: 2D Minimum Tension Gridding.

Once the 2D Minimum Tension Gridding window is open, follow the steps below:

1) Load the file in the *Scattered Data* text box. If the scattered data file selected contains more than one Z-field, select the required Z-field in the file using the *Field* option menu (Step 1 Figure 23).

2) Check X, Y and Z ranges and select grid cell spacing (X and Y dimensions) based on the desired level of precision required for the output grid. In the example a grid spacing of 50 m has been selected (Step 2 Figure 23).

3) Run the *Normal Minimum Tension* calculation from the *Calculate* pull-down menu on the menu bar and save the output file (.2grd): *Calculate > Normal Minimum tension* (Step 3 Figure 23).

Once the calculation has finished, you will be able to display the 2D grid in the 3D Viewer window (Figure 24).

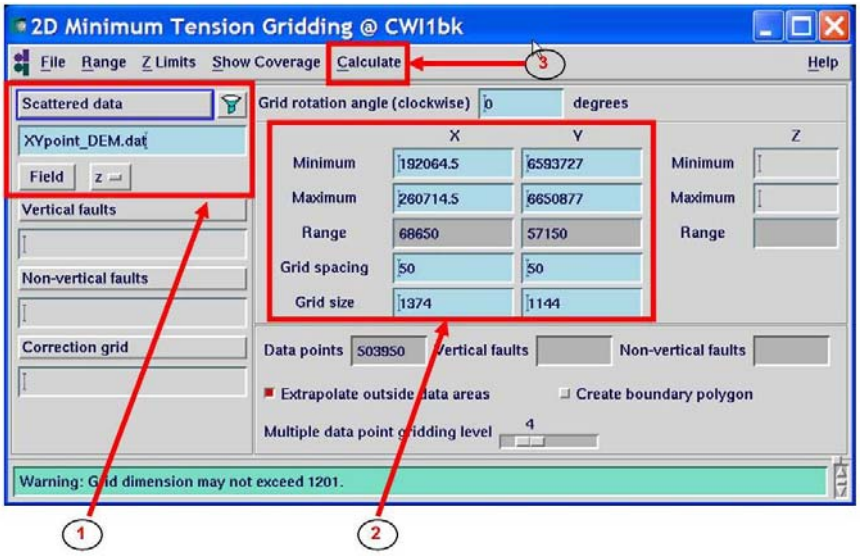

Figure 23: Steps 1-3 to calculate a 2D grid with 2D Minimum Tension Gridding.

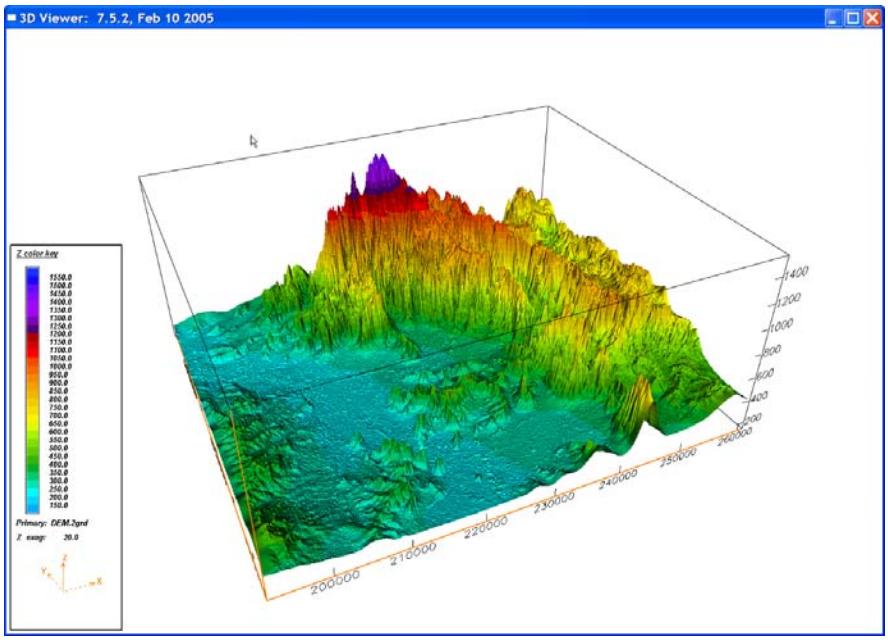

Figure 24: The 2D minimum tension DEM grid displayed in the 3D Viewer.

Data Sorting

In areas of steep mountains surrounded by flat alluvial plains the gradient of the DEM grid can be used to sort the data. The sorting method requires 3 steps using the Formula Processor, Grid Filtering and then the Formula Processor. These steps are explained in detail below. Each step that uses the Formula Processor consists of two or more lines of scripting. These scripts have been saved as formula files (*.fml*).

Open the *Formula Processor* window by selecting *Formula Processor* from the *Utilities* pull-down menu on the main *EarthVision* window (Figure 25) and follow the 3 steps detailed below.

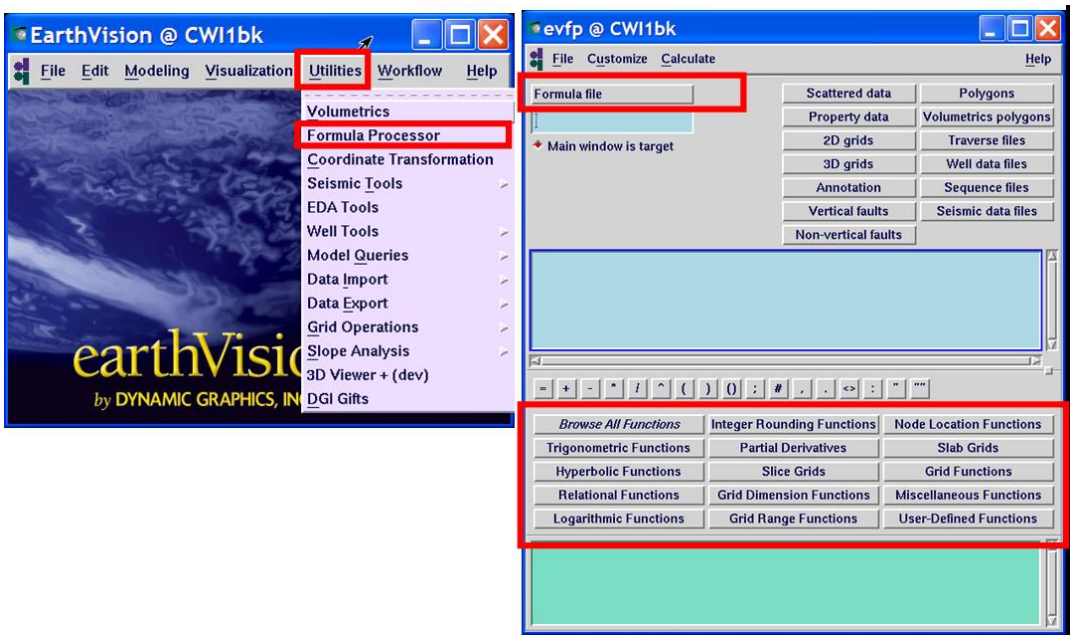

Figure 25: Formula Processor window and *Formula file* and functions push-buttons.

Step1

Select the *Formula file* push-button and navigate to your folder to find and enter the first formula (*step1.fml*) using the *File* selection button (Figure 25). In the large scrolling text window below the *File selection* buttons a formula will appear to complete step 1:

```
X.2grd=partialX(DEM.2grd);
Y.2grd=partialY(DEM.2grd);
slope.2grd=X.2grd+Y.2grd;
highslope_pos.2grd=lt(slope.2grd,-0.022,1,slope.2grd);
highslope_neg.2grd=gt(highslope_pos.2grd,0.022,1,0);
```

The first two lines of this step calculate the partial derivatives of the DEM in the X and Y directions and returns two grids (X.2grd and Y.2grd). Figure 26 shows a geometrical interpretation of partial derivatives for a given point (X, Y, Z=f(X, Y)) on the DEM surface. The partial derivatives f_x and f_y tells us the slope of the tangent plane in the X and Y directions. Figure 27 shows the partial derivative grids X.2grd and Y.2grd in the *3D Viewer* calculated from the Maules Creek DEM 2D minimum tension grid.

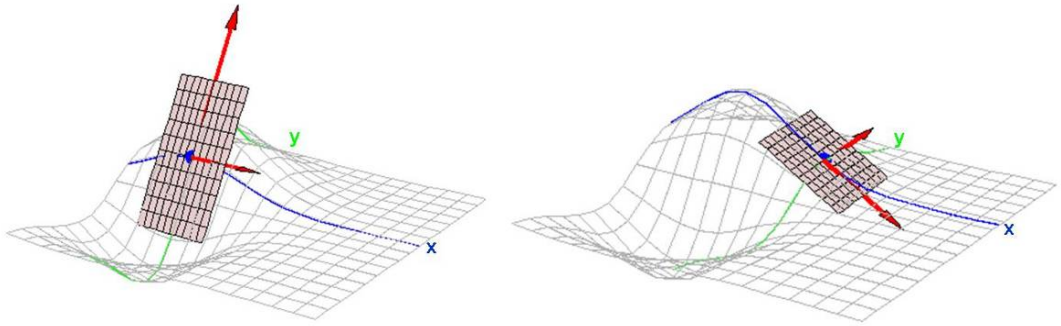

Figure 26: Geometric interpretation of partial derivatives. (modified from http://www.math.umn.edu/~rogness/multivar/, University of Minnesota).

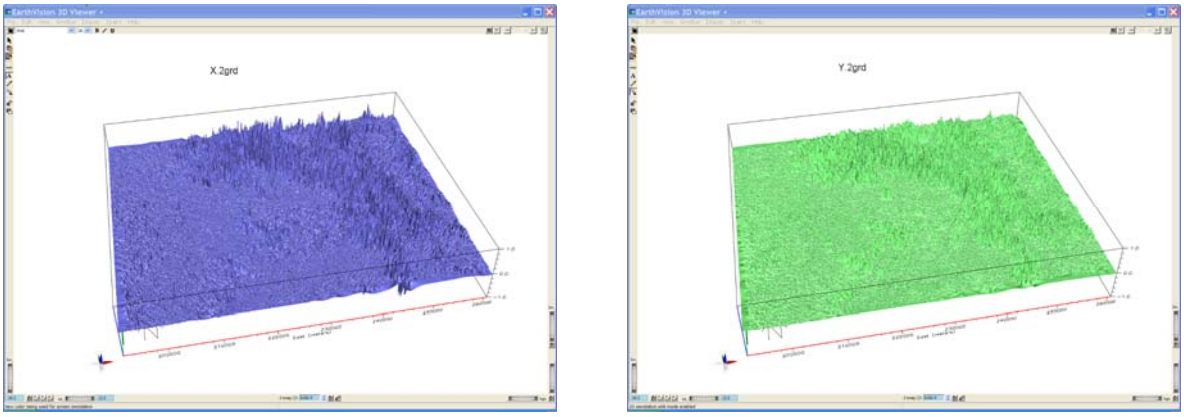

Figure 27: Grids resulting from the calculation of partial derivatives of the DEM in X and Y directions (*X.2grd* and Y.2grd after running *step1.fml* in the Formula Processor).

The third line of the formula file *step1.fml* combines the two grids into a single 2D grid (*slope.2grd*) in order to highlight the areas of sloping rock (Figure 28). The slope grid is then separated into rock outcrops (index 1) and alluvial zone (index 0) using the *greater than* (*gt*) and *less than (lt)* functions. The filtering value of 0.022 is an arbitrary value set based on the grid cell size and external reference information at key locations (i.e. based on geological maps, aerial photos and ground truthing) Figure 29 shows the plan view of the output grids after this step.

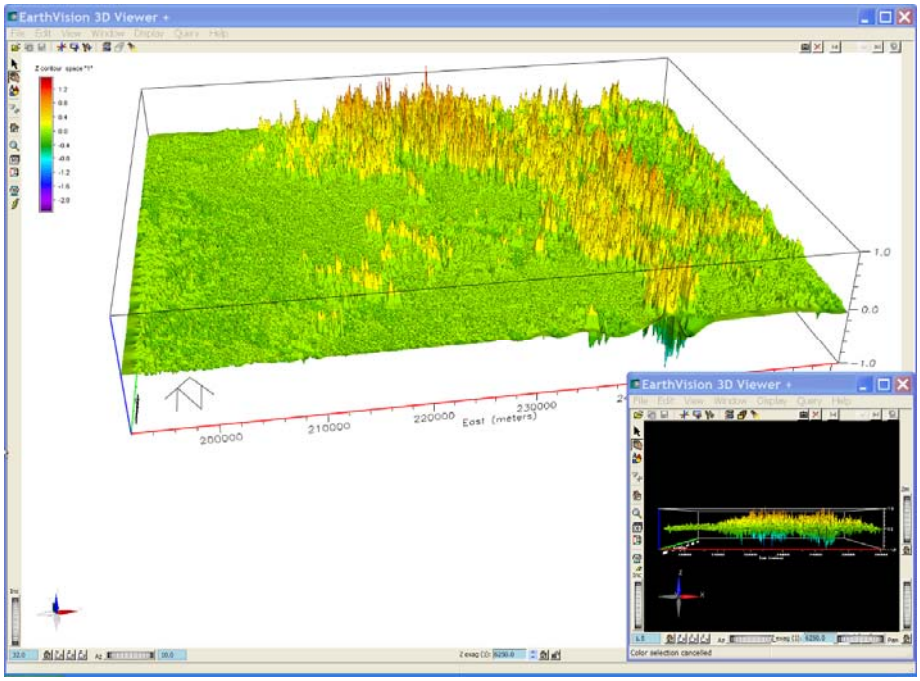

Figure 28: Slope.2grd, resulting from the sum of X.2grd and Y.2grd, highlighting the high gradient rock outcrops (A second view of the same grid in the lower right corner displays the negative values: blue).

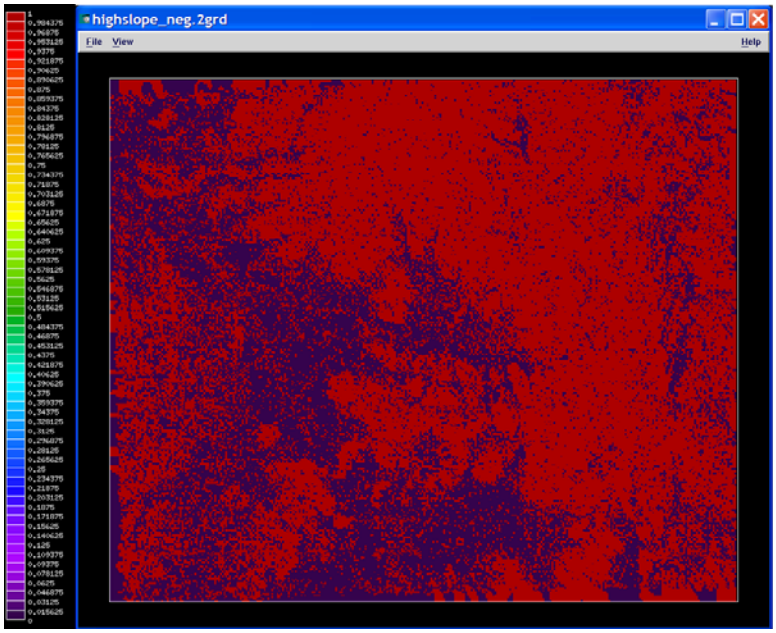

Figure 29: Plan view of the highslope_neg grid.

Step2

The second step uses the *Grid Filtering Utility* to smooth the noisy grid created in the last stage of step1. From the main window select *Utility* > *Grid Operations* > *Grid Filtering* (Figure 30).

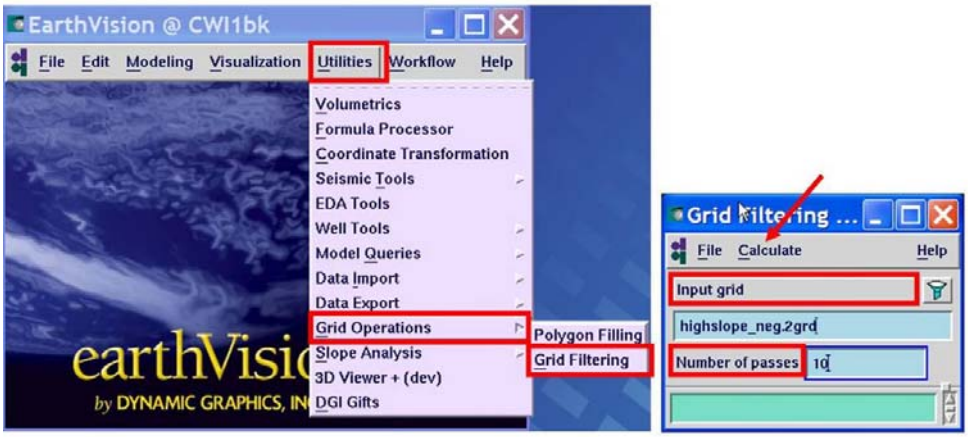

Figure 30: Opening the Grid Filtering window and setting the number of filtering passes.

In the *Grid Filtering* window you have to enter the last grid obtained in step1 (*highslope_neg.2grd* in the example). The number of passes refers to the number of times the filter runs over the grid to return a smoothed value at each grid node. The degree of filtering applied is based on a subjective interpretation using existing knowledge of the area under examination. The resulting surface needs to be evaluated since different degrees of filter can significantly change the output data (see *EarthVision* User's Guide – Utilities for a more detailed explanation of the Grid Filtering program). For this example 10 passes were selected based on trial and error and comparison with a geological map of the study area. After setting the number of passes select the *Calculate* push-button to perform the calculation. The output grid is written to the user-specified grid file name (*filter.2grd* in this example; Figure 31).

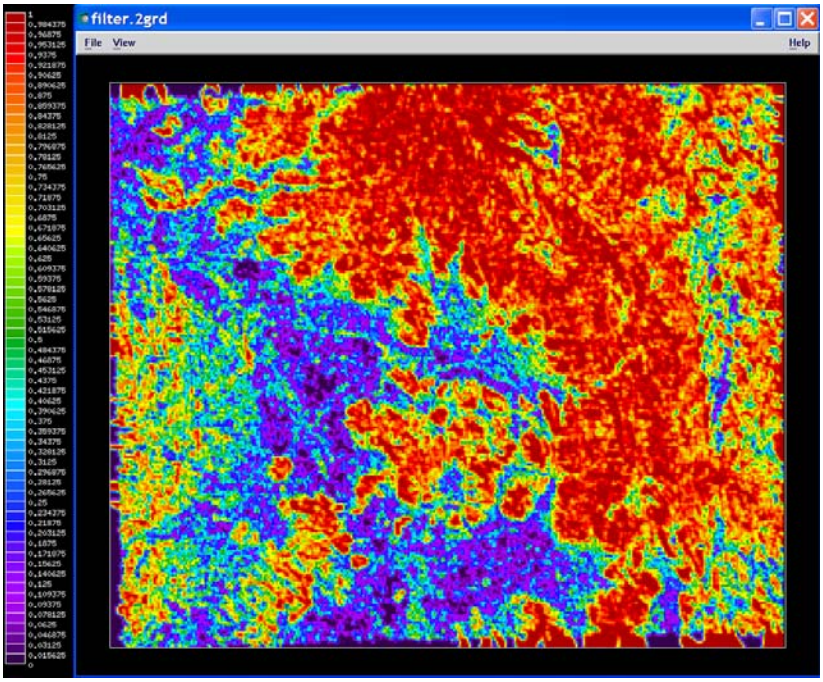

Figure 31: Plan view of the filter.2grd after the ten grid filtering passes.

Step3

Back in the Formula Processor window load *step3.fml*. In the text window the formula below will appear:

```
rock.2grd=gt(filter.2grd,0.5,DEM.2grd,1E20);
alluvial.2grd=lt(filter.2grd,0.5,DEM.2grd,1E20);
```

This script uses the *greater than (gt)* and *less than (lt)* functions to sort all values greater than 0.5 into a rock outcrop grid (rock.2grd, Figure 32) and all values less than 0.5 into an alluvial sediment grid (alluvial.2grd, Figure 33). Where the category (rock or alluvium) is present the original DEM value is returned, and when the class is absent a null value (1E20) is set at the grid node. The sorted and combined categories are displayed in Figure 34. From a geological perspective the alluvial.2grd is a combination of alluvial and colluvial sediments (upper right portion in Figure 33 and 34). After the alluvial grid is exported to a scattered data file (Figure 35) the colluvial data points can be isolated using a polygon selection in the Graphic Editor.

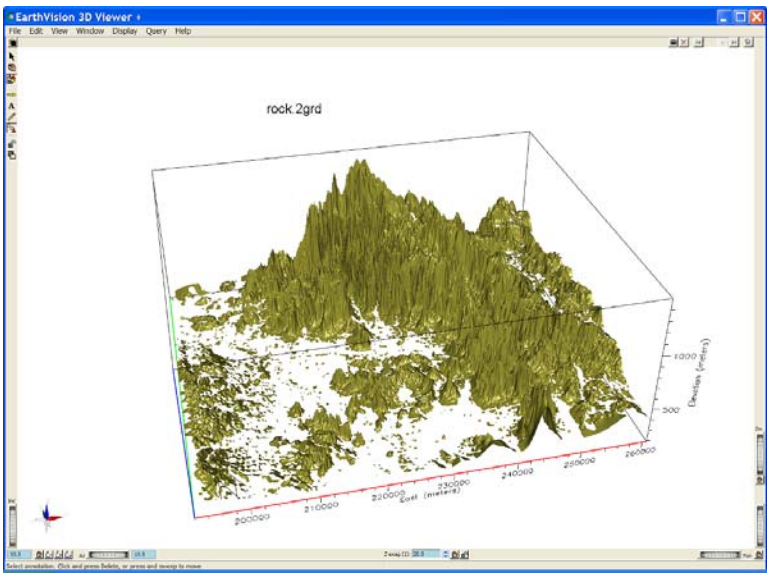

Figure 32: Final grid of the rock outcrop.

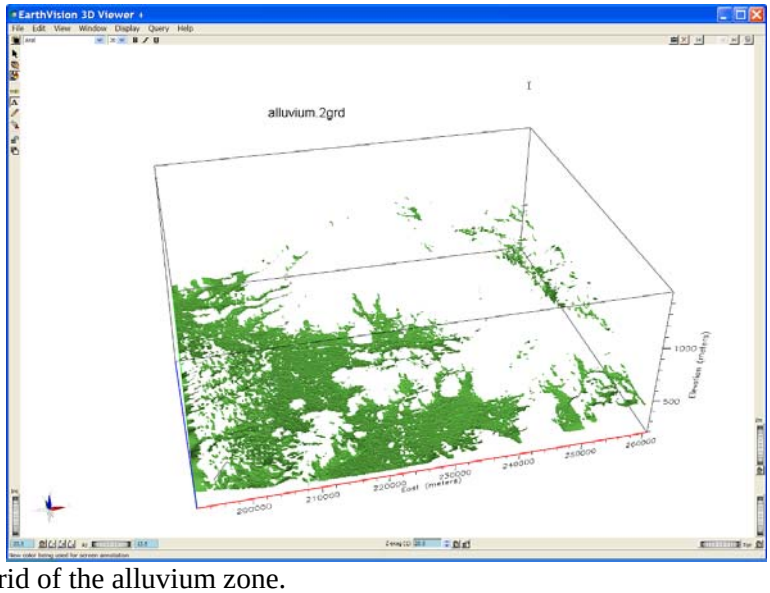

Figure 33: Final grid of the alluvium zone.

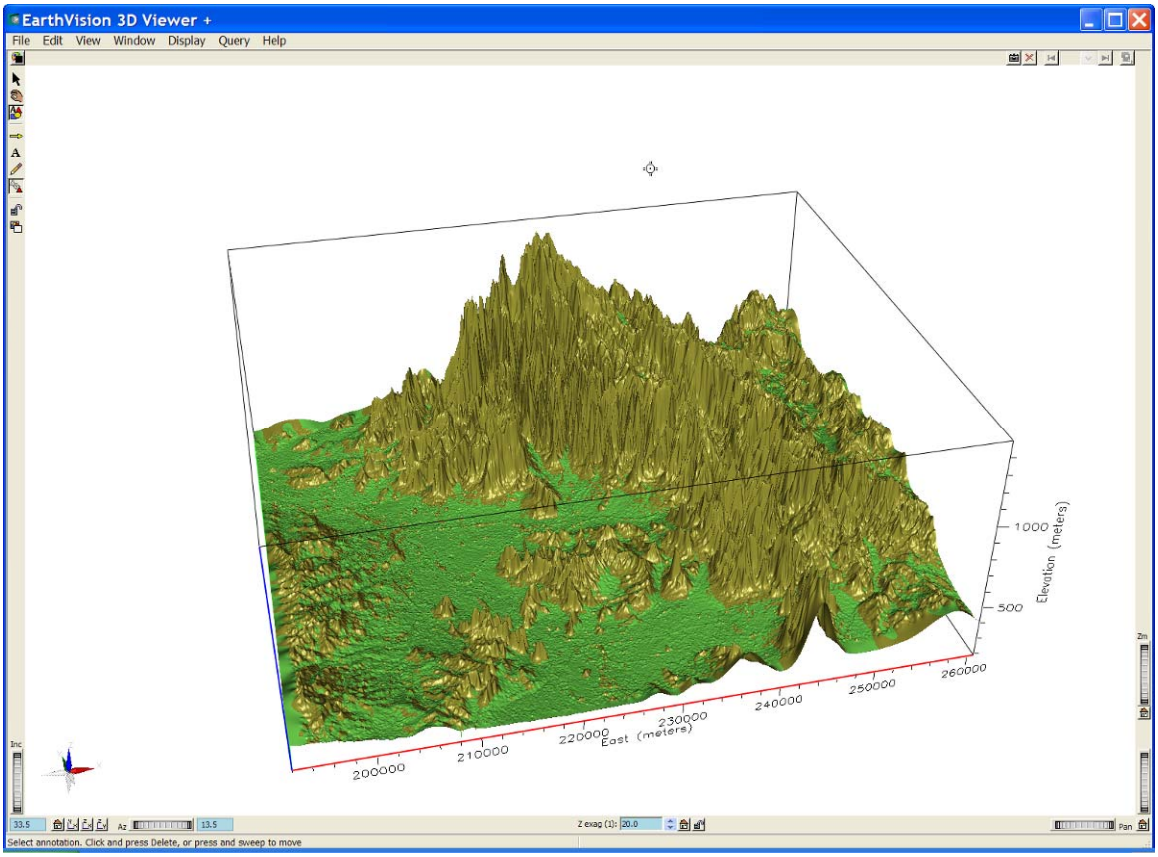

Figure 34: DEM grid sorted into rock and alluvium zones.

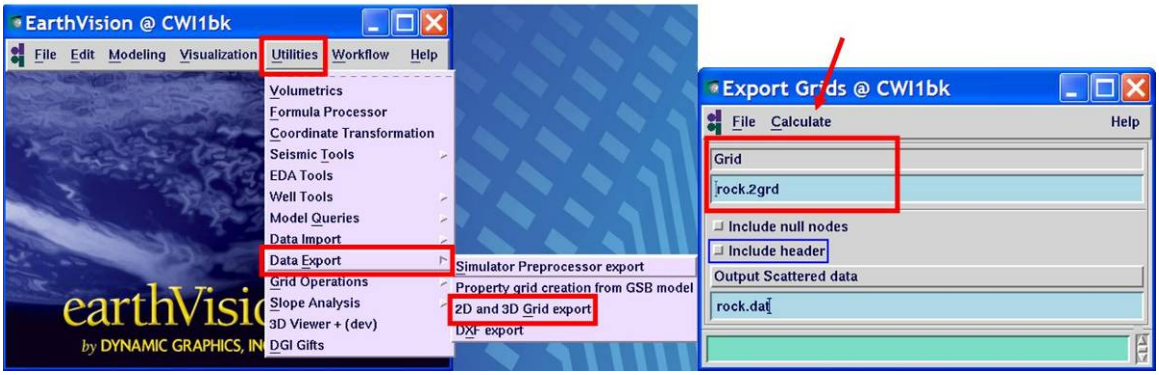

Figure 35: The *2D and 3D Grid export* window.

Script files used in *EarthVision*

Here is the list of *script files (.sh)* and *formula processor files (.fml)* for repeating the calculations.

Script files

DEM:

```
#!sh.exe
# Cause script to exit on errors.
set -e

FEATURE=ev_ps_win
ev_2grid -o "DEM.2grd" -F $FEATURE -r
192064.530000,260714.530000,6593726.726000,6650876.726000 -s 1374,1144 -d "XYpoint_DEM.dat" -f
"z" -G "DEM.2grpt" -m 4
```

Step1:

```
#!sh.exe
# Cause script to exit on errors.
set -e

ev_fpfp -u -F ev_ps_win  << EOF
X.2grd=partialX(DEM.2grd);
Y.2grd=partialY(DEM.2grd);
slope.2grd=X.2grd+Y.2grd;
highslope_pos.2grd=lt(slope.2grd,-0.022,1,slope.2grd);
highslope_neg.2grd=gt(highslope_pos.2grd,0.022,1,0);
EOF
```

Step2:

```
#!sh.exe
# Cause script to exit on errors.
set -e

ev_filter -n 10 -o filter.2grd highslope_neg.2grd
```

Step3:

```
#!sh.exe
# Cause script to exit on errors.
set -e

ev_fpfp -u -F ev_ps_win  << EOF
rock.2grd=gt(filter.2grd,0.5,DEM.2grd,1E20);
alluvial.2grd=lt(filter.2grd,0.5,DEM.2grd,1E20);

EOF
```

Step4:

```
#!sh.exe
# Cause script to exit on errors.
set -e

GRID='rock.2grd'
INCLUDENULLS=''
INCLUDEHEADER='-x'
OUTPUT='rock.dat'

ev_export $INCLUDENULLS $INCLUDEHEADER -o $OUTPUT $GRID
```

Step5:

```
#!sh.exe
# Cause script to exit on errors.
set -e

GRID='alluvial.2grd'
INCLUDENULLS=''
INCLUDEHEADER=''
OUTPUT='alluvium.dat'

ev_export $INCLUDENULLS $INCLUDEHEADER -o $OUTPUT $GRID
```

Formula Processor files

Step1:

```
X.2grd=partialX(DEM.2grd);
Y.2grd=partialY(DEM.2grd);
slope.2grd=X.2grd+Y.2grd;
highslope_pos.2grd=lt(slope.2grd,-0.022,1,slope.2grd);
highslope_neg.2grd=gt(highslope_pos.2grd,0.022,1,0);
```

Step2:

```
rock.2grd=gt(filter.2grd,0.5,DEM.2grd,1E20);
alluvial.2grd=lt(filter.2grd,0.5,DEM.2grd,1E20);
```

A2.5 References

ArcGIS 9.2 Manual
EarthVision 7.5 User's Guide

A2.6 Internet References

http://www.esri.com
http://www.dgi.com/
http://www.connectedwaters.unsw.edu.au/
http://srtm.csi.cgiar.org/
http://srtm.csi.cgiar.org/SELECTION/inputCoord.asp
http://www.lands.nsw.gov.au/survey_maps/geodesy/gda/geod_software
http://www.math.umn.edu/~rogness/multivar/index.shtml

Appendix 3

Crystallize
3D Geological Modelling

Author
B. Kelly

A3.1 Introduction

Presented in this appendix is a complete example of the workflow for constructing a 3D geological model of a catchment using *Mathematica*. This work was presented at the International *Mathematica* User Conference, Champaign, Illinois, USA, October 2009.

The Mathematica notebook and associated data files can be downloaded from
http://www.wolfram.com/news/events/userconf2009/presentations.html

This notebook can be easily adapted for constructing models in other catchments, by changing the input files and coordinates. Below are copies of the slides from the presentation.

Catchment Scale 3D Geological Models from Sparse Data Sets

Bryce F. J. Kelly
The University of New South Wales, Australia
Connected Waters Initiative
National Centre for Groundwater Research and Training

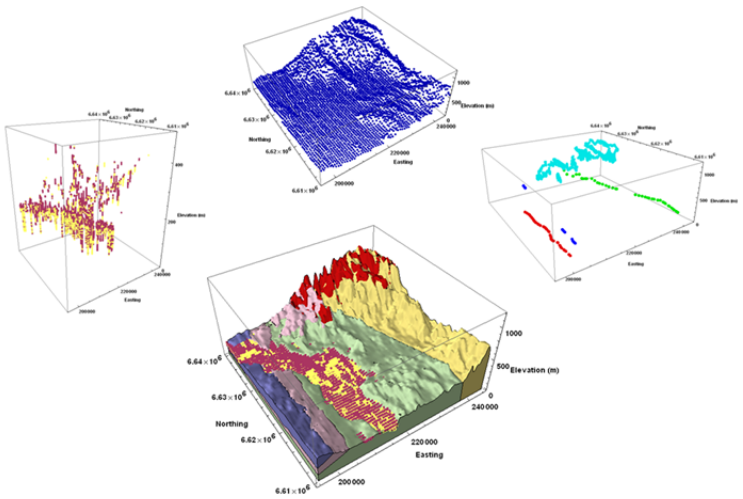

Introduction

Three dimensional models of regional geological structures and the properties of each unit are important for numerous earth science applications. Such models are essential for :

- defining the distribution of base metals,
- delineating hydrocarbon traps,
- determining the volume of groundwater contamination plumes, and
- creating the framework for hydrogeological water balance models.

This presentation illustrates how to build 3D geological models using *Mathematica*. The data processing steps are demonstrated on a catchment scale model that was constructed to define the hydrogeological framework for a regional groundwater investigation in an environmentally stressed aquifer in Australia.

Geological Data Sets

The 3D geological models are built from sparse data sets including :

- borehole lithological logs,
- geological maps,
- geophysical surveys, and
- field measurements of geological surfaces (defined by their strike and dip).

Sample points are often irregularly distributed in space.

Mathematica provides a single environment to edit and sort the data, grid the sparse data, interpolate surfaces and then view the 3D conceptual geological model.

Gridding Irregularly Spaced 2D Data

The Need for Sparse Data Interpolation

The final 3D geological models are built using the function **RegionPlot3D**. To plot the region that corresponds to the geological feature of interest an approximate function over the x,y domain needs to be defined for each surface used to delineate the limits of the region.

An approximate function for a surface is determined using the **Interpolation** function. The data passed to **Interpolation** need to be on a regular grid (also called a mesh or rectangular grid).

Mathematica does not have built in functions for interpolating irregularly spaced point data onto a regular grid described by a list of triplets.

Two gridding functions are defined: nearest neighbor and inverse distance. Both of these algorithms are refinements of the functions published by Haneberg (2004).

Defining the Dimensions of the Region of Interest

3D geological models are built using a combination of 2D and 3D grids.

The domain dimensions are defined here and used throughout the calculations below.

```
xmin = 195 000; xmax = 245 000; xspace = 500;
ymin = 6 610 000; ymax = 6 640 000; yspace = 500;
zmin = 0; zmax = 1200;
zspace = 5;
```

The dimensions of the 2D grid used for many of the calculations are also defined.

```
grid2D = Flatten[Table[{x, y}, {x, xmin, xmax, xspace}, {y, ymin, ymax, yspace}], 1];
```

```
ListPlot[grid2D, AxesOrigin → {xmin, ymin}, PlotStyle → PointSize[0.008],
 AspectRatio → 1,
 AxesLabel → {"Easting", "Northing"}, ImageSize → {350, 350}]
```

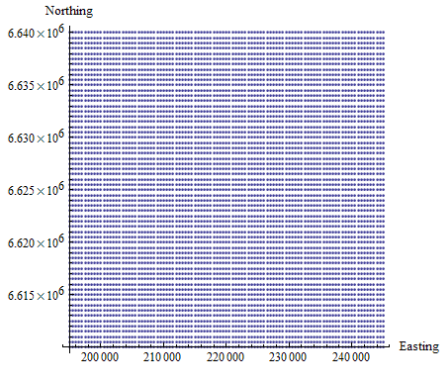

2D Nearest Neighbor Gridding of Irregularly Spaced Data

Some of the geological data sets are dense and need little interpolation. For these data sets nearest neighbor gridding is used.

The function **NearestNeighborGrid2D** defined below interpolates/extrapolates 2D data sets onto a regular grid and then the function **Interpolation** is applied to the grid list to define an approximate function at all locations over the domain. An approximate function is returned by **NearestNeighborGrid2D**.

Inputs for the new function **NearestNeighborGrid2D** are the 2D surface data, $\{\{x_1,y_1,z_1\},\{x_2,y_2,z_2\}, \ldots\}$, and the regular grid list, $\{\{x_1,y_1\},\{x_2,y_2\}, \ldots\}$.

```
NearestNeighborGrid2D[datain_, gridin_] :=
 Module[{nnfunction, nn2Dmap, nn2Ddatagrid, nn2Dfunction},
  nnfunction = Nearest[datain[[All, {1, 2}]] → datain[[All, 3]]];
  nn2Dmap = Map[nnfunction, gridin][[All, 1]];
  nn2Ddatagrid = Partition[Flatten[Riffle[gridin, nn2Dmap]], 3];
  nn2Dfunction = Interpolation[nn2Ddatagrid, Method → "Hermite",
    InterpolationOrder → 3];
  Return[nn2Dfunction]]
```

2D Inverse Distance Gridding of Irregularly Spaced Data: Defined

Inverse distance gridding is commonly used to grid geological data (Yamamoto 1998).

The value at the grid node, $z_{x,y}$, is determined via:

$$z_{x,y} = \frac{\sum_{i=1}^{k} \frac{z_i}{d_i^p}}{\sum_{i=1}^{k} \frac{1}{d_i^p}}$$

where d_i is the Euclidean distance between the node and the i-th data point, k is the number of neighboring points, and p is the power of distance.

2D Inverse Distance Gridding of Irregularly Spaced Data: The Function

Haneberg (2004) published a *Mathematica* algorithm for gridding irregularly spaced data using inverse distance gridding. Below is a modified inverse distance algorithm that takes advantage of the functions **Nearest** and **EuclideanDistance**, and uses no **Do** loops for faster calculation times.

Inputs for the new function **InverseDistanceGrid2D** are the 2D surface data, $\{\{x_1,y_1,z_1\},\{x_2,y_2,z_2\}, \ldots\}$, the number of nearest points to use, the power of distance (typically 1, 2 or 3), and the regular grid list, $\{\{x_1,y_1\},\{x_2,y_2\}, \ldots\}$.

Within the **InverseDistanceGrid2D** module the data are interpolated/extrapolated onto a regular grid and then the function **Interpolation** is applied to the grid list to define an approximate function at all locations over the domain. An approximate function is returned by **InverseDistanceGrid2D**.

```
InverseDistanceGrid2D[datain_, k_, p_, gridin_] :=
 Module[{nfunction, xyz, xy, z, d, zestimate, zgrid, zfunction},
  nfunction = Nearest[datain[[All, {1, 2}]] → datain[[All]]];
  xyz = Map[nfunction[{#, #}, k] &, gridin];
  xy = xyz[[All, All, {1, 2}]];
  z = xyz[[All, All, 3]];
  d = Table[EuclideanDistance[gridin[[i]], xy[[i, j]]], {i, Length[gridin]},
    {j, Length[xy[[1]]]}];
  zestimate = Apply[Plus, z / d^p, 1] / Apply[Plus, 1 / d^p, 1];
  zgrid = Table[{gridin[[i, 1]], gridin[[i, 2]], zestimate[[i]]},
    {i, Length[gridin]}];
  zfunction = Interpolation[zgrid, Method → "Spline", InterpolationOrder → 3];
  Return[zfunction]]
```

Building the 3D Facies Model

Import the Digital Elevation Model (DEM)

Digital Elevation Models (DEM) are available from many government geological organizations.

The USGS provides DEM data for the whole globe.

The DEM of the Maules Creek catchment is imported and then reduced in size for the demonstration.

```
SetDirectory["F:\\Bryce\\1 work\\mathematica\\3Dgeology\\BryceKellyMIUC2009"];
dem = Drop[Import["maulesdem.csv"], 1];
subdem = Table[Extract[dem, i], {i, 1, Length[dem], 50}];
```

View the DEM in 3D

The DEM is plotted below using the function **ListPlot3D.** In the image the dark brown areas are the fertile vertosol soils where irrigated crops are grown. In the south east corner coal mines are being developed. The dimensions of the catchment are approximately 40 km by 30 km.

```
ListPlot3D[subdem, PlotRange → {{xmin, xmax}, {ymin, ymax}, {zmin, zmax}},
 Mesh → None, ColorFunction → (Blend[{{0, RGBColor[0.356863, 0.180392, 0]},
      {0.07, RGBColor[0.737255, 0.737255, 0.478431]},
      {0.15, RGBColor[0.443137, 0.572549, 0.180392]}}, #3] &),
 AxesLabel → {"Easting", "Northing", "Elevation (m)"},
 ViewPoint → {-1.75, -1.5, 2.5}, ImageSize → {500, 450}]
```

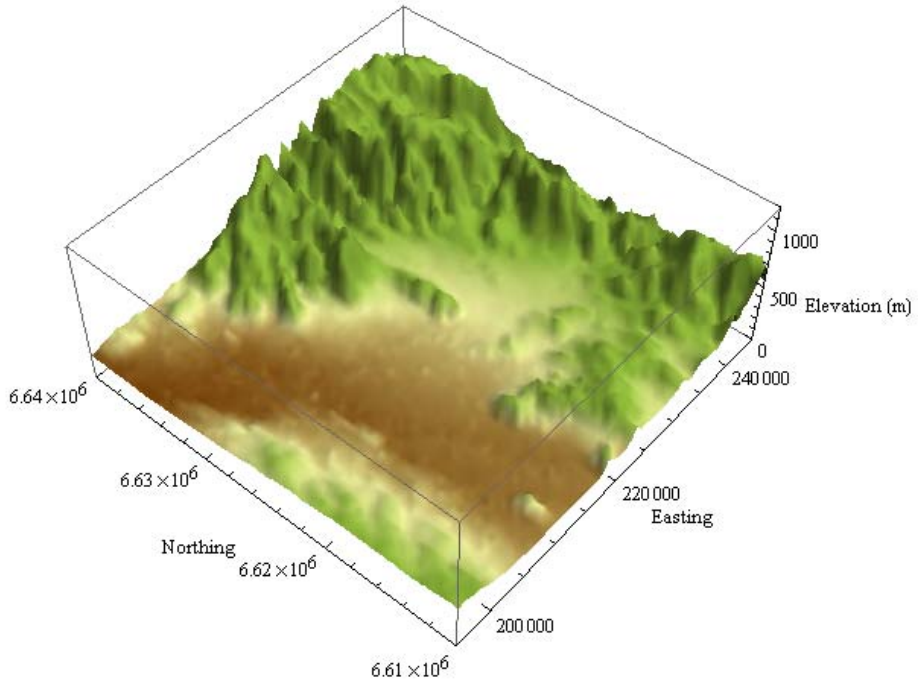

Sort the DEM into Rock and Alluvium Zones

The DEM needs to be sorted into areas that represent the rock and the alluvium. This is done by taking advantage of the fact that alluvial areas are relatively flat and at low elevations. The model is divided into two domains and the data are then sorted based on the elevation.

Alternative methods for sorting the data are variance, median and gradient filters. In this terrain the simple elevation cutoff is acceptable.

There are thin unconsolidated sediments in the eastern portion of the catchment. This demonstration focuses on the alluvial sediments in the main paleochannel.

```
rock = {};
alluvium = {};
Do[If[subdem[[i, 1]] ≤ 210 000 && subdem[[i, 3]] < 245,
  AppendTo[alluvium, subdem[[i]]],
  If[210 000 < subdem[[i, 1]] < 220 000 && subdem[[i, 3]] < 280,
   AppendTo[alluvium, subdem[[i]]],
   If[220 000 < subdem[[i, 1]] && subdem[[i, 3]] < 280,
    AppendTo[alluvium, subdem[[i]]], AppendTo[rock, subdem[[i]]]]]],
 {i, Length[subdem]}]

rockpointplot = ListPointPlot3D[rock,
   PlotRange → {{xmin, xmax}, {ymin, ymax}, {zmin, zmax}},
   PlotStyle → PointSize[0.01]];
alluviumpointplot = ListPointPlot3D[alluvium,
   PlotRange → {{xmin, xmax}, {ymin, ymax}, {zmin, zmax}},
   PlotStyle → {Lighter[Yellow], PointSize[0.01]}];
Show[rockpointplot, alluviumpointplot,
 AxesLabel → {"Easting", "Northing", "Elevation (m)"},
 ImageSize → {500, 450}, ViewPoint → {-1.75, -1.5, 2.5}]
```

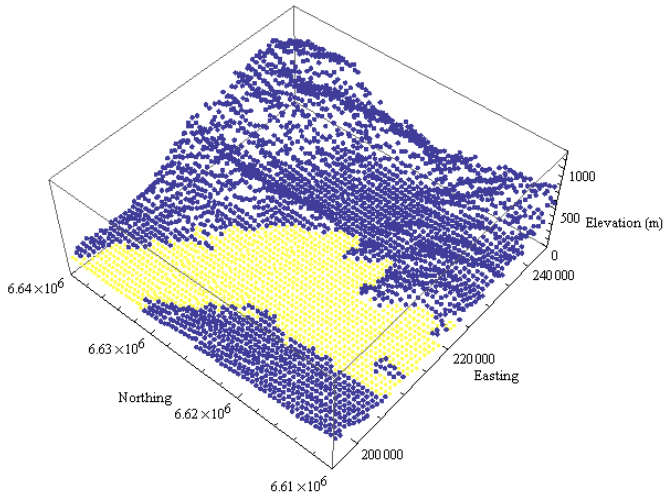

Import the Bedrock Picks from the Boreholes

Whenever a borehole is drilled in New South Wales (NSW), Australia, a record of the lithology is kept by the NSW State Government.

Some of these boreholes intersect the bedrock. These borehole rock top picks are combined with the DEM rock data.

These points define the extent of the bedrock surface, the bottom of the alluvium (unconsolidated sediments).

```
boreholerockpoints = Drop[Import["maulesbedrocktops.csv"], 1][[All, {2, 3, 7}]];
rocksurfacepoints = Join[rock, boreholerockpoints];
```

```
ListPointPlot3D[rocksurfacepoints,
 PlotRange → {{xmin, xmax}, {ymin, ymax}, {zmin, zmax}},
 PlotStyle → PointSize[0.01],
 AxesLabel → {"Easting", "Northing", "Elevation (m)"},
 ImageSize → {500, 450}, ViewPoint → {-1.75, -1.5, 2.5}]
```

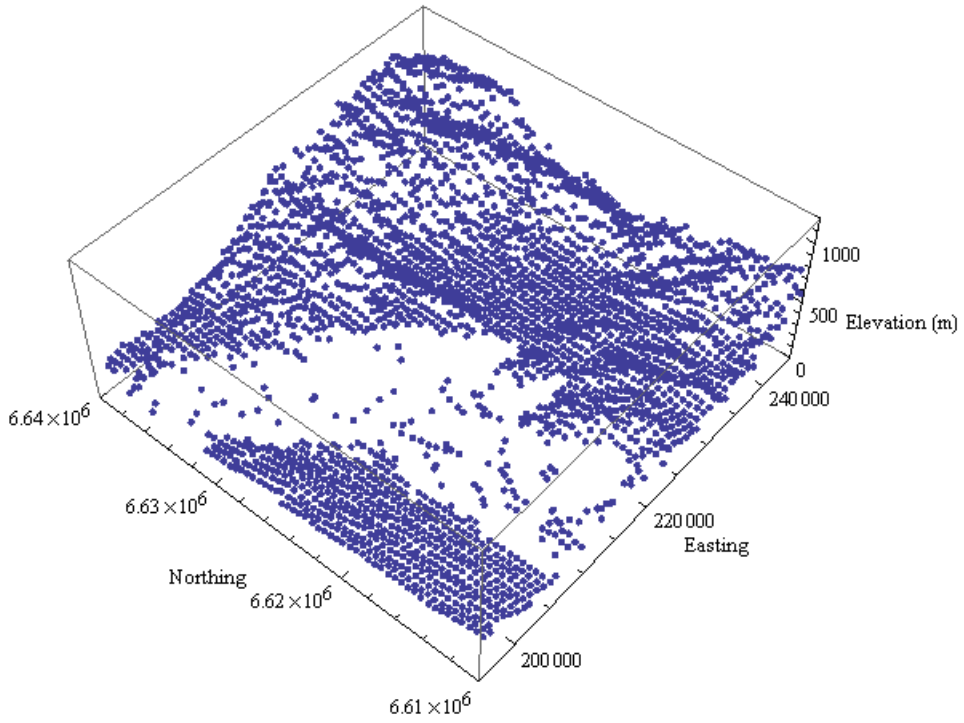

Grid the Rock Surface Data

To define the base of the aquifer the rock surface data are gridded using the function **InverseDistanceGrid2D**.

We can then highlight the pre-Tertiary paleochannel (the base of the alluvial aquifer) by using the function **RegionPlot3D**.

The predicate is: z < rockfunction[x, y]

```
ksearch = 3; power = 2;
rockfunction = InverseDistanceGrid2D[rocksurfacepoints, ksearch, power, grid2D];

rockregionplot3D = RegionPlot3D[z < rockfunction[x, y], {x, xmin, xmax},
  {y, ymin, ymax}, {z, zmin, zmax}, Mesh → None, PlotPoints → 75,
  BoxRatios → {1, 1, 0.5}, ColorFunction → "DarkBands",
  AxesLabel → {"Easting", "Northing", "Elevation (m)"},
  ViewPoint →  {-1.75, -1.5, 2.5}, ImageSize → {500, 450}]
```

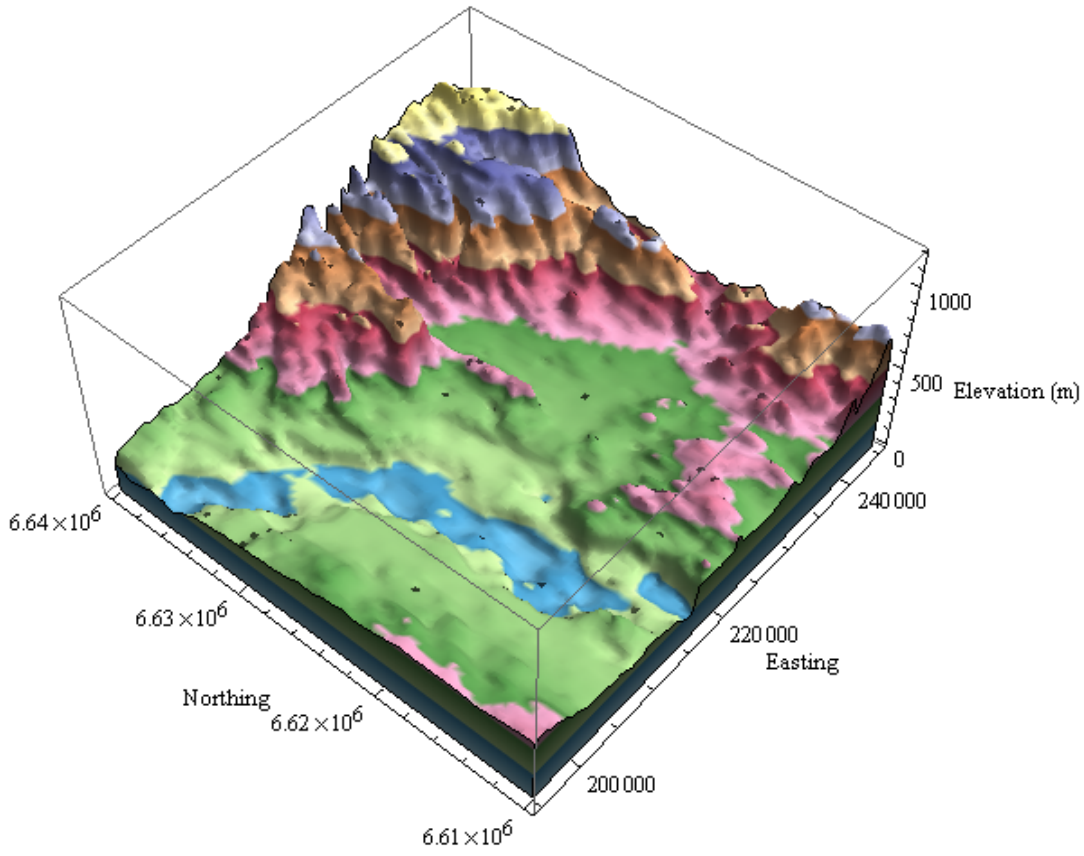

A RegionPlot3D Image of the 3D Surface Model

The sorted alluvial data set is gridded using the new function **NearestNeighborGrid2D**.

```
alluviumfunction = NearestNeighborGrid2D[alluvium, grid2D];
```

Now that each surface is defined by a continuous approximate function over the x,y domain a 3D plot of the rock and alluvium can be calculated using **RegionPlot3D**.

The predicate for the alluvium is: z < alluviumfunction[x, y] && z > rockfunction[x, y]

```
alluviumregionplot3D =
  RegionPlot3D[z < alluviumfunction[x, y] && z > rockfunction[x, y],
   {x, xmin, 220 000}, {y, ymin, ymax}, {z, 120, 500}, PlotStyle → Lighter[Yellow],
   Mesh → None, PlotPoints → 75, PerformanceGoal → "Quality"];
Show[rockregionplot3D, alluviumregionplot3D, ViewPoint → {-1.0, -1.5, 0.75},
 ImageSize → {500, 450}]
```

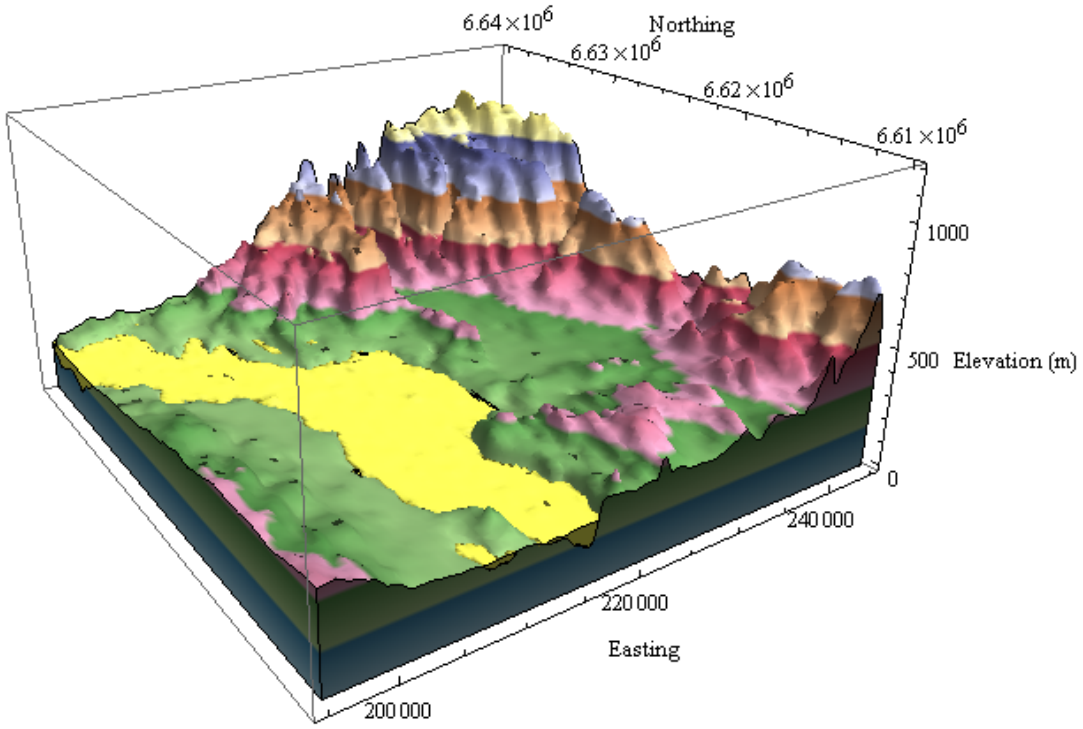

Import the Borehole Facies Data

The next step is to fill in the alluvial region with the facies data.

For this example the clay is one class (purple) and the high water yielding sands and gravels are the second class (yellow).

```
faciesdata = Drop[Import["maulesfacies.csv"], 1];
clay = Cases[faciesdata, {_, _, _, 1}];
sandgravel = Cases[faciesdata, {_, _, _, 2}];
ListPointPlot3D[{clay[[All, {1, 2, 3}]], sandgravel[[All, {1, 2, 3}]]},
 PlotRange → {{xmin, xmax}, {ymin, ymax}, {zmin, 500}},
 PlotStyle → {Directive[RGBColor[0.666667, 0.207843, 0.380392], PointSize[0.01]],
   Directive[Lighter[Yellow, 0.4], PointSize[0.01]]},
 AxesLabel → {"Easting", "Northing", "Elevation (m)"},
 ViewPoint → {-1.0, -1.5, 0.75}, BoxRatios → {1, 1, 1.25},
 ImageSize → {450, 450} ]
```

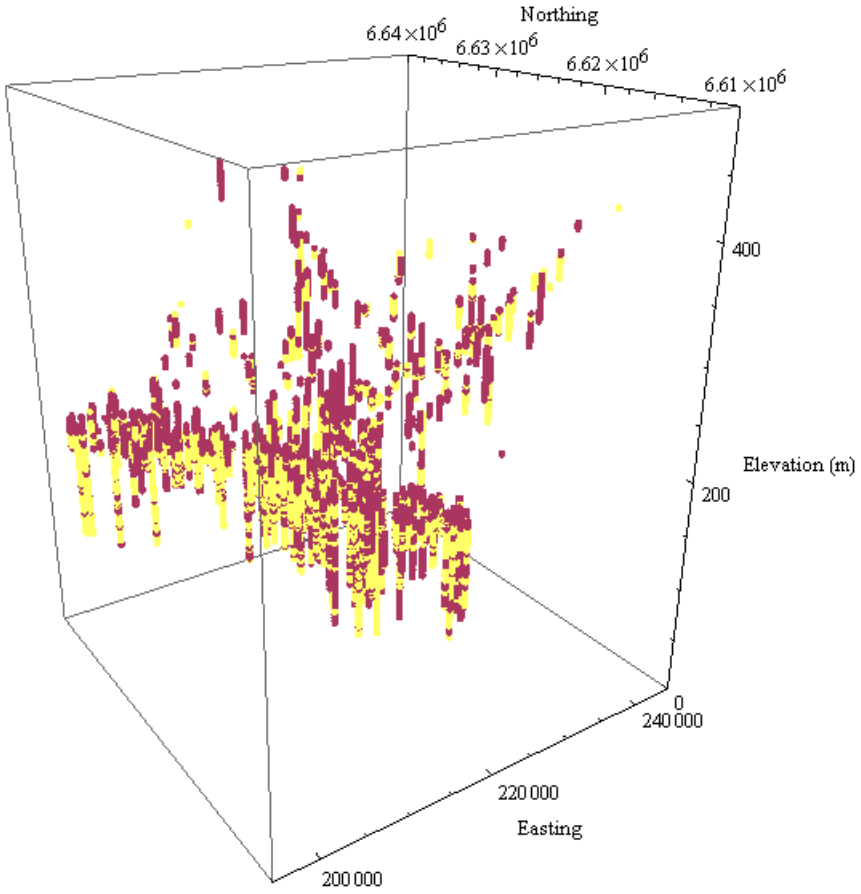

Defining the Dimensions of the 3D Grid

The regular 3D grid list, $\{\{x_1,y_1,z_1\},\{x_2,y_2,z_2\}, \ldots\}$, is defined and the nodes limited to those that fall within the limits of the alluvium.

```
grid3D = Flatten[Table[{x, y, z}, {x, xmin, 225 000, 500}, {y, ymin, ymax, 500},
    {z, zmin, 400, 5}], 2];

sort[{x_, y_, z_}] := If[z > rockfunction[x, y] && z < alluviumfunction[x, y], 1, 0];
inout = Map[sort, grid3D];
inoutlist = Partition[Flatten[Riffle[grid3D, inout]], 4];
insidenodes = Cases[inoutlist, {_, _, _, 1}][[All, {1, 2, 3}]];

ListPointPlot3D[insidenodes,
 PlotRange → {{xmin, xmax}, {ymin, ymax}, {zmin, 400}},
 AxesLabel → {"Easting", "Northing", "Elevation (m)"},
 PlotStyle → PointSize[0.006], ViewPoint → {-1.0, -1.5, 0.75},
 BoxRatios → {1, 1, 1.25}, ImageSize → {450, 450}]
```

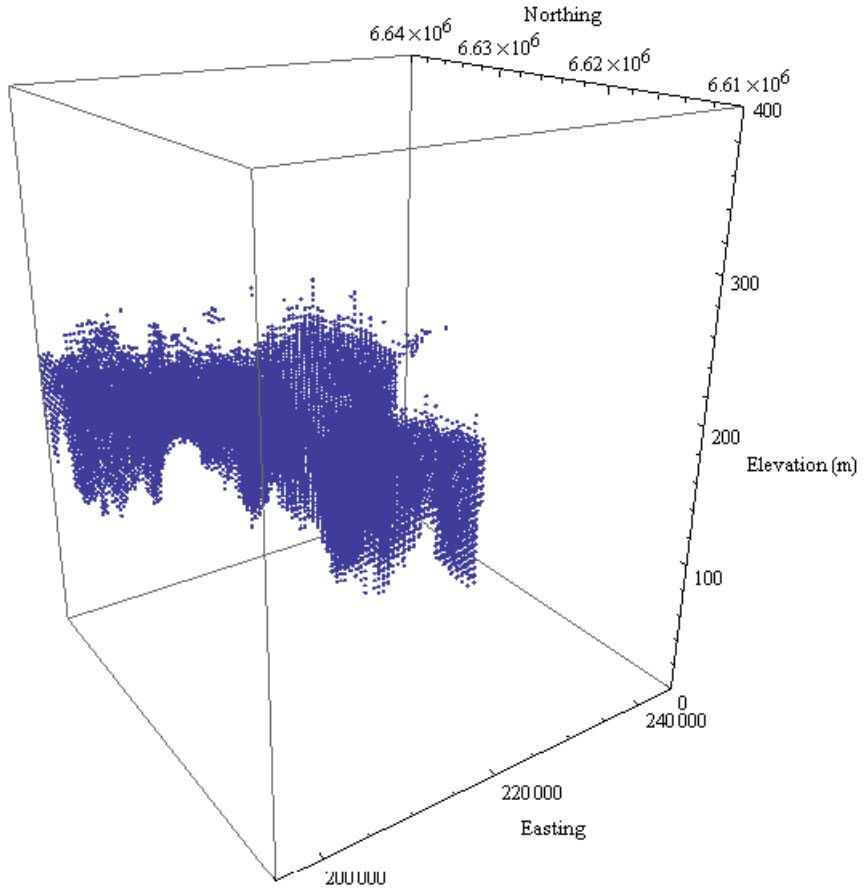

3D Nearest Neighbor Gridding of Borehole Facies Data

The facies class assigned to each grid node is estimated from the borehole facies data using 3D nearest neighbor gridding.

This simple categorical classification technique has proven to be a robust method in many sedimentary environments (Tartakovsky, 2007).

Gridding the facies data enhances the visual continuity of the sand/gravel and clay lenses.

```
faciesfunction = Nearest[faciesdata[[All, {1, 2, 3}]] → faciesdata[[All, 4]]];
faciesNNlist = Map[faciesfunction, insidenodes][[All, 1]];
faciesNNgrid3Dinside = Partition[Flatten[Riffle[insidenodes, faciesNNlist]], 4];

clayNN = Cases[faciesNNgrid3Dinside, {_, _, _, 1}];
sandgravelNN = Cases[faciesNNgrid3Dinside, {_, _, _, 2}];
faciespoints3D =
 ListPointPlot3D[{clayNN[[All, {1, 2, 3}]], sandgravelNN[[All, {1, 2, 3}]]},
  PlotRange → {{xmin, xmax}, {ymin, ymax}, {zmin, 400}},
  PlotStyle → {Directive[RGBColor[0.666667, 0.207843, 0.380392],
     PointSize[0.007]], Directive[Lighter[Yellow, 0.4], PointSize[0.008]]},
  AxesLabel → {"Easting", "Northing", "Elevation (m)"},
  ViewPoint → {-1.0, -1.5, 0.75}, BoxRatios → {1, 1, 1.25}, ImageSize → {450, 450}]
```

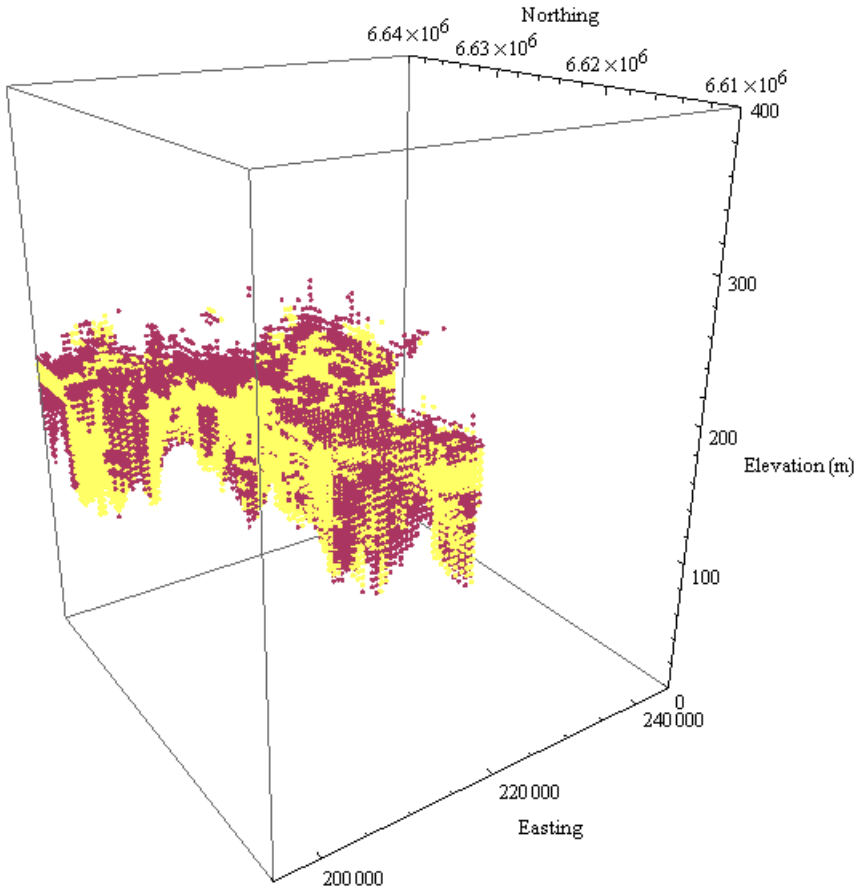

3D Geological Facies Model

Displayed below is the final facies model. The facies data points fill the paleovalley. This model can be exported into groundwater flow modeling programs.

```
Show[rockregionplot3D, faciespoints3D, ViewPoint → {-1.0, -1.5, 0.75},
 ImageSize → {600, 550}]
```

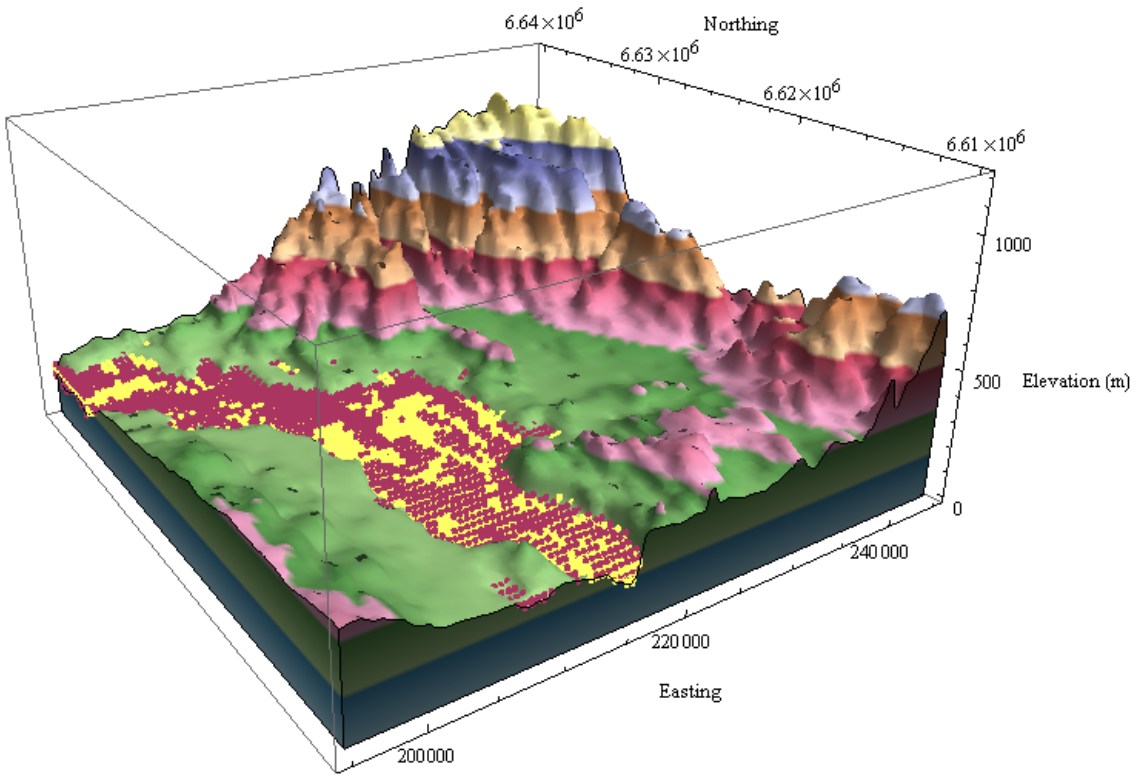

Slice the 3D Facies Model

The 3D facies model can be sliced to examine the facies distribution along lines of interest.

```
xslice = 205 000; yslice = 6 622 000;
ztop = 300; zbottom = 100;
faciesslice =
  ListPointPlot3D[{clayNN[[All, {1, 2, 3}]], sandgravelNN[[All, {1, 2, 3}]]},
   PlotRange → {{xslice, xmax}, {yslice, ymax}, {zbottom, ztop}},
   PlotStyle → {Directive[RGBColor[0.666667, 0.207843, 0.380392],
      PointSize[0.015]], Directive[Lighter[Yellow], PointSize[0.015]]}];
rockslice = RegionPlot3D[z < rockfunction[x, y], {x, xslice, xmax},
   {y, yslice, ymax}, {z, zbottom, ztop}, Mesh → None, PlotPoints → 50,
   PlotStyle → RGBColor[0.392157, 0.576471, 1]];
Show[rockslice, faciesslice, AxesLabel → {"Easting", "Northing", "Elevation (m)"},
 Lighting → "Neutral", ViewPoint → {-2, -2, 0}, ImageSize → {500, 500} ]
```

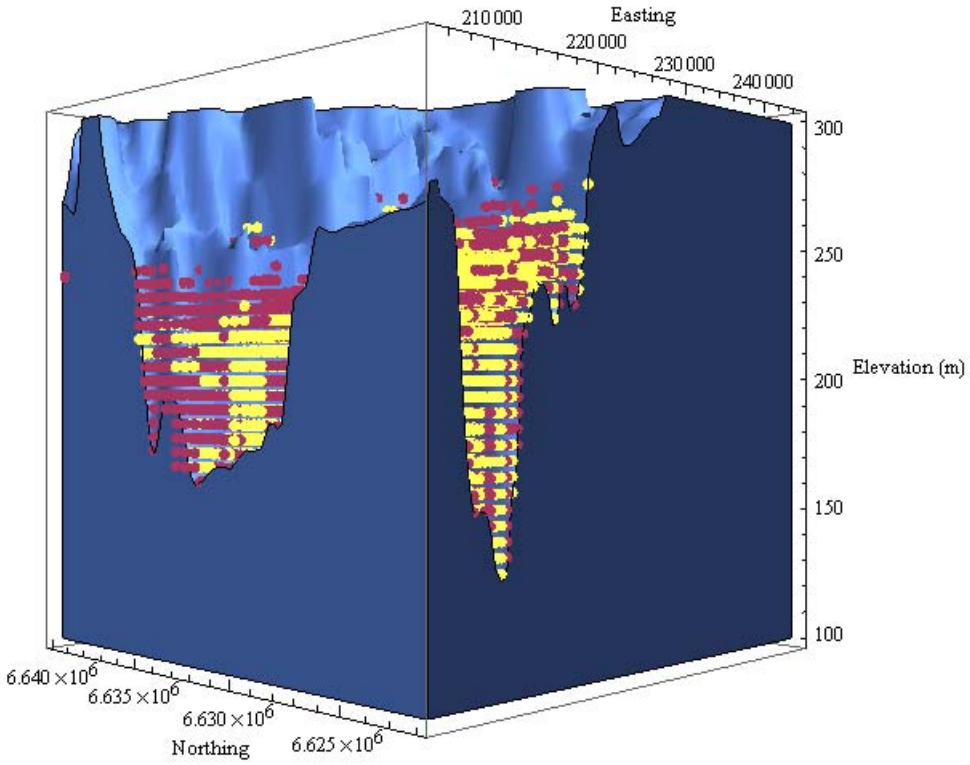

Building the Geological Structural Model

Maules Creek Geological Map

Below is the geological map of Maules Creek.

The major geological periods are labeled in yellow on the map. The red lines show portions of the map where details of the strike and dip of the contact surface have been obtained. The outline of the Tertiary basalt was also digitized.

From this sparse data set a 3D geological structural model based on the geological period boundaries will be constructed.

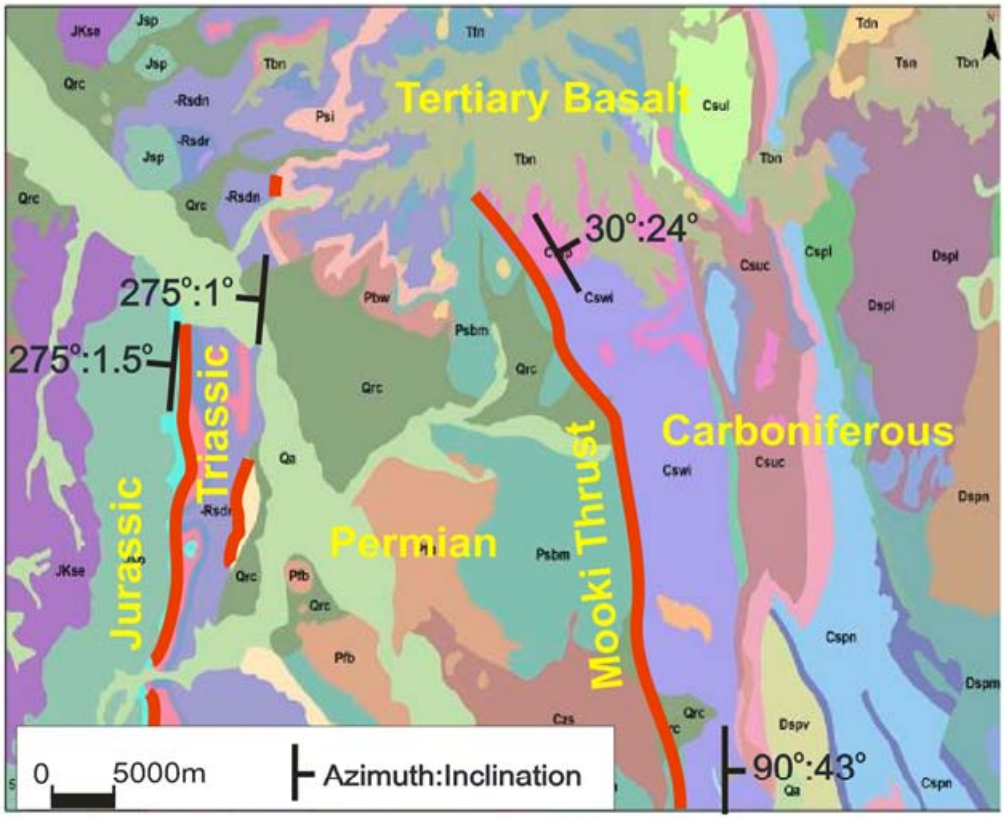

Import the Geological Structural Data

At selected locations on the upper surface of geological structures the dip inclination and dip azimuth are recorded. The structures can be geological period boundaries, the top of formations, or fault surfaces.

These data sets provide sparse details on the shape of the geological surfaces that define the volume of the geological elements of interest.

For the period boundaries and fault surface data sets at each point the coordinates (x,y,z), azimuth and inclination are loaded. Azimuth values range from 0 to 360, north is 0, east is 90. Inclination values range from 0 to 90, where 0 is horizontal and 90 is vertically down.

The base of the Tertiary basalt is defined by projecting the digitized map points onto the DEM. Each point representing the outline of the Tertiary basalt boundary is then defined by the triplet {x,y,z}.

Below the structural data for the Maules Creek catchment are imported and displayed.

```
topTriassic = Drop[Import["TopTriassic.csv"], 1];
topPermian = Drop[Import["TopPermian.csv"], 1];
faultMookiThrust = Drop[Import["MookiThrust.csv"], 1];
bottomTertiaryBasalt = Drop[Import["BottomTertiaryBasalt.csv"], 1];
pointsTertiaryBasalt = bottomTertiaryBasalt[[All, {2, 3, 4}]];
ListPointPlot3D[{topTriassic[[All, {2, 3, 4}]], topPermian[[All, {2, 3, 4}]],
  faultMookiThrust[[All, {2, 3, 4}]], pointsTertiaryBasalt},
 PlotRange → {{xmin, xmax}, {ymin, ymax}, {zmin, zmax}},
 PlotStyle → {Directive[Darker[Red, 0.1], PointSize[0.012]],
   Directive[Blue, PointSize[0.012]],
   Directive[Darker[Green, 0.1], PointSize[0.012]],
   Directive[Darker[Cyan, 0.1], PointSize[0.007]]},
 AxesLabel → {"Easting", "Northing", "Elevation (m)"},
 ViewPoint → {-1.0, -1.5, 0.75}, ImageSize → {500, 400}]
```

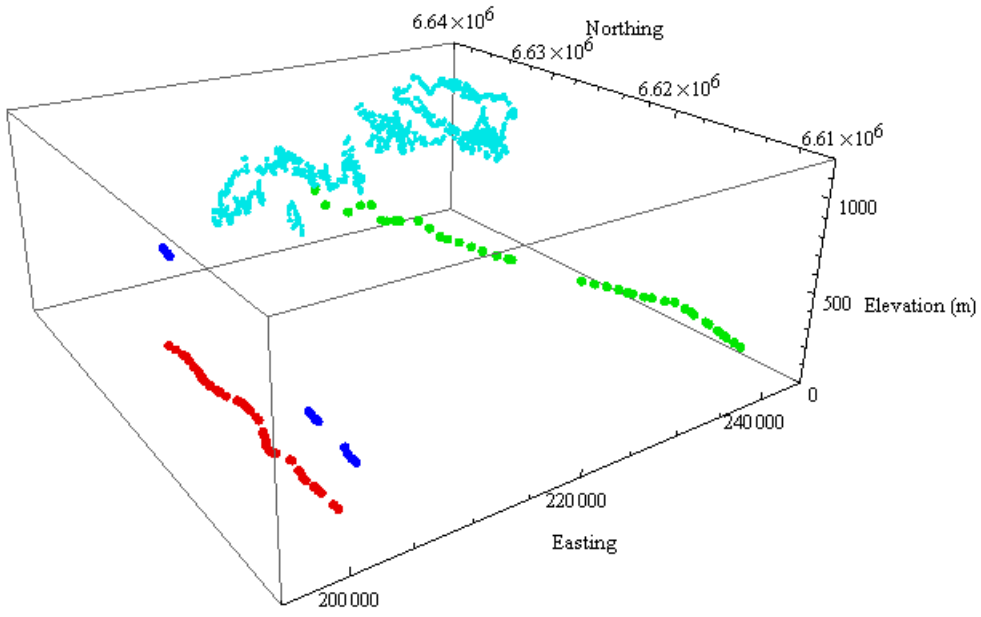

Projection of Field and Map Data

Starting at the measurement point (x_0,y_0,z_0), the n-th point (x_n,y_n,z_n) projected along the linear line in the down dip direction is calculated using the trigonometric equations:

$x_n = x_0 + \text{Cos[inclination] Sin[azimuth] n s},$
$y_n = y_0 + \text{Cos[inclination] Cos[azimuth] n s},$
$z_n = z_0 - \text{Sin[inclination]},$

where s is the size of the interval between each point.

A set of points is projected both up and down dip from the field or digitized data location.

The function **GeoPointProjectLine** is defined and applied to each of the structural data sets.This process is described in more detail in de Kemp (1998), Bistacchi et al. (2008) and Zanchi et al. (2009).

```
GeoPointProjectLine[geodatain_, stepin_, countin_] :=
 Module[{step, projectdown, projectup, projectiontable},
  projectdown = Flatten[N[Table[{
       geodatain[[i, 2]] + (Cos[geodatain[[i, 5]] °] * Sin[geodatain[[i, 6]] °]) stepir
       geodatain[[i, 3]] + (Cos[geodatain[[i, 5]] °] * Cos[geodatain[[i, 6]] °])
         stepin n,
       geodatain[[i, 4]] - Sin[geodatain[[i, 5]] °] stepin n},
      {i, Length[geodatain]}, {n, 0, countin}]], 1];
  projectup = Flatten[N[Table[{
       geodatain[[i, 2]] - (Cos[geodatain[[i, 5]] °] * Sin[geodatain[[i, 6]] °]) stepir
       geodatain[[i, 3]] - (Cos[geodatain[[i, 5]] °] * Cos[geodatain[[i, 6]] °])
         stepin n,
       geodatain[[i, 4]] + Sin[geodatain[[i, 5]] °] stepin n},
      {i, Length[geodatain]}, {n, 0, countin}]], 1];
  projectiontable = Join[projectup, projectdown];
  Return[projectiontable]]
```

The Projected Data

Below is a 3D plot of the projected data after the function **GeoPointProjectLine** has been applied to the sparse geological structural data sets.

Data points are projected beyond the domain of interest to control the shape of the grids to be calculated.

```
step = 1000; count = 50;
linesTriassic = GeoPointProjectLine[topTriassic, step, count];
linesPermian = GeoPointProjectLine[topPermian, step, count];
linesMookiThrust = GeoPointProjectLine[faultMookiThrust, 200, 15];

ListPointPlot3D[{linesTriassic, linesPermian, linesMookiThrust,
  pointsTertiaryBasalt},
 PlotRange → {{xmin, xmax}, {ymin, ymax}},
 PlotStyle → {Directive[Darker[Red, 0.1], PointSize[0.006]],
   Directive[Blue, PointSize[0.006]],
   Directive[Darker[Green, 0.3], PointSize[0.006]],
   Directive[Darker[Cyan, 0.1], PointSize[0.006]]},
 AxesLabel → {"Easting", "Northing", "Elevation (m)"},
 ViewPoint → {-1.0, -1.5, 0.75}, ImageSize → {500, 450}]
```

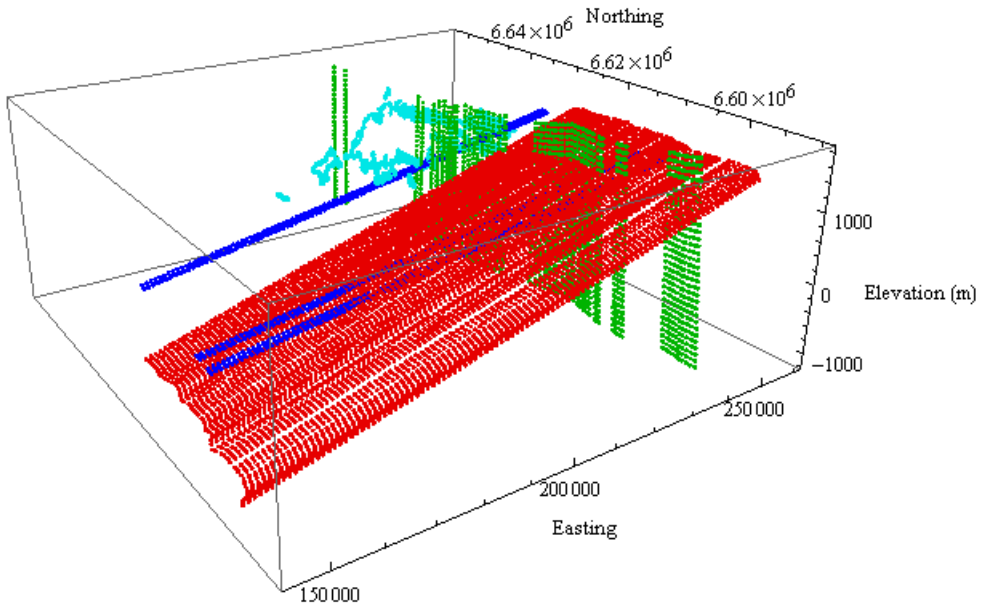

Grid the Projected Data

Each projected data set can now be gridded using the new functions **NearestNeighborGrid2D** and **InverseDistanceGrid2D**.

The Tertiary basalt data are gridded using nearest neighbor, while the projected data sets that define the structural tops of the Jurassic and Permian, along with the Mooki Thrust are gridded using inverse distance.

```
ksearch = 3; power = 2;
grid2Dc =
  Partition[Flatten[Table[{x, y}, {x, xmin, xmax, 1000}, {y, ymin, ymax, 1000}]], 2];
fPermian = InverseDistanceGrid2D[linesPermian, ksearch, power, grid2Dc];
fTriassic = InverseDistanceGrid2D[linesTriassic, ksearch, power, grid2Dc];
fMookiThrust = InverseDistanceGrid2D[linesMookiThrust, ksearch, power, grid2Dc];
fTertiaryBasalt = NearestNeighborGrid2D[pointsTertiaryBasalt, grid2Dc];

Plot3D[{fTriassic[x, y], fPermian[x, y], fMookiThrust[x, y],
  fTertiaryBasalt[x, y]}, {x, xmin, xmax}, {y, ymin, ymax},
 PlotStyle → {Darker[Red, 0.1], Blue, Darker[Green, 0.3], Darker[Cyan, 0.1]},
 PlotPoints → 50, Mesh → None,
 AxesLabel → {"Easting", "Northing", "Elevation (m)"},
 ViewPoint → {1, -2, -0.1}, ImageSize → {500, 300},
 Lighting → {{"Directional", GrayLevel[0.95], {220 000, 6 620 000, 5000}},
   {"Directional", GrayLevel[0.8], {350 000, 6 630 000, -500}},
   {"Directional", GrayLevel[0.8], {210 000, 6 660 000, -5000}}}]
```

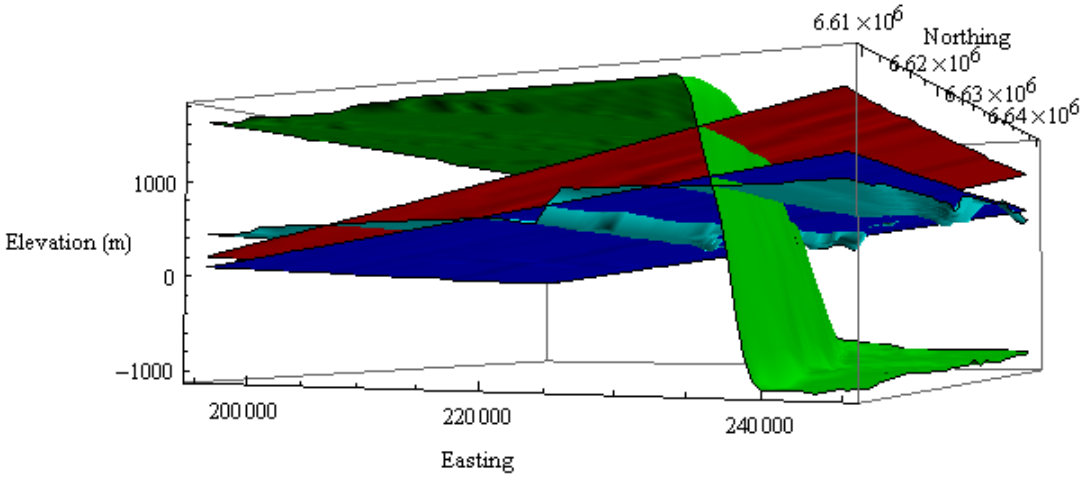

Constructing the Geological Regions

Each region of the geological model is defined using the function **RegionPlot3D**.

Using a set of relational and logical operators for the predicate the geological history is replicated.

```
regionTertiaryBasalt =
  RegionPlot3D[z > fTertiaryBasalt[x, y] && z < rockfunction[x, y],
   {x, 215 000, xmax}, {y, 6 630 000, ymax}, {z, zmin, zmax}, Mesh → None,
   PlotPoints → 75, PlotStyle → RGBColor[0.729412, 0.0392157, 0.0392157]];

regionJurassic =
  RegionPlot3D[z > fTriassic[x, y] && z < rockfunction[x, y] && z < fMookiThrust[x, y],
   {x, xmin, xmax}, {y, ymin, ymax}, {z, zmin, zmax}, Mesh → None,
   PlotPoints → 75, PlotStyle → RGBColor[0.470588, 0.470588, 0.737255]];

regionTriassic =
  RegionPlot3D[z < fTriassic[x, y] && z > fPermian[x, y] && z < rockfunction[x, y] &&
    z < fTertiaryBasalt[x, y] && z < fMookiThrust[x, y], {x, xmin, xmax},
   {y, ymin, ymax}, {z, zmin, zmax}, Mesh → None, PlotPoints → 75,
   PlotStyle → Lighter[RGBColor[0.823529, 0.576471, 0.670588]]];

regionPermian =
  RegionPlot3D[z < fPermian[x, y] && z < rockfunction[x, y] &&
    z < fTertiaryBasalt[x, y] && z < fMookiThrust[x, y], {x, xmin, xmax},
   {y, ymin, ymax}, {z, zmin, zmax}, Mesh → None, PlotPoints → 75,
   PlotStyle → Lighter[RGBColor[0.556863, 0.733333, 0.443137]]];

regionMookiThrust =
  RegionPlot3D[z > fMookiThrust[x, y] && z < rockfunction[x, y] &&
    z < fTertiaryBasalt[x, y], {x, xmin, xmax}, {y, ymin, ymax}, {z, zmin, zmax},
   Mesh → None, PlotPoints → 75, PlotStyle → RGBColor[0.894118, 0.827451, 0.454902]];
```

3D Geological Structural Model

The above calculated, but not displayed, geological period region images are combined into the single 3D geological structural model shown below.

Each geological period is represented as a solid color. The color key used below is: Tertiary basalt (red), Jurassic (blue), Triassic (pink), Permian (green), and Carboniferous (yellow).

```
structuralmodel = Show[regionJurassic, regionTriassic, regionPermian,
  regionMookiThrust, regionTertiaryBasalt,
  AxesLabel → {"Easting", "Northing", "Elevation (m)"},
  BoxRatios → {1, 1, 0.5},
  Lighting → {{"Directional", GrayLevel[0.95], {220 000, 6 600 000, 500}},
    {"Directional", GrayLevel[0.8], {150 000, 6 630 000, 500}},
    {"Directional", GrayLevel[0.8], {210 000, 6 660 000, 5000}}},
  ViewPoint → {-1.0, -1.5, 1.5}, ImageSize → {500, 450}]
```

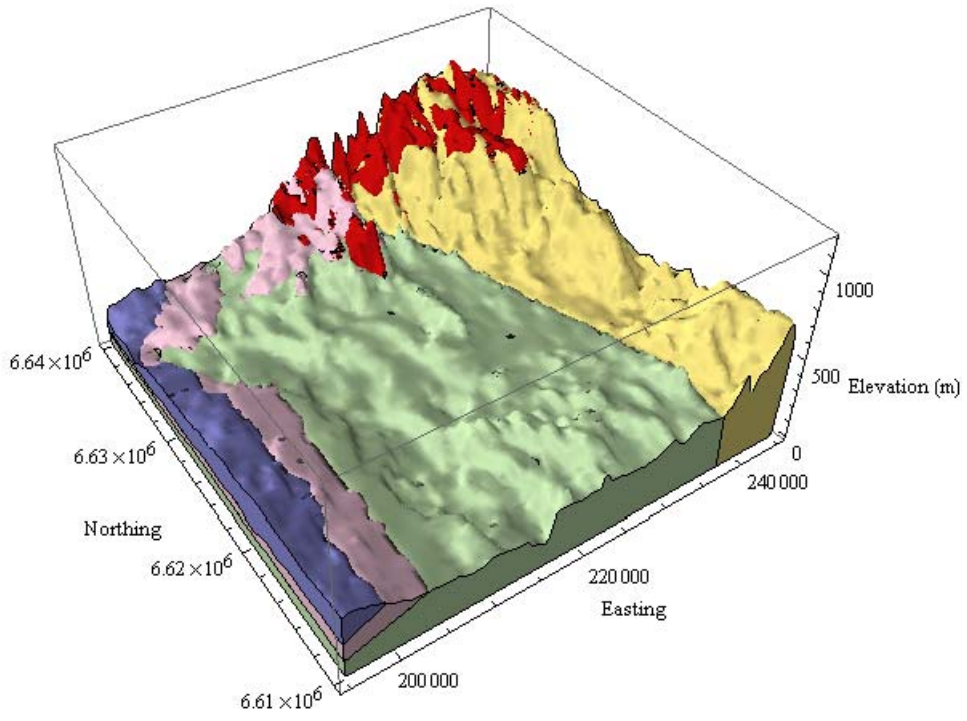

3D Geological Structural and Facies Model

The last step is to combine the facies and structural models into a single 3D geological model.

These models are the starting point for further geological investigations. They can be used to:

- present our conceptualization of the regional geological history,
- determine the volume of the aquifer,
- predict the lithology at new borehole locations, and
- provide the framework for regional water balance modeling.

As more details are obtained about the catchment the models can be easily updated or refined.

Finally, collating the information into 3D images allows for the easy communication of geological information to the wider community.

```
Show[structuralmodel, faciespoints3D]
```

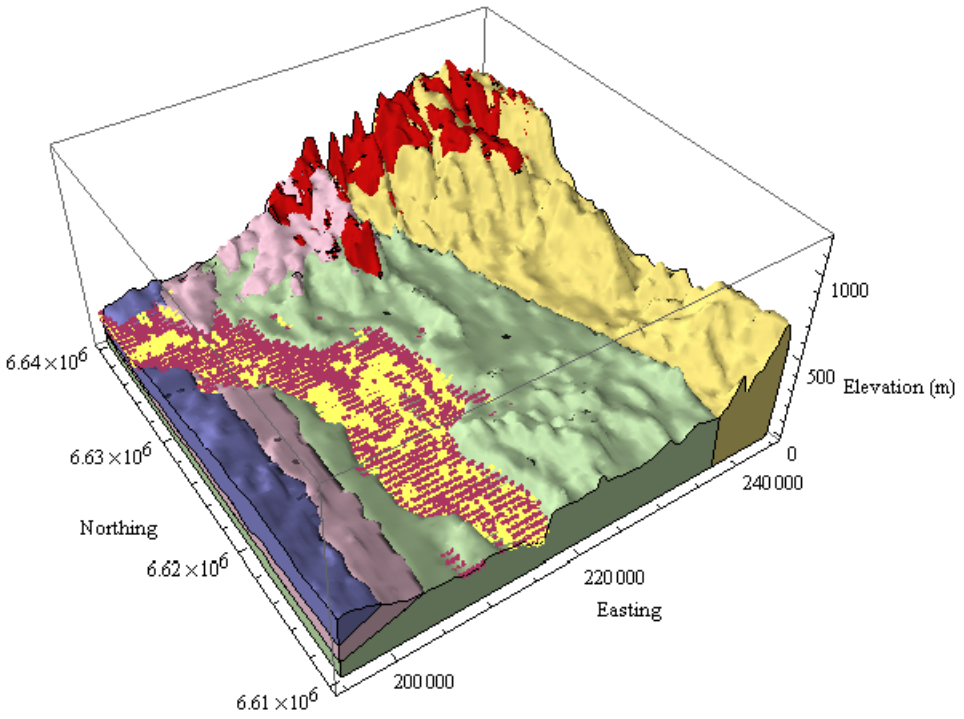

Acknowledgments

The financial support of the Australian Government National Water Commission, Australian Research Council, Cotton Catchment Communities CRC and the Namoi Catchment Management Authority is acknowledged.

I would also like to thank Dr B. Giambastiani for her assistance with preparing the data sets used in this presentation, and Professor I. Acworth for the coordination and administration of the grants.

References

Bistacchi A., Massironi M., Dal Piaz G.V., Dal Piaz G., Monopoli B., Schiavo A., Toffolon G. (2008) 3D fold and fault reconstruction with an uncertainty model: An example from an Alpine tunnel case study. *Computers and Geosciences,* 34(4): 351-372.

de Kemp E.A. (1998) Three-dimensional projection of curvilinear geological features through direction cosine interpolation of structural field observations. *Computers and Geosciences,* 24(3): 269-284.

Haneberg, W.C. (2004) *Computational Geosciences with Mathematica*. Springer-Verlag Berlin Heidelberg. ISBN 3-540-40245-4.

Tartakovsky D.M., Wohlberg B., Guadagninni A. (2007) Nearest-Neighbor Classification for Facies Delineation. *Water Resources Research,* 43 DOI 10.1029/2007WR005968.

Yamamoto, J.K. (1998) A Review of Numerical Methods for the Interpolation of Geological Data. *An. Acad. Bras. Ci.*, 70(1): 91-116.

Zanchi A., Francesca S., Stefano Z., Simone S., Graziano G. (2009) 3D reconstruction of complex geological bodies: Examples from the Alps. *Computers and Geosciences,* 35(1): 49-69.

Appendix 4

Crystallize
Populating a FEFLOW Mesh with Property Data

Authors
B. Kelly and B. Giambastiani

A4.1 Introduction

This *Crystallize* notebook demonstrates how to populate a FEFLOW mesh with property data. For this example the lithology index is assigned to the FEFLOW volume element centre using nearest neighbour gridding. The nearest neighbour is determined using the Euclidean distance. The driller core logs reported on the NSW State Government groundwater Pinneena CD were interpreted assigning the index 1 to log intervals dominated by clay, and 2 to log intervals dominated by sand and gravel.

Although it is possible to generate a finite element mesh in *Mathematica* for the moment there are better tools for generating a finite element mesh in FEFLOW. FEFLOW has interpolation algorithms, but they lack the flexibility of the gridding algorithms available in *Mathematica* or in SGEMS.

A4.2 Calculation

Set the working directory for the project

```
SetDirectory[
  "G:\\NWC_FinalReportUNSW3DHydrogeology\\Appendix4_CrystallizeFEFLOWmesh"];
```

Assign the dimensions that will be used in all the 3D plots.

```
xmin = 205 000; xmax = 225 000; xspace = 500;
ymin = 6 605 000; ymax = 6 635 000; yspace = 500;
zmin = 100; zmax = 600; zspace = 5;
```

Import the borehole lithology index data and the FEFLOW mesh.

```
faciesdata = Drop[Import["maulesfacies.csv"], 1];
femesh = Import["FEFLOW_centroid_mesh.csv", "CSV"];
grid = femesh[[All, {3, 4, 5}]];
```

Examine the bore logs in 3D. For this example the clay is one class (purple) and the high water yielding sands and gravels are the second class (yellow).

```
clay = Cases[faciesdata, {_, _, _, 1}];
sandgravel = Cases[faciesdata, {_, _, _, 2}];
ListPointPlot3D[{clay[[All, {1, 2, 3}]], sandgravel[[All, {1, 2, 3}]]},
 PlotRange → {{xmin, xmax}, {ymin, ymax}, {zmin, 500}},
 PlotStyle → {Directive[RGBColor[0.666667, 0.207843, 0.380392], PointSize[0.01]],
   Directive[Lighter[Yellow, 0.4], PointSize[0.01]]},
 AxesLabel → {"Easting", "Northing", "Elevation (m)"},
 ViewPoint → {-1.0, -1.5, 0.75}, BoxRatios → {1, 1, 1.25},
 ImageSize → {450, 450} ]
```

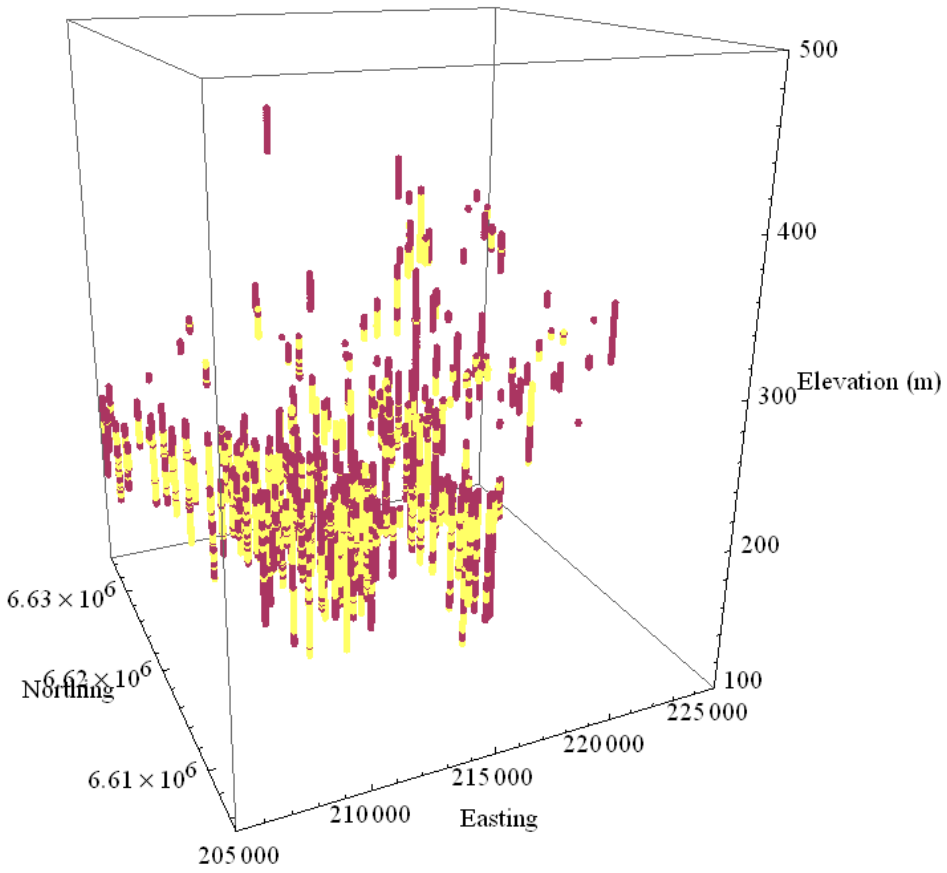

Take a look at the FEFLOW mesh

```
ListPointPlot3D[grid, PlotRange → {{xmin, xmax}, {ymin, ymax}, {zmin, 500}},
 PlotStyle → {Directive[RGBColor[0, 0, 1], PointSize[0.003]]},
 AxesLabel → {"Easting", "Northing", "Elevation (m)"},
 ViewPoint → {-1.0, -1.5, 0.75}, BoxRatios → {1, 1, 1.25},
 ImageSize → {450, 450} ]
```

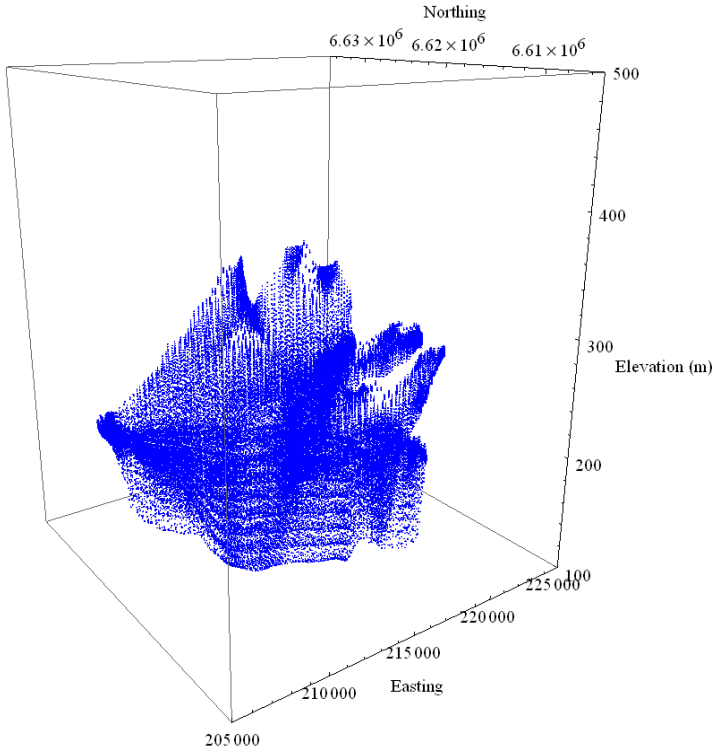

Populate the FEFLOW meash using nearest neighbour gridding (Note: this calculation takes approximately 5 minutes).

```
faciesfunction =
 Nearest[faciesdata[[All, {1, 2, 3}]] → faciesdata[[All, 4]]];
faciesNNlist = Map[faciesfunction, grid][[All, 1]];
faciesNNgrid3D = Partition[Flatten[Riffle[grid, faciesNNlist]], 4];
```

Plot in 3D the indexed facies mesh.

```
clayNN = Cases[faciesNNgrid3D, {_, _, _, 1}];
sandgravelNN = Cases[faciesNNgrid3D, {_, _, _, 2}];
faciespoints3D =
 ListPointPlot3D[{clayNN[[All, {1, 2, 3}]],
   sandgravelNN[[All, {1, 2, 3}]]},
  PlotRange → {{xmin, xmax}, {ymin, ymax}, {zmin, 400}},
  PlotStyle →
   {Directive[RGBColor[0.666667, 0.207843, 0.380392],
     PointSize[0.007]], Directive[Lighter[Yellow, 0.4],
     PointSize[0.008]]},
  AxesLabel → {"Easting", "Northing", "Elevation (m)"},
  ViewPoint → {-1.0, -1.5, 0.75}, BoxRatios → {1, 1, 1.25},
  ImageSize → {450, 450}]
```

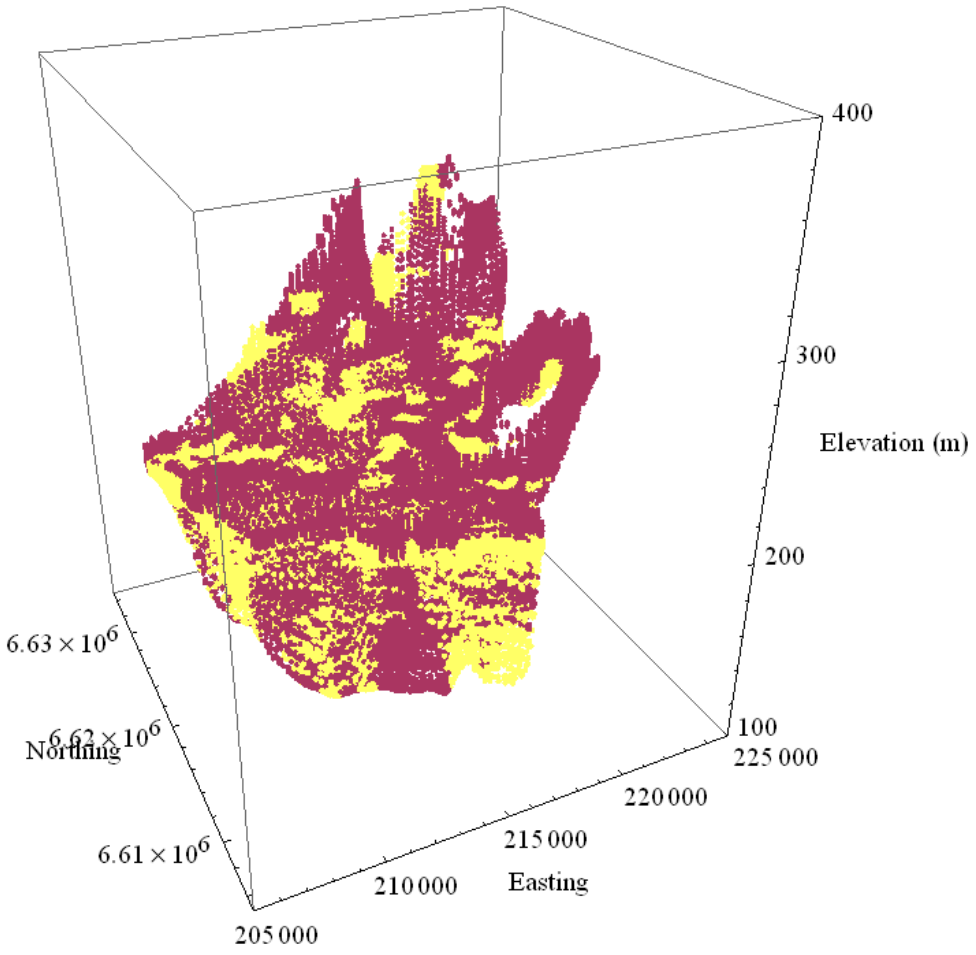

Add a new index value column to the originally imported FEFLOW mesh matrix.

```
feknnnode = faciesNNgrid3D[[All, 4]];
fepoints = Partition[Flatten[Riffle[femesh, feknnnode]], 6];
```

The next step is to import the location of the streams. The polygon file in the ArcGIS database was converted to a list of points and exported. The next few lines import the stream data file and then makes a plot of the points.

```
streampoints = Import["streams_nonamoi_filled_09july_09.csv", "CSV"];
streampointsplot = streampoints[[All, {2, 3}]];
ListPlot[streampointsplot, Axes → True, AxesLabel → {"Easting", "Northing"} ,
 PlotLabel → "Stream Points" , AxesOrigin → {xmin, ymin}]
```

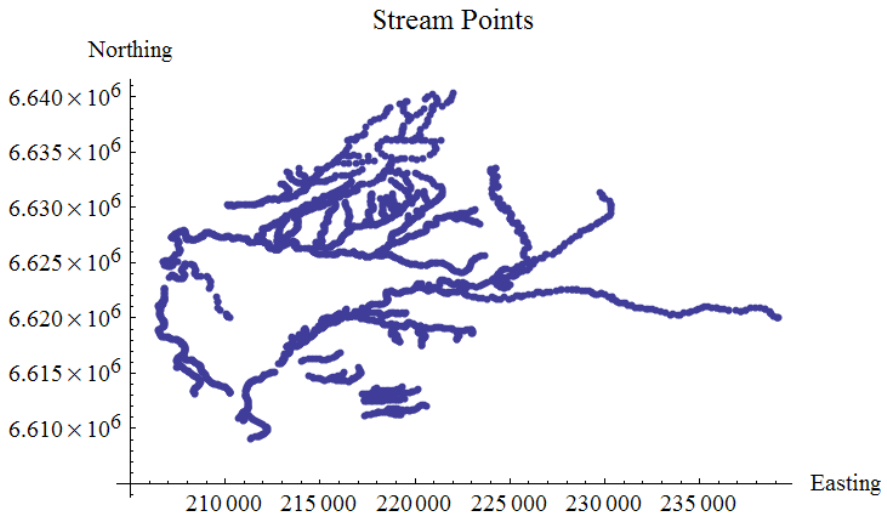

Find points adjacent to the stream data set, and check that they are classified as hydraulically conductive sediments. This calculation takes about 15 minutes.

```
Do[
 Do[
  If[fepoints[[j, 2]] < 3,
   If[EuclideanDistance[fepoints[[j, {3, 4}]], streampoints [[i, {2, 3}]]] < 300,
    fepoints[[j]] = {fepoints[[j, 1]], fepoints[[j, 2]], fepoints[[j, 3]],
      fepoints[[j, 4]], fepoints[[j, 5]], 5},
    fepoints[[j]]], 0
  ],
  {i, 1, Length[streampoints], 1}
 ],
 {j, 1, Length[fepoints], 1}
]

fepointsclean = Partition[Flatten[fepoints], 6]
```

Export the 3D facies mesh with the inserted streams.

```
Export["knn1_maulesstreamsonly_2FE_23July09.csv", fepointsclean];
```

Plot in 3D the facies mesh with the inserted streams.

```
clayNN2 = Cases[fepointsclean, {_, _, _, _, _, 1}];
sandgravelNN2 = Cases[fepointsclean, {_, _, _, _, _, 2}];
stream2 = Cases[fepointsclean, {_, _, _, _, _, 5}];
faciespoints3D2 =
 ListPointPlot3D[{clayNN2[[All, {3, 4, 5}]],
   sandgravelNN2[[All, {3, 4, 5}]], stream2[[All, {3, 4, 5}]]},
  PlotRange → {{xmin, xmax}, {ymin, ymax}, {zmin, 400}},
  PlotStyle →
   {Directive[RGBColor[0.666667, 0.207843, 0.380392],
     PointSize[0.007]], Directive[Lighter[Yellow, 0.4],
     PointSize[0.008]], Directive[Blue, PointSize[0.008]]},
  AxesLabel → {"Easting", "Northing", "Elevation (m)"},
  ViewPoint → {-1.0, -1.5, 0.75}, BoxRatios → {1, 1, 1.25},
  ImageSize → {450, 450}]
```

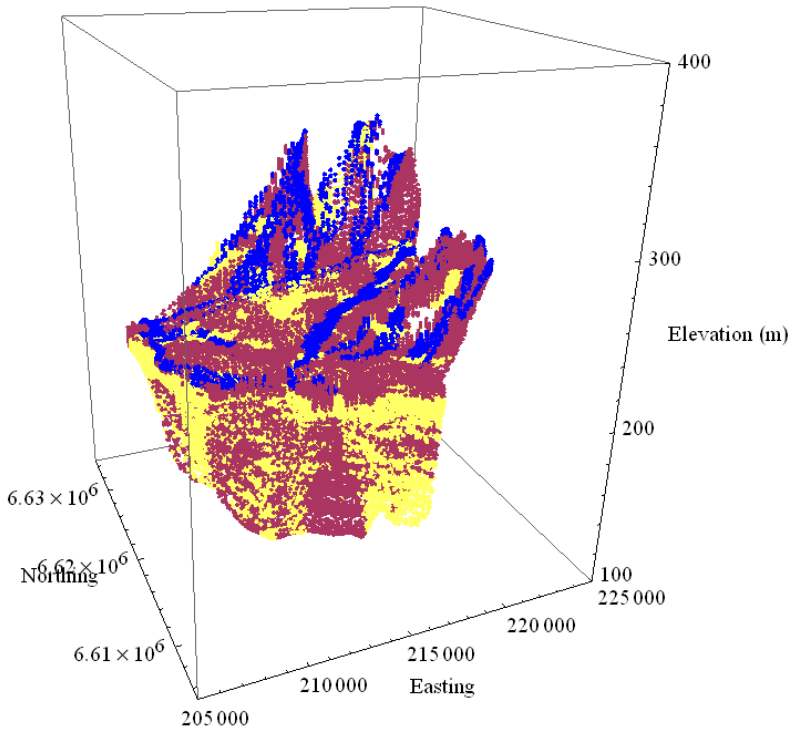

Export each FEFLOW layer to a separate comma separated file.

```
Do[
 slicematrix = {};
 Do[If[ fepointsclean[[i, 2]] == j, AppendTo[slicematrix, fepointsclean[[i]]], i],
  {i, 1, Length[fepointsclean]}];
 index = ToString[j];
 exportname = StringJoin["knn1_FEFLOW_layer_", index, ".csv"];
 Export[exportname, slicematrix], {j, 1, 9}]
```

Generate a 3D plot of each FEFLOW layer.

```
plotslice = {}; Do[slicematrix = {};
 Do[If[ fepointsclean[[i, 2]] == j, AppendTo[slicematrix, fepointsclean[[i]]], i],
  {i, 1, Length[fepointsclean]}];
 If[j < 3,
  clayNN2 = Cases[slicematrix, {_, _, _, _, _, 1}];
  sandgravelNN2 = Cases[slicematrix, {_, _, _, _, _, 2}];
  stream2 = Cases[slicematrix, {_, _, _, _, _, 5}];
  faciespoints3D2 =
   ListPointPlot3D[{clayNN2[[All, {3, 4, 5}]], sandgravelNN2[[All, {3, 4, 5}]],
     stream2[[All, {3, 4, 5}]]},
    PlotRange → {{xmin, xmax}, {ymin, ymax}, {zmin, 400}},
    PlotStyle → {Directive[RGBColor[0.666667, 0.207843, 0.380392],
       PointSize[0.007]], Directive[Lighter[Yellow, 0.2], PointSize[0.009]],
      Directive[Blue, PointSize[0.008]]},
    AxesLabel → {"Easting", "Northing", "Elevation (m)"}, BoxRatios → {1, 1, 1.25},
    ImageSize → {450, 450}];, clayNN2 = Cases[slicematrix, {_, _, _, _, _, 1}];
  sandgravelNN2 = Cases[slicematrix, {_, _, _, _, _, 2}];
  faciespoints3D2 =
   ListPointPlot3D[{clayNN2[[All, {3, 4, 5}]], sandgravelNN2[[All, {3, 4, 5}]]},
    PlotRange → {{xmin, xmax}, {ymin, ymax}, {zmin, 400}},
    PlotStyle → {Directive[RGBColor[0.666667, 0.207843, 0.380392],
       PointSize[0.007]], Directive[Lighter[Yellow, 0.2], PointSize[0.009]]},
    AxesLabel → {"Easting", "Northing", "Elevation (m)"}, BoxRatios → {1, 1, 1.25},
    ImageSize → {450, 450}]];
 AppendTo[plotslice, faciespoints3D2];,
 {j, 1, 9}];
plotslice
```

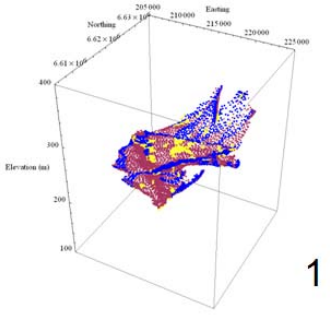
Easting
205 000
210 000
215 000
220 000
225 000
Northing
6.63 × 10^6
6.62 × 10^6
6.61 × 10^6
Elevation (m)
400
300
200
100
1

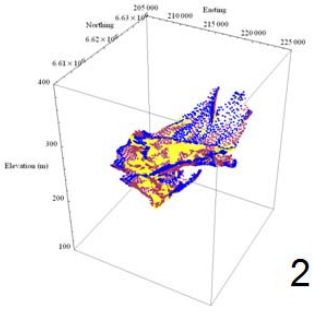
Easting
205 000
210 000
215 000
220 000
225 000
Northing
6.63 × 10^6
6.62 × 10^6
6.61 × 10^6
Elevation (m)
400
300
200
100
2

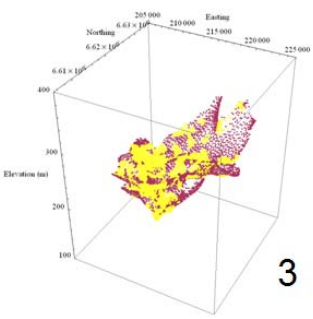
Easting
205 000
210 000
215 000
220 000
225 000
Northing
6.63 × 10^6
6.62 × 10^6
6.61 × 10^6
Elevation (m)
400
300
200
100
3

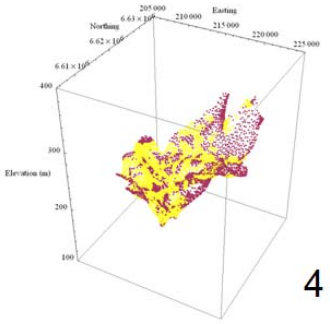
Easting
205 000
210 000
215 000
220 000
225 000
Northing
6.63 × 10^6
6.62 × 10^6
6.61 × 10^6
Elevation (m)
400
300
200
100
4

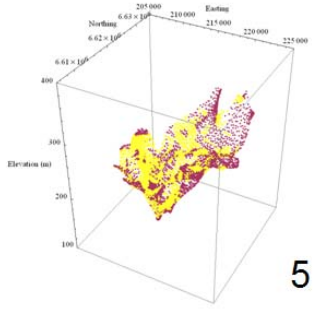
Easting
205 000
210 000
215 000
220 000
225 000
Northing
6.63 × 10^6
6.62 × 10^6
6.61 × 10^6
Elevation (m)
400
300
200
100
5

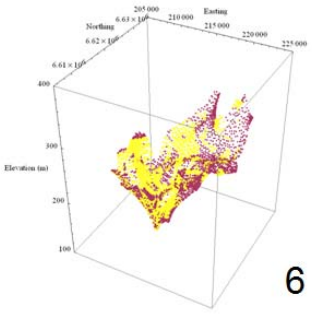
Easting
205 000
210 000
215 000
220 000
225 000
Northing
6.63 × 10^6
6.62 × 10^6
6.61 × 10^6
Elevation (m)
400
300
200
100
6

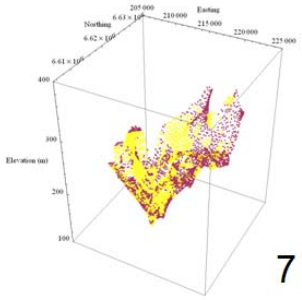
Easting
205 000
210 000
215 000
220 000
225 000
Northing
6.63 × 10^6
6.62 × 10^6
6.61 × 10^6
Elevation (m)
400
300
200
100
7

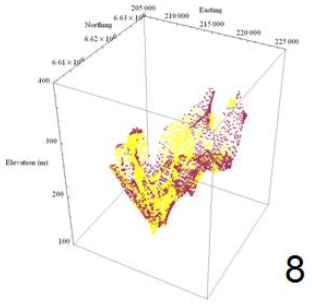
Easting
205 000
210 000
215 000
220 000
225 000
Northing
6.63 × 10^6
6.62 × 10^6
6.61 × 10^6
Elevation (m)
400
300
200
100
8

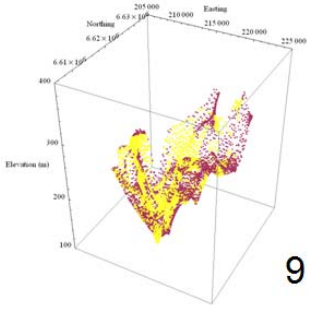
Easting
205 000
210 000
215 000
220 000
225 000
Northing
6.63 × 10^6
6.62 × 10^6
6.61 × 10^6
Elevation (m)
400
300
200
100
9

Appendix 4

Crystallize
Populating a FEFLOW Mesh with Property Data

Authors
B. Kelly and B. Giambastiani

A4.1 Introduction

This *Crystallize* notebook demonstrates how to populate a FEFLOW mesh with property data. For this example the lithology index is assigned to the FEFLOW volume element centre using nearest neighbour gridding. The nearest neighbour is determined using the Euclidean distance. The driller core logs reported on the NSW State Government groundwater Pinneena CD were interpreted assigning the index 1 to log intervals dominated by clay, and 2 to log intervals dominated by sand and gravel.

Although it is possible to generate a finite element mesh in *Mathematica* for the moment there are better tools for generating a finite element mesh in FEFLOW. FEFLOW has interpolation algorithms, but they lack the flexibility of the gridding algorithms available in *Mathematica* or in SGEMS.

A4.2 Calculation

Set the working directory for the project

```
SetDirectory[
  "G:\\NWC_FinalReportUNSW3DHydrogeology\\Appendix4_CrystallizeFEFLOWmesh"];
```

Assign the dimensions that will be used in all the 3D plots.

```
xmin = 205 000; xmax = 225 000; xspace = 500;
ymin = 6 605 000; ymax = 6 635 000; yspace = 500;
zmin = 100; zmax = 600; zspace = 5;
```

Import the borehole lithology index data and the FEFLOW mesh.

```
faciesdata = Drop[Import["maulesfacies.csv"], 1];
femesh = Import["FEFLOW_centroid_mesh.csv", "CSV"];
grid = femesh[[All, {3, 4, 5}]];
```

Examine the bore logs in 3D. For this example the clay is one class (purple) and the high water yielding sands and gravels are the second class (yellow).

```
clay = Cases[faciesdata, {_, _, _, 1}];
sandgravel = Cases[faciesdata, {_, _, _, 2}];
ListPointPlot3D[{clay[[All, {1, 2, 3}]], sandgravel[[All, {1, 2, 3}]]},
 PlotRange → {{xmin, xmax}, {ymin, ymax}, {zmin, 500}},
 PlotStyle → {Directive[RGBColor[0.666667, 0.207843, 0.380392], PointSize[0.01]],
   Directive[Lighter[Yellow, 0.4], PointSize[0.01]]},
 AxesLabel → {"Easting", "Northing", "Elevation (m)"},
 ViewPoint → {-1.0, -1.5, 0.75}, BoxRatios → {1, 1, 1.25},
 ImageSize → {450, 450} ]
```

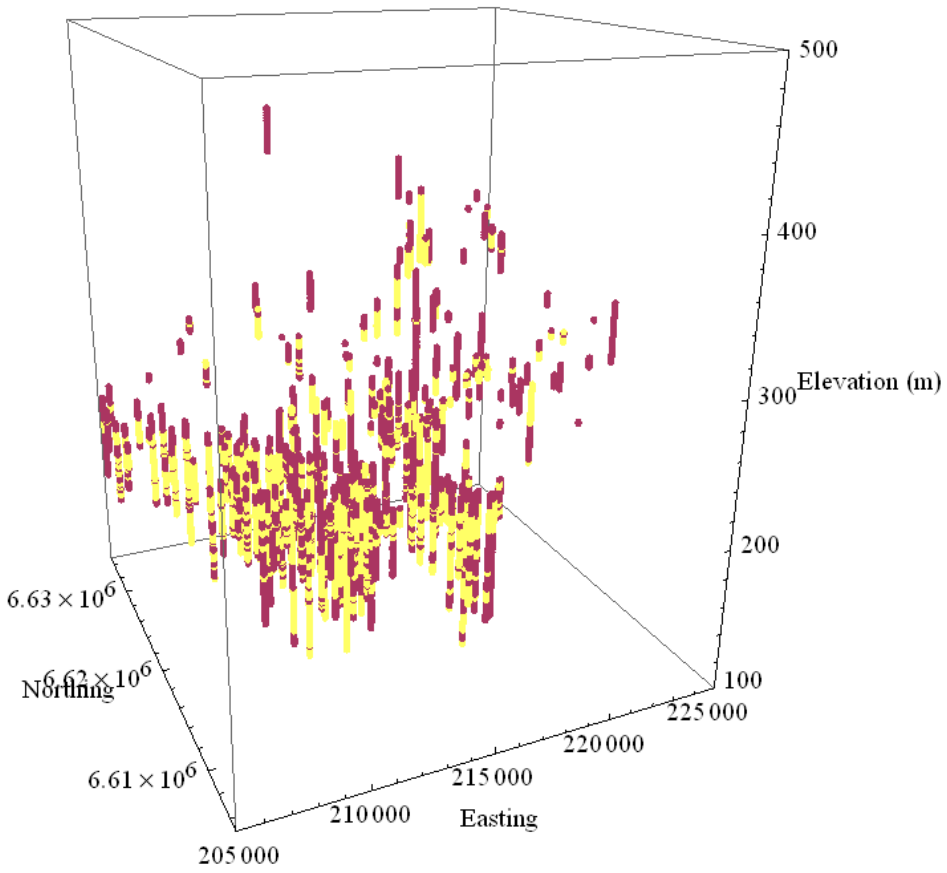

Take a look at the FEFLOW mesh

```
ListPointPlot3D[grid, PlotRange → {{xmin, xmax}, {ymin, ymax}, {zmin, 500}},
 PlotStyle → {Directive[RGBColor[0, 0, 1], PointSize[0.003]]},
 AxesLabel → {"Easting", "Northing", "Elevation (m)"},
 ViewPoint → {-1.0, -1.5, 0.75}, BoxRatios → {1, 1, 1.25},
 ImageSize → {450, 450} ]
```

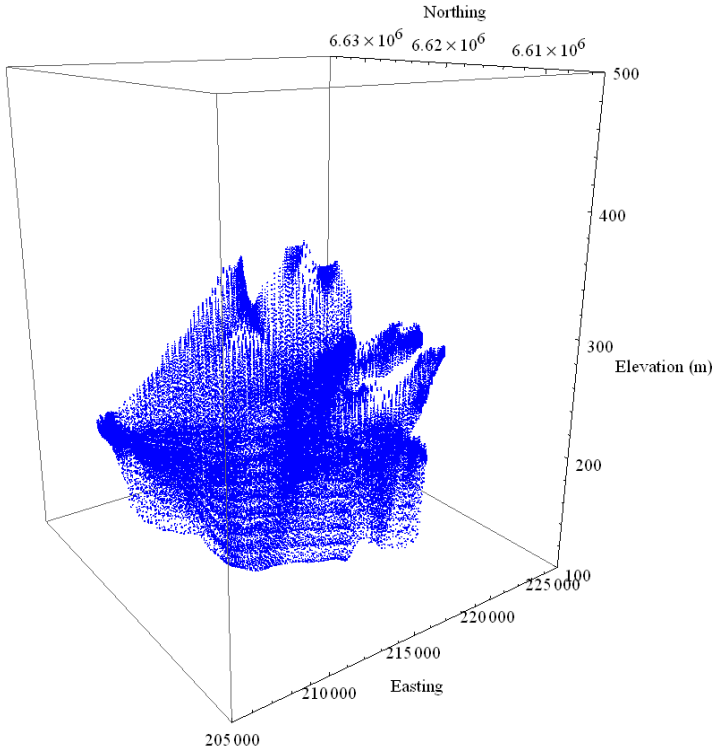

Populate the FEFLOW meash using nearest neighbour gridding (Note: this calculation takes approximately 5 minutes).

```
faciesfunction =
 Nearest[faciesdata[[All, {1, 2, 3}]] → faciesdata[[All, 4]]];
faciesNNlist = Map[faciesfunction, grid][[All, 1]];
faciesNNgrid3D = Partition[Flatten[Riffle[grid, faciesNNlist]], 4];
```

Plot in 3D the indexed facies mesh.

```
clayNN = Cases[faciesNNgrid3D, {_, _, _, 1}];
sandgravelNN = Cases[faciesNNgrid3D, {_, _, _, 2}];
faciespoints3D =
 ListPointPlot3D[{clayNN[[All, {1, 2, 3}]],
   sandgravelNN[[All, {1, 2, 3}]]},
  PlotRange → {{xmin, xmax}, {ymin, ymax}, {zmin, 400}},
  PlotStyle →
   {Directive[RGBColor[0.666667, 0.207843, 0.380392],
     PointSize[0.007]], Directive[Lighter[Yellow, 0.4],
     PointSize[0.008]]},
  AxesLabel → {"Easting", "Northing", "Elevation (m)"},
  ViewPoint → {-1.0, -1.5, 0.75}, BoxRatios → {1, 1, 1.25},
  ImageSize → {450, 450}]
```

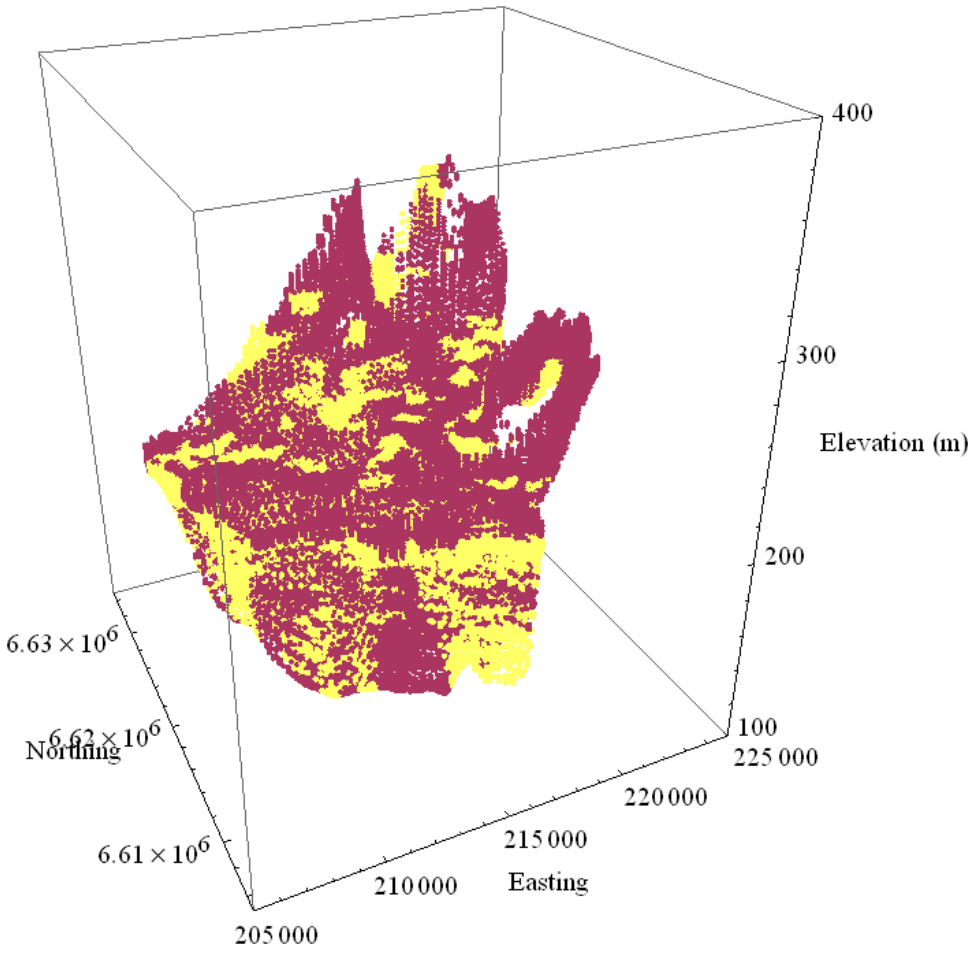

Add a new index value column to the originally imported FEFLOW mesh matrix.

```
feknnnode = faciesNNgrid3D[[All, 4]];
fepoints = Partition[Flatten[Riffle[femesh, feknnnode]], 6];
```

The next step is to import the location of the streams. The polygon file in the ArcGIS database was converted to a list of points and exported. The next few lines import the stream data file and then makes a plot of the points.

```
streampoints = Import["streams_nonamoi_filled_09july_09.csv", "CSV"];
streampointsplot = streampoints[[All, {2, 3}]];
ListPlot[streampointsplot, Axes → True, AxesLabel → {"Easting", "Northing"} ,
 PlotLabel → "Stream Points" , AxesOrigin → {xmin, ymin}]
```

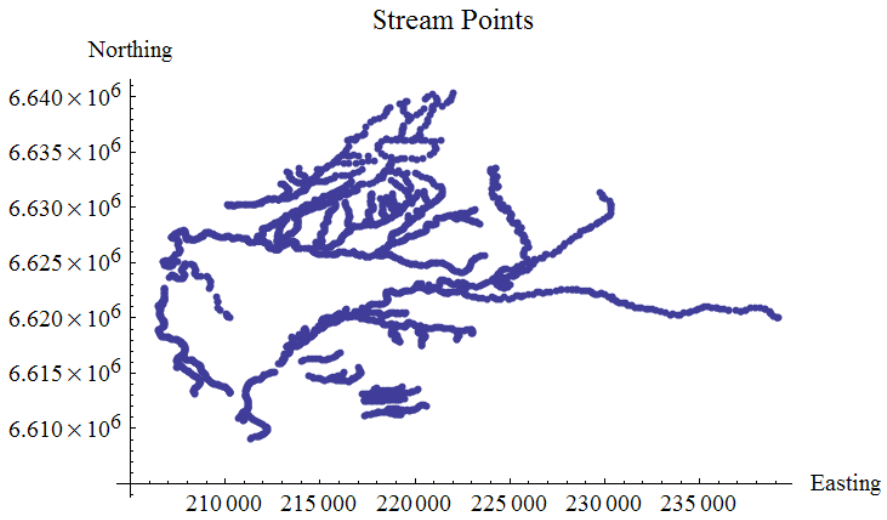

Find points adjacent to the stream data set, and check that they are classified as hydraulically conductive sediments. This calculation takes about 15 minutes.

```
Do[
 Do[
  If[fepoints[[j, 2]] < 3,
   If[EuclideanDistance[fepoints[[j, {3, 4}]], streampoints [[i, {2, 3}]]] < 300,
    fepoints[[j]] = {fepoints[[j, 1]], fepoints[[j, 2]], fepoints[[j, 3]],
      fepoints[[j, 4]], fepoints[[j, 5]], 5},
    fepoints[[j]]], 0
  ],
  {i, 1, Length[streampoints], 1}
 ],
 {j, 1, Length[fepoints], 1}
]

fepointsclean = Partition[Flatten[fepoints], 6]
```

Export the 3D facies mesh with the inserted streams.

```
Export["knn1_maulesstreamsonly_2FE_23July09.csv", fepointsclean];
```

Plot in 3D the facies mesh with the inserted streams.

```
clayNN2 = Cases[fepointsclean, {_, _, _, _, _, 1}];
sandgravelNN2 = Cases[fepointsclean, {_, _, _, _, _, 2}];
stream2 = Cases[fepointsclean, {_, _, _, _, _, 5}];
faciespoints3D2 =
 ListPointPlot3D[{clayNN2[[All, {3, 4, 5}]],
   sandgravelNN2[[All, {3, 4, 5}]], stream2[[All, {3, 4, 5}]]},
  PlotRange → {{xmin, xmax}, {ymin, ymax}, {zmin, 400}},
  PlotStyle →
   {Directive[RGBColor[0.666667, 0.207843, 0.380392],
     PointSize[0.007]], Directive[Lighter[Yellow, 0.4],
     PointSize[0.008]], Directive[Blue, PointSize[0.008]]},
  AxesLabel → {"Easting", "Northing", "Elevation (m)"},
  ViewPoint → {-1.0, -1.5, 0.75}, BoxRatios → {1, 1, 1.25},
  ImageSize → {450, 450}]
```

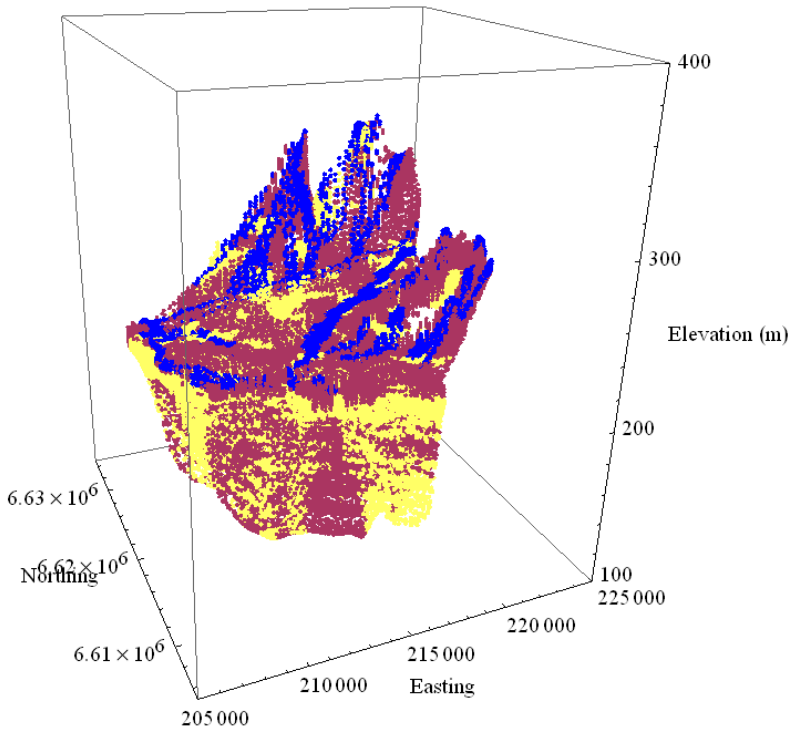

Export each FEFLOW layer to a separate comma separated file.

```
Do[
 slicematrix = {};
 Do[If[ fepointsclean[[i, 2]] == j, AppendTo[slicematrix, fepointsclean[[i]]], i],
  {i, 1, Length[fepointsclean]}];
 index = ToString[j];
 exportname = StringJoin["knn1_FEFLOW_layer_", index, ".csv"];
 Export[exportname, slicematrix], {j, 1, 9}]
```

Generate a 3D plot of each FEFLOW layer.

```
plotslice = {}; Do[slicematrix = {};
 Do[If[ fepointsclean[[i, 2]] == j, AppendTo[slicematrix, fepointsclean[[i]]], i],
  {i, 1, Length[fepointsclean]}];
 If[j < 3,
  clayNN2 = Cases[slicematrix, {_, _, _, _, _, 1}];
  sandgravelNN2 = Cases[slicematrix, {_, _, _, _, _, 2}];
  stream2 = Cases[slicematrix, {_, _, _, _, _, 5}];
  faciespoints3D2 =
   ListPointPlot3D[{clayNN2[[All, {3, 4, 5}]], sandgravelNN2[[All, {3, 4, 5}]],
     stream2[[All, {3, 4, 5}]]},
    PlotRange → {{xmin, xmax}, {ymin, ymax}, {zmin, 400}},
    PlotStyle → {Directive[RGBColor[0.666667, 0.207843, 0.380392],
       PointSize[0.007]], Directive[Lighter[Yellow, 0.2], PointSize[0.009]],
      Directive[Blue, PointSize[0.008]]},
    AxesLabel → {"Easting", "Northing", "Elevation (m)"}, BoxRatios → {1, 1, 1.25},
    ImageSize → {450, 450}];, clayNN2 = Cases[slicematrix, {_, _, _, _, _, 1}];
  sandgravelNN2 = Cases[slicematrix, {_, _, _, _, _, 2}];
  faciespoints3D2 =
   ListPointPlot3D[{clayNN2[[All, {3, 4, 5}]], sandgravelNN2[[All, {3, 4, 5}]]},
    PlotRange → {{xmin, xmax}, {ymin, ymax}, {zmin, 400}},
    PlotStyle → {Directive[RGBColor[0.666667, 0.207843, 0.380392],
       PointSize[0.007]], Directive[Lighter[Yellow, 0.2], PointSize[0.009]]},
    AxesLabel → {"Easting", "Northing", "Elevation (m)"}, BoxRatios → {1, 1, 1.25},
    ImageSize → {450, 450}]];
 AppendTo[plotslice, faciespoints3D2];,
 {j, 1, 9}];
plotslice
```

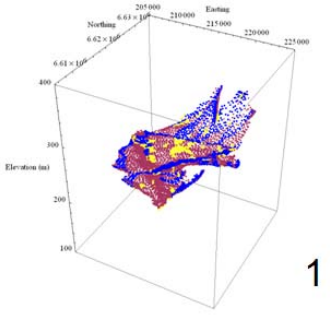
Easting
205 000
210 000
215 000
220 000
225 000
Northing
6.63 × 10^6
6.62 × 10^6
6.61 × 10^6
Elevation (m)
400
300
200
100
1

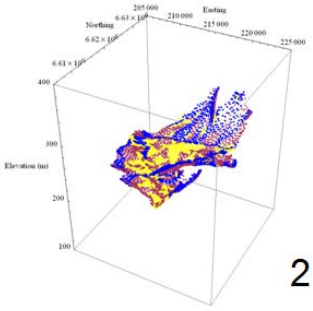
Easting
205 000
210 000
215 000
220 000
225 000
Northing
6.63 × 10^6
6.62 × 10^6
6.61 × 10^6
Elevation (m)
400
300
200
100
2

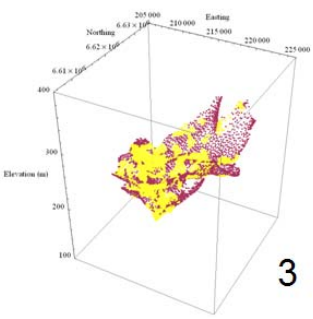
Easting
205 000
210 000
215 000
220 000
225 000
Northing
6.63 × 10^6
6.62 × 10^6
6.61 × 10^6
Elevation (m)
400
300
200
100
3

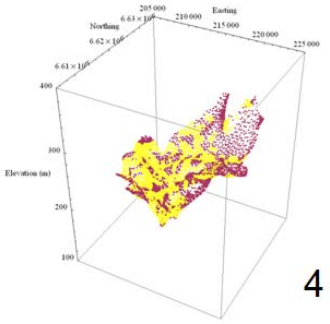
Easting
205 000
210 000
215 000
220 000
225 000
Northing
6.63 × 10^6
6.62 × 10^6
6.61 × 10^6
Elevation (m)
400
300
200
100
4

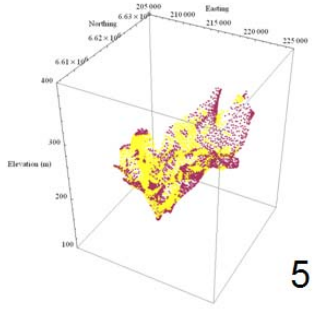
Easting
205 000
210 000
215 000
220 000
225 000
Northing
6.63 × 10^6
6.62 × 10^6
6.61 × 10^6
Elevation (m)
400
300
200
100
5

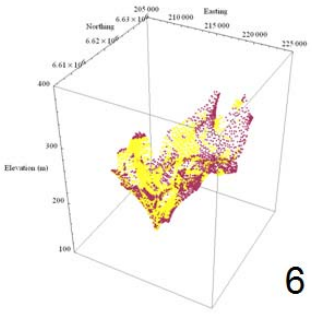
Easting
205 000
210 000
215 000
220 000
225 000
Northing
6.63 × 10^6
6.62 × 10^6
6.61 × 10^6
Elevation (m)
400
300
200
100
6

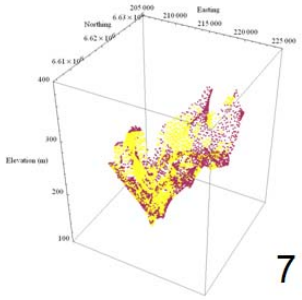
Easting
205 000
210 000
215 000
220 000
225 000
Northing
6.63 × 10^6
6.62 × 10^6
6.61 × 10^6
Elevation (m)
400
300
200
100
7

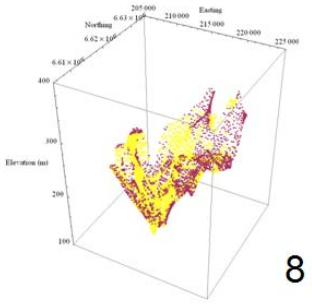
Easting
205 000
210 000
215 000
220 000
225 000
Northing
6.63 × 10^6
6.62 × 10^6
6.61 × 10^6
Elevation (m)
400
300
200
100
8

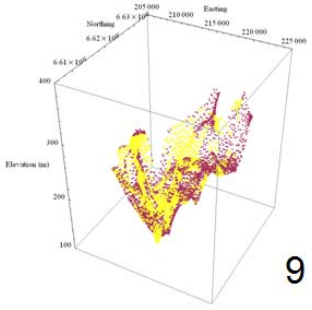
Easting
205 000
210 000
215 000
220 000
225 000
Northing
6.63 × 10^6
6.62 × 10^6
6.61 × 10^6
Elevation (m)
400
300
200
100
9

Appendix 5
A Groundwater Flow Model of the Maules Creek Catchment

Beatrice M.S. Giambastiani, Andrew M. McCallum, Martin S. Andersen,
Bryce F.J. Kelly, R. Ian Acworth

April 19, 2010

University of New South Wales, Connected Waters Initiative, Sydney Australia

Contents

Executive Summary

A groundwater flow model was developed for the Maules Creek alluvial aquifer situated in the Namoi Valley (NSW, Australia). The main objectives were to provide a better understanding of the dynamics of the alluvial aquifer in the Maules Creek Catchment and to provide integrated modelling of catchment water resources, including the simulation and assessment of pumping.

The model was developed using the FEFLOW 5.4 finite element subsurface flow and transport simulation system. The hydrogeological system is represented by 9 layers bounded by bedrock that is assumed to be impermeable. Hydrologic stresses include diffuse recharge, irrigation recharge, stream-aquifer interaction, lateral groundwater inflow/outflow and groundwater pumping. The hydraulic head distribution for 1978, obtained from a steady state model, was used as the initial condition for the transient model which was run from January 1978 to April 2007.

The hydraulic conductivity distribution in the model was assigned on the basis of a 3D geological model built with EarthVision® and Mathematica™ using bore logs from the NSW Office of Water database.

Model calibration was performed by a trial-and-error method based on matching modelled bore hydrographs with measured hydrographs. The calibration period was from 1982 to 2007. Overall the model performance is good with the model correctly capturing the recovered water levels after each irrigation season, as well as the long-term trends shown in the measured hydrographs. However, in areas where the groundwater abstraction-induced drawdown is large (up to 8-10 m) the seasonal dynamic is not completely captured by the model.

For assessing the effect of groundwater abstraction on the stream-aquifer interaction, two hypothetical scenarios were run: without groundwater pumping and with a 2-fold increase in pumping rate. The total groundwater influx to the river versus time and water budgets were computed for each scenario and compared with the calibration model.

The groundwater model has provided a better understanding of the alluvial aquifer system and its dynamics. The numerical simulations show the impact of irrigation on the hydraulic head distribution and baseflow to the river. Limitations and possible methods of resolving model uncertainties and improving calibration performance were also investigated and reported.

1 Introduction

This report documents the development of a groundwater flow model for the Maules Creek Catchment in the Upper Namoi Valley, NSW (Australia).

This modelling project is part of a significant research program involving field work, data analysis and modelling studies (`http://www.connectedwaters.unsw.edu.au`). The main objectives were to provide a better understanding of the dynamics of the alluvial aquifer in the Maules Creek Catchment and to provide integrated modelling of the catchment water resources, including the simulation and assessment of pumping.

Maules Creek, a sub-catchment of the Namoi Valley, has a surface area of approximately 1500 km^2 and is located on the western slopes of the Great Dividing Range south-east of the township of Narrabri, NSW, Australia. It is bound to the east by the New England Fold Belt and the Great Dividing Range, to the north by the Nandewar Range and Mount Kaputar (altitude: 1510 m), to the south by the Leard State Forest and Gins Leap Gap, and to the west by a low ridge of hills (Fig. 1).

The climate is semi-arid. In the lower part of the catchment along the Namoi River, flood irrigation farming relies on surface water supplies from Split Rock and Keepit Dams, delivered via the Namoi River, and on extensive groundwater extraction from a palaeochannel of the Namoi River to grow cotton, sorghum and wheat. Groundwater in the Upper Namoi Valley is over allocated with regard to its sustainable yield, with zones of extraction in excess of recharge. Consequently, users are competing for groundwater, especially during peak periods of groundwater extraction in spring and summer (CSIRO, 2007; Sinclair et al., 2005).

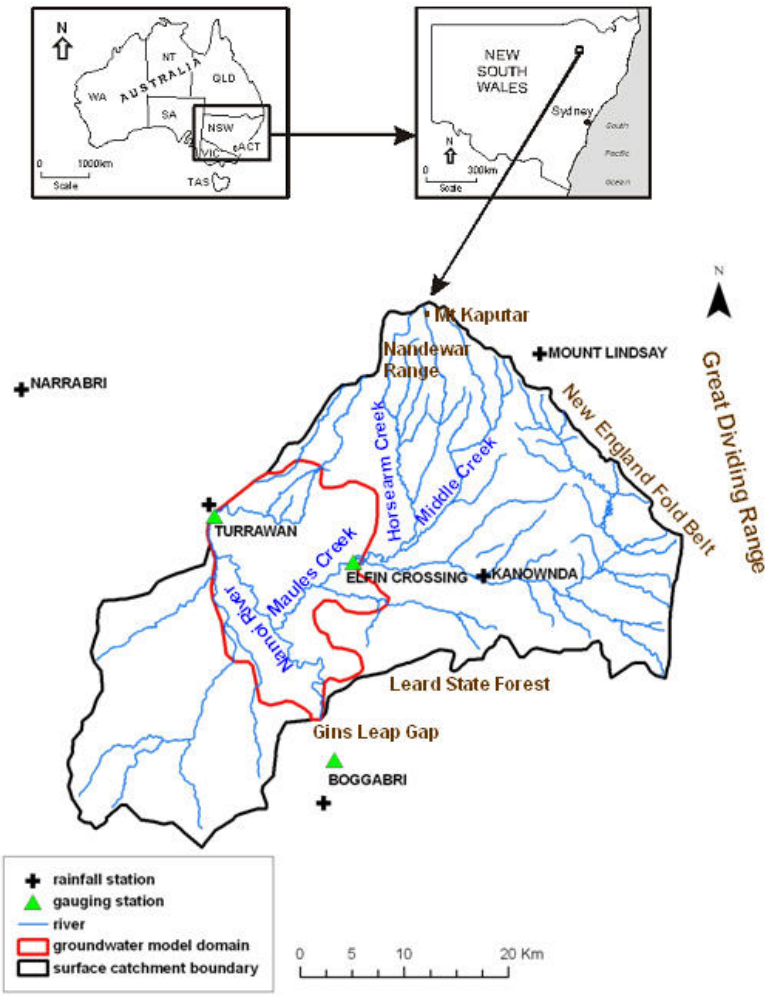

Figure 1: Location of the Maules Creek study area in New South Wales, Australia.

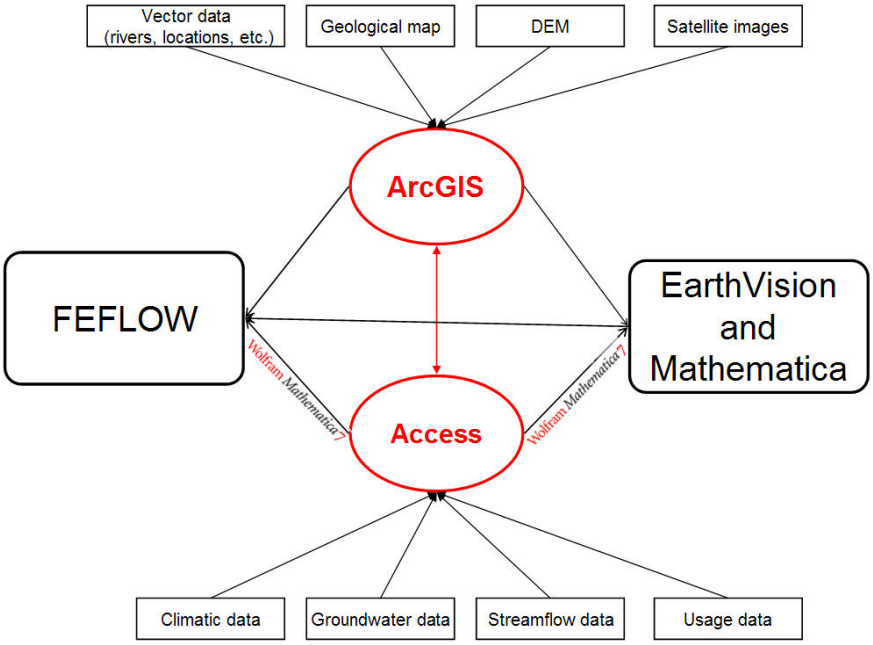

Figure 2: Schematic showing the data types and relationship of software used in the project.

In 2006 the NSW Department of Natural Resources developed a numerical groundwater model of the Upper Namoi Valley (DNR, 2006) using Modflow-96 finite difference software (McDonald and Harbaugh, 1998). The model conceptualisation of the aquifer is a two layer system bounded by impermeable bedrock. The upper layer is set as unconfined and the lower one as semi-confined. Since it is a large scale groundwater model, the grid is coarser than the one used in the present study, and the hydrological stresses and boundary conditions were assessed differently.

In this project the model was developed using the FEFLOW 5.4 finite element subsurface flow and transport simulation code (Diersch, 2005) using an entirely different conceptualisation. This report presents the description of the catchment geometry, hydrogeology and the data analysis and processing methods used for the development of the transient groundwater flow model of Maules Creek Catchment. The calibration is demonstrated in both qualitative and quantitative terms, based on matching modelled bore hydrographs with measured hydrographs. The results of two scenarios are presented: without pumping and a 2-fold increase in pumping rate in order to assess the effect of groundwater abstraction on the stream-aquifer interactions. Finally, model uncertainty and parameter sensitivity are discussed and possible methods of improving calibration performance are also reported.

Figure 2 shows a block schematic relationship of all the utilised data sources and various software used in the project.

2 Data Analysis and Hydrogeological Setting

2.1 Available data

Data relevant to the catchment area from various sources were used to develop and calibrate the model. A brief description of each data source is provided in Table 1; how these data were used specifically is detailed throughout the report at relevant sections.

2.2 Hydrology

2.2.1 Precipitation and Evapotranspiration

Precipitation in the catchment varies temporally within the catchment. Within a year precipitation is generally at a maximum in the summer and winter months with minimums between (Figure 3).

Table 1: Data sources.

Data	Source	Description
Groundwater Levels	NSW Office of Water	Water level (1970-2008) for 37 monitoring boreholes
Abstraction Volumes	NSW Office of Water	1996-2008
Monitoring and Abstraction bore construction details	NSW Office of Water	Construction details for all boreholes and data on screens
Streamflows	NSW Office of Water	Daily data from 3 gauging stations (1950-2008)
Precipitation and Evapotranspiration	SILO and BOM	Daily data from 5 weather stations (1889-2009)
Digital Elevation Model	CGIAR-CSI	SRTM 90 m DEM (3 arcsec)
GPS Surveys	WRL	GPS surveys of boreholes and river topography from several field campaigns (WRL team)
Geological Map	GA	Map of Australia (1:250000)
River Polylines	GA	River and stream distribution
Satellite Image	CMA	Satellite images of Manilla and Narrabri
Soil Map	CMA	Soil type distribution in Namoi Catchment (2008)
Land Use Map	CMA	Land use distribution in Namoi Catchment (2008)
Geological Model	UNSW	3D geological model of the Maules Creek Catchment

However, there are large interannual variations.

Like precipitation, evapotranspiration also varies temporally, with maximum values in the summer and lowest values in the winter (Fig. 4).

Precipitation and evapotranspiration also vary spatially across the catchment due to the orographic effect of the mountain range. Precipitation is highest on the mountain range and lowest on the plain; evapotranspiration is highest on the plain and lowest on the mountain range.

2.2.2 Streamflow

This spatial difference in precipitation and evapotranspiration is important for catchment hydrology. Most of the precipitation which falls on the plain either evaporates or infiltrates into the soil (diffuse recharge); runoff within the plain is insignificant due to the very low slopes. In contrast, precipitation which falls on the mountainous region either infiltrates into the shallow soils or becomes runoff and streamflow. This runoff may infiltrate the aquifer further downslope in the foothills. These differences in pathways control the surface water as well as the groundwater hydrology of the catchment. Flows in Maules Creek and its two main tributaries Horsearm and Middle Creek (see Figure 1) are unregulated. The upper reaches of Maules Creek and tributaries drain the fractured rock of the Nandewar Range. However, only during severe storms and associated flooding does Maules Creek and its tributaries flow across the alluvial fan between the mountains and the confluence of Maules and Horsearm Creeks at Elfin Crossing. There is one gauging station on Maules Creek, at Elfin Crossing (DNR code: 419051). At low flow conditions the surface water flow in Maules Creek at Elfin Crossing is exclusively controlled by surface and ground water interactions (Sinclair et al. 2005; Andersen and Acworth 2009), since the reaches above and below Elfin Crossing dry out when the creek is not in flood. Flow rarely reaches the junction of Maules Creek and the Namoi River; only during severe storms with associated flooding does Maules Creek flow to the Namoi River. The flow in the middle section of Maules Creek can be considered an expression of the groundwater table (Andersen and Acworth, 2009).

The Namoi River flows into the catchment from the south draining a catchment of approximately 23,000 km^2. The flow upstream is regulated at Keepit Dam. The Namoi River is gauged at two locations at either end of the sub-catchment. The Boggabri gauge (DNR code: 419012) is located on

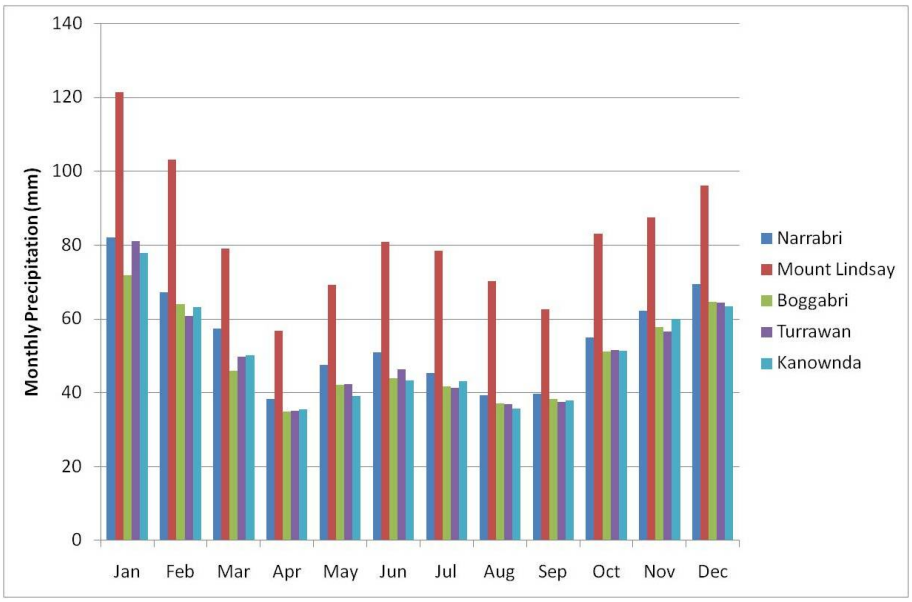

Figure 3: Monthly precipitation for five stations (See Figure 1 for the locations).

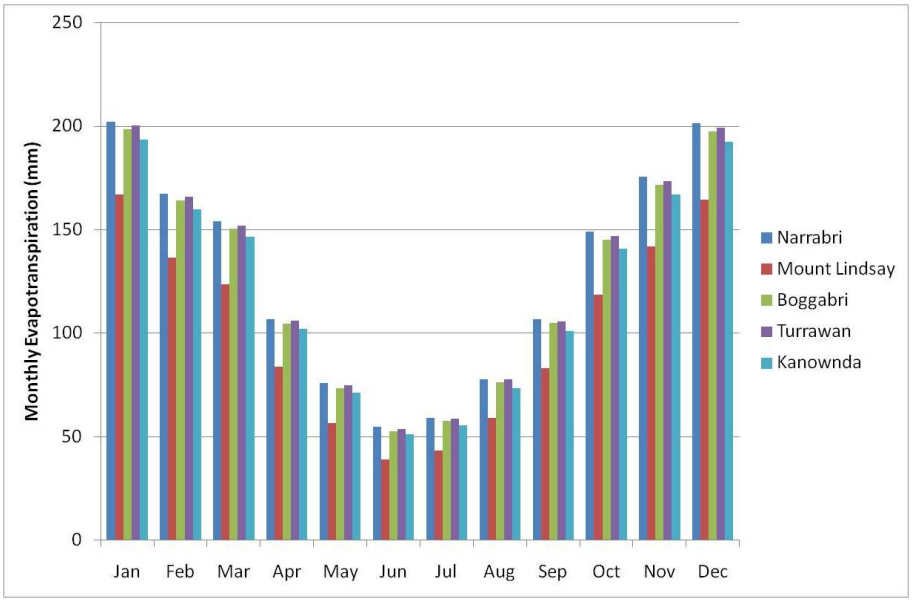

Figure 4: Monthly evapotranspiration for five stations (See Figure 1 for the locations).

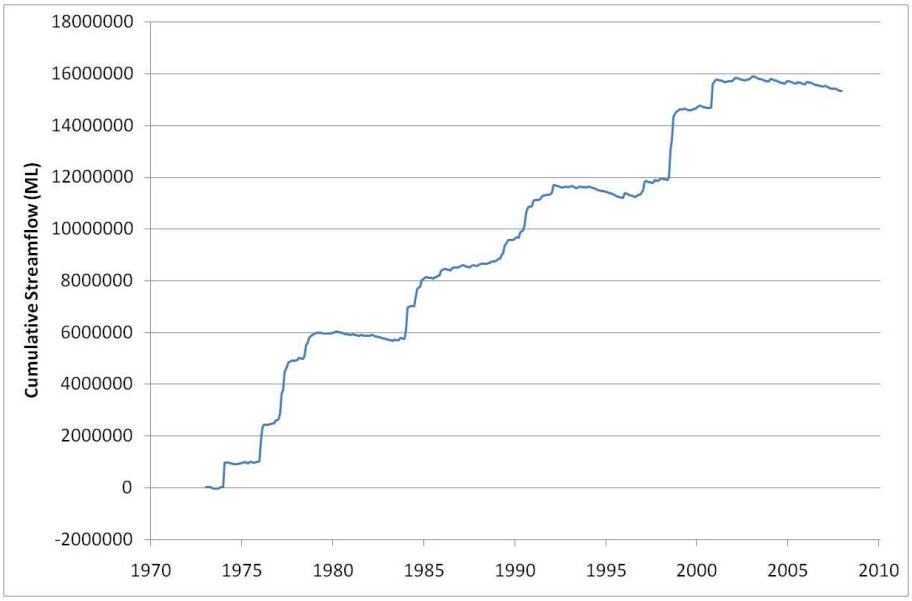

Figure 5: Cumulative streamflow curve for Boggabri (1973 to 2007) calculated from the median streamflow data. The slope of this curve shows the trends within the data set.

the Namoi River upstream of Gins Leap, a narrow (1000 m) constriction in the valley. The Turrawan gauge (DNR code: 419023) is at the northern end of the catchment (Figure 1). The stretch of river between Boggabri and Turrawan therefore acts as a conduit for a very large upstream catchment in addition to receiving water from the Maules Creek Catchment.

The historical pattern of flow in the Namoi River can be seen in a cumulative streamflow curve (Fig. 5). Positive trends indicate periods of above median streamflow, with negative trends indicate periods of below median streamflow. Positive steps indicate periods of flooding; flat portions of the curve indicate periods of typical streamflow.

As well as the historical flows in the river, it is possible to look at the mass balance of the river over time, as there are two gauges, at either end of the catchment, thereby showing whether the river is gaining or losing overall (Figure 6). Between the early 1970s and the late 1980s more water discharged (typically up to 20% more) at Turrawan than entered at Boggabri. This must be due to contributions to the streamflow from the aquifer as baseflow or from catchment surface water runoff. It is likely that during this pre-development period (before 1985) there was more reliance on surface water diversions for farming within the catchment. Without these diversions the percentage of water leaving the catchment would be even higher. In the post-development period the general trend is reversed, with less water apparently leaving the catchment than entering it, suggesting that the river is losing water to the aquifer.

2.3 Geology and Hydrogeology

2.3.1 General Setting

The Namoi Catchment is bounded on the eastern side by Devonian and Carboniferous sedimentary and Cenozoic volcanic rocks that form the Great Dividing Range, in the south by the Permian sedimentary and Tertiary volcanics of the Liverpool Range, and on the west by the southern extension of the Cenozoic volcanics of the Warrumbungle Range and the westerly dipping Cretaceous and Jurassic sedimentary units of the Great Artesian Basin (GAB). To the north the Namoi Catchment is divided from the Gwydir Catchment by Tertiary volcanics and uplifted Permian sedimentary formations (NSWDMR, 2002).

The hydrogeology of the region has been discussed by Gates (1980), William (1986), Lavitt (1999), Young et al. (2002),Kelly et al. (2006), The (2008), Bowling (2009). The alluvial aquifer system consists of unconsolidated sediments deposited on a pre-Tertiary erosional surface, which represents the basement of the hydrogeological system. The unconsolidated sediments have been divided into two al-

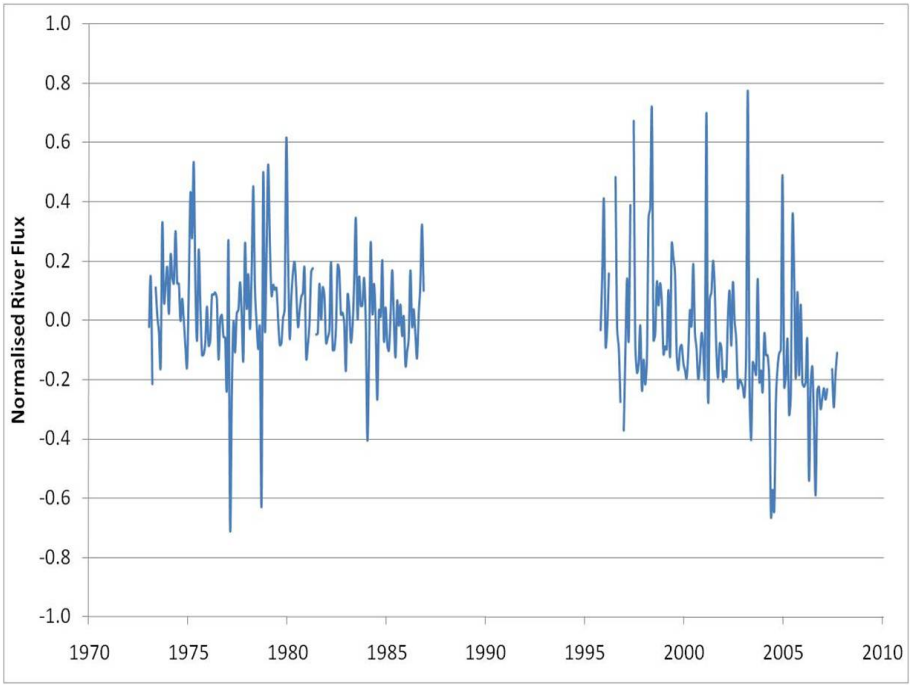

Figure 6: Flow difference between Turrawan and Boggabri gauging stations. Positive values indicate more water entering the catchment at Boggabri than leaving at Turrawan, and vice versa. The missing portion of the curve from the late 1980s to the mid 1990s is due to lack of available data at one or both gauging stations during this period.

luvial formations: the Narrabri Formation overlying the Gunnedah Formation. The Narrabri Formation consists of extensive overbank clays with some channel sands and gravel deposited by levied meandering streams. The clay dominated formation contains high-salinity, low yielding aquifers. The Gunnedah Formation consists of sands and gravel with interbedded clays deposited by braided streams. The sand and gravel dominated formation contains lower-salinity, high-yielding aquifers. This formation predominantly fills the older palaeochannels, with the highest yielding aquifers being in deep palaeochannels containing coarse sediments deposited by high energy streams (Gates, 1980; William, 1986).

2.3.2 Groundwater Levels

Groundwater abstraction started within the catchment in the mid 1980's. Evidence of that can be seen in the groundwater level data by comparing groundwater head data during two periods: pre onset of pumping (1973-1984) and post onset of pumping (1985-2007) (McCallum et al., 2009).

In the pre-development period the average groundwater head decline was 0.08 m/year, and ranged from –0.04 (i.e. head rise) to 0.22 m/year. This decline seems to be due to climatic factors.

In the post-development period analysed the decline increased to 0.2 m/year, and ranged from 0.01 to 0.48 m/year. Figure 7 shows the spatial distribution of the rate of decline during the two periods. The post-development pattern of drawdown appears to coincide with the geology with the greatest drawdown located within the palaeochannel located beneath and to the east of the Namoi River where the majority of irrigation abstraction bores are located.

3 Conceptualisation and Model Development

A numerical groundwater flow model is the mathematical representation of an aquifer that is based on a conceptual model of that system. A set of equations which describes the physical processes of groundwater flow in the system is solved using numerical methods. The computer code FEFLOW has been used to simulate 3 dimensional groundwater flow in the catchment. FEFLOW is a finite element groundwater modelling software package for modelling fluid flow and transport of dissolved constituents

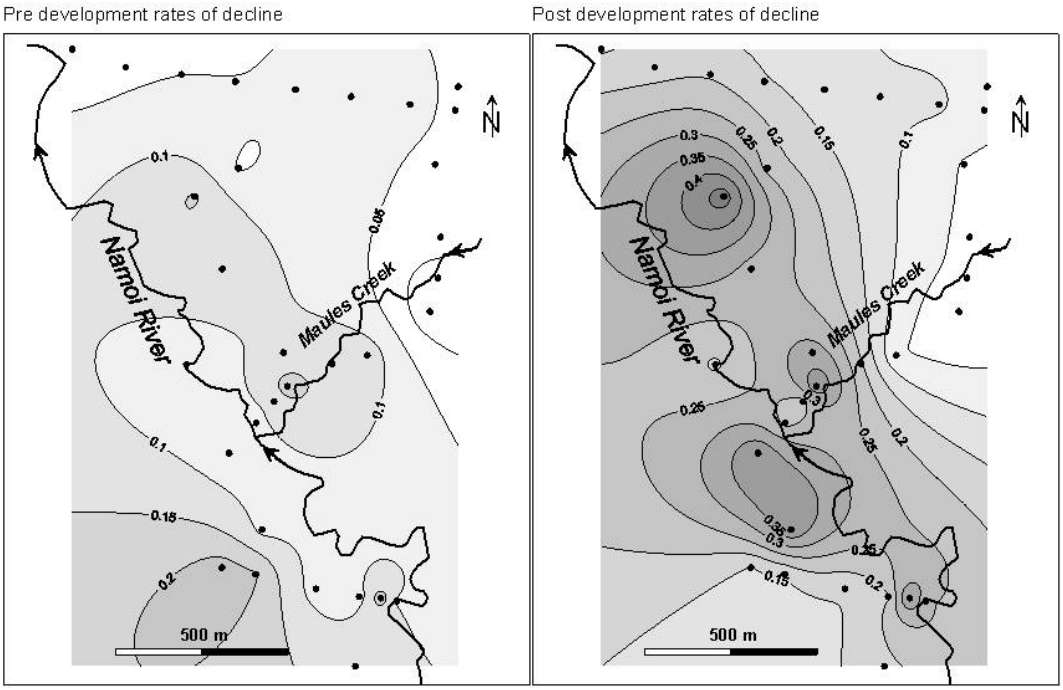

Figure 7: Rate of groundwater level decline (m/year) during pre-development period (1973-1984) on the left and post-development period (1085-2007) on the right.

and/or heat transport processes in the subsurface. It allows simulation of 2D and 3D complex systems, with saturated and/or unsaturated flow (Diersch, 2005). Typically groundwater numerical modelling codes are based on the finite difference schemes for spatial discretisation. By contrast FEFLOW uses the finite element method and was selected as the preferred model code for this reason. The fundamental advantage of this is the flexibility of the mesh. Adaptation of the mesh allows for the rivers to be better represented with a finer mesh locally, as well as for a better representation of the complex alluvial geology.

3.1 Conceptual Model

The groundwater conceptual model is a simplified interpretation of the characteristics and dynamics of the physical hydrogeologic system. On the basis of the available data, a conceptual model was developed for the Maules Creek unconsolidated alluvial aquifer (Figure 8). The model domain was chosen essentially to cover the alluvial aquifer between Gins Leaps in the south and the northern edge of the Maules Creek Catchment. Four sources of information were used: a 3D geological structural model built in EarthVision using all bore logs available in the NSW Office of Water database, a satellite image (where rock outcrops could be identified; changes in geology were also identifiable in the changes in the vegetation type), the geological map of Australia (scale 1:250,000) and a facies model built using Mathematica™. The eastern extent of the model domain was placed at Maules Creek just upstream of Elfin Crossing due to the limited knowledge of the area further to the east and the lack of monitoring boreholes for calibration of the model (Figure 9).

The model consists of a multilayered sedimentary aquifer bounded by impermeable bedrock, assuming zero flux into/out of the basement. The upper part is assumed to be unconfined.

The alluvial aquifer geology was divided into two classes: 1) sand and gravel and 2) clay and silt. The geology distribution was determined using nearest neighbour gridding of the indexed lithological bore logs. The model conceptualisation thus deviates from the classic layered representation of aquifer and aquitard previously described and used for this catchment by other studies (Gates, 1980; William, 1986; DNR, 2006). Refer to the Section 3.6 for details.

Hydrologic stresses include diffuse recharge, irrigation recharge, stream-aquifer interaction, lateral groundwater inflow/outflow and groundwater pumping. Each of the fluxes into and out of the alluvial

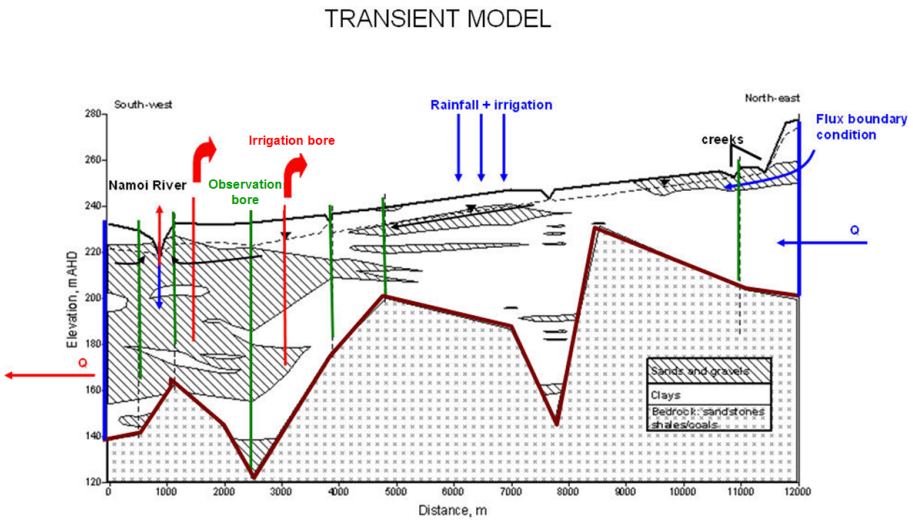

Figure 8: Conceptual model of Maules Creek (modified from Andersen and Acworth, 2009). The output components of the water budget are red and the input components are blue.

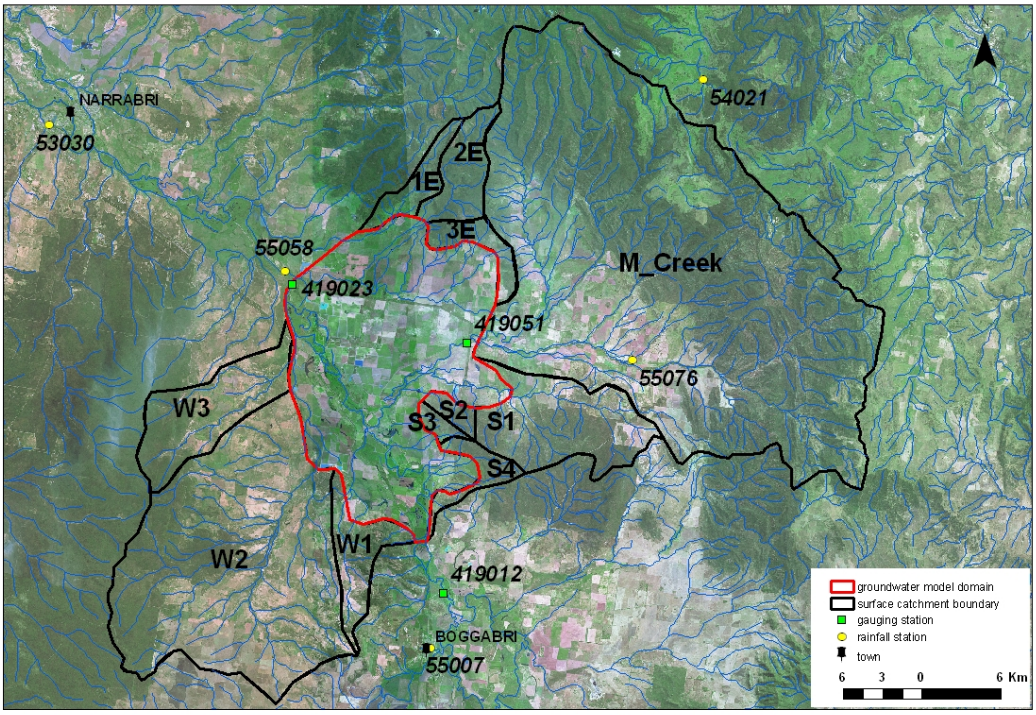

Figure 9: Groundwater model domain (in red) and Maules Creek surface water catchment boundary (in black). Also shown in this image are the locations of the five weather stations and three river/stream gauging stations. Sub-catchments are defined around each major stream to enable the estimation of the sub-catchment contribution to the groundwater model boundary.

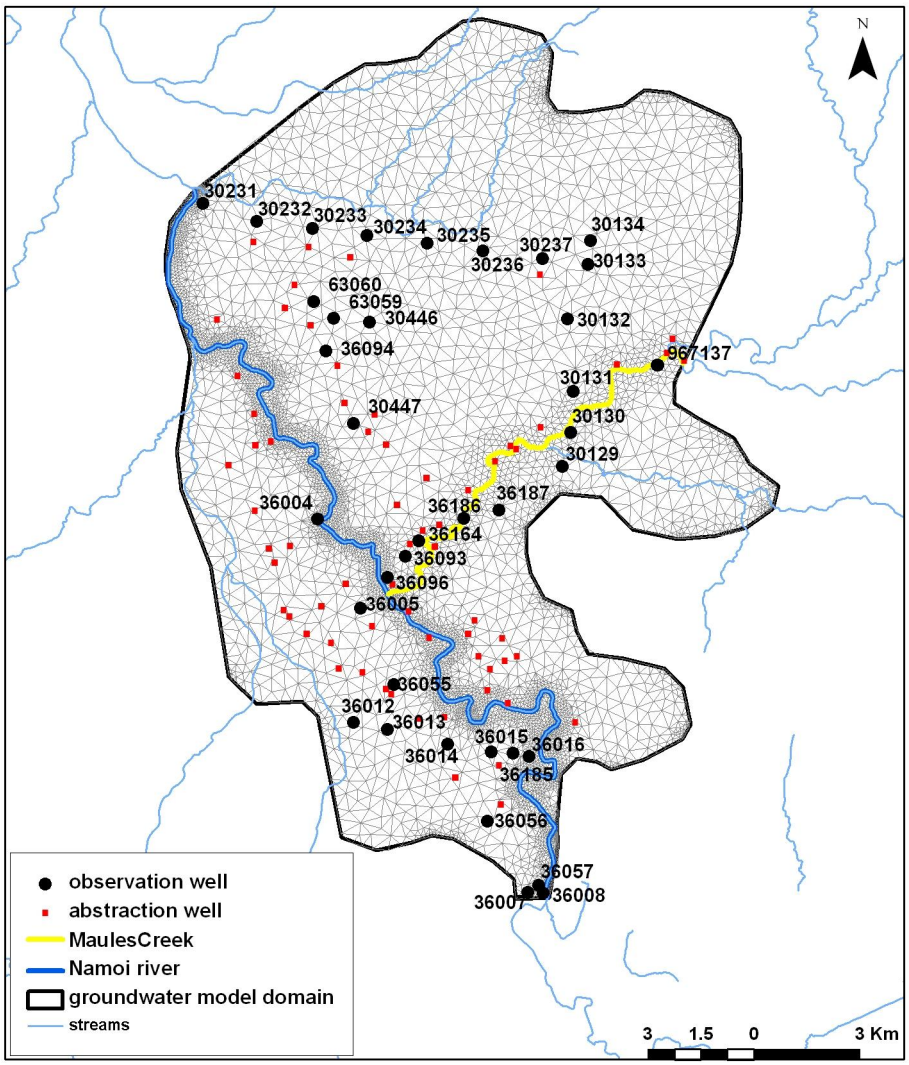

Figure 10: FEFLOW finite element mesh of the Maules Creek Catchment. Number refer to NSW Office of Water observation boreholes. Plotted in the figure are also abstraction bores implemented in the model.

aquifer is discussed in the following sections. It should be noted that the overbank flows related to floods occurring during the period of simulation (1978-2007) are not modeled. These flows are potentially important for recharge.

A total of 68 irrigation bores and 37 groundwater monitoring boreholes (total of 64 observation points to calibrate the model) were implemented within the model domain (Figure 10).

3.2 Model Geometry

3.2.1 Finite Element Mesh

A triangular finite element mesh of the model domain was generated using triangle algorithm (Shewchuk, 1996; 2002) and refined around the rivers and abstraction bores. Along the Namoi River, where the mesh has been refined to allow for more accurate stream-aquifer interactions, the average target element length is 50 m. In the rest of the domain the element sizes are variable with an average size of about 400 m for each side of the triangular element and variable volume depending on the thickness of the layer. A minimum angle of 30 degrees was used for each triangle, aiming to obtain a more uniform structure of the mesh. The mesh consists of 187290 6-nodal prismatic finite elements and 106560 nodes (Figures 10 and 11).

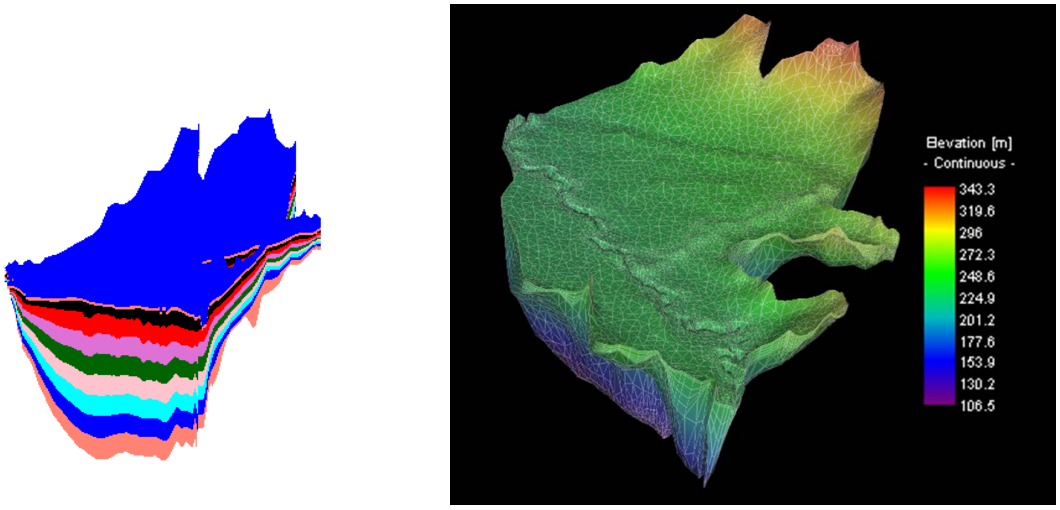

Figure 11: Three dimensional view of the FEFLOW groundwater model domain for Maules Creek. Left figure shows the 3D-layer configuration consisting of 9 layers (10 slices); right figure shows mesh geometry in 3D.

3.2.2 3D Layer Configuration

The 3D-layer configuration consists of 9 layers (10 slices) (Fig. 11). The upper slice of the model is based on a digital elevation model (SRTM 90m DEM, CGIAR-CSI website) of the ground surface, surveyed bore elevations and GPS surveys of Namoi River and Maules Creek topography (by WRL team during several field trips).

In order to define the aquifer limit (i.e. the bedrock slice), a DEM was imported via ArcGIS into EarthVision and sorted into 2 domains, alluvium and rock outcrop, based on the topographic gradient (Giambastiani and Kelly, 2009). The rock outcrop data then were combined with bedrock top elevation from all available geological bore logs and gridded as a single surface. The DEM and the bedrock layers were designed to coincide in the horizontal plane.

The second slice is located 2 m below the top slice and is needed to implement the transfer boundary condition for the Namoi River. The area between the second and last slice was then divided into 8 equally spaced layers.

3.2.3 Problem Class

Conceptually the aquifer is regarded as saturated and unconfined and the top slice accordingly set to be 'phreatic' as an option in FEFLOW. Slices 2-4 are set to be 'unspecified' whereas all the other slices are set to be 'fixed'.

A 'fixed' slice is used to define the top of a confined aquifer. It simulates a rigid slice which is stationary along a stratigraphic unit and cannot move. In this case, natural constraints are activated that force the water table to remain above any fixed slice.

An 'unspecified' slice is used for movable meshes. With this setting, FEFLOW adapts the slice automatically depending on the definition of the adjacent slices. 'Unspecified' means that FEFLOW will choose whether the layer is confined or not, allowing the water table to cross layers.

A phreatic surface simulates a free surface which means that an element cell can become partially unsaturated and the integration of the volumetric element and the hydraulic conductivity will be reduced according to the proportion of the partial saturation (water table in the element/height of the element). A residual water depth of 0.04 m for dry elements has been used as a constraint to prevent the elements from completely drying. This minimum water level can be considered as an initial saturation of the layer and it is used for computing the transmissivity of the corresponding area. The residual water level, selected by trial-and-error, is 2% of the first layer thickness.

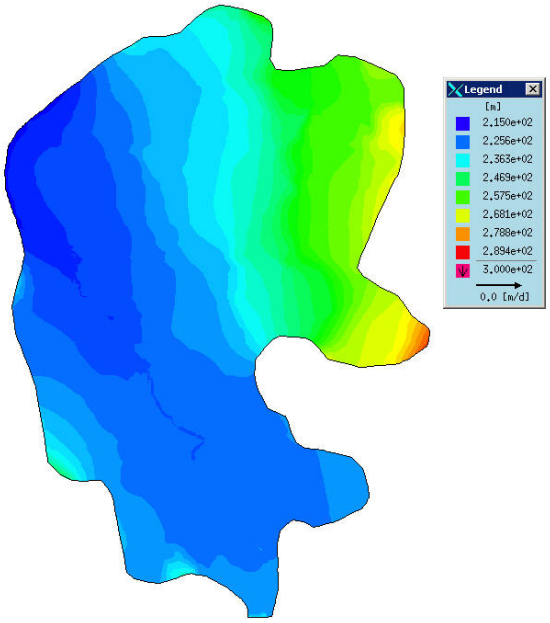

Figure 12: 1978 hydraulic head distribution computed by a steady state model and used as the initial condition for the transient model.

3.3 Temporal and Control Data

The simulation period runs from January 1978 to April 2007. A start date in 1978 was chosen in order to start the simulation before the onset of groundwater pumping, that is, where the hydrologic conditions approximate steady state.

The model time discretisation is based on an automatic time step control. The forward Adams-Bashforth/backward trapezoid predictor scheme was used for controlling the time step length. This scheme is based on the expected error and frees the user from prescribing proper time step lengths. An initial time step length of 1 day was used.

Of the many possible FEFLOW norms for describing the modelling error, the Euclidean L2 integral (RMS) norm was selected to calculate an integral error quantity. The error tolerance is dimensionless and is calculated by dividing the accepted tolerance in the hydraulic head by the maximum hydraulic head in the model domain at the beginning of the simulation. The smaller the error tolerance value, the higher the accuracy and the greater the numerical effort (Diersch, 2007). The tolerance derivation in the hydraulic head set for the groundwater model is 1 m. This can be described as the maximum error allowed during the calculation.

3.4 Initial Head

The hydraulic head distribution for 1978, obtained from a steady state model, was used as the initial condition for the transient model (refer to the previous report of this series: "Maules Creek Project: Steady-State Groundwater model" by Giambastiani et al., 2009). Figure 12 shows the 1978 hydraulic head distribution modelled by the steady state model and used as the initial condition for the transient model.

3.5 Boundary Conditions

Boundary conditions are mathematical constraints imposed on the model to represent in space and time the relationship of water transfer between the model flow domain and the external environment. Table 2 summaries the types of boundary conditions used in the model and Figure 13 shows the locations of the boundary conditions in the model domain. The boundary conditions are explained in the sub-sections that follow and shown in Figures 14and 15.

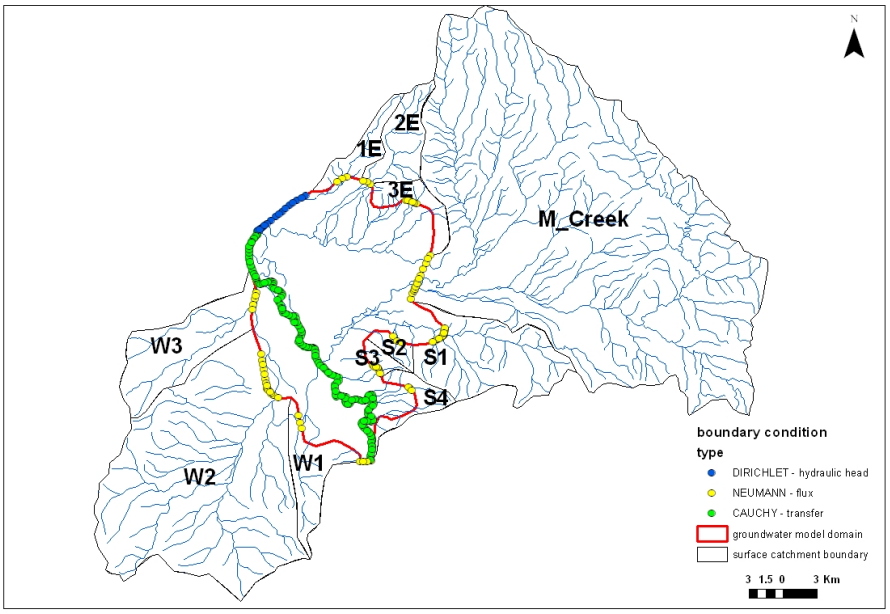

Figure 13: Distribution of boundary conditions.

Table 2: Summary of boundary conditions.

	Boundary Type	Application	Note
Aquifer Basement	No flow	-	-
Northern Boundary	Head (Dirichlet)	all slices	constant
Southern Boundary	Flux (Neumann)	all slices	constant
Eastern Boundary (at Elfin Crossing)	Flux (Neumann)	all slices	time series (Figure 14a)
Aquifer Boundary (1E, 2E,3E; S1, S2, S3, S4; |W1, W2, W3)	Flux (Neumann)	slice 1 and 2	time series (Figures 14b-d)
Namoi River Boundary	Transfer (Cauchy)	slice 1 and 2	time series (Figure 17)
Abstraction Bores	Specified flow	varies (depends on the depth of the screen)	time series (Figure 18)
Diffuse Recharge and Irrigation Recharge	Flux	slice 1	time series (Figure 15 a-b)

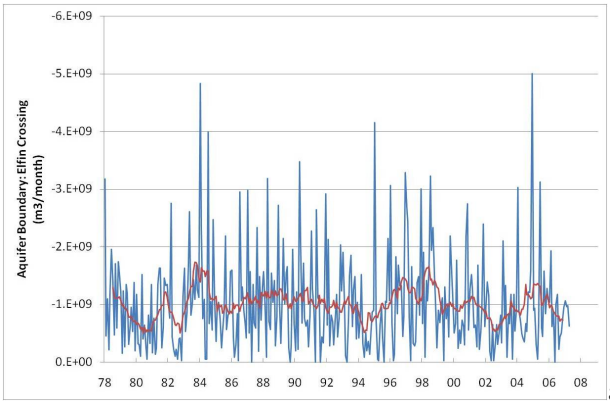

a)

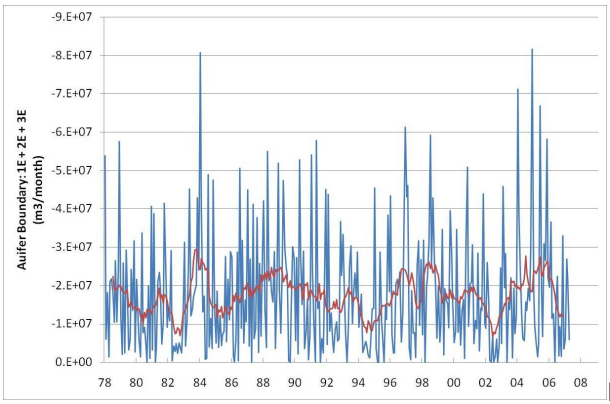

b)

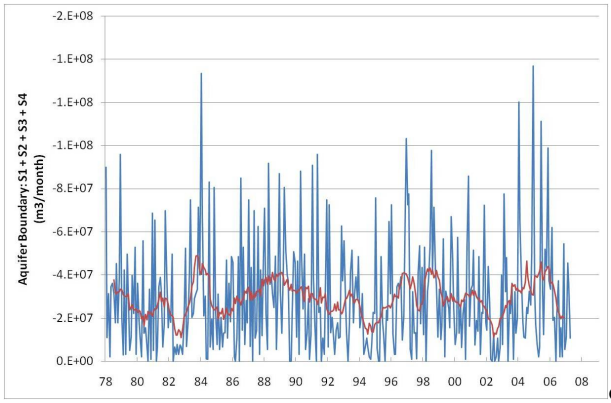

c)

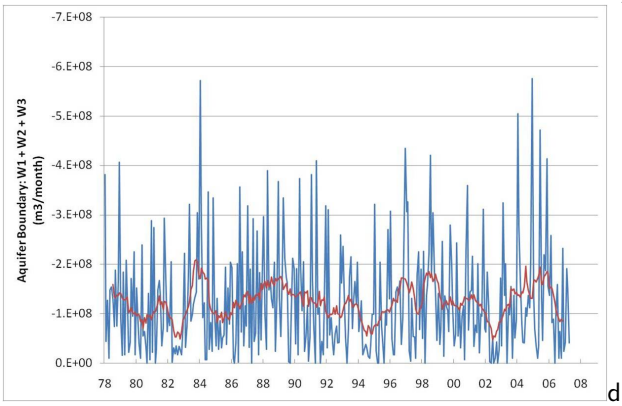

d)

Figure 14: Flux boundary conditions time series (y axes is the flux in m^3/month and x axes is the year from 1978 to 2007). Refer to Figure 13 for the location of the sub-catchments. The red line shows the 12 monthly average and the blue line is the total flux entering the model from boundaries.

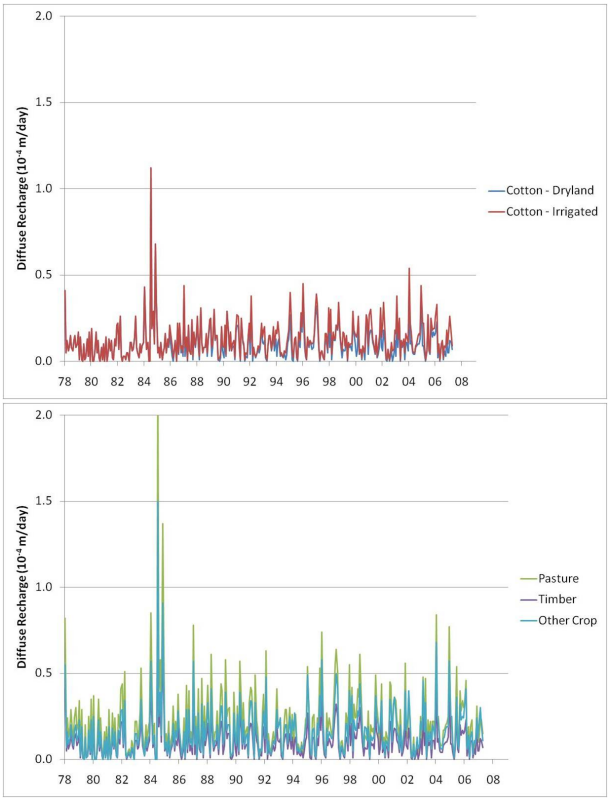

Figure 15: Diffuse recharge time series of 5 land use categories used.

3.5.1 Aquifer Basement

The basement was assumed to be impermeable and the flux into/out of the basement to be zero. This is a justifiable assumption as the difference in flow between the overlying alluvium and the bedrock would generally be expected to be greater than two orders of magnitude (Anderson and Woessner, 1992).

3.5.2 Northern Boundary

Since flow at the northern boundary is not perpendicular to the boundary, it is not possible to compute the flux through this boundary accurately. Instead, the northern boundary was treated as a fixed head boundary with values approximately 5-7 m below the DEM in order to let the water leave the system.

3.5.3 Southern Boundary

An estimate of groundwater flow into the model domain through Gins Leap Gap in the southern boundary was calculated based on a Darcian approach, using an average hydraulic gradient over 1978, a range of hydraulic conductivity values (from $5x10^{-4}$m/s to 10^{-3} m/s) and cross-sectional areas based on the FEFLOW mesh (Figure 16).

3.5.4 Eastern Boundary at Elfin Crossing

In order to define the eastern boundary at Elfin Crossing (Maules Creek) it was assumed that diffuse recharge in the area outside the groundwater domain, but inside the surface water catchment, became influx at the boundary.

Estimates of diffuse recharge were based on soil moisture deficit water balance calculations based on precipitation, evapotranspiration data, soil type and crop type parameters (see Section 3.5.8 for the detailed explanation). The calculations resulted in a time series of net recharge (Figure 14 a).

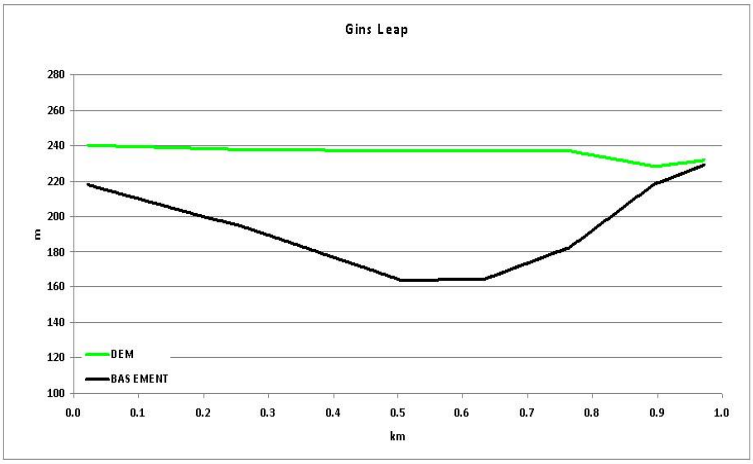

Figure 16: Aquifer areal cross-section of Southern Boundary at Gins Leap Gap (see 1 for location).

The eastern boundary is conceptually difficult to describe because the sub-catchment contains both a mountainous area and a plain area, each of which had different precipitation and evapotranspiration data. In addition the plain is underlain by a shallow aquifer of which very little is known. To overcome this, the sub-catchment was further subdivided into "Plain" and "Mountainous" areas. Data from rain station 55076 were used for the Plain area. For the Mountainous area, recharge was estimated by using linear interpolation of the precipitation and evapotranspiration data between climate stations 55076 and 54021.

An average recharge expressed as percentage of rainfall was calculated for each sub-catchment outside the model boundary. The average percentages were calculated on a daily basis over the whole period of the simulation (1978-2007). Finally, the recharge (mm) was multiplied by the sub-catchment area (m^2) to calculate a total flux of water (m^3). This flux was then evenly distributed across the model time period (m^3/day). At the model boundary this flux was applied as a flux boundary (m/day) by dividing the flux (m^3/day) by the cross sectional area on which the fluxes were applied (m^2). This boundary flux was adjusted during the calibration phase of the modelling (refer to Section 4 for discussion).

3.5.5 Aquifer Boundary

These boundaries, in reality the edge of the alluvial aquifer, were treated in a similar way to the eastern boundary. The way in which the computed flux was applied was different however: the boundary fluxes were applied around the main creeks and only on the shallow part of the aquifer (first 2 layers) assuming that the water is runoff from the higher bedrock terrain rather than groundwater recharge.

Fluxes along the boundary of the model domain were treated as an adjustable parameter to be assessed during model calibration. Figures 14 b-d show the flux boundary condition time series for the edge of the alluvial aquifer.

3.5.6 Namoi River

The Namoi River was treated as a transfer boundary condition (or Cauchy-type) with a prescribed hydraulic head. Two steps were required to do this: adjustment of the DEM and spatial and temporal estimation of hydraulic head data for all river nodes.

The digital terrain model (DEM) was corrected to incorporate a true streambed level for the Namoi River based on GPS surveys carried out in 2008 and 2009 by the WRL team. The next step was to define the river head at each node within the model domain. This was done by calculating the average head at Boggabri and Turrawan for each month. The ratio of these was also calculated for each month, and the median ratio of B/T was found to be 0.8. This factor was then used to fill in gaps in the Turrawan data set based on the Boggabri data set (see Figure 6). A continuous time series of river stage at Turrawan was thus created. Where the river stage was less than 0.3 m (essentially meaning no flow)

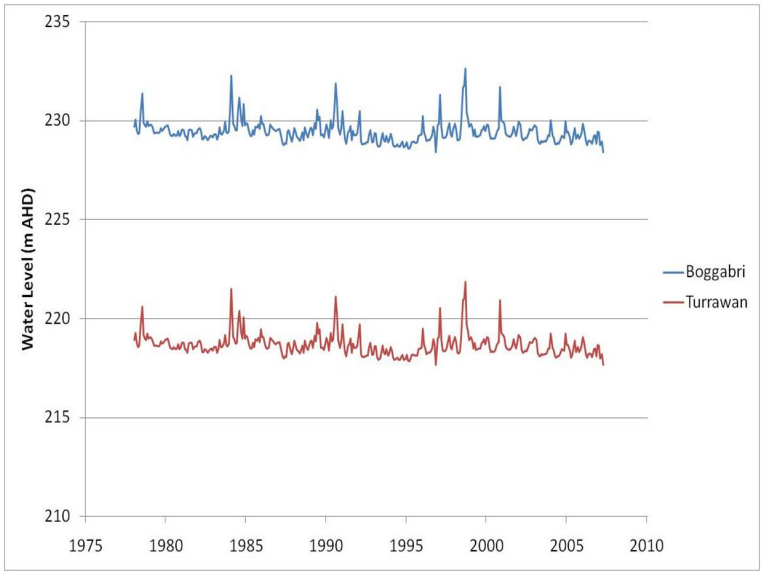

Figure 17: River heads at Boggabri and Turrawan which were used to create time series for all river nodes along the Namoi River.

the model stage was set to be 0.0 m. This time series was then simply added to the river bed elevation. River heads were linearly interpolated along the river between these nodes using FEFLOW. Figure 17 shows the river heads at Boggabri and Turrawan stations used to create time-varying functions for the Namoi river.

3.5.7 Abstraction Bores

Within the model domain 68 major groundwater abstraction bores, with multilevel screens tapping into the transmissive water-bearing zones, were implemented (Figure 10). Annual abstraction data were available for each bore (Figure 18). Monthly time series were created by distributing the annual abstraction over the year using monthly irrigation patterns (Figure 19, DNR, 2006). The time series were assigned to the slices in FEFLOW corresponding to the screened depths of each abstraction.

3.5.8 Diffuse Recharge

Theory Diffuse recharge was calculated based on daily soil moisture balance calculations with coefficients introduced to represent specific crop (crop coefficient, Kc) and reduced evapotranspiration (water stress coefficient, Ks) when there is limited moisture availability.

It has been assumed no throughflow (lateral flow within unsaturated zone), no runoff and that all deep percolation is equivalent to recharge that reaches the watertable at depth (Figure 20). The input to the soil moisture balance is the infiltration which depends on precipitation and the main output is the actual total evapotranspiration. The reference crop transpiration (ETo) data were obtained from SILO (Bureau of Meteorology website) for each weather station and has been estimated using the FAO version of the Penman-Monteith equation (Allen et al., 1998). Grass is used as the reference crop, since it grows throughout the year. Because different crops require different amounts of water, and crops can be under stress due to limited water availability, the crop evapotranspiration of a particular crop (ETc), is estimated via:

$$ETc = KcKsETo \tag{1}$$

where Kc and Ks are, respectively, the crop coefficient and water stress coefficient for evapotranspiration. Each crop type has a unique Kc value and these were obtained from Allen et al. (1998). Ks depends on the soil moisture deficit (SMD) which is the equivalent depth of water required to bring the soil up to field capacity, and is calculated from:

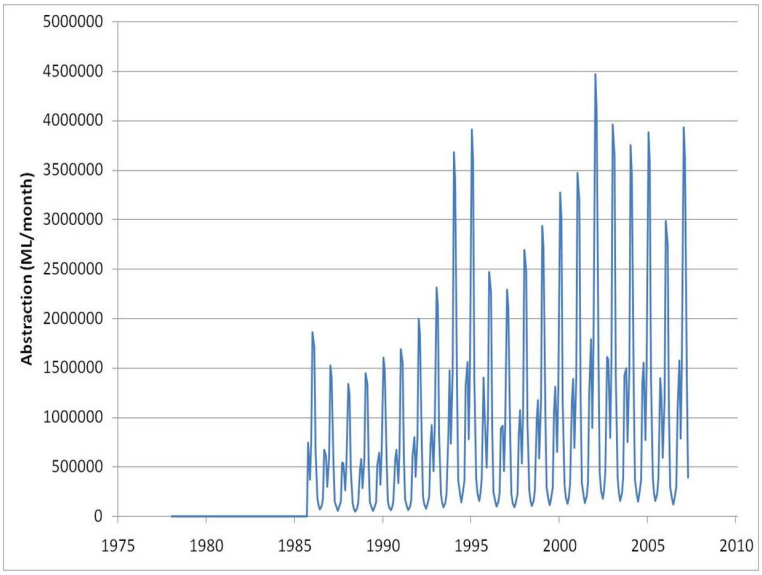

Figure 18: Total abstracted water volume.

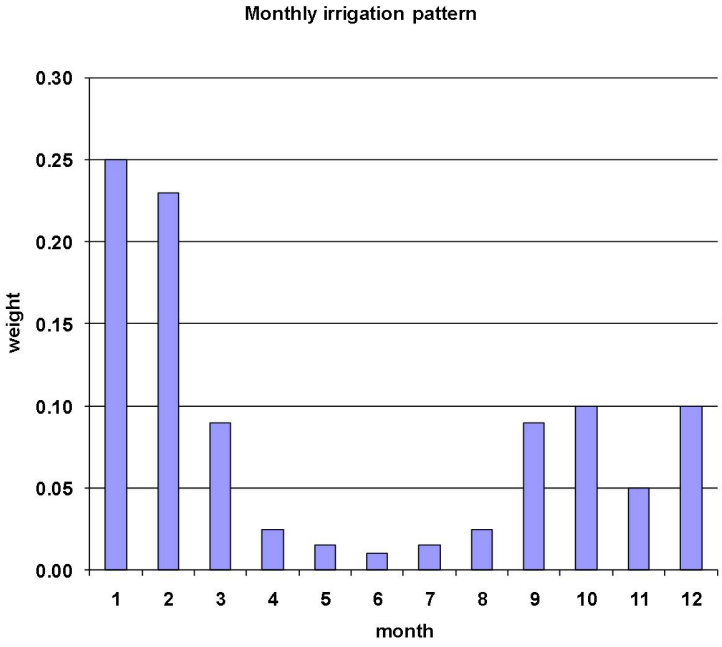

Figure 19: Assumed monthly irrigation pattern (from DNR, 2006).

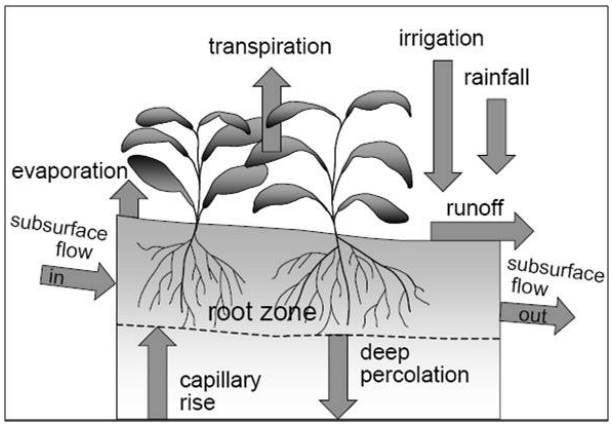

Figure 20: Soil water balance of the root zone (Allen et al., 1998).

$$SMD = \theta fc – \theta wp \tag{2}$$

where θfc is the field capacity defined as the amount of water that a well-drained soil can hold against gravitational forces and θwp is the wilting point defined as the soil moisture content below which plant roots cannot extract moisture. Different soils have different moisture holding properties. The Total Available Water (TAW, units mm) for a given crop on a given soil is:

$$TAW = 1000(\theta fc – \theta wp)Zr \tag{3}$$

where Zr is the rooting depth (m). The fraction of the TAW that a crop can extract without suffering water stress is called the 'Readily Available Water' (RAW, units mm) and is calculated from:

$$RAW = pTAW \tag{4}$$

where p is the average fraction of TAW that can be depleted before the moisture content falls below the threshold value. In order to calculate the crop evapotranspiration rate (ETc) four situations need to be considered (Rushton, 2005):

1. SMD' $<$ RAW or infiltration (precipitation and/or irrigation recharge) $\geq$ ETo, where SMD' is the soil moisture deficit for the previous day, then Ks=1 and the actual evapotranspiration is equal to ETc = KcETo;
2. TAW $\geq$ SMD' $\geq$ RAW and infiltration $<$ ETo, then ETc = Kc Ks ETo and Ks is calculated using the soil moisture deficit for the previous day;
3. Ks = (TAW – SMD')/(TAW-RAW); and
4. SMD' $>$ TAW no infiltration occurs.

Soil Type and Land Use As explained in the section above, the amount of recharge depends on climatic parameters, as well as soil type and land use. To convert 1D recharge estimates (m/year) to volume of total catchment recharge, the area over which to apply each recharge estimate was determined.

Figures 21 and 22 show the soil type and land use distribution in the Maules Creek Catchment. The combination of landuse and soil type results in many classes for which area and recharge should be calculated. In order to simplify the calculation, the number of land use classes was reduced to 5: 'cotton' (dry-land and flood irrigation), 'pasture' (rotated grazing; non irrigated crop), 'timber' and 'other crop' (wheat, oats, sorghum, etc.; irrigated land). Clay and silt were considered the main soil types in the catchment and grouped as one.

The adopted coefficients for the calculations of all different crops are shown in Table 3. These areas are assumed to be constant throughout the simulation period (1978-2007).

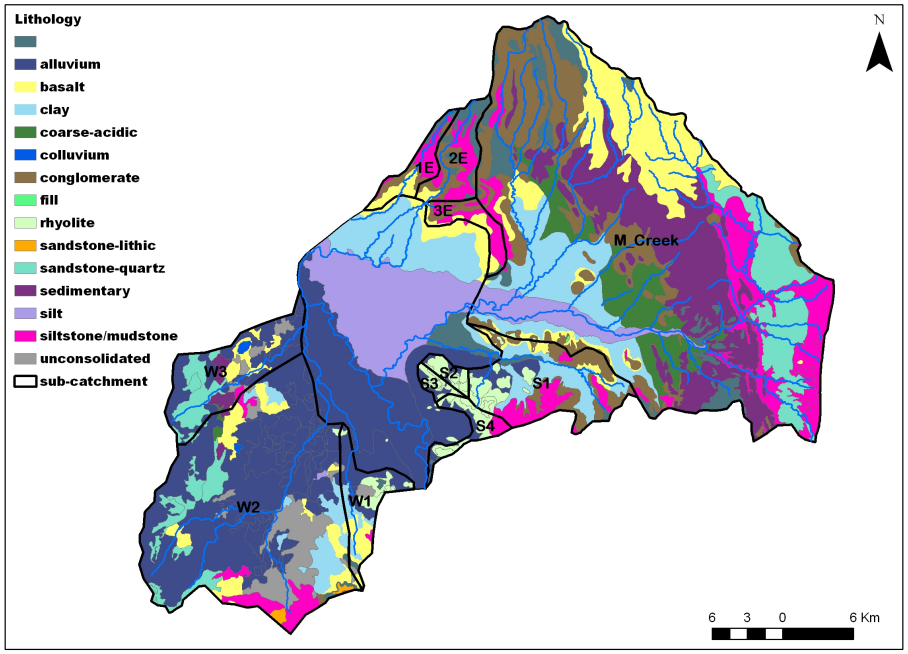

Figure 21: Maules Creek Catchment soil type map (provided by the Namoi CMA).

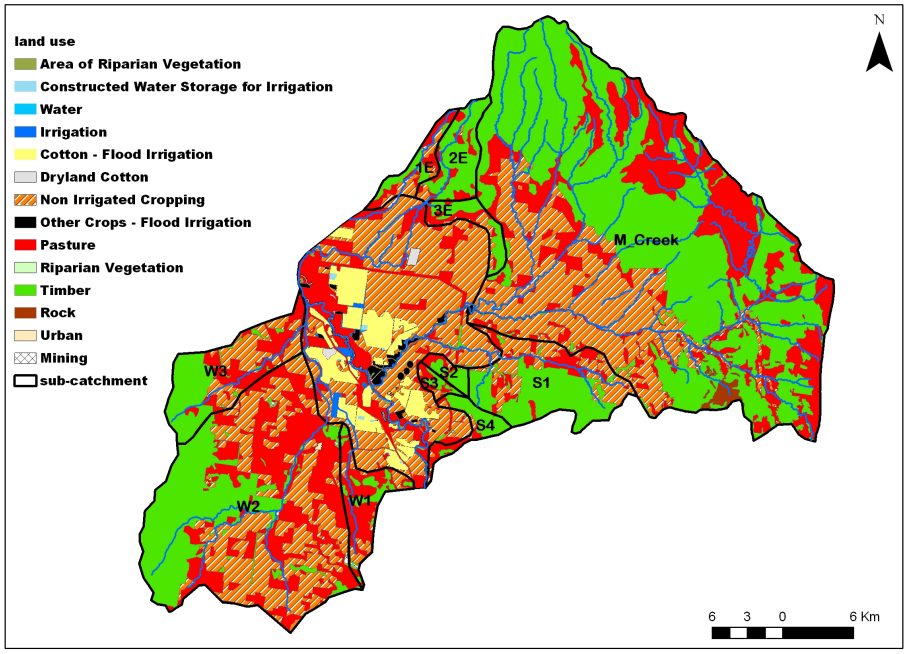

Figure 22: Maules Creek land use (provided by the Namoi CMA).

Table 3: Parameter values used for the soil moisture balance calculation (values from Allen et al., 1998).

	Cotton		Pasture		Timber		Other crop	
	Range	Used	Range	Used	Range	Used	Range	Used
Kc_ini	1	0.98	0.4	0.8	1	1	-	0.8
Kc_mid	1.15-1.2		0.85-1.05		1		1-1.15	
Kc_end	0.70-0.5		0.85		1		0.25-0.4	
Zr (m)	1-17	1.35	0.5-1.5	1	1-1.5	1.25	1-2	1.5
p	0.65	0.65	0.6	0.6	0.7	0.7	0.55	0.55
fc-wp clay-silt (m^3/m^3)	0.12-0.2	0.13	0.12-0.21	0.13	0.12-0.2	0.13	0.12-0.2	0.13
TAW(mm)	-	176	-	130	-	163	-	195
RAW (mm)	-	114	-	78	-	114	-	107

Table 4: Average of recharge as percentage of average rainfall for the land use classes used in the model domain.

Land use	Recharge (% of P)
Cotton_Flood Irrigation	3% + irrigation recharge
Dryland Cotton	3%
Pasture	6%
Timber	3%
Other crop	4% + irrigation recharge

Figure 23 shows the land use as it has been simplified and applied on the first layer of the FEFLOW mesh. Diffuse recharge is applied in FEFLOW to the surface of the finite element and internally multiplied with the element area resulting in a flow (m^3/d).

Table 4 shows the average of recharge as percentage of rainfall for the 5 crops considered in the model domain as calculated on daily basis using climatic data from the station 55076 over the period of simulation (1978-2007).

The recharge rate was treated as an adjustable parameter to be assessed during model calibration. Figure 15 shows the diffuse recharge time series used for the 5 land use categories.

3.5.9 Irrigation Recharge

Leakage from irrigated crops is a further source of recharge to the aquifer system. In this model irrigation recharge is implemented merging irrigation data with the diffuse recharge explained above. The irrigation recharge area within the model were applied only on the land use categories: 'cotton-flood irrigation' and 'other crop' classes (Figure 23) and are based on the simplification of the land use map explained in the section above. These areas are assumed to be constant throughout the simulation period.

Net irrigation recharge rate was calculated as 3% of the abstraction rate. This annual recharge flux was distributed across the monthly stress period based on the seasonal irrigation pattern shown in Figure 19.

3.6 Aquifer Parameters

FEFLOW requires hydraulic conductivity, diffuse recharge, specific yield, specific storage and leakage coefficient (or transfer rate) to be specified for each element. All parameters used for the groundwater model are summarised in Table 5 and explained below.

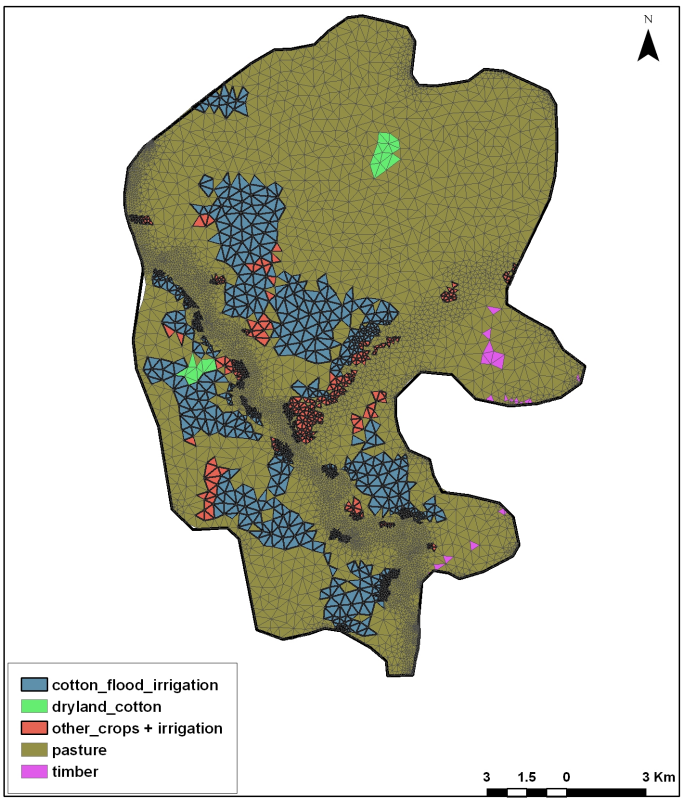

Figure 23: Land use implemented on the FEFLOW mesh.

Table 5: Aquifer parameter values.

Parameter	Value	Application	Source
Kxx = Kyy	Sand = 10^{-3}m/s, Clay = 8x10^{-5}m/s; Sand = 10^{-3}m/s, Clay = 10^{-6}m/s;	Layer 1 Layers 2-9	Core-logs, pumping tests, trial-and-error method, typical values
Anisotropy	0.1	Layers 1-9	Typical values
Specific Yield	Sand = 0.1 Clay = 0.01	Layers 1-9	Typical values and trial-and-error method
Specific Storage	10^{-5}1/m	Layers 1-9	Typical values and pumping tests
Transfer rate	In = 0.5 d^{-1} Out = 1 d^{-1}	First 2 layers (related to Cauchy boundary conditions)	Trail-and-error method

3.6.1 Hydraulic Conductivity Distribution

The borehole driller lithology logs (from NSW Office of Water, NSWG, 2007) were indexed into low and high conductivity sediments. The element centres of the FEFLOW mesh were populated using the categorical gridding method 'Nearest Neighbour' (Tartakovsky et al., 2007). This is the simplest categorical gridding method, and requires only few assumptions. The value assigned to the element centre is the nearest neighbour from the borehole logs, based on the Euclidean distance between the element centre and neighbouring borehole points. This calculation was coded in the Mathematica™ scripting language. Each lithology index was then assigned a hydraulic conductivity value and imported into FEFLOW. In FEFLOW the hydraulic conductivity values were assigned to the closest finite element mesh centre using inverse distance weighting. and a search count of 1. More information about the geological model can be found in Appendix 3 "Crystallize: Catchment Scale 3D Geological Models from Sparse Data Sets".

Hydraulic conductivities of the model domain were assigned on the basis of stratigraphic information, pumping test data and the calibration of the model (refer to: "Maules Creek Project: Steady-State Groundwater Model", Giambastiani et al., 2009). The measured range of hydraulic conductivity used in the trial-and error calibration method was 10^{-6}m/s to 10^{-3}m/s.

Values of horizontal and vertical hydraulic conductivity selected for the model are listed in Table 5. Note that the K-value of $8x10^{-5}$m/s for the clay in the top layer is higher than the one used deeper in the model. This value represents the hydraulic conductivity of typical cracking clay Vertosols present in the Namoi Catchment (Vervoot et al., 2003). This specific soil type, present on the river plains, can have large cracks (and hence a high hydraulic conductivity) through which large amounts of water can quickly infiltrate to the subsoil (Collis-George, 1997, McKay et al., 1993). The hydraulic conductivities in the horizontal x and y directions are uniform while the vertical hydraulic conductivity is an order of magnitude lower for all layers (i.e. an anisotropy of 0.1).

As explained in the previous report for the steady state model (Giambastiani et al., 2009); high water fluxes along with a steep topographic gradient and low transmissivity (low K and low model thickness) along the model boundary caused the hydraulic head to build up and prevented a good calibration performance. This required the implementation of high conductivity zones around major creeks for the first 2 layers in order to distribute the applied boundary fluxes into the model domain. The validity of implementing these higher conductivity zones around the major creeks was verified by field observations.

Figure 24 shows the hydraulic conductivity distribution for each layer in the model domain. In Figure 25 two cross-sections have been plotted showing the hydraulic conductivity distribution over depth from west to east (cross-section 1) and from north to south (cross-section 2).

3.6.2 Specific Yield and Specific Storage

The specific yield was assigned based on the geology distribution with a value of 0.1 for the sand and 0.01 for the clay units. These values are within the typical range of values for these types of sediment (Freeze and Cherry, 1979; Fetter, 2001). The specific storage was assigned as a global value (i.e. no spatial distribution) and was assumed to be $10^{-5}m^{-1}$. For saturated flow problems with a phreatic surface FEFLOW uses both the specific yield and the specific storage.

3.6.3 Transfer Rate

In FEFLOW leakage between streams and the shallow aquifer system is simulated using transfer rate parameters. The rate and direction of flow depend on the difference in head between the stream and the aquifer and the hydraulic conductivity of the river bed.

Transfer rates are handled as transfer flow boundary conditions and are calculated from the hydraulic conductivity (K) and thickness of colmation layer (d) of the riverbed based on these relations:

$\Phi_{in} \approx K_{in}/d$ [d^{-1}]

and

$\Phi_{out} \approx K_{out}/d$ [d^{-1}]

The transfer rate in and out are different because clogging layers in rivers generally tend to have higher conductivity during out-flowing conditions compared to inflow, where suspended material in the surface water clog the pores (Diersch, 2005). Values are listed in Table 5.

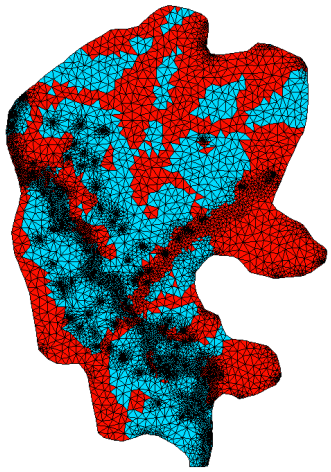

(a) layer 1

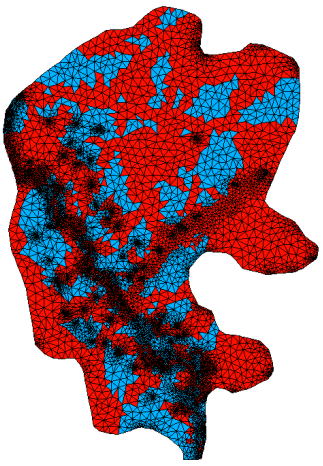

(b) layer 2

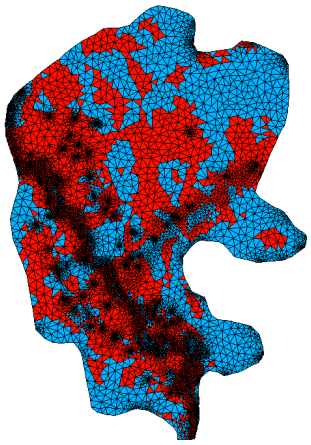

(c) layer 3

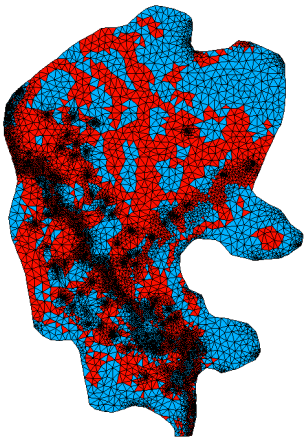

(d) layer 4

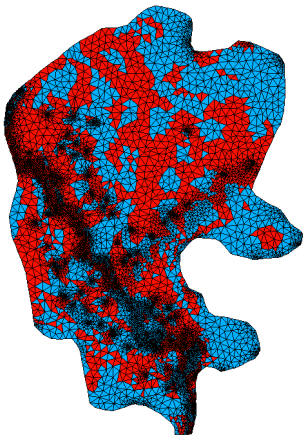

(e) layer 5

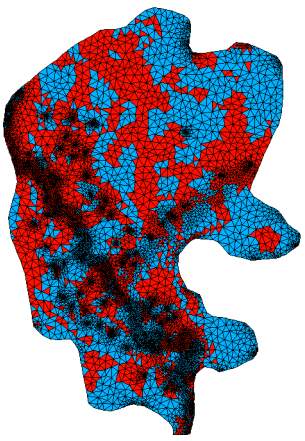

(f) layer 6

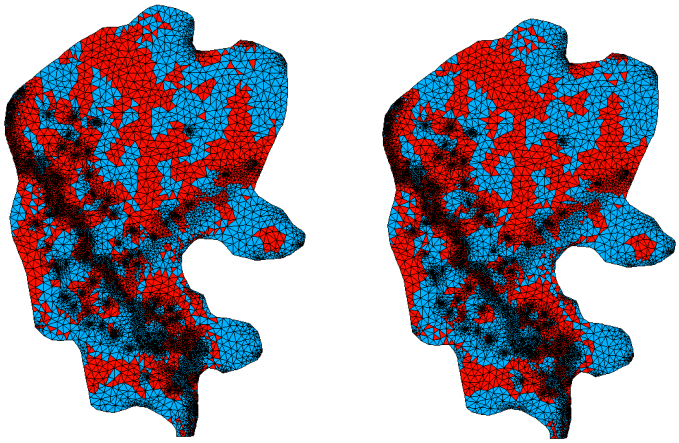

(a) layer 7

(b) layer 8

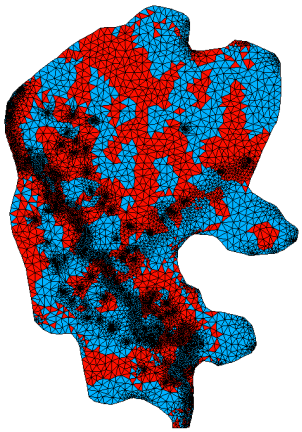

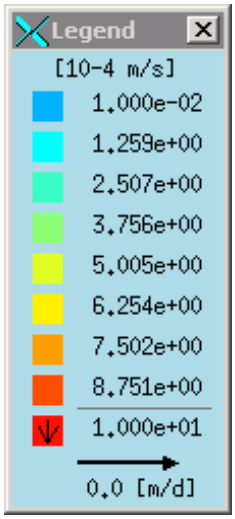

(c) layer 9

Figure 24: Hydraulic conductivity distribution (Kxx and Kyy) for each model layer (sand in red and clay in blue).

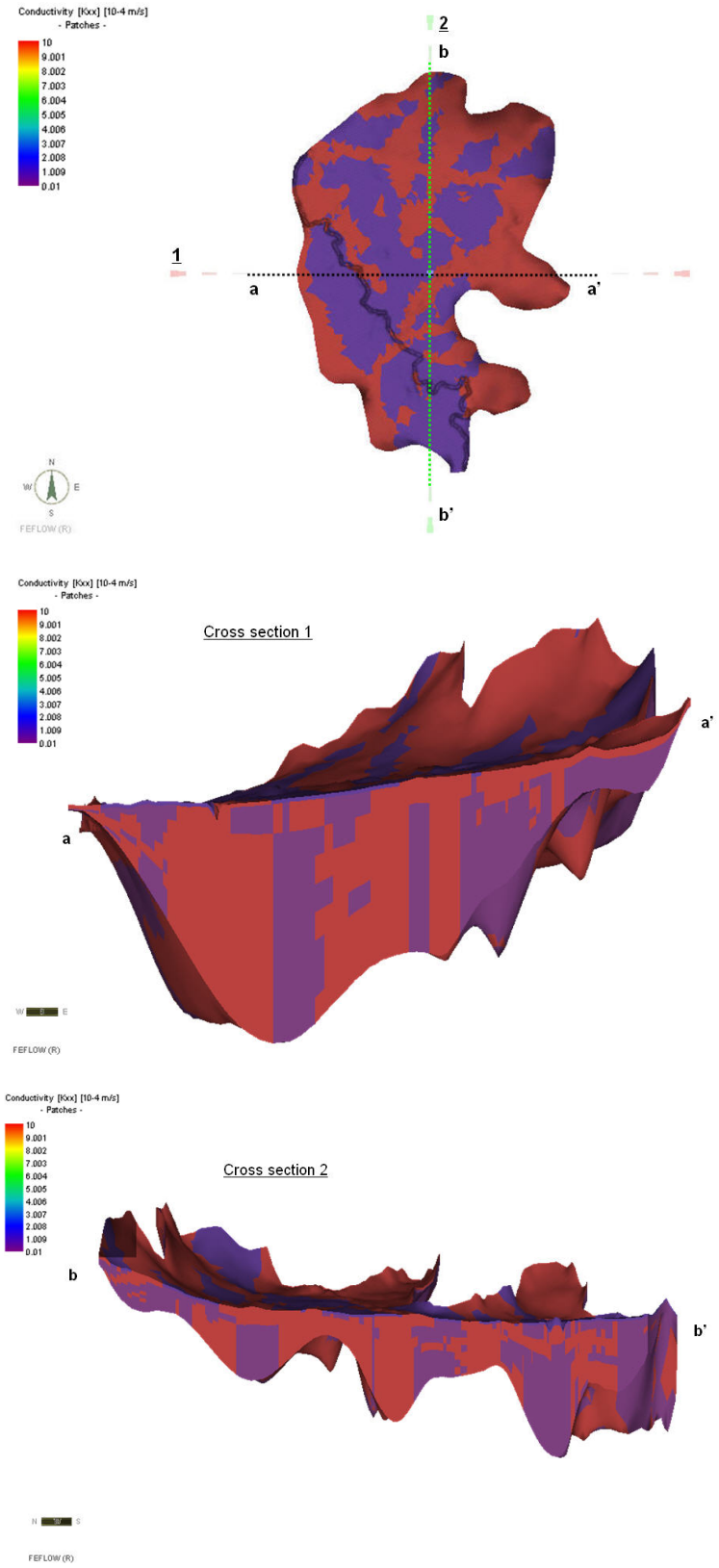

Figure 25: Locations of cross-sections in the model domain and hydraulic conductivity distribution (Kxx and Kyy) across the model domain (sand in red and clay in purple).

The thickness of the colmation layer (d) is 2m according to the thickness of layer 1 where the transfer rate is defined. The hydraulic conductivity of the river bed used in the model is 10^{-5}m/s.

4 Calibration and Sensitivity Analysis

4.1 General

Groundwater flow models are calibrated by adjusting uncertain model parameters and fluxes within realistic limits in order to obtain a reasonable match between modelled data and measured data.

Model calibration was performed by trial-and-error with the objective of matching modelled bore hydrographs with measured hydrographs. The calibration period is from 1982 to 2007 because the head condition at early times (1978-1982) in the eastern part of the model domain contains high water levels as a result of the 1978 hydraulic head distribution of the steady state model.

Approximately 60 individual FEFLOW simulations were run during development of the final calibrated model. The calibration process involved adjustments and changing of model parameters over successive model runs. The details of these are provided in the following sections and documented in the Model Journal.

Subsequently 28 FEFLOW sensitivity tests were run to provide a global picture of relative sensitivity to key parameters. The results of the global sensitivity are shown and discussed in Section 4.4.

4.2 Calibration Process

4.2.1 Observation Boreholes

A total of 64 observation points (of 37 multipipe monitoring boreholes) were implemented for the purpose of comparing modelled and measured heads. Each observation point was located in space using x and y GPS surveys and screen interval information from the NSW Office of Water construction database.

Each observation point was implemented on the FEFLOW mesh slice which better represents the depth of the top of screened interval which was considered the representative depth for the measured head in the aquifer. See Figure 10 for locations of all observation boreholes in the Maules Creek Catchment.

4.2.2 Calibrated Parameters

The calibration process involved adjustment and assessment of the following model parameters:

- hydraulic conductivity values;
- specific yield and specific storage;
- transfer rate values in and out of the Namoi River; and
- flow boundary conditions and diffuse recharge.

Table 6 shows the range of values used to calibrate each aquifer parameter.

During the calibration process it became clear that high water fluxes along with a steep topographic gradient and low transmissivity (low K and model thickness) along the model boundary caused the hydraulic head to build up. To achieve a good calibration performance it was necessary to increase the hydraulic conductivity of the sand units previously adopted in the steady state (10^{-3}m/s instead of 7.5 10^{-4}m/s initially adopted).

In order to improve matching between modelled and measured drawdown in the bores which are affected by groundwater abstraction, specific yield and specific storage values were varied in a range of possible values based on the literature (Fetter, 2001; Freeze and Cherry, 1979). It was found that even with values close to the limit of acceptable values, the seasonal drawdown and calibration were not significantly improved. The system acts more like an unconfined aquifer and changes in the specific yield values have a greater influence on water storage.

Table 6: Range of value used to calibrate the model.

Parameter	Range	Adopted
K sand	10^{-3}- 10^{-4}m/s	See table 5
K clay	10^{-7}- 10^{-5}m/s	See table 5
Specific Yield sand	10 -30 %	See table 5
Specific Yield clay	0 - 5 %	See table 5
Specific Storage	10^{-4}- 10^{-9}1/d	See table 5
Transfer Rate In and Out	10^{-4}- 10^{-6}m/s	See table 5
Flux and diffuse recharge	divided by factor 2 and 5	flux and diffuse recharge, calculated as described in Section 3.5.8, divided by 5

Transfer rate values in and out of the Namoi River were varied in a range of 10^{-4}- 10^{-6}m/s. The values adopted for the transient model are the same used for the steady state. These values were selected after sensitivity tests (detailed explanation in the previous report, Giambastiani et al., 2009).

The aquifer parameters described in the previous sections of the report are the actual model values used in the transient model. No further adjustment of these parameters was required. Boundary fluxes and diffuse recharge, however, were treated as adjustable. In fact, during the calibration process, hydraulic head was shown to be very sensitive to both diffuse recharge and boundary fluxes. So the previously calculated boundary fluxes and diffuse recharge, explained in Section 3.5.8, were reduced during the calibration process to get the best match between the modelled and measured hydraulic heads. The final calibrated model used a division factor of 5, with calibrated fluxes and diffuse recharge much less than initially estimated.

4.2.3 Non-uniqueness Problem

Every groundwater model is non-unique, that is, different sets of model inputs and parameters can result in similar if not identical model outputs (MDBC, 2001, Ritchey and Rumbaugh, 1996). During calibration there are many variables that can be changed and so it can be difficult to assess which combination, each giving an apparently calibrated model, is the preferred one. In this situation, while the model may appear to be calibrated its ability to make predictions will be limited. For example, theoretically it can be shown if that concurrent and proportional changes in recharge and conductivity can lead to identical model results (Ritchey and Rumbaugh, 1996). However, if an unrealistic recharge value is used, the usefulness of the model in predicting the aquifer response to climatic changes will be limited.

This problem was addressed by the following three approaches. Areas of high and low conductivity were defined using a relatively high resolution geological model. This, in part, constrained the possible solutions to a greater degree than is normally achieved in groundwater modelling. Further, as described in Section 4.2.2 above, aquifer parameters (conductivity and specific yield/storage) were adjusted within reasonable limits and were consistent with measured values. Finally, the model attempts to capture the dynamics of a highly stressed aquifer system. The rule of thumb "constant recharge over conductivity gives identical models" is not valid for the present model. The aquifer has varying boundary fluxes and diffuse recharge rates. It also experiences large pumping stresses as well as interaction with a major river. The model is thus calibrated to a dynamic situation which covers a variety of distinct hydrological conditions.

4.3 Calibrated Model

4.3.1 Modelled and Measured Water Level

Model calibration performance was assessed qualitatively by comparing modelled and measured hydrographs and quantitatively by calculating the root mean square error (RMS) for each observation borehole and the statistics of head residuals for the whole calibration period (1982-2007).

A major difficulty with calibration measures is the alignment of measured and modelled data. Consequently, as a post-processing activity, the modelled data were shifted to times and interpolated to get

values at the correct date for which measured data were recorded. Hydrographs and calculated RMS for all observation points in the model domain are presented in Appendix 5A. It should be noted that the calibration is not applicable on boreholes GW063060, GW063059 and GW967137 due to the lack of sufficient measured data and in the hydrographs only the modelled values are reported.

Overall the model performance is good, with the model correctly capturing the recovered water levels after each irrigation season, as well as the long-term trends shown in the measured hydrographs. However, in areas where the magnitude of pumping induced drawdown is large (up to 8-10 m) the seasonal dynamic is not closely captured by the model (see example hydrographs GW030232 pipe 2 and 3; GW030233 pipe 2 and 3; GW030446 pipe 2; GW030447 pipe 1).

In the measured data, many of the hydrographs start to decline more steeply at about year 2000 however this is not always the case in the modelled data. The decline is due to a number of factors: this period corresponds to a regional drought; during drought there is little or no rain, and therefore there will be little deep drainage (diffuse recharge) occurring. Also the influx of water entering the aquifer from side slope runoff (mountain front recharge) is reduced. During this period there has not been a large flood in the Namoi, which is also an important mechanism for recharge. Meanwhile, groundwater abstraction is ongoing, thus causing a decline in hydraulic heads. A possible explanation is that the model is not fully capturing the combination of all the above processes which are occuring in reality. The mismatch between measured and modelled heads may be due to the way in which the diffuse recharge and boundary fluxes are computed and implemented. That is, these volumes were calculated by creating time series by multiplying the precipitation by a set percentage (the percentage having been calculated using a soil moisture defecit model – see Section 3.5.8). During drought this percentage will decrease, leading to less flux of water into the model. Another explanation is that the groundwater abstraction records for this period are underestimated. Further research into these processes is required.

In the measured data there is often a difference in the response of different pipes at the same location, whereas this is not always captured in the model. This is likely due to the geological distribution which does not capture the semi-continuous confining layers which are present in reality.

A good calibration and small RMS error were achieved for boreholes closer to the Namoi River (such as GW030231 pipe 1 and 2; GW036004 pipe 1 and 2; GW036096 pipe 1, GW036056 pipe 1, etc.).

Calibration is less reliable in the eastern part of the model domain (GW030131 and GW030130) especially due to large flux at Maules Creek boundary associated with low K units which do not let the fluxes enter and distribute along the model. As a result, hydraulic heads build up.

The statistics such as RMS error are based on head residuals. A systematic error will bias the statistics. In fact there are cases such as borehole GW036187 when a modelled hydrograph agrees very well with the measured hydrograph in pattern and amplitude but differs in absolute magnitude (i.e. two similar curves run parallel to each other). In this case the head-based statistics will suggest a poor calibration when in fact the calibration might be good (MDBC, 2001). Legitimate elevation residuals can also result from model discretisation and interpolation of the location of modelled and measured sites. It has to be remembered that observation points have been applied on the closest slice which best represented the depth of the screen top. However, due to the model discretisation, in some cases the real depth and model nodes are not exactly at the same place. Considering all observation points in the model domain, the biggest mismatch between real depth and model nodes is 1.2 m with an average of 0.6 m.

To account for these effects, some form of normalisation is appropriate. The technique used in this study is the standard correlation function between the two time series (modelled and measured) (Zheng and Bennett, 1995). This technique returns a linear correlation coefficient 'r' which lies between -1 and 1. A value of 1 indicates a perfect linear correlation, with the modelled and measured values increasing and decreasing together. A value of -1 also indicates a perfect linear correlation with the modelled and measured values changing in the opposite direction. A value of 'r' near zero is an indication of no correlation. Better calibrated models tend to have values close to 1. The global 'r' values calculated for the model is 0.94, indicating a good correlation.

The results of the statistics and standard correlation function for the calibrated model over the period of calibration (1982-2007) are shown in Table 2 in Appendix 5A.

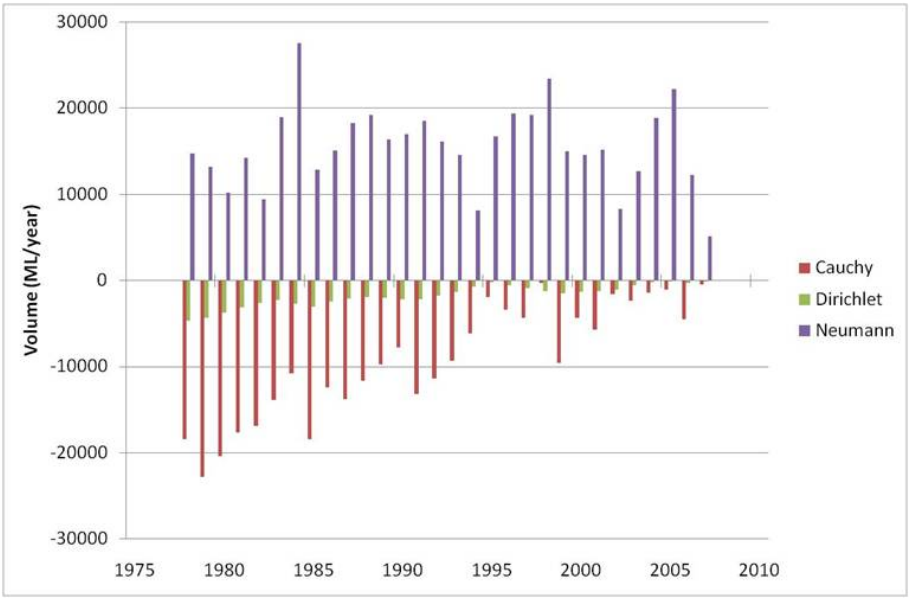

Figure 26: Components of the water balance: boundary conditions.

4.3.2 Water Budget

Water balances are calculated for the model calibration period (1982 to 2008). Figures 26 to 28 illustrate this as a series of volume balances: positive values means a gain in volume to the system, while a negative value means a loss of volume from the system.

The fluxes for the 'Dirichlet' (head), 'Neuman' (flux) and 'Cauchy' (transfer) type boundaries are shown in Figure 26. The largest inflow component over the calibration period was boundary fluxes. Water leaves the aquifer system via the northern boundary ('Dirichlet' type) and the river ('Cauchy' type). More water leaves via the river than the northern boundary as would be expected hydrologically, however this volume has been decreasing with time. Also evident in this figure is the delayed response of the aquifer system to stresses: for example, the large influx of water in 1984 via the boundaries resulted in a large outflux of water in 1985 via the river.

Figure 27 shows the water balance for the boundary conditions ('Dirichlet', 'Neuman' and 'Cauchy' summed for each year) as well as for the diffuse recharge and bore abstraction. These form all components of the water balance of the aquifer system. The difference between them ("Imbalance" in blue) is therefore the change in storage in the aquifer system. Shown in this figure is the importance of groundwater abstraction as a hydrological stress, which causes a large outflux of water each year (in purple) which is much larger than the influx due to diffuse recharge (in green) and more consistent than the influx due to the boundary fluxes (in red).

The water balance results can also be presented as a cumulative plot, as has been done in Figure 28. This allows the cumulative magnitudes of the components in the water balance to be seen at any particular time. From this it can be seen that over the whole modelling period, nearly 200000 ML and approximately 50000 ML water entered the aquifer system via, respectively, all the boundaries and diffuse recharge, respectively, while approximately 250000 ML water left the aquifer system via abstraction bores, leaving a small negative imbalance for the sytem.

4.3.3 River Exchange

Figure 29 shows the flux to and from the river and groundwater flux for the modelling period. A positive value indicates a volume gain to the aquifer system while a negative value a volume loss from the aquifer system. The pumping record for the modelled period is shown in red. Prior to 1985 there was little or no pumping, while after that time the pumping volume changes for each irrigation season. Also shown in the figure (in blue) is the fact that for the majority of the modelled period the aquifer loses water to the river (i.e. a gaining river). However, there is a general diminuishing flux to the river.

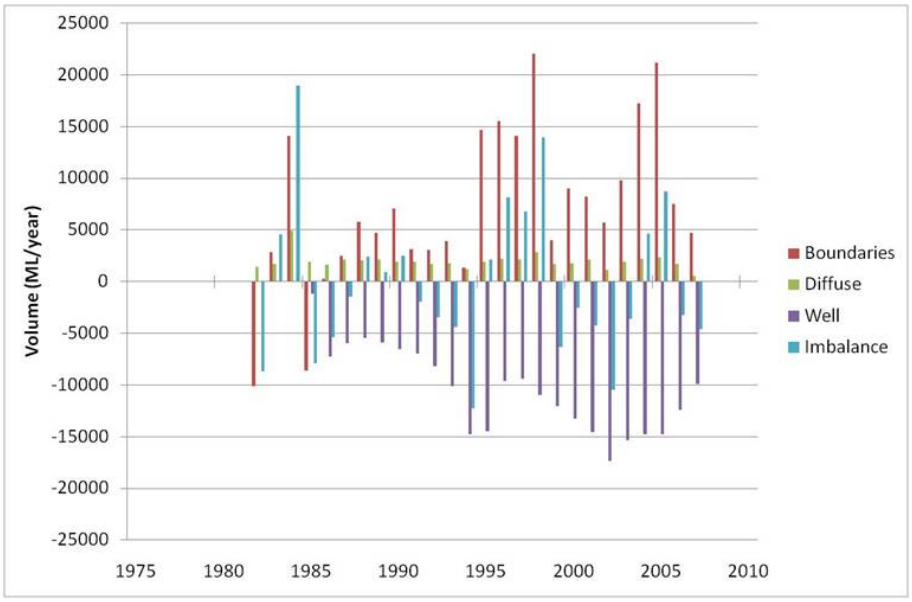

Figure 27: Complete water balance.

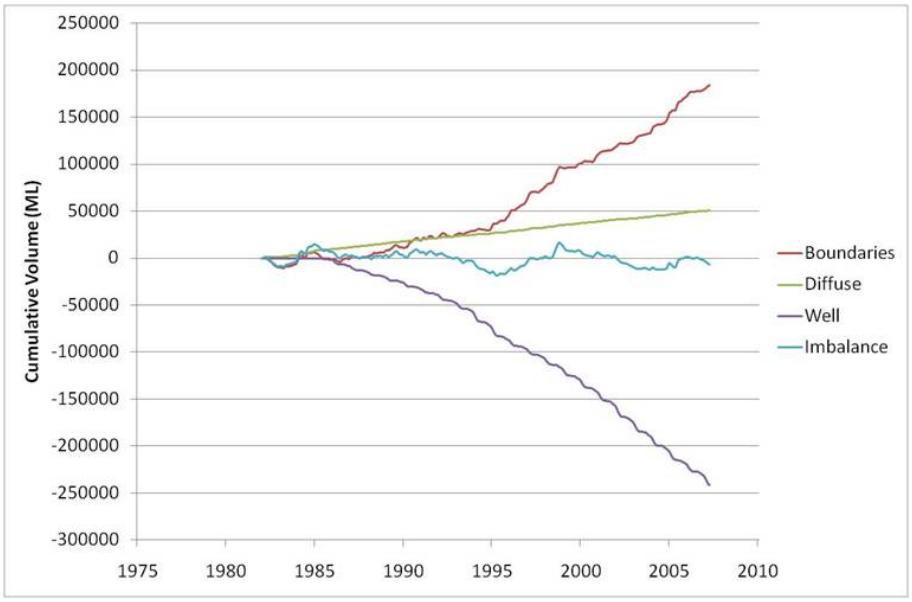

Figure 28: Water balance shown as a cumulative plot.

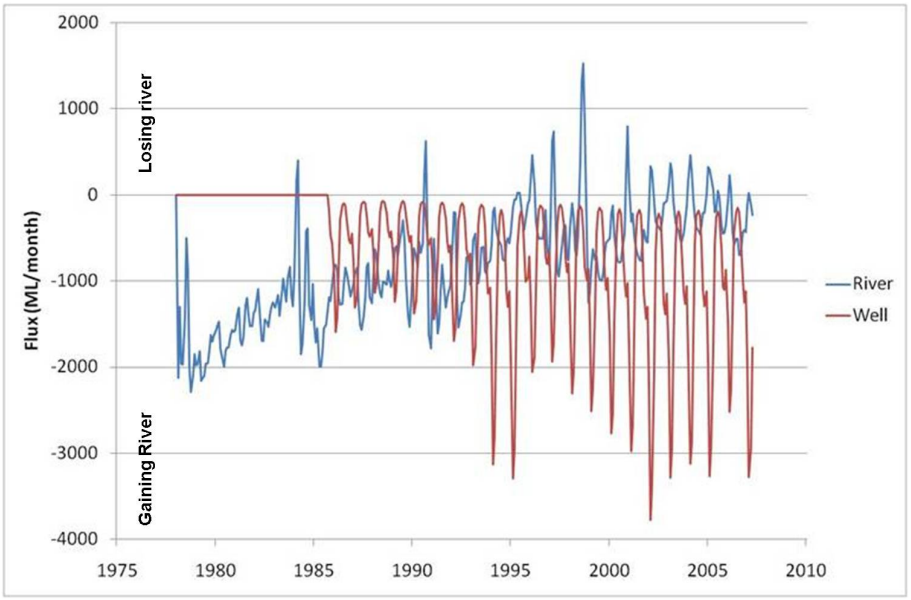

Figure 29: Flux versus time for river-aquifer interaction and groundwater abstraction from bores

During the last decade of modelling there are periods where the aquifer gains water from the river (i.e. a losing river). This is due to the lowered groundwater heads caused by the groundwater pumping in each irrigation season. Prior to this period the only other times the aquifer gained water from the river in the model was during the large flow events in 1984 and around 1990 (where the sustained high river stage would have induced a losing river situation).

4.4 Sensitivity Analysis

A sensitivity analysis was undertaken to quantify the impact on the simulated response of the aquifer due to variations in the model parameters and hydraulic stresses, thus identifying which parameters are most sensitive in determining aquifer behavior.

A partial sensitivity test was initially carried out during the trial-and-error calibration of the steady state (refer to previous report by Giambastiani et al., 2009) to enhance the understanding of the aquifer and accelerate the calibration process. Here a second and more complete sensitivity analysis was performed after the calibration of the transient state in order to indicate the sensitivity of key parameters on the aquifer system.

The following parameters in the model were changed from the base case (calibrated model) to test the sensitivity of the model:

- horizontal and vertical (Kxx, Kyy) hydraulic conductivities (Kzz);
- specific yield (Sy);
- specific storage (Ss);
- transfer rate value (river);
- flux boundary conditions; and
- diffuse recharge.

These parameters were changed in turn by multiplying and dividing the base value of the calibrated model by a factor of 5 and 10. For each simulation the RMS error is calculated and listed in table 7.

Figure 30 shows global sensitivities of the calibration performance indicator RMS error of the head residual to variations in model parameters and hydrological stresses. To facilitate comparison all curves are plotted at the same horizontal and vertical scales.

Table 7: Calculated RMS of head residuals for each sensitivity test.

	RMS(m)						
parameter multiplier	Kxx	Kzz	Sy	Ss	Transfer rate	Recharge	Flux
0.1	14.4	2.4	2.8	2.4	2.9	2.4	5.5
0.2	10.2	2.5	2.6	2.4	2.6	2.4	4.8
1 (base case)	2.4	2.4	2.4	2.4	2.4	2.4	2.4
5	5.9	2.4	2.8	2.4	2.5	2.7	16.2
10	6.9	2.4	3.1	2.4	2.5	3.4	37.1

Table 8: Sensitivity coefficients in terms of root mean square error (RMS) with respect to model parameters.

	normalized RMS						
parameter multiplier	Kxx	Kzz	Sy	Ss	Transfer rate	Recharge	Flux
0.1	49.18	0.00	0.06	0.00	0.07	0.00	0.42
0.2	15.84	0.00	0.02	0.00	0.03	0.00	0.37
1 (base case)	0.00	0.00	0.00	0.00	0.00	0.00	0.00
5	0.28	0.00	0.05	0.00	0.00	0.01	2.29
10	0.18	0.00	0.11	0.00	0.00	0.01	5.75

The results of the sensitivity test show that the present model calibration (i.e. parameter multiplier of 1 in Figure 30) returns the lowest RMS value as expected. Figure 30 also shows that the calibration performance is most sensitive to the horizontal hydraulic conductivity and least sensitive to the confined storage coefficient and vertically hydraulic conductivity where increasing and decreasing the base value by an order of magnitude does not affect the performance of the groundwater system. With respect to diffuse recharge and fluxes along the boundaries, the performance is much more sensitive to increasing than to decreasing the calibrated settings and the performance is more sensitive to fluxes applied along the model domain than diffuse recharge.

Alternatively, a sensitivity coefficient is calculated for each test. This is done by first calculating the deviation of the RMS error from the base case and normalising by its base case. The resulting value is then divided by the factor of change in paramater value. With this calculation all sensitivity coefficients have the same units and can be compared (Table 8).

As already shown in Figure 30, Table 8 highlights that the calibration performance is most sensitive to horizontal hydraulic conductivity and fluxes along the boundary. The model is more sensitive to an increase than decrease in conductivity, and a decrease rather than an increase in flux compared to the preferred calibrated model indicated in those figures.

5 Scenarios

5.1 General

The main purpose of running scenarios was to assess the impact of groundwater abstraction on the aquifer system. To do this, two scenarios were run: in the first the pumping rate was set at 200% of that used for the calibrated model; in the second, the pumping was set at 0%. For the first scenario it was assumed that the increase in pumping was limited to existing bores only. For both scenarios all other parameters were the same as used for the calibrated model.

5.2 Water Balance

Figure 31 shows the overall water balance for each of the scenarios. For both scenarios the quantity of water entering from the flux boundaries and diffuse recharge remained approximately constant compared to the calibrated model (the differences being mainly due to numerical errors; in the case of "No Pumping" the diffuse recharge was slightly lower due to no irrigation return).

For the "Double Pumping" scenario the fluxes leaving the aquifer via the northern boundary and river were both reduced, while for the "No Pumping" scenario these fluxes were increased. This demonstrates how pumping intercepts water that would otherwise leave the catchment and be potentially used downstream.

5.3 Example Hydrographs

Shown in Figure 32 (a-c) are example hydrographs which illustrate spatial outcomes from the scenarios.

Bore 36004 is located adjacent to the Namoi River, bore 36094 approximately 2.4 km from the river and in an area where irrigation occurs, and bore 30237 is located remotely from the river, outside the irrigation zone and close to the model boundary.

In the case of bores 36004, 36094 and 30237 the main stressors on the system are, respectively, the varying head condition on the river (i.e. river interaction), the pumping/diffuse recharge, and the varying flux condition at the model boundary (i.e. mountain front recharge).

For all three locations, the "No Pumping" scenario resulted in hydrographs with higher heads compared to the "Base case" while the "Double Pumping" resulted in lower heads overall. The "Double Pumping" scenario resulted in greater seasonal drawdowns, particularly at bore 36094. Interestingly, the drawdowns modelled for this scenario more accurately reflect the measured data.

The "No Pumping" scenario shows the effect of climate on the aquifer system. At all three locations there is intra and inter year variability, due to climatically dependent variability in river stage, diffuse recharge, and boundary fluxes. At bore 36004 the effect of the river head is evident, while at bore 30237 the effect of the varying boundary flux is evident. At bore 36094, which is the most affected bore of the three for the "Double Pumping" scenario in terms of reduced heads and increased drawdowns, there is only minor variability (head of about 224 m AHD for entire period).

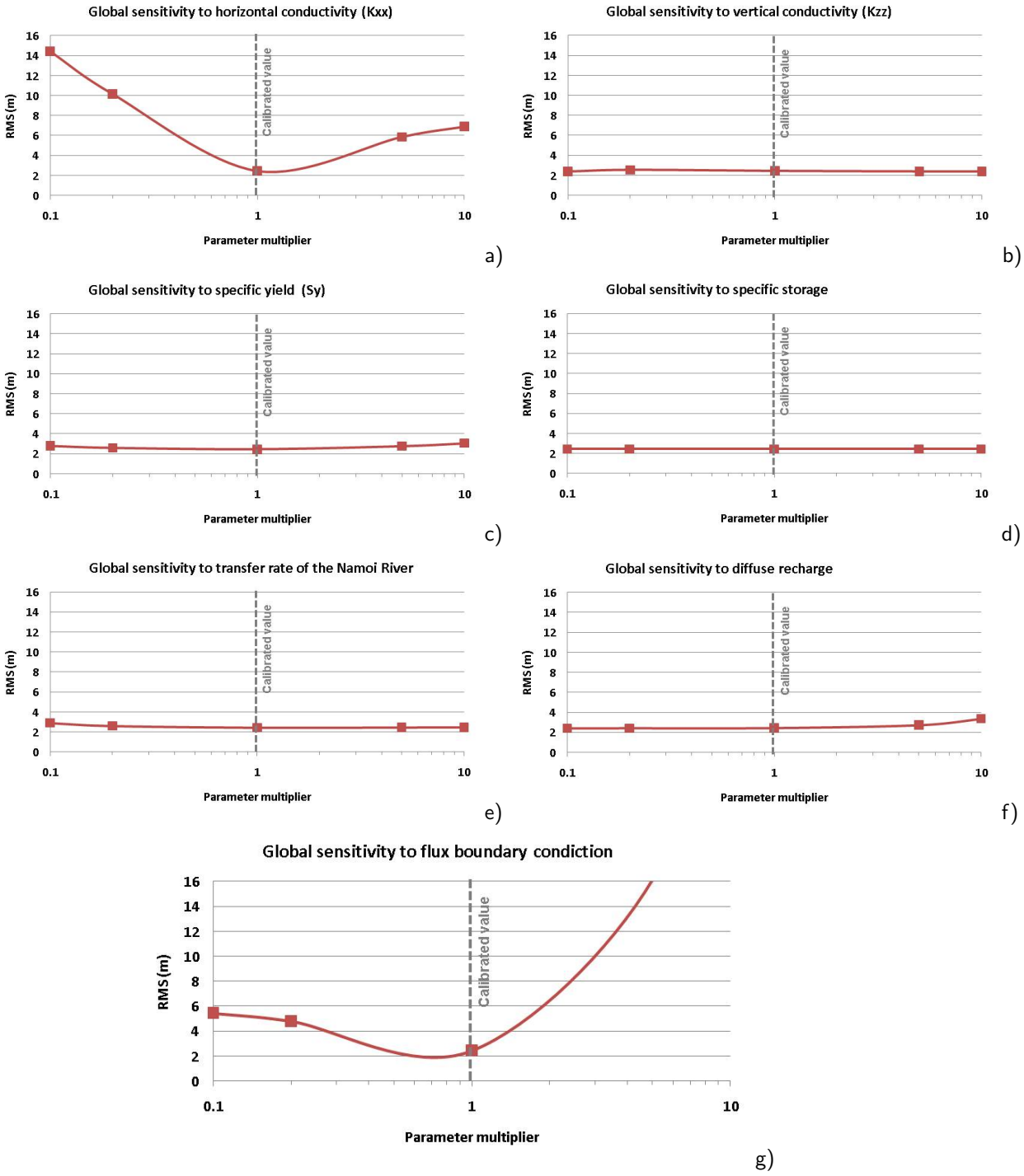

Figure 30: Curves showing the sensitivity analysis of the calibration performance indicator RMS of head residual (for the whole model domain over the whole period of simulation) to the parameters: (a) horizontal hydraulic conductivity; (b) vertical hydraulic conductivity; (c) specific yield; (d) specific storage; (e) transfer rate in and out; (f) diffuse recharge; (g) flux boundary conditions.

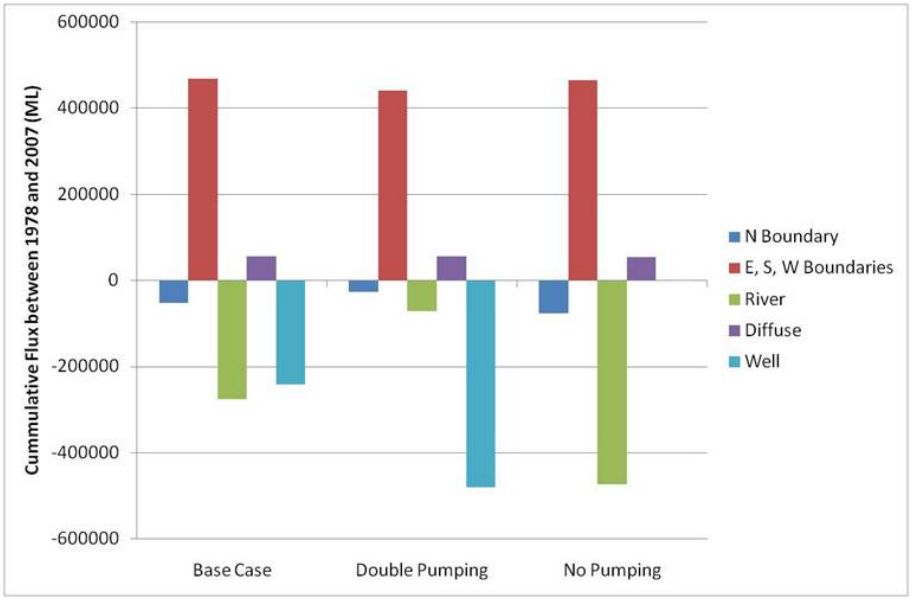

Figure 31: General water balance (positive = water gained by aquifer).

5.4 River-Aquifer Interaction

The sensitivity of the river-aquifer interaction to groundwater pumping is shown in Figure 33. For the "No Pumping" scenario there is a consistent upward trend meaning that the river gains water from the aquifer in general. For the "Base Case" this trend starts to level off after the introduction of pumping in the mid 1980s, while for the "Double Pumping" scenario this trend reverses direction in the early 1990s. At the end of the model scenario (i.e. April 2007) the flux to the river is diminished for the "Base Case" compared to the "No Pumping" scenario and greatly diminished for the "Double Pumping" scenario.

It should be noted that the model is not truly dynamically coupled since the change in flux to/from the stream does not result in a change in stream stage and hence change the flux. See recommendations on this aspect in Section 6.2.

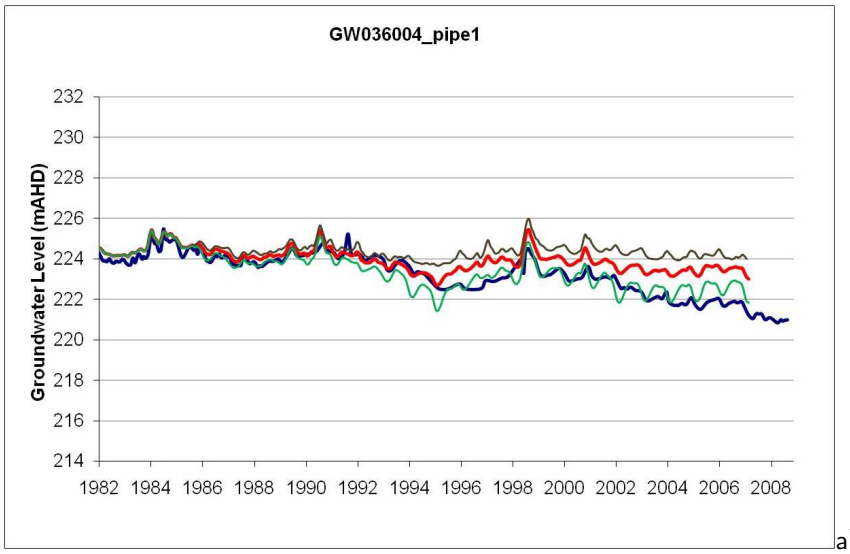

a)

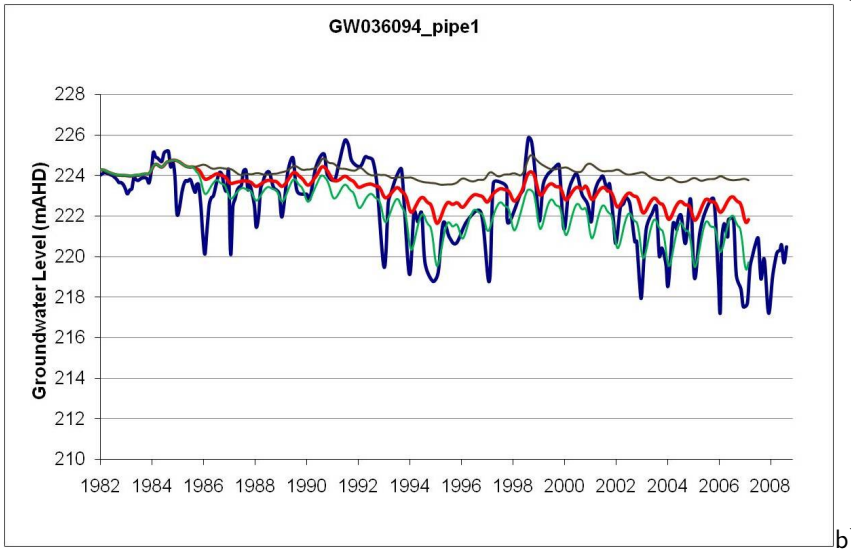

b)

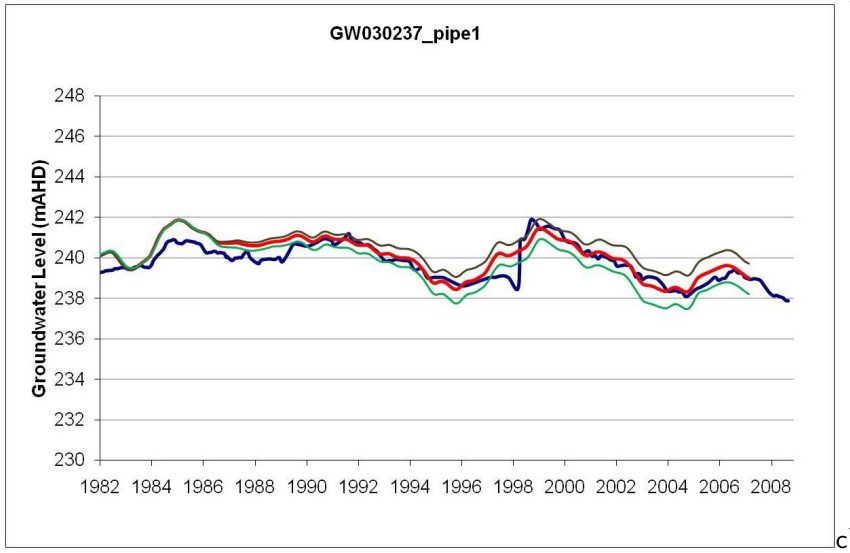

c)

Figure 32: Examples of modelled and measured hydrographs for each scenario (Key: Brown – No Pumping; Red – Base Case; Green – Double Pumping; Blue – Measured Heads).

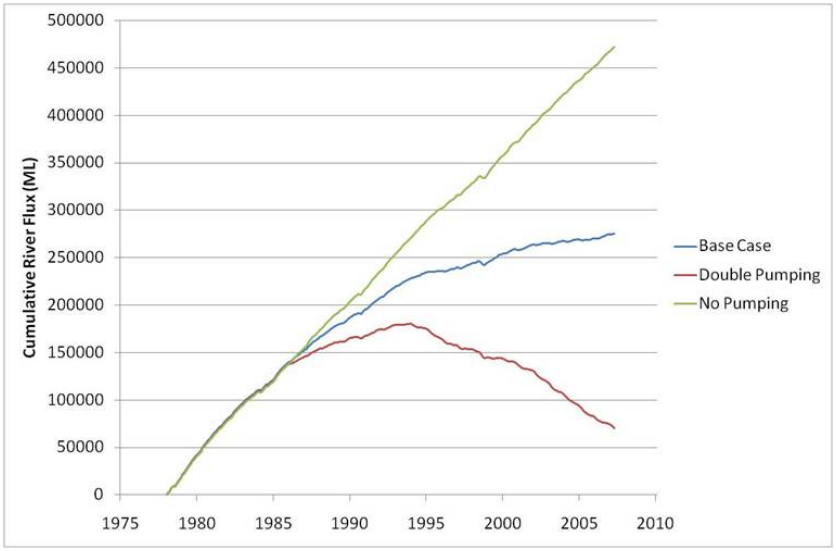

Figure 33: Cumulative river flux versus time (note: positive slope indicates water gained by river).

6 Conclusions and Recommendations

6.1 Conclusions

The main objectives of this study were to provide a better understanding of the dynamics of the alluvial aquifer in the Maules Creek Catchment and to provide an integrated modelling approach of the catchment water resources, including the simulation and assessment of pumping. From the model the following can be concluded.

A well calibrated model was obtained. As demonstrated statistically in Section 4 and Appendix 5A, the model is generally well calibrated with the model correctly capturing the recovered water levels after each irrigation season, as well as the long-term trends shown in the measured hydrographs. However, in areas where the groundwater abstraction-induced drawdown is large (up to 8-10 m) the seasonal dynamic is not captured well by the model. The calibration is based on all available boreholes, which is in contrast to previous modelling done for the area. However, this may mean that it is better calibrated in some areas, but poorly in other areas.

It should also be remembered though that model calibration is not necessarily unique: many different possible sets of model inputs can produce nearly identical modelled aquifer head distribution for a given model (MDBC, 2001). The calibration is less reliable in the eastern part of the model domain due to a lack of data. In order to reduce the mismatch between measured and modelled hydraulic heads in this area of the model domain see the following recommendations (Section 6.2).

General dynamics of the aquifer system are captured by the model. All components of the hydrological cycle were included in the model which attempts to model the transient conditions for three decades. This has led to a better understanding of how the components are interrelated and which are the main drivers of the system. For example, the Namoi River acts as a sink of water and controls the flow of water from east to west; this flux is much greater than that from south to north.

Groundwater pumping affects the aquifer system. As shown by the scenarios, groundwater abstraction for irrigation and other purposes impacts on the hydrological system in at least two ways. First, hydraulic heads are decreasing over time. This has implications for the sustainability of the water resource. Under the current climatic conditions, the current rate of pumping is dewatering the aquifer. Second, the river-aquifer interaction is effected by groundwater abstraction. In the no-pumping scenario the river gains water from the aquifer overall with some variation due to climatic variations. As the pumping rate is increased the river eventually becomes losing. Initially the losing conditions are only occurring during the irrigation seasons, but eventually the losing conditions will occur most of the time. This has implications for groundwater dependent ecosystems and for water resource management: connections between surface and ground water must be accounted for. Water consumed within the Maules Creek Catchment is not available for downstream users or the aquatic environment.

The use of daily soil moisture water balance calculation has been a useful way of determining the diffuse recharge. The soil moisture balance was based on a FAO version of the Penman-Monteith equation. This allowed for a more detailed calculations of the soil moisture balance (and hence recharge) than has been done in previous groundwater models for the same region. However, this calculation appears to be a factor of 5 too large as compared to diffuse recharge used in the calibrated model and is perhaps the cause of the apparent over-estimation of input fluxes for the post 2000 drought period. This indicates systematic errors and a potential lack of fundamental process understanding for the catchment. See recommendations in the following Section 6.2.

The calculation of the fluxes entering from outside the groundwater model domain but inside the surface water catchment is critical to the accurate modelling of the aquifer system. External fluxes and diffuse recharge were calculated by using climatic data in a daily soil moisture balance calculation. This allowed for the determination of time varying boundary fluxes, including orographic effects on rainfall caused by the mountain range. The largest uncertainty in the model is associated with these fluxes. The choice of appropriate coefficients in the water balance calculation, such as crop coefficient, land use and type of soil, influences significantly the diffuse recharge as a percentage of rainfall and thus the amount of recharge coming from the sub-catchments into the model domain.

The 3D geological model is a good foundation for the groundwater model. A significant difference in the approach used in this model compared with common modelling approaches for this region was the distribution of hydraulic conductivity. A more realistic hydraulic conductivity derived from the stratigraphic data as a function of three-dimensional geological modelling was used successfully.

In an heterogeneous alluvial aquifer a geology based on 3D hydraulic conductivity distribution permits a more realistic representation of the groundwater flow system. The general multilayered model conceptualisation of the alluvial aquifer previously used for the Maules Creek Catchment has been replaced by a distribution that better represents the heterogeneity of the unconsolidated aquifer. Notwithstanding the sophistication of the geological model, it was still necessary to adjust the conductivities around the creeks and in the upper clay zone to allow for water from the boundaries and upper surface to enter the model domain.

Representation of river-aquifer interaction by modelling. The transient nature of the coupling between the aquifer and water levels in the Namoi River was achieved in this model, including the effects of groudnwater abstraction on baseflow to the river. Further work is yet to be carried out on the implementation of streams in the model (see Section 6.2).

6.2 Recommendations

Groundwater models are an important tool in the understanding of complex groundwater systems. However, reasonable modelling results are dependent on appropriate data input and due consideration of model limitations and assumptions. The model presented in this report has been useful for understanding the alluvial aquifer system in the Maules Creek Catchment. It has also raised awareness of certain limitations and gaps in data and process understanding. To address these issues the following are recommended as future tasks which should be undertaken.

Continue to monitor groundwater levels. The groundwater model was calibrated against historical water level measurements. The move towards more frequent and telemetered monitoring should be encouraged. This will allow for a better temporal resolution of the aquifer response to stresses such as recharge by floods and pumping. The current monitoring rate of 3 or 4 times per year is insufficient for analysing these processes. Additional considerations for monitoring is that the groundwater monitoring boreholes are ageing. In time these will need to be replaced. Planning for the maintenance and/or replacement of the bores should be considered by government agencies. In some areas there is a need for additional new boreholes to be drilled. This is particularly the case in the area to the east of Elfin Crossing as well as in the region near the northern boundary.

Continue to monitor surface water levels/fluxes. Similar to the situation with groundwater levels, data on surface water level and flow are important for calibration of the model and should continue to be collected. Currently the stage vs flow curves are not well calibrated for high flows and stages. This has implications for the estimation of flood recharge.

Continue to monitor groundwater and surface water abstractions. The pumping scenarios (Section 5) demonstrated the sensitivity of the groundwater baseflow to the groundwater abstraction rate. To properly define this relationship and make quantitative conclusions regarding the surface water or

groundwater resources, it is important therefore that the abstractions are accurately recorded now and into the future. More detailed information is required about the crops planted, pumping rates at the irrigation bores, and irrigation days; including how much of the irrigation water is sourced from groundwater and how much is extracted from the river.

Determine the impact of the geological model uncertainty on the groundwater model output. It is recommended that the impact of the geological uncertainty be determined. This could be done by running the current base case parameters with a series of different geological models each based on different interpolation techniques including categorical, geostatistical and deterministic algorithms and quantifying which method returns a better calibration performance. Another way to improve the calibration will be increasing the number of layers in the 3D layer configuration in order to refine the vertical discretisation and better represent heterogeneity of the system, specifically the semicontinous confining layers which are present in reality. However, this will significally increase the computation time. Changing hydraulic conductivity locally will improve the match between modelled and measured values in those areas where the calibration is poor (i.e. eastern part of the model domain). However this procedure performed by a trial-and-error method would be very time-consuming and it could be automated using inverse estimation software (PEST). Extensive guidelines for automated calibration on a zonal basis or using pilot points have been developed by Hill (1998), Doherty (2004) and Knapton et al. (2009).

Address the non-uniqueness problem with additional data. As outlined in Section 4.2.3 above, all models have issues with non-uniqueness. This has been addressed in a variety of ways as previously described. An additional method would be to use field data describing the water residence times (based on Carbon 14 and tritium dating of the groundwater) and compare that to the modelled residence times to constrain flow rates along modelled pathlines and modify the aquifer parameters and boundary fluxes accordingly.

Better conceptualise the surface water groundwater interaction. The current river-aquifer interaction in the model is not a proper dynamic mass balance since the river is treated as an infinite source or sink (i.e. reduced baseflow does not lead to reduced riverflow and thus river heads). A coupled approach using Mike 11 linked to FEFLOW would overcome this limitation and perhaps improve the calibration. Further, as the Namoi River is regulated there are periods during which the reach within Maules Creek Catchment is in reality dry. Presently this is modelled as the water level being at the base of the river bed elevation. As the river boundary is defined as a transfer boundary between the first and second slices and the heads are defined on the first slice, this means that the river becomes an infinite source of water even when it is actually dry. Also, during large floods significant overbank flow does occur. In reality part of this water could infiltrate the flood plain and become recharge to the shallow aquifer. This is not modelled with the current model set-up. Finally, preliminary field data indicate that the transfer hydraulic conductivity is not a constant in time: clogging (or colmation) will occur during long period of low flow (i.e. reducing hydraulic conductivity), whereas floods can scour the streambed and remove the colmation layer and increase the hydraulic conductivity in the period that follows. Consequently, a way of allowing a variable river bed hydraulic conductivity may have to be implemented.

Better assess mountain front recharge. It has been demonstrated that one of the two most sensitive parameters is the flux at the boundaries from mountainous hard rock areas. There is a scarcity of literature relating to the best way of modelling alluvial aquifers in a larger catchment where there are large volumes of water from mountain front runoff/infiltration. More importantly there is a real need for the quantification of these processes and their resulting fluxes in the field.

Better understanding and hence modelling of the hydrological processes east of Elfin Crossing. At discussed above, the model domain extended just to the east of Elfin Crossing although the alluvial aquifer extends further eastwards. How this section of the aquifer works is not well understood. From a surface and ground water interaction point of view it is highly significant: the large eastern catchment means that large fluxes pass through this boundary, and the constriction at the boundary means that in reality the groundwater becomes surface water flow at Elfin Crossing only to return as groundwater recharge further downstream in Maules Creek. How the rainfall, runoff, infiltration, groundwater flux and surface water flux relate in this section of the catchment needs to be understood before it can be appropriately modelled. Again, there is a need for field investigations to provide this information.

7 Acknowledgements

The authors would like to thank the Australian Government National Water Commission and the Cotton Catchment Communities CRC for their financial support.

References

Allen, R., Pereira, L., Raes, D., Smith, M., 1998. Crop evapotranspiration guidelines for computing crop water requirement. FAO Irrigation and Drainage, Rome, Italy, paper no.56.

Andersen, M., Acworth, R., 2009. Stream-aquifer interactions in the Maules Creek Catchment, Namoi Valley, New South Wales, Australia. Hydrogeology Journal 17, DOI 10.1007/s10040–009–0500–9.

Anderson, M., Woessner, W., 1992. Applied Groundwater Modeling. Academic Press, San Diego.

Bowling, A., 2009. A 3D spatial and temporal analysis of groundwater hydrographs in the Mooki Catchment, NSW, Australia. B. Sc. Honours Thesis.

Collis-George, N., 1997. Infiltration equation for simple soil systems. Water Resources Research 13, 395–403.

CSIRO, 2007. Water availability in the Namoi - A report to the Australian Government from the CSIRO Murray-Darling Basin Sustainable Yield Project. Tech. rep.

Diersch, H., 2005. FEFLOW - Finite Element Subsurface Flow and Transport Simulation System. URL `http://www.feflow.info/manuals.html`

Diersch, H., 2007. Error norms used in feflow. FEFLOW - Finite Element Subsurface Flow & Transport Simulation System, White Papers 1, 117–119.
URL `http://www.feflow.info/manuals.html`

DNR, 2006. Upper Namoi groundwater flow model - Groundwater Management Area 004; Zones 2, 3, 4, 5, 11 and 12. Tech. rep., Department of Natural Resources, NSW Government.

Doherty, J., 2004. PEST Model-Independent Parameter Estimation User Manual: 5th Edition. Watermark numerical computing Edition.

Fetter, C., 2001. Applied Hydrogeology (4th Edition). Prentice Hall.

Freeze, R., Cherry, J., 1979. Groundwater. Prentice-Hall.

Gates, G., 1980. The hydrogeology of the unconsolidated sediments in the Mooki Valley, New South Wales. Master's thesis, The University of New South Wales.

Giambastiani, B., Kelly, B., 2009. Importing and separating a Digital Elevation Model (DEM) for near surface geological models in EarthVision. School of Biological, Earth and Environmental Sciences, University of New South Wales.
URL `http://www.connectedwaters.unsw.edu.au/`

Giambastiani, B., McCallum, A., Andersen, M., Kelly, B., Acworth, R., 2009. Maules Creek project: Steady-state groundwater model, Water Research Laboratory, School of Civil and Environmental Engineering, University of New South Wales.

Hill, M., 1998. Methods and guidelines for effective model calibration. Water-resources investigations report 98-4005, USGS.

Kelly, B., Merrick, N., Dent, B., Milne-Home, W., Yates, D., 2006. A scoping study on groundwater knowledge and gaps in the Namoi Catchment Management Area. National Center for Groundwater Management Report, NCGM, Cotton Catchment Communities CRC, University of Technology, Sydney, 77 pages.

Knapton, A., Cox, G., MacHunter, S., Szylkarski, S., 2009. Two case studies of the development and implementation of integrated river - groundwater models in the top end of Australia. In: FEFLOW User Conference 2009.

Lavitt, N., 1999. Integrated approach to geology, hydrogeology and hydrochemistry in the Lower Mooki River Catchment. Ph.D. thesis, The University of New South Wales.

McCallum, A., Andersen, M., Bryce, B., Giambastiani, B., Acworth, R., 2009. Hydrologic investigations of surface water groundwater interactions in a sub-catchment in the Namoi Valley, NSW, Australia. In: Publ., I. (Ed.), Trends and Sustainability of Groundwater in Highly Stressed Aquifer. Proc. of Symposium JS.2 at the Joint IAHS & IAH Convention, Hyderabad, India, September 2009. Vol. 329.

McDonald, M., Harbaugh, A., 1998. A modular three-dimensional finite-difference ground-water flow model. In: USGS Techniques of Water Resources Investigations. Book 6. Ch. A1, p. 586.

McKay, L., Cherry, J., Gilham, R., 1993. Field experiments in a fractures clay till . Hydraulic conductivity and fracture aperture. Water Resources Research 29, Issue 4, 1149–1162.

MDBC, January 2001. Groundwater flow modelling guideline. Technical report, Murray-Darling Basin Commission, Aquaterra Consulting Pty Ltd.
URL http://www2.mdbc.gov.au/__data/page/127/model_guide.pdf

NSWDMR, 2002. Geology - integration and upgrade. NSW Western Regional Assessments - Brigalow Belt South Bioregion (stage 2). Geological Survey of New South Wales., NSW Department of Mineral Resources, 156 pp.

NSWG, 2007. Historic data cd PINNEENA for groundwater works.
URL http://waterinfo.nsw.gov.au/pinneena/gw.shtml

Ritchey, J., Rumbaugh, J., 1996. Subsurface fluid flow (ground-water and vadose zone) modeling. ASTM Special Technical Publication 1288.

Rushton, K., 2005. Groundwater Hydrology. Wiley.
URL http://www3.interscience.wiley.com/cgi-bin/bookhome/112094150/

Shewchuk, J., 1996. Triangle: Engineering a 2D Quality Mesh Generator and Delaunay Triangulator. In: Lin, M. C., Manocha, D. (Eds.), Applied Computational Geometry: Towards Geometric Engineering. Vol. 1148 of Lecture Notes in Computer Science. Springer-Berlin, pp. 203–222.

Shewchuk, J., 2002. Delaunay Refinement for Triangular Mesh Generation. Computational Geometry: Theory and Applications 22 (1-3), 21–27.

Sinclair, P., Barrett, C., Williams, R., 2005. Impact of groundwater extraction on Maules Creek: Upper Namoi Valley, NSW, Australia. In: Acworth, R., Merrick, N., Macky, G. (Eds.), Where water meet. Proceedings of the NZHS-IAH-NZSSS 2005 Conference, Auckland, 29 November - 1 December 2005.

Tartakovsky, D., Wohlberg, B., Guadagnini, A., 2007. Nearest-neighbor classification for facies delineation. Water Resources Research 43(7), DOI 10.1029/2007WR005968.

The, C., 2008. A 3D spatial and temporal analysis of bore hydrograph data in the Lower Namoi Catchment. B. Sc. Honours Thesis.

Vervoot, R., Cattle, S., Minasny, B., 2003. The hydrology of Vertosols used for cotton production: Hydraulic, structural and fundamental soil properties. Australian Journal of Soil Research 41, 1255–1272.

William, R., 1986. The Cainozoic geology, hydrogeology and hydrochemistry of the unconsolidated sediments associated with the Namoi River in the Lower Namoi Valley, NSW. Hydrogeology report 1986/4, Department of Water Resources.

Young, R., Young, A., Price, D., Wray, R., 2002. Geomorphology of the Namoi alluvial plain, northwestern New South Wales. Australian Journal of Earth Sciences 49, 509–523.

Zheng, C., Bennett, G., 1995. Applied Contaminant Transport Modeling - Theory and Practice. ITP, p. 440.

Appendix 5A - Modelled and Measured Hydrographs

Modelled and measured hydrographs for observation boreholes in the model domain. In the graphs the blue line is the measured water level in the monitoring bore and the red line the water level simulated by the FEFLOW model.

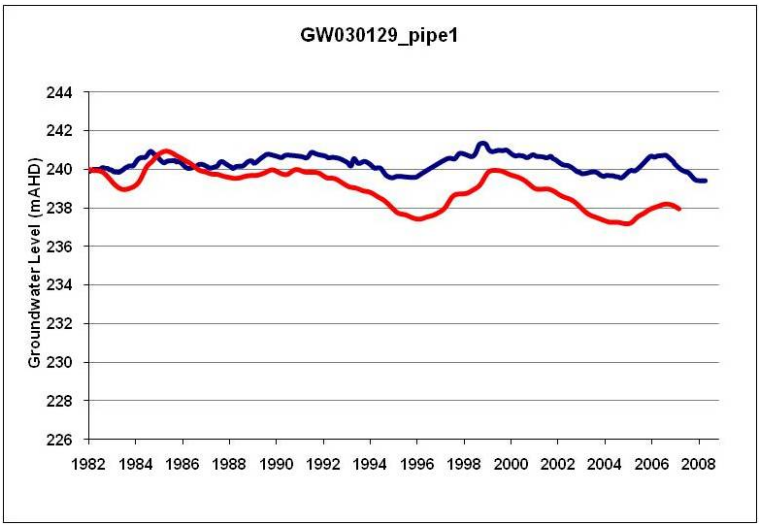

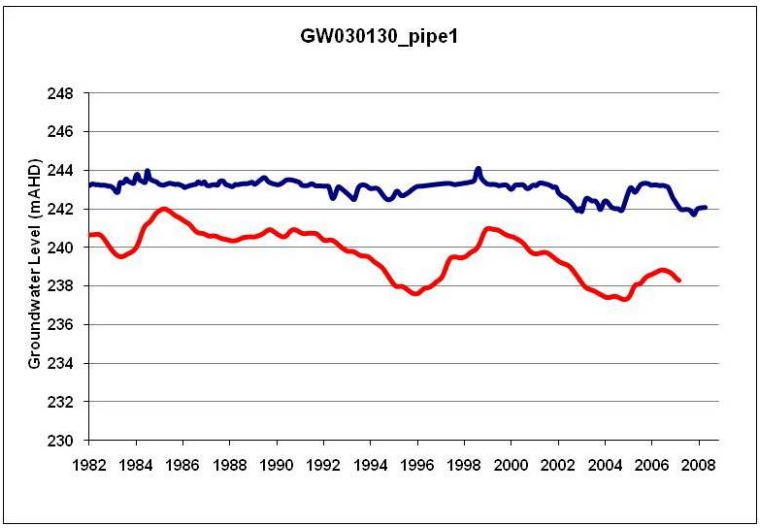

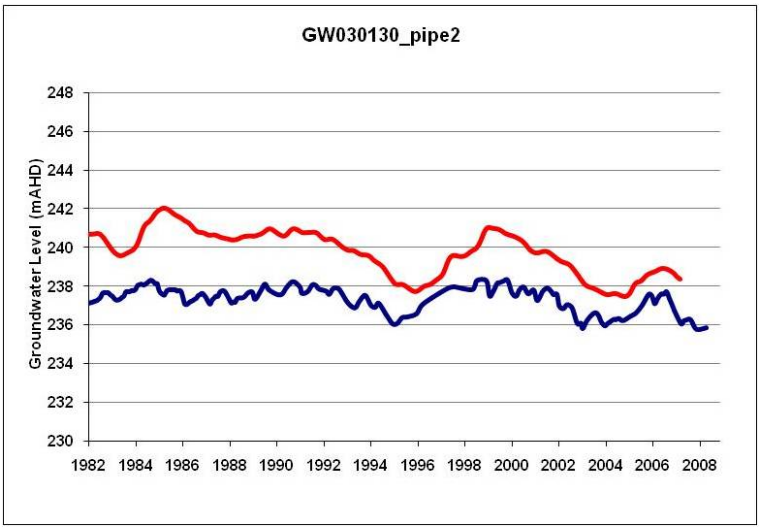

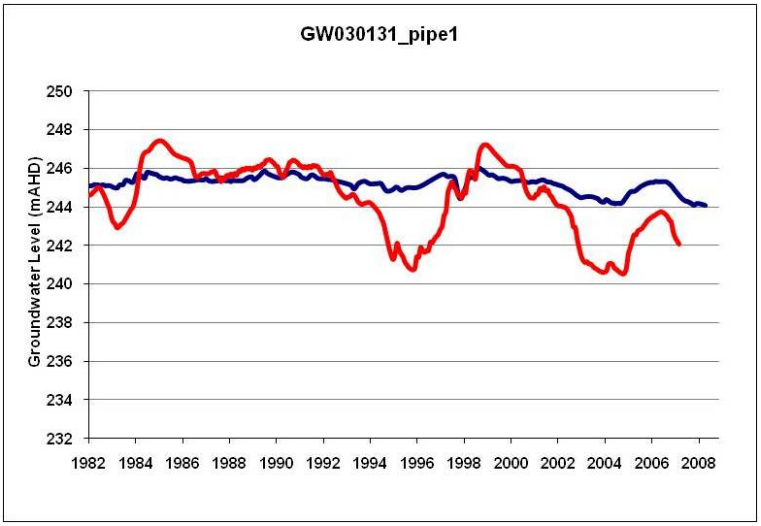
GW030131_pipe1
Groundwater Level (mAHD)
250
248
246
244
242
240
238
236
234
232
1982 1984 1986 1988 1990 1992 1994 1996 1998 2000 2002 2004 2006 2008

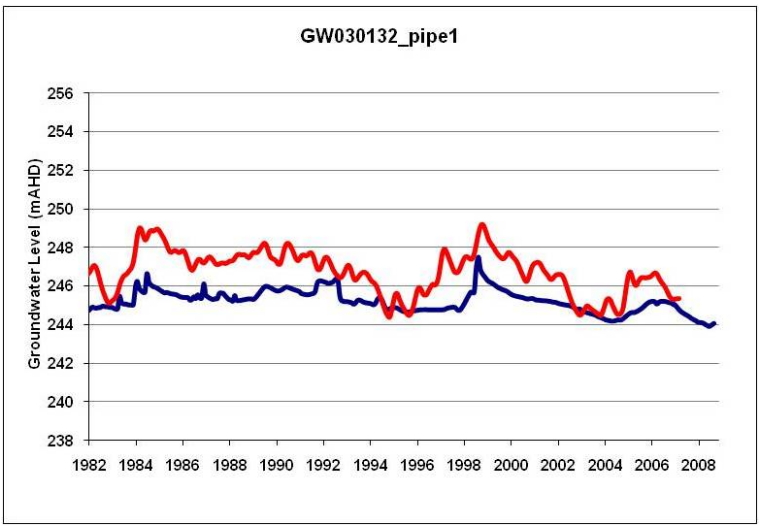
GW030132_pipe1
Groundwater Level (mAHD)
256
254
252
250
248
246
244
242
240
238
1982 1984 1986 1988 1990 1992 1994 1996 1998 2000 2002 2004 2006 2008

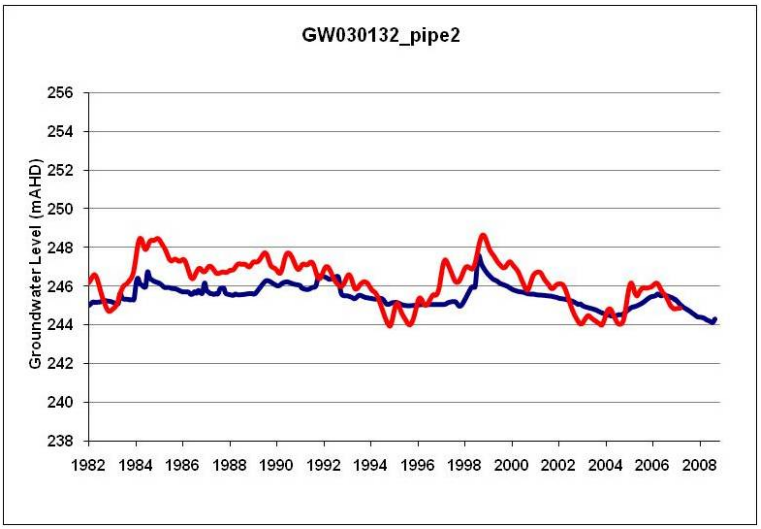
GW030132_pipe2
Groundwater Level (mAHD)
256
254
252
250
248
246
244
242
240
238
1982 1984 1986 1988 1990 1992 1994 1996 1998 2000 2002 2004 2006 2008

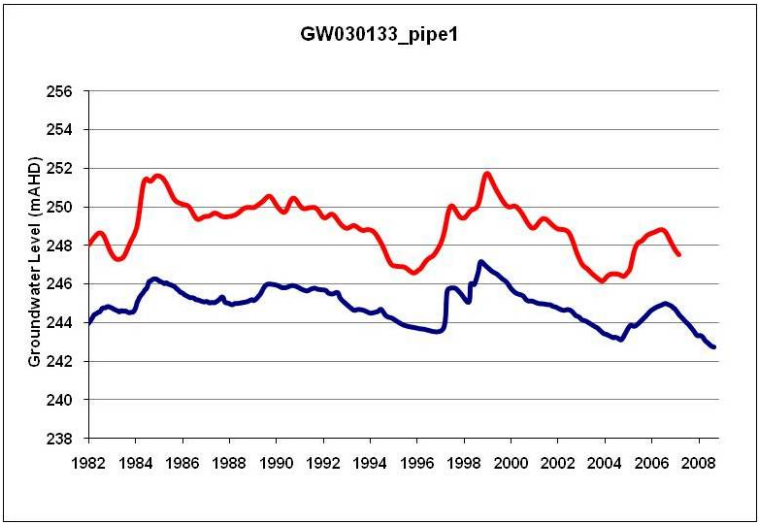
GW030133_pipe1
Groundwater Level (mAHD)
256
254
252
250
248
246
244
242
240
238
1982 1984 1986 1988 1990 1992 1994 1996 1998 2000 2002 2004 2006 2008

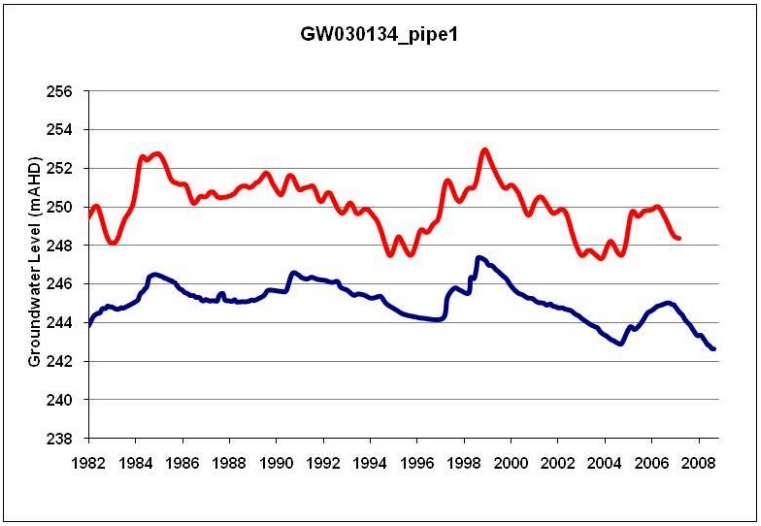
GW030134_pipe1
Groundwater Level (mAHD)
256
254
252
250
248
246
244
242
240
238
1982 1984 1986 1988 1990 1992 1994 1996 1998 2000 2002 2004 2006 2008

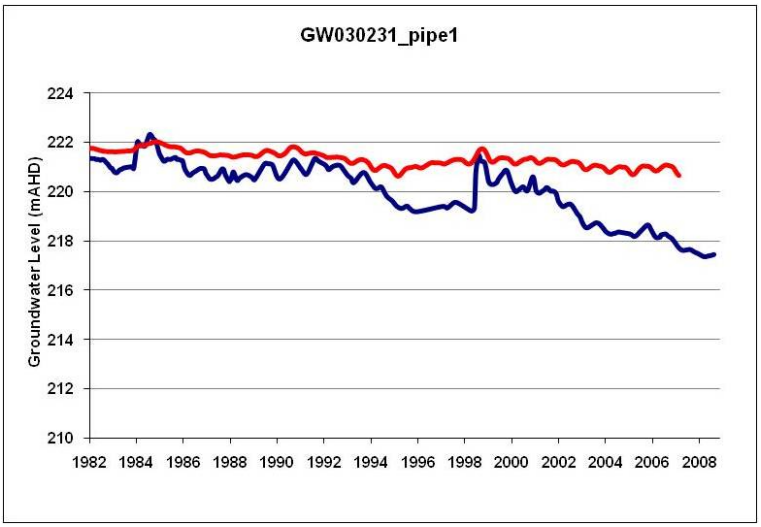
GW030231_pipe1
Groundwater Level (mAHD)
224
222
220
218
216
214
212
210
1982 1984 1986 1988 1990 1992 1994 1996 1998 2000 2002 2004 2006 2008

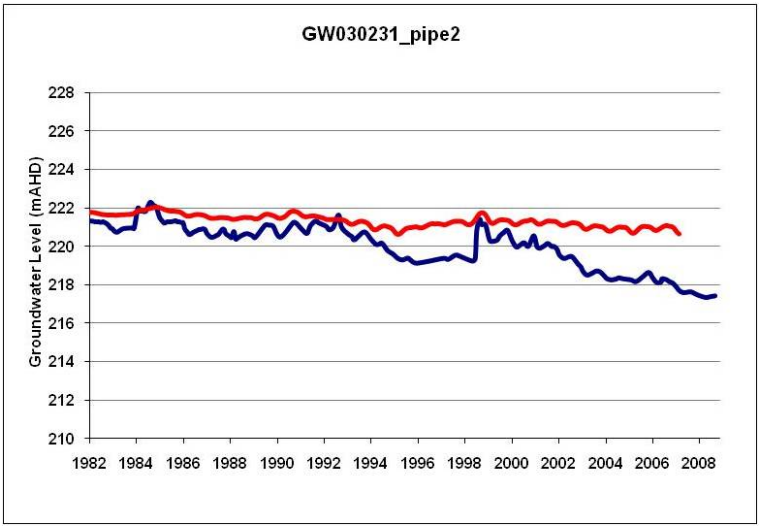
GW030231_pipe2
Groundwater Level (mAHD)
228
226
224
222
220
218
216
214
212
210
1982 1984 1986 1988 1990 1992 1994 1996 1998 2000 2002 2004 2006 2008

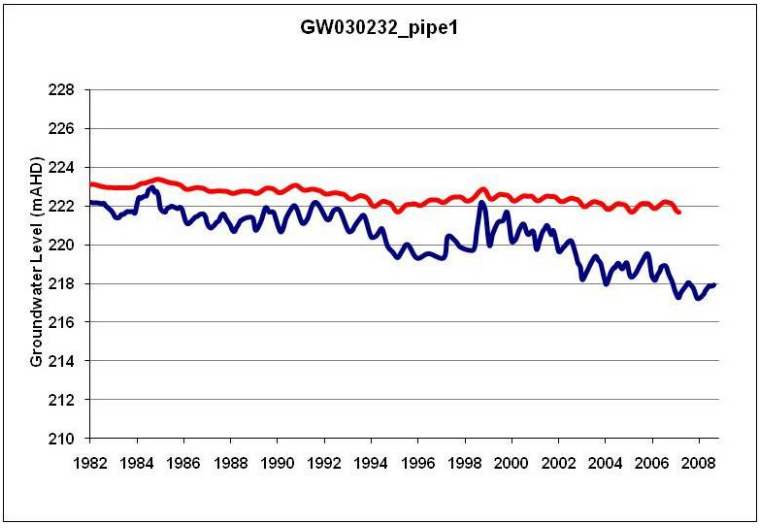
GW030232_pipe1
Groundwater Level (mAHD)
228
226
224
222
220
218
216
214
212
210
1982 1984 1986 1988 1990 1992 1994 1996 1998 2000 2002 2004 2006 2008

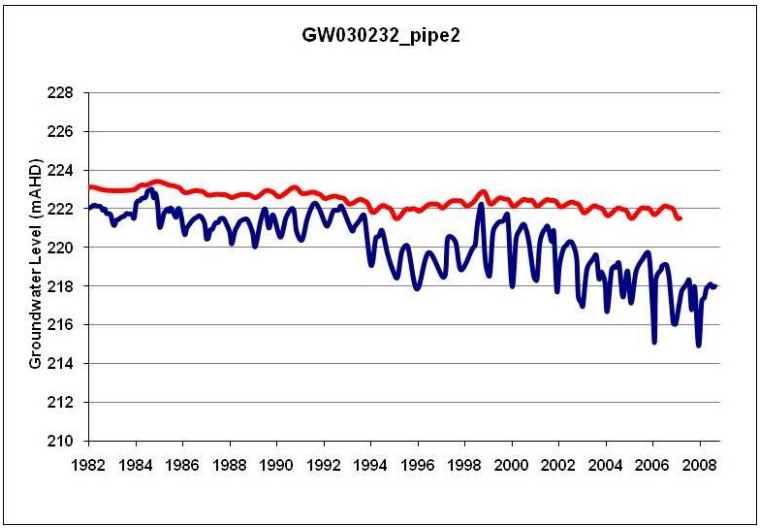
GW030232_pipe2
Groundwater Level (mAHD)
228
226
224
222
220
218
216
214
212
210
1982 1984 1986 1988 1990 1992 1994 1996 1998 2000 2002 2004 2006 2008

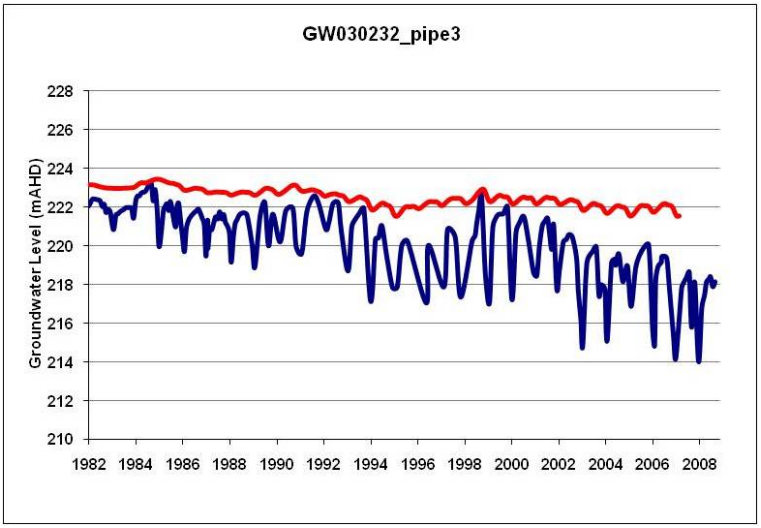
GW030232_pipe3
Groundwater Level (mAHD)
228
226
224
222
220
218
216
214
212
210
1982 1984 1986 1988 1990 1992 1994 1996 1998 2000 2002 2004 2006 2008

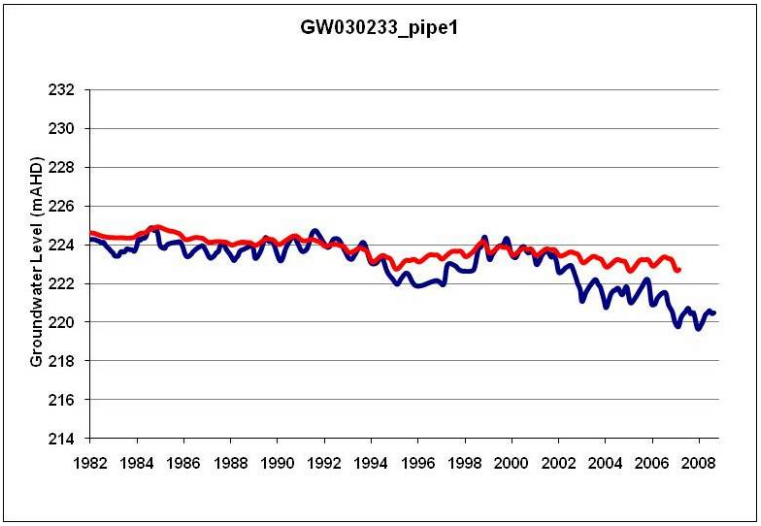
GW030233_pipe1
Groundwater Level (mAHD)
232
230
228
226
224
222
220
218
216
214
1982 1984 1986 1988 1990 1992 1994 1996 1998 2000 2002 2004 2006 2008

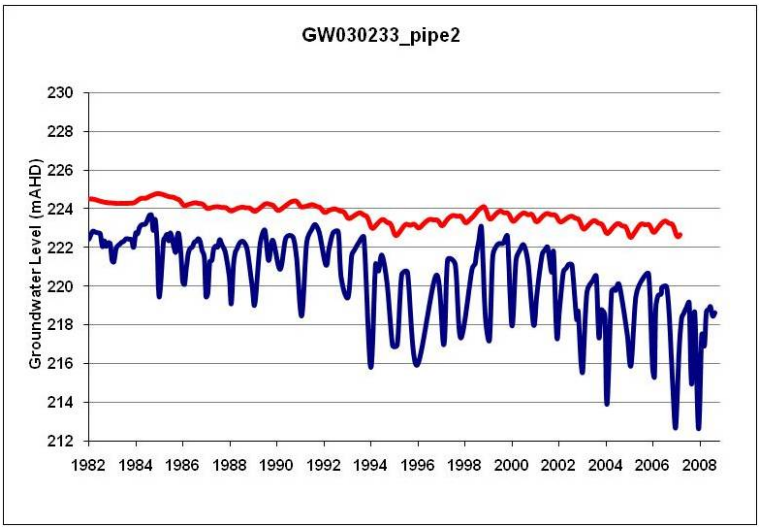
GW030233_pipe2
Groundwater Level (mAHD)
230
228
226
224
222
220
218
216
214
212
1982 1984 1986 1988 1990 1992 1994 1996 1998 2000 2002 2004 2006 2008

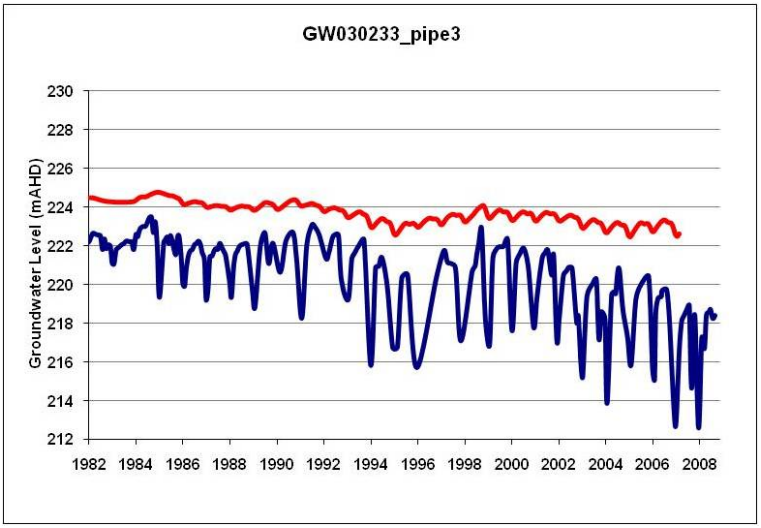
GW030233_pipe3
Groundwater Level (mAHD)
230
228
226
224
222
220
218
216
214
212
1982 1984 1986 1988 1990 1992 1994 1996 1998 2000 2002 2004 2006 2008

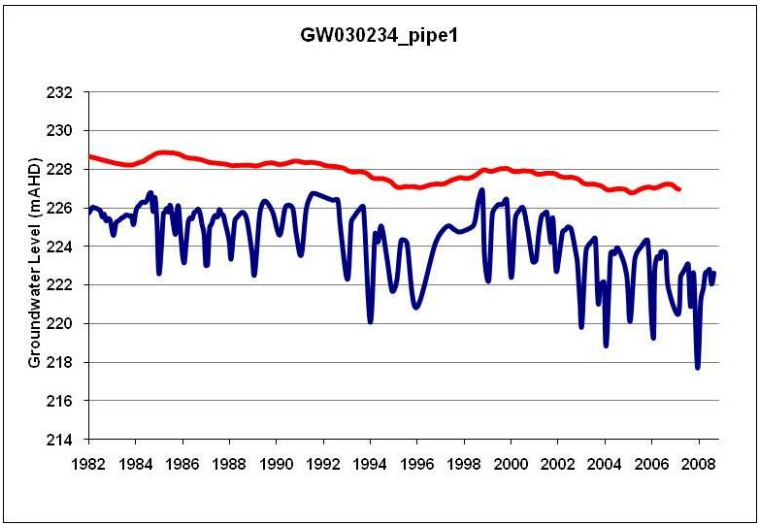
GW030234_pipe1
Groundwater Level (mAHD)
232
230
228
226
224
222
220
218
216
214
1982 1984 1986 1988 1990 1992 1994 1996 1998 2000 2002 2004 2006 2008

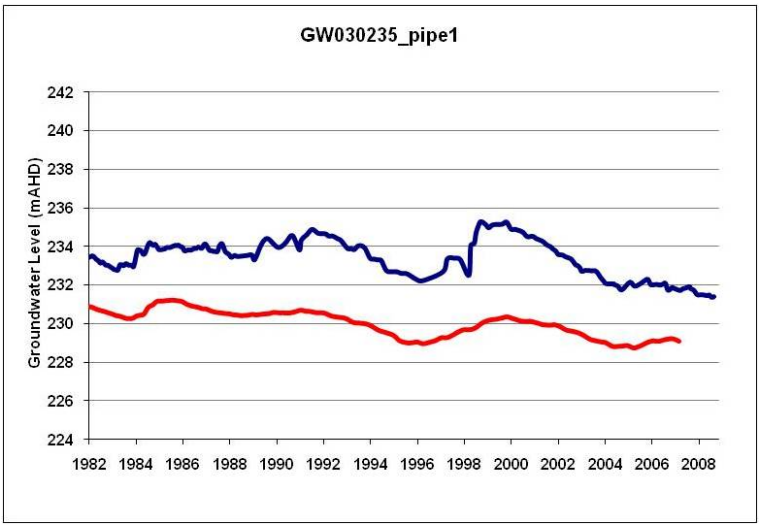
GW030235_pipe1
Groundwater Level (mAHD)
242
240
238
236
234
232
230
228
226
224
1982 1984 1986 1988 1990 1992 1994 1996 1998 2000 2002 2004 2006 2008

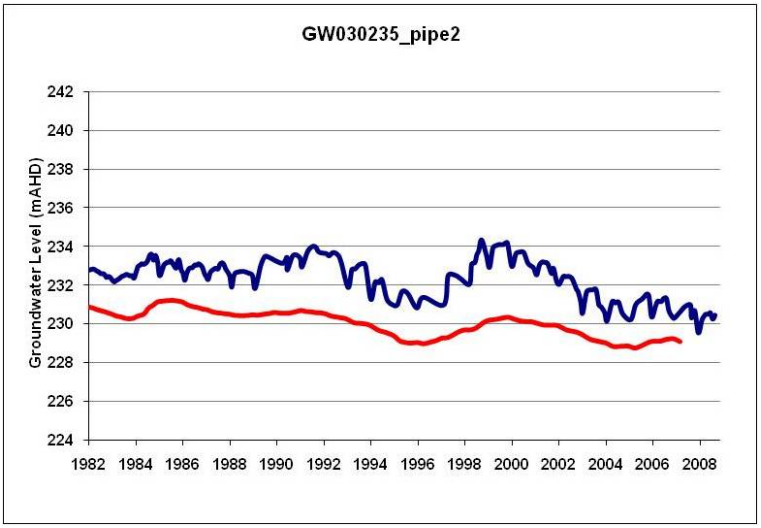
GW030235_pipe2
Groundwater Level (mAHD)
242
240
238
236
234
232
230
228
226
224
1982 1984 1986 1988 1990 1992 1994 1996 1998 2000 2002 2004 2006 2008

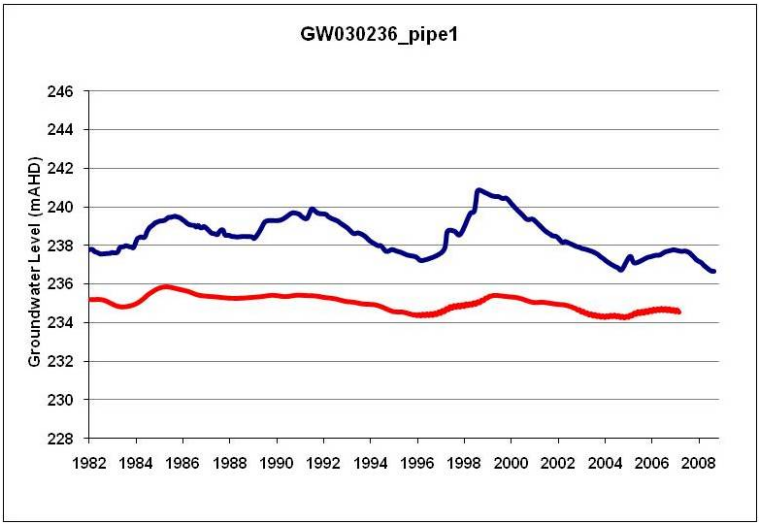
GW030236_pipe1
Groundwater Level (mAHD)
246
244
242
240
238
236
234
232
230
228
1982 1984 1986 1988 1990 1992 1994 1996 1998 2000 2002 2004 2006 2008

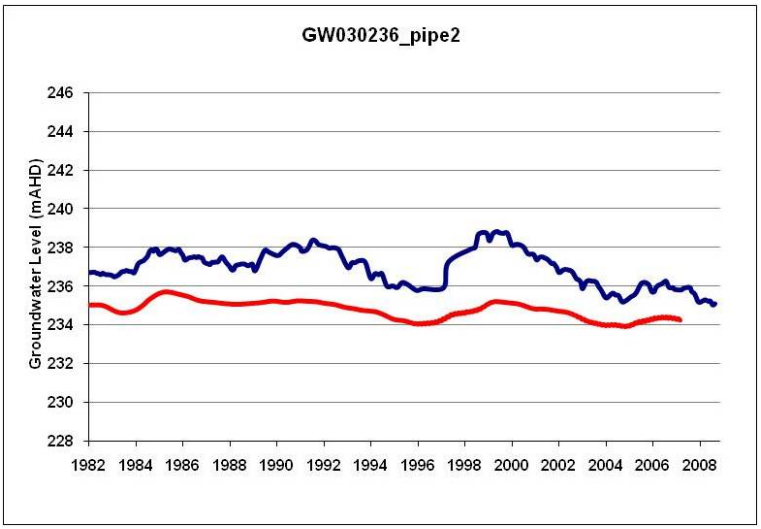
GW030236_pipe2
Groundwater Level (mAHD)
246
244
242
240
238
236
234
232
230
228
1982 1984 1986 1988 1990 1992 1994 1996 1998 2000 2002 2004 2006 2008

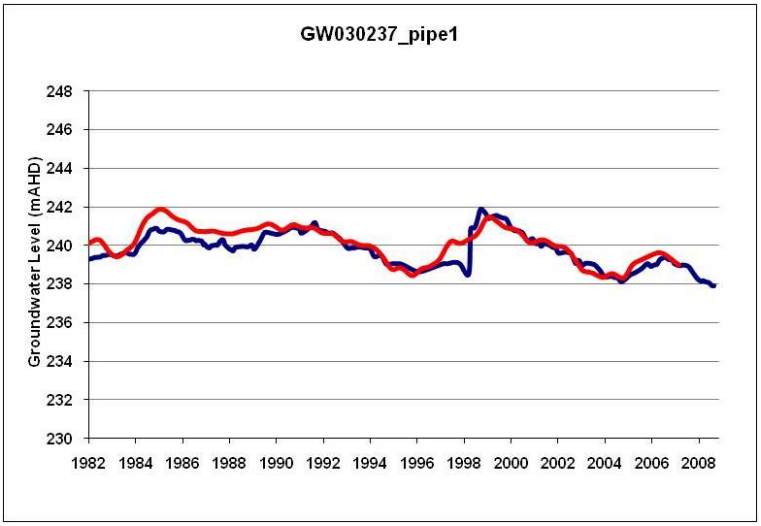
GW030237_pipe1
Groundwater Level (mAHD)
248
246
244
242
240
238
236
234
232
230
1982 1984 1986 1988 1990 1992 1994 1996 1998 2000 2002 2004 2006 2008

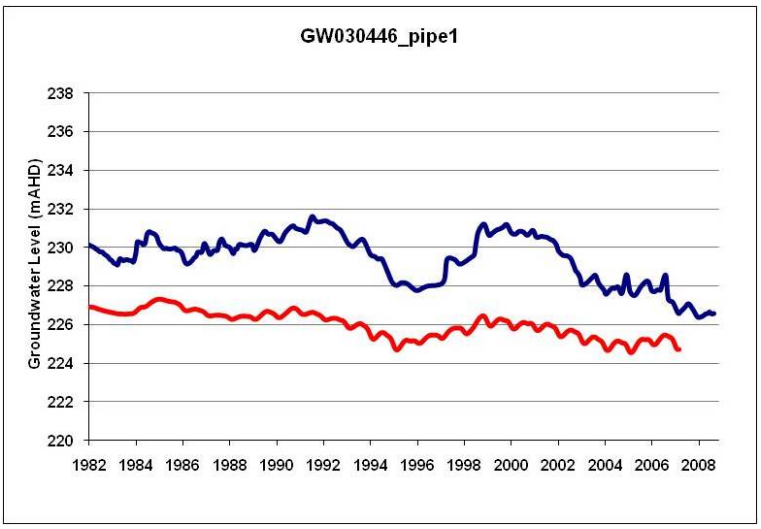
GW030446_pipe1
Groundwater Level (mAHD)
238
236
234
232
230
228
226
224
222
220
1982 1984 1986 1988 1990 1992 1994 1996 1998 2000 2002 2004 2006 2008

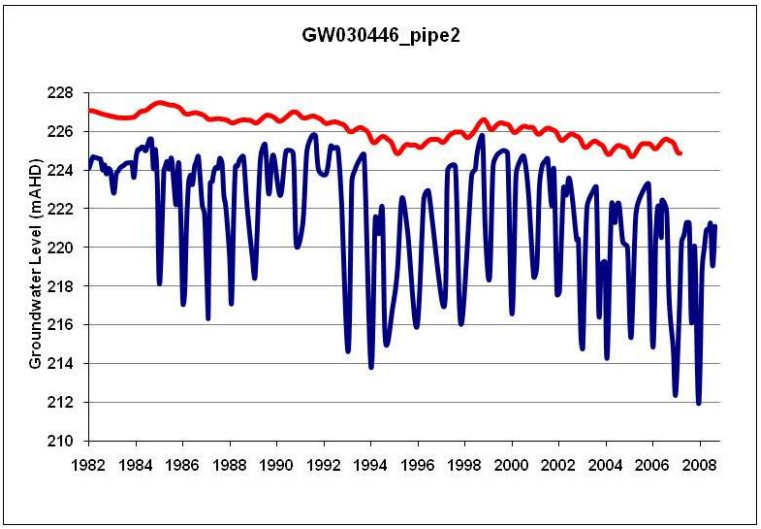
GW030446_pipe2
Groundwater Level (mAHD)
228
226
224
222
220
218
216
214
212
210
1982 1984 1986 1988 1990 1992 1994 1996 1998 2000 2002 2004 2006 2008

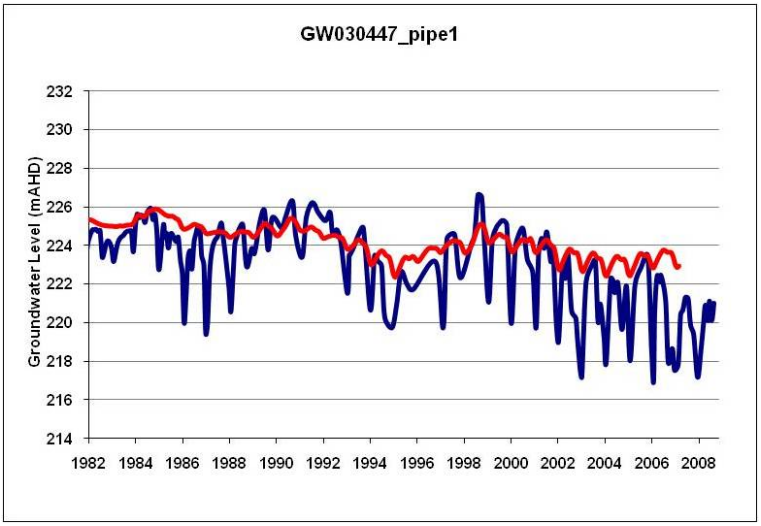
GW030447_pipe1
Groundwater Level (mAHD)
232
230
228
226
224
222
220
218
216
214
1982 1984 1986 1988 1990 1992 1994 1996 1998 2000 2002 2004 2006 2008

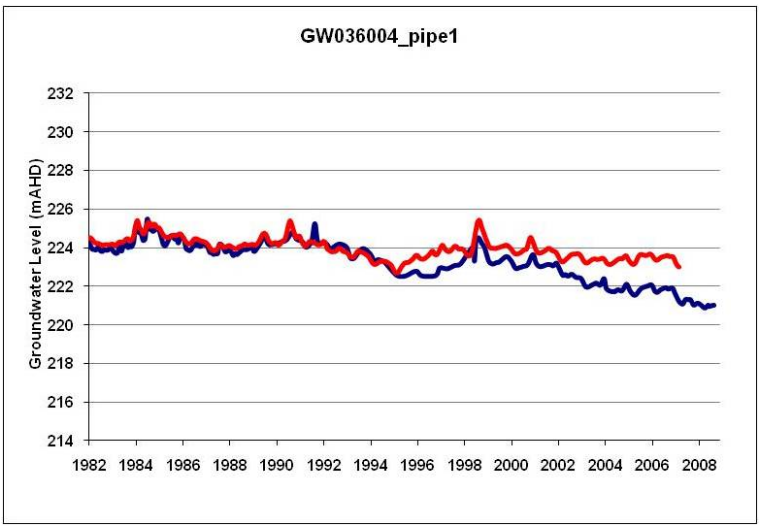
GW036004_pipe1
Groundwater Level (mAHD)
232
230
228
226
224
222
220
218
216
214
1982 1984 1986 1988 1990 1992 1994 1996 1998 2000 2002 2004 2006 2008

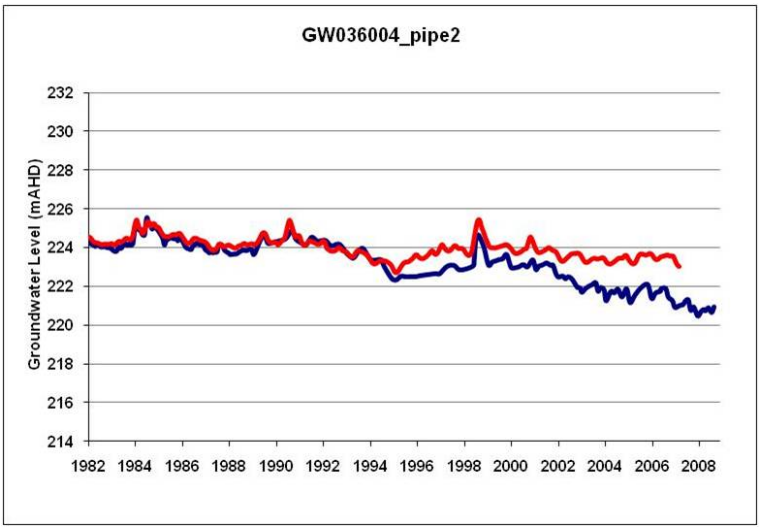
GW036004_pipe2
Groundwater Level (mAHD)
232
230
228
226
224
222
220
218
216
214
1982 1984 1986 1988 1990 1992 1994 1996 1998 2000 2002 2004 2006 2008

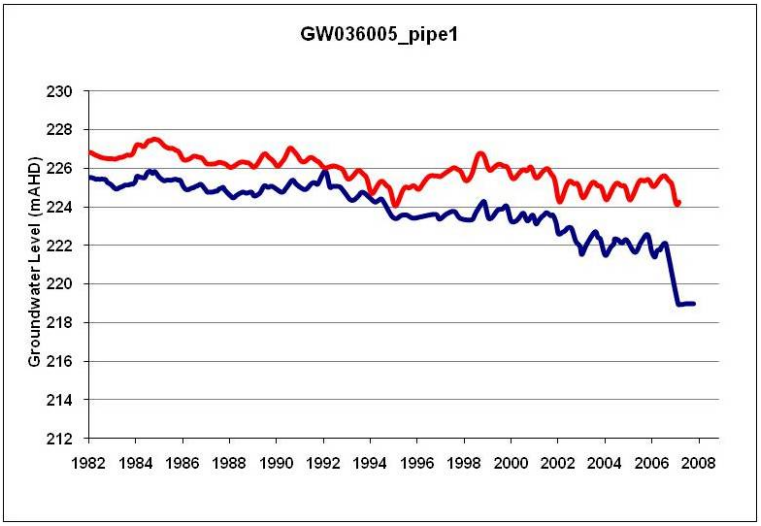
GW036005_pipe1
Groundwater Level (mAHD)
230
228
226
224
222
220
218
216
214
212
1982 1984 1986 1988 1990 1992 1994 1996 1998 2000 2002 2004 2006 2008

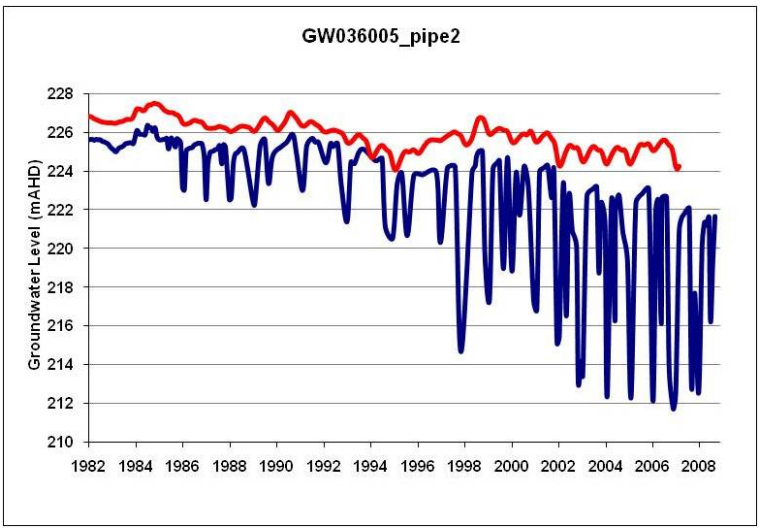
GW036005_pipe2
Groundwater Level (mAHD)
228
226
224
222
220
218
216
214
212
210
1982 1984 1986 1988 1990 1992 1994 1996 1998 2000 2002 2004 2006 2008

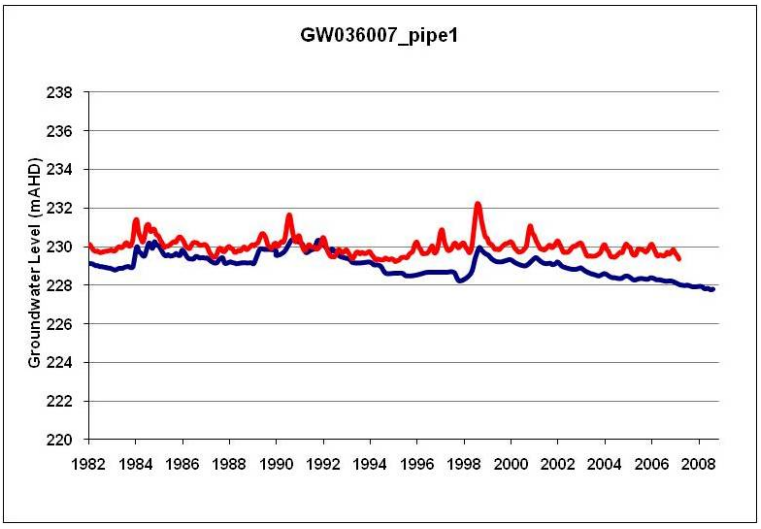
GW036007_pipe1
Groundwater Level (mAHD)
238
236
234
232
230
228
226
224
222
220
1982 1984 1986 1988 1990 1992 1994 1996 1998 2000 2002 2004 2006 2008

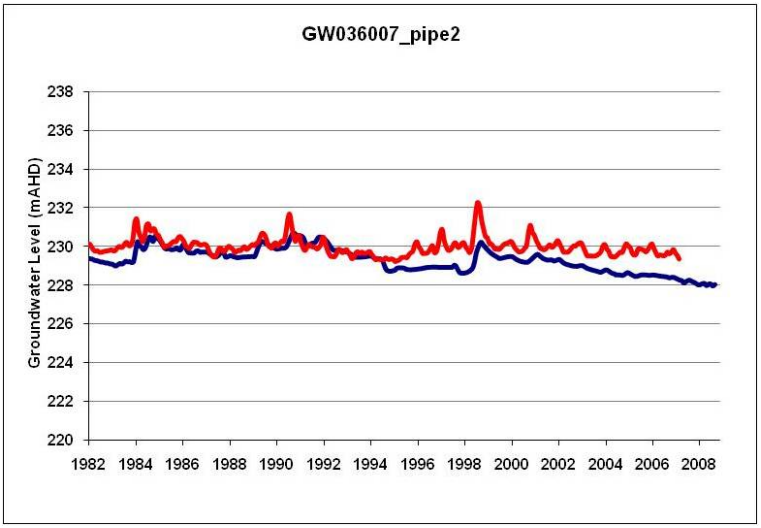
GW036007_pipe2
Groundwater Level (mAHD)
238
236
234
232
230
228
226
224
222
220
1982 1984 1986 1988 1990 1992 1994 1996 1998 2000 2002 2004 2006 2008

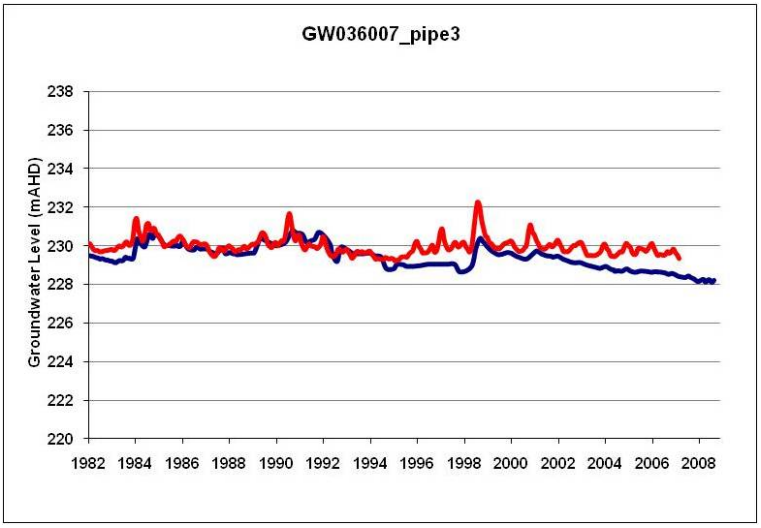
GW036007_pipe3
Groundwater Level (mAHD)
238
236
234
232
230
228
226
224
222
220
1982 1984 1986 1988 1990 1992 1994 1996 1998 2000 2002 2004 2006 2008

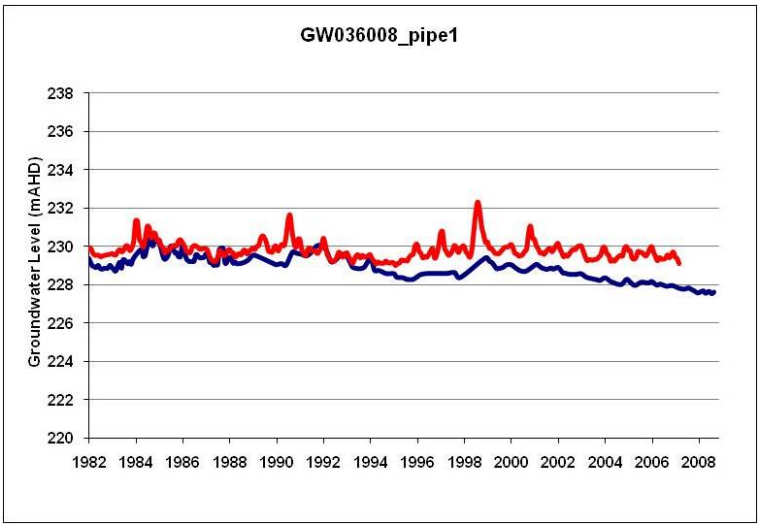
GW036008_pipe1
Groundwater Level (mAHD)
238
236
234
232
230
228
226
224
222
220
1982 1984 1986 1988 1990 1992 1994 1996 1998 2000 2002 2004 2006 2008

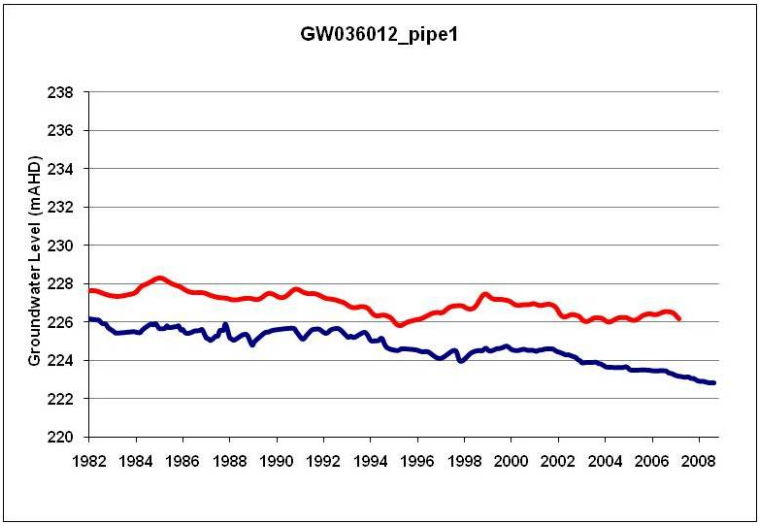
GW036012_pipe1
Groundwater Level (mAHD)
238
236
234
232
230
228
226
224
222
220
1982 1984 1986 1988 1990 1992 1994 1996 1998 2000 2002 2004 2006 2008

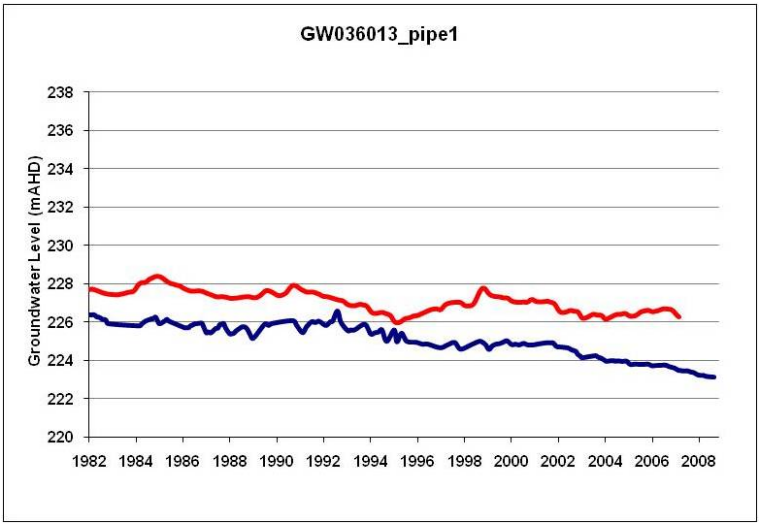
GW036013_pipe1
Groundwater Level (mAHD)
238
236
234
232
230
228
226
224
222
220
1982 1984 1986 1988 1990 1992 1994 1996 1998 2000 2002 2004 2006 2008

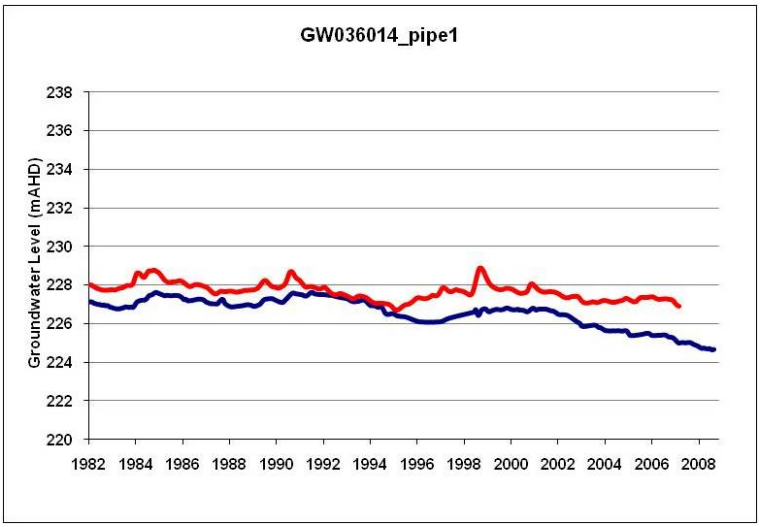
GW036014_pipe1
Groundwater Level (mAHD)
238
236
234
232
230
228
226
224
222
220
1982 1984 1986 1988 1990 1992 1994 1996 1998 2000 2002 2004 2006 2008

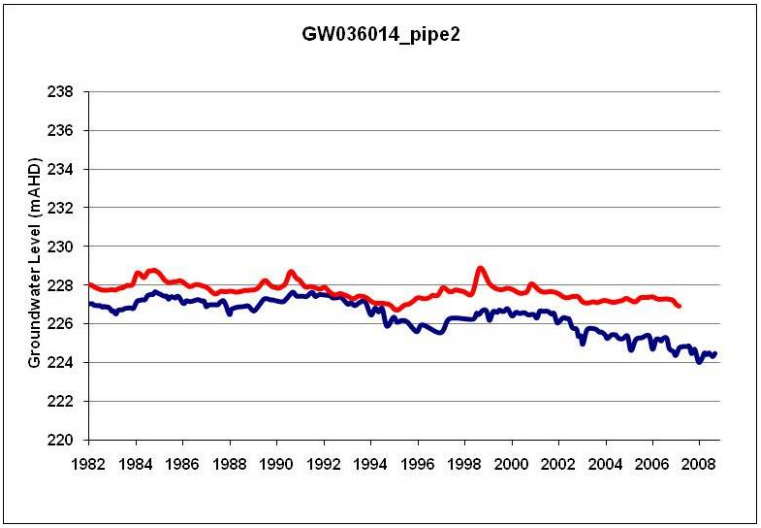
GW036014_pipe2
Groundwater Level (mAHD)
238
236
234
232
230
228
226
224
222
220
1982 1984 1986 1988 1990 1992 1994 1996 1998 2000 2002 2004 2006 2008

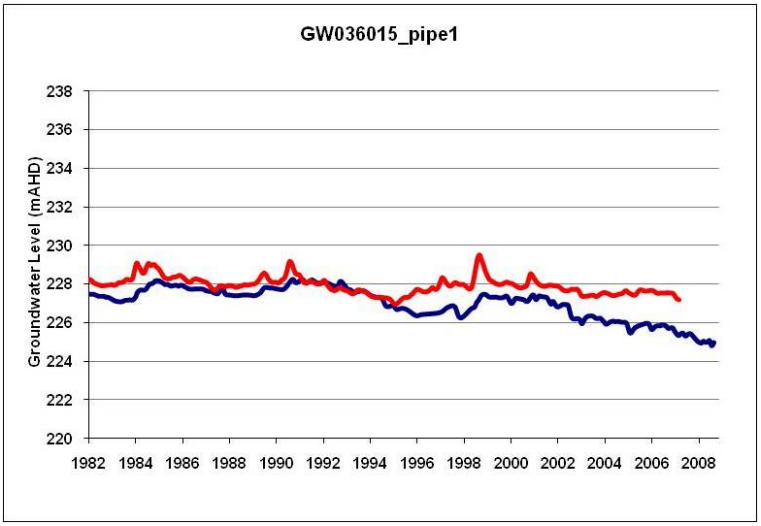
GW036015_pipe1
Groundwater Level (mAHD)
238
236
234
232
230
228
226
224
222
220
1982 1984 1986 1988 1990 1992 1994 1996 1998 2000 2002 2004 2006 2008

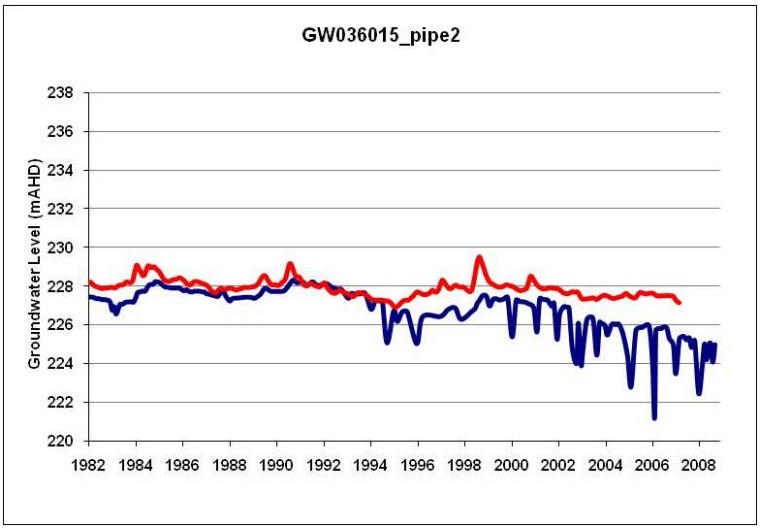
GW036015_pipe2
Groundwater Level (mAHD)
238
236
234
232
230
228
226
224
222
220
1982 1984 1986 1988 1990 1992 1994 1996 1998 2000 2002 2004 2006 2008

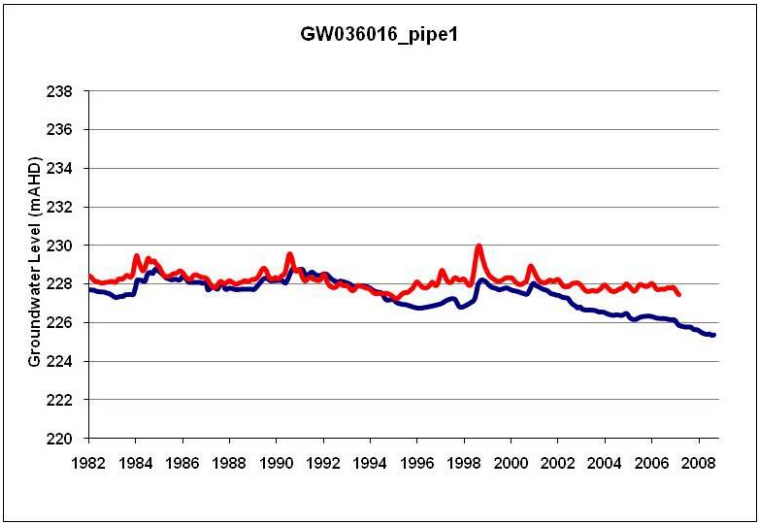
GW036016_pipe1
Groundwater Level (mAHD)
238
236
234
232
230
228
226
224
222
220
1982 1984 1986 1988 1990 1992 1994 1996 1998 2000 2002 2004 2006 2008

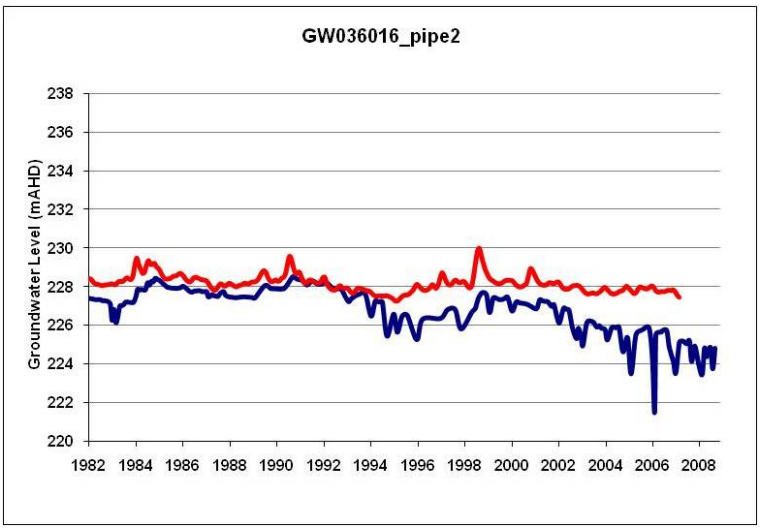
GW036016_pipe2
Groundwater Level (mAHD)
238
236
234
232
230
228
226
224
222
220
1982 1984 1986 1988 1990 1992 1994 1996 1998 2000 2002 2004 2006 2008

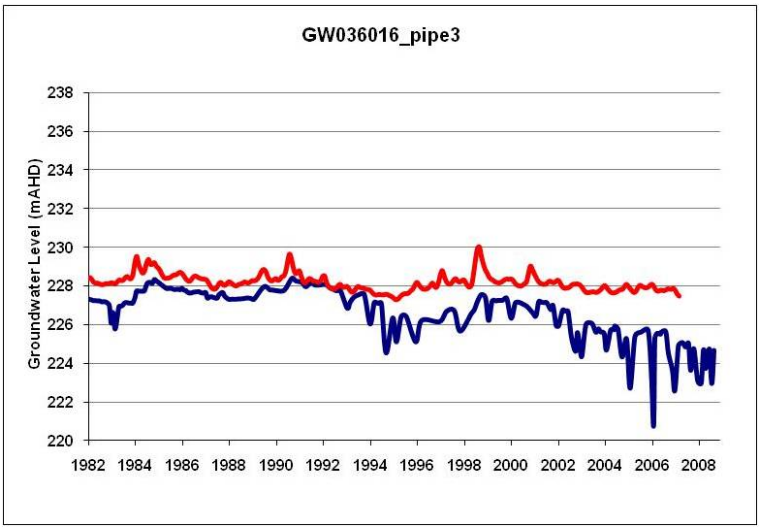
GW036016_pipe3
Groundwater Level (mAHD)
238
236
234
232
230
228
226
224
222
220
1982 1984 1986 1988 1990 1992 1994 1996 1998 2000 2002 2004 2006 2008

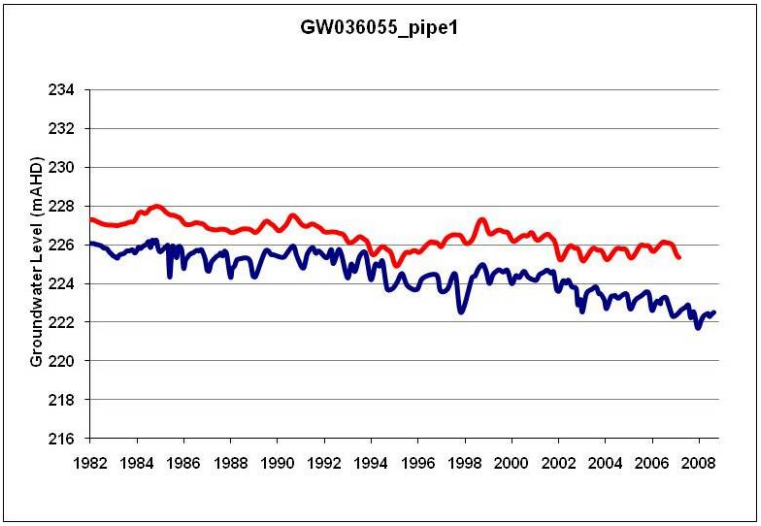
GW036055_pipe1
Groundwater Level (mAHD)
234
232
230
228
226
224
222
220
218
216
1982 1984 1986 1988 1990 1992 1994 1996 1998 2000 2002 2004 2006 2008

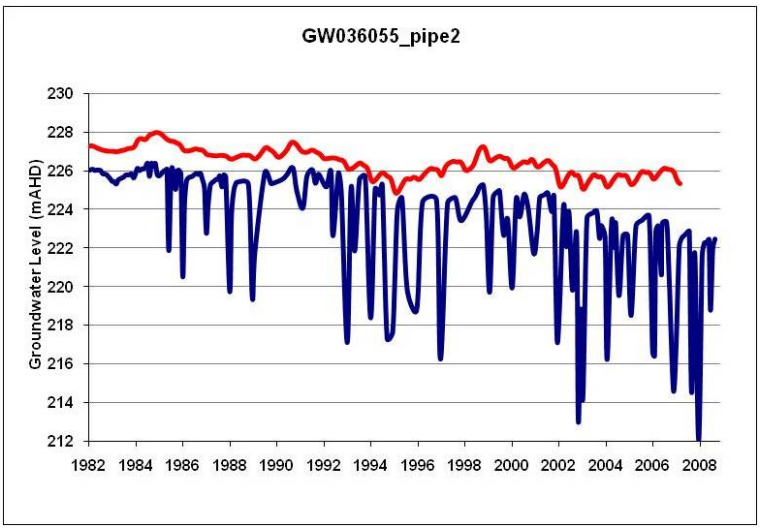
GW036055_pipe2
Groundwater Level (mAHD)
230
228
226
224
222
220
218
216
214
212
1982 1984 1986 1988 1990 1992 1994 1996 1998 2000 2002 2004 2006 2008

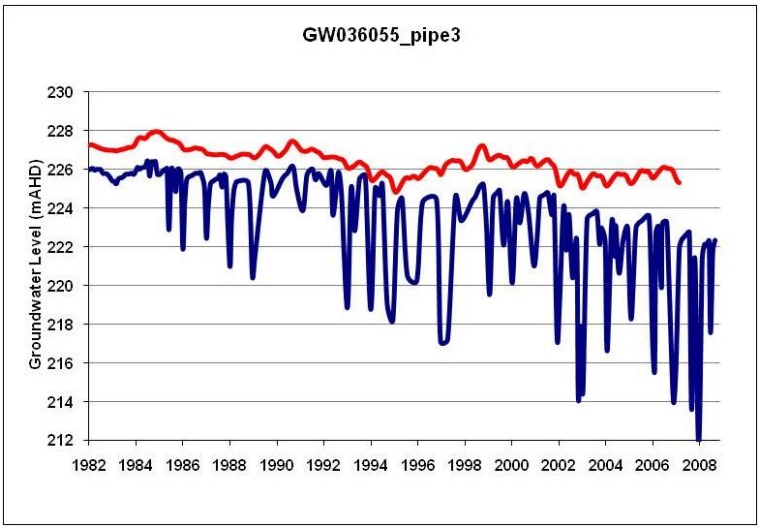
GW036055_pipe3
Groundwater Level (mAHD)
230
228
226
224
222
220
218
216
214
212
1982 1984 1986 1988 1990 1992 1994 1996 1998 2000 2002 2004 2006 2008

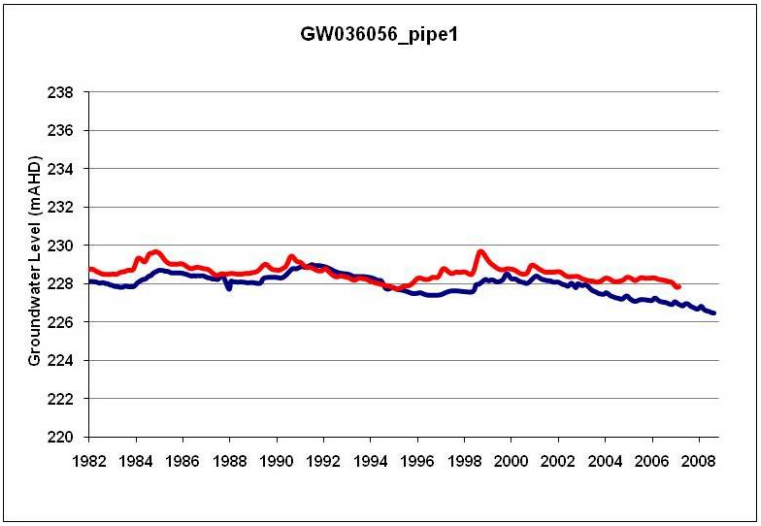
GW036056_pipe1
Groundwater Level (mAHD)
238
236
234
232
230
228
226
224
222
220
1982 1984 1986 1988 1990 1992 1994 1996 1998 2000 2002 2004 2006 2008

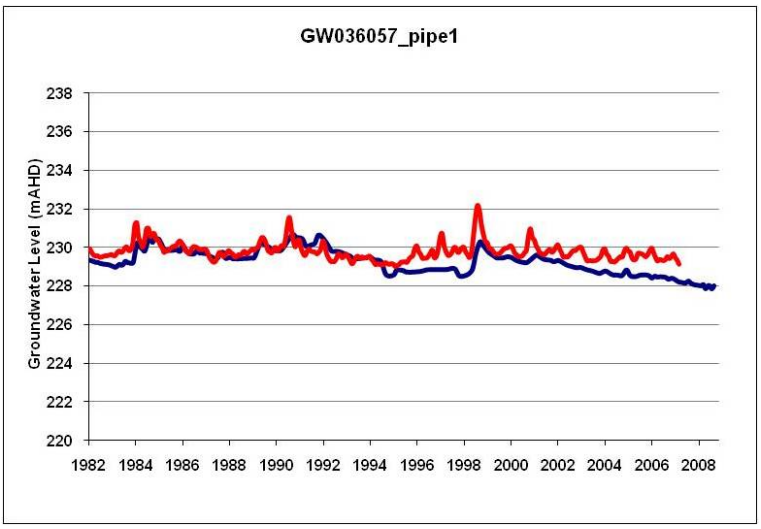
GW036057_pipe1
Groundwater Level (mAHD)
238
236
234
232
230
228
226
224
222
220
1982 1984 1986 1988 1990 1992 1994 1996 1998 2000 2002 2004 2006 2008

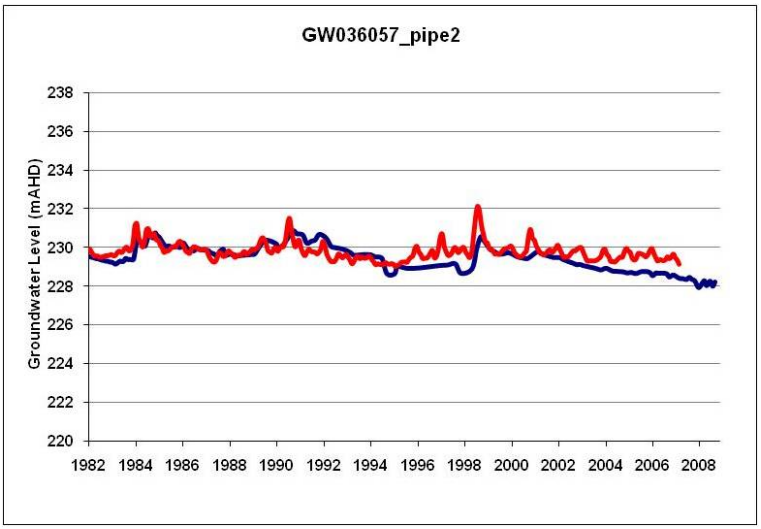
GW036057_pipe2
Groundwater Level (mAHD)
238
236
234
232
230
228
226
224
222
220
1982 1984 1986 1988 1990 1992 1994 1996 1998 2000 2002 2004 2006 2008

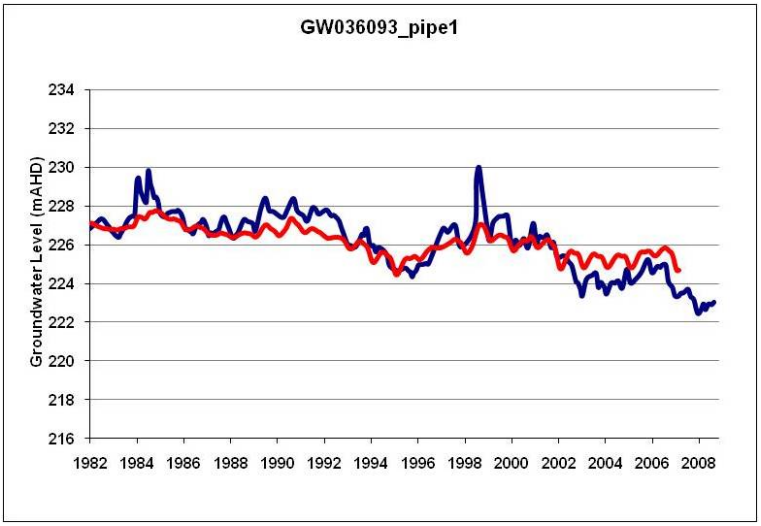
GW036093_pipe1
Groundwater Level (mAHD)
234
232
230
228
226
224
222
220
218
216
1982 1984 1986 1988 1990 1992 1994 1996 1998 2000 2002 2004 2006 2008

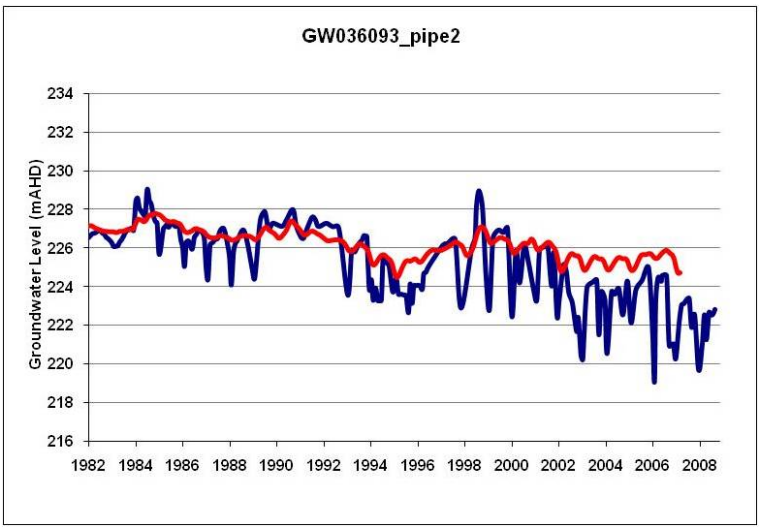
GW036093_pipe2
Groundwater Level (mAHD)
234
232
230
228
226
224
222
220
218
216
1982 1984 1986 1988 1990 1992 1994 1996 1998 2000 2002 2004 2006 2008

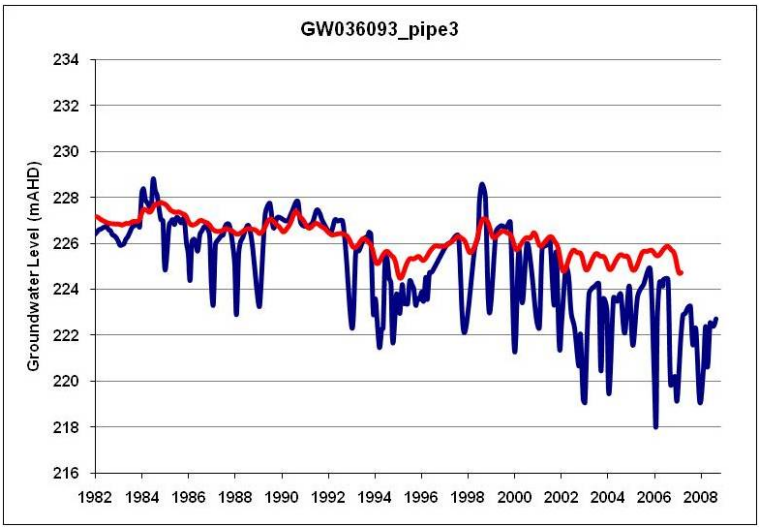
GW036093_pipe3
Groundwater Level (mAHD)
234
232
230
228
226
224
222
220
218
216
1982 1984 1986 1988 1990 1992 1994 1996 1998 2000 2002 2004 2006 2008

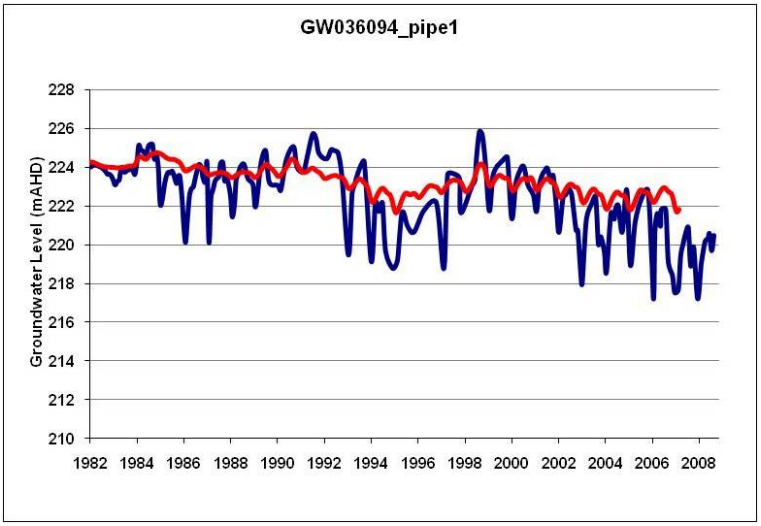
GW036094_pipe1
Groundwater Level (mAHD)
228
226
224
222
220
218
216
214
212
210
1982 1984 1986 1988 1990 1992 1994 1996 1998 2000 2002 2004 2006 2008

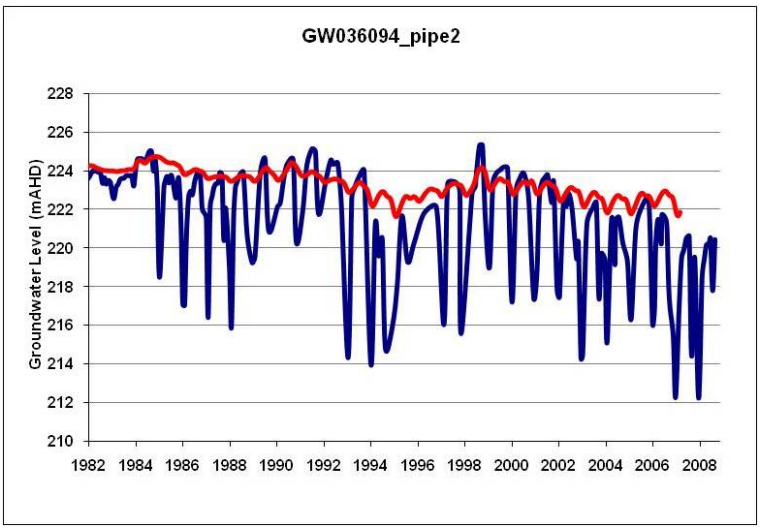
GW036094_pipe2
Groundwater Level (mAHD)
228
226
224
222
220
218
216
214
212
210
1982 1984 1986 1988 1990 1992 1994 1996 1998 2000 2002 2004 2006 2008

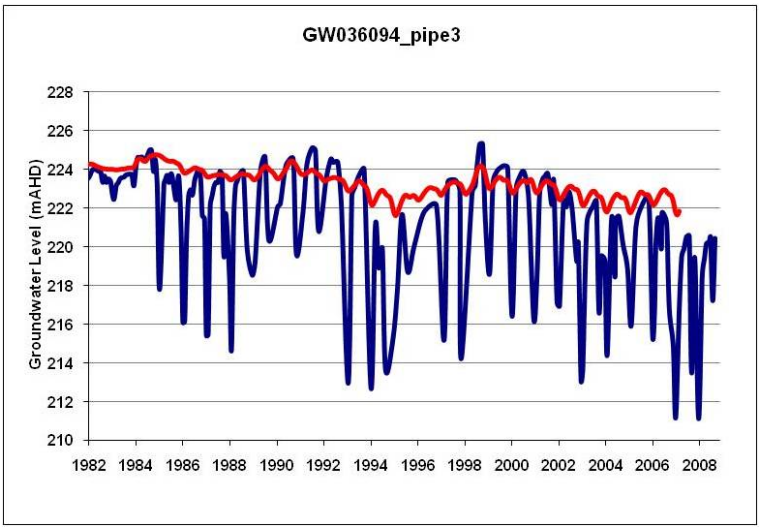
GW036094_pipe3
Groundwater Level (mAHD)
228
226
224
222
220
218
216
214
212
210
1982 1984 1986 1988 1990 1992 1994 1996 1998 2000 2002 2004 2006 2008

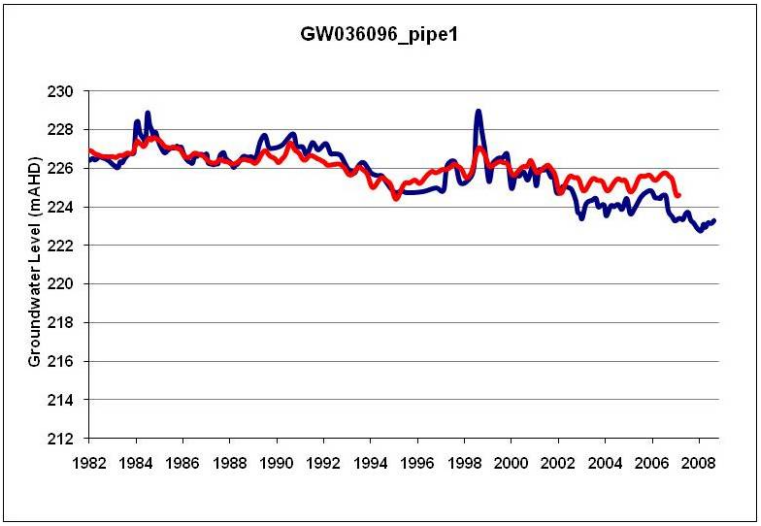
GW036096_pipe1
Groundwater Level (mAHD)
230
228
226
224
222
220
218
216
214
212
1982 1984 1986 1988 1990 1992 1994 1996 1998 2000 2002 2004 2006 2008

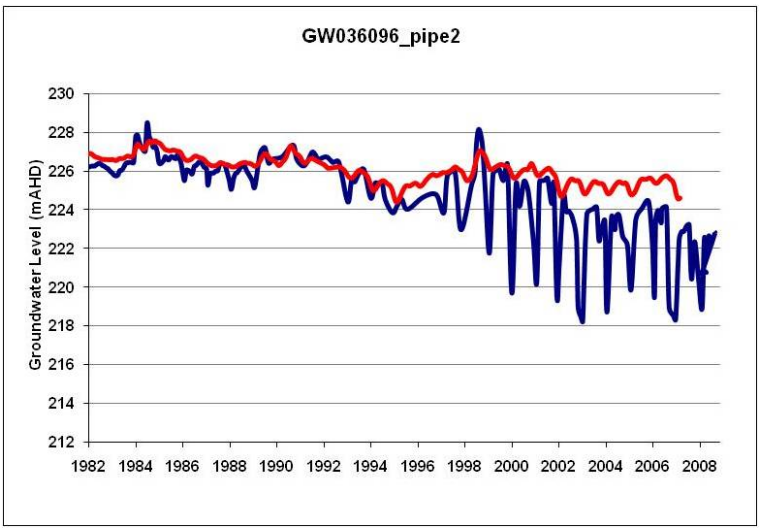
GW036096_pipe2
Groundwater Level (mAHD)
230
228
226
224
222
220
218
216
214
212
1982 1984 1986 1988 1990 1992 1994 1996 1998 2000 2002 2004 2006 2008

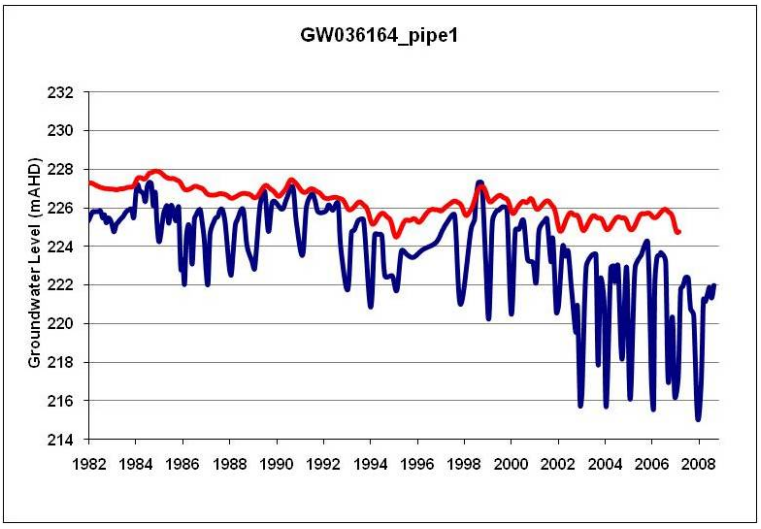
GW036164_pipe1
Groundwater Level (mAHD)
232
230
228
226
224
222
220
218
216
214
1982 1984 1986 1988 1990 1992 1994 1996 1998 2000 2002 2004 2006 2008

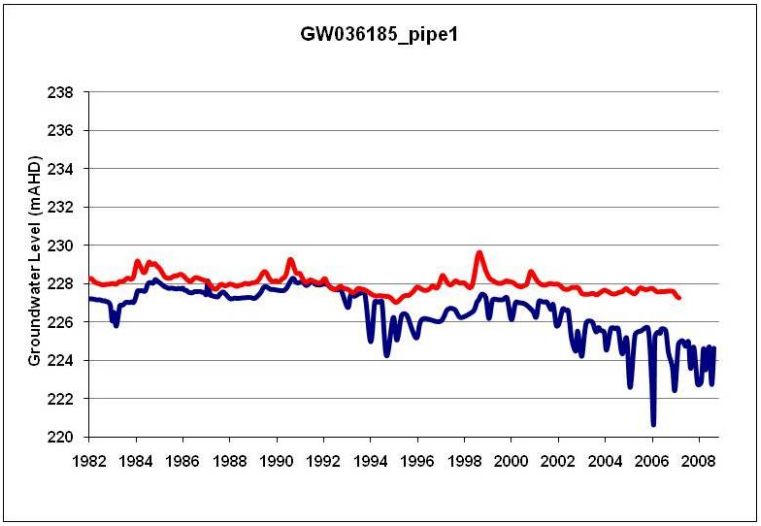
GW036185_pipe1
Groundwater Level (mAHD)
238
236
234
232
230
228
226
224
222
220
1982 1984 1986 1988 1990 1992 1994 1996 1998 2000 2002 2004 2006 2008

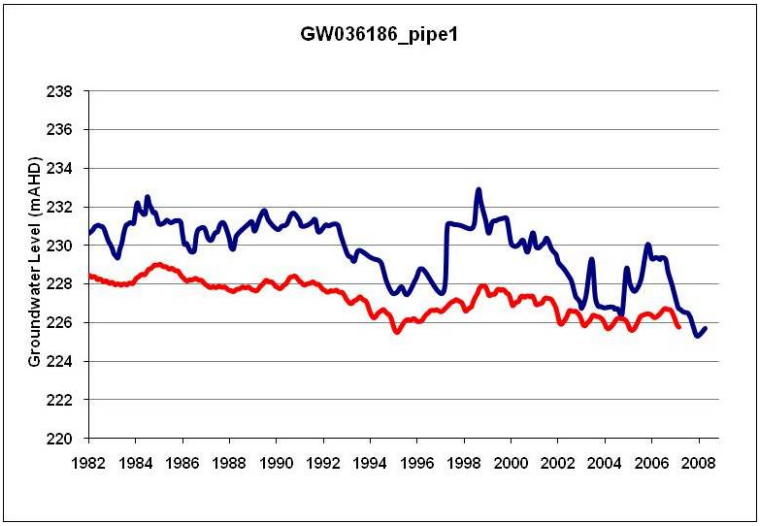
GW036186_pipe1
Groundwater Level (mAHD)
238
236
234
232
230
228
226
224
222
220
1982 1984 1986 1988 1990 1992 1994 1996 1998 2000 2002 2004 2006 2008

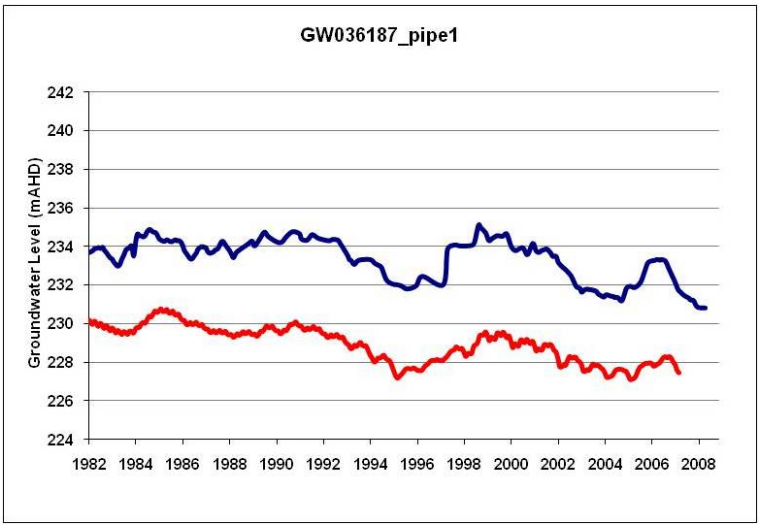
GW036187_pipe1
Groundwater Level (mAHD)
242
240
238
236
234
232
230
228
226
224
1982 1984 1986 1988 1990 1992 1994 1996 1998 2000 2002 2004 2006 2008

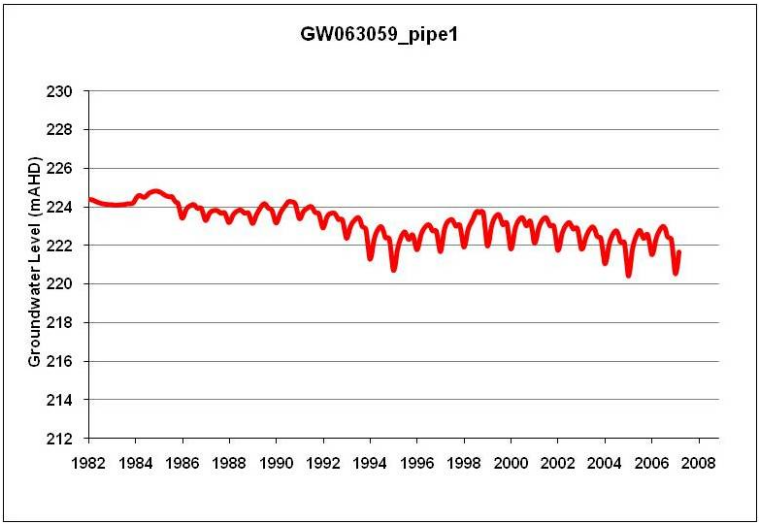
GW063059_pipe1
Groundwater Level (mAHD)
230
228
226
224
222
220
218
216
214
212
1982 1984 1986 1988 1990 1992 1994 1996 1998 2000 2002 2004 2006 2008

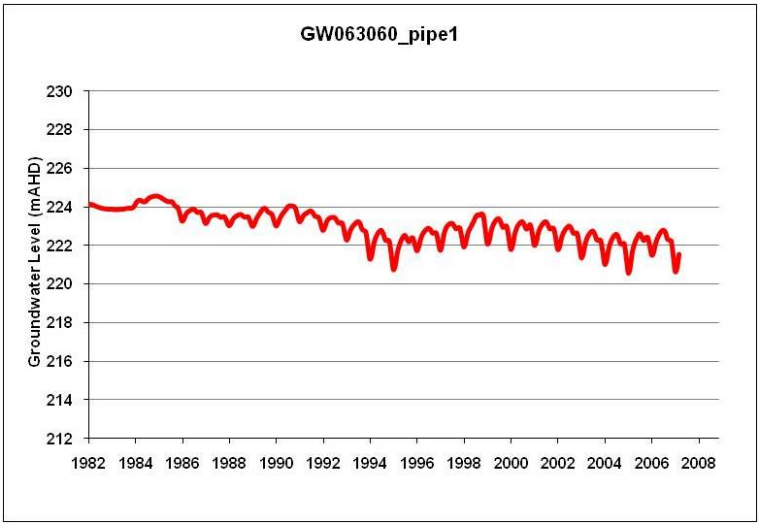
GW063060_pipe1
Groundwater Level (mAHD)
230
228
226
224
222
220
218
216
214
212
1982 1984 1986 1988 1990 1992 1994 1996 1998 2000 2002 2004 2006 2008

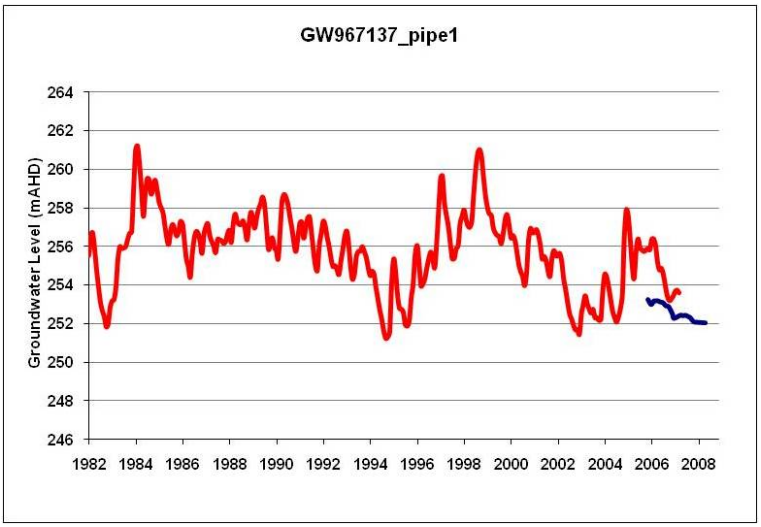
GW967137_pipe1
Groundwater Level (mAHD)
264
262
260
258
256
254
252
250
248
246
1982 1984 1986 1988 1990 1992 1994 1996 1998 2000 2002 2004 2006 2008

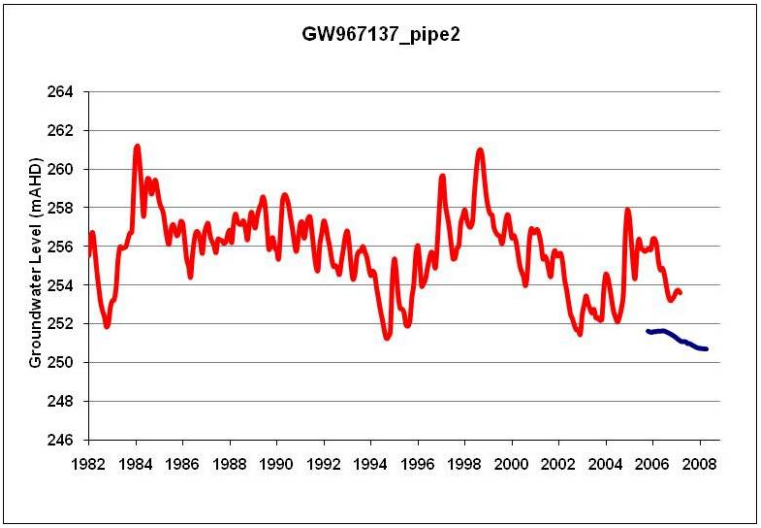
GW967137_pipe2
Groundwater Level (mAHD)
264
262
260
258
256
254
252
250
248
246
1982
1984
1986
1988
1990
1992
1994
1996
1998
2000
2002
2004
2006
2008

Table 5A-1 - Root mean square error and correlation coefficient values for the observation boreholes in the model domain.

Bore ID	pipe	RMS error	Corr.Coeff	Bore ID	pipe	RMS error	Corr.Coeff
GW030129	1	1.4	0.4	GW036008	1	0.9	0.5
GW030130	1	3.3	0.7	GW036012	1	2.2	0.8
GW030130	2	2.7	0.7	GW036013	1	2.0	0.8
GW030131	1	1.6	0.8	GW036014	1	1.1	0.7
GW030132	1	1.7	0.8	GW036014	2	1.3	0.7
GW030132	2	1.1	0.8	GW036015	1	1.0	0.6
GW030133	1	4.1	0.9	GW036015	2	1.4	0.5
GW030134	1	5.0	0.8	GW036016	1	0.8	0.6
GW030231	1	1.3	0.9	GW036016	2	1.5	0.5
GW030231	2	1.4	0.9	GW036016	3	1.8	0.5
GW030232	1	2.0	0.9	GW036055	1	1.9	0.8
GW030232	2	2.3	0.9	GW036055	2	3.7	0.7
GW030232	3	2.6	0.8	GW036055	3	3.7	0.7
GW030233	1	0.9	0.9	GW036056	1	0.7	0.6
GW030233	2	3.5	0.8	GW036057	1	0.6	0.6
GW030233	3	3.5	0.8	GW036057	2	0.5	0.6
GW030234	1	3.6	0.6	GW036093	1	0.8	0.9
GW030235	1	3.4	0.6	GW036093	2	1.6	0.8
GW030235	2	2.5	0.7	GW036093	3	2.0	0.8
GW030236	1	3.6	0.7	GW036094	1	1.5	0.8
GW030236	2	2.3	0.8	GW036094	2	2.9	0.7
GW030237	1	0.6	0.9	GW036094	3	3.4	0.6
GW030446	1	3.6	0.7	GW036096	1	0.7	0.9
GW030446	2	5.0	0.5	GW036096	2	2.0	0.8
GW030447	1	2.0	0.7	GW036164	1	3.1	0.7
GW036004	1	0.8	0.9	GW036185	1	1.7	0.6
GW036004	2	0.9	0.9	GW036186	1	2.7	0.8
GW036005	1	2.0	0.9	GW036187	1	4.5	0.8
GW036005	2	4.1	0.7	GW063059	1	n/a	n/a
GW036007	1	0.9	0.6	GW063060	1	n/a	n/a
GW036007	2	0.7	0.6	GW967137	1	n/a	n/a
GW036007	3	0.6	0.6	GW967137	1	n/a	n/a
MIN_RMS	0.5						
MAX_RMS	5.0						
AVERAGE_RMS	2.1						

Table 5A-2 - Error calibration performance measures for the model over the whole period of calibration (1982-2007). Refer to MDBC (2001) for the statistics equations and explanation.

STATISTICS		VALUE
ROOT MEAN SQUARE (m)	RMS	2.44
ROOT MEAN FRACTION SQUARE (%)	RMFS	1.08
SCALED RMFS (%)	SRMFS	6.76
SCALED RMS (%)	SRMS	6.70
COEFFICIENT OF DETERMINATION	CD	1.13
STANDARD CORRELATION FUNCTION	r	0.95

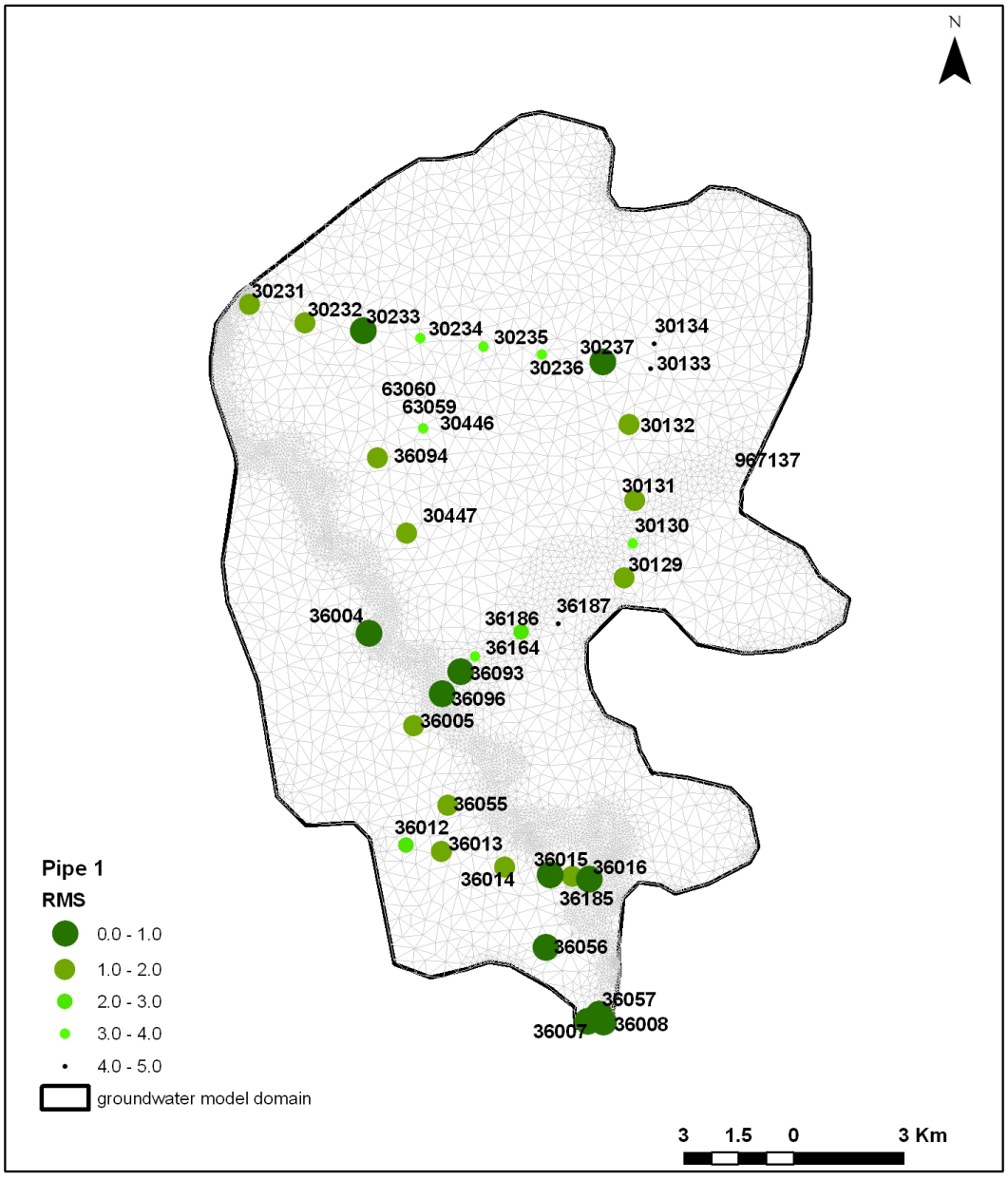
N
30231
30232
30233
30234
30235
30236
30237
30134
30133
63060
63059
30446
30132
36094
967137
30131
30447
30130
30129
36004
36186
36187
36164
36093
36096
36005
36055
36012
36013
36014
36015
36016
36185
36056
36057
36007
36008
Pipe 1
RMS
0.0 - 1.0
1.0 - 2.0
2.0 - 3.0
3.0 - 4.0
4.0 - 5.0
groundwater model domain
3 1.5 0 3 Km

a)

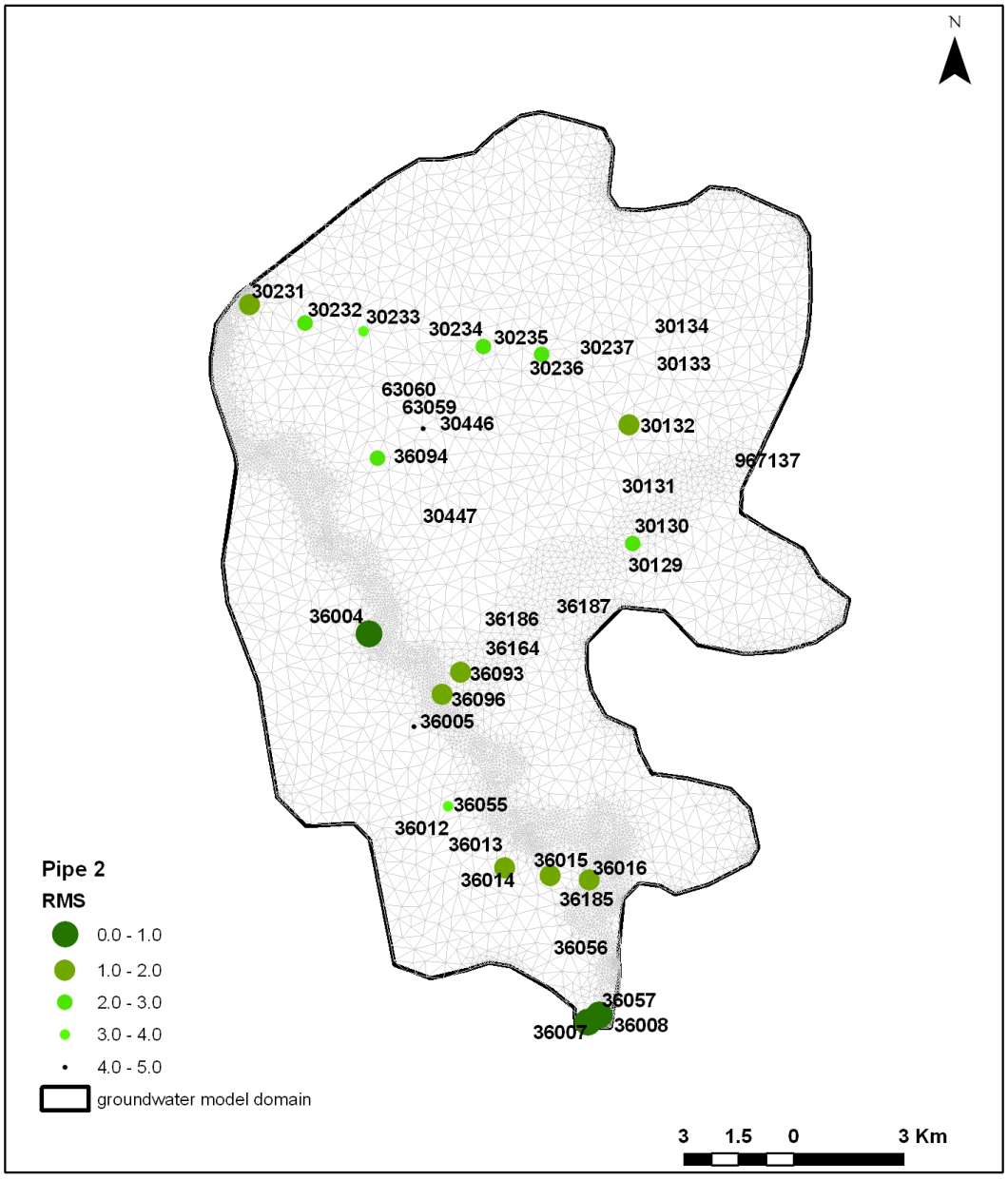
N
30231
30232
30233
30234
30235
30237
30134
30236
30133
63060
63059
30446
30132
36094
967137
30131
30447
30130
30129
36187
36004
36186
36164
36093
36096
36005
36055
36012
36013
36015
36016
36014
36185
36056
36057
36008
36007
Pipe 2
RMS
0.0 - 1.0
1.0 - 2.0
2.0 - 3.0
3.0 - 4.0
4.0 - 5.0
groundwater model domain
3 1.5 0 3 Km

b)

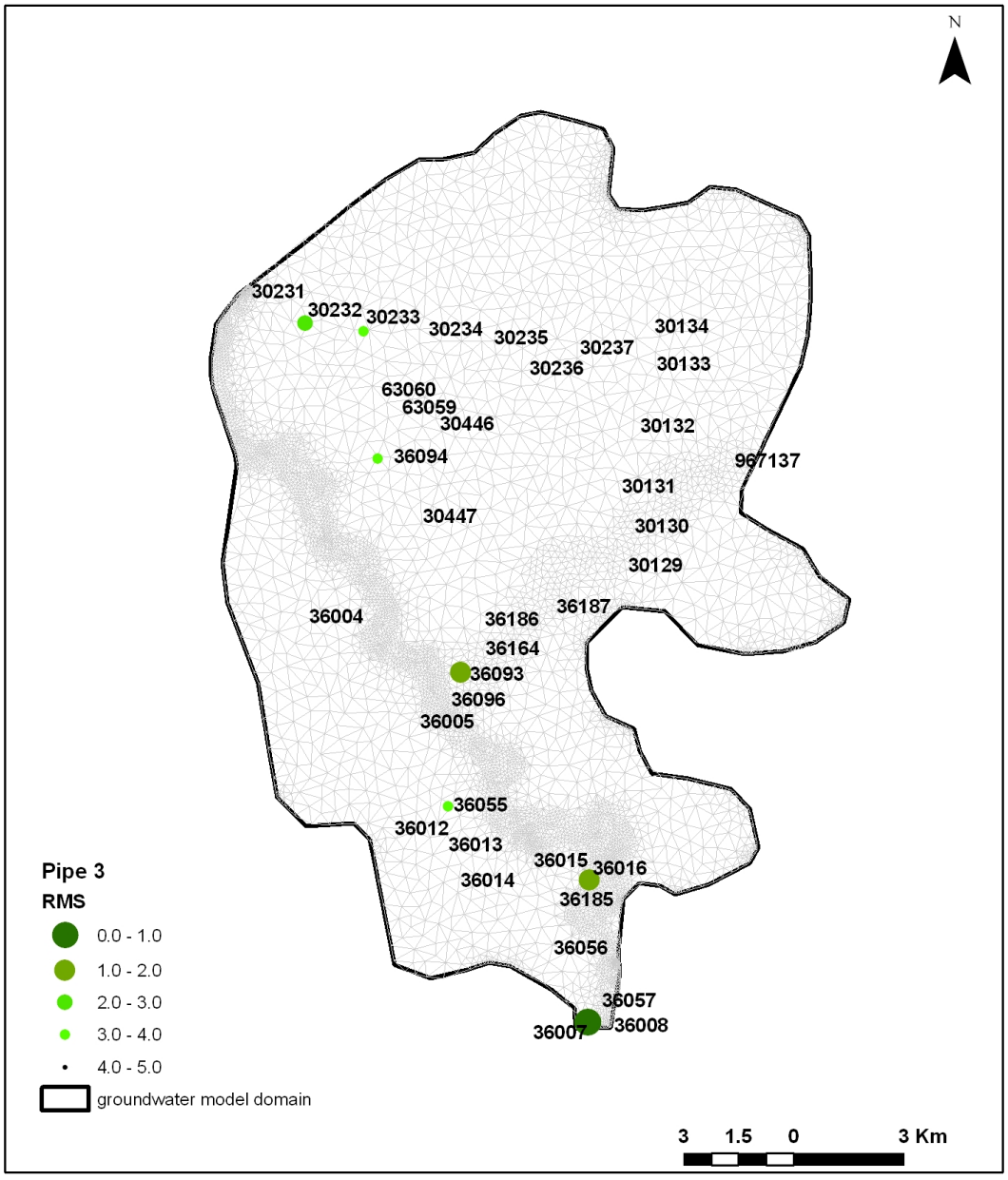

c)

Figure 5A-1: Evaluation of the calibration based on RMS error for pipe 1 (a), 2 (b) and 3 (c). The symbol size indicates the RMS value, the bigger the size the better the calibration based on the RMS error. Refer to Table 5A-1 for the values.

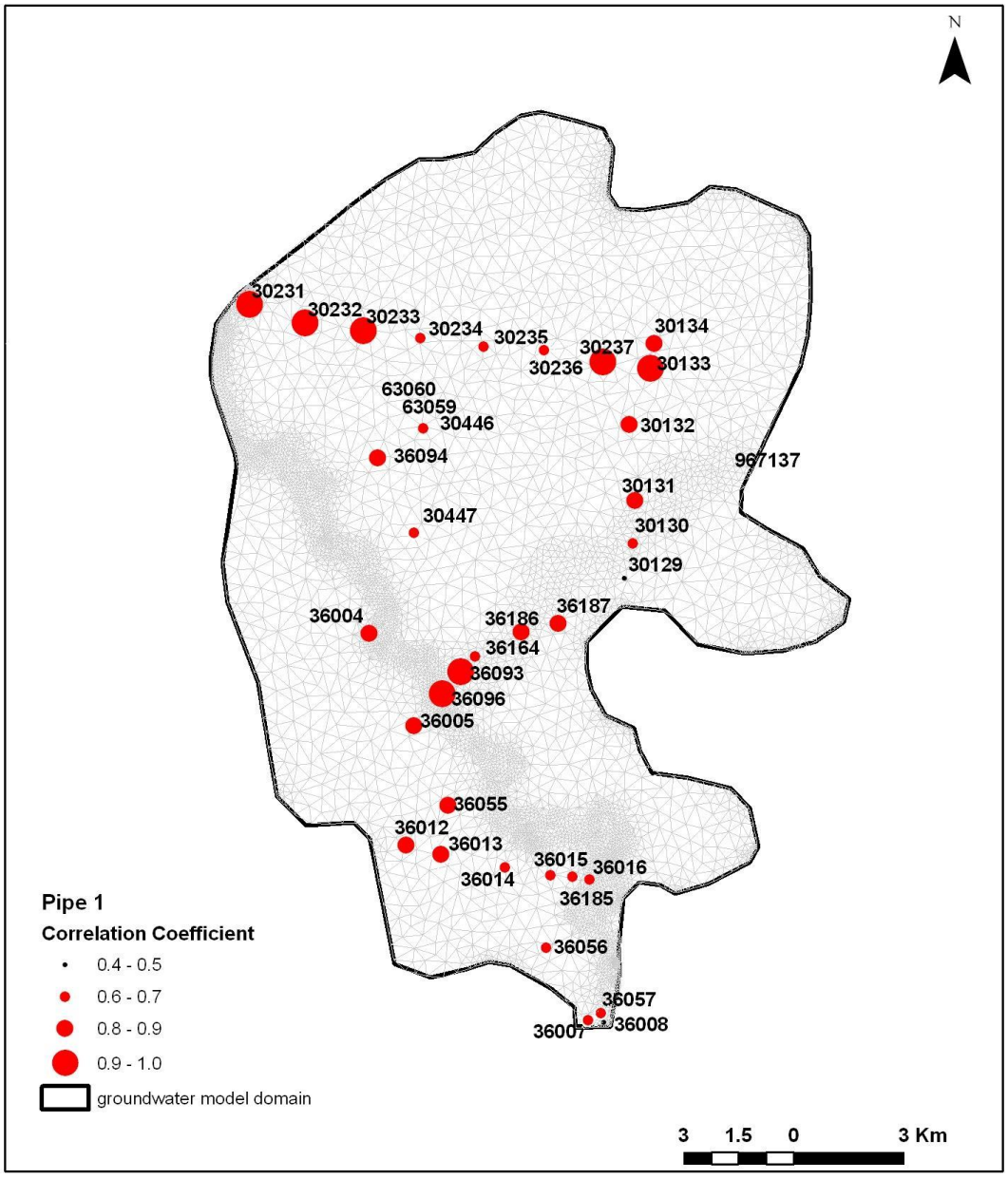
N
30231
30232
30233
30234
30235
30134
30237
30236
30133
63060
63059
30446
30132
36094
967137
30131
30447
30130
30129
36004
36186
36187
36164
36093
36096
36005
36055
36012
36013
36015
36016
36014
36185
36056
36057
36008
36007
Pipe 1
Correlation Coefficient
0.4 - 0.5
0.6 - 0.7
0.8 - 0.9
0.9 - 1.0
groundwater model domain
3 1.5 0 3 Km

a)

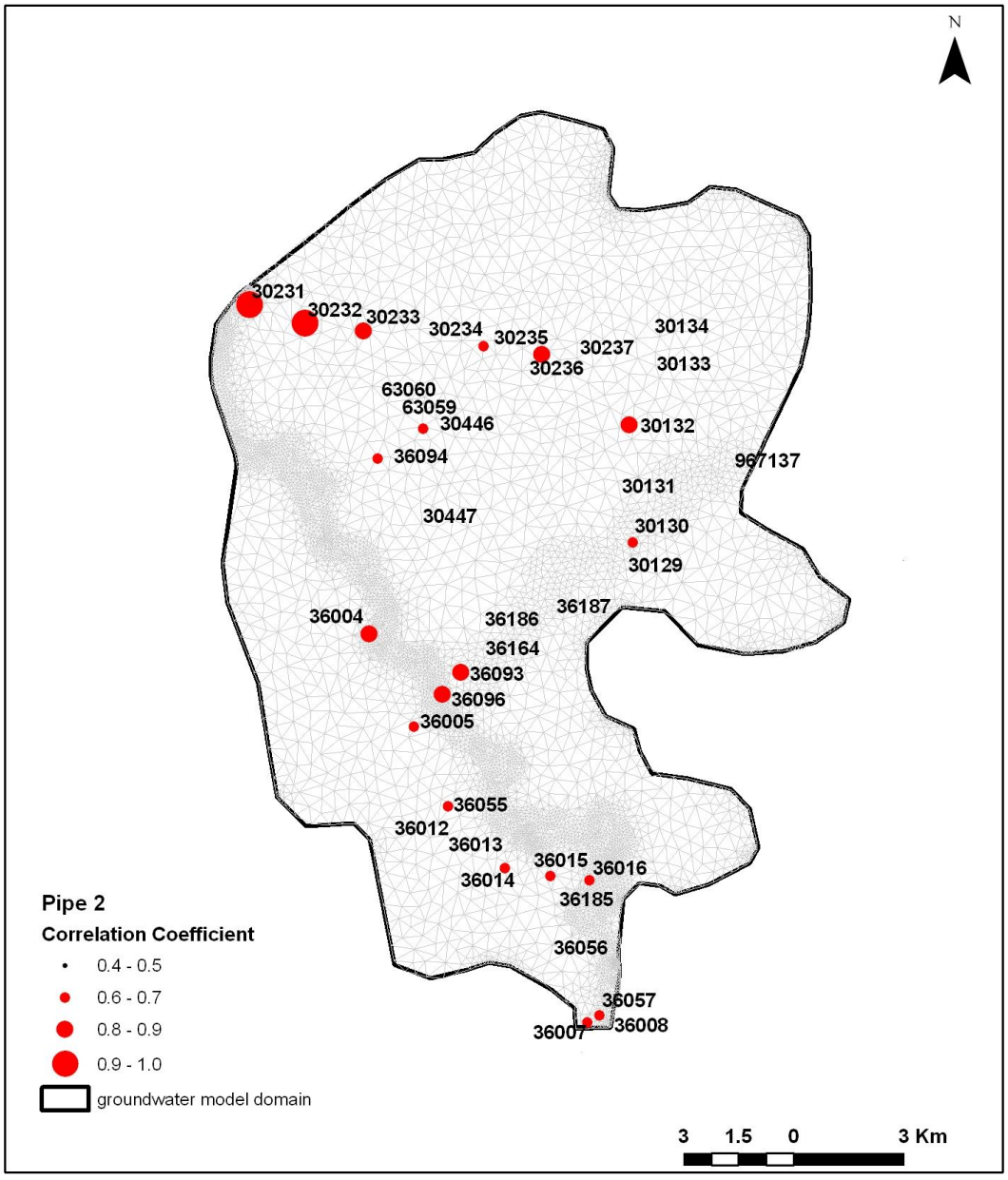
N
30231
30232
30233
30234
30235
30237
30134
30236
30133
63060
63059
30446
30132
36094
967137
30131
30447
30130
30129
36187
36004
36186
36164
36093
36096
36005
36055
36012
36013
36015
36016
36014
36185
36056
36057
36008
36007
Pipe 2
Correlation Coefficient
0.4 - 0.5
0.6 - 0.7
0.8 - 0.9
0.9 - 1.0
groundwater model domain
3 1.5 0 3 Km

b)

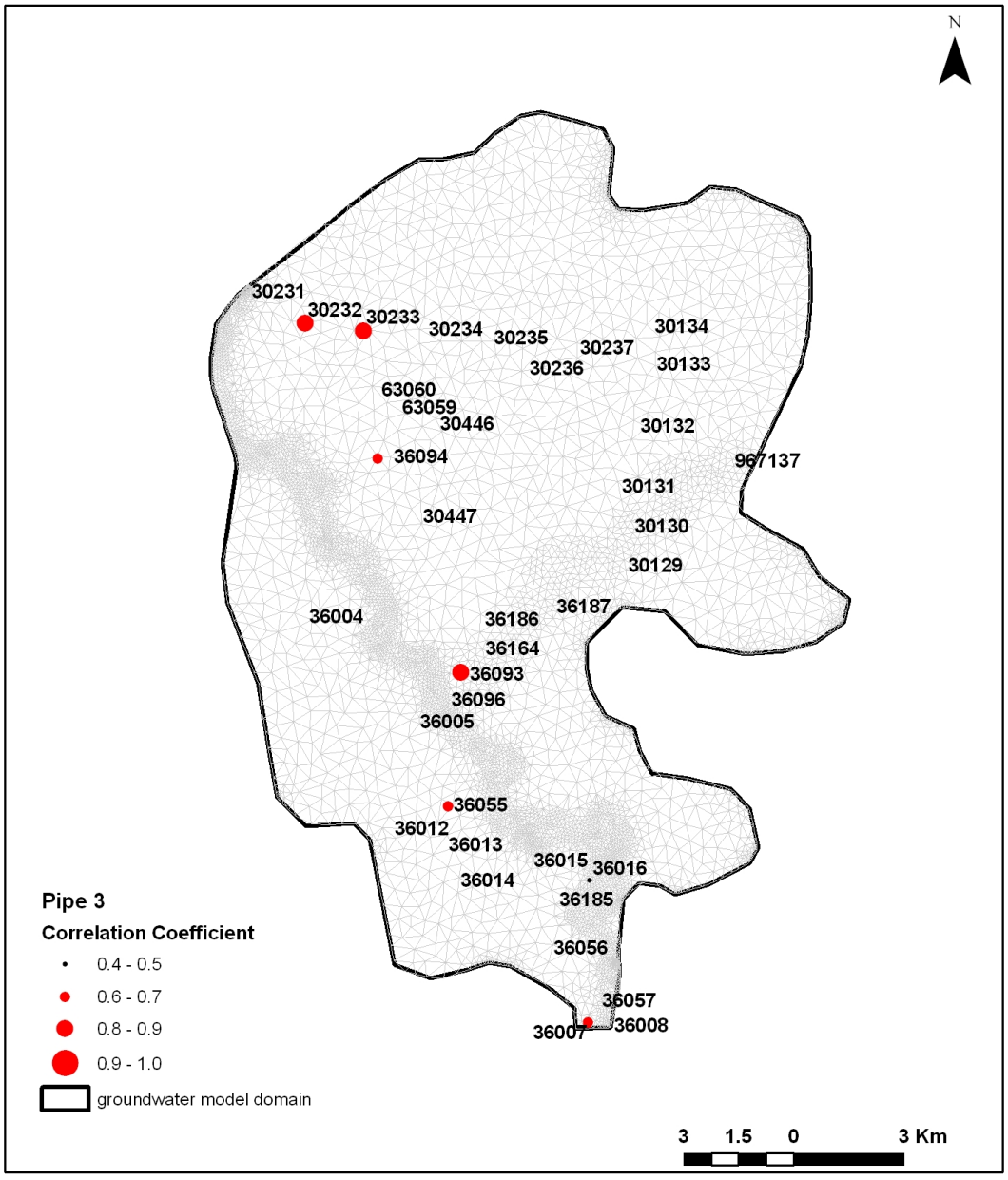

c)

Figure 5A-2: Evaluation of the calibration based on correlation coefficient values for pipe 1 (a), 2 (b) and 3 (c). The symbol size indicates the correlation coefficient, the bigger the size the better the calibration. Refer to Table 5A-1 for the values.

Model Journal

The following table tracks the modelling progress by listing the changes made as the model was developed and calibrated. Only the major changes in development and calibration are listed.

Run	Issue	Model changes	Comments Results	Filename & Patch
A0			See previous report	steady_state.fem
A1	To test one pumping bore in the steady state	Refine mesh around pumping bore; set pumping bore	Observed drawdown in the obs. boreholes adjacent to the pumping bore	1pw_steady_state.fem
B1	Test one pumping bore in the transient model	Set time&control data for a transient simulation Set time-series for the pumping bore; Automatic time step control function	Check final water budget for the aquifer	1pw_transient_model.fem
B2	Set 56 irrigation bores for which data were provided by NSW Office of Water	Set time series for all pumping bores; Refine mesh around bores	Mismatch between total modelled abstracted water and measured data due to a slice which becomes dry during the computation; Drawdown not evident yet	allw_transient model.fem; time series_abstraction.pow
B3	Set diffuse recharge and irrigation recharge based on 5 classes of land use	Set time-series for each land use (5)	Trend between modelled and measured hydrographs is replicated but not calibrated yet; no distinction between shallow and deep aquifer	allw_diffrech.fem;
B4	Set time varying transfer BC for the Namoi River	Set time-varying head of the river considering the values at the gauging stations (419023, 419012) and by linear interpolating values along the river; Sy = 0.2 for sand and 0.02 for clay; Ss = $10^{-4}m^{-1}$		all_diffrech_river.fem; folders 'specific_storage' and 'storativity' with all .dat files; Time_series_diffuserecharge_00.pow

B5	Set time varying flux BC along the boundary of the model	Set 12 more pumping bores in the model domain (not having any screen information for these bores, data of the closest bores were applied); Set time-series for each sub-catchment where the flux BC are applied. For each of the sub-catchments, the net recharge was calculated using the SMD calculation explained in Section 3.5.8.	First run with all time-varying parameters and hydrologic stresses; Too much water entering the system, hydraulic head rises up	T00.fem; Time_series_fluxes_00.pow
C1	Change of the problem class setting	Slices 2-4 set as 'unspecified' and slices 5-10 as 'fixed' because the water level never reaches that depth and in order to confine the deeper portion of the aquifer.	Computation time reduced; Deep slices are fixed, abstraction bores do not run dry anymore and the amount of extracted water at the end of the modelled period is the same of the NSW Office of Water measured data; Delay in the aquifer response based on the saturation of the layers; Still peaks in hydraulic heads	T01.fem
C2	Ss and K adjustments	Ss= $10^{-5}m^{-1}$; Ksand = $10^{-4}m/s$	Drawdown increases; Better match between modelled and measured values	T02.fem

C3	River adjustment	DEM was adjusted to incorporate a true streambed level for the Namoi River. Method: first a DGPS survey of the water level was conducted along the river from Boggabri to Turrawan (February 2009). These survey points was then interpolated using a 1D linear interpolation along the length of the river. Since the gauging stations at Boggabri and Turrawan read, on average, 1m for the period the survey was undertaken, this resulting interpolation represented the 1m water level at each node for this reach of the Namoi River. To create the streambed level, 1m was subtracted at each node. The DEM was then corrected to incorporate the true riverbed values. New time-series of the transient BC of the Namoi River		T03.fem; bottom_river_NAMOI.trp; Namoi_WL_GPS_2009.trp; Time_series_stream_height.pow
C4	K sand adjustment	K sand = 10^{-4}m/s	Increasing K value helps to reduce mismatch between modelled and measured hydrographs but hydraulic head is still too high	T04.fem
C5	Specific yield adjustment	Sy sand = 0.1 Sy clay=0.01	Not significant changes in the calibration	
C6	Locally changes in K	K values for sand and clay were reduced of an order of magnitude in the deep portion of the aquifer (slices 5-10) in order to increase the drawdown	Not significant changes in the drawdown; Increase in the groundwater peaks due to the diffuse recharge	

C7	Change in diffuse recharge and fluxes	Set new time-series for the diffuse recharge and fluxes. To distribute the recharge in a more uniform way through time, the average recharge as a percentage of rainfall over the whole period of simulation were used instead of daily values as calculated previously with the daily SMD calculation. The amount of water applied is the same as before but water is more equally distributed.	Improved fit to recovery level and decrease in groundwater peaks.	T05.fem; Time_series_fluxes_%.pow; Time_series_diffrech_%.pow
C8	Diffuse recharge and fluxes adjustments	Diffuse recharge and fluxes of the previous simulation were divided by a factor of 5 to get a better fit between modelled and measured values. Irrigation recharge was set 3% of the abstraction rate (instead of the previous 5%)	Best calibration	base_case.fem; base_case_diffrech.pow; base_case_fluxes.pow
D1	Scenarios	Two scenarios: without pumping (and without irrigation recharge) and with double pumping rate	See comments in Section 5	without_pumping.fem; double_pumping.fem; Time_series_diffrech_NOirr_rech.pow; Time_series_double_abstraction.pow;
E1	Sensitivity tests	All sensitivity tests explained in Section 4.4.		folder 'sensitivity_test' with all .fem file

Appendix 6a

Crystallize

FEFLOW Post Processing of Hydrograph Data
Function Time Series

Authors
B. Kelly, B. Giambastiani and A. McCallum

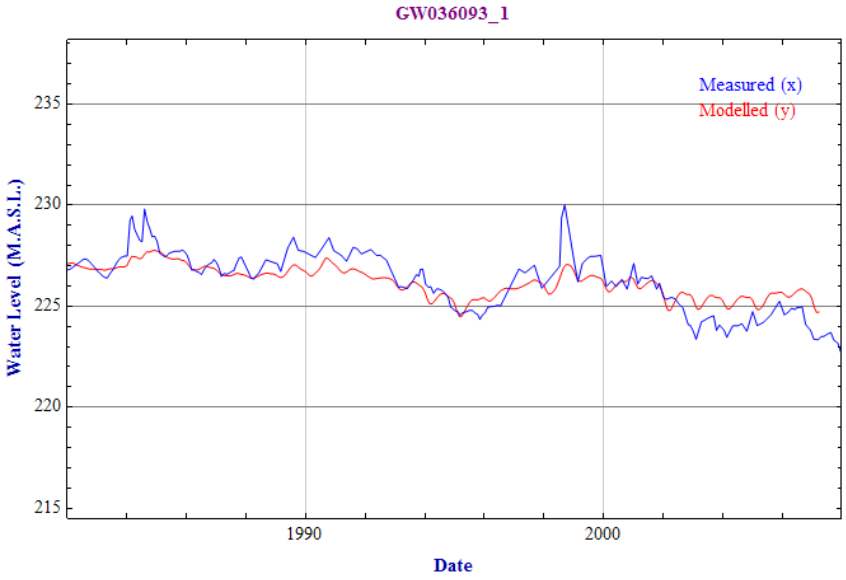

A.6.1 Introduction

This notebook plots measured versus modelled groundwater hydrographs. The degree of correlation between the two hydrographs is also determined. FEFLOW does not have tools for the comprehensive analysis of the hydrograph data. This ***Crystallize*** notebook demonstrates how *Mathematica* scripts can be written to automate the statistical analysis of any groundwater model. The correlation coefficient is just one statistical measure used to help with the evaluation of a groundwater model. A correlation coefficient of zero means there is no linear relationship between the two variables, a value of one indicates a perfect match. For an introductory discussion on statistics refer to:

Gonick, L. and Smith W. (1993) "The Cartoon Guide to Statistics", HarperPerennial

For a detailed discussion on the interpretation of the statistics, details on the correlation coefficient and signal analysis refer to:

Ruskeepaa, H. (2009) "Mathematica Navigator: Mathematics, Statistics, and Graphics", 3rd Edition, Elsevier.

Costain, J.K. and Coruh, C. (2004) "Basic Theory of Exploration Seismology: with Mathematica Notebooks and Examples on CD-ROM", Elsevier.

There are many other statistical measures that can be used to evaluate the quality of a groundwater model. A comprehensive listing of the statistical measures commonly used for assessing the quality of measured versus modelled groundwater hydrograph is presented in:

Middlemis, H., Merrick, N.P. and Ross, J.B. (2000). "Murray-Darling Basin Commission groundwater flow modelling guidelines". Murray-Darling Basin Commission, Aquaterra Consulting Pty Ltd, Perth.
http://www2.mdbc.gov.au/nrm/groundwater/groundwater_guides.html
http://www2.mdbc.gov.au/__data/page/127/model_guide.pdf

A.6.2 Loading the Data

The first two lines of script below load the data. The third line makes a list of all the bores in the input files. These data files contain the columns of data that detail the field measured groundwater head and the FEFLOW modelled groundwater head. If this notebook is used on data files that have different columns for the time and groundwater head data then the columns called in the scripts below would need to be changed.

```
feflowData =
  Drop[
   Import[
    "G:\\NWC_FinalReportUNSW3DHydrogeology\\Appendix8_CrystallizeFEFLOWHydrographs\\MaulesCkFEFLOWhydrographs.csv"],
   1];
measuredData =
  Drop[
   Import[
    "G:\\NWC_FinalReportUNSW3DHydrogeology\\Appendix8_CrystallizeFEFLOWHydrographs\\MaulesCkMeasuredHydrographs.csv"
    ], 1];

allbores = DeleteDuplicates[feflowData[[All, 2]]]
```

```
{GW036008_1, GW036007_1, GW036007_2, GW036007_3, GW036057_1, GW036057_2, GW036056_1, GW036016_1,
 GW036016_2, GW036016_3, GW036185_1, GW036015_1, GW036015_2, GW036014_1, GW036014_2, GW036013_1,
 GW036012_1, GW036055_1, GW036055_2, GW036055_3, GW036005_1, GW036005_2, GW036096_1, GW036096_2,
 GW036093_1, GW036093_2, GW036093_3, GW036164_1, GW036004_1, GW036004_2, GW036186_1, GW036187_1,
 GW030129_1, GW030130_1, GW030130_2, GW030447_1, GW030131_1, GW967137_1, GW967137_2, GW036094_3,
 GW036094_2, GW036094_1, GW030446_1, GW030446_2, GW030132_1, GW030132_2, GW063059_1, GW063060_1,
 GW030133_1, GW030237_1, GW030236_1, GW030236_2, GW030235_1, GW030235_2, GW030134_1, GW030234_1,
 GW030233_1, GW030233_2, GW030233_3, GW030232_1, GW030232_2, GW030232_3, GW030231_1, GW030231_2}
```

A.6.3 Plotting the Data and Calculating the Correlation Coefficient

This block of script generates the plots and determines the statistical correlation coefficient between the measured groundwater hydrograph and the FEFLOW modelled hydrograph. The statistical algorithms are from:

Daniel de Souza Carvalho "Correlation and Covariance of Random Discrete Signals" from the Wolfram Demonstrations Project,
http://demonstrations.wolfram.com/CorrelationAndCovarianceOfFandomDiscreteSignals.

```
imagelist = {};
correlationlist = {};
Do[
 gw = allbores[[m]]; gwnumber = ToExpression[StringTake[gw, {3, 8}]]; gwpipe = ToExpression[StringTake[gw, {10}]] / 1.;
 set1 = Cases[feflowData, {_, gw, _, _}][[All, {3, 4}]];
 set2 = Cases[measuredData, {gwnumber, gwpipe, _, _, _, _, _, _}][[All, {5, 8}]];
 If[Length[set2 ] > 1,
  string = Column[{Style["Measured (x)", Blue], Style["Modelled (y)", Red]}];
  plot = DateListPlot[{set1, set2}, PlotStyle → {Red, Blue}, GridLines → Automatic, ImageSize → {300, 300},
    PlotRange → {{{1982}, {2008}},
      {Max[set1[[All, 2]]] + 10, Min[set1[[All, 2]]] - 10}}, Joined → True, Frame → True, FrameLabel → {Style["Date",
       Bold, Darker[Blue]], Style["Water Level (M.A.S.L.)", Bold, Darker[Blue]], Style[gw, Bold, Purple]},
    Epilog :→ Text[string, {{2005}, Max[set1[[All, 2]] + 7]}]];
  scaleddata1 = Table[{N[AbsoluteTime[set1[[i, 1]]]], Abs[set1[[i, 2]]]}, {i, 1, Length[set1]}];
  function1 = Interpolation[scaleddata1, Method → "Spline", InterpolationOrder → 1];
  scaleddata2 = Table[{N[AbsoluteTime[set2[[i, 1]]]], Abs[set2[[i, 2]]]}, {i, 1, Length[set2]}];
  function2 = Interpolation[scaleddata2, Method → "Spline", InterpolationOrder → 1];
  min1 = Min[scaleddata1[[All, 1]]]; min2 = Min[scaleddata2[[All, 1]]];
  max1 = Max[scaleddata1[[All, 1]]]; max2 = Max[scaleddata2[[All, 1]]];
  If[min1 < min2 , rmina = min2, rmina = min1];
  If[max1 > max2, rmaxa = max2, rmaxa = max1];
  rstep = (rmaxa - rmina) / 1000;
  abs1980 = AbsoluteTime[{1982, 1, 1, 0, 0, 0}]; abs2007 = AbsoluteTime[{2007, 4, 1, 0, 0, 0}];
  If[rmina < abs1980 , rmin = abs1980, rmin = rmina];
  If[rmaxa > abs2007, rmax = abs2007, rmax = rmaxa];
  interpset1 = Table[{i, function1[i]}, {i, rmin, rmax, rstep}]; interpset2 = Table[{i, function2[i]}, {i, rmin, rmax, rstep}];
  lx = Table[function1[i], {i, rmin, rmax, rstep}]; ly = Table[function2[i], {i, rmin, rmax, rstep}];

   AppendTo[imagelist, Grid[{{Show[plot, ImageSize → {300, 300}], "    ",
       Text@TraditionalForm@Grid[{
          {x̄, " = ", HoldForm[1/N] ∑_{i=1}^{N} x_i, " = ", NumberForm[#, {5, 4}, NumberPadding → {"", "0"}] &@(xm = N[Mean[lx]])},
          {ȳ, " = ", HoldForm[1/N] ∑_{i=1}^{N} y_i, " = ", NumberForm[#, {5, 4}, NumberPadding → {"", "0"}] &@(ym = N[Mean[ly]])},
          {x̄ ȳ, " = ", HoldForm[1/N] ∑_{i=1}^{N} (x_i * y_i), " = ", NumberForm[#, {5, 4}, NumberPadding → {"", "0"}] &@
            (xym = N[Mean[lx * ly]])},
          {σ̂_x, " = ", √(HoldForm[1/(N - 1)] * ∑_{i=1}^{N} (x_i - x̄)^2), " = ", NumberForm[#, {5, 4}, NumberPadding → {"", "0"}] &@
            (xstddev = N[StandardDeviation[lx]])},
          {σ̂_y, " = ", √(HoldForm[1/(N - 1)] * ∑_{i=1}^{N} (y_i - ȳ)^2), " = ", NumberForm[#, {5, 4}, NumberPadding → {"", "0"}] &@
            (ystddev = N[StandardDeviation[ly]])},
          {σ̂_xy, " = ", HoldForm[1/(N - 1)] * ∑_{i=1}^{N} (x_i - x̄) (y_i - ȳ), " = ",
           NumberForm[#, {5, 4}, NumberPadding → {"", "0"}] &@(N[Covariance[lx, ly]])},
          {ρ̂, " = ", σ̂_xy / (σ̂_x σ̂_y), " = ", NumberForm[#, {5, 4}, NumberPadding → {"", "0"}] &@(N[Correlation[lx, ly]])}
         }, Alignment → Left, ItemSize → {{3, 1.5, 11, 1.5, 10}, Automatic}]}}]];
  AppendTo[correlationlist, {gw, N[Correlation[lx, ly]]}];
  , 0];,|{m, 1, Length[allbores]}]
imagelist
```

Below are the hydrograph plots generated by the above script for the Maules Creek FEFLOW model data sets. The statistics calculated are the mean head, mean (measured head *x* modelled head), standard deviation, covariance and the correlation coefficient.

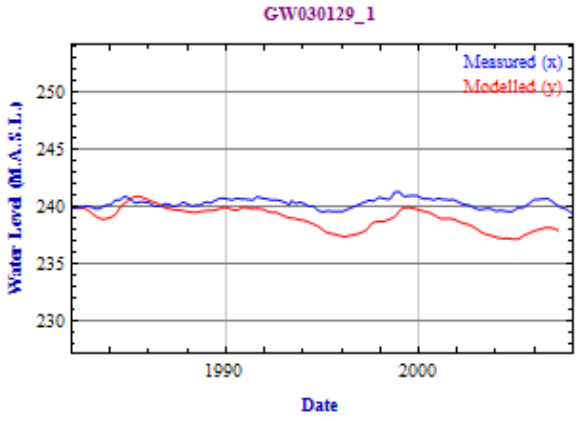

$$\bar{x} = \frac{1}{N}\sum_{i=1}^{N} x_i = 239.0200$$

$$\bar{y} = \frac{1}{N}\sum_{i=1}^{N} y_i = 240.3400$$

$$\overline{xy} = \frac{1}{N}\sum_{i=1}^{N} x_i y_i = 57445.0000$$

$$\hat{\sigma}_x = \sqrt{\frac{1}{N-1}\sum_{i=1}^{N} (x_i - \bar{x})^2} = 0.9812$$

$$\hat{\sigma}_y = \sqrt{\frac{1}{N-1}\sum_{i=1}^{N} (y_i - \bar{y})^2} = 0.4020$$

$$\hat{\sigma}_{xy} = \frac{1}{N-1}\sum_{i=1}^{N} (x_i - \bar{x})(y_i - \bar{y}) = 0.2167$$

$$\hat{\rho} = \frac{\hat{\sigma}_{xy}}{\hat{\sigma}_x \hat{\sigma}_y} = 0.5493$$

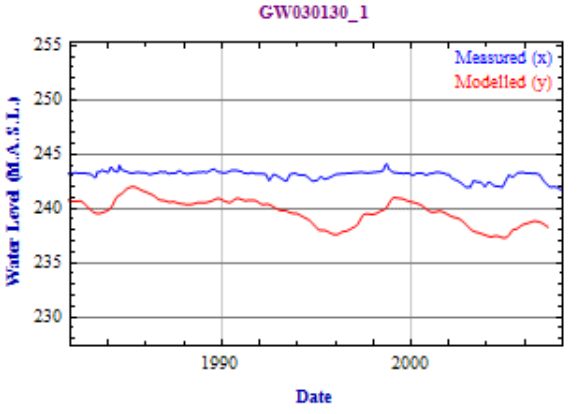

$$\bar{x} = \frac{1}{N}\sum_{i=1}^{N} x_i = 239.7000$$

$$\bar{y} = \frac{1}{N}\sum_{i=1}^{N} y_i = 243.1100$$

$$\overline{xy} = \frac{1}{N}\sum_{i=1}^{N} x_i y_i = 58272.0000$$

$$\hat{\sigma}_x = \sqrt{\frac{1}{N-1}\sum_{i=1}^{N} (x_i - \bar{x})^2} = 1.2197$$

$$\hat{\sigma}_y = \sqrt{\frac{1}{N-1}\sum_{i=1}^{N} (y_i - \bar{y})^2} = 0.3885$$

$$\hat{\sigma}_{xy} = \frac{1}{N-1}\sum_{i=1}^{N} (x_i - \bar{x})(y_i - \bar{y}) = 0.3034$$

$$\hat{\rho} = \frac{\hat{\sigma}_{xy}}{\hat{\sigma}_x \hat{\sigma}_y} = 0.6403$$

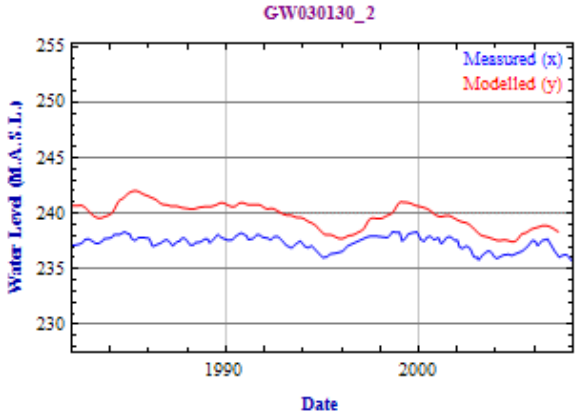

$$\bar{x} = \frac{1}{N}\sum_{i=1}^{N} x_i = 239.7600$$

$$\bar{y} = \frac{1}{N}\sum_{i=1}^{N} y_i = 237.3700$$

$$\overline{xy} = \frac{1}{N}\sum_{i=1}^{N} x_i y_i = 56912.0000$$

$$\hat{\sigma}_x = \sqrt{\frac{1}{N-1}\sum_{i=1}^{N} (x_i - \bar{x})^2} = 1.1883$$

$$\hat{\sigma}_y = \sqrt{\frac{1}{N-1}\sum_{i=1}^{N} (y_i - \bar{y})^2} = 0.6042$$

$$\hat{\sigma}_{xy} = \frac{1}{N-1}\sum_{i=1}^{N} (x_i - \bar{x})(y_i - \bar{y}) = 0.5436$$

$$\hat{\rho} = \frac{\hat{\sigma}_{xy}}{\hat{\sigma}_x \hat{\sigma}_y} = 0.7571$$

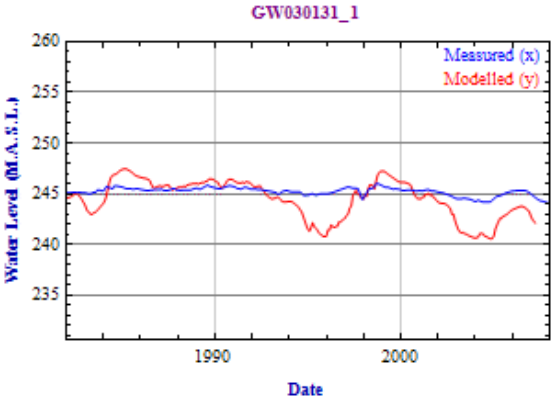

$$\bar{x} = \frac{1}{N}\sum_{i=1}^{N} x_i = 244.4700$$

$$\bar{y} = \frac{1}{N}\sum_{i=1}^{N} y_i = 245.2300$$

$$\overline{xy} = \frac{1}{N}\sum_{i=1}^{N} x_i y_i = 59952.0000$$

$$\hat{\sigma}_x = \sqrt{\frac{1}{N-1}\sum_{i=1}^{N} (x_i - \bar{x})^2} = 1.8938$$

$$\hat{\sigma}_y = \sqrt{\frac{1}{N-1}\sum_{i=1}^{N} (y_i - \bar{y})^2} = 0.3721$$

$$\hat{\sigma}_{xy} = \frac{1}{N-1}\sum_{i=1}^{N} (x_i - \bar{x})(y_i - \bar{y}) = 0.5800$$

$$\hat{\rho} = \frac{\hat{\sigma}_{xy}}{\hat{\sigma}_x \hat{\sigma}_y} = 0.8231$$

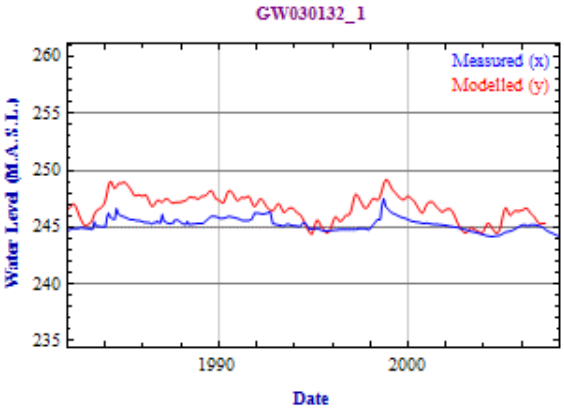

$$\bar{x} = \frac{1}{N}\sum_{i=1}^{N} x_i = 246.7200$$

$$\bar{y} = \frac{1}{N}\sum_{i=1}^{N} y_i = 245.2800$$

$$\overline{xy} = \frac{1}{N}\sum_{i=1}^{N} x_i y_i = 60517.0000$$

$$\hat{\sigma}_x = \sqrt{\frac{1}{N-1}\sum_{i=1}^{N} (x_i - \bar{x})^2} = 1.1363$$

$$\hat{\sigma}_y = \sqrt{\frac{1}{N-1}\sum_{i=1}^{N} (y_i - \bar{y})^2} = 0.5370$$

$$\hat{\sigma}_{xy} = \frac{1}{N-1}\sum_{i=1}^{N} (x_i - \bar{x})(y_i - \bar{y}) = 0.4777$$

$$\hat{\rho} = \frac{\hat{\sigma}_{xy}}{\hat{\sigma}_x \hat{\sigma}_y} = 0.7829$$

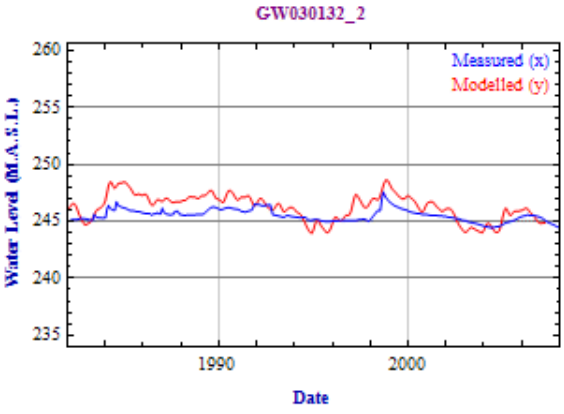

$$\bar{x} = \frac{1}{N}\sum_{i=1}^{N} x_i = 246.2500$$

$$\bar{y} = \frac{1}{N}\sum_{i=1}^{N} y_i = 245.5400$$

$$\overline{xy} = \frac{1}{N}\sum_{i=1}^{N} x_i y_i = 60463.0000$$

$$\hat{\sigma}_x = \sqrt{\frac{1}{N-1}\sum_{i=1}^{N} (x_i - \bar{x})^2} = 1.1319$$

$$\hat{\sigma}_y = \sqrt{\frac{1}{N-1}\sum_{i=1}^{N} (y_i - \bar{y})^2} = 0.5210$$

$$\hat{\sigma}_{xy} = \frac{1}{N-1}\sum_{i=1}^{N} (x_i - \bar{x})(y_i - \bar{y}) = 0.4725$$

$$\hat{\rho} = \frac{\hat{\sigma}_{xy}}{\hat{\sigma}_x \hat{\sigma}_y} = 0.8012$$

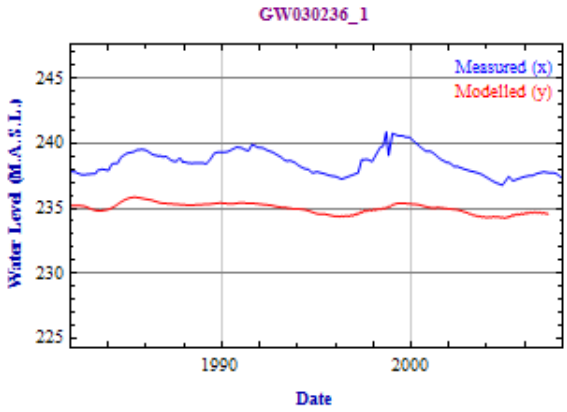

$$\bar{x} = \frac{1}{N}\sum_{i=1}^{N} x_i = 235.0100$$

$$\bar{y} = \frac{1}{N}\sum_{i=1}^{N} y_i = 238.5600$$

$$\overline{xy} = \frac{1}{N}\sum_{i=1}^{N} x_i y_i = 56064.0000$$

$$\hat{\sigma}_x = \sqrt{\frac{1}{N-1}\sum_{i=1}^{N} (x_i - \bar{x})^2} = 0.3999$$

$$\hat{\sigma}_y = \sqrt{\frac{1}{N-1}\sum_{i=1}^{N} (y_i - \bar{y})^2} = 0.9318$$

$$\hat{\sigma}_{xy} = \frac{1}{N-1}\sum_{i=1}^{N} (x_i - \bar{x})(y_i - \bar{y}) = 0.2929$$

$$\hat{\rho} = \frac{\hat{\sigma}_{xy}}{\hat{\sigma}_x \hat{\sigma}_y} = 0.7859$$

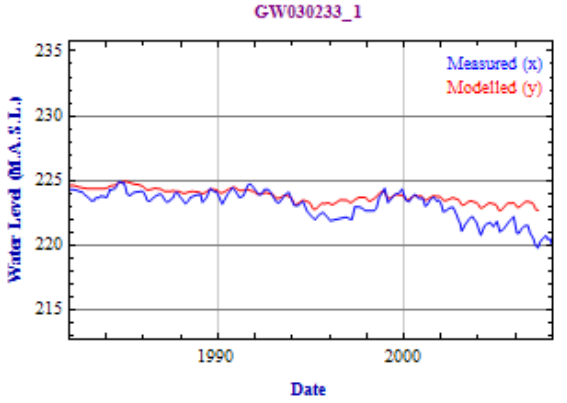

$$\bar{x} = \frac{1}{N}\sum_{i=1}^{N} x_i = 223.8000$$

$$\bar{y} = \frac{1}{N}\sum_{i=1}^{N} y_i = 223.1400$$

$$\overline{xy} = \frac{1}{N}\sum_{i=1}^{N} x_i y_i = 49940.0000$$

$$\hat{\sigma}_x = \sqrt{\frac{1}{N-1}\sum_{i=1}^{N} (x_i - \bar{x})^2} = 0.5310$$

$$\hat{\sigma}_y = \sqrt{\frac{1}{N-1}\sum_{i=1}^{N} (y_i - \bar{y})^2} = 1.0451$$

$$\hat{\sigma}_{xy} = \frac{1}{N-1}\sum_{i=1}^{N} (x_i - \bar{x})(y_i - \bar{y}) = 0.4818$$

$$\hat{\rho} = \frac{\hat{\sigma}_{xy}}{\hat{\sigma}_x \hat{\sigma}_y} = 0.8682$$

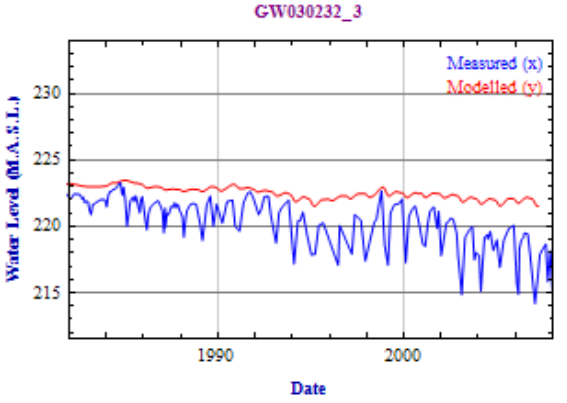

$$\bar{x} = \frac{1}{N}\sum_{i=1}^{N} x_i = 222.5000$$

$$\bar{y} = \frac{1}{N}\sum_{i=1}^{N} y_i = 220.2800$$

$$\overline{xy} = \frac{1}{N}\sum_{i=1}^{N} x_i y_i = 49013.0000$$

$$\hat{\sigma}_x = \sqrt{\frac{1}{N-1}\sum_{i=1}^{N} (x_i - \bar{x})^2} = 0.4570$$

$$\hat{\sigma}_y = \sqrt{\frac{1}{N-1}\sum_{i=1}^{N} (y_i - \bar{y})^2} = 1.6869$$

$$\hat{\sigma}_{xy} = \frac{1}{N-1}\sum_{i=1}^{N} (x_i - \bar{x})(y_i - \bar{y}) = 0.6170$$

$$\hat{\rho} = \frac{\hat{\sigma}_{xy}}{\hat{\sigma}_x \hat{\sigma}_y} = 0.8002$$

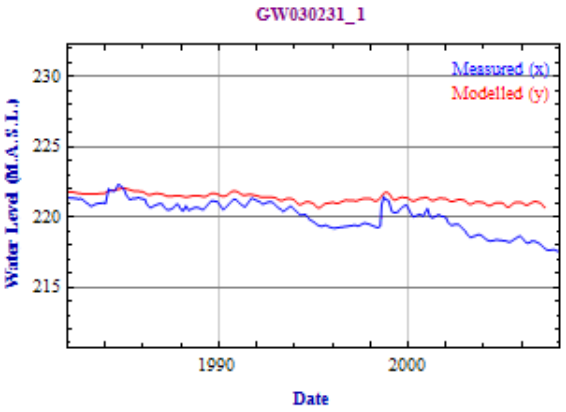

$$\bar{x} = \frac{1}{N}\sum_{i=1}^{N} x_i = 221.3400$$

$$\bar{y} = \frac{1}{N}\sum_{i=1}^{N} y_i = 220.1400$$

$$\overline{xy} = \frac{1}{N}\sum_{i=1}^{N} x_i y_i = 48726.0000$$

$$\hat{\sigma}_x = \sqrt{\frac{1}{N-1}\sum_{i=1}^{N} (x_i - \bar{x})^2} = 0.3179$$

$$\hat{\sigma}_y = \sqrt{\frac{1}{N-1}\sum_{i=1}^{N} (y_i - \bar{y})^2} = 1.0522$$

$$\hat{\sigma}_{xy} = \frac{1}{N-1}\sum_{i=1}^{N} (x_i - \bar{x})(y_i - \bar{y}) = 0.2976$$

$$\hat{\rho} = \frac{\hat{\sigma}_{xy}}{\hat{\sigma}_x \hat{\sigma}_y} = 0.8898$$

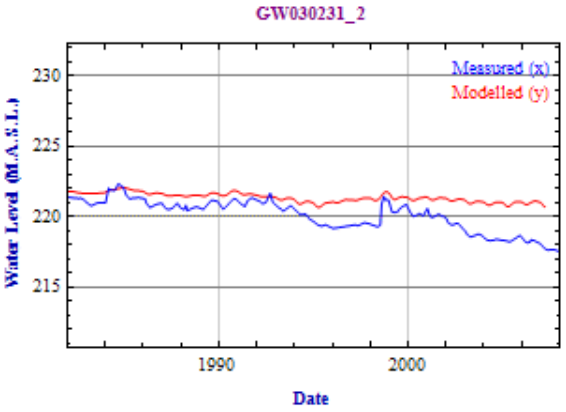

$$\bar{x} = \frac{1}{N}\sum_{i=1}^{N} x_i = 221.3400$$

$$\bar{y} = \frac{1}{N}\sum_{i=1}^{N} y_i = 220.1400$$

$$\overline{xy} = \frac{1}{N}\sum_{i=1}^{N} x_i y_i = 48727.0000$$

$$\hat{\sigma}_x = \sqrt{\frac{1}{N-1}\sum_{i=1}^{N} (x_i - \bar{x})^2} = 0.3180$$

$$\hat{\sigma}_y = \sqrt{\frac{1}{N-1}\sum_{i=1}^{N} (y_i - \bar{y})^2} = 1.0584$$

$$\hat{\sigma}_{xy} = \frac{1}{N-1}\sum_{i=1}^{N} (x_i - \bar{x})(y_i - \bar{y}) = 0.2987$$

$$\hat{\rho} = \frac{\hat{\sigma}_{xy}}{\hat{\sigma}_x \hat{\sigma}_y} = 0.8874$$

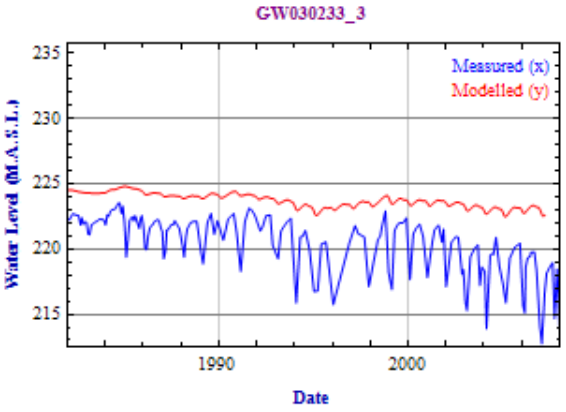

$$\bar{x} = \frac{1}{N}\sum_{i=1}^{N} x_i = 223.7100$$

$$\bar{y} = \frac{1}{N}\sum_{i=1}^{N} y_i = 220.4500$$

$$\overline{xy} = \frac{1}{N}\sum_{i=1}^{N} x_i y_i = 49317.0000$$

$$\hat{\sigma}_x = \sqrt{\frac{1}{N-1}\sum_{i=1}^{N} (x_i - \bar{x})^2} = 0.5390$$

$$\hat{\sigma}_y = \sqrt{\frac{1}{N-1}\sum_{i=1}^{N} (y_i - \bar{y})^2} = 1.9598$$

$$\hat{\sigma}_{xy} = \frac{1}{N-1}\sum_{i=1}^{N} (x_i - \bar{x})(y_i - \bar{y}) = 0.8273$$

$$\hat{\rho} = \frac{\hat{\sigma}_{xy}}{\hat{\sigma}_x \hat{\sigma}_y} = 0.7832$$

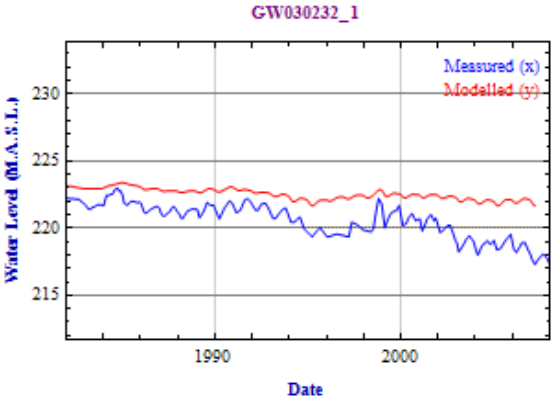

$$\bar{x} = \frac{1}{N}\sum_{i=1}^{N} x_i = 222.5200$$

$$\bar{y} = \frac{1}{N}\sum_{i=1}^{N} y_i = 220.6200$$

$$\overline{xy} = \frac{1}{N}\sum_{i=1}^{N} x_i y_i = 49094.0000$$

$$\hat{\sigma}_x = \sqrt{\frac{1}{N-1}\sum_{i=1}^{N} (x_i - \bar{x})^2} = 0.4078$$

$$\hat{\sigma}_y = \sqrt{\frac{1}{N-1}\sum_{i=1}^{N} (y_i - \bar{y})^2} = 1.2037$$

$$\hat{\sigma}_{xy} = \frac{1}{N-1}\sum_{i=1}^{N} (x_i - \bar{x})(y_i - \bar{y}) = 0.4490$$

$$\hat{\rho} = \frac{\hat{\sigma}_{xy}}{\hat{\sigma}_x \hat{\sigma}_y} = 0.9147$$

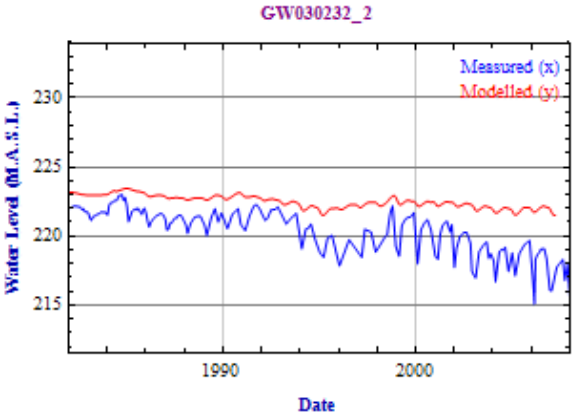

$$\bar{x} = \frac{1}{N}\sum_{i=1}^{N} x_i = 222.4900$$

$$\bar{y} = \frac{1}{N}\sum_{i=1}^{N} y_i = 220.3600$$

$$\overline{xy} = \frac{1}{N}\sum_{i=1}^{N} x_i y_i = 49028.0000$$

$$\hat{\sigma}_x = \sqrt{\frac{1}{N-1}\sum_{i=1}^{N} (x_i - \bar{x})^2} = 0.4552$$

$$\hat{\sigma}_y = \sqrt{\frac{1}{N-1}\sum_{i=1}^{N} (y_i - \bar{y})^2} = 1.4505$$

$$\hat{\sigma}_{xy} = \frac{1}{N-1}\sum_{i=1}^{N} (x_i - \bar{x})(y_i - \bar{y}) = 0.5678$$

$$\hat{\rho} = \frac{\hat{\sigma}_{xy}}{\hat{\sigma}_x \hat{\sigma}_y} = 0.8599$$

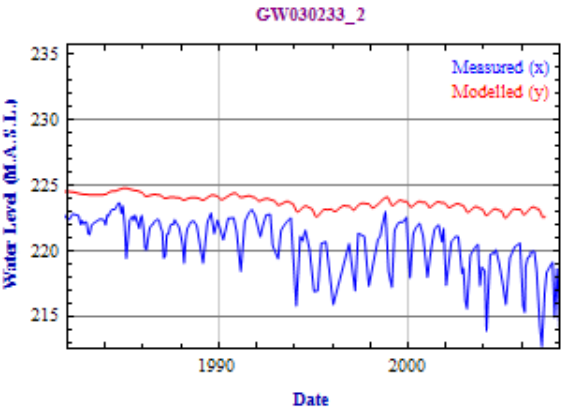

$$\bar{x} = \frac{1}{N}\sum_{i=1}^{N} x_i = 223.7400$$

$$\bar{y} = \frac{1}{N}\sum_{i=1}^{N} y_i = 220.5600$$

$$\overline{xy} = \frac{1}{N}\sum_{i=1}^{N} x_i y_i = 49348.0000$$

$$\hat{\sigma}_x = \sqrt{\frac{1}{N-1}\sum_{i=1}^{N} (x_i - \bar{x})^2} = 0.5309$$

$$\hat{\sigma}_y = \sqrt{\frac{1}{N-1}\sum_{i=1}^{N} (y_i - \bar{y})^2} = 1.9674$$

$$\hat{\sigma}_{xy} = \frac{1}{N-1}\sum_{i=1}^{N} (x_i - \bar{x})(y_i - \bar{y}) = 0.8303$$

$$\hat{\rho} = \frac{\hat{\sigma}_{xy}}{\hat{\sigma}_x \hat{\sigma}_y} = 0.7949$$

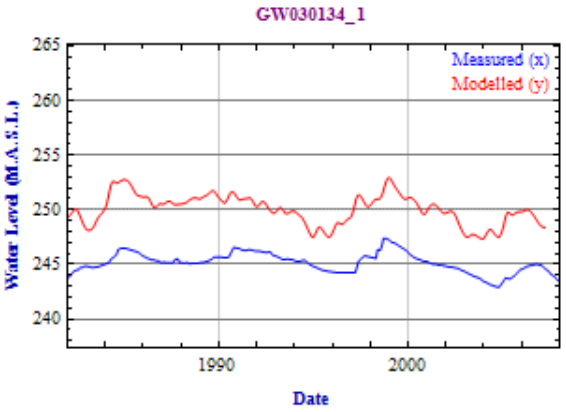

$$\bar{x} = \frac{1}{N}\sum_{i=1}^{N} x_i = 250.0400$$

$$\bar{y} = \frac{1}{N}\sum_{i=1}^{N} y_i = 245.1800$$

$$\overline{xy} = \frac{1}{N}\sum_{i=1}^{N} x_i y_i = 61304.0000$$

$$\hat{\sigma}_x = \sqrt{\frac{1}{N-1}\sum_{i=1}^{N} (x_i - \bar{x})^2} = 1.3589$$

$$\hat{\sigma}_y = \sqrt{\frac{1}{N-1}\sum_{i=1}^{N} (y_i - \bar{y})^2} = 0.8988$$

$$\hat{\sigma}_{xy} = \frac{1}{N-1}\sum_{i=1}^{N} (x_i - \bar{x})(y_i - \bar{y}) = 0.9729$$

$$\hat{\rho} = \frac{\hat{\sigma}_{xy}}{\hat{\sigma}_x \hat{\sigma}_y} = 0.7966$$

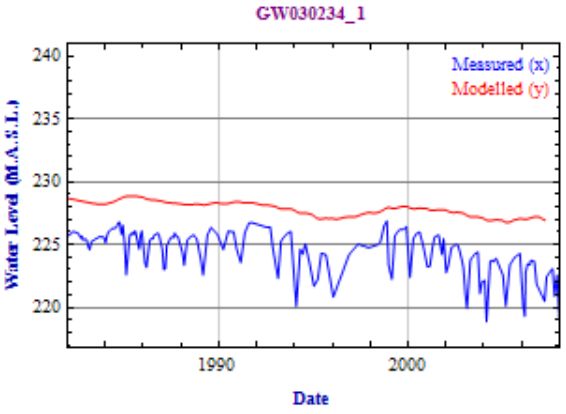

$$\bar{x} = \frac{1}{N}\sum_{i=1}^{N} x_i = 227.8400$$

$$\bar{y} = \frac{1}{N}\sum_{i=1}^{N} y_i = 224.5000$$

$$\overline{xy} = \frac{1}{N}\sum_{i=1}^{N} x_i y_i = 51150.0000$$

$$\hat{\sigma}_x = \sqrt{\frac{1}{N-1}\sum_{i=1}^{N} (x_i - \bar{x})^2} = 0.5674$$

$$\hat{\sigma}_y = \sqrt{\frac{1}{N-1}\sum_{i=1}^{N} (y_i - \bar{y})^2} = 1.5619$$

$$\hat{\sigma}_{xy} = \frac{1}{N-1}\sum_{i=1}^{N} (x_i - \bar{x})(y_i - \bar{y}) = 0.5926$$

$$\hat{\rho} = \frac{\hat{\sigma}_{xy}}{\hat{\sigma}_x \hat{\sigma}_y} = 0.6687$$

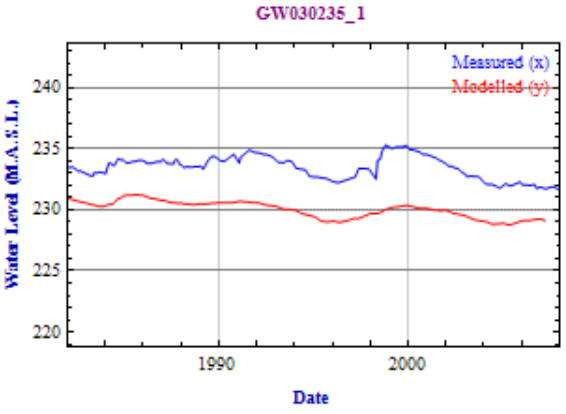

$$\bar{x} = \frac{1}{N}\sum_{i=1}^{N} x_i = 230.0200$$

$$\bar{y} = \frac{1}{N}\sum_{i=1}^{N} y_i = 233.4900$$

$$\overline{xy} = \frac{1}{N}\sum_{i=1}^{N} x_i y_i = 53707.0000$$

$$\hat{\sigma}_x = \sqrt{\frac{1}{N-1}\sum_{i=1}^{N} (x_i - \bar{x})^2} = 0.6826$$

$$\hat{\sigma}_y = \sqrt{\frac{1}{N-1}\sum_{i=1}^{N} (y_i - \bar{y})^2} = 0.9163$$

$$\hat{\sigma}_{xy} = \frac{1}{N-1}\sum_{i=1}^{N} (x_i - \bar{x})(y_i - \bar{y}) = 0.4528$$

$$\hat{\rho} = \frac{\hat{\sigma}_{xy}}{\hat{\sigma}_x \hat{\sigma}_y} = 0.7240$$

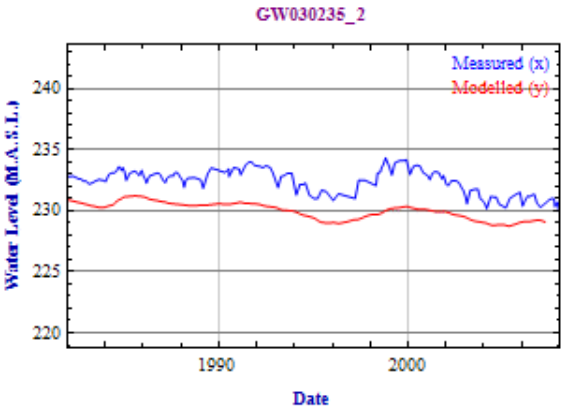

$$\bar{x} = \frac{1}{N}\sum_{i=1}^{N} x_i = 230.0000$$

$$\bar{y} = \frac{1}{N}\sum_{i=1}^{N} y_i = 232.4200$$

$$\overline{xy} = \frac{1}{N}\sum_{i=1}^{N} x_i y_i = 53456.0000$$

$$\hat{\sigma}_x = \sqrt{\frac{1}{N-1}\sum_{i=1}^{N} (x_i - \bar{x})^2} = 0.6826$$

$$\hat{\sigma}_y = \sqrt{\frac{1}{N-1}\sum_{i=1}^{N} (y_i - \bar{y})^2} = 0.9841$$

$$\hat{\sigma}_{xy} = \frac{1}{N-1}\sum_{i=1}^{N} (x_i - \bar{x})(y_i - \bar{y}) = 0.5309$$

$$\hat{\rho} = \frac{\hat{\sigma}_{xy}}{\hat{\sigma}_x \hat{\sigma}_y} = 0.7903$$

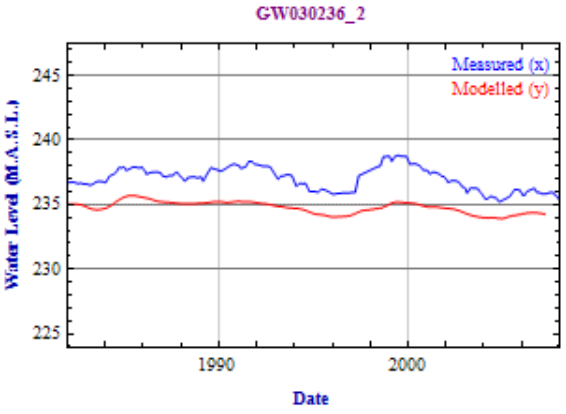

$$\bar{x} = \frac{1}{N}\sum_{i=1}^{N} x_i = 234.7700$$

$$\bar{y} = \frac{1}{N}\sum_{i=1}^{N} y_i = 237.0500$$

$$\overline{xy} = \frac{1}{N}\sum_{i=1}^{N} x_i y_i = 55654.0000$$

$$\hat{\sigma}_x = \sqrt{\frac{1}{N-1}\sum_{i=1}^{N} (x_i - \bar{x})^2} = 0.4582$$

$$\hat{\sigma}_y = \sqrt{\frac{1}{N-1}\sum_{i=1}^{N} (y_i - \bar{y})^2} = 0.8806$$

$$\hat{\sigma}_{xy} = \frac{1}{N-1}\sum_{i=1}^{N} (x_i - \bar{x})(y_i - \bar{y}) = 0.3341$$

$$\hat{\rho} = \frac{\hat{\sigma}_{xy}}{\hat{\sigma}_x \hat{\sigma}_y} = 0.8279$$

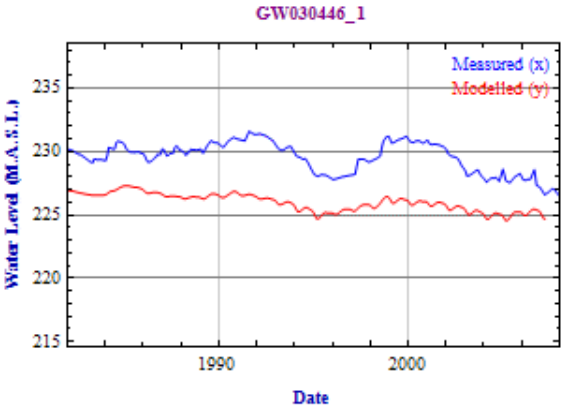

$$\bar{x} = \frac{1}{N}\sum_{i=1}^{N} x_i = 225.9900$$

$$\bar{y} = \frac{1}{N}\sum_{i=1}^{N} y_i = 229.6100$$

$$\overline{xy} = \frac{1}{N}\sum_{i=1}^{N} x_i y_i = 51890.0000$$

$$\hat{\sigma}_x = \sqrt{\frac{1}{N-1}\sum_{i=1}^{N} (x_i - \bar{x})^2} = 0.6828$$

$$\hat{\sigma}_y = \sqrt{\frac{1}{N-1}\sum_{i=1}^{N} (y_i - \bar{y})^2} = 1.1533$$

$$\hat{\sigma}_{xy} = \frac{1}{N-1}\sum_{i=1}^{N} (x_i - \bar{x})(y_i - \bar{y}) = 0.5834$$

$$\hat{\rho} = \frac{\hat{\sigma}_{xy}}{\hat{\sigma}_x \hat{\sigma}_y} = 0.7409$$

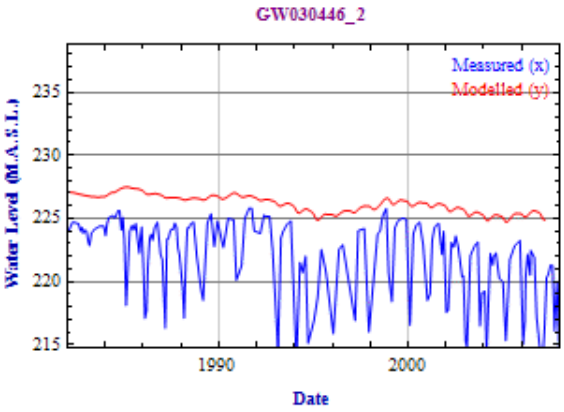

$$\bar{x} = \frac{1}{N}\sum_{i=1}^{N} x_i = 226.1600$$

$$\bar{y} = \frac{1}{N}\sum_{i=1}^{N} y_i = 221.9400$$

$$\overline{xy} = \frac{1}{N}\sum_{i=1}^{N} x_i y_i = 50195.0000$$

$$\hat{\sigma}_x = \sqrt{\frac{1}{N-1}\sum_{i=1}^{N} (x_i - \bar{x})^2} = 0.6856$$

$$\hat{\sigma}_y = \sqrt{\frac{1}{N-1}\sum_{i=1}^{N} (y_i - \bar{y})^2} = 2.8396$$

$$\hat{\sigma}_{xy} = \frac{1}{N-1}\sum_{i=1}^{N} (x_i - \bar{x})(y_i - \bar{y}) = 1.1360$$

$$\hat{\rho} = \frac{\hat{\sigma}_{xy}}{\hat{\sigma}_x \hat{\sigma}_y} = 0.5835$$

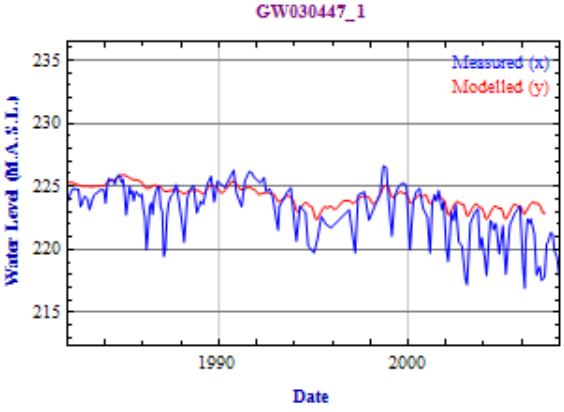

$$\bar{x} = \frac{1}{N}\sum_{i=1}^{N} x_i = 224.2200$$

$$\bar{y} = \frac{1}{N}\sum_{i=1}^{N} y_i = 223.1600$$

$$\overline{xy} = \frac{1}{N}\sum_{i=1}^{N} x_i y_i = 50038.0000$$

$$\hat{\sigma}_x = \sqrt{\frac{1}{N-1}\sum_{i=1}^{N} (x_i - \bar{x})^2} = 0.8246$$

$$\hat{\sigma}_y = \sqrt{\frac{1}{N-1}\sum_{i=1}^{N} (y_i - \bar{y})^2} = 1.9638$$

$$\hat{\sigma}_{xy} = \frac{1}{N-1}\sum_{i=1}^{N} (x_i - \bar{x})(y_i - \bar{y}) = 1.2234$$

$$\hat{\rho} = \frac{\hat{\sigma}_{xy}}{\hat{\sigma}_x \hat{\sigma}_y} = 0.7555$$

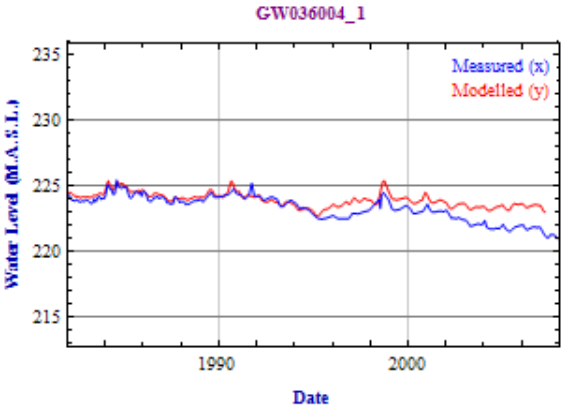

$$\bar{x} = \frac{1}{N}\sum_{i=1}^{N} x_i = 223.9600$$

$$\bar{y} = \frac{1}{N}\sum_{i=1}^{N} y_i = 223.3800$$

$$\overline{xy} = \frac{1}{N}\sum_{i=1}^{N} x_i y_i = 50030.0000$$

$$\hat{\sigma}_x = \sqrt{\frac{1}{N-1}\sum_{i=1}^{N} (x_i - \bar{x})^2} = 0.5330$$

$$\hat{\sigma}_y = \sqrt{\frac{1}{N-1}\sum_{i=1}^{N} (y_i - \bar{y})^2} = 0.9159$$

$$\hat{\sigma}_{xy} = \frac{1}{N-1}\sum_{i=1}^{N} (x_i - \bar{x})(y_i - \bar{y}) = 0.4024$$

$$\hat{\rho} = \frac{\hat{\sigma}_{xy}}{\hat{\sigma}_x \hat{\sigma}_y} = 0.8241$$

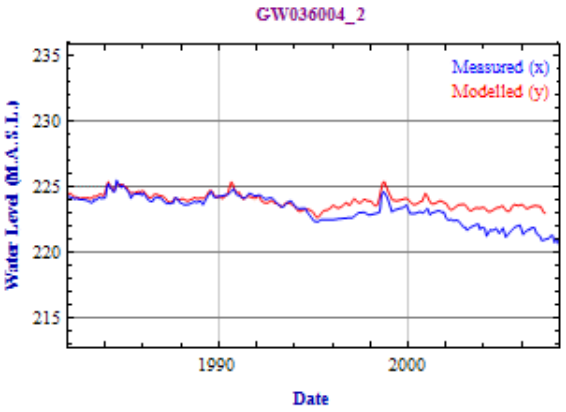

$$\bar{x} = \frac{1}{N}\sum_{i=1}^{N} x_i = 223.9600$$

$$\bar{y} = \frac{1}{N}\sum_{i=1}^{N} y_i = 223.3500$$

$$\overline{xy} = \frac{1}{N}\sum_{i=1}^{N} x_i y_i = 50022.0000$$

$$\hat{\sigma}_x = \sqrt{\frac{1}{N-1}\sum_{i=1}^{N} (x_i - \bar{x})^2} = 0.5335$$

$$\hat{\sigma}_y = \sqrt{\frac{1}{N-1}\sum_{i=1}^{N} (y_i - \bar{y})^2} = 1.0123$$

$$\hat{\sigma}_{xy} = \frac{1}{N-1}\sum_{i=1}^{N} (x_i - \bar{x})(y_i - \bar{y}) = 0.4500$$

$$\hat{\rho} = \frac{\hat{\sigma}_{xy}}{\hat{\sigma}_x \hat{\sigma}_y} = 0.8332$$

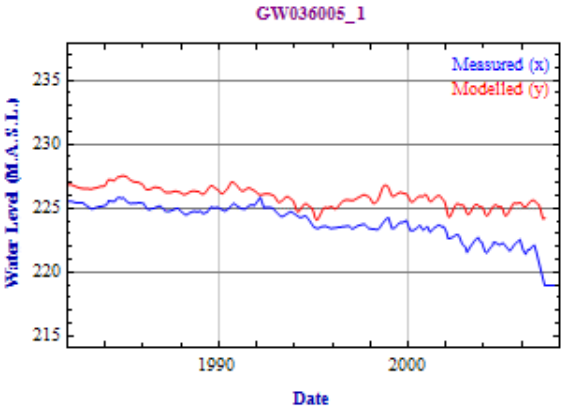

$$\bar{x} = \frac{1}{N}\sum_{i=1}^{N} x_i = 225.9000$$

$$\bar{y} = \frac{1}{N}\sum_{i=1}^{N} y_i = 223.9700$$

$$\overline{xy} = \frac{1}{N}\sum_{i=1}^{N} x_i y_i = 50596.0000$$

$$\hat{\sigma}_x = \sqrt{\frac{1}{N-1}\sum_{i=1}^{N} (x_i - \bar{x})^2} = 0.7625$$

$$\hat{\sigma}_y = \sqrt{\frac{1}{N-1}\sum_{i=1}^{N} (y_i - \bar{y})^2} = 1.2790$$

$$\hat{\sigma}_{xy} = \frac{1}{N-1}\sum_{i=1}^{N} (x_i - \bar{x})(y_i - \bar{y}) = 0.7970$$

$$\hat{\rho} = \frac{\hat{\sigma}_{xy}}{\hat{\sigma}_x \hat{\sigma}_y} = 0.8172$$

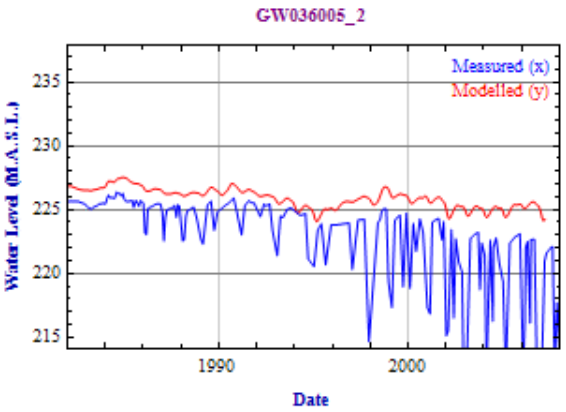

$$\bar{x} = \frac{1}{N}\sum_{i=1}^{N} x_i = 225.8900$$

$$\bar{y} = \frac{1}{N}\sum_{i=1}^{N} y_i = 223.0000$$

$$\overline{xy} = \frac{1}{N}\sum_{i=1}^{N} x_i y_i = 50377.0000$$

$$\hat{\sigma}_x = \sqrt{\frac{1}{N-1}\sum_{i=1}^{N} (x_i - \bar{x})^2} = 0.7632$$

$$\hat{\sigma}_y = \sqrt{\frac{1}{N-1}\sum_{i=1}^{N} (y_i - \bar{y})^2} = 3.0337$$

$$\hat{\sigma}_{xy} = \frac{1}{N-1}\sum_{i=1}^{N} (x_i - \bar{x})(y_i - \bar{y}) = 1.4932$$

$$\hat{\rho} = \frac{\hat{\sigma}_{xy}}{\hat{\sigma}_x \hat{\sigma}_y} = 0.6449$$

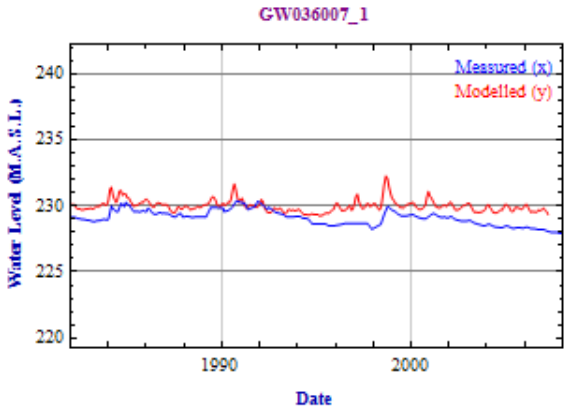

$$\bar{x} = \frac{1}{N}\sum_{i=1}^{N} x_i = 229.9800$$

$$\bar{y} = \frac{1}{N}\sum_{i=1}^{N} y_i = 229.1200$$

$$\overline{xy} = \frac{1}{N}\sum_{i=1}^{N} x_i y_i = 52693.0000$$

$$\hat{\sigma}_x = \sqrt{\frac{1}{N-1}\sum_{i=1}^{N} (x_i - \bar{x})^2} = 0.4442$$

$$\hat{\sigma}_y = \sqrt{\frac{1}{N-1}\sum_{i=1}^{N} (y_i - \bar{y})^2} = 0.5424$$

$$\hat{\sigma}_{xy} = \frac{1}{N-1}\sum_{i=1}^{N} (x_i - \bar{x})(y_i - \bar{y}) = 0.1288$$

$$\hat{\rho} = \frac{\hat{\sigma}_{xy}}{\hat{\sigma}_x \hat{\sigma}_y} = 0.5346$$

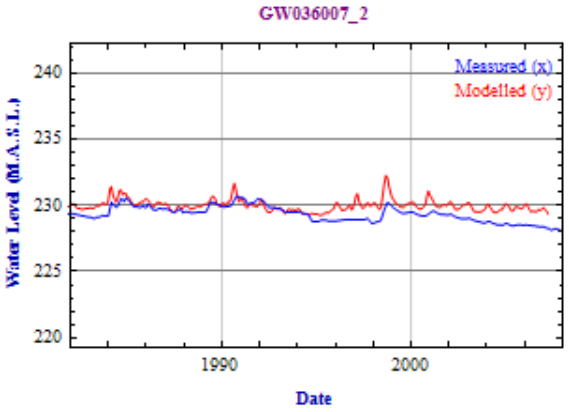

$$\bar{x} = \frac{1}{N}\sum_{i=1}^{N} x_i = 229.9800$$

$$\bar{y} = \frac{1}{N}\sum_{i=1}^{N} y_i = 229.3600$$

$$\overline{xy} = \frac{1}{N}\sum_{i=1}^{N} x_i y_i = 52748.0000$$

$$\hat{\sigma}_x = \sqrt{\frac{1}{N-1}\sum_{i=1}^{N} (x_i - \bar{x})^2} = 0.4442$$

$$\hat{\sigma}_y = \sqrt{\frac{1}{N-1}\sum_{i=1}^{N} (y_i - \bar{y})^2} = 0.5704$$

$$\hat{\sigma}_{xy} = \frac{1}{N-1}\sum_{i=1}^{N} (x_i - \bar{x})(y_i - \bar{y}) = 0.1361$$

$$\hat{\rho} = \frac{\hat{\sigma}_{xy}}{\hat{\sigma}_x \hat{\sigma}_y} = 0.5370$$

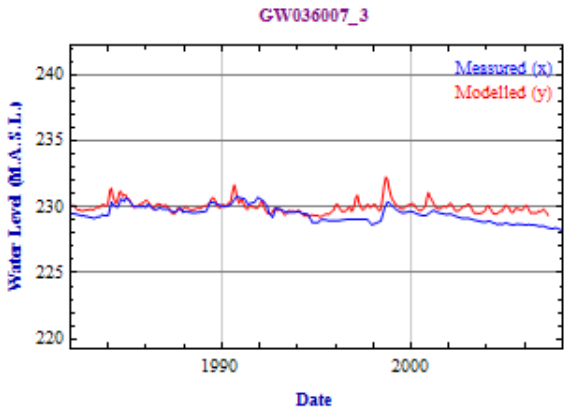

$$\bar{x} = \frac{1}{N}\sum_{i=1}^{N} x_i = 229.9800$$

$$\bar{y} = \frac{1}{N}\sum_{i=1}^{N} y_i = 229.4800$$

$$\overline{xy} = \frac{1}{N}\sum_{i=1}^{N} x_i y_i = 52777.0000$$

$$\hat{\sigma}_x = \sqrt{\frac{1}{N-1}\sum_{i=1}^{N} (x_i - \bar{x})^2} = 0.4442$$

$$\hat{\sigma}_y = \sqrt{\frac{1}{N-1}\sum_{i=1}^{N} (y_i - \bar{y})^2} = 0.5669$$

$$\hat{\sigma}_{xy} = \frac{1}{N-1}\sum_{i=1}^{N} (x_i - \bar{x})(y_i - \bar{y}) = 0.1399$$

$$\hat{\rho} = \frac{\hat{\sigma}_{xy}}{\hat{\sigma}_x \hat{\sigma}_y} = 0.5557$$

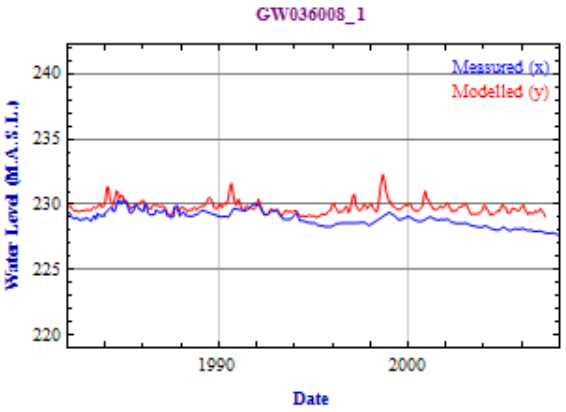

$$\bar{x} = \frac{1}{N}\sum_{i=1}^{N} x_i = 229.7700$$

$$\bar{y} = \frac{1}{N}\sum_{i=1}^{N} y_i = 228.9400$$

$$\overline{xy} = \frac{1}{N}\sum_{i=1}^{N} x_i y_i = 52604.0000$$

$$\hat{\sigma}_x = \sqrt{\frac{1}{N-1}\sum_{i=1}^{N} (x_i - \bar{x})^2} = 0.4662$$

$$\hat{\sigma}_y = \sqrt{\frac{1}{N-1}\sum_{i=1}^{N} (y_i - \bar{y})^2} = 0.5472$$

$$\hat{\sigma}_{xy} = \frac{1}{N-1}\sum_{i=1}^{N} (x_i - \bar{x})(y_i - \bar{y}) = 0.1100$$

$$\hat{\rho} = \frac{\hat{\sigma}_{xy}}{\hat{\sigma}_x \hat{\sigma}_y} = 0.4311$$

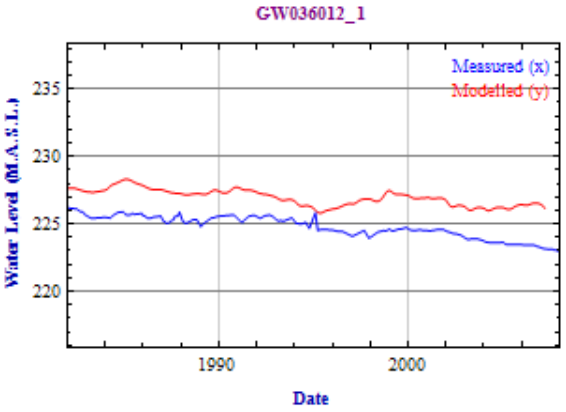

$$\bar{x} = \frac{1}{N}\sum_{i=1}^{N} x_i = 226.9500$$

$$\bar{y} = \frac{1}{N}\sum_{i=1}^{N} y_i = 224.8300$$

$$\overline{xy} = \frac{1}{N}\sum_{i=1}^{N} x_i y_i = 51026.0000$$

$$\hat{\sigma}_x = \sqrt{\frac{1}{N-1}\sum_{i=1}^{N} (x_i - \bar{x})^2} = 0.6009$$

$$\hat{\sigma}_y = \sqrt{\frac{1}{N-1}\sum_{i=1}^{N} (y_i - \bar{y})^2} = 0.7663$$

$$\hat{\sigma}_{xy} = \frac{1}{N-1}\sum_{i=1}^{N} (x_i - \bar{x})(y_i - \bar{y}) = 0.3602$$

$$\hat{\rho} = \frac{\hat{\sigma}_{xy}}{\hat{\sigma}_x \hat{\sigma}_y} = 0.7822$$

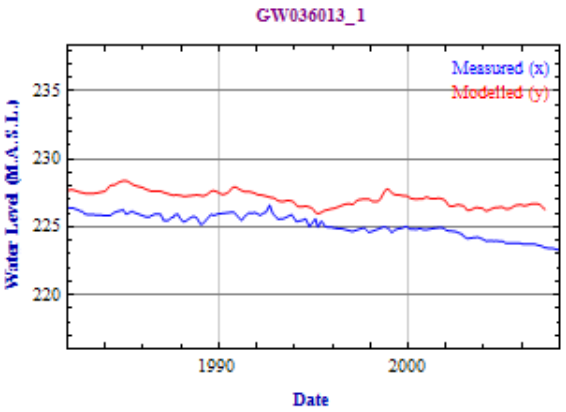

$$\bar{x} = \frac{1}{N}\sum_{i=1}^{N} x_i = 227.1000$$

$$\bar{y} = \frac{1}{N}\sum_{i=1}^{N} y_i = 225.1800$$

$$\overline{xy} = \frac{1}{N}\sum_{i=1}^{N} x_i y_i = 51139.0000$$

$$\hat{\sigma}_x = \sqrt{\frac{1}{N-1}\sum_{i=1}^{N} (x_i - \bar{x})^2} = 0.5606$$

$$\hat{\sigma}_y = \sqrt{\frac{1}{N-1}\sum_{i=1}^{N} (y_i - \bar{y})^2} = 0.7703$$

$$\hat{\sigma}_{xy} = \frac{1}{N-1}\sum_{i=1}^{N} (x_i - \bar{x})(y_i - \bar{y}) = 0.3176$$

$$\hat{\rho} = \frac{\hat{\sigma}_{xy}}{\hat{\sigma}_x \hat{\sigma}_y} = 0.7355$$

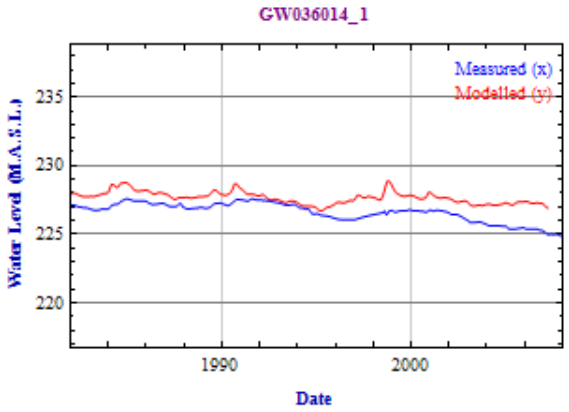

$$\bar{x} = \frac{1}{N}\sum_{i=1}^{N} x_i = 227.6800$$

$$\bar{y} = \frac{1}{N}\sum_{i=1}^{N} y_i = 226.6600$$

$$\overline{xy} = \frac{1}{N}\sum_{i=1}^{N} x_i y_i = 51607.0000$$

$$\hat{\sigma}_x = \sqrt{\frac{1}{N-1}\sum_{i=1}^{N} (x_i - \bar{x})^2} = 0.4414$$

$$\hat{\sigma}_y = \sqrt{\frac{1}{N-1}\sum_{i=1}^{N} (y_i - \bar{y})^2} = 0.6419$$

$$\hat{\sigma}_{xy} = \frac{1}{N-1}\sum_{i=1}^{N} (x_i - \bar{x})(y_i - \bar{y}) = 0.1851$$

$$\hat{\rho} = \frac{\hat{\sigma}_{xy}}{\hat{\sigma}_x \hat{\sigma}_y} = 0.6534$$

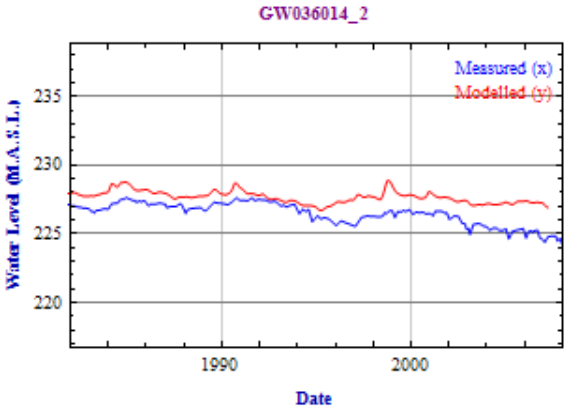

$$\bar{x} = \frac{1}{N}\sum_{i=1}^{N} x_i = 227.6800$$

$$\bar{y} = \frac{1}{N}\sum_{i=1}^{N} y_i = 226.5100$$

$$\overline{xy} = \frac{1}{N}\sum_{i=1}^{N} x_i y_i = 51571.0000$$

$$\hat{\sigma}_x = \sqrt{\frac{1}{N-1}\sum_{i=1}^{N} (x_i - \bar{x})^2} = 0.4414$$

$$\hat{\sigma}_y = \sqrt{\frac{1}{N-1}\sum_{i=1}^{N} (y_i - \bar{y})^2} = 0.7619$$

$$\hat{\sigma}_{xy} = \frac{1}{N-1}\sum_{i=1}^{N} (x_i - \bar{x})(y_i - \bar{y}) = 0.2289$$

$$\hat{\rho} = \frac{\hat{\sigma}_{xy}}{\hat{\sigma}_x \hat{\sigma}_y} = 0.6805$$

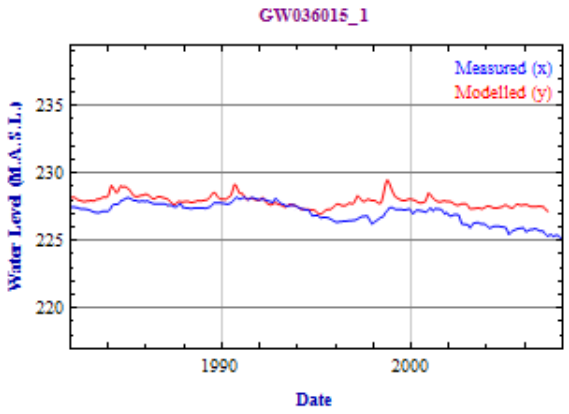

$$\bar{x} = \frac{1}{N}\sum_{i=1}^{N} x_i = 227.9100$$

$$\bar{y} = \frac{1}{N}\sum_{i=1}^{N} y_i = 227.1000$$

$$\overline{xy} = \frac{1}{N}\sum_{i=1}^{N} x_i y_i = 51758.0000$$

$$\hat{\sigma}_x = \sqrt{\frac{1}{N-1}\sum_{i=1}^{N} (x_i - \bar{x})^2} = 0.4391$$

$$\hat{\sigma}_y = \sqrt{\frac{1}{N-1}\sum_{i=1}^{N} (y_i - \bar{y})^2} = 0.7200$$

$$\hat{\sigma}_{xy} = \frac{1}{N-1}\sum_{i=1}^{N} (x_i - \bar{x})(y_i - \bar{y}) = 0.1893$$

$$\hat{\rho} = \frac{\hat{\sigma}_{xy}}{\hat{\sigma}_x \hat{\sigma}_y} = 0.5987$$

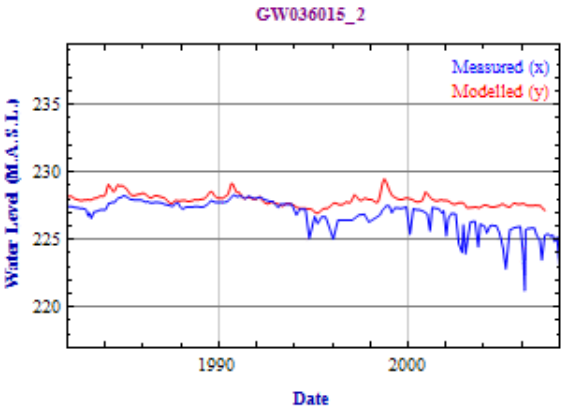

$$\bar{x} = \frac{1}{N}\sum_{i=1}^{N} x_i = 227.9100$$

$$\bar{y} = \frac{1}{N}\sum_{i=1}^{N} y_i = 226.9000$$

$$\overline{xy} = \frac{1}{N}\sum_{i=1}^{N} x_i y_i = 51713.0000$$

$$\hat{\sigma}_x = \sqrt{\frac{1}{N-1}\sum_{i=1}^{N} (x_i - \bar{x})^2} = 0.4390$$

$$\hat{\sigma}_y = \sqrt{\frac{1}{N-1}\sum_{i=1}^{N} (y_i - \bar{y})^2} = 1.0351$$

$$\hat{\sigma}_{xy} = \frac{1}{N-1}\sum_{i=1}^{N} (x_i - \bar{x})(y_i - \bar{y}) = 0.2623$$

$$\hat{\rho} = \frac{\hat{\sigma}_{xy}}{\hat{\sigma}_x \hat{\sigma}_y} = 0.5772$$

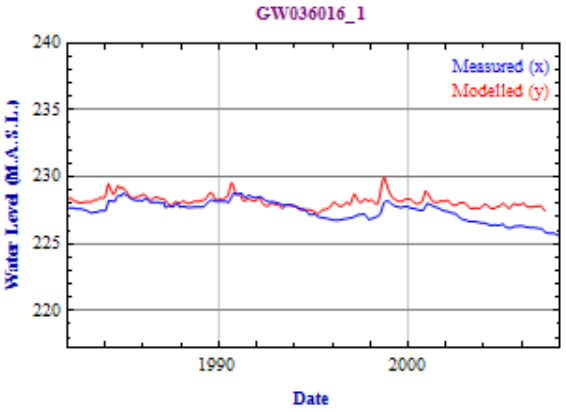

$$\bar{x} = \frac{1}{N}\sum_{i=1}^{N} x_i = 228.1600$$

$$\bar{y} = \frac{1}{N}\sum_{i=1}^{N} y_i = 227.5100$$

$$\overline{xy} = \frac{1}{N}\sum_{i=1}^{N} x_i y_i = 51909.0000$$

$$\hat{\sigma}_x = \sqrt{\frac{1}{N-1}\sum_{i=1}^{N} (x_i - \bar{x})^2} = 0.4336$$

$$\hat{\sigma}_y = \sqrt{\frac{1}{N-1}\sum_{i=1}^{N} (y_i - \bar{y})^2} = 0.7047$$

$$\hat{\sigma}_{xy} = \frac{1}{N-1}\sum_{i=1}^{N} (x_i - \bar{x})(y_i - \bar{y}) = 0.1867$$

$$\hat{\rho} = \frac{\hat{\sigma}_{xy}}{\hat{\sigma}_x \hat{\sigma}_y} = 0.6109$$

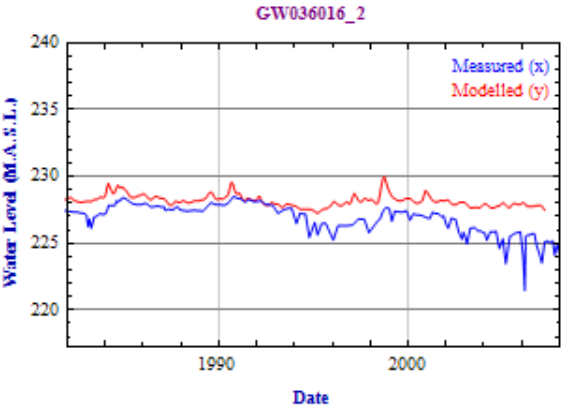

$$\bar{x} = \frac{1}{N}\sum_{i=1}^{N} x_i = 228.1600$$

$$\bar{y} = \frac{1}{N}\sum_{i=1}^{N} y_i = 226.9100$$

$$\overline{xy} = \frac{1}{N}\sum_{i=1}^{N} x_i y_i = 51774.0000$$

$$\hat{\sigma}_x = \sqrt{\frac{1}{N-1}\sum_{i=1}^{N} (x_i - \bar{x})^2} = 0.4336$$

$$\hat{\sigma}_y = \sqrt{\frac{1}{N-1}\sum_{i=1}^{N} (y_i - \bar{y})^2} = 1.0277$$

$$\hat{\sigma}_{xy} = \frac{1}{N-1}\sum_{i=1}^{N} (x_i - \bar{x})(y_i - \bar{y}) = 0.2486$$

$$\hat{\rho} = \frac{\hat{\sigma}_{xy}}{\hat{\sigma}_x \hat{\sigma}_y} = 0.5578$$

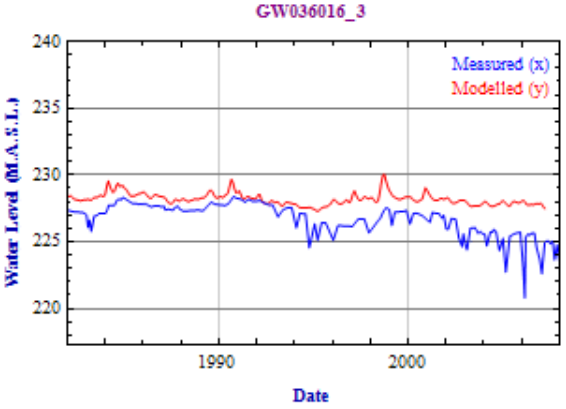

$$\bar{x} = \frac{1}{N}\sum_{i=1}^{N} x_i = 228.1900$$

$$\bar{y} = \frac{1}{N}\sum_{i=1}^{N} y_i = 226.7600$$

$$\overline{xy} = \frac{1}{N}\sum_{i=1}^{N} x_i y_i = 51745.0000$$

$$\hat{\sigma}_x = \sqrt{\frac{1}{N-1}\sum_{i=1}^{N} (x_i - \bar{x})^2} = 0.4369$$

$$\hat{\sigma}_y = \sqrt{\frac{1}{N-1}\sum_{i=1}^{N} (y_i - \bar{y})^2} = 1.1192$$

$$\hat{\sigma}_{xy} = \frac{1}{N-1}\sum_{i=1}^{N} (x_i - \bar{x})(y_i - \bar{y}) = 0.2585$$

$$\hat{\rho} = \frac{\hat{\sigma}_{xy}}{\hat{\sigma}_x \hat{\sigma}_y} = 0.5287$$

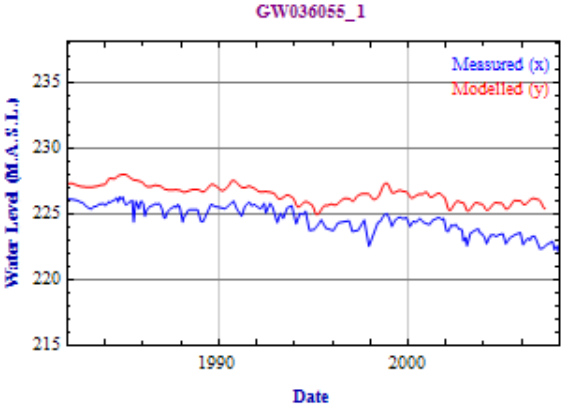

$$\bar{x} = \frac{1}{N}\sum_{i=1}^{N} x_i = 226.4800$$

$$\bar{y} = \frac{1}{N}\sum_{i=1}^{N} y_i = 224.6300$$

$$\overline{xy} = \frac{1}{N}\sum_{i=1}^{N} x_i y_i = 50873.0000$$

$$\hat{\sigma}_x = \sqrt{\frac{1}{N-1}\sum_{i=1}^{N} (x_i - \bar{x})^2} = 0.6775$$

$$\hat{\sigma}_y = \sqrt{\frac{1}{N-1}\sum_{i=1}^{N} (y_i - \bar{y})^2} = 0.9719$$

$$\hat{\sigma}_{xy} = \frac{1}{N-1}\sum_{i=1}^{N} (x_i - \bar{x})(y_i - \bar{y}) = 0.5418$$

$$\hat{\rho} = \frac{\hat{\sigma}_{xy}}{\hat{\sigma}_x \hat{\sigma}_y} = 0.8229$$

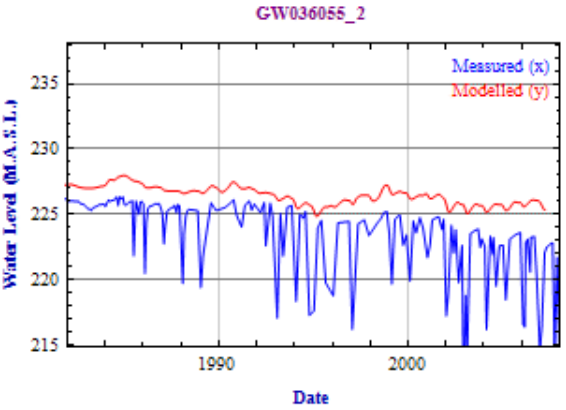

$$\bar{x} = \frac{1}{N}\sum_{i=1}^{N} x_i = 226.4600$$

$$\bar{y} = \frac{1}{N}\sum_{i=1}^{N} y_i = 223.5500$$

$$\overline{xy} = \frac{1}{N}\sum_{i=1}^{N} x_i y_i = 50625.0000$$

$$\hat{\sigma}_x = \sqrt{\frac{1}{N-1}\sum_{i=1}^{N} (x_i - \bar{x})^2} = 0.6911$$

$$\hat{\sigma}_y = \sqrt{\frac{1}{N-1}\sum_{i=1}^{N} (y_i - \bar{y})^2} = 2.4819$$

$$\hat{\sigma}_{xy} = \frac{1}{N-1}\sum_{i=1}^{N} (x_i - \bar{x})(y_i - \bar{y}) = 1.1842$$

$$\hat{\rho} = \frac{\hat{\sigma}_{xy}}{\hat{\sigma}_x \hat{\sigma}_y} = 0.6904$$

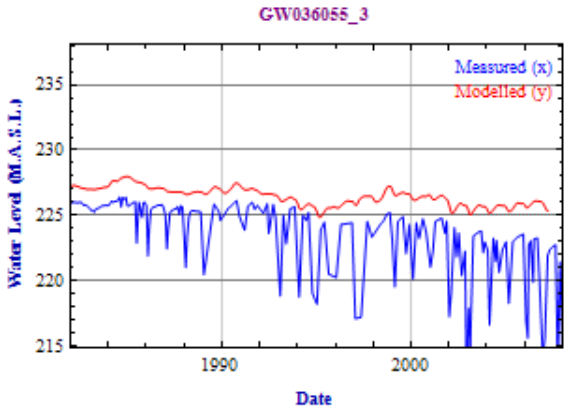

$$\bar{x} = \frac{1}{N}\sum_{i=1}^{N} x_i = 226.4600$$

$$\bar{y} = \frac{1}{N}\sum_{i=1}^{N} y_i = 223.5200$$

$$\overline{xy} = \frac{1}{N}\sum_{i=1}^{N} x_i y_i = 50620.0000$$

$$\hat{\sigma}_x = \sqrt{\frac{1}{N-1}\sum_{i=1}^{N} (x_i - \bar{x})^2} = 0.6904$$

$$\hat{\sigma}_y = \sqrt{\frac{1}{N-1}\sum_{i=1}^{N} (y_i - \bar{y})^2} = 2.4632$$

$$\hat{\sigma}_{xy} = \frac{1}{N-1}\sum_{i=1}^{N} (x_i - \bar{x})(y_i - \bar{y}) = 1.1578$$

$$\hat{\rho} = \frac{\hat{\sigma}_{xy}}{\hat{\sigma}_x \hat{\sigma}_y} = 0.6808$$

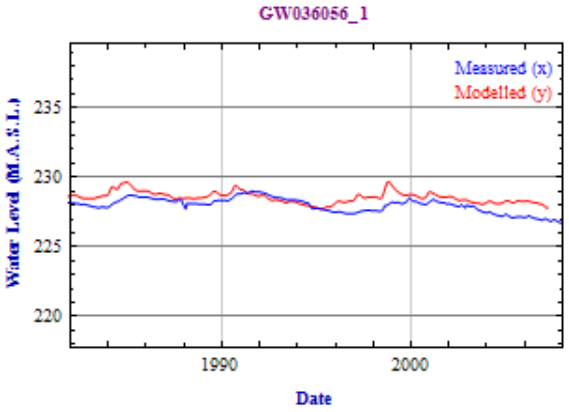

$$\bar{x} = \frac{1}{N}\sum_{i=1}^{N} x_i = 228.5500$$

$$\bar{y} = \frac{1}{N}\sum_{i=1}^{N} y_i = 228.0200$$

$$\overline{xy} = \frac{1}{N}\sum_{i=1}^{N} x_i y_i = 52115.0000$$

$$\hat{\sigma}_x = \sqrt{\frac{1}{N-1}\sum_{i=1}^{N} (x_i - \bar{x})^2} = 0.3986$$

$$\hat{\sigma}_y = \sqrt{\frac{1}{N-1}\sum_{i=1}^{N} (y_i - \bar{y})^2} = 0.4960$$

$$\hat{\sigma}_{xy} = \frac{1}{N-1}\sum_{i=1}^{N} (x_i - \bar{x})(y_i - \bar{y}) = 0.1164$$

$$\hat{\rho} = \frac{\hat{\sigma}_{xy}}{\hat{\sigma}_x \hat{\sigma}_y} = 0.5888$$

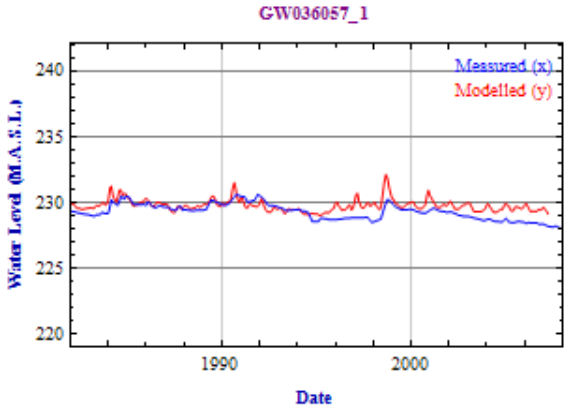

$$\bar{x} = \frac{1}{N}\sum_{i=1}^{N} x_i = 229.8000$$

$$\bar{y} = \frac{1}{N}\sum_{i=1}^{N} y_i = 229.3400$$

$$\overline{xy} = \frac{1}{N}\sum_{i=1}^{N} x_i y_i = 52704.0000$$

$$\hat{\sigma}_x = \sqrt{\frac{1}{N-1}\sum_{i=1}^{N} (x_i - \bar{x})^2} = 0.4501$$

$$\hat{\sigma}_y = \sqrt{\frac{1}{N-1}\sum_{i=1}^{N} (y_i - \bar{y})^2} = 0.5770$$

$$\hat{\sigma}_{xy} = \frac{1}{N-1}\sum_{i=1}^{N} (x_i - \bar{x})(y_i - \bar{y}) = 0.1400$$

$$\hat{\rho} = \frac{\hat{\sigma}_{xy}}{\hat{\sigma}_x \hat{\sigma}_y} = 0.5392$$

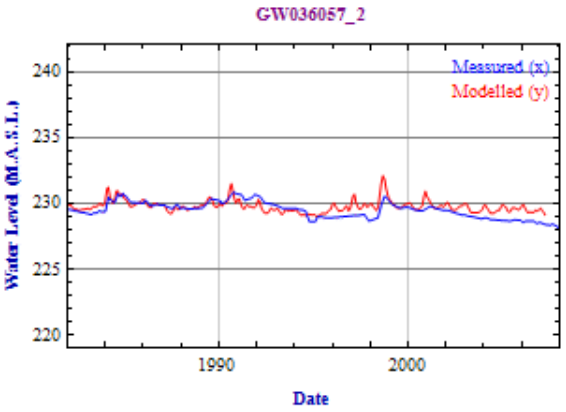

$$\bar{x} = \frac{1}{N}\sum_{i=1}^{N} x_i = 229.7800$$

$$\bar{y} = \frac{1}{N}\sum_{i=1}^{N} y_i = 229.5200$$

$$\overline{xy} = \frac{1}{N}\sum_{i=1}^{N} x_i y_i = 52738.0000$$

$$\hat{\sigma}_x = \sqrt{\frac{1}{N-1}\sum_{i=1}^{N} (x_i - \bar{x})^2} = 0.4489$$

$$\hat{\sigma}_y = \sqrt{\frac{1}{N-1}\sum_{i=1}^{N} (y_i - \bar{y})^2} = 0.5898$$

$$\hat{\sigma}_{xy} = \frac{1}{N-1}\sum_{i=1}^{N} (x_i - \bar{x})(y_i - \bar{y}) = 0.1457$$

$$\hat{\rho} = \frac{\hat{\sigma}_{xy}}{\hat{\sigma}_x \hat{\sigma}_y} = 0.5502$$

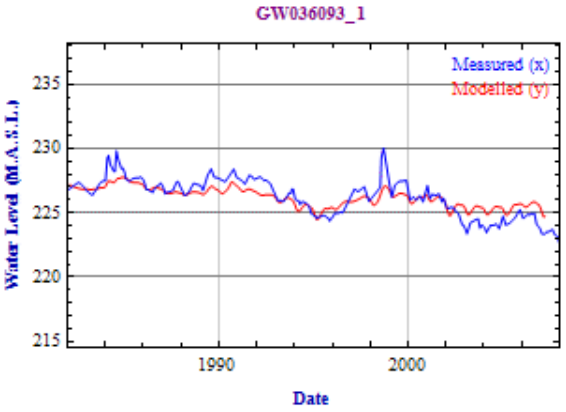

$$\bar{x} = \frac{1}{N}\sum_{i=1}^{N} x_i = 226.2100$$

$$\bar{y} = \frac{1}{N}\sum_{i=1}^{N} y_i = 226.3500$$

$$\overline{xy} = \frac{1}{N}\sum_{i=1}^{N} x_i y_i = 51203.0000$$

$$\hat{\sigma}_x = \sqrt{\frac{1}{N-1}\sum_{i=1}^{N} (x_i - \bar{x})^2} = 0.7400$$

$$\hat{\sigma}_y = \sqrt{\frac{1}{N-1}\sum_{i=1}^{N} (y_i - \bar{y})^2} = 1.3852$$

$$\hat{\sigma}_{xy} = \frac{1}{N-1}\sum_{i=1}^{N} (x_i - \bar{x})(y_i - \bar{y}) = 0.9104$$

$$\hat{\rho} = \frac{\hat{\sigma}_{xy}}{\hat{\sigma}_x \hat{\sigma}_y} = 0.8881$$

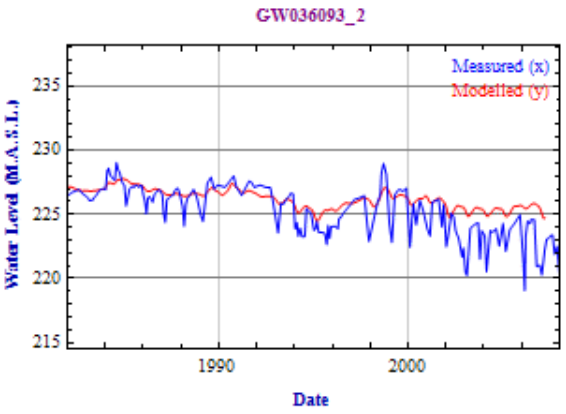

$$\bar{x} = \frac{1}{N}\sum_{i=1}^{N} x_i = 226.2100$$

$$\bar{y} = \frac{1}{N}\sum_{i=1}^{N} y_i = 225.4400$$

$$\overline{xy} = \frac{1}{N}\sum_{i=1}^{N} x_i y_i = 50998.0000$$

$$\hat{\sigma}_x = \sqrt{\frac{1}{N-1}\sum_{i=1}^{N} (x_i - \bar{x})^2} = 0.7412$$

$$\hat{\sigma}_y = \sqrt{\frac{1}{N-1}\sum_{i=1}^{N} (y_i - \bar{y})^2} = 1.7785$$

$$\hat{\sigma}_{xy} = \frac{1}{N-1}\sum_{i=1}^{N} (x_i - \bar{x})(y_i - \bar{y}) = 1.0792$$

$$\hat{\rho} = \frac{\hat{\sigma}_{xy}}{\hat{\sigma}_x \hat{\sigma}_y} = 0.8187$$

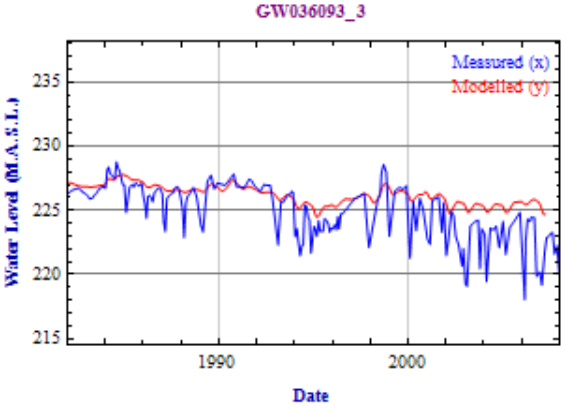

$$\bar{x} = \frac{1}{N}\sum_{i=1}^{N} x_i = 226.2100$$

$$\bar{y} = \frac{1}{N}\sum_{i=1}^{N} y_i = 225.1000$$

$$\overline{xy} = \frac{1}{N}\sum_{i=1}^{N} x_i y_i = 50922.0000$$

$$\hat{\sigma}_x = \sqrt{\frac{1}{N-1}\sum_{i=1}^{N} (x_i - \bar{x})^2} = 0.7425$$

$$\hat{\sigma}_y = \sqrt{\frac{1}{N-1}\sum_{i=1}^{N} (y_i - \bar{y})^2} = 1.9618$$

$$\hat{\sigma}_{xy} = \frac{1}{N-1}\sum_{i=1}^{N} (x_i - \bar{x})(y_i - \bar{y}) = 1.1470$$

$$\hat{\rho} = \frac{\hat{\sigma}_{xy}}{\hat{\sigma}_x \hat{\sigma}_y} = 0.7875$$

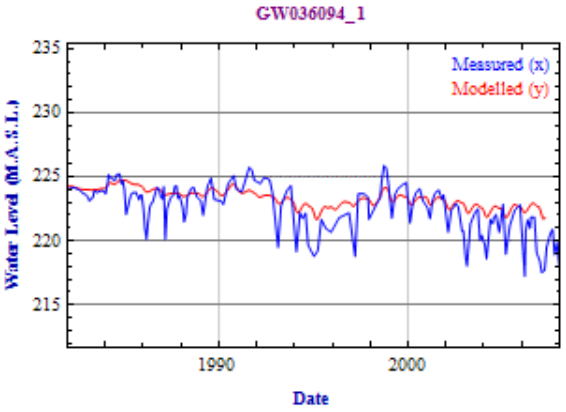

$$\bar{x} = \frac{1}{N}\sum_{i=1}^{N} x_i = 223.3200$$

$$\bar{y} = \frac{1}{N}\sum_{i=1}^{N} y_i = 222.6800$$

$$\overline{xy} = \frac{1}{N}\sum_{i=1}^{N} x_i y_i = 49732.0000$$

$$\hat{\sigma}_x = \sqrt{\frac{1}{N-1}\sum_{i=1}^{N} (x_i - \bar{x})^2} = 0.6987$$

$$\hat{\sigma}_y = \sqrt{\frac{1}{N-1}\sum_{i=1}^{N} (y_i - \bar{y})^2} = 1.7046$$

$$\hat{\sigma}_{xy} = \frac{1}{N-1}\sum_{i=1}^{N} (x_i - \bar{x})(y_i - \bar{y}) = 0.9497$$

$$\hat{\rho} = \frac{\hat{\sigma}_{xy}}{\hat{\sigma}_x \hat{\sigma}_y} = 0.7974$$

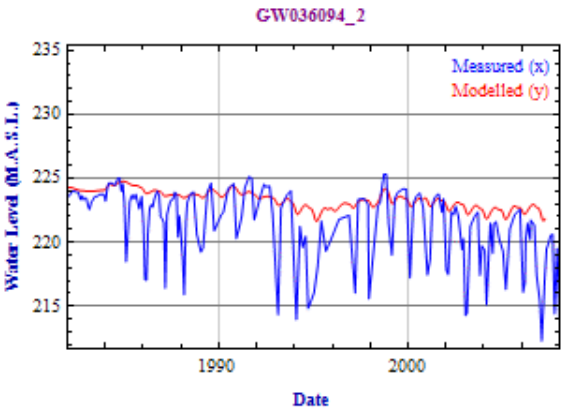

$$\bar{x} = \frac{1}{N}\sum_{i=1}^{N} x_i = 223.3300$$

$$\bar{y} = \frac{1}{N}\sum_{i=1}^{N} y_i = 221.5100$$

$$\overline{xy} = \frac{1}{N}\sum_{i=1}^{N} x_i y_i = 49471.0000$$

$$\hat{\sigma}_x = \sqrt{\frac{1}{N-1}\sum_{i=1}^{N} (x_i - \bar{x})^2} = 0.7025$$

$$\hat{\sigma}_y = \sqrt{\frac{1}{N-1}\sum_{i=1}^{N} (y_i - \bar{y})^2} = 2.5481$$

$$\hat{\sigma}_{xy} = \frac{1}{N-1}\sum_{i=1}^{N} (x_i - \bar{x})(y_i - \bar{y}) = 1.2130$$

$$\hat{\rho} = \frac{\hat{\sigma}_{xy}}{\hat{\sigma}_x \hat{\sigma}_y} = 0.6776$$

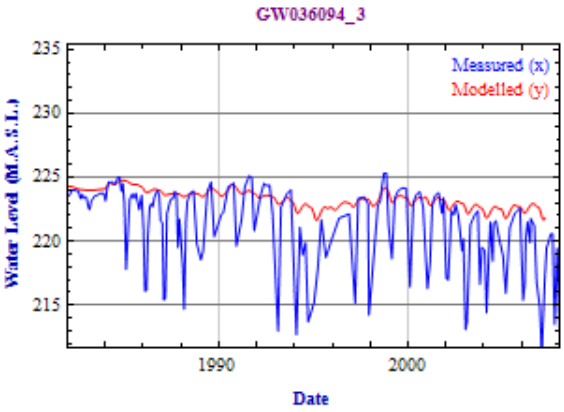

$$\bar{x} = \frac{1}{N}\sum_{i=1}^{N} x_i = 223.3300$$

$$\bar{y} = \frac{1}{N}\sum_{i=1}^{N} y_i = 221.2700$$

$$\overline{xy} = \frac{1}{N}\sum_{i=1}^{N} x_i y_i = 49417.0000$$

$$\hat{\sigma}_x = \sqrt{\frac{1}{N-1}\sum_{i=1}^{N} (x_i - \bar{x})^2} = 0.7026$$

$$\hat{\sigma}_y = \sqrt{\frac{1}{N-1}\sum_{i=1}^{N} (y_i - \bar{y})^2} = 2.8286$$

$$\hat{\sigma}_{xy} = \frac{1}{N-1}\sum_{i=1}^{N} (x_i - \bar{x})(y_i - \bar{y}) = 1.2784$$

$$\hat{\rho} = \frac{\hat{\sigma}_{xy}}{\hat{\sigma}_x \hat{\sigma}_y} = 0.6433$$

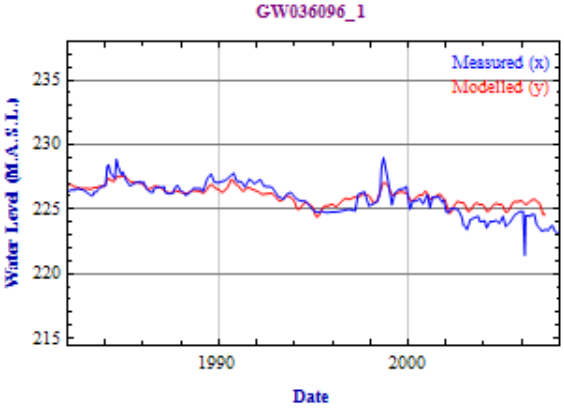

$$\bar{x} = \frac{1}{N}\sum_{i=1}^{N} x_i = 226.0700$$

$$\bar{y} = \frac{1}{N}\sum_{i=1}^{N} y_i = 225.9000$$

$$\overline{xy} = \frac{1}{N}\sum_{i=1}^{N} x_i y_i = 51068.0000$$

$$\hat{\sigma}_x = \sqrt{\frac{1}{N-1}\sum_{i=1}^{N} (x_i - \bar{x})^2} = 0.6924$$

$$\hat{\sigma}_y = \sqrt{\frac{1}{N-1}\sum_{i=1}^{N} (y_i - \bar{y})^2} = 1.1914$$

$$\hat{\sigma}_{xy} = \frac{1}{N-1}\sum_{i=1}^{N} (x_i - \bar{x})(y_i - \bar{y}) = 0.7285$$

$$\hat{\rho} = \frac{\hat{\sigma}_{xy}}{\hat{\sigma}_x \hat{\sigma}_y} = 0.8830$$

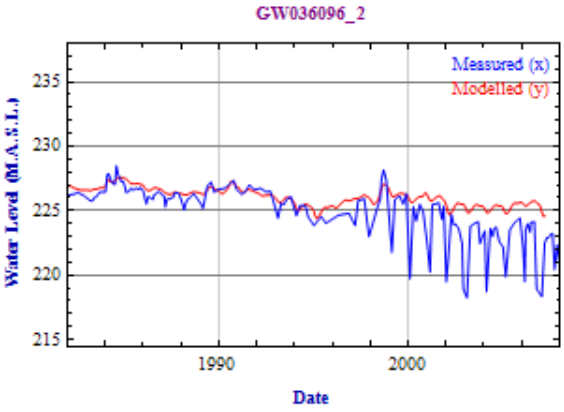

$$\bar{x} = \frac{1}{N}\sum_{i=1}^{N} x_i = 226.0600$$

$$\bar{y} = \frac{1}{N}\sum_{i=1}^{N} y_i = 225.0000$$

$$\overline{xy} = \frac{1}{N}\sum_{i=1}^{N} x_i y_i = 50866.0000$$

$$\hat{\sigma}_x = \sqrt{\frac{1}{N-1}\sum_{i=1}^{N} (x_i - \bar{x})^2} = 0.6932$$

$$\hat{\sigma}_y = \sqrt{\frac{1}{N-1}\sum_{i=1}^{N} (y_i - \bar{y})^2} = 1.9100$$

$$\hat{\sigma}_{xy} = \frac{1}{N-1}\sum_{i=1}^{N} (x_i - \bar{x})(y_i - \bar{y}) = 0.9969$$

$$\hat{\rho} = \frac{\hat{\sigma}_{xy}}{\hat{\sigma}_x \hat{\sigma}_y} = 0.7530$$

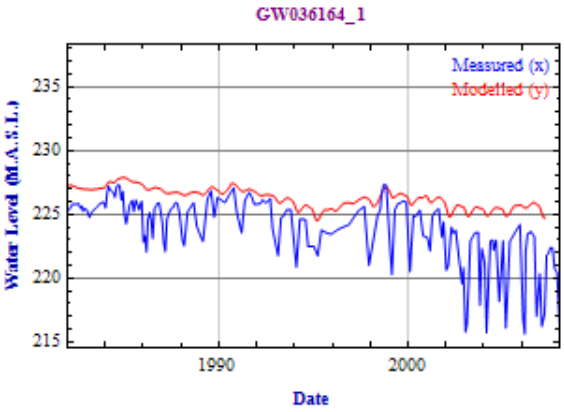

$$\bar{x} = \frac{1}{N}\sum_{i=1}^{N} x_i = 226.2900$$

$$\bar{y} = \frac{1}{N}\sum_{i=1}^{N} y_i = 224.0400$$

$$\overline{xy} = \frac{1}{N}\sum_{i=1}^{N} x_i y_i = 50697.0000$$

$$\hat{\sigma}_x = \sqrt{\frac{1}{N-1}\sum_{i=1}^{N} (x_i - \bar{x})^2} = 0.7742$$

$$\hat{\sigma}_y = \sqrt{\frac{1}{N-1}\sum_{i=1}^{N} (y_i - \bar{y})^2} = 2.2292$$

$$\hat{\sigma}_{xy} = \frac{1}{N-1}\sum_{i=1}^{N} (x_i - \bar{x})(y_i - \bar{y}) = 1.2290$$

$$\hat{\rho} = \frac{\hat{\sigma}_{xy}}{\hat{\sigma}_x \hat{\sigma}_y} = 0.7121$$

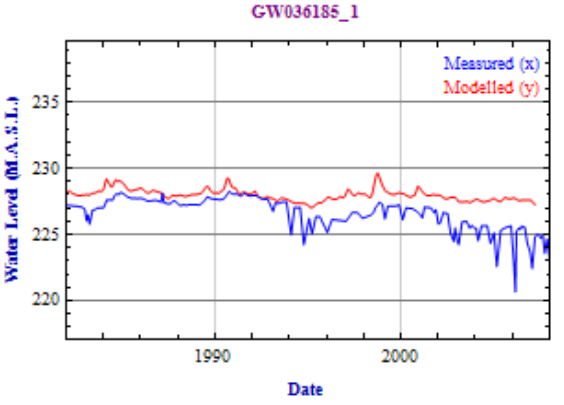

$$\bar{x} = \frac{1}{N}\sum_{i=1}^{N} x_i = 227.9900$$

$$\bar{y} = \frac{1}{N}\sum_{i=1}^{N} y_i = 226.6700$$

$$\overline{xy} = \frac{1}{N}\sum_{i=1}^{N} x_i y_i = 51678.0000$$

$$\hat{\sigma}_x = \sqrt{\frac{1}{N-1}\sum_{i=1}^{N} (x_i - \bar{x})^2} = 0.4383$$

$$\hat{\sigma}_y = \sqrt{\frac{1}{N-1}\sum_{i=1}^{N} (y_i - \bar{y})^2} = 1.1264$$

$$\hat{\sigma}_{xy} = \frac{1}{N-1}\sum_{i=1}^{N} (x_i - \bar{x})(y_i - \bar{y}) = 0.2983$$

$$\hat{\rho} = \frac{\hat{\sigma}_{xy}}{\hat{\sigma}_x \hat{\sigma}_y} = 0.6043$$

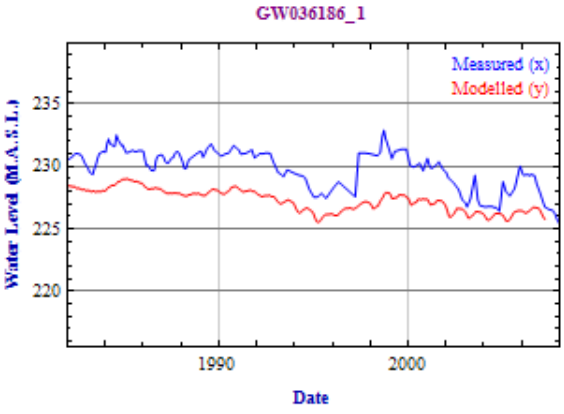

$$\bar{x} = \frac{1}{N}\sum_{i=1}^{N} x_i = 227.3000$$

$$\bar{y} = \frac{1}{N}\sum_{i=1}^{N} y_i = 229.8900$$

$$\overline{xy} = \frac{1}{N}\sum_{i=1}^{N} x_i y_i = 52254.0000$$

$$\hat{\sigma}_x = \sqrt{\frac{1}{N-1}\sum_{i=1}^{N} (x_i - \bar{x})^2} = 0.8756$$

$$\hat{\sigma}_y = \sqrt{\frac{1}{N-1}\sum_{i=1}^{N} (y_i - \bar{y})^2} = 1.4730$$

$$\hat{\sigma}_{xy} = \frac{1}{N-1}\sum_{i=1}^{N} (x_i - \bar{x})(y_i - \bar{y}) = 1.0873$$

$$\hat{\rho} = \frac{\hat{\sigma}_{xy}}{\hat{\sigma}_x \hat{\sigma}_y} = 0.8430$$

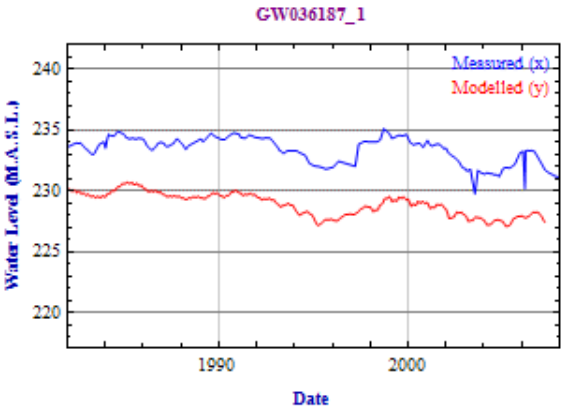

$$\bar{x} = \frac{1}{N}\sum_{i=1}^{N} x_i = 228.9300$$

$$\bar{y} = \frac{1}{N}\sum_{i=1}^{N} y_i = 233.4400$$

$$\overline{xy} = \frac{1}{N}\sum_{i=1}^{N} x_i y_i = 53442.0000$$

$$\hat{\sigma}_x = \sqrt{\frac{1}{N-1}\sum_{i=1}^{N} (x_i - \bar{x})^2} = 0.9274$$

$$\hat{\sigma}_y = \sqrt{\frac{1}{N-1}\sum_{i=1}^{N} (y_i - \bar{y})^2} = 1.0406$$

$$\hat{\sigma}_{xy} = \frac{1}{N-1}\sum_{i=1}^{N} (x_i - \bar{x})(y_i - \bar{y}) = 0.8092$$

$$\hat{\rho} = \frac{\hat{\sigma}_{xy}}{\hat{\sigma}_x \hat{\sigma}_y} = 0.8385$$

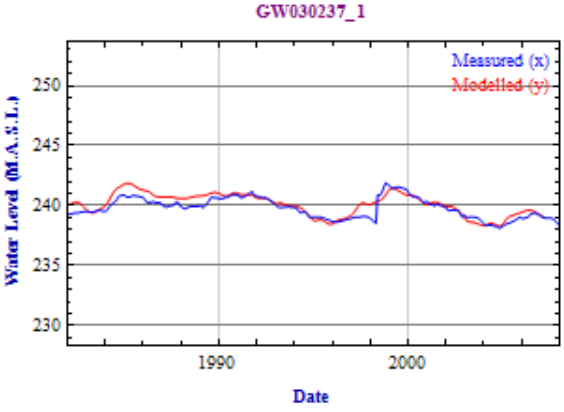

$$\bar{x} = \frac{1}{N}\sum_{i=1}^{N} x_i = 240.1000$$

$$\bar{y} = \frac{1}{N}\sum_{i=1}^{N} y_i = 239.8300$$

$$\overline{xy} = \frac{1}{N}\sum_{i=1}^{N} x_i y_i = 57584.0000$$

$$\hat{\sigma}_x = \sqrt{\frac{1}{N-1}\sum_{i=1}^{N} (x_i - \bar{x})^2} = 0.9136$$

$$\hat{\sigma}_y = \sqrt{\frac{1}{N-1}\sum_{i=1}^{N} (y_i - \bar{y})^2} = 0.8535$$

$$\hat{\sigma}_{xy} = \frac{1}{N-1}\sum_{i=1}^{N} (x_i - \bar{x})(y_i - \bar{y}) = 0.6843$$

$$\hat{\rho} = \frac{\hat{\sigma}_{xy}}{\hat{\sigma}_x \hat{\sigma}_y} = 0.8775$$

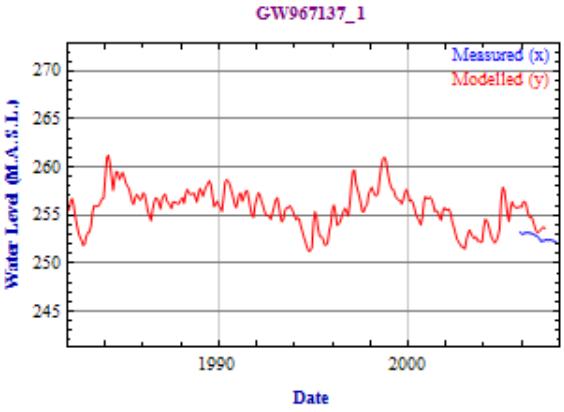

$$\bar{x} = \frac{1}{N}\sum_{i=1}^{N} x_i = 254.6100$$

$$\bar{y} = \frac{1}{N}\sum_{i=1}^{N} y_i = 252.8800$$

$$\overline{xy} = \frac{1}{N}\sum_{i=1}^{N} x_i y_i = 64386.0000$$

$$\hat{\sigma}_x = \sqrt{\frac{1}{N-1}\sum_{i=1}^{N} (x_i - \bar{x})^2} = 1.1149$$

$$\hat{\sigma}_y = \sqrt{\frac{1}{N-1}\sum_{i=1}^{N} (y_i - \bar{y})^2} = 0.3218$$

$$\hat{\sigma}_{xy} = \frac{1}{N-1}\sum_{i=1}^{N} (x_i - \bar{x})(y_i - \bar{y}) = 0.2656$$

$$\hat{\rho} = \frac{\hat{\sigma}_{xy}}{\hat{\sigma}_x \hat{\sigma}_y} = 0.7403$$

Appendix 6b

Crystallize
FEFLOW Post Processing of Hydrograph Data
Point Time Series

Authors
B. Kelly, B. Giambastiani and A. McCallum

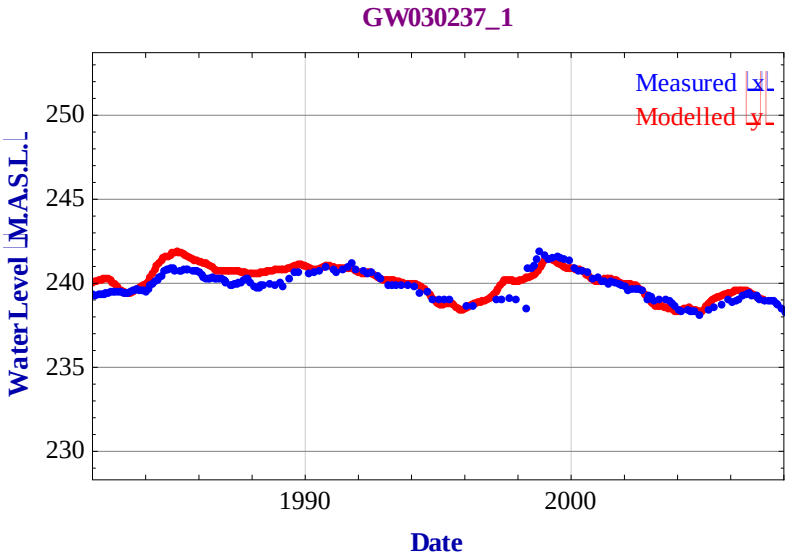

A.6b.1 Introduction

This notebook plots measured versus modelled groundwater hydrographs. The degree of correlation between the two hydrographs is also determined. FEFLOW does not have tools for the comprehensive analysis of the hydrograph data. This ***Crystallize*** notebook demonstrates how *Mathematica* scripts can be written to automate the statistical analysis of any groundwater model. The correlation coefficient is just one statistical measure used to help with the evaluation of a groundwater model. A correlation coefficient of zero means there is no linear relationship between the two variables, a value of one indicates a perfect match. For an introductory discussion on statistics refer to:

Gonick, L. and Smith W. (1993) "The Cartoon Guide to Statistics", HarperPerennial

For a detailed discussion on the interpretation of the statistics, details on the correlation coefficient and signal analysis refer to:

Ruskeepaa, H. (2009) "Mathematica Navigator: Mathematics, Statistics, and Graphics", 3rd Edition, Elsevier.

Costain, J.K. and Coruh, C. (2004) "Basic Theory of Exploration Seismology: with Mathematica Notebooks and Examples on CD-ROM", Elsevier.

There are many other statistical measures that can be used to evaluate the quality of a groundwater model. A comprehensive listing of the statistical measures commonly used for assessing the quality of measured versus modelled groundwater hydrograph is presented in:

Middlemis, H., Merrick, N.P. and Ross, J.B. (2000). "Murray-Darling Basin Commission groundwater flow modelling guidelines". Murray-Darling Basin Commission, Aquaterra Consulting Pty Ltd, Perth.
http://www2.mdbc.gov.au/nrm/groundwater/groundwater_guides.html
http://www2.mdbc.gov.au/__data/page/127/model_guide.pdf

This version calculates the correlation coefficient as recommended in the Middlemis et al. (2000). It calculates the correlation between the borehole measured head and the predicted head at the corresponding time of the field measurement.

A.6b.2 Loading the Data

The first two lines of script below load the data. The third line makes a list of all the bores in the input files. These data files contain the columns of data that detail the field measured groundwater head and the FEFLOW modelled groundwater head. If this notebook is used on data files that have different columns for the time and groundwater head data then the columns called in the scripts below would need to be changed.

```
feflowData =
  Drop[
   Import[
    "I:\\NWC\\NWC_FinalReportUNSW3DHydrogeology\\Appendix6b_CrystallizeFEFLOWHydrographs\\MaulesCkFEFLOWhydrographs.
      csv"], 1];
measuredData =
  Drop[Import["I:\\NWC\\NWC_FinalReportUNSW3DHydrogeology\\Appendix6b_CrystallizeFEFLOWHydrographs\\
      MaulesCkMeasuredHydrographs.csv"], 1];

allbores = DeleteDuplicates[feflowData[[All, 2]]]
```

```
{GW036008_1, GW036007_1, GW036007_2, GW036007_3, GW036057_1, GW036057_2, GW036056_1, GW036016_1,
 GW036016_2, GW036016_3, GW036185_1, GW036015_1, GW036015_2, GW036014_1, GW036014_2, GW036013_1,
 GW036012_1, GW036055_1, GW036055_2, GW036055_3, GW036005_1, GW036005_2, GW036096_1, GW036096_2,
 GW036093_1, GW036093_2, GW036093_3, GW036164_1, GW036004_1, GW036004_2, GW036186_1, GW036187_1,
 GW030129_1, GW030130_1, GW030130_2, GW030447_1, GW030131_1, GW967137_1, GW967137_2, GW036094_3,
 GW036094_2, GW036094_1, GW030446_1, GW030446_2, GW030132_1, GW030132_2, GW063059_1, GW063060_1,
 GW030133_1, GW030237_1, GW030236_1, GW030236_2, GW030235_1, GW030235_2, GW030134_1, GW030234_1,
 GW030233_1, GW030233_2, GW030233_3, GW030232_1, GW030232_2, GW030232_3, GW030231_1, GW030231_2}
```

A.6.3 Plotting the Data and Calculating the Correlation Coefficient

This block of script generates the plots and determines the statistical correlation coefficient between the measured groundwater hydrograph and the FEFLOW modelled hydrograph. The statistical algorithms are from:

Daniel de Souza Carvalho "Correlation and Covariance of Random Discrete Signals" from the Wolfram Demonstrations Project,
http://demonstrations.wolfram.com/CorrelationAndCovarianceOfFandomDiscreteSignals.

```
imagelist = {};
correlationlist = {};
Do[
 gw = allbores[[m]]; gwnumber = ToExpression[StringTake[gw, {3, 8}]]; gwpipe = ToExpression[StringTake[gw, {10}]] / 1.;
 set1 = Cases[feflowData, {_, gw, _, _}][[All, {3, 4}]];
 set2 = Cases[measuredData, {gwnumber, gwpipe, _, _, _, _, _, _}][[All, {5, 8}]];
 If[Length[set2 ] > 1,
  string = Column[{Style["Measured (x)", Blue], Style["Modelled (y)", Red]}];
  plot = DateListPlot[{set1, set2}, PlotStyle → {Red, Blue}, GridLines → Automatic, ImageSize → {300, 300},
    PlotRange → {{{1982}, {2008}},
      {Max[set1[[All, 2]]] + 10, Min[set1[[All, 2]]] - 10}}, Joined → False, Frame → True, FrameLabel → {Style["Date",
       Bold, Darker[Blue]], Style["Water Level (M.A.S.L.)", Bold, Darker[Blue]], Style[gw, Bold, Purple]},
    Epilog :→ Text[string, {{2005}, Max[set1[[All, 2]] + 7]}]];
  scaleddata1 = Table[{N[AbsoluteTime[set1[[i, 1]]]], Abs[set1[[i, 2]]]}, {i, 1, Length[set1]}];
  function1 = Interpolation[scaleddata1, Method → "Spline", InterpolationOrder → 1];
  scaleddata2 = Table[{N[AbsoluteTime[set2[[i, 1]]]], Abs[set2[[i, 2]]]}, {i, 1, Length[set2]}];
  function2 = Interpolation[scaleddata2, Method → "Spline", InterpolationOrder → 1];
  min1 = Min[scaleddata1[[All, 1]]]; min2 = Min[scaleddata2[[All, 1]]]; max1 = Max[scaleddata1[[All, 1]]];
  max2 = Max[scaleddata2[[All, 1]]];
  If[min1 < min2 , rmina = min2, rmina = min1]; If[max1 > max2, rmaxa = max2, rmaxa = max1];
  rstep = (rmaxa - rmina) / 1000;
  abs1980 = AbsoluteTime[{1982, 1, 1, 0, 0, 0}]; abs2007 = AbsoluteTime[{2007, 4, 1, 0, 0, 0}];
  If[rmina < abs1980 , rmin = abs1980, rmin = rmina];
  If[rmaxa > abs2007, rmax = abs2007, rmax = rmaxa];
  lx = {}; ly = {};
  Do[If[scaleddata2[[i, 1]] >= rmin && scaleddata2[[i, 1]] ≤ rmax,
     AppendTo[lx, function1[scaleddata2[[i, 1]]]];
     AppendTo[ly, scaleddata2[[i, 2]]];
    ], {i, Length[scaleddata2]}]
  AppendTo[imagelist, Grid[{{Show[plot, ImageSize → {300, 300}], "   ",
      Text@TraditionalForm@Grid[{
         {x̄, " = ", HoldForm[1/N] ∑_{i=1}^{N} x_i, " = ", NumberForm[#, {5, 4}, NumberPadding → {"", "0"}] &@(xm = N[Mean[lx]])},
         {ȳ, " = ", HoldForm[1/N] ∑_{i=1}^{N} y_i, " = ", NumberForm[#, {5, 4}, NumberPadding → {"", "0"}] &@(ym = N[Mean[ly]])},
         {x̄ ȳ, " = ", HoldForm[1/N] ∑_{i=1}^{N} (x_i * y_i), " = ", NumberForm[#, {5, 4}, NumberPadding → {"", "0"}] &@
           (xym = N[Mean[lx * ly]])},
         {σ̂_x, " = ", √(HoldForm[1/(N - 1)] * ∑_{i=1}^{N} (x_i - x̄)^2), " = ", NumberForm[#, {5, 4}, NumberPadding → {"", "0"}] &@
           (xstddev = N[StandardDeviation[lx]])},
         {σ̂_y, " = ", √(HoldForm[1/(N - 1)] * ∑_{i=1}^{N} (y_i - ȳ)^2), " = ", NumberForm[#, {5, 4}, NumberPadding → {"", "0"}] &@
           (ystddev = N[StandardDeviation[ly]])},
         {σ̂_xy, " = ", HoldForm[1/(N - 1)] * ∑_{i=1}^{N} (x_i - x̄) (y_i - ȳ), " = ",
          NumberForm[#, {5, 4}, NumberPadding → {"", "0"}] &@(N[Covariance[lx, ly]])},
         {ρ̂, " = ", σ̂_xy/(σ̂_x σ̂_y), " = ", NumberForm[#, {5, 4}, NumberPadding → {"", "0"}] &@(N[Correlation[lx, ly]])}
        }, Alignment → Left, ItemSize → {{3, 1.5, 11, 1.5, 10}, Automatic}]}}]];
  AppendTo[correlationlist, {gw, N[Correlation[lx, ly]]}];
 ], {m, 1, Length[allbores]}]
```

Below are the hydrograph plots generated by the above script for the Maules Creek FEFLOW model data sets. The statistics calculated are the mean head, mean (measured head *x* modelled head), standard deviation, covariance and the correlation coefficient.

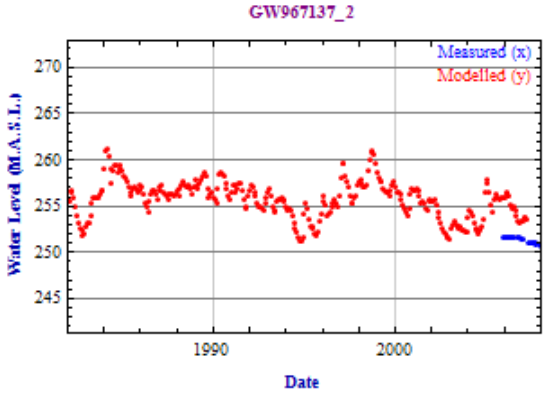

$$\bar{x} = \frac{1}{N}\sum_{i=1}^{N} x_i = 254.8600$$

$$\bar{y} = \frac{1}{N}\sum_{i=1}^{N} y_i = 251.5700$$

$$\overline{xy} = \frac{1}{N}\sum_{i=1}^{N} x_i y_i = 64116.0000$$

$$\hat{\sigma}_x = \sqrt{\frac{1}{N-1}\sum_{i=1}^{N}(x_i - \bar{x})^2} = 1.2123$$

$$\hat{\sigma}_y = \sqrt{\frac{1}{N-1}\sum_{i=1}^{N}(y_i - \bar{y})^2} = 0.0992$$

$$\hat{\sigma}_{xy} = \frac{1}{N-1}\sum_{i=1}^{N}(x_i - \bar{x})(y_i - \bar{y}) = 0.0756$$

$$\hat{\rho} = \frac{\hat{\sigma}_{xy}}{\hat{\sigma}_x \hat{\sigma}_y} = 0.6287$$

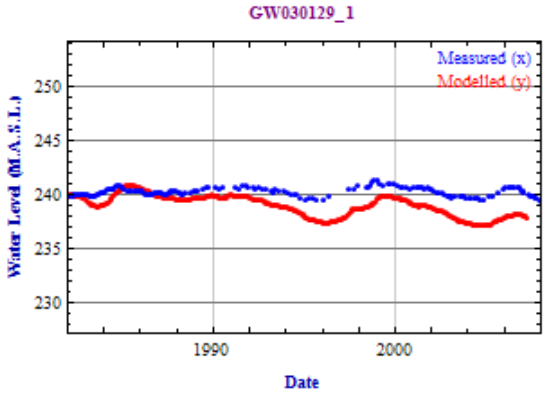

$$\bar{x} = \frac{1}{N}\sum_{i=1}^{N} x_i = 239.2100$$

$$\bar{y} = \frac{1}{N}\sum_{i=1}^{N} y_i = 240.3200$$

$$\overline{xy} = \frac{1}{N}\sum_{i=1}^{N} x_i y_i = 57488.0000$$

$$\hat{\sigma}_x = \sqrt{\frac{1}{N-1}\sum_{i=1}^{N}(x_i - \bar{x})^2} = 0.9510$$

$$\hat{\sigma}_y = \sqrt{\frac{1}{N-1}\sum_{i=1}^{N}(y_i - \bar{y})^2} = 0.3871$$

$$\hat{\sigma}_{xy} = \frac{1}{N-1}\sum_{i=1}^{N}(x_i - \bar{x})(y_i - \bar{y}) = 0.1550$$

$$\hat{\rho} = \frac{\hat{\sigma}_{xy}}{\hat{\sigma}_x \hat{\sigma}_y} = 0.4209$$

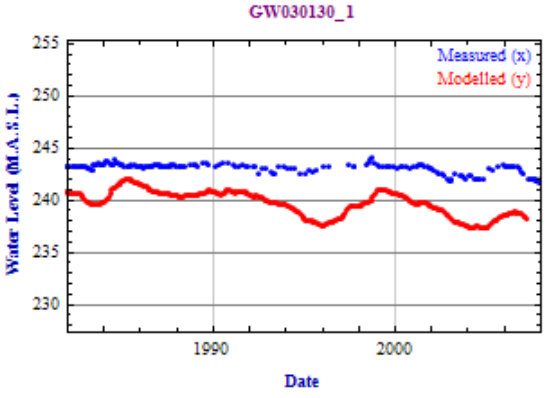

$$\bar{x} = \frac{1}{N}\sum_{i=1}^{N} x_i = 239.9400$$

$$\bar{y} = \frac{1}{N}\sum_{i=1}^{N} y_i = 243.1400$$

$$\overline{xy} = \frac{1}{N}\sum_{i=1}^{N} x_i y_i = 58338.0000$$

$$\hat{\sigma}_x = \sqrt{\frac{1}{N-1}\sum_{i=1}^{N}(x_i - \bar{x})^2} = 1.1753$$

$$\hat{\sigma}_y = \sqrt{\frac{1}{N-1}\sum_{i=1}^{N}(y_i - \bar{y})^2} = 0.4094$$

$$\hat{\sigma}_{xy} = \frac{1}{N-1}\sum_{i=1}^{N}(x_i - \bar{x})(y_i - \bar{y}) = 0.3214$$

$$\hat{\rho} = \frac{\hat{\sigma}_{xy}}{\hat{\sigma}_x \hat{\sigma}_y} = 0.6680$$

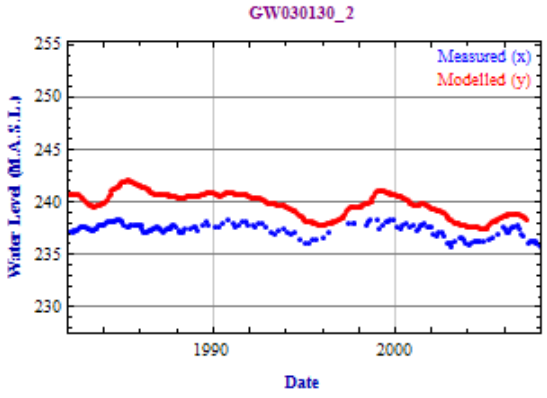

$$\bar{x} = \frac{1}{N}\sum_{i=1}^{N} x_i = 239.9900$$

$$\bar{y} = \frac{1}{N}\sum_{i=1}^{N} y_i = 237.4000$$

$$\overline{xy} = \frac{1}{N}\sum_{i=1}^{N} x_i y_i = 56974.0000$$

$$\hat{\sigma}_x = \sqrt{\frac{1}{N-1}\sum_{i=1}^{N} (x_i - \bar{x})^2} = 1.1584$$

$$\hat{\sigma}_y = \sqrt{\frac{1}{N-1}\sum_{i=1}^{N} (y_i - \bar{y})^2} = 0.5861$$

$$\hat{\sigma}_{xy} = \frac{1}{N-1}\sum_{i=1}^{N} (x_i - \bar{x})(y_i - \bar{y}) = 0.5016$$

$$\hat{\rho} = \frac{\hat{\sigma}_{xy}}{\hat{\sigma}_x \hat{\sigma}_y} = 0.7388$$

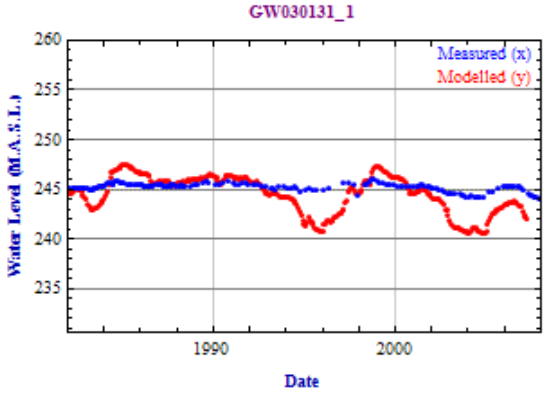

$$\bar{x} = \frac{1}{N}\sum_{i=1}^{N} x_i = 244.7100$$

$$\bar{y} = \frac{1}{N}\sum_{i=1}^{N} y_i = 245.2500$$

$$\overline{xy} = \frac{1}{N}\sum_{i=1}^{N} x_i y_i = 60016.0000$$

$$\hat{\sigma}_x = \sqrt{\frac{1}{N-1}\sum_{i=1}^{N} (x_i - \bar{x})^2} = 1.8042$$

$$\hat{\sigma}_y = \sqrt{\frac{1}{N-1}\sum_{i=1}^{N} (y_i - \bar{y})^2} = 0.3720$$

$$\hat{\sigma}_{xy} = \frac{1}{N-1}\sum_{i=1}^{N} (x_i - \bar{x})(y_i - \bar{y}) = 0.5698$$

$$\hat{\rho} = \frac{\hat{\sigma}_{xy}}{\hat{\sigma}_x \hat{\sigma}_y} = 0.8490$$

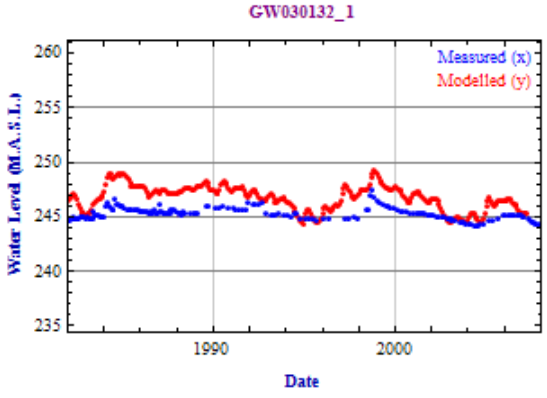

$$\bar{x} = \frac{1}{N}\sum_{i=1}^{N} x_i = 246.8100$$

$$\bar{y} = \frac{1}{N}\sum_{i=1}^{N} y_i = 245.3200$$

$$\overline{xy} = \frac{1}{N}\sum_{i=1}^{N} x_i y_i = 60548.0000$$

$$\hat{\sigma}_x = \sqrt{\frac{1}{N-1}\sum_{i=1}^{N} (x_i - \bar{x})^2} = 1.1694$$

$$\hat{\sigma}_y = \sqrt{\frac{1}{N-1}\sum_{i=1}^{N} (y_i - \bar{y})^2} = 0.5431$$

$$\hat{\sigma}_{xy} = \frac{1}{N-1}\sum_{i=1}^{N} (x_i - \bar{x})(y_i - \bar{y}) = 0.5009$$

$$\hat{\rho} = \frac{\hat{\sigma}_{xy}}{\hat{\sigma}_x \hat{\sigma}_y} = 0.7887$$

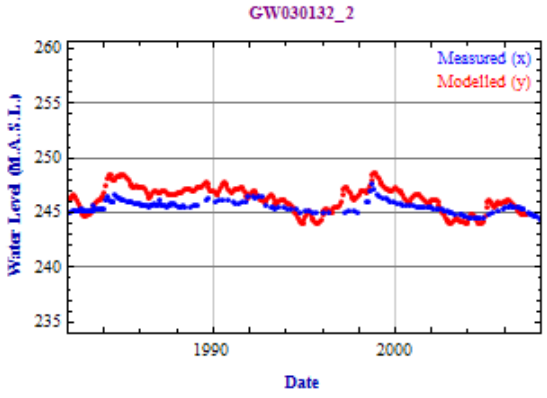

$$\bar{x} = \frac{1}{N}\sum_{i=1}^{N} x_i = 246.3400$$

$$\bar{y} = \frac{1}{N}\sum_{i=1}^{N} y_i = 245.5700$$

$$\overline{xy} = \frac{1}{N}\sum_{i=1}^{N} x_i y_i = 60496.0000$$

$$\hat{\sigma}_x = \sqrt{\frac{1}{N-1}\sum_{i=1}^{N} (x_i - \bar{x})^2} = 1.1609$$

$$\hat{\sigma}_y = \sqrt{\frac{1}{N-1}\sum_{i=1}^{N} (y_i - \bar{y})^2} = 0.5223$$

$$\hat{\sigma}_{xy} = \frac{1}{N-1}\sum_{i=1}^{N} (x_i - \bar{x})(y_i - \bar{y}) = 0.4891$$

$$\hat{\rho} = \frac{\hat{\sigma}_{xy}}{\hat{\sigma}_x \hat{\sigma}_y} = 0.8067$$

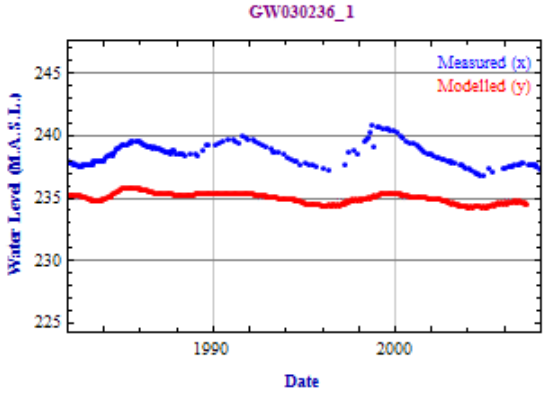

$$\bar{x} = \frac{1}{N}\sum_{i=1}^{N} x_i = 235.0800$$

$$\bar{y} = \frac{1}{N}\sum_{i=1}^{N} y_i = 238.5900$$

$$\overline{xy} = \frac{1}{N}\sum_{i=1}^{N} x_i y_i = 56089.0000$$

$$\hat{\sigma}_x = \sqrt{\frac{1}{N-1}\sum_{i=1}^{N} (x_i - \bar{x})^2} = 0.3877$$

$$\hat{\sigma}_y = \sqrt{\frac{1}{N-1}\sum_{i=1}^{N} (y_i - \bar{y})^2} = 0.9006$$

$$\hat{\sigma}_{xy} = \frac{1}{N-1}\sum_{i=1}^{N} (x_i - \bar{x})(y_i - \bar{y}) = 0.2529$$

$$\hat{\rho} = \frac{\hat{\sigma}_{xy}}{\hat{\sigma}_x \hat{\sigma}_y} = 0.7244$$

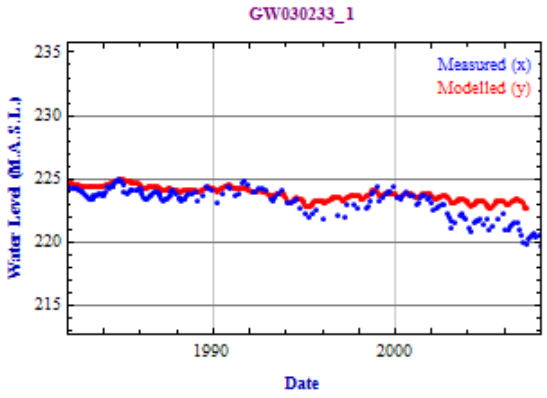

$$\bar{x} = \frac{1}{N}\sum_{i=1}^{N} x_i = 223.9300$$

$$\bar{y} = \frac{1}{N}\sum_{i=1}^{N} y_i = 223.2700$$

$$\overline{xy} = \frac{1}{N}\sum_{i=1}^{N} x_i y_i = 49997.0000$$

$$\hat{\sigma}_x = \sqrt{\frac{1}{N-1}\sum_{i=1}^{N} (x_i - \bar{x})^2} = 0.5485$$

$$\hat{\sigma}_y = \sqrt{\frac{1}{N-1}\sum_{i=1}^{N} (y_i - \bar{y})^2} = 1.0509$$

$$\hat{\sigma}_{xy} = \frac{1}{N-1}\sum_{i=1}^{N} (x_i - \bar{x})(y_i - \bar{y}) = 0.5012$$

$$\hat{\rho} = \frac{\hat{\sigma}_{xy}}{\hat{\sigma}_x \hat{\sigma}_y} = 0.8695$$

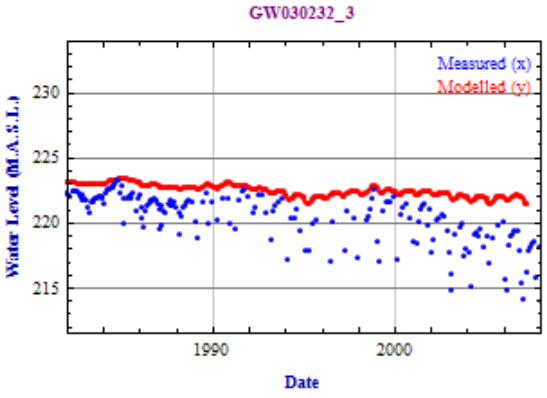

$$\bar{x} = \frac{1}{N}\sum_{i=1}^{N} x_i = 222.6000$$

$$\bar{y} = \frac{1}{N}\sum_{i=1}^{N} y_i = 220.5300$$

$$\overline{xy} = \frac{1}{N}\sum_{i=1}^{N} x_i y_i = 49090.0000$$

$$\hat{\sigma}_x = \sqrt{\frac{1}{N-1}\sum_{i=1}^{N} (x_i - \bar{x})^2} = 0.4740$$

$$\hat{\sigma}_y = \sqrt{\frac{1}{N-1}\sum_{i=1}^{N} (y_i - \bar{y})^2} = 1.8555$$

$$\hat{\sigma}_{xy} = \frac{1}{N-1}\sum_{i=1}^{N} (x_i - \bar{x})(y_i - \bar{y}) = 0.6953$$

$$\hat{\rho} = \frac{\hat{\sigma}_{xy}}{\hat{\sigma}_x \hat{\sigma}_y} = 0.7905$$

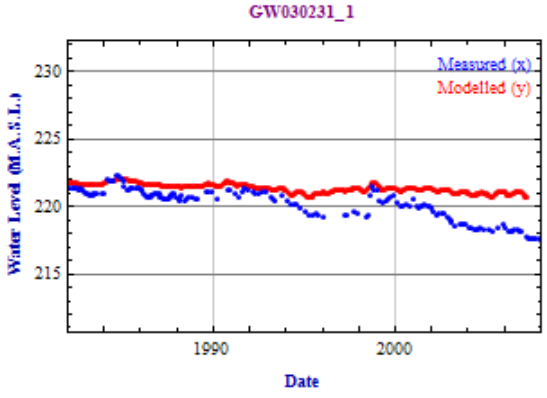

$$\bar{x} = \frac{1}{N}\sum_{i=1}^{N} x_i = 221.4000$$

$$\bar{y} = \frac{1}{N}\sum_{i=1}^{N} y_i = 220.3100$$

$$\overline{xy} = \frac{1}{N}\sum_{i=1}^{N} x_i y_i = 48777.0000$$

$$\hat{\sigma}_x = \sqrt{\frac{1}{N-1}\sum_{i=1}^{N} (x_i - \bar{x})^2} = 0.3277$$

$$\hat{\sigma}_y = \sqrt{\frac{1}{N-1}\sum_{i=1}^{N} (y_i - \bar{y})^2} = 1.0701$$

$$\hat{\sigma}_{xy} = \frac{1}{N-1}\sum_{i=1}^{N} (x_i - \bar{x})(y_i - \bar{y}) = 0.3176$$

$$\hat{\rho} = \frac{\hat{\sigma}_{xy}}{\hat{\sigma}_x \hat{\sigma}_y} = 0.9058$$

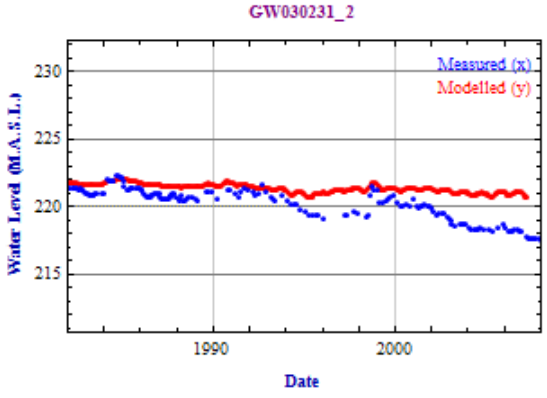

$$\bar{x} = \frac{1}{N}\sum_{i=1}^{N} x_i = 221.4100$$

$$\bar{y} = \frac{1}{N}\sum_{i=1}^{N} y_i = 220.3100$$

$$\overline{xy} = \frac{1}{N}\sum_{i=1}^{N} x_i y_i = 48778.0000$$

$$\hat{\sigma}_x = \sqrt{\frac{1}{N-1}\sum_{i=1}^{N} (x_i - \bar{x})^2} = 0.3278$$

$$\hat{\sigma}_y = \sqrt{\frac{1}{N-1}\sum_{i=1}^{N} (y_i - \bar{y})^2} = 1.0741$$

$$\hat{\sigma}_{xy} = \frac{1}{N-1}\sum_{i=1}^{N} (x_i - \bar{x})(y_i - \bar{y}) = 0.3180$$

$$\hat{\rho} = \frac{\hat{\sigma}_{xy}}{\hat{\sigma}_x \hat{\sigma}_y} = 0.9032$$

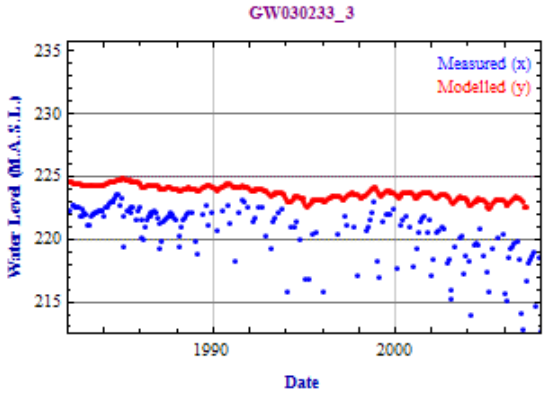

$$\bar{x} = \frac{1}{N}\sum_{i=1}^{N} x_i = 223.8200$$

$$\bar{y} = \frac{1}{N}\sum_{i=1}^{N} y_i = 220.7300$$

$$\overline{xy} = \frac{1}{N}\sum_{i=1}^{N} x_i y_i = 49405.0000$$

$$\hat{\sigma}_x = \sqrt{\frac{1}{N-1}\sum_{i=1}^{N} (x_i - \bar{x})^2} = 0.5598$$

$$\hat{\sigma}_y = \sqrt{\frac{1}{N-1}\sum_{i=1}^{N} (y_i - \bar{y})^2} = 2.0933$$

$$\hat{\sigma}_{xy} = \frac{1}{N-1}\sum_{i=1}^{N} (x_i - \bar{x})(y_i - \bar{y}) = 0.9046$$

$$\hat{\rho} = \frac{\hat{\sigma}_{xy}}{\hat{\sigma}_x \hat{\sigma}_y} = 0.7719$$

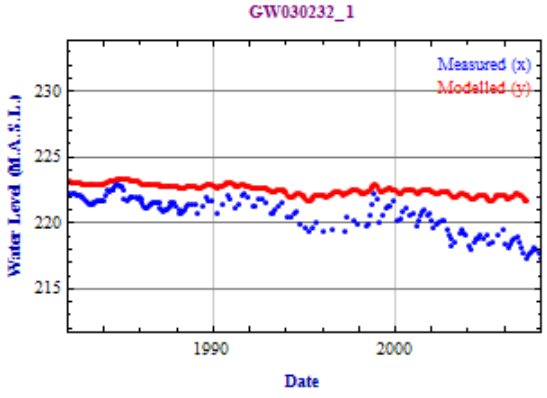

$$\bar{x} = \frac{1}{N}\sum_{i=1}^{N} x_i = 222.6100$$

$$\bar{y} = \frac{1}{N}\sum_{i=1}^{N} y_i = 220.8300$$

$$\overline{xy} = \frac{1}{N}\sum_{i=1}^{N} x_i y_i = 49160.0000$$

$$\hat{\sigma}_x = \sqrt{\frac{1}{N-1}\sum_{i=1}^{N} (x_i - \bar{x})^2} = 0.4213$$

$$\hat{\sigma}_y = \sqrt{\frac{1}{N-1}\sum_{i=1}^{N} (y_i - \bar{y})^2} = 1.2491$$

$$\hat{\sigma}_{xy} = \frac{1}{N-1}\sum_{i=1}^{N} (x_i - \bar{x})(y_i - \bar{y}) = 0.4851$$

$$\hat{\rho} = \frac{\hat{\sigma}_{xy}}{\hat{\sigma}_x \hat{\sigma}_y} = 0.9218$$

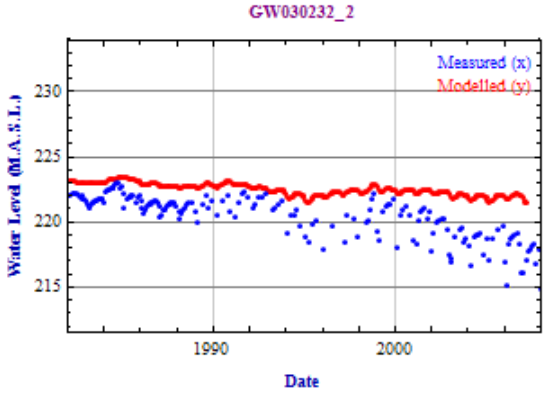

$$\bar{x} = \frac{1}{N}\sum_{i=1}^{N} x_i = 222.5800$$

$$\bar{y} = \frac{1}{N}\sum_{i=1}^{N} y_i = 220.5700$$

$$\overline{xy} = \frac{1}{N}\sum_{i=1}^{N} x_i y_i = 49097.0000$$

$$\hat{\sigma}_x = \sqrt{\frac{1}{N-1}\sum_{i=1}^{N} (x_i - \bar{x})^2} = 0.4744$$

$$\hat{\sigma}_y = \sqrt{\frac{1}{N-1}\sum_{i=1}^{N} (y_i - \bar{y})^2} = 1.5674$$

$$\hat{\sigma}_{xy} = \frac{1}{N-1}\sum_{i=1}^{N} (x_i - \bar{x})(y_i - \bar{y}) = 0.6400$$

$$\hat{\rho} = \frac{\hat{\sigma}_{xy}}{\hat{\sigma}_x \hat{\sigma}_y} = 0.8606$$

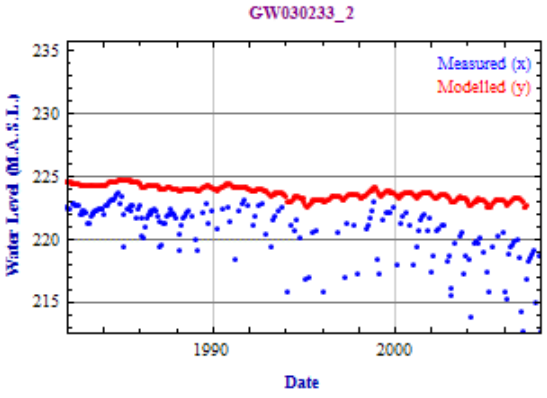

$$\bar{x} = \frac{1}{N}\sum_{i=1}^{N} x_i = 223.8500$$

$$\bar{y} = \frac{1}{N}\sum_{i=1}^{N} y_i = 220.8600$$

$$\overline{xy} = \frac{1}{N}\sum_{i=1}^{N} x_i y_i = 49440.0000$$

$$\hat{\sigma}_x = \sqrt{\frac{1}{N-1}\sum_{i=1}^{N} (x_i - \bar{x})^2} = 0.5512$$

$$\hat{\sigma}_y = \sqrt{\frac{1}{N-1}\sum_{i=1}^{N} (y_i - \bar{y})^2} = 2.1063$$

$$\hat{\sigma}_{xy} = \frac{1}{N-1}\sum_{i=1}^{N} (x_i - \bar{x})(y_i - \bar{y}) = 0.8991$$

$$\hat{\rho} = \frac{\hat{\sigma}_{xy}}{\hat{\sigma}_x \hat{\sigma}_y} = 0.7744$$

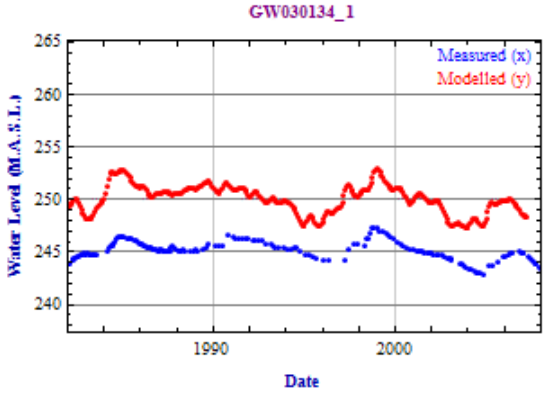

$$\bar{x} = \frac{1}{N}\sum_{i=1}^{N} x_i = 250.1700$$

$$\bar{y} = \frac{1}{N}\sum_{i=1}^{N} y_i = 245.2300$$

$$\overline{xy} = \frac{1}{N}\sum_{i=1}^{N} x_i y_i = 61352.0000$$

$$\hat{\sigma}_x = \sqrt{\frac{1}{N-1}\sum_{i=1}^{N} (x_i - \bar{x})^2} = 1.3907$$

$$\hat{\sigma}_y = \sqrt{\frac{1}{N-1}\sum_{i=1}^{N} (y_i - \bar{y})^2} = 0.8906$$

$$\hat{\sigma}_{xy} = \frac{1}{N-1}\sum_{i=1}^{N} (x_i - \bar{x})(y_i - \bar{y}) = 0.9887$$

$$\hat{\rho} = \frac{\hat{\sigma}_{xy}}{\hat{\sigma}_x \hat{\sigma}_y} = 0.7983$$

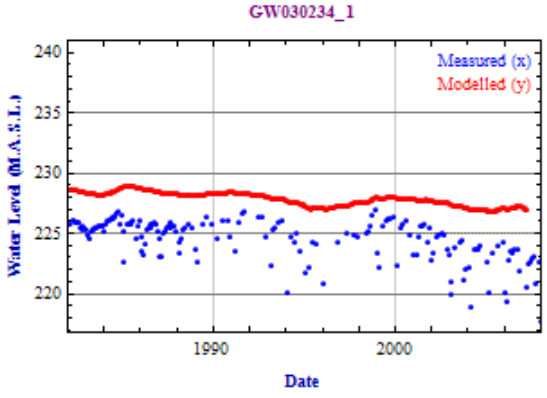

$$\bar{x} = \frac{1}{N}\sum_{i=1}^{N} x_i = 227.9800$$

$$\bar{y} = \frac{1}{N}\sum_{i=1}^{N} y_i = 224.6500$$

$$\overline{xy} = \frac{1}{N}\sum_{i=1}^{N} x_i y_i = 51217.0000$$

$$\hat{\sigma}_x = \sqrt{\frac{1}{N-1}\sum_{i=1}^{N} (x_i - \bar{x})^2} = 0.5680$$

$$\hat{\sigma}_y = \sqrt{\frac{1}{N-1}\sum_{i=1}^{N} (y_i - \bar{y})^2} = 1.6317$$

$$\hat{\sigma}_{xy} = \frac{1}{N-1}\sum_{i=1}^{N} (x_i - \bar{x})(y_i - \bar{y}) = 0.5736$$

$$\hat{\rho} = \frac{\hat{\sigma}_{xy}}{\hat{\sigma}_x \hat{\sigma}_y} = 0.6189$$

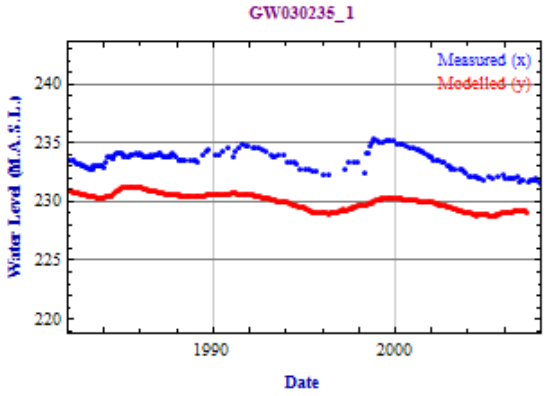

$$\bar{x} = \frac{1}{N}\sum_{i=1}^{N} x_i = 230.1700$$

$$\bar{y} = \frac{1}{N}\sum_{i=1}^{N} y_i = 233.5500$$

$$\overline{xy} = \frac{1}{N}\sum_{i=1}^{N} x_i y_i = 53757.0000$$

$$\hat{\sigma}_x = \sqrt{\frac{1}{N-1}\sum_{i=1}^{N} (x_i - \bar{x})^2} = 0.6671$$

$$\hat{\sigma}_y = \sqrt{\frac{1}{N-1}\sum_{i=1}^{N} (y_i - \bar{y})^2} = 0.8494$$

$$\hat{\sigma}_{xy} = \frac{1}{N-1}\sum_{i=1}^{N} (x_i - \bar{x})(y_i - \bar{y}) = 0.3602$$

$$\hat{\rho} = \frac{\hat{\sigma}_{xy}}{\hat{\sigma}_x \hat{\sigma}_y} = 0.6357$$

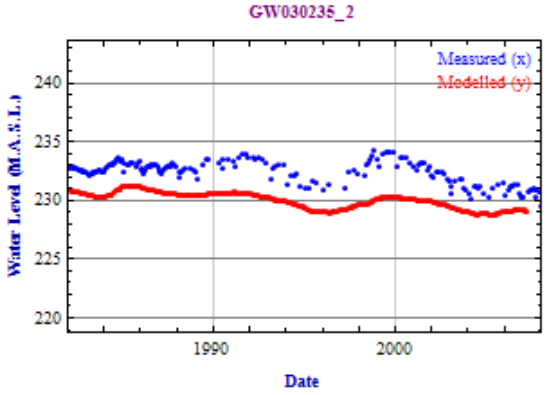

$$\bar{x} = \frac{1}{N}\sum_{i=1}^{N} x_i = 230.1500$$

$$\bar{y} = \frac{1}{N}\sum_{i=1}^{N} y_i = 232.5200$$

$$\overline{xy} = \frac{1}{N}\sum_{i=1}^{N} x_i y_i = 53516.0000$$

$$\hat{\sigma}_x = \sqrt{\frac{1}{N-1}\sum_{i=1}^{N} (x_i - \bar{x})^2} = 0.6664$$

$$\hat{\sigma}_y = \sqrt{\frac{1}{N-1}\sum_{i=1}^{N} (y_i - \bar{y})^2} = 0.9156$$

$$\hat{\sigma}_{xy} = \frac{1}{N-1}\sum_{i=1}^{N} (x_i - \bar{x})(y_i - \bar{y}) = 0.4417$$

$$\hat{\rho} = \frac{\hat{\sigma}_{xy}}{\hat{\sigma}_x \hat{\sigma}_y} = 0.7239$$

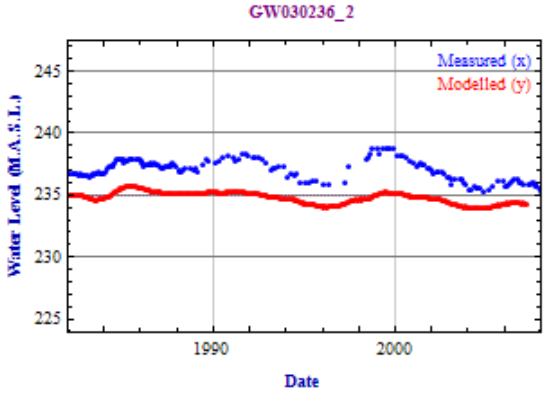

$$\bar{x} = \frac{1}{N}\sum_{i=1}^{N} x_i = 234.8600$$

$$\bar{y} = \frac{1}{N}\sum_{i=1}^{N} y_i = 237.0800$$

$$\overline{xy} = \frac{1}{N}\sum_{i=1}^{N} x_i y_i = 55681.0000$$

$$\hat{\sigma}_x = \sqrt{\frac{1}{N-1}\sum_{i=1}^{N} (x_i - \bar{x})^2} = 0.4468$$

$$\hat{\sigma}_y = \sqrt{\frac{1}{N-1}\sum_{i=1}^{N} (y_i - \bar{y})^2} = 0.8189$$

$$\hat{\sigma}_{xy} = \frac{1}{N-1}\sum_{i=1}^{N} (x_i - \bar{x})(y_i - \bar{y}) = 0.2949$$

$$\hat{\rho} = \frac{\hat{\sigma}_{xy}}{\hat{\sigma}_x \hat{\sigma}_y} = 0.8059$$

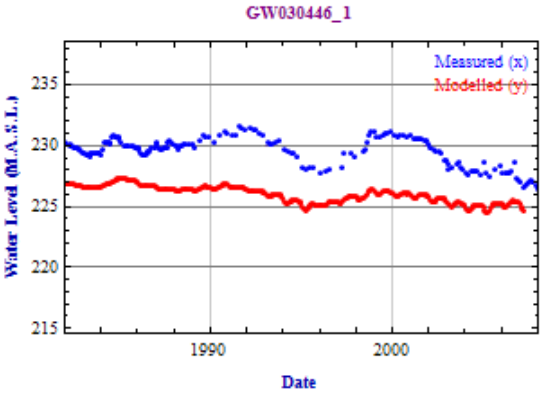

$\bar{x}$	=	$\frac{1}{N}\sum_{i=1}^{N} x_i$	=	226.1400
$\bar{y}$	=	$\frac{1}{N}\sum_{i=1}^{N} y_i$	=	229.6600
$\bar{xy}$	=	$\frac{1}{N}\sum_{i=1}^{N} x_i y_i$	=	51934.0000
$\hat{\sigma}_x$	=	$\sqrt{\frac{1}{N-1}\sum_{i=1}^{N}(x_i-\bar{x})^2}$	=	0.6932
$\hat{\sigma}_y$	=	$\sqrt{\frac{1}{N-1}\sum_{i=1}^{N}(y_i-\bar{y})^2}$	=	1.0718
$\hat{\sigma}_{xy}$	=	$\frac{1}{N-1}\sum_{i=1}^{N}(x_i-\bar{x})(y_i-\bar{y})$	=	0.5076
$\hat{\rho}$	=	$\frac{\hat{\sigma}_{xy}}{\hat{\sigma}_x \hat{\sigma}_y}$	=	0.6832

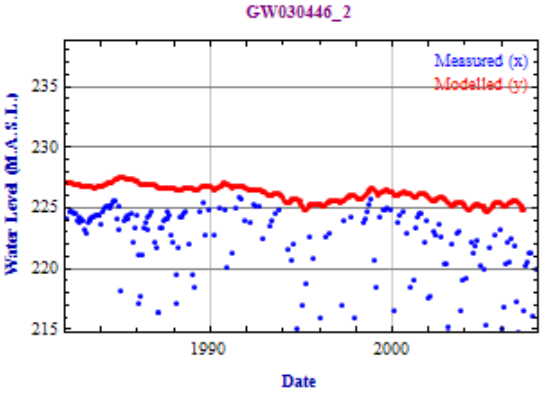

$\bar{x}$	=	$\frac{1}{N}\sum_{i=1}^{N} x_i$	=	226.3000
$\bar{y}$	=	$\frac{1}{N}\sum_{i=1}^{N} y_i$	=	222.2200
$\bar{xy}$	=	$\frac{1}{N}\sum_{i=1}^{N} x_i y_i$	=	50289.0000
$\hat{\sigma}_x$	=	$\sqrt{\frac{1}{N-1}\sum_{i=1}^{N}(x_i-\bar{x})^2}$	=	0.6990
$\hat{\sigma}_y$	=	$\sqrt{\frac{1}{N-1}\sum_{i=1}^{N}(y_i-\bar{y})^2}$	=	3.1107
$\hat{\sigma}_{xy}$	=	$\frac{1}{N-1}\sum_{i=1}^{N}(x_i-\bar{x})(y_i-\bar{y})$	=	1.1795
$\hat{\rho}$	=	$\frac{\hat{\sigma}_{xy}}{\hat{\sigma}_x \hat{\sigma}_y}$	=	0.5424

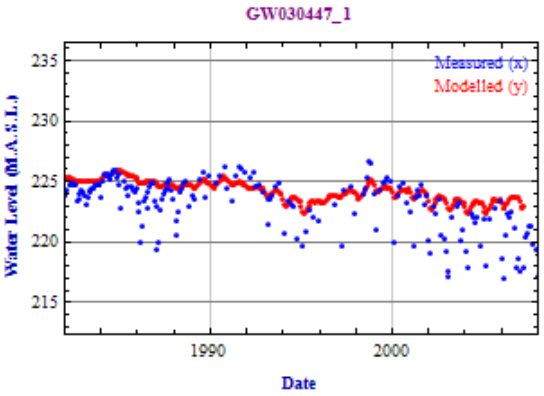

$\bar{x}$	=	$\frac{1}{N}\sum_{i=1}^{N} x_i$	=	224.3800
$\bar{y}$	=	$\frac{1}{N}\sum_{i=1}^{N} y_i$	=	223.2200
$\bar{xy}$	=	$\frac{1}{N}\sum_{i=1}^{N} x_i y_i$	=	50088.0000
$\hat{\sigma}_x$	=	$\sqrt{\frac{1}{N-1}\sum_{i=1}^{N}(x_i-\bar{x})^2}$	=	0.8545
$\hat{\sigma}_y$	=	$\sqrt{\frac{1}{N-1}\sum_{i=1}^{N}(y_i-\bar{y})^2}$	=	2.1411
$\hat{\sigma}_{xy}$	=	$\frac{1}{N-1}\sum_{i=1}^{N}(x_i-\bar{x})(y_i-\bar{y})$	=	1.3372
$\hat{\rho}$	=	$\frac{\hat{\sigma}_{xy}}{\hat{\sigma}_x \hat{\sigma}_y}$	=	0.7309

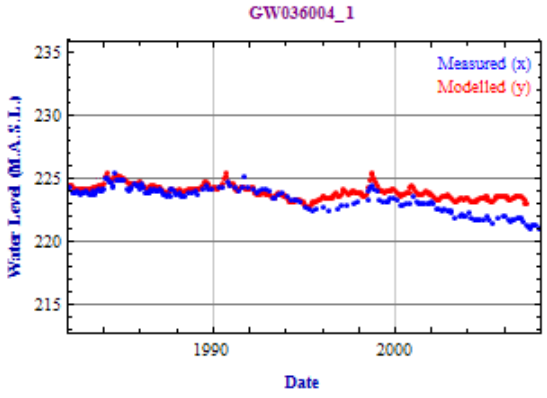

$$\bar{x} = \frac{1}{N}\sum_{i=1}^{N} x_i = 224.0600$$

$$\bar{y} = \frac{1}{N}\sum_{i=1}^{N} y_i = 223.5100$$

$$\overline{xy} = \frac{1}{N}\sum_{i=1}^{N} x_i y_i = 50079.0000$$

$$\hat{\sigma}_x = \sqrt{\frac{1}{N-1}\sum_{i=1}^{N} (x_i - \bar{x})^2} = 0.5456$$

$$\hat{\sigma}_y = \sqrt{\frac{1}{N-1}\sum_{i=1}^{N} (y_i - \bar{y})^2} = 0.9362$$

$$\hat{\sigma}_{xy} = \frac{1}{N-1}\sum_{i=1}^{N} (x_i - \bar{x})(y_i - \bar{y}) = 0.4390$$

$$\hat{\rho} = \frac{\hat{\sigma}_{xy}}{\hat{\sigma}_x \hat{\sigma}_y} = 0.8596$$

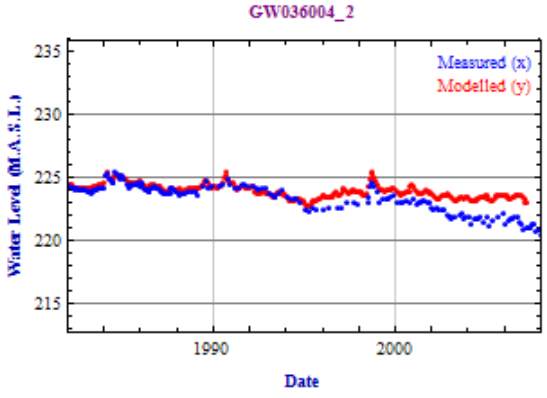

$$\bar{x} = \frac{1}{N}\sum_{i=1}^{N} x_i = 224.0600$$

$$\bar{y} = \frac{1}{N}\sum_{i=1}^{N} y_i = 223.4900$$

$$\overline{xy} = \frac{1}{N}\sum_{i=1}^{N} x_i y_i = 50074.0000$$

$$\hat{\sigma}_x = \sqrt{\frac{1}{N-1}\sum_{i=1}^{N} (x_i - \bar{x})^2} = 0.5476$$

$$\hat{\sigma}_y = \sqrt{\frac{1}{N-1}\sum_{i=1}^{N} (y_i - \bar{y})^2} = 1.0466$$

$$\hat{\sigma}_{xy} = \frac{1}{N-1}\sum_{i=1}^{N} (x_i - \bar{x})(y_i - \bar{y}) = 0.4929$$

$$\hat{\rho} = \frac{\hat{\sigma}_{xy}}{\hat{\sigma}_x \hat{\sigma}_y} = 0.8601$$

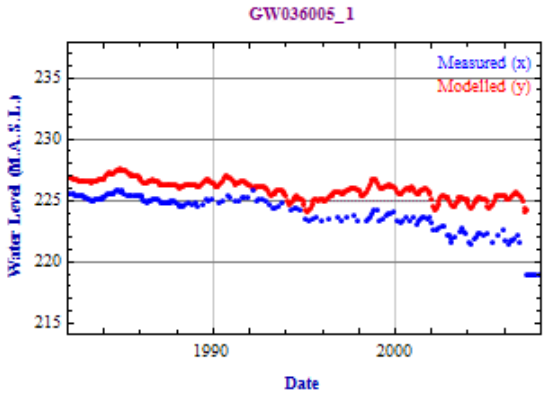

$$\bar{x} = \frac{1}{N}\sum_{i=1}^{N} x_i = 226.0800$$

$$\bar{y} = \frac{1}{N}\sum_{i=1}^{N} y_i = 224.1900$$

$$\overline{xy} = \frac{1}{N}\sum_{i=1}^{N} x_i y_i = 50685.0000$$

$$\hat{\sigma}_x = \sqrt{\frac{1}{N-1}\sum_{i=1}^{N} (x_i - \bar{x})^2} = 0.7685$$

$$\hat{\sigma}_y = \sqrt{\frac{1}{N-1}\sum_{i=1}^{N} (y_i - \bar{y})^2} = 1.2821$$

$$\hat{\sigma}_{xy} = \frac{1}{N-1}\sum_{i=1}^{N} (x_i - \bar{x})(y_i - \bar{y}) = 0.8468$$

$$\hat{\rho} = \frac{\hat{\sigma}_{xy}}{\hat{\sigma}_x \hat{\sigma}_y} = 0.8595$$

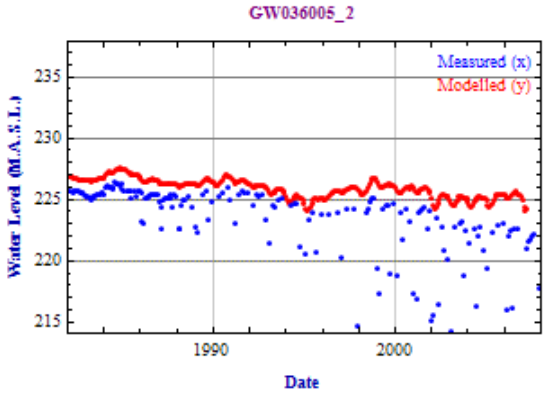

$$\bar{x} = \frac{1}{N}\sum_{i=1}^{N} x_i = 226.0400$$

$$\bar{y} = \frac{1}{N}\sum_{i=1}^{N} y_i = 223.2100$$

$$\overline{xy} = \frac{1}{N}\sum_{i=1}^{N} x_i y_i = 50457.0000$$

$$\hat{\sigma}_x = \sqrt{\frac{1}{N-1}\sum_{i=1}^{N} (x_i - \bar{x})^2} = 0.7875$$

$$\hat{\sigma}_y = \sqrt{\frac{1}{N-1}\sum_{i=1}^{N} (y_i - \bar{y})^2} = 3.4420$$

$$\hat{\sigma}_{xy} = \frac{1}{N-1}\sum_{i=1}^{N} (x_i - \bar{x})(y_i - \bar{y}) = 1.8306$$

$$\hat{\rho} = \frac{\hat{\sigma}_{xy}}{\hat{\sigma}_x \hat{\sigma}_y} = 0.6753$$

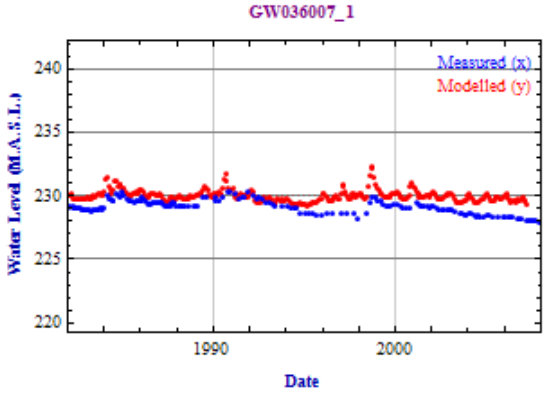

$$\bar{x} = \frac{1}{N}\sum_{i=1}^{N} x_i = 229.9900$$

$$\bar{y} = \frac{1}{N}\sum_{i=1}^{N} y_i = 229.1600$$

$$\overline{xy} = \frac{1}{N}\sum_{i=1}^{N} x_i y_i = 52705.0000$$

$$\hat{\sigma}_x = \sqrt{\frac{1}{N-1}\sum_{i=1}^{N} (x_i - \bar{x})^2} = 0.4232$$

$$\hat{\sigma}_y = \sqrt{\frac{1}{N-1}\sum_{i=1}^{N} (y_i - \bar{y})^2} = 0.5142$$

$$\hat{\sigma}_{xy} = \frac{1}{N-1}\sum_{i=1}^{N} (x_i - \bar{x})(y_i - \bar{y}) = 0.1286$$

$$\hat{\rho} = \frac{\hat{\sigma}_{xy}}{\hat{\sigma}_x \hat{\sigma}_y} = 0.5907$$

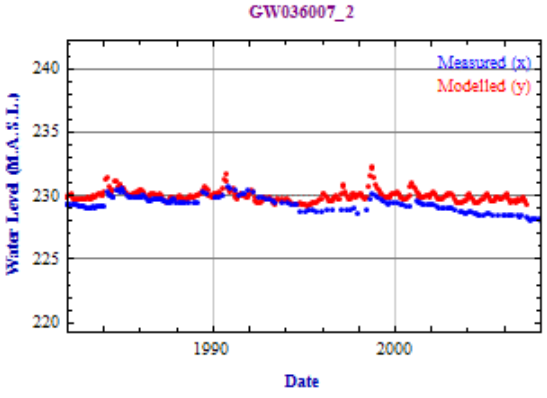

$$\bar{x} = \frac{1}{N}\sum_{i=1}^{N} x_i = 229.9900$$

$$\bar{y} = \frac{1}{N}\sum_{i=1}^{N} y_i = 229.4000$$

$$\overline{xy} = \frac{1}{N}\sum_{i=1}^{N} x_i y_i = 52761.0000$$

$$\hat{\sigma}_x = \sqrt{\frac{1}{N-1}\sum_{i=1}^{N} (x_i - \bar{x})^2} = 0.4217$$

$$\hat{\sigma}_y = \sqrt{\frac{1}{N-1}\sum_{i=1}^{N} (y_i - \bar{y})^2} = 0.5476$$

$$\hat{\sigma}_{xy} = \frac{1}{N-1}\sum_{i=1}^{N} (x_i - \bar{x})(y_i - \bar{y}) = 0.1385$$

$$\hat{\rho} = \frac{\hat{\sigma}_{xy}}{\hat{\sigma}_x \hat{\sigma}_y} = 0.5999$$

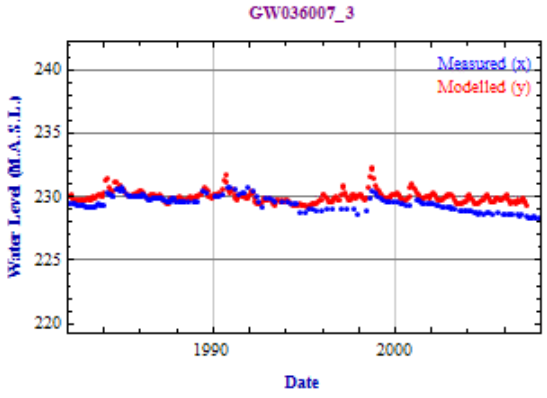

$$\bar{x} = \frac{1}{N}\sum_{i=1}^{N} x_i = 229.9900$$

$$\bar{y} = \frac{1}{N}\sum_{i=1}^{N} y_i = 229.5300$$

$$\overline{xy} = \frac{1}{N}\sum_{i=1}^{N} x_i y_i = 52791.0000$$

$$\hat{\sigma}_x = \sqrt{\frac{1}{N-1}\sum_{i=1}^{N} (x_i - \bar{x})^2} = 0.4231$$

$$\hat{\sigma}_y = \sqrt{\frac{1}{N-1}\sum_{i=1}^{N} (y_i - \bar{y})^2} = 0.5436$$

$$\hat{\sigma}_{xy} = \frac{1}{N-1}\sum_{i=1}^{N} (x_i - \bar{x})(y_i - \bar{y}) = 0.1395$$

$$\hat{\rho} = \frac{\hat{\sigma}_{xy}}{\hat{\sigma}_x \hat{\sigma}_y} = 0.6064$$

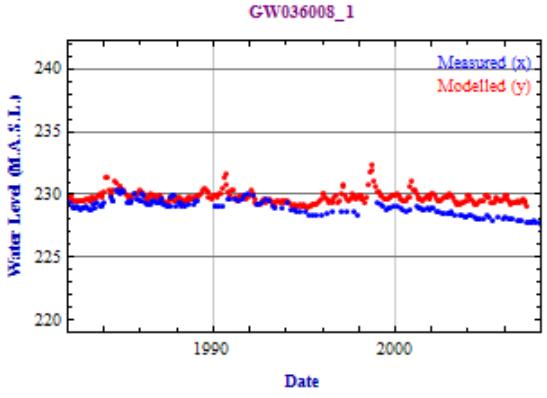

$$\bar{x} = \frac{1}{N}\sum_{i=1}^{N} x_i = 229.7200$$

$$\bar{y} = \frac{1}{N}\sum_{i=1}^{N} y_i = 229.0100$$

$$\overline{xy} = \frac{1}{N}\sum_{i=1}^{N} x_i y_i = 52607.0000$$

$$\hat{\sigma}_x = \sqrt{\frac{1}{N-1}\sum_{i=1}^{N} (x_i - \bar{x})^2} = 0.3438$$

$$\hat{\sigma}_y = \sqrt{\frac{1}{N-1}\sum_{i=1}^{N} (y_i - \bar{y})^2} = 0.5692$$

$$\hat{\sigma}_{xy} = \frac{1}{N-1}\sum_{i=1}^{N} (x_i - \bar{x})(y_i - \bar{y}) = 0.1083$$

$$\hat{\rho} = \frac{\hat{\sigma}_{xy}}{\hat{\sigma}_x \hat{\sigma}_y} = 0.5536$$

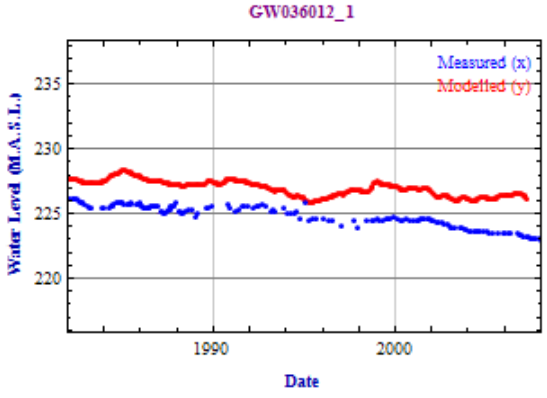

$$\bar{x} = \frac{1}{N}\sum_{i=1}^{N} x_i = 227.0600$$

$$\bar{y} = \frac{1}{N}\sum_{i=1}^{N} y_i = 224.9100$$

$$\overline{xy} = \frac{1}{N}\sum_{i=1}^{N} x_i y_i = 51068.0000$$

$$\hat{\sigma}_x = \sqrt{\frac{1}{N-1}\sum_{i=1}^{N} (x_i - \bar{x})^2} = 0.6343$$

$$\hat{\sigma}_y = \sqrt{\frac{1}{N-1}\sum_{i=1}^{N} (y_i - \bar{y})^2} = 0.8016$$

$$\hat{\sigma}_{xy} = \frac{1}{N-1}\sum_{i=1}^{N} (x_i - \bar{x})(y_i - \bar{y}) = 0.4129$$

$$\hat{\rho} = \frac{\hat{\sigma}_{xy}}{\hat{\sigma}_x \hat{\sigma}_y} = 0.8122$$

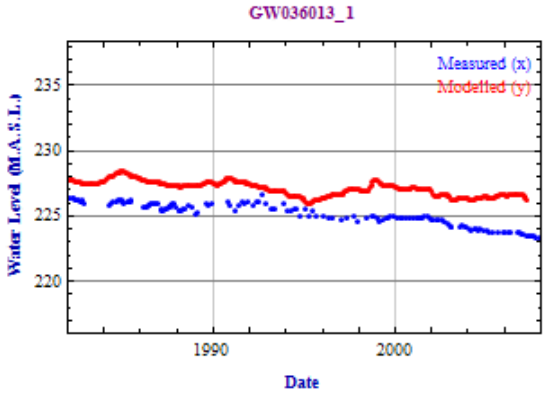

$$\bar{x} = \frac{1}{N}\sum_{i=1}^{N} x_i = 227.1500$$

$$\bar{y} = \frac{1}{N}\sum_{i=1}^{N} y_i = 225.2100$$

$$\overline{xy} = \frac{1}{N}\sum_{i=1}^{N} x_i y_i = 51155.0000$$

$$\hat{\sigma}_x = \sqrt{\frac{1}{N-1}\sum_{i=1}^{N} (x_i - \bar{x})^2} = 0.5869$$

$$\hat{\sigma}_y = \sqrt{\frac{1}{N-1}\sum_{i=1}^{N} (y_i - \bar{y})^2} = 0.8063$$

$$\hat{\sigma}_{xy} = \frac{1}{N-1}\sum_{i=1}^{N} (x_i - \bar{x})(y_i - \bar{y}) = 0.3600$$

$$\hat{\rho} = \frac{\hat{\sigma}_{xy}}{\hat{\sigma}_x \hat{\sigma}_y} = 0.7607$$

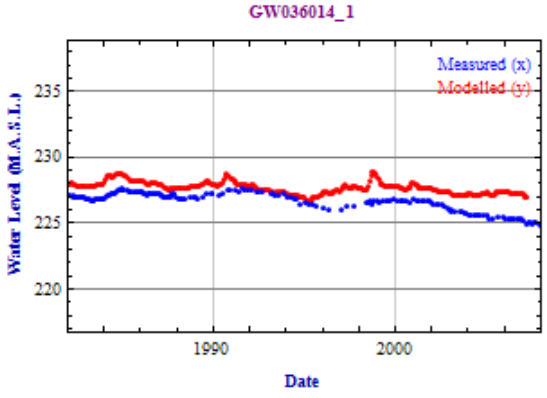

$$\bar{x} = \frac{1}{N}\sum_{i=1}^{N} x_i = 227.7500$$

$$\bar{y} = \frac{1}{N}\sum_{i=1}^{N} y_i = 226.7300$$

$$\overline{xy} = \frac{1}{N}\sum_{i=1}^{N} x_i y_i = 51638.0000$$

$$\hat{\sigma}_x = \sqrt{\frac{1}{N-1}\sum_{i=1}^{N} (x_i - \bar{x})^2} = 0.4515$$

$$\hat{\sigma}_y = \sqrt{\frac{1}{N-1}\sum_{i=1}^{N} (y_i - \bar{y})^2} = 0.6347$$

$$\hat{\sigma}_{xy} = \frac{1}{N-1}\sum_{i=1}^{N} (x_i - \bar{x})(y_i - \bar{y}) = 0.1973$$

$$\hat{\rho} = \frac{\hat{\sigma}_{xy}}{\hat{\sigma}_x \hat{\sigma}_y} = 0.6886$$

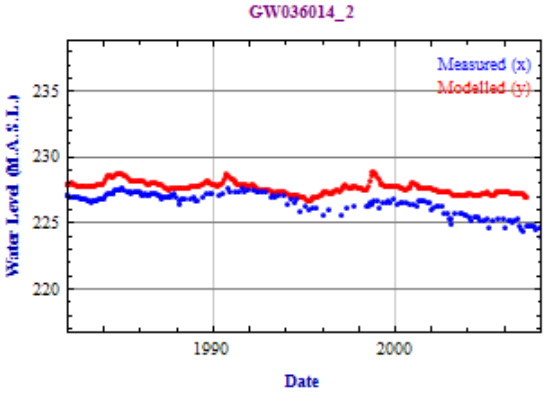

$$\bar{x} = \frac{1}{N}\sum_{i=1}^{N} x_i = 227.7500$$

$$\bar{y} = \frac{1}{N}\sum_{i=1}^{N} y_i = 226.6000$$

$$\overline{xy} = \frac{1}{N}\sum_{i=1}^{N} x_i y_i = 51607.0000$$

$$\hat{\sigma}_x = \sqrt{\frac{1}{N-1}\sum_{i=1}^{N} (x_i - \bar{x})^2} = 0.4504$$

$$\hat{\sigma}_y = \sqrt{\frac{1}{N-1}\sum_{i=1}^{N} (y_i - \bar{y})^2} = 0.7601$$

$$\hat{\sigma}_{xy} = \frac{1}{N-1}\sum_{i=1}^{N} (x_i - \bar{x})(y_i - \bar{y}) = 0.2406$$

$$\hat{\rho} = \frac{\hat{\sigma}_{xy}}{\hat{\sigma}_x \hat{\sigma}_y} = 0.7026$$

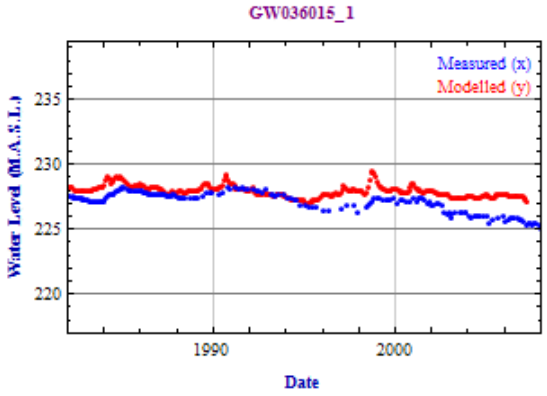

$$\bar{x} = \frac{1}{N}\sum_{i=1}^{N} x_i = 227.9700$$

$$\bar{y} = \frac{1}{N}\sum_{i=1}^{N} y_i = 227.1700$$

$$\overline{xy} = \frac{1}{N}\sum_{i=1}^{N} x_i y_i = 51789.0000$$

$$\hat{\sigma}_x = \sqrt{\frac{1}{N-1}\sum_{i=1}^{N} (x_i - \bar{x})^2} = 0.4513$$

$$\hat{\sigma}_y = \sqrt{\frac{1}{N-1}\sum_{i=1}^{N} (y_i - \bar{y})^2} = 0.7062$$

$$\hat{\sigma}_{xy} = \frac{1}{N-1}\sum_{i=1}^{N} (x_i - \bar{x})(y_i - \bar{y}) = 0.1963$$

$$\hat{\rho} = \frac{\hat{\sigma}_{xy}}{\hat{\sigma}_x \hat{\sigma}_y} = 0.6159$$

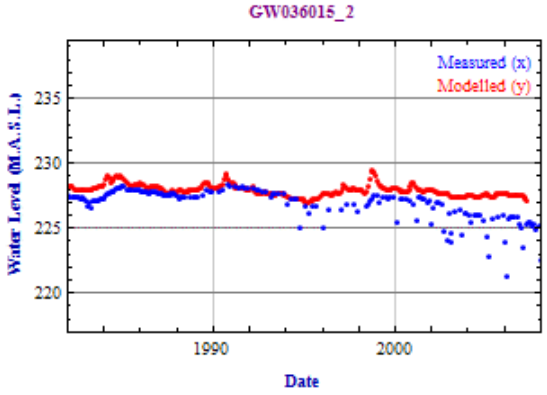

$$\bar{x} = \frac{1}{N}\sum_{i=1}^{N} x_i = 227.9700$$

$$\bar{y} = \frac{1}{N}\sum_{i=1}^{N} y_i = 226.9700$$

$$\overline{xy} = \frac{1}{N}\sum_{i=1}^{N} x_i y_i = 51742.0000$$

$$\hat{\sigma}_x = \sqrt{\frac{1}{N-1}\sum_{i=1}^{N} (x_i - \bar{x})^2} = 0.4507$$

$$\hat{\sigma}_y = \sqrt{\frac{1}{N-1}\sum_{i=1}^{N} (y_i - \bar{y})^2} = 1.1159$$

$$\hat{\sigma}_{xy} = \frac{1}{N-1}\sum_{i=1}^{N} (x_i - \bar{x})(y_i - \bar{y}) = 0.2781$$

$$\hat{\rho} = \frac{\hat{\sigma}_{xy}}{\hat{\sigma}_x \hat{\sigma}_y} = 0.5530$$

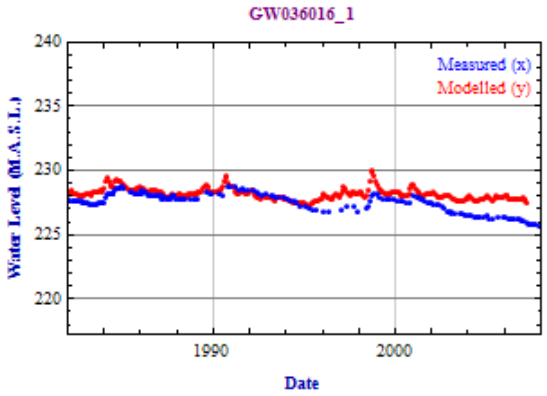

$$\bar{x} = \frac{1}{N}\sum_{i=1}^{N} x_i = 228.2100$$

$$\bar{y} = \frac{1}{N}\sum_{i=1}^{N} y_i = 227.5700$$

$$\overline{xy} = \frac{1}{N}\sum_{i=1}^{N} x_i y_i = 51932.0000$$

$$\hat{\sigma}_x = \sqrt{\frac{1}{N-1}\sum_{i=1}^{N} (x_i - \bar{x})^2} = 0.4483$$

$$\hat{\sigma}_y = \sqrt{\frac{1}{N-1}\sum_{i=1}^{N} (y_i - \bar{y})^2} = 0.6890$$

$$\hat{\sigma}_{xy} = \frac{1}{N-1}\sum_{i=1}^{N} (x_i - \bar{x})(y_i - \bar{y}) = 0.1938$$

$$\hat{\rho} = \frac{\hat{\sigma}_{xy}}{\hat{\sigma}_x \hat{\sigma}_y} = 0.6273$$

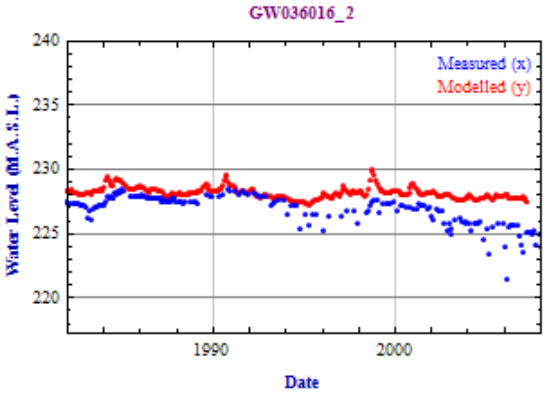

$$\bar{x} = \frac{1}{N}\sum_{i=1}^{N} x_i = 228.2100$$

$$\bar{y} = \frac{1}{N}\sum_{i=1}^{N} y_i = 226.9800$$

$$\overline{xy} = \frac{1}{N}\sum_{i=1}^{N} x_i y_i = 51798.0000$$

$$\hat{\sigma}_x = \sqrt{\frac{1}{N-1}\sum_{i=1}^{N} (x_i - \bar{x})^2} = 0.4475$$

$$\hat{\sigma}_y = \sqrt{\frac{1}{N-1}\sum_{i=1}^{N} (y_i - \bar{y})^2} = 1.0833$$

$$\hat{\sigma}_{xy} = \frac{1}{N-1}\sum_{i=1}^{N} (x_i - \bar{x})(y_i - \bar{y}) = 0.2563$$

$$\hat{\rho} = \frac{\hat{\sigma}_{xy}}{\hat{\sigma}_x \hat{\sigma}_y} = 0.5287$$

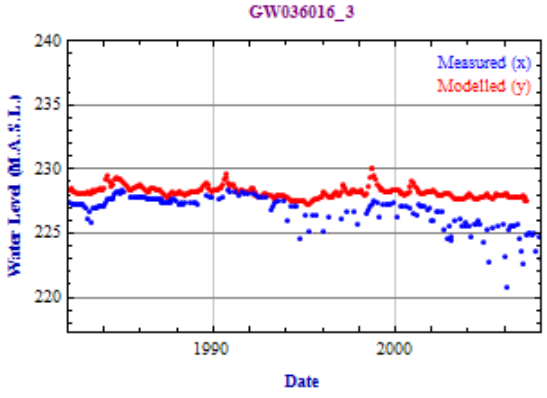

$$\bar{x} = \frac{1}{N}\sum_{i=1}^{N} x_i = 228.2300$$

$$\bar{y} = \frac{1}{N}\sum_{i=1}^{N} y_i = 226.8300$$

$$\overline{xy} = \frac{1}{N}\sum_{i=1}^{N} x_i y_i = 51770.0000$$

$$\hat{\sigma}_x = \sqrt{\frac{1}{N-1}\sum_{i=1}^{N} (x_i - \bar{x})^2} = 0.4510$$

$$\hat{\sigma}_y = \sqrt{\frac{1}{N-1}\sum_{i=1}^{N} (y_i - \bar{y})^2} = 1.1973$$

$$\hat{\sigma}_{xy} = \frac{1}{N-1}\sum_{i=1}^{N} (x_i - \bar{x})(y_i - \bar{y}) = 0.2654$$

$$\hat{\rho} = \frac{\hat{\sigma}_{xy}}{\hat{\sigma}_x \hat{\sigma}_y} = 0.4914$$

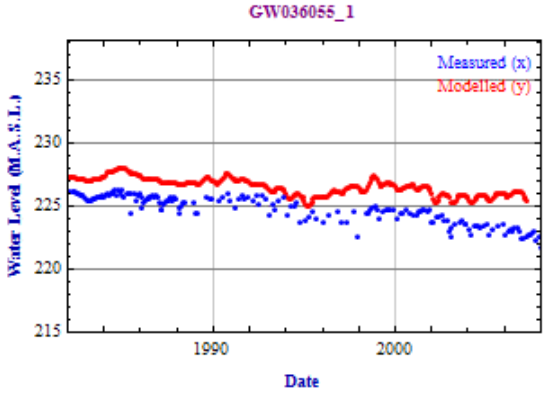

$$\bar{x} = \frac{1}{N}\sum_{i=1}^{N} x_i = 226.6100$$

$$\bar{y} = \frac{1}{N}\sum_{i=1}^{N} y_i = 224.7800$$

$$\overline{xy} = \frac{1}{N}\sum_{i=1}^{N} x_i y_i = 50939.0000$$

$$\hat{\sigma}_x = \sqrt{\frac{1}{N-1}\sum_{i=1}^{N} (x_i - \bar{x})^2} = 0.7025$$

$$\hat{\sigma}_y = \sqrt{\frac{1}{N-1}\sum_{i=1}^{N} (y_i - \bar{y})^2} = 1.0272$$

$$\hat{\sigma}_{xy} = \frac{1}{N-1}\sum_{i=1}^{N} (x_i - \bar{x})(y_i - \bar{y}) = 0.6074$$

$$\hat{\rho} = \frac{\hat{\sigma}_{xy}}{\hat{\sigma}_x \hat{\sigma}_y} = 0.8417$$

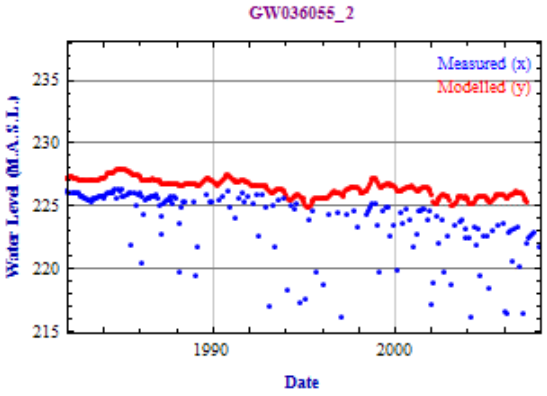

$$\bar{x} = \frac{1}{N}\sum_{i=1}^{N} x_i = 226.5900$$

$$\bar{y} = \frac{1}{N}\sum_{i=1}^{N} y_i = 223.7900$$

$$\overline{xy} = \frac{1}{N}\sum_{i=1}^{N} x_i y_i = 50709.0000$$

$$\hat{\sigma}_x = \sqrt{\frac{1}{N-1}\sum_{i=1}^{N} (x_i - \bar{x})^2} = 0.7199$$

$$\hat{\sigma}_y = \sqrt{\frac{1}{N-1}\sum_{i=1}^{N} (y_i - \bar{y})^2} = 2.8208$$

$$\hat{\sigma}_{xy} = \frac{1}{N-1}\sum_{i=1}^{N} (x_i - \bar{x})(y_i - \bar{y}) = 1.3470$$

$$\hat{\rho} = \frac{\hat{\sigma}_{xy}}{\hat{\sigma}_x \hat{\sigma}_y} = 0.6633$$

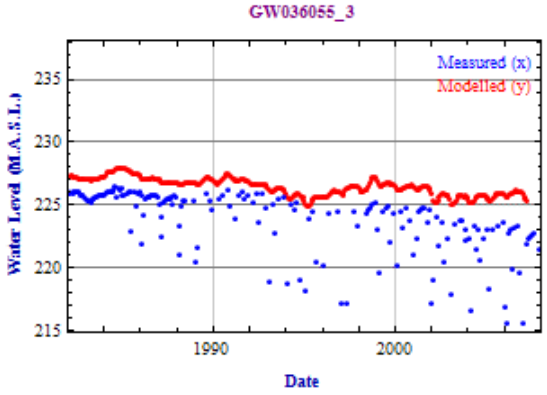

$$\bar{x} = \frac{1}{N}\sum_{i=1}^{N} x_i = 226.5900$$

$$\bar{y} = \frac{1}{N}\sum_{i=1}^{N} y_i = 223.7800$$

$$\overline{xy} = \frac{1}{N}\sum_{i=1}^{N} x_i y_i = 50707.0000$$

$$\hat{\sigma}_x = \sqrt{\frac{1}{N-1}\sum_{i=1}^{N} (x_i - \bar{x})^2} = 0.7191$$

$$\hat{\sigma}_y = \sqrt{\frac{1}{N-1}\sum_{i=1}^{N} (y_i - \bar{y})^2} = 2.7561$$

$$\hat{\sigma}_{xy} = \frac{1}{N-1}\sum_{i=1}^{N} (x_i - \bar{x})(y_i - \bar{y}) = 1.3419$$

$$\hat{\rho} = \frac{\hat{\sigma}_{xy}}{\hat{\sigma}_x \hat{\sigma}_y} = 0.6771$$

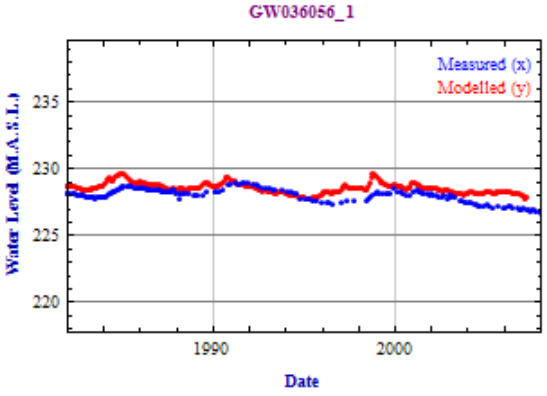

$$\bar{x} = \frac{1}{N}\sum_{i=1}^{N} x_i = 228.6100$$

$$\bar{y} = \frac{1}{N}\sum_{i=1}^{N} y_i = 228.0600$$

$$\overline{xy} = \frac{1}{N}\sum_{i=1}^{N} x_i y_i = 52137.0000$$

$$\hat{\sigma}_x = \sqrt{\frac{1}{N-1}\sum_{i=1}^{N} (x_i - \bar{x})^2} = 0.4067$$

$$\hat{\sigma}_y = \sqrt{\frac{1}{N-1}\sum_{i=1}^{N} (y_i - \bar{y})^2} = 0.4676$$

$$\hat{\sigma}_{xy} = \frac{1}{N-1}\sum_{i=1}^{N} (x_i - \bar{x})(y_i - \bar{y}) = 0.1171$$

$$\hat{\rho} = \frac{\hat{\sigma}_{xy}}{\hat{\sigma}_x \hat{\sigma}_y} = 0.6155$$

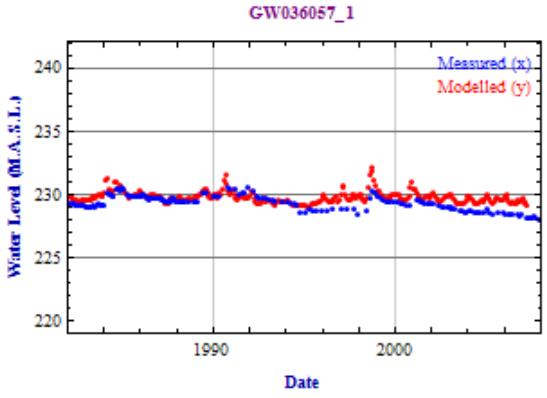

$$\bar{x} = \frac{1}{N}\sum_{i=1}^{N} x_i = 229.8100$$

$$\bar{y} = \frac{1}{N}\sum_{i=1}^{N} y_i = 229.4000$$

$$\overline{xy} = \frac{1}{N}\sum_{i=1}^{N} x_i y_i = 52717.0000$$

$$\hat{\sigma}_x = \sqrt{\frac{1}{N-1}\sum_{i=1}^{N} (x_i - \bar{x})^2} = 0.4247$$

$$\hat{\sigma}_y = \sqrt{\frac{1}{N-1}\sum_{i=1}^{N} (y_i - \bar{y})^2} = 0.5516$$

$$\hat{\sigma}_{xy} = \frac{1}{N-1}\sum_{i=1}^{N} (x_i - \bar{x})(y_i - \bar{y}) = 0.1364$$

$$\hat{\rho} = \frac{\hat{\sigma}_{xy}}{\hat{\sigma}_x \hat{\sigma}_y} = 0.5824$$

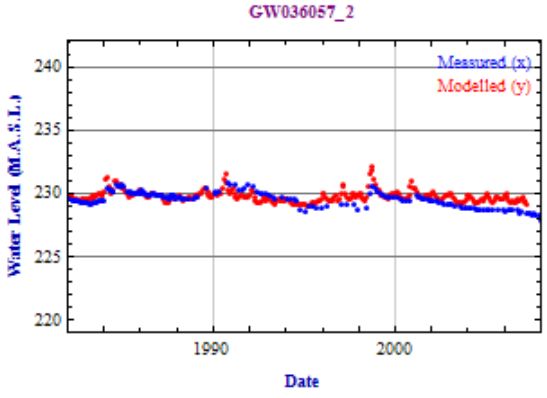

$$\bar{x} = \frac{1}{N}\sum_{i=1}^{N} x_i = 229.7800$$

$$\bar{y} = \frac{1}{N}\sum_{i=1}^{N} y_i = 229.5700$$

$$\overline{xy} = \frac{1}{N}\sum_{i=1}^{N} x_i y_i = 52750.0000$$

$$\hat{\sigma}_x = \sqrt{\frac{1}{N-1}\sum_{i=1}^{N} (x_i - \bar{x})^2} = 0.4232$$

$$\hat{\sigma}_y = \sqrt{\frac{1}{N-1}\sum_{i=1}^{N} (y_i - \bar{y})^2} = 0.5628$$

$$\hat{\sigma}_{xy} = \frac{1}{N-1}\sum_{i=1}^{N} (x_i - \bar{x})(y_i - \bar{y}) = 0.1403$$

$$\hat{\rho} = \frac{\hat{\sigma}_{xy}}{\hat{\sigma}_x \hat{\sigma}_y} = 0.5890$$

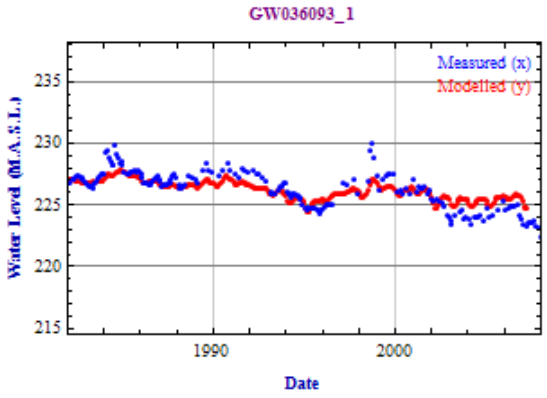

$$\bar{x} = \frac{1}{N}\sum_{i=1}^{N} x_i = 226.2500$$

$$\bar{y} = \frac{1}{N}\sum_{i=1}^{N} y_i = 226.3700$$

$$\overline{xy} = \frac{1}{N}\sum_{i=1}^{N} x_i y_i = 51217.0000$$

$$\hat{\sigma}_x = \sqrt{\frac{1}{N-1}\sum_{i=1}^{N} (x_i - \bar{x})^2} = 0.7914$$

$$\hat{\sigma}_y = \sqrt{\frac{1}{N-1}\sum_{i=1}^{N} (y_i - \bar{y})^2} = 1.4268$$

$$\hat{\sigma}_{xy} = \frac{1}{N-1}\sum_{i=1}^{N} (x_i - \bar{x})(y_i - \bar{y}) = 1.0013$$

$$\hat{\rho} = \frac{\hat{\sigma}_{xy}}{\hat{\sigma}_x \hat{\sigma}_y} = 0.8868$$

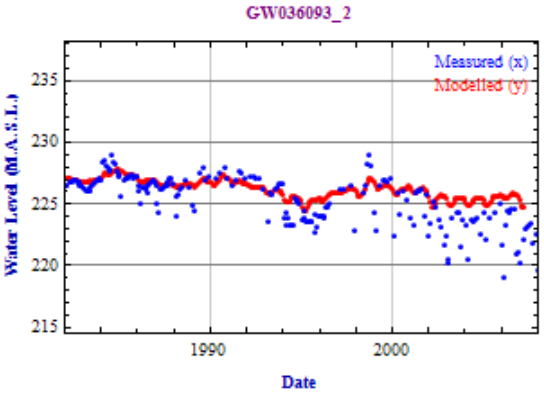

$$\bar{x} = \frac{1}{N}\sum_{i=1}^{N} x_i = 226.2500$$

$$\bar{y} = \frac{1}{N}\sum_{i=1}^{N} y_i = 225.4500$$

$$\overline{xy} = \frac{1}{N}\sum_{i=1}^{N} x_i y_i = 51010.0000$$

$$\hat{\sigma}_x = \sqrt{\frac{1}{N-1}\sum_{i=1}^{N} (x_i - \bar{x})^2} = 0.7910$$

$$\hat{\sigma}_y = \sqrt{\frac{1}{N-1}\sum_{i=1}^{N} (y_i - \bar{y})^2} = 1.9061$$

$$\hat{\sigma}_{xy} = \frac{1}{N-1}\sum_{i=1}^{N} (x_i - \bar{x})(y_i - \bar{y}) = 1.2089$$

$$\hat{\rho} = \frac{\hat{\sigma}_{xy}}{\hat{\sigma}_x \hat{\sigma}_y} = 0.8018$$

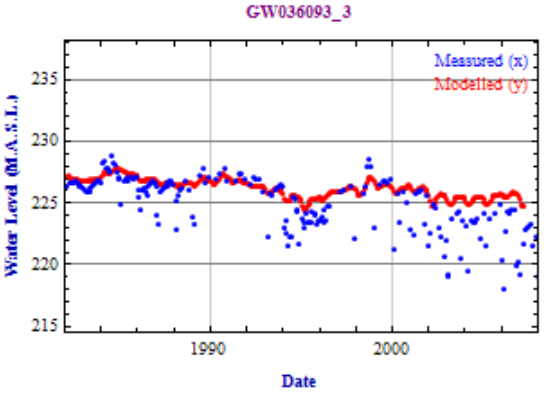

$$\bar{x} = \frac{1}{N}\sum_{i=1}^{N} x_i = 226.2500$$

$$\bar{y} = \frac{1}{N}\sum_{i=1}^{N} y_i = 225.1100$$

$$\overline{xy} = \frac{1}{N}\sum_{i=1}^{N} x_i y_i = 50933.0000$$

$$\hat{\sigma}_x = \sqrt{\frac{1}{N-1}\sum_{i=1}^{N} (x_i - \bar{x})^2} = 0.7956$$

$$\hat{\sigma}_y = \sqrt{\frac{1}{N-1}\sum_{i=1}^{N} (y_i - \bar{y})^2} = 2.1311$$

$$\hat{\sigma}_{xy} = \frac{1}{N-1}\sum_{i=1}^{N} (x_i - \bar{x})(y_i - \bar{y}) = 1.2980$$

$$\hat{\rho} = \frac{\hat{\sigma}_{xy}}{\hat{\sigma}_x \hat{\sigma}_y} = 0.7656$$

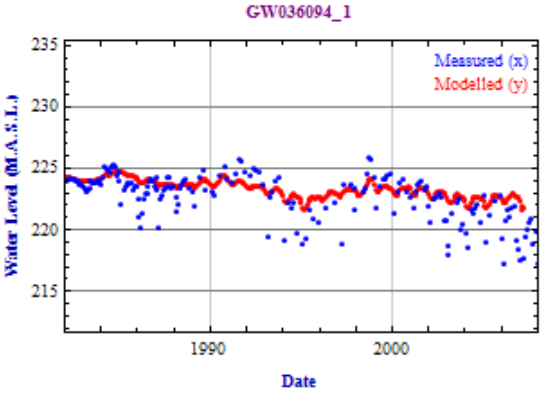

$$\bar{x} = \frac{1}{N}\sum_{i=1}^{N} x_i = 223.4600$$

$$\bar{y} = \frac{1}{N}\sum_{i=1}^{N} y_i = 222.8200$$

$$\overline{xy} = \frac{1}{N}\sum_{i=1}^{N} x_i y_i = 49792.0000$$

$$\hat{\sigma}_x = \sqrt{\frac{1}{N-1}\sum_{i=1}^{N} (x_i - \bar{x})^2} = 0.7195$$

$$\hat{\sigma}_y = \sqrt{\frac{1}{N-1}\sum_{i=1}^{N} (y_i - \bar{y})^2} = 1.7987$$

$$\hat{\sigma}_{xy} = \frac{1}{N-1}\sum_{i=1}^{N} (x_i - \bar{x})(y_i - \bar{y}) = 0.9968$$

$$\hat{\rho} = \frac{\hat{\sigma}_{xy}}{\hat{\sigma}_x \hat{\sigma}_y} = 0.7702$$

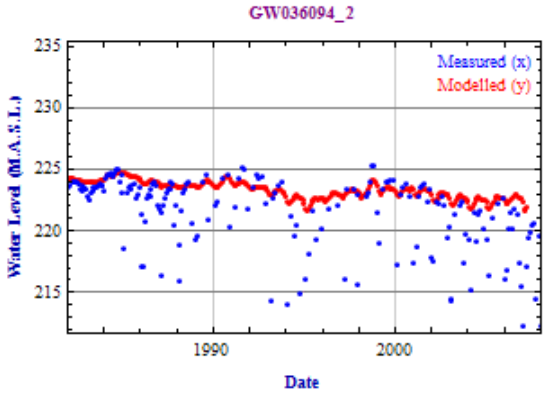

$$\bar{x} = \frac{1}{N}\sum_{i=1}^{N} x_i = 223.4600$$

$$\bar{y} = \frac{1}{N}\sum_{i=1}^{N} y_i = 221.7500$$

$$\overline{xy} = \frac{1}{N}\sum_{i=1}^{N} x_i y_i = 49555.0000$$

$$\hat{\sigma}_x = \sqrt{\frac{1}{N-1}\sum_{i=1}^{N} (x_i - \bar{x})^2} = 0.7237$$

$$\hat{\sigma}_y = \sqrt{\frac{1}{N-1}\sum_{i=1}^{N} (y_i - \bar{y})^2} = 2.8038$$

$$\hat{\sigma}_{xy} = \frac{1}{N-1}\sum_{i=1}^{N} (x_i - \bar{x})(y_i - \bar{y}) = 1.3316$$

$$\hat{\rho} = \frac{\hat{\sigma}_{xy}}{\hat{\sigma}_x \hat{\sigma}_y} = 0.6563$$

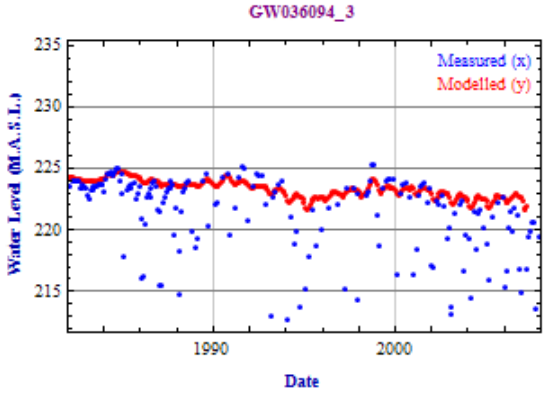

$$\bar{x} = \frac{1}{N}\sum_{i=1}^{N} x_i = 223.4600$$

$$\bar{y} = \frac{1}{N}\sum_{i=1}^{N} y_i = 221.5200$$

$$\overline{xy} = \frac{1}{N}\sum_{i=1}^{N} x_i y_i = 49504.0000$$

$$\hat{\sigma}_x = \sqrt{\frac{1}{N-1}\sum_{i=1}^{N} (x_i - \bar{x})^2} = 0.7237$$

$$\hat{\sigma}_y = \sqrt{\frac{1}{N-1}\sum_{i=1}^{N} (y_i - \bar{y})^2} = 3.1353$$

$$\hat{\sigma}_{xy} = \frac{1}{N-1}\sum_{i=1}^{N} (x_i - \bar{x})(y_i - \bar{y}) = 1.4085$$

$$\hat{\rho} = \frac{\hat{\sigma}_{xy}}{\hat{\sigma}_x \hat{\sigma}_y} = 0.6207$$

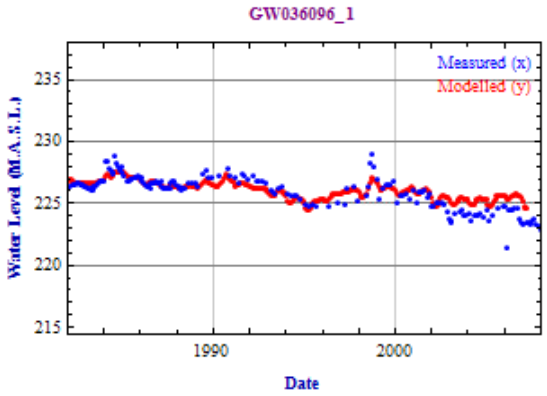

$$\bar{x} = \frac{1}{N}\sum_{i=1}^{N} x_i = 226.2000$$

$$\bar{y} = \frac{1}{N}\sum_{i=1}^{N} y_i = 226.0200$$

$$\overline{xy} = \frac{1}{N}\sum_{i=1}^{N} x_i y_i = 51125.0000$$

$$\hat{\sigma}_x = \sqrt{\frac{1}{N-1}\sum_{i=1}^{N} (x_i - \bar{x})^2} = 0.7104$$

$$\hat{\sigma}_y = \sqrt{\frac{1}{N-1}\sum_{i=1}^{N} (y_i - \bar{y})^2} = 1.2523$$

$$\hat{\sigma}_{xy} = \frac{1}{N-1}\sum_{i=1}^{N} (x_i - \bar{x})(y_i - \bar{y}) = 0.7826$$

$$\hat{\rho} = \frac{\hat{\sigma}_{xy}}{\hat{\sigma}_x \hat{\sigma}_y} = 0.8797$$

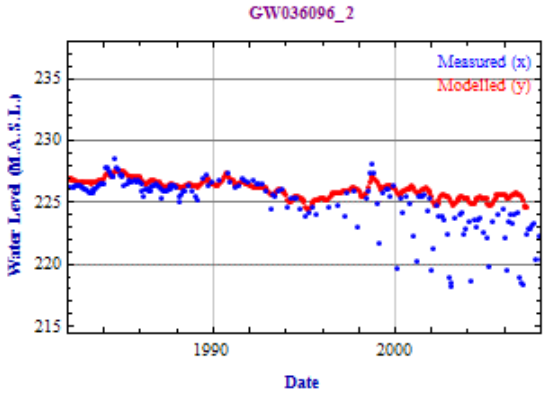

$$\bar{x} = \frac{1}{N}\sum_{i=1}^{N} x_i = 226.2000$$

$$\bar{y} = \frac{1}{N}\sum_{i=1}^{N} y_i = 225.1300$$

$$\overline{xy} = \frac{1}{N}\sum_{i=1}^{N} x_i y_i = 50925.0000$$

$$\hat{\sigma}_x = \sqrt{\frac{1}{N-1}\sum_{i=1}^{N} (x_i - \bar{x})^2} = 0.7112$$

$$\hat{\sigma}_y = \sqrt{\frac{1}{N-1}\sum_{i=1}^{N} (y_i - \bar{y})^2} = 2.1229$$

$$\hat{\sigma}_{xy} = \frac{1}{N-1}\sum_{i=1}^{N} (x_i - \bar{x})(y_i - \bar{y}) = 1.1382$$

$$\hat{\rho} = \frac{\hat{\sigma}_{xy}}{\hat{\sigma}_x \hat{\sigma}_y} = 0.7538$$

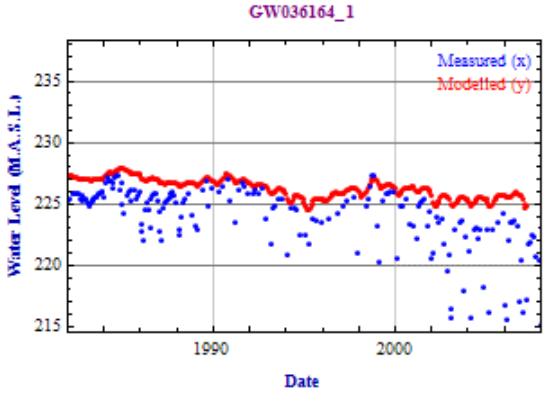

$$\bar{x} = \frac{1}{N}\sum_{i=1}^{N} x_i = 226.4400$$

$$\bar{y} = \frac{1}{N}\sum_{i=1}^{N} y_i = 224.1300$$

$$\overline{xy} = \frac{1}{N}\sum_{i=1}^{N} x_i y_i = 50754.0000$$

$$\hat{\sigma}_x = \sqrt{\frac{1}{N-1}\sum_{i=1}^{N} (x_i - \bar{x})^2} = 0.7951$$

$$\hat{\sigma}_y = \sqrt{\frac{1}{N-1}\sum_{i=1}^{N} (y_i - \bar{y})^2} = 2.5260$$

$$\hat{\sigma}_{xy} = \frac{1}{N-1}\sum_{i=1}^{N} (x_i - \bar{x})(y_i - \bar{y}) = 1.3993$$

$$\hat{\rho} = \frac{\hat{\sigma}_{xy}}{\hat{\sigma}_x \hat{\sigma}_y} = 0.6967$$

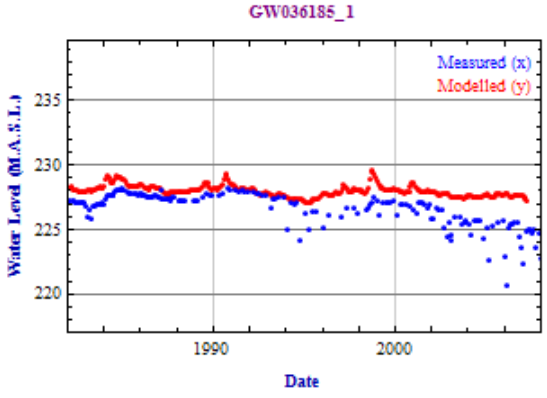

$$\bar{x} = \frac{1}{N}\sum_{i=1}^{N} x_i = 228.0500$$

$$\bar{y} = \frac{1}{N}\sum_{i=1}^{N} y_i = 226.7400$$

$$\overline{xy} = \frac{1}{N}\sum_{i=1}^{N} x_i y_i = 51708.0000$$

$$\hat{\sigma}_x = \sqrt{\frac{1}{N-1}\sum_{i=1}^{N} (x_i - \bar{x})^2} = 0.4523$$

$$\hat{\sigma}_y = \sqrt{\frac{1}{N-1}\sum_{i=1}^{N} (y_i - \bar{y})^2} = 1.2155$$

$$\hat{\sigma}_{xy} = \frac{1}{N-1}\sum_{i=1}^{N} (x_i - \bar{x})(y_i - \bar{y}) = 0.3164$$

$$\hat{\rho} = \frac{\hat{\sigma}_{xy}}{\hat{\sigma}_x \hat{\sigma}_y} = 0.5755$$

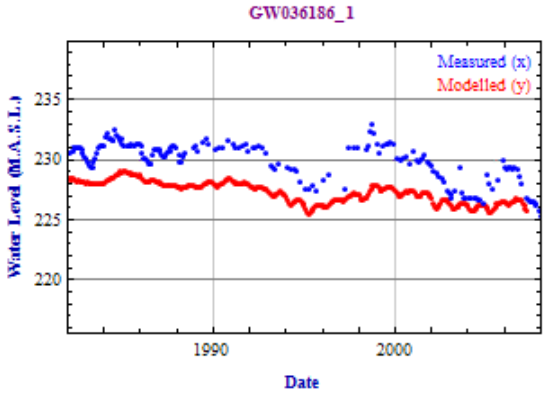

$$\bar{x} = \frac{1}{N}\sum_{i=1}^{N} x_i = 227.4800$$

$$\bar{y} = \frac{1}{N}\sum_{i=1}^{N} y_i = 230.0600$$

$$\overline{xy} = \frac{1}{N}\sum_{i=1}^{N} x_i y_i = 52336.0000$$

$$\hat{\sigma}_x = \sqrt{\frac{1}{N-1}\sum_{i=1}^{N} (x_i - \bar{x})^2} = 0.8930$$

$$\hat{\sigma}_y = \sqrt{\frac{1}{N-1}\sum_{i=1}^{N} (y_i - \bar{y})^2} = 1.4662$$

$$\hat{\sigma}_{xy} = \frac{1}{N-1}\sum_{i=1}^{N} (x_i - \bar{x})(y_i - \bar{y}) = 1.0798$$

$$\hat{\rho} = \frac{\hat{\sigma}_{xy}}{\hat{\sigma}_x \hat{\sigma}_y} = 0.8247$$

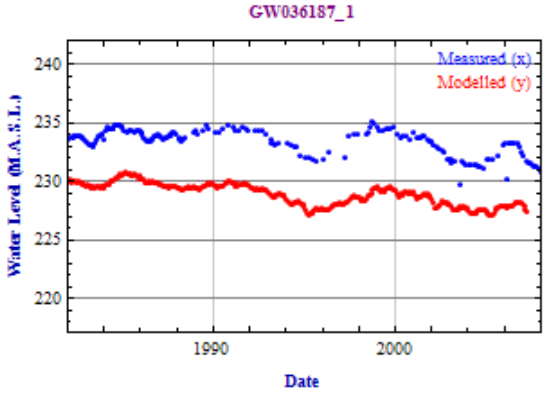

$$\bar{x} = \frac{1}{N}\sum_{i=1}^{N} x_i = 229.1100$$

$$\bar{y} = \frac{1}{N}\sum_{i=1}^{N} y_i = 233.5200$$

$$\overline{xy} = \frac{1}{N}\sum_{i=1}^{N} x_i y_i = 53505.0000$$

$$\hat{\sigma}_x = \sqrt{\frac{1}{N-1}\sum_{i=1}^{N} (x_i - \bar{x})^2} = 0.9405$$

$$\hat{\sigma}_y = \sqrt{\frac{1}{N-1}\sum_{i=1}^{N} (y_i - \bar{y})^2} = 1.0149$$

$$\hat{\sigma}_{xy} = \frac{1}{N-1}\sum_{i=1}^{N} (x_i - \bar{x})(y_i - \bar{y}) = 0.7664$$

$$\hat{\rho} = \frac{\hat{\sigma}_{xy}}{\hat{\sigma}_x \hat{\sigma}_y} = 0.8029$$

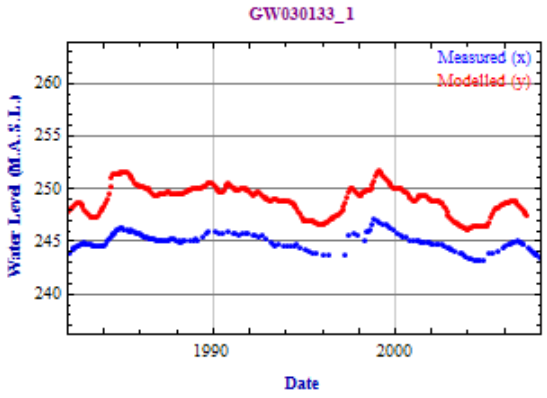

$$\bar{x} = \frac{1}{N}\sum_{i=1}^{N} x_i = 249.0600$$

$$\bar{y} = \frac{1}{N}\sum_{i=1}^{N} y_i = 245.0400$$

$$\overline{xy} = \frac{1}{N}\sum_{i=1}^{N} x_i y_i = 61031.0000$$

$$\hat{\sigma}_x = \sqrt{\frac{1}{N-1}\sum_{i=1}^{N} (x_i - \bar{x})^2} = 1.3563$$

$$\hat{\sigma}_y = \sqrt{\frac{1}{N-1}\sum_{i=1}^{N} (y_i - \bar{y})^2} = 0.7892$$

$$\hat{\sigma}_{xy} = \frac{1}{N-1}\sum_{i=1}^{N} (x_i - \bar{x})(y_i - \bar{y}) = 0.9770$$

$$\hat{\rho} = \frac{\hat{\sigma}_{xy}}{\hat{\sigma}_x \hat{\sigma}_y} = 0.9127$$

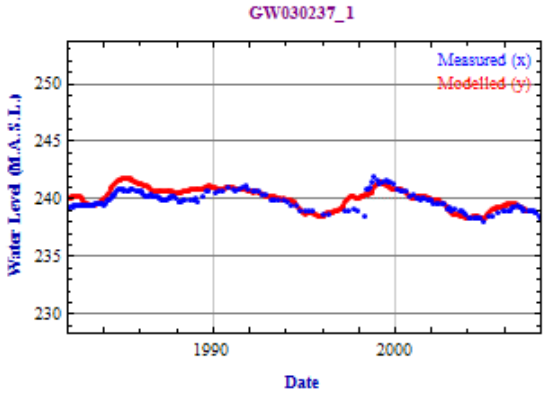

$$\bar{x} = \frac{1}{N}\sum_{i=1}^{N} x_i = 240.2400$$

$$\bar{y} = \frac{1}{N}\sum_{i=1}^{N} y_i = 239.9100$$

$$\overline{xy} = \frac{1}{N}\sum_{i=1}^{N} x_i y_i = 57638.0000$$

$$\hat{\sigma}_x = \sqrt{\frac{1}{N-1}\sum_{i=1}^{N} (x_i - \bar{x})^2} = 0.8816$$

$$\hat{\sigma}_y = \sqrt{\frac{1}{N-1}\sum_{i=1}^{N} (y_i - \bar{y})^2} = 0.7965$$

$$\hat{\sigma}_{xy} = \frac{1}{N-1}\sum_{i=1}^{N} (x_i - \bar{x})(y_i - \bar{y}) = 0.6050$$

$$\hat{\rho} = \frac{\hat{\sigma}_{xy}}{\hat{\sigma}_x \hat{\sigma}_y} = 0.8615$$

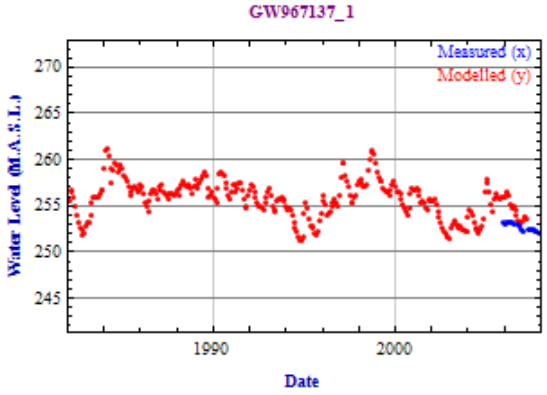

$$\bar{x} = \frac{1}{N}\sum_{i=1}^{N} x_i = 254.8800$$

$$\bar{y} = \frac{1}{N}\sum_{i=1}^{N} y_i = 252.9700$$

$$\overline{xy} = \frac{1}{N}\sum_{i=1}^{N} x_i y_i = 64475.0000$$

$$\hat{\sigma}_x = \sqrt{\frac{1}{N-1}\sum_{i=1}^{N} (x_i - \bar{x})^2} = 1.2133$$

$$\hat{\sigma}_y = \sqrt{\frac{1}{N-1}\sum_{i=1}^{N} (y_i - \bar{y})^2} = 0.3138$$

$$\hat{\sigma}_{xy} = \frac{1}{N-1}\sum_{i=1}^{N} (x_i - \bar{x})(y_i - \bar{y}) = 0.2843$$

$$\hat{\rho} = \frac{\hat{\sigma}_{xy}}{\hat{\sigma}_x \hat{\sigma}_y} = 0.7465$$

Appendix 7a

Crystallize
Plot One Hydrograph Set from the Maules Creek Database

Authors
B. Kelly and B. Giambastiani

A7a.1 Introduction

This ***Crystallize*** notebook plots a single groundwater hydrograph set at one Groundwater Works location in the Maules Creek catchment using data from the NSW Water Information Pinneena Groundwater Works CD. To be able to run this notebook the database Malues_Creek_database_Feb2010 needs to be linked and listed in the MS Windows ODBC control panel. In *Mathematica* select **Evaluation > Evaluate Notebook** from the main menu to generate plots of all the hydrographs. To change the hydrograph set that is plotted, change the GW####### in the cell with the read header **BoreHydrographPlot**

The next two cells set the working directory and load in the ***Crystallize*** package that plots a groundwater hydrograph set from the Maules Creek database.

A7a.2 Generating the Graph

```
In[1]:= SetDirectory["G:\\NWC_FinalReportUNSW3DHydrogeology\\Appendix7_CrystallizeHydrographs"];
        Needs["CrystallizeBoreHydrographMaulesCk`"]

In[3]:= BoreHydrographPlot["GW036094"]
```

Out[3]=

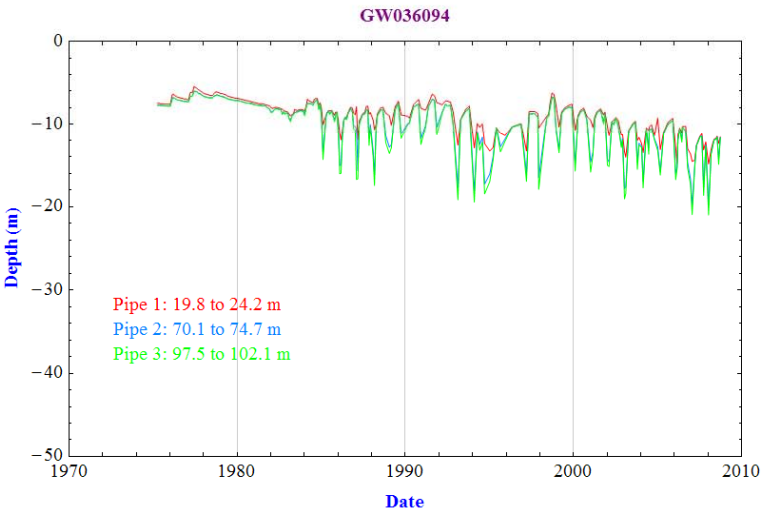

Appendix 7b

Crystallize
Plot all Hydrographs from the Maules Creek Database

Authors
B. Kelly and B. Giambastiani

A7b.1 Introduction

This ***Crystallize*** notebook plots all groundwater hydrographs in the Maules Creek Catchment using the data from the NSW Water Information Pinneena Groundwater Works CD. To be able to run this notebook the database Malues_Creek_database_Feb2010 needs to be linked and listed in the MS Windows ODBC control panel. In *Mathematica* select **Evaluation > Evaluate Notebook** from the main menu to generate plots of all the groundwater hydrographs. A copy of the plots is saved in the folder "Images", which needs to be created before running the program. It takes about 30 seconds to calculate all the graphs.

A7b.2 Generating the Graphs

```
In[1]:= SetDirectory["G:\\NWC_FinalReportUNSW3DHydrogeology\\Appendix7_CrystallizeHydrographs"];
        Needs["CrystallizeAllBoreHydrographsMaulesCk`"]
```

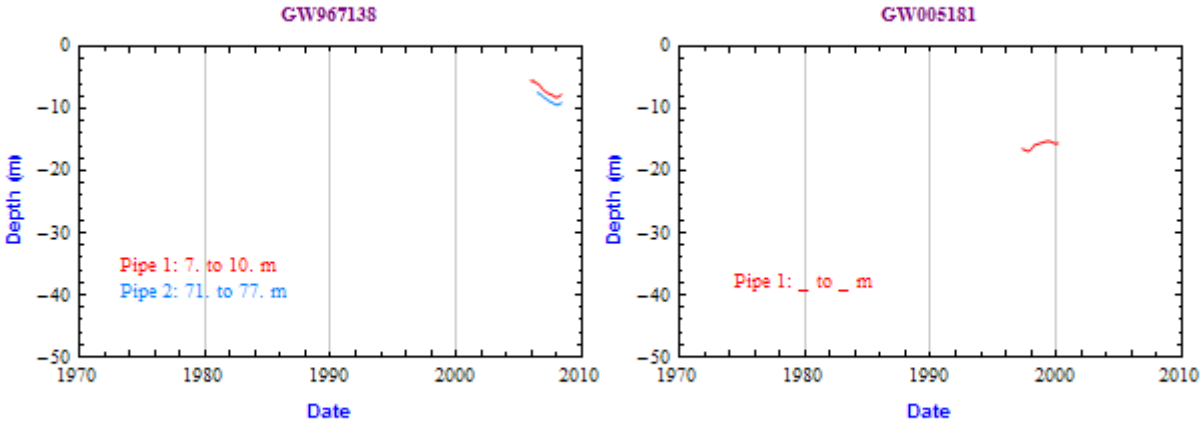

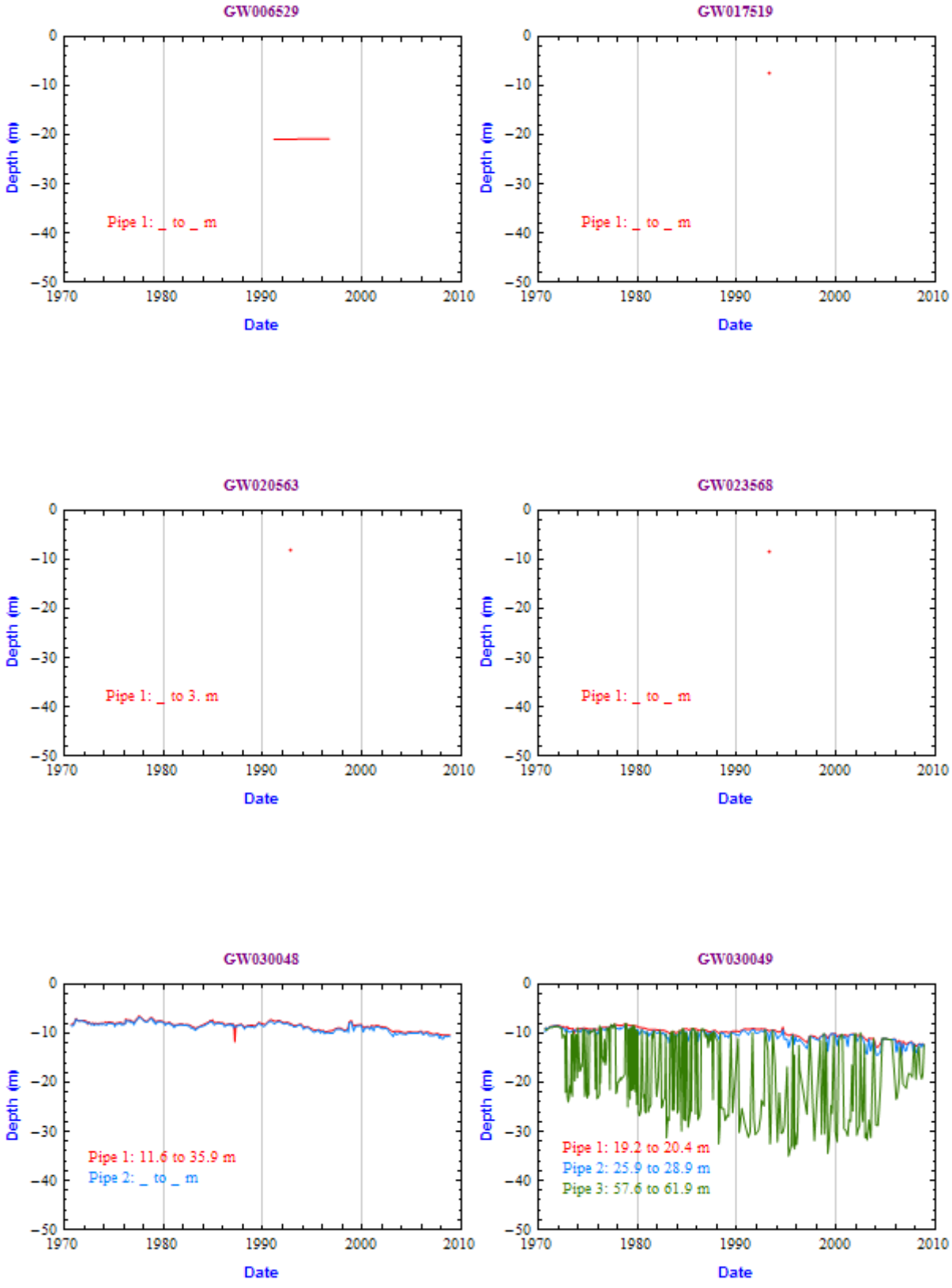
GW006529
Depth (m)
Date
Pipe 1: _ to _ m
GW017519
Depth (m)
Date
Pipe 1: _ to _ m
GW020563
Depth (m)
Date
Pipe 1: _ to 3. m
GW023568
Depth (m)
Date
Pipe 1: _ to _ m
GW030048
Depth (m)
Date
Pipe 1: 11.6 to 35.9 m
Pipe 2: _ to _ m
GW030049
Depth (m)
Date
Pipe 1: 19.2 to 20.4 m
Pipe 2: 25.9 to 28.9 m
Pipe 3: 57.6 to 61.9 m

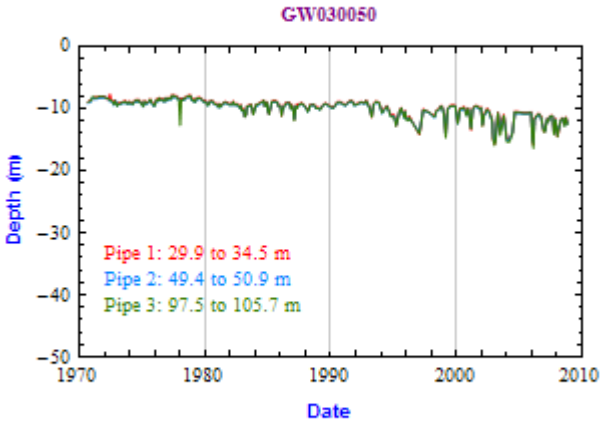
GW030050
Depth (m)
0
−10
−20
−30
−40
−50
1970
1980
1990
2000
2010
Date
Pipe 1: 29.9 to 34.5 m
Pipe 2: 49.4 to 50.9 m
Pipe 3: 97.5 to 105.7 m

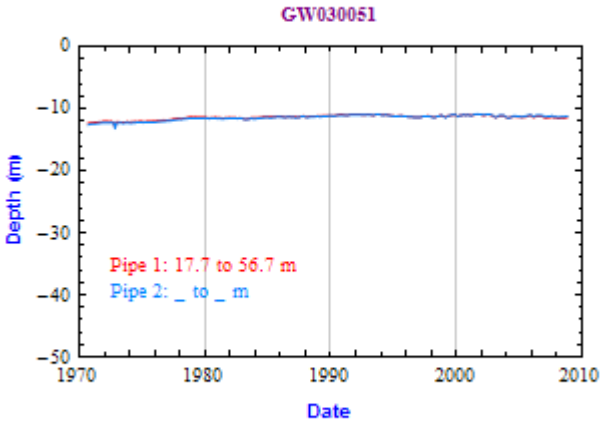
GW030051
Depth (m)
0
−10
−20
−30
−40
−50
1970
1980
1990
2000
2010
Date
Pipe 1: 17.7 to 56.7 m
Pipe 2: _ to _ m

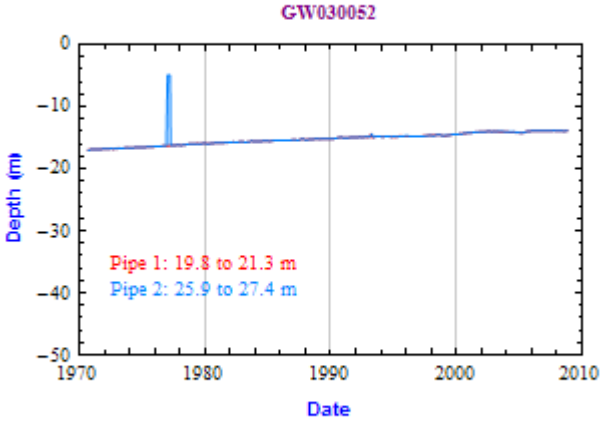
GW030052
Depth (m)
0
−10
−20
−30
−40
−50
1970
1980
1990
2000
2010
Date
Pipe 1: 19.8 to 21.3 m
Pipe 2: 25.9 to 27.4 m

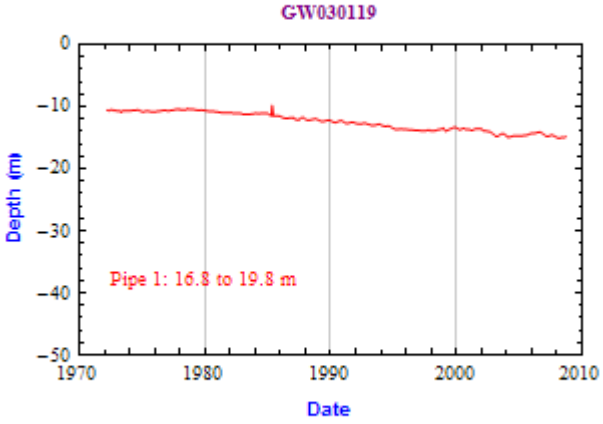
GW030119
Depth (m)
0
−10
−20
−30
−40
−50
1970
1980
1990
2000
2010
Date
Pipe 1: 16.8 to 19.8 m

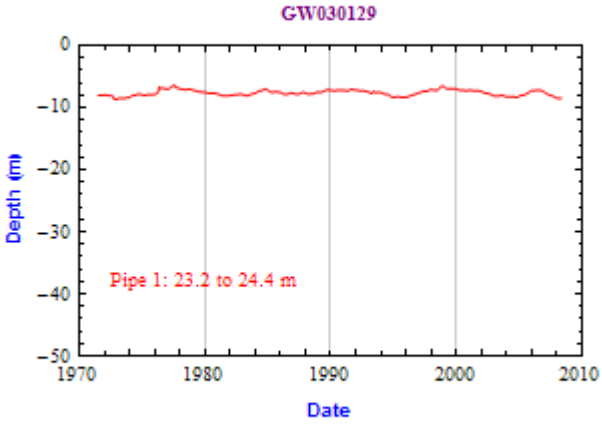
GW030129
Depth (m)
0
−10
−20
−30
−40
−50
1970
1980
1990
2000
2010
Date
Pipe 1: 23.2 to 24.4 m

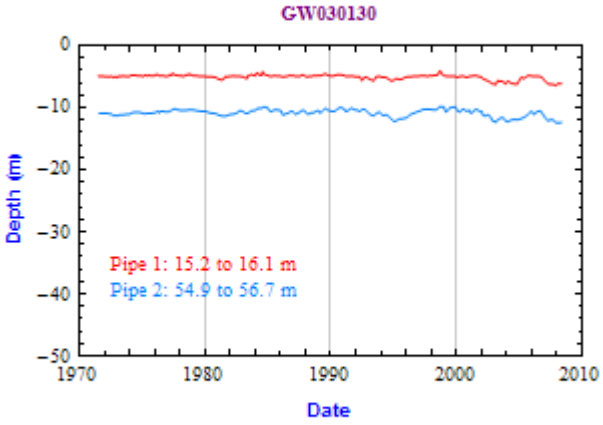
GW030130
Depth (m)
0
−10
−20
−30
−40
−50
1970
1980
1990
2000
2010
Date
Pipe 1: 15.2 to 16.1 m
Pipe 2: 54.9 to 56.7 m

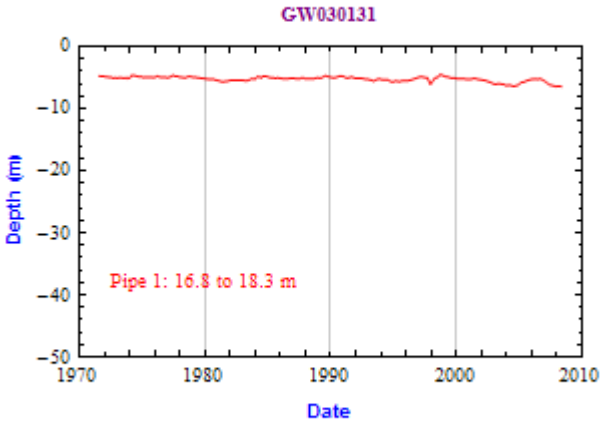
GW030131
Depth (m)
0
−10
−20
−30
−40
−50
1970
1980
1990
2000
2010
Date
Pipe 1: 16.8 to 18.3 m

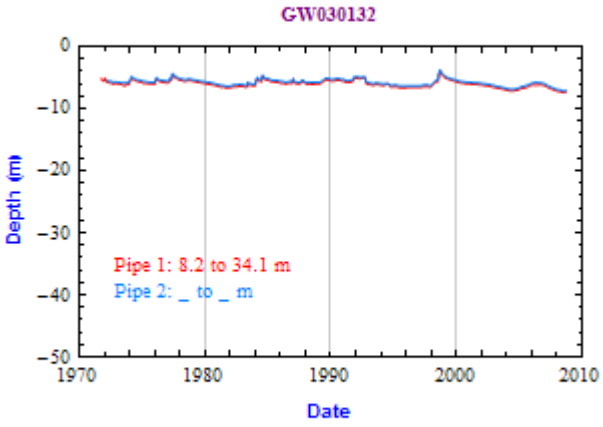
GW030132
Depth (m)
0
−10
−20
−30
−40
−50
1970
1980
1990
2000
2010
Date
Pipe 1: 8.2 to 34.1 m
Pipe 2: _ to _ m

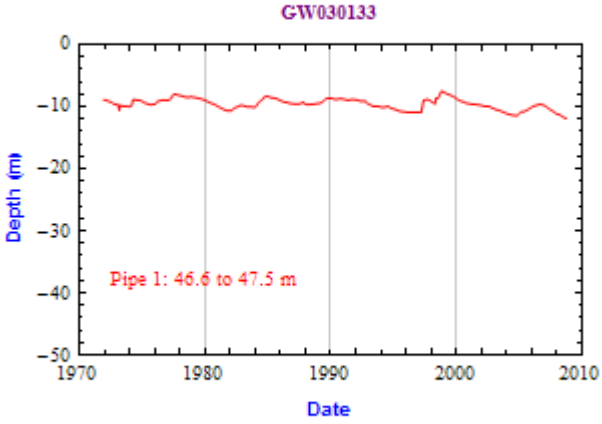
GW030133
Depth (m)
0
−10
−20
−30
−40
−50
1970
1980
1990
2000
2010
Date
Pipe 1: 46.6 to 47.5 m

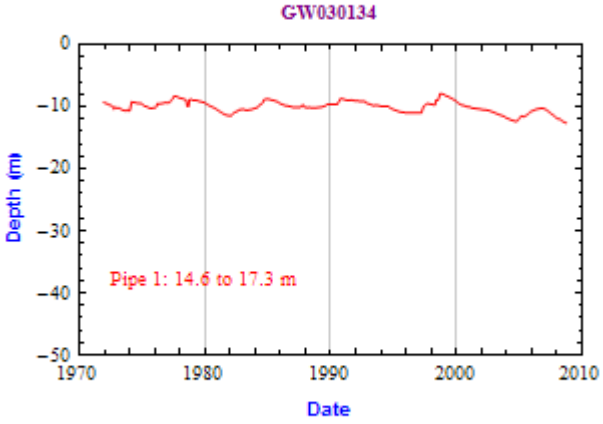
GW030134
Depth (m)
0
−10
−20
−30
−40
−50
1970
1980
1990
2000
2010
Date
Pipe 1: 14.6 to 17.3 m

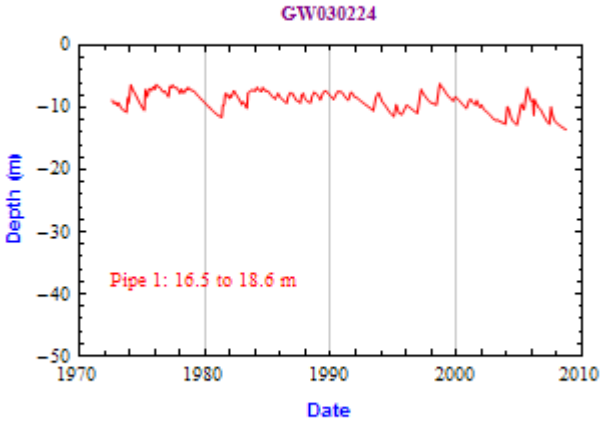
GW030224
Depth (m)
0
−10
−20
−30
−40
−50
1970
1980
1990
2000
2010
Date
Pipe 1: 16.5 to 18.6 m

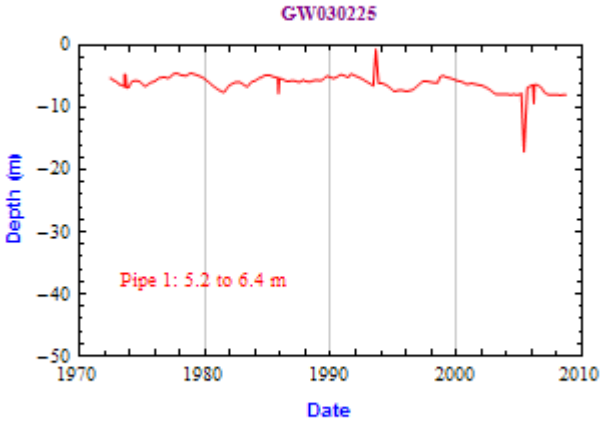
GW030225
Depth (m)
0
−10
−20
−30
−40
−50
1970
1980
1990
2000
2010
Date
Pipe 1: 5.2 to 6.4 m

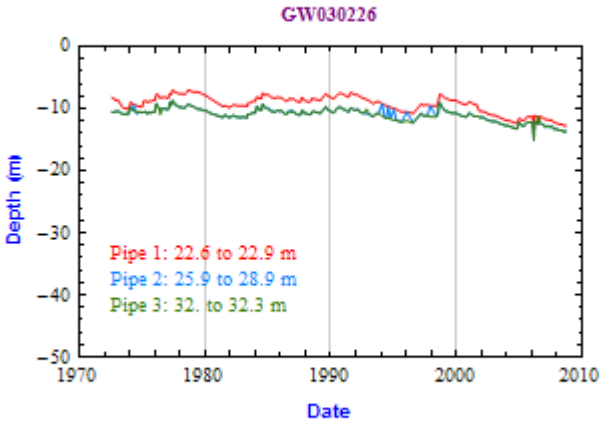
GW030226
Depth (m)
0
−10
−20
−30
−40
−50
1970
1980
1990
2000
2010
Date
Pipe 1: 22.6 to 22.9 m
Pipe 2: 25.9 to 28.9 m
Pipe 3: 32. to 32.3 m

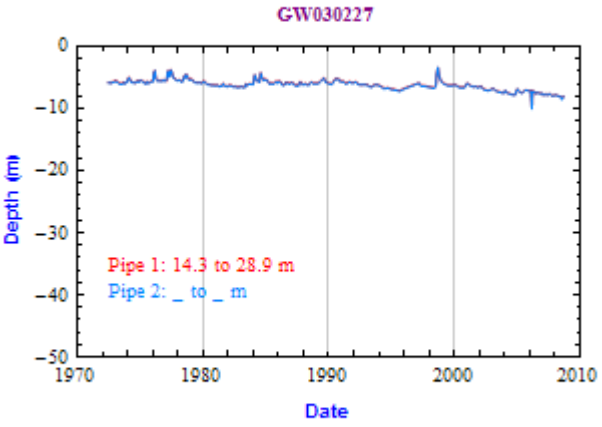
GW030227
Depth (m)
0
−10
−20
−30
−40
−50
1970
1980
1990
2000
2010
Date
Pipe 1: 14.3 to 28.9 m
Pipe 2: _ to _ m

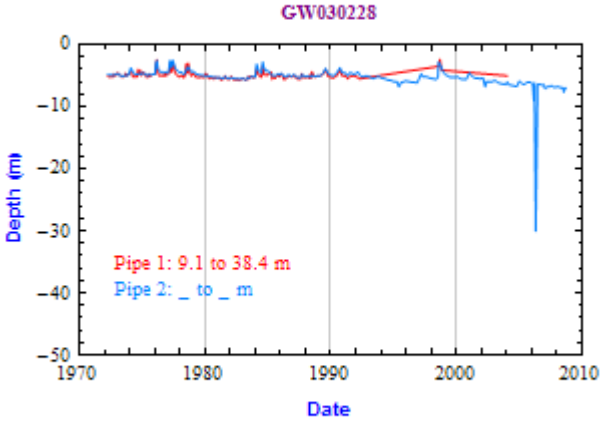
GW030228
Depth (m)
0
−10
−20
−30
−40
−50
1970
1980
1990
2000
2010
Date
Pipe 1: 9.1 to 38.4 m
Pipe 2: _ to _ m

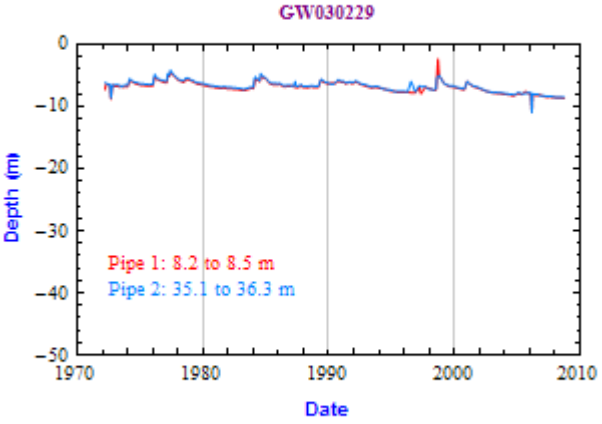
GW030229
Depth (m)
0
−10
−20
−30
−40
−50
1970
1980
1990
2000
2010
Date
Pipe 1: 8.2 to 8.5 m
Pipe 2: 35.1 to 36.3 m

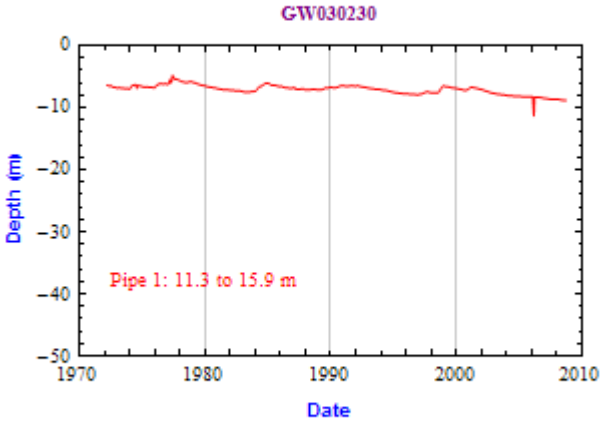
GW030230
Depth (m)
0
−10
−20
−30
−40
−50
1970
1980
1990
2000
2010
Date
Pipe 1: 11.3 to 15.9 m

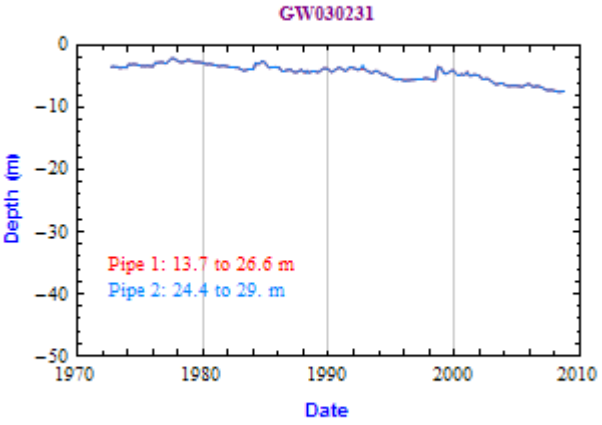
GW030231
Depth (m)
0
−10
−20
−30
−40
−50
1970
1980
1990
2000
2010
Date
Pipe 1: 13.7 to 26.6 m
Pipe 2: 24.4 to 29. m

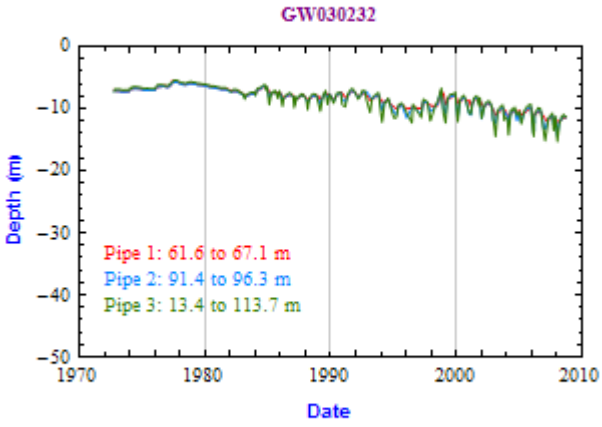
GW030232
Depth (m)
0
−10
−20
−30
−40
−50
1970
1980
1990
2000
2010
Date
Pipe 1: 61.6 to 67.1 m
Pipe 2: 91.4 to 96.3 m
Pipe 3: 13.4 to 113.7 m

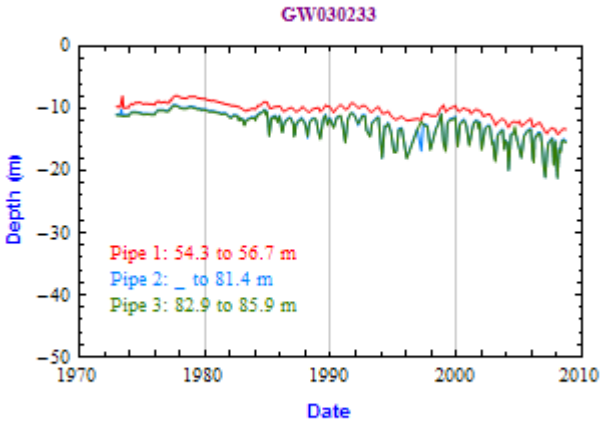
GW030233
Depth (m)
0
−10
−20
−30
−40
−50
1970
1980
1990
2000
2010
Date
Pipe 1: 54.3 to 56.7 m
Pipe 2: _ to 81.4 m
Pipe 3: 82.9 to 85.9 m

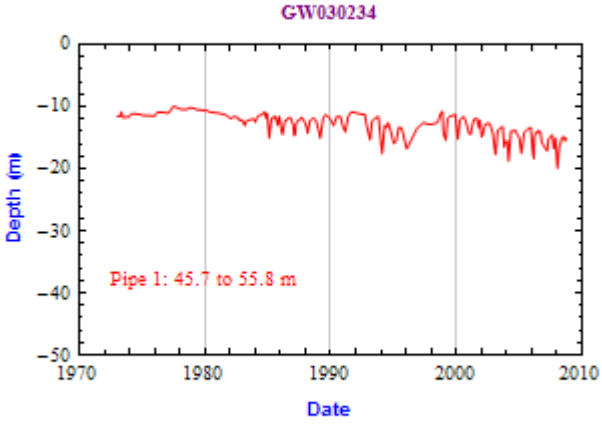
GW030234
Depth (m)
0
−10
−20
−30
−40
−50
1970
1980
1990
2000
2010
Date
Pipe 1: 45.7 to 55.8 m

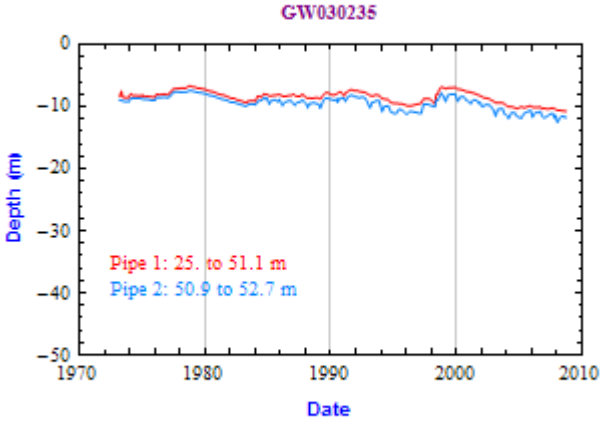
GW030235
Depth (m)
0
−10
−20
−30
−40
−50
1970
1980
1990
2000
2010
Date
Pipe 1: 25. to 51.1 m
Pipe 2: 50.9 to 52.7 m

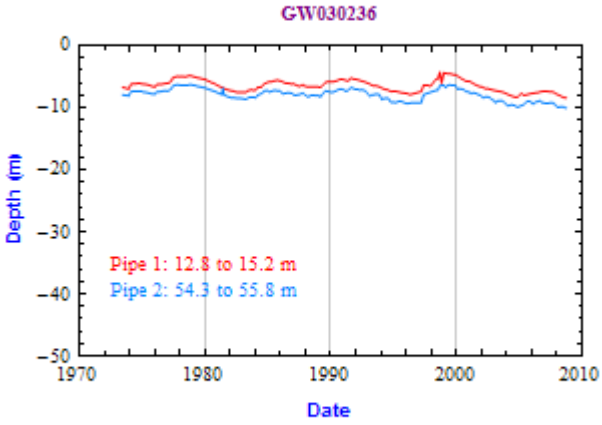
GW030236
Depth (m)
0
−10
−20
−30
−40
−50
1970
1980
1990
2000
2010
Date
Pipe 1: 12.8 to 15.2 m
Pipe 2: 54.3 to 55.8 m

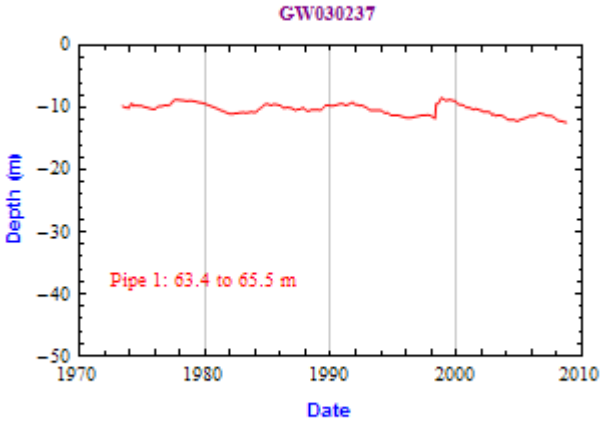
GW030237
Depth (m)
0
−10
−20
−30
−40
−50
1970
1980
1990
2000
2010
Date
Pipe 1: 63.4 to 65.5 m

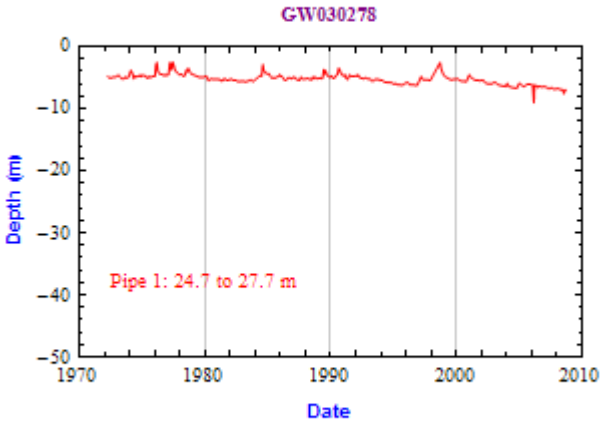
GW030278
Depth (m)
0
−10
−20
−30
−40
−50
1970
1980
1990
2000
2010
Date
Pipe 1: 24.7 to 27.7 m

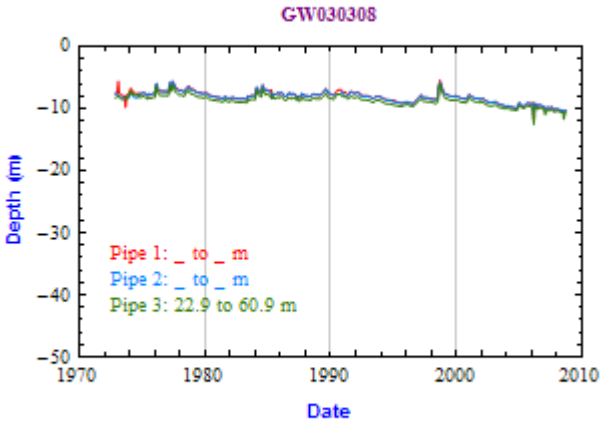
GW030308
Depth (m)
0
−10
−20
−30
−40
−50
1970
1980
1990
2000
2010
Date
Pipe 1: _ to _ m
Pipe 2: _ to _ m
Pipe 3: 22.9 to 60.9 m

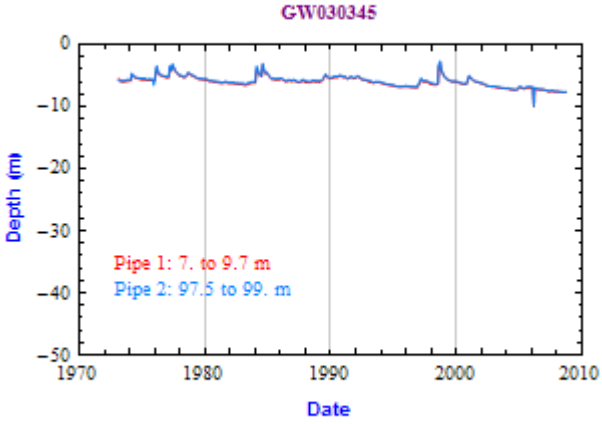
GW030345
Depth (m)
0
−10
−20
−30
−40
−50
1970
1980
1990
2000
2010
Date
Pipe 1: 7. to 9.7 m
Pipe 2: 97.5 to 99. m

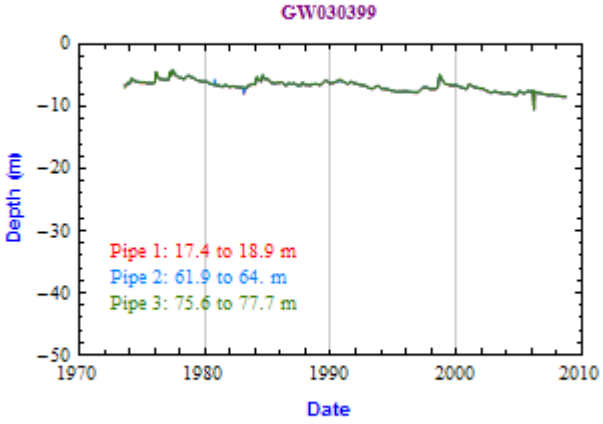
GW030399
Depth (m)
0
−10
−20
−30
−40
−50
1970
1980
1990
2000
2010
Date
Pipe 1: 17.4 to 18.9 m
Pipe 2: 61.9 to 64. m
Pipe 3: 75.6 to 77.7 m

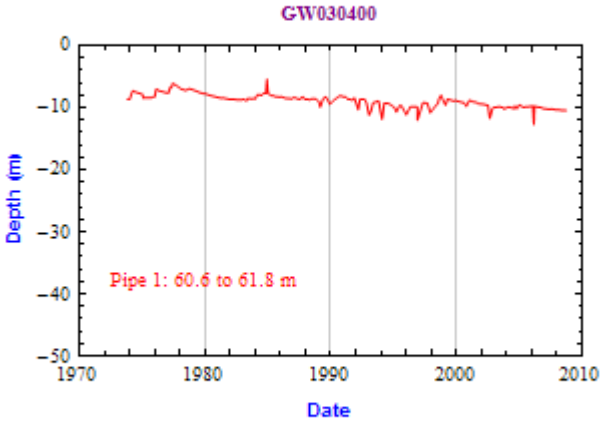
GW030400
Depth (m)
0
−10
−20
−30
−40
−50
1970
1980
1990
2000
2010
Date
Pipe 1: 60.6 to 61.8 m

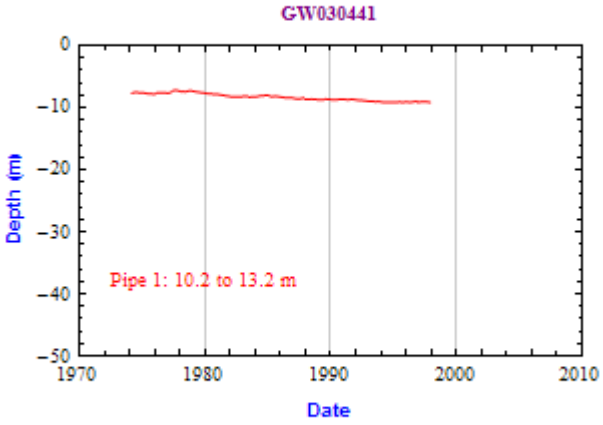
GW030441
Depth (m)
0
−10
−20
−30
−40
−50
1970
1980
1990
2000
2010
Date
Pipe 1: 10.2 to 13.2 m

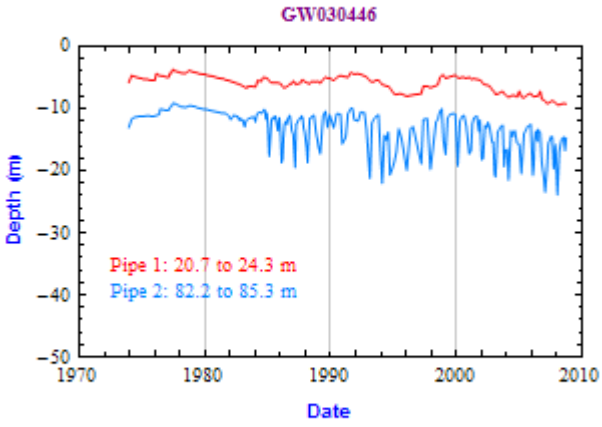
GW030446
Depth (m)
0
−10
−20
−30
−40
−50
1970
1980
1990
2000
2010
Date
Pipe 1: 20.7 to 24.3 m
Pipe 2: 82.2 to 85.3 m

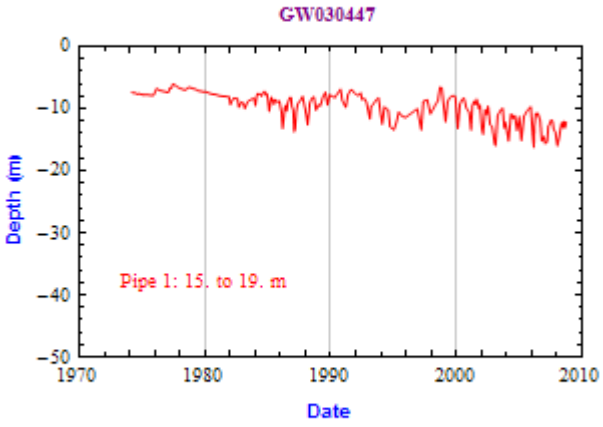
GW030447
Depth (m)
0
−10
−20
−30
−40
−50
1970
1980
1990
2000
2010
Date
Pipe 1: 15. to 19. m

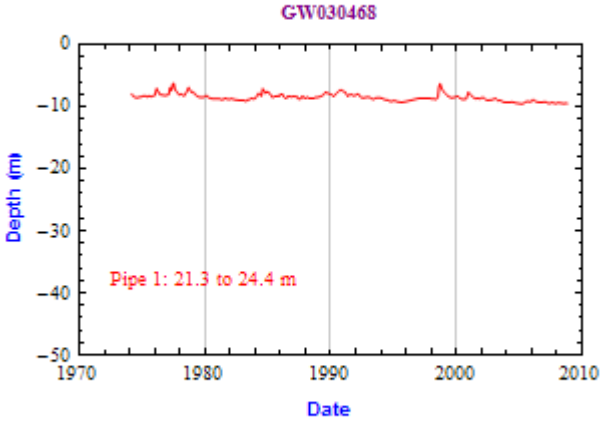
GW030468
Depth (m)
0
−10
−20
−30
−40
−50
1970
1980
1990
2000
2010
Date
Pipe 1: 21.3 to 24.4 m

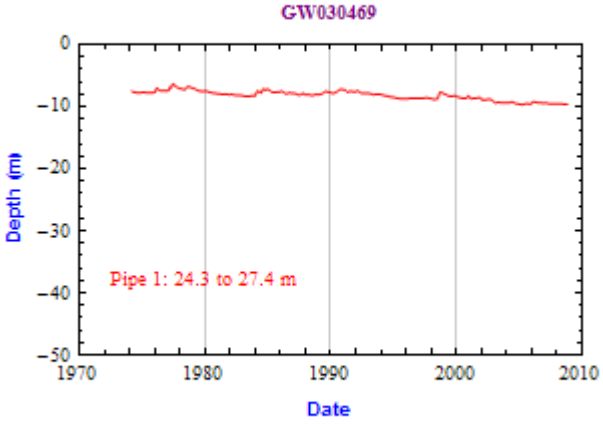
GW030469
Depth (m)
0
−10
−20
−30
−40
−50
1970
1980
1990
2000
2010
Date
Pipe 1: 24.3 to 27.4 m

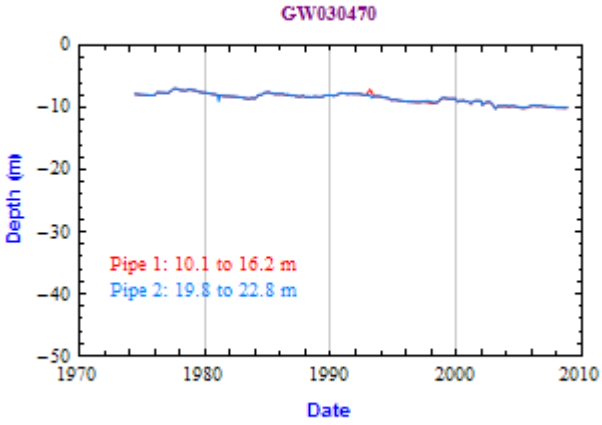
GW030470
Depth (m)
0
−10
−20
−30
−40
−50
1970
1980
1990
2000
2010
Date
Pipe 1: 10.1 to 16.2 m
Pipe 2: 19.8 to 22.8 m

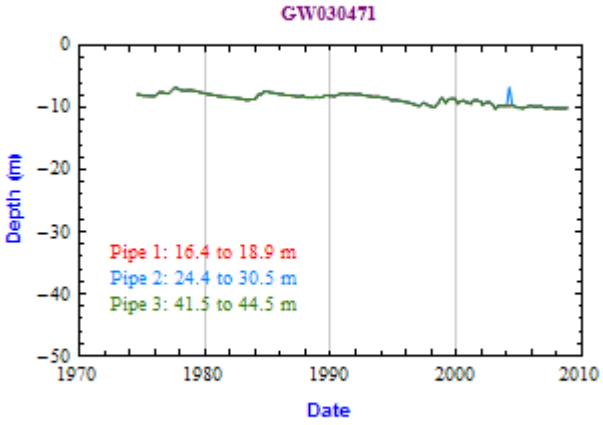
GW030471
Depth (m)
0
−10
−20
−30
−40
−50
1970
1980
1990
2000
2010
Date
Pipe 1: 16.4 to 18.9 m
Pipe 2: 24.4 to 30.5 m
Pipe 3: 41.5 to 44.5 m

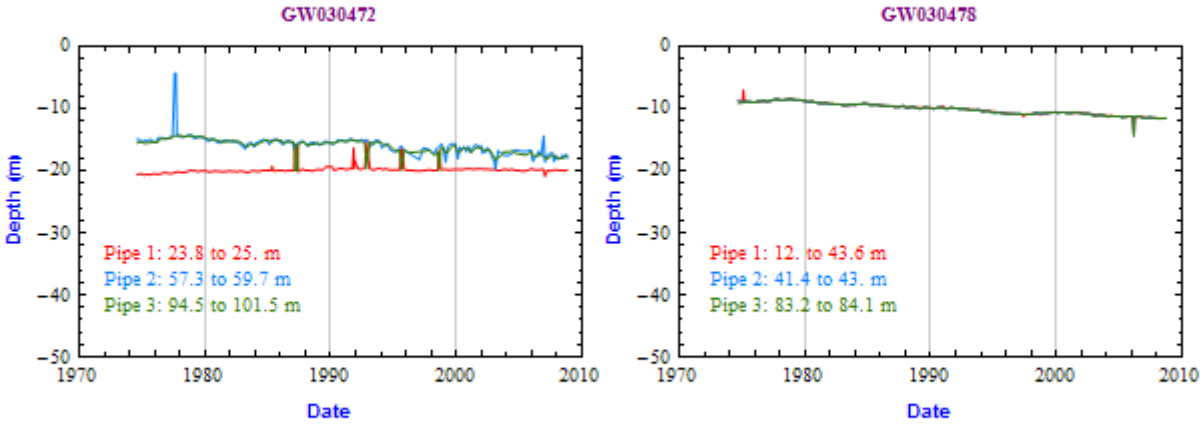
GW030472
Depth (m)
0
−10
−20
−30
−40
−50
1970
1980
1990
2000
2010
Date
Pipe 1: 23.8 to 25. m
Pipe 2: 57.3 to 59.7 m
Pipe 3: 94.5 to 101.5 m
GW030478
Depth (m)
Date
Pipe 1: 12. to 43.6 m
Pipe 2: 41.4 to 43. m
Pipe 3: 83.2 to 84.1 m

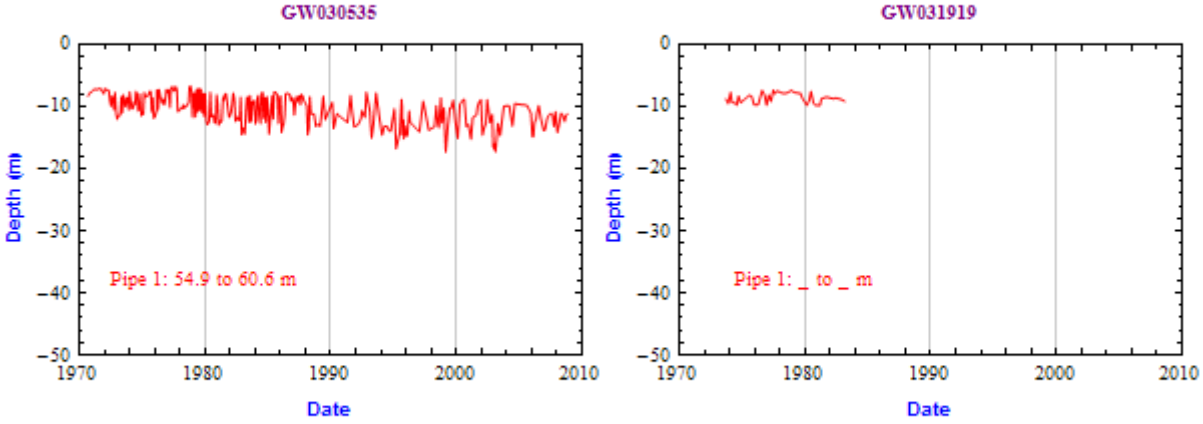
GW030535
Depth (m)
0
−10
−20
−30
−40
−50
1970
1980
1990
2000
2010
Date
Pipe 1: 54.9 to 60.6 m
GW031919
Depth (m)
Date
Pipe 1: _ to _ m

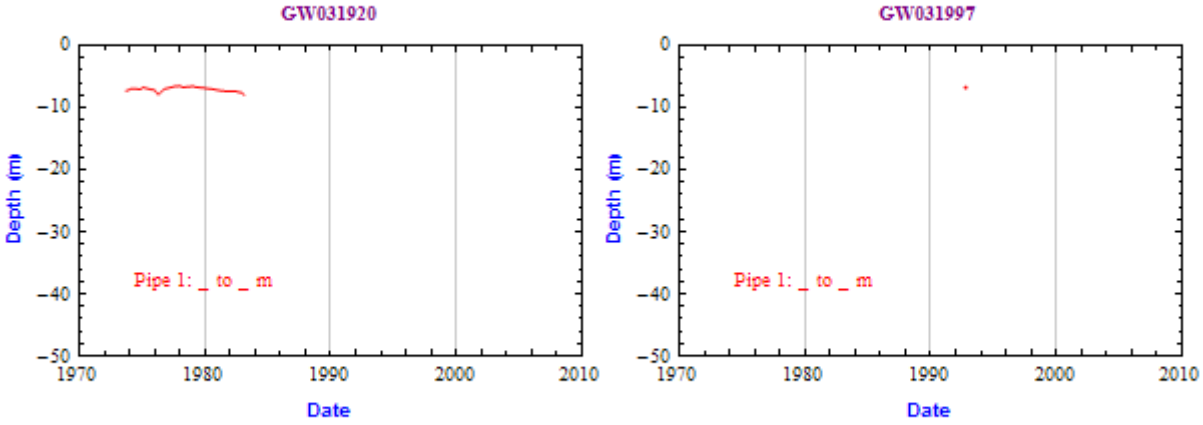
GW031920
Depth (m)
0
−10
−20
−30
−40
−50
1970
1980
1990
2000
2010
Date
Pipe 1: _ to _ m
GW031997
Depth (m)
Date
Pipe 1: _ to _ m

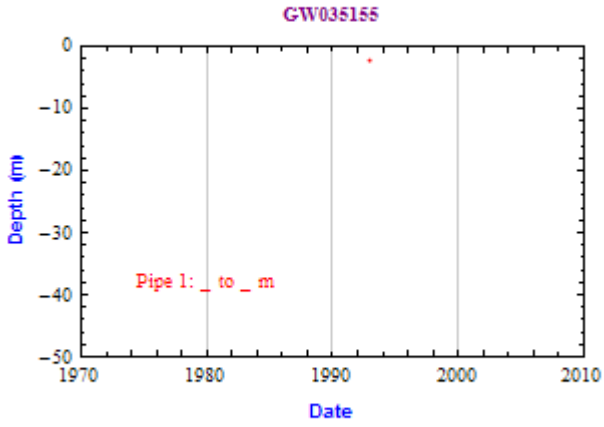
GW035155
Depth (m)
0
−10
−20
−30
−40
−50
1970
1980
1990
2000
2010
Date
Pipe 1: _ to _ m

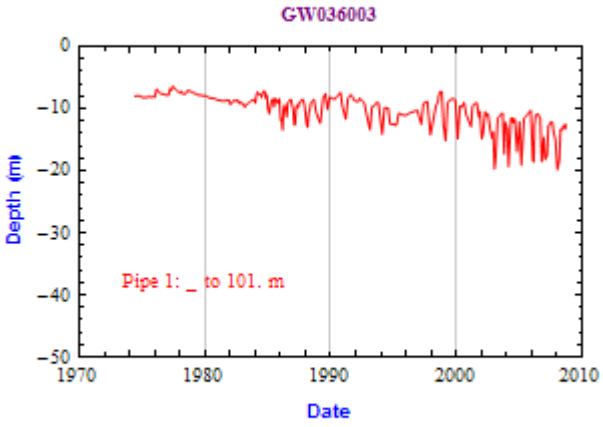
GW036003
Depth (m)
0
−10
−20
−30
−40
−50
1970
1980
1990
2000
2010
Date
Pipe 1: _ to 101. m

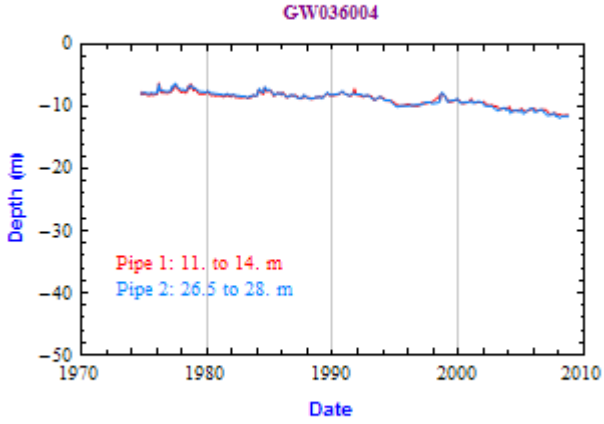
GW036004
Depth (m)
0
−10
−20
−30
−40
−50
1970
1980
1990
2000
2010
Date
Pipe 1: 11. to 14. m
Pipe 2: 26.5 to 28. m

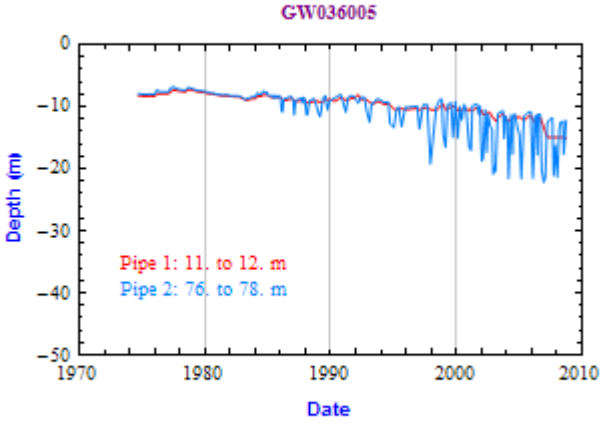
GW036005
Depth (m)
0
−10
−20
−30
−40
−50
1970
1980
1990
2000
2010
Date
Pipe 1: 11. to 12. m
Pipe 2: 76. to 78. m

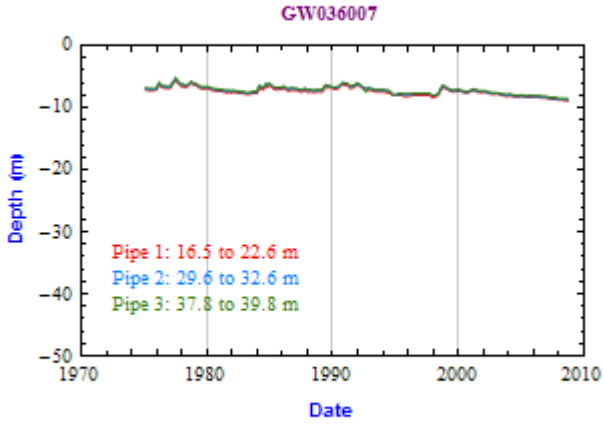
GW036007
Depth (m)
0
−10
−20
−30
−40
−50
1970
1980
1990
2000
2010
Date
Pipe 1: 16.5 to 22.6 m
Pipe 2: 29.6 to 32.6 m
Pipe 3: 37.8 to 39.8 m

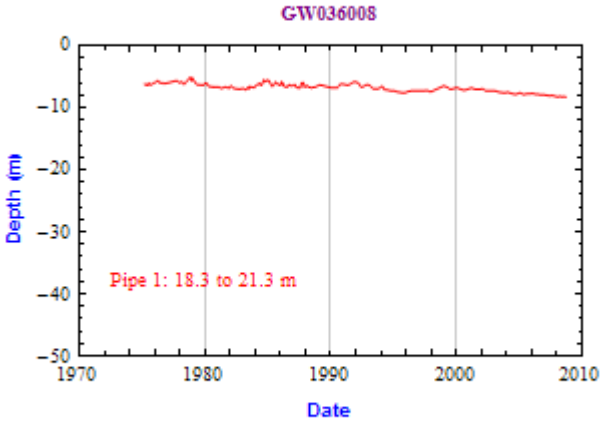
GW036008
Depth (m)
0
−10
−20
−30
−40
−50
1970
1980
1990
2000
2010
Date
Pipe 1: 18.3 to 21.3 m

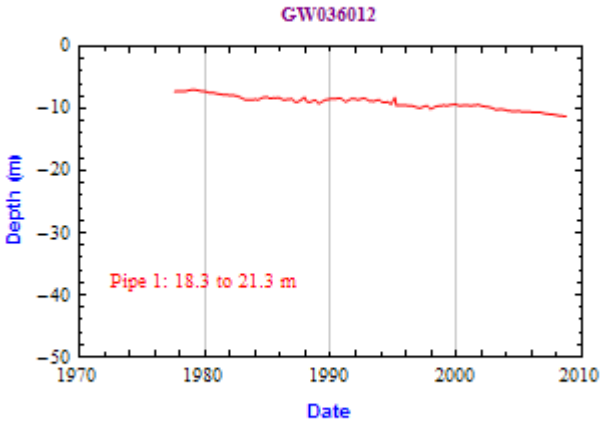
GW036012
Depth (m)
0
−10
−20
−30
−40
−50
1970
1980
1990
2000
2010
Date
Pipe 1: 18.3 to 21.3 m

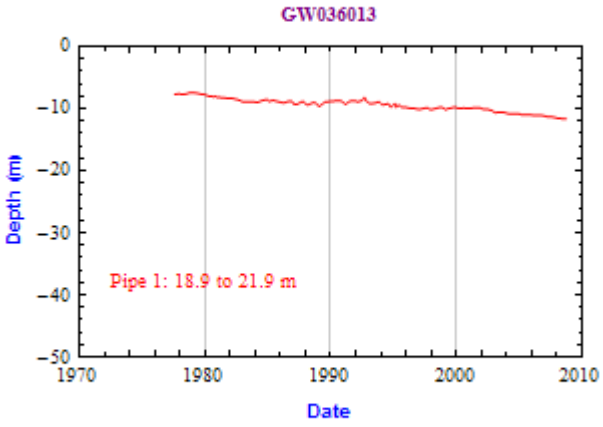
GW036013
Depth (m)
0
−10
−20
−30
−40
−50
1970
1980
1990
2000
2010
Date
Pipe 1: 18.9 to 21.9 m

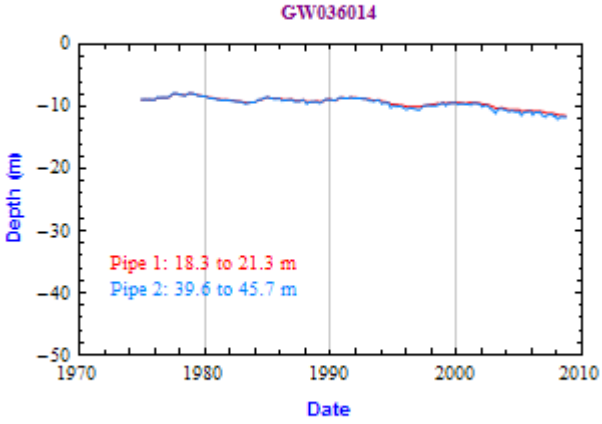
GW036014
Depth (m)
0
−10
−20
−30
−40
−50
1970
1980
1990
2000
2010
Date
Pipe 1: 18.3 to 21.3 m
Pipe 2: 39.6 to 45.7 m

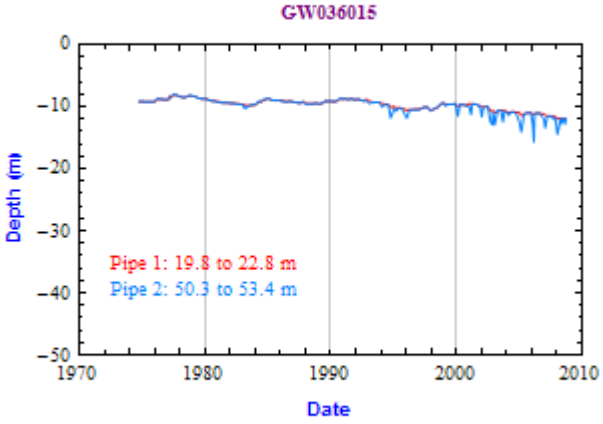
GW036015
Depth (m)
0
−10
−20
−30
−40
−50
1970
1980
1990
2000
2010
Date
Pipe 1: 19.8 to 22.8 m
Pipe 2: 50.3 to 53.4 m

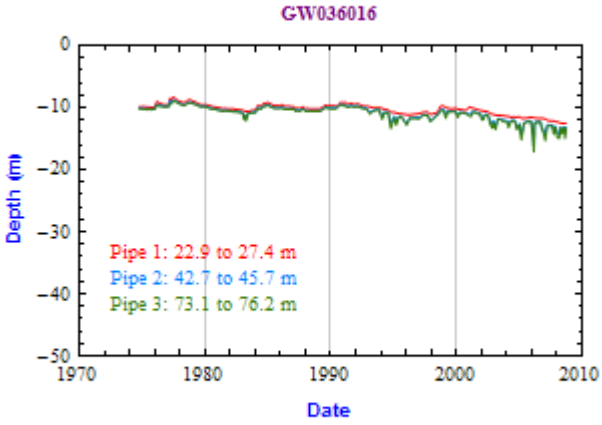
GW036016
Depth (m)
0
−10
−20
−30
−40
−50
1970
1980
1990
2000
2010
Date
Pipe 1: 22.9 to 27.4 m
Pipe 2: 42.7 to 45.7 m
Pipe 3: 73.1 to 76.2 m

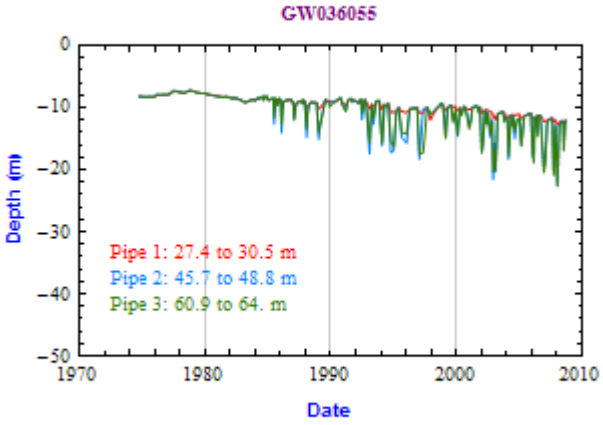
GW036055
Depth (m)
0
−10
−20
−30
−40
−50
1970
1980
1990
2000
2010
Date
Pipe 1: 27.4 to 30.5 m
Pipe 2: 45.7 to 48.8 m
Pipe 3: 60.9 to 64. m

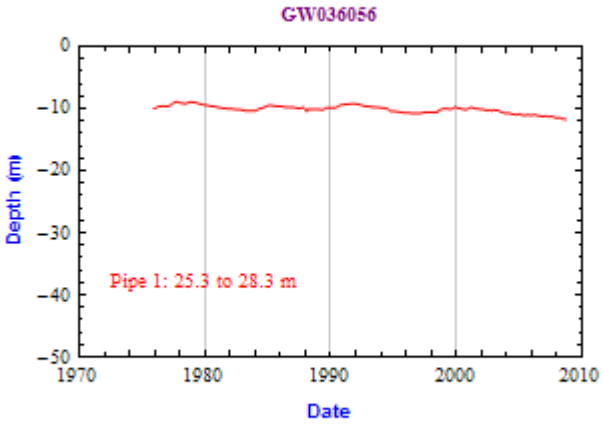
GW036056
Depth (m)
0
−10
−20
−30
−40
−50
1970
1980
1990
2000
2010
Date
Pipe 1: 25.3 to 28.3 m

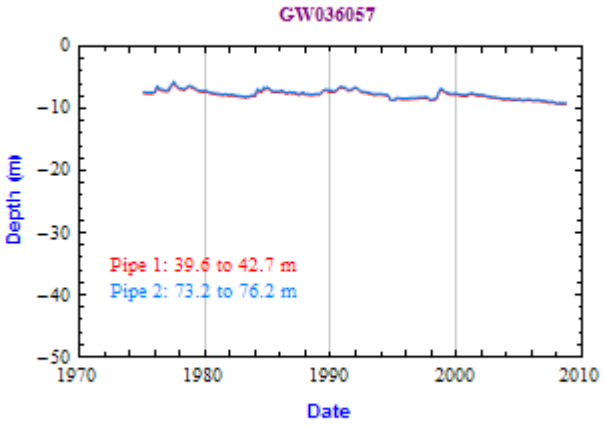
GW036057
Depth (m)
0
−10
−20
−30
−40
−50
1970
1980
1990
2000
2010
Date
Pipe 1: 39.6 to 42.7 m
Pipe 2: 73.2 to 76.2 m

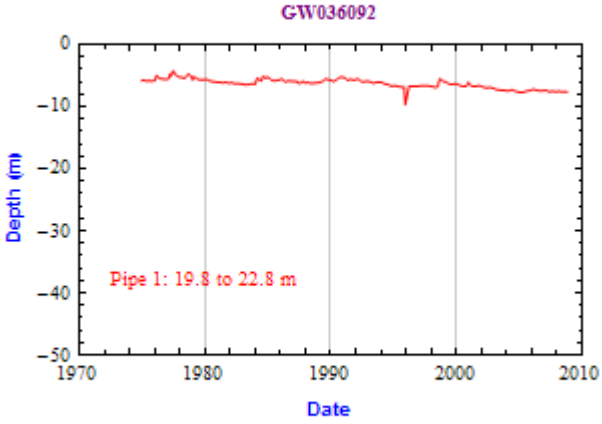
GW036092
Depth (m)
0
−10
−20
−30
−40
−50
1970
1980
1990
2000
2010
Date
Pipe 1: 19.8 to 22.8 m

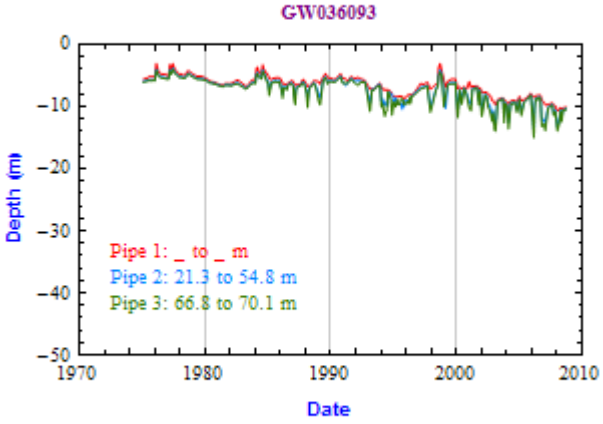
GW036093
Depth (m)
0
−10
−20
−30
−40
−50
1970
1980
1990
2000
2010
Date
Pipe 1: _ to _ m
Pipe 2: 21.3 to 54.8 m
Pipe 3: 66.8 to 70.1 m

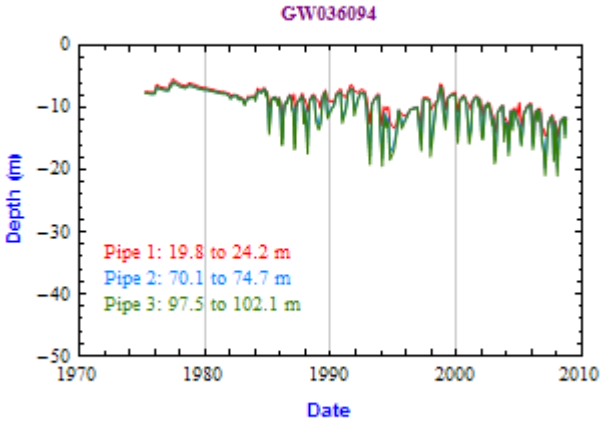
GW036094
Depth (m)
0
−10
−20
−30
−40
−50
1970
1980
1990
2000
2010
Date
Pipe 1: 19.8 to 24.2 m
Pipe 2: 70.1 to 74.7 m
Pipe 3: 97.5 to 102.1 m

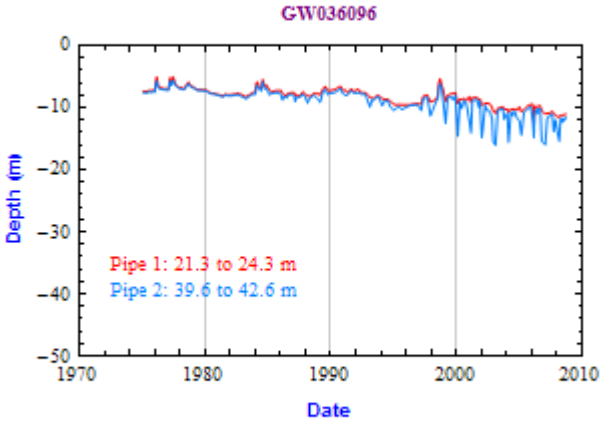
GW036096
Depth (m)
0
−10
−20
−30
−40
−50
1970
1980
1990
2000
2010
Date
Pipe 1: 21.3 to 24.3 m
Pipe 2: 39.6 to 42.6 m

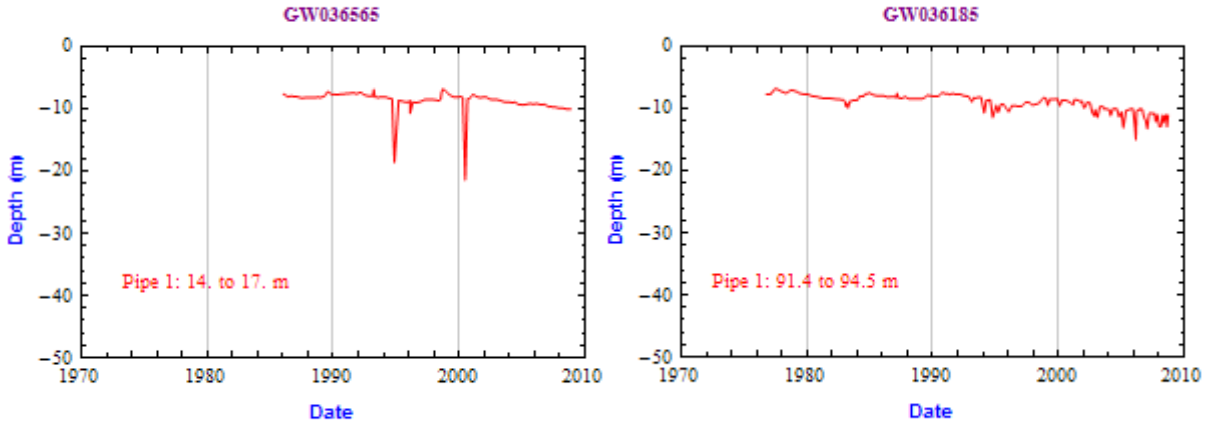
GW036565
Depth (m)
0
−10
−20
−30
−40
−50
1970
1980
1990
2000
2010
Date
Pipe 1: 14. to 17. m

GW036185
Depth (m)
0
−10
−20
−30
−40
−50
1970
1980
1990
2000
2010
Date
Pipe 1: 91.4 to 94.5 m

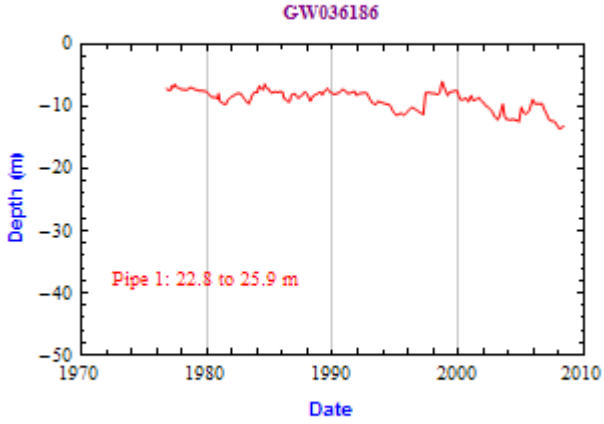
GW036186
Depth (m)
0
−10
−20
−30
−40
−50
1970
1980
1990
2000
2010
Date
Pipe 1: 22.8 to 25.9 m

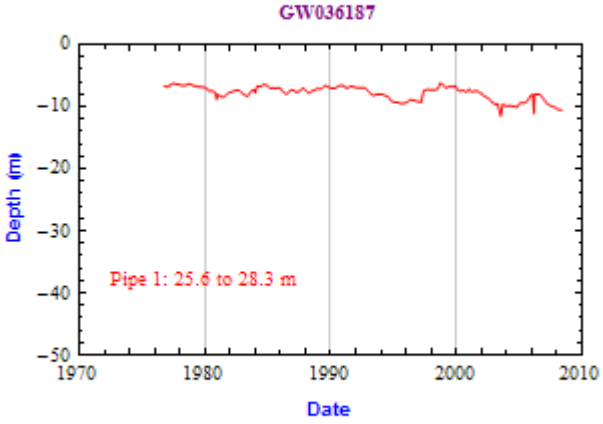
GW036187
Depth (m)
0
−10
−20
−30
−40
−50
1970
1980
1990
2000
2010
Date
Pipe 1: 25.6 to 28.3 m

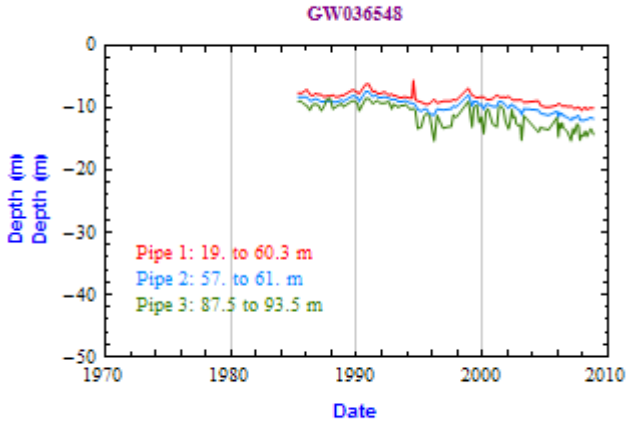
GW036548
Depth (m)
Depth (m)
0
−10
−20
−30
−40
−50
1970
1980
1990
2000
2010
Date
Pipe 1: 19. to 60.3 m
Pipe 2: 57. to 61. m
Pipe 3: 87.5 to 93.5 m

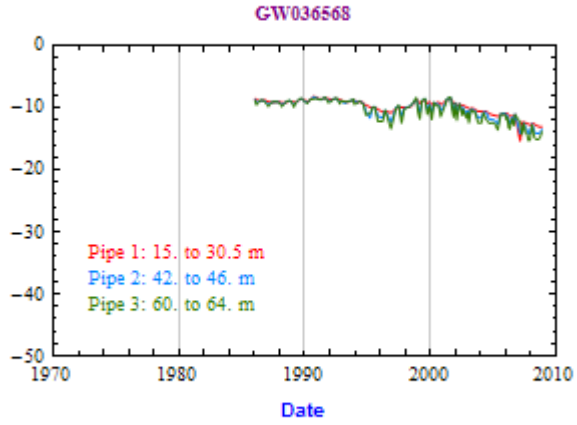
GW036568
0
−10
−20
−30
−40
−50
1970
1980
1990
2000
2010
Date
Pipe 1: 15. to 30.5 m
Pipe 2: 42. to 46. m
Pipe 3: 60. to 64. m

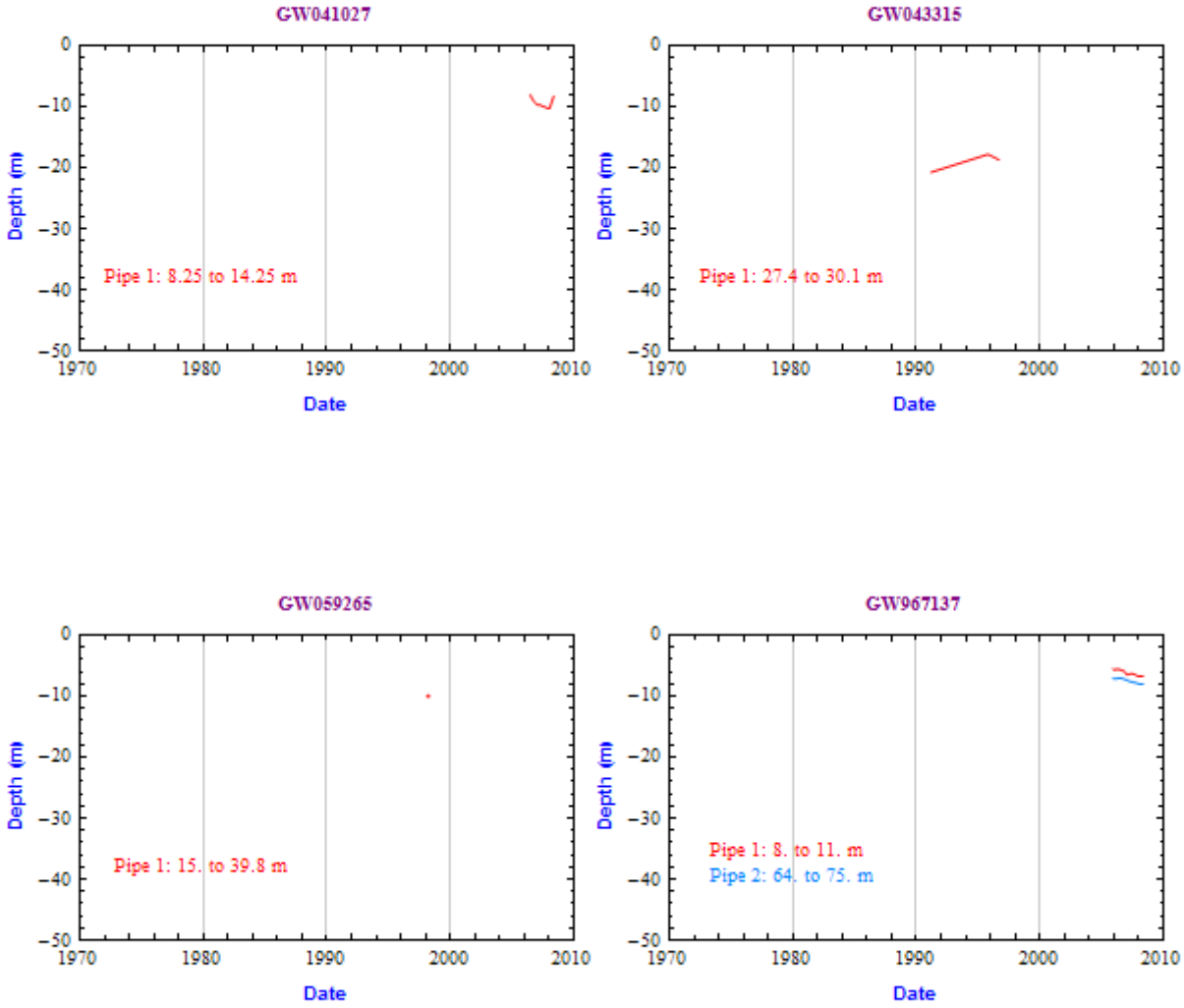
GW041027
Depth (m)
0
−10
−20
−30
−40
−50
1970
1980
1990
2000
2010
Date
Pipe 1: 8.25 to 14.25 m
GW043315
Depth (m)
Date
Pipe 1: 27.4 to 30.1 m
GW059265
Depth (m)
Date
Pipe 1: 15. to 39.8 m
GW967137
Depth (m)
Date
Pipe 1: 8. to 11. m
Pipe 2: 64. to 75. m

Appendix 8a

Crystallize

Plot in 3D the Change in the Recovered Groundwater Level

Authors
B. Kelly and B. Giambastiani

A8a.1 Introduction

This ***Crystallize*** notebook plots the change in the measured recovered groundwater level in the Maules Creek catchment and adjacent reach of the Namoi River using the data from the NSW Water Information Pinneena Groundwater Works CD (Figure 1).

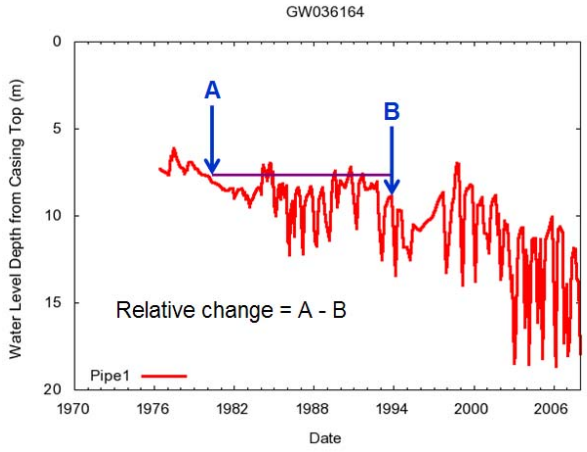

Figure 1: Determining the relative change in the recovered water level.

To be able to run this notebook the database Malues_Creek_database_Feb2010 needs to be linked and listed in the MS Windows ODBC control panel. In *Mathematica* select **Evaluation > Evaluate Notebook** from the main menu to generate the 3D plot.

In the 3D plot the change (delta) in the measured water level is positioned at the midpoint of the slotted interval.

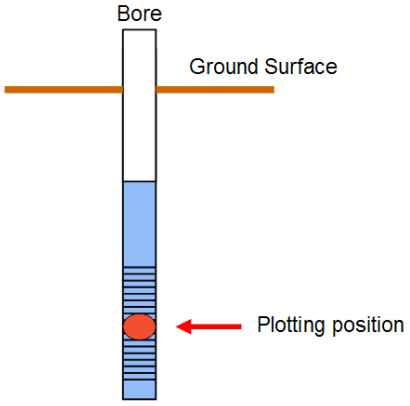

Figure 2: Position of the points in the 3D plot calculated below.

If you place the mouse point over a colored point in the 3D plot a listing of the details relating to that point will display. The items in the list are: groundwater works number, pipe number, easting, northing, elevation of the midpoint of the slotted interval, and the difference in the recovered measured groundwater level between the two selected years (positive values indicate a rising level, negative values a falling level).

If you click on a point in the 3D plot the bore hydrograph set corresponding to that point will open in the new window.

To change the date of the starting and ending years, edit the dates next to the variable names listed in the first two lines below. Note: Measurements range from 1970 to 2008.

A8a.2 Application Code and Output

Below is the input code for generating the plot and the output for the years 1986 and 2006.

In[1]:=
```
startyear = 1987;
endyear = 2007;
SetDirectory["G:\\NWC_FinalReportUNSW3DHydrogeology\\Appendix8_Crystallize3DGroundwater"];
Needs["Crystallize3DGroundwaterHeadTrends`"]
```

Out[4]=

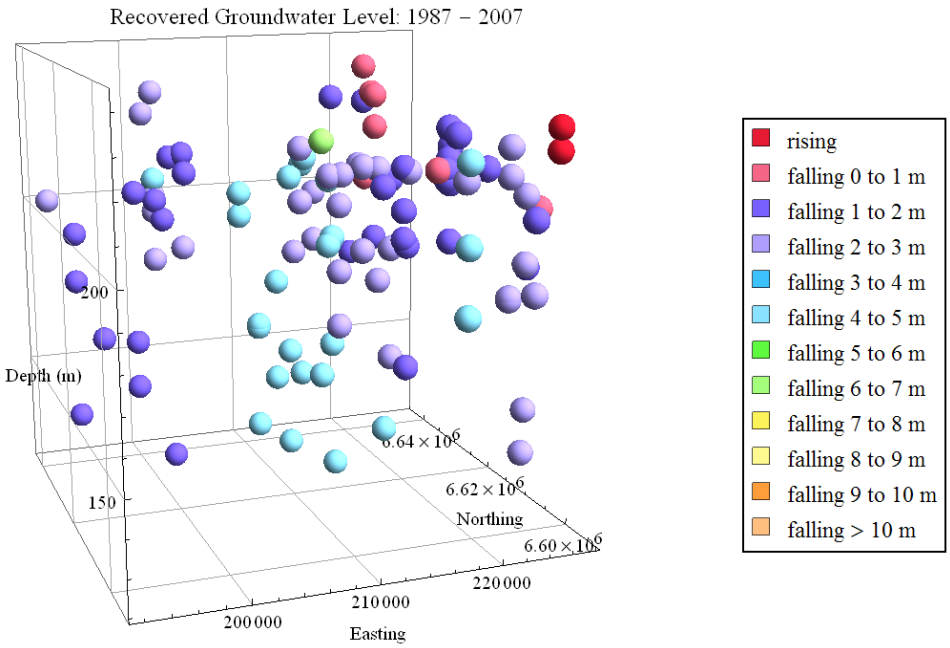

A8a.3 Interactive Examples

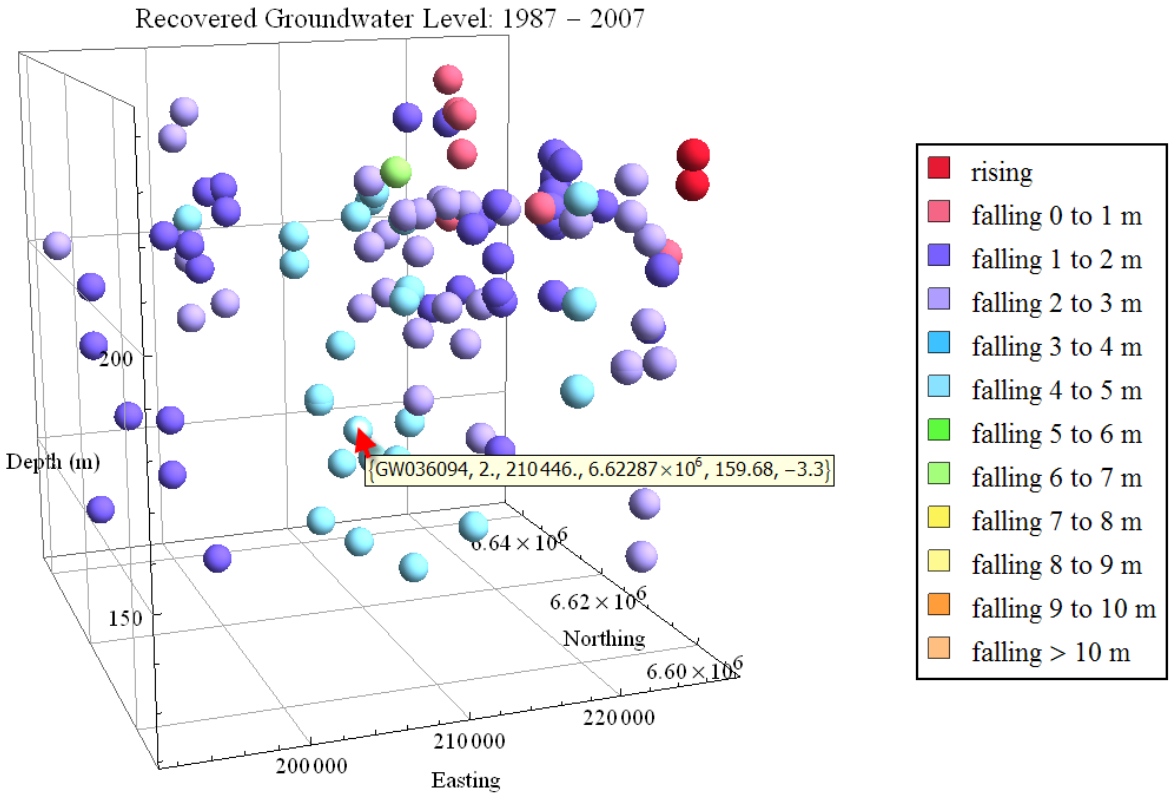

Figure 4. An example of the point details that appear when the mouse pointer is placed over a point in the 3D plot. The items in the list are: groundwater works number, pipe number, easting, northing, elevation of the midpoint of the slotted interval, and the difference in the recovered measured groundwater level between the two selected years (positive values indicate a rising level, negative values a falling level).

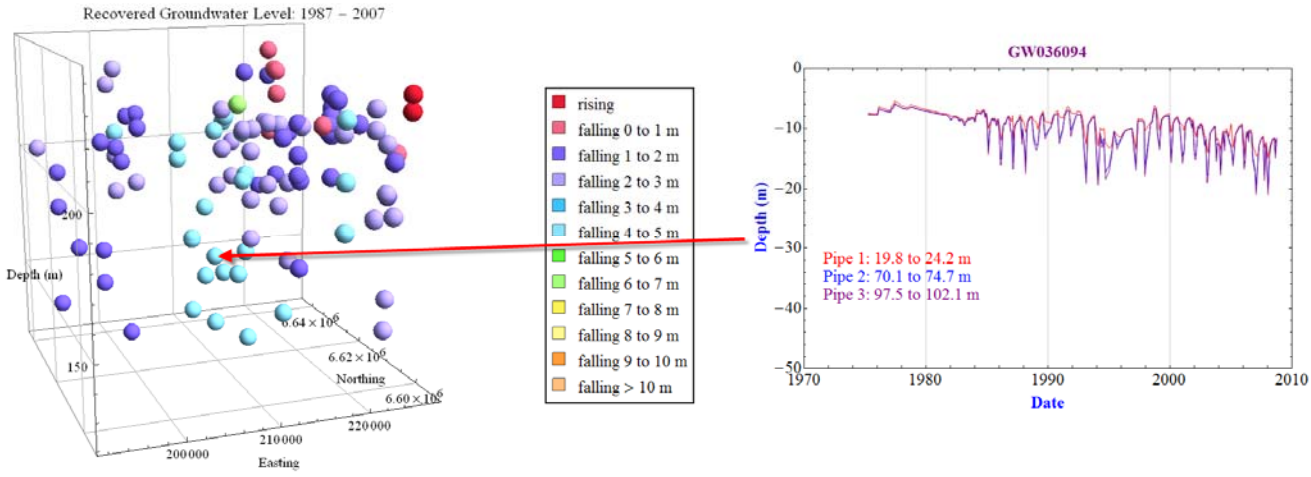

Figure 5. An example of a bore hydrograph set which appears when you click on a point in the 3D plot.

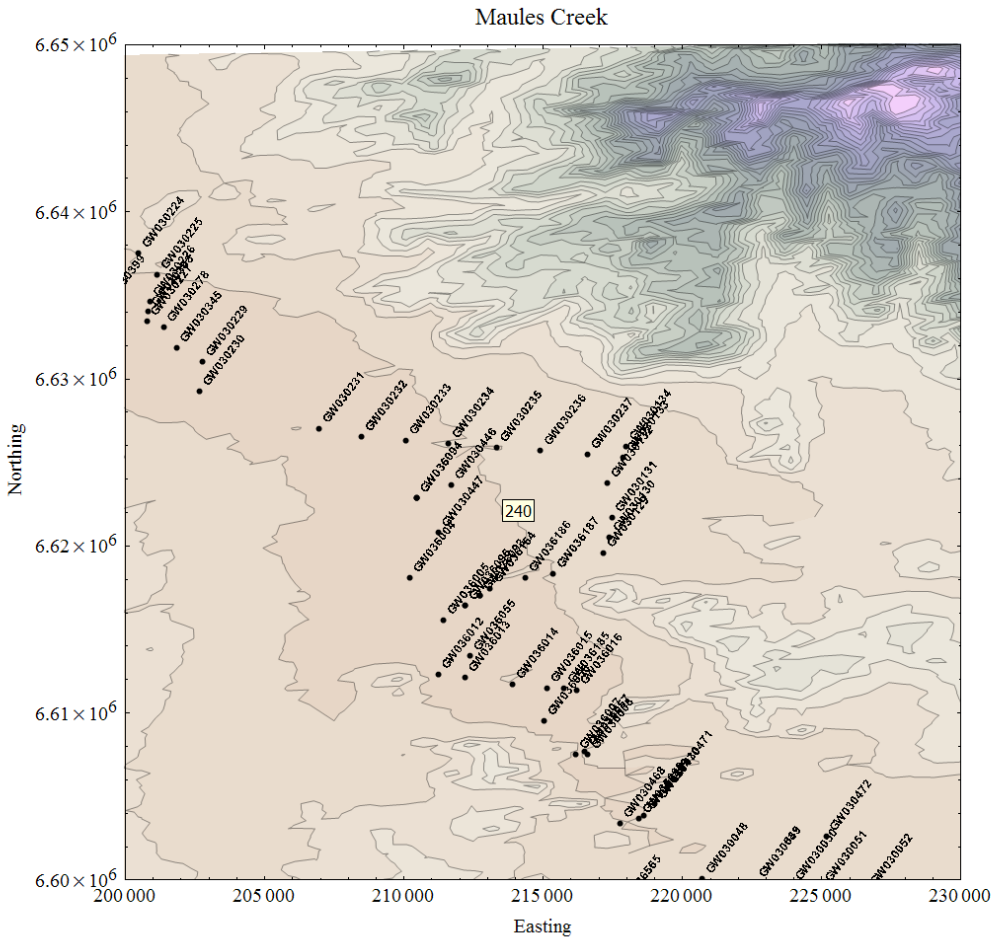

Figure 6. Location map of the bores in the Maules Creek database. When the mouse pointer is placed over a contour line the elevation appears in a yellow text box.

Appendix 8b

Crystallize

Plot in 3D the Fluctuation in the Groundwater Level for a Selected Year

Authors
B. Kelly and B. Giambastiani

A8b.1 Introduction

This ***Crystallize*** notebook plots the absolute fluctuation in the groundwater level for a selected year in the Maules Creek Catchment and adjacent reach of the Namoi River using the data from the NSW Water Information Pinneena Groundwater Works CD (Figure 1).

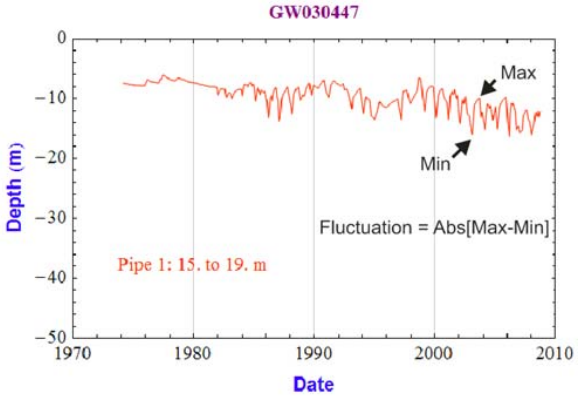

Figure 1: Determining the groundwater level fluctuation for a give

To be able to run this notebook the database Malues_Creek_database_Feb2010 needs to be linked and listed in the MS Windows ODBC control panel. In *Mathematica* select **Evaluation > Evaluate Notebook** from the main menu to generate the 3D plot.

In the 3D plot the absolute fluctuation in the groundwater level is positioned at the midpoint of the slotted interval for plotting (Figure 2).

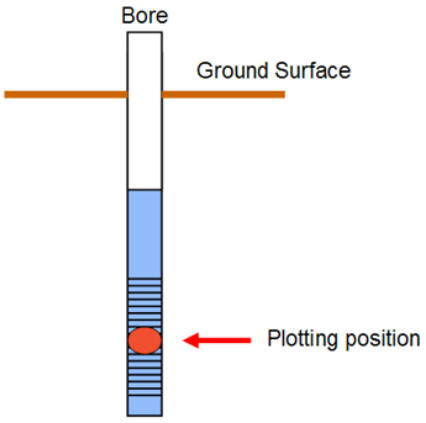

Figure 2: Position of the points in the 3D plot calculated below.

If the mouse pointer is placed over a coloured point in the 3D plot, a listing of the details relating to that point will be displayed. The items in this list are: groundwater works number, pipe number, easting, northing, ground surface elevation, elevation of the midpoint of the slotted interval, the minimum level, maximum level and the absolute fluctuation for the selected year.

If you click on a point in the 3D plot the bore hydrograph set corresponding to that point will open in the new window.

To change the year edit the year string next to the variable name "year" in the line below. Note: Measurements range from 1970 to 2008.

A8b.2 Application Code and Output

Below is the input code for generating the plot and the output for the year 2004.

```
In[1]:= year = 2004;
        SetDirectory["G:\\NWC_FinalReportUNSW3DHydrogeology\\Appendix8_Crystallize3DGroundwater"];
        Needs["Crystallize3DGroundwaterHeadFluctuation`"]
```

Out[3]=

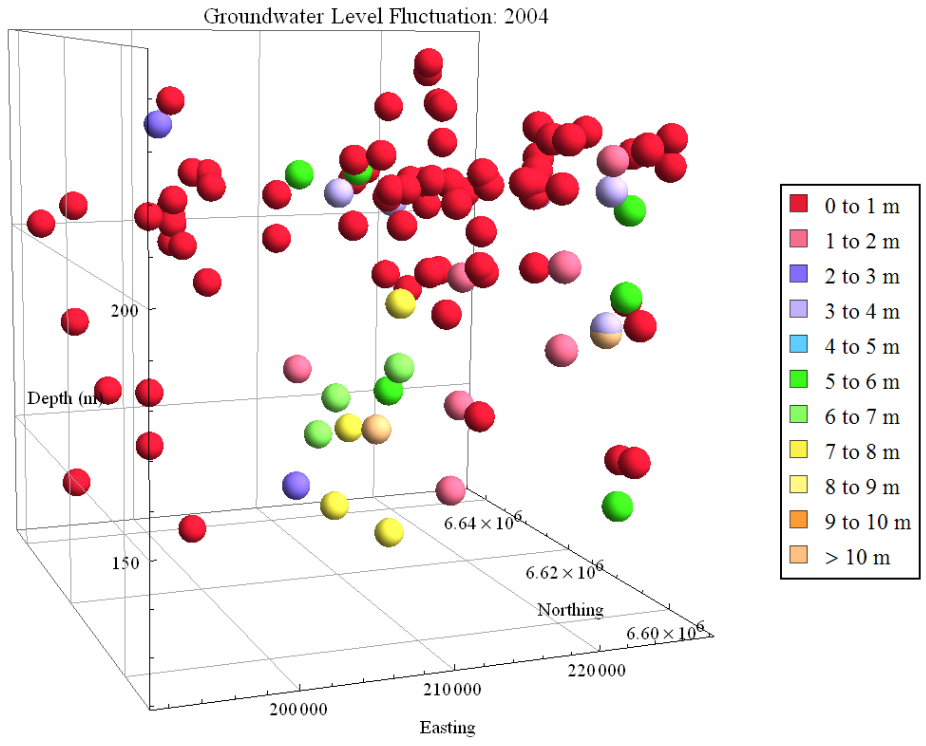

A8b.3 Interactive Examples

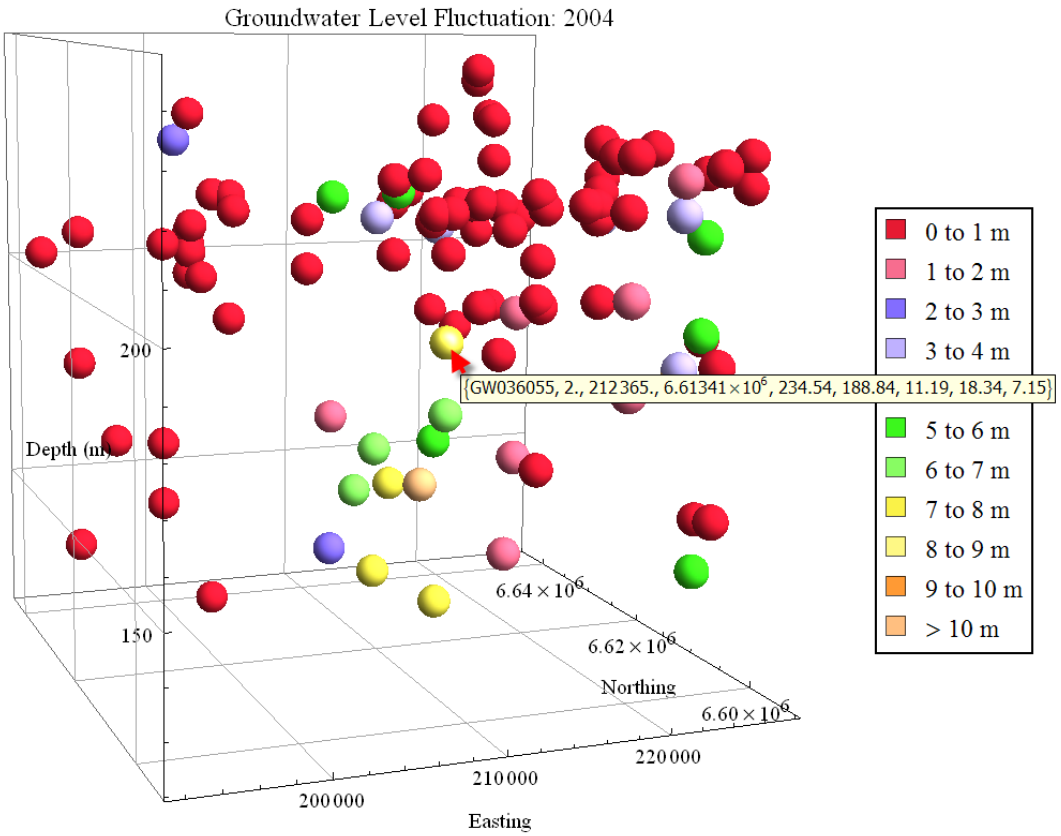

Figure 4. An example of the point details that appear when the mouse pointer is placed over a point in the 3D plot. The items in this list are: groundwater works number, pipe number, easting, northing, ground surface elevation, elevation of the midpoint of the slotted interval, the minimum level, maximum level and the absolute fluctuation for the selected year.

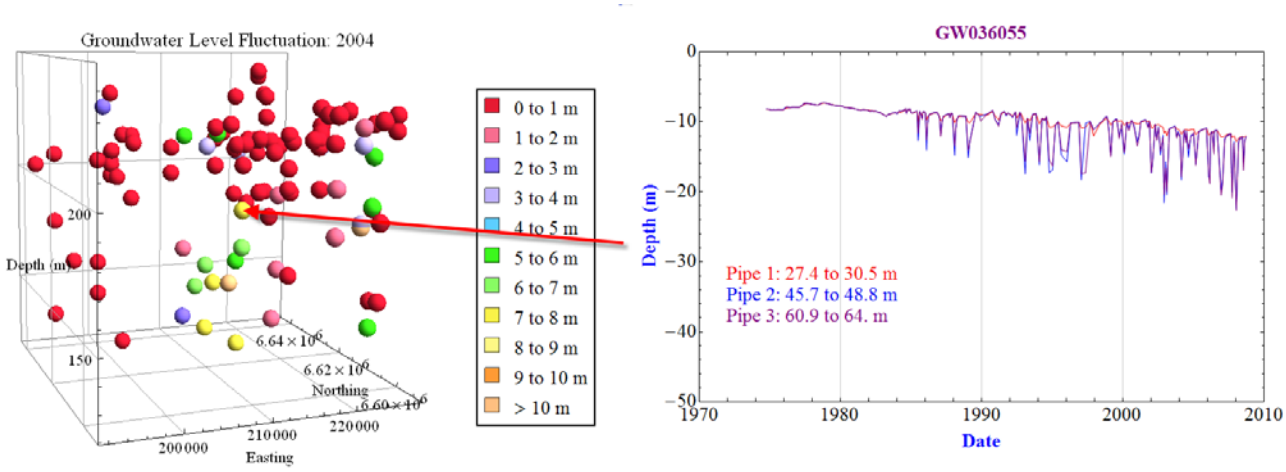

Figure 5. An example of a bore hydrograph set which appears when you click on a point in the 3D plot.

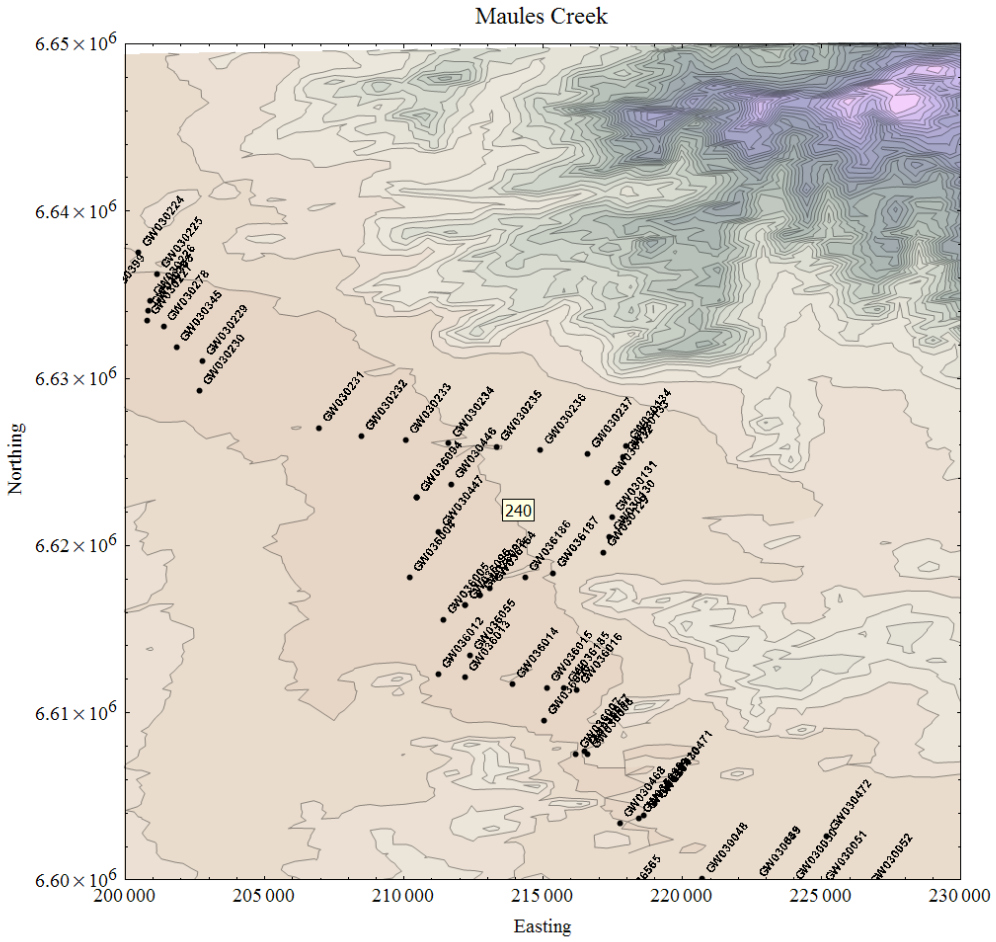

Figure 6. Location map of the bores in the Maules Creek database. When the mouse pointer is placed over a contour line the elevation appears in a yellow text box.

Appendix 9

Maules Creek Time Lapse Video of Groundwater Head

Authors
B. Kelly, B. Giambastiani and A. McCallum

A9.1 Introduction

Below are the frames from the Maules Creek time-lapse video of the groundwater head. This video is available from: http://www.connectedwaters.unsw.edu.au/resources/video/video_maules.html

An animated gif file has also been included in this folder along with the original MS PowerPoint document used to construct each video frame.

In this video the bedrock surface (combined outcrop and palaeochannel) and coloured data points that represent the groundwater head, were generated using EarthVision. These can now be generated using *Mathematica* as discussed in the report. The histograms of the rainfall, streamflow and groundwater usage were generated using *Mathematica*.

This video demonstrates visually the connection between rainfall, streamflow, groundwater usage and the measured groundwater levels in the NSW State Government groundwater monitoring boreholes throughout the Maules Creek catchment and adjacent reach of the Namoi River.

A9.2 Video Frames

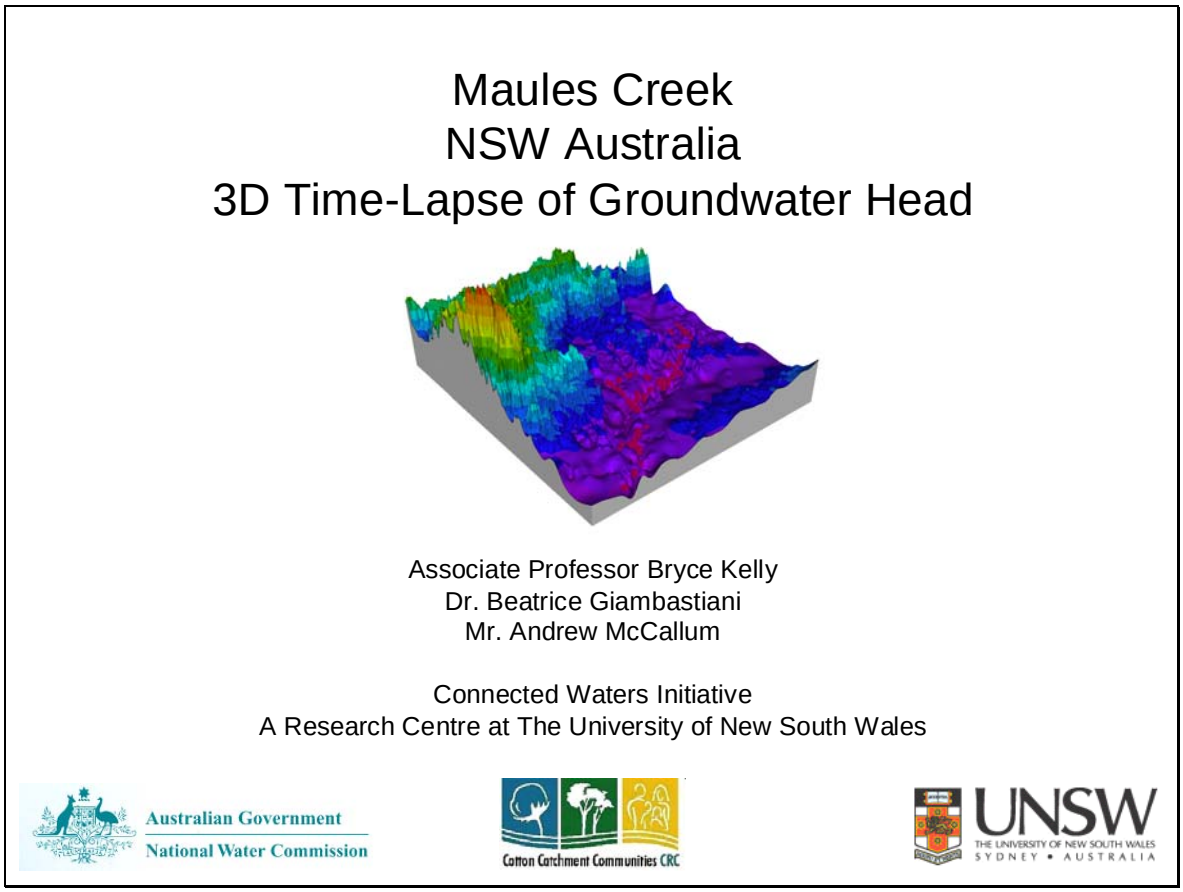

3D Geology

The following time-lapse images of groundwater head measurements will show readings taken in NSW government groundwater monitoring bores. The sample points have been located in their true position in space.

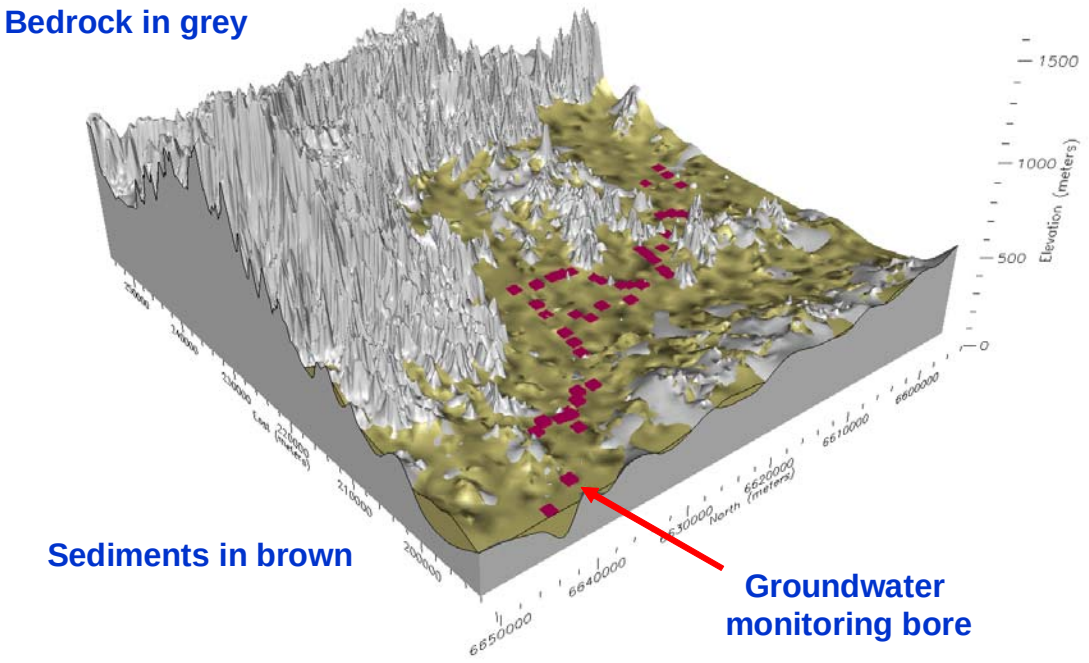

Sediments Removed

The sediments that fill the palaeochannels have been removed to clearly display all sampling intervals.

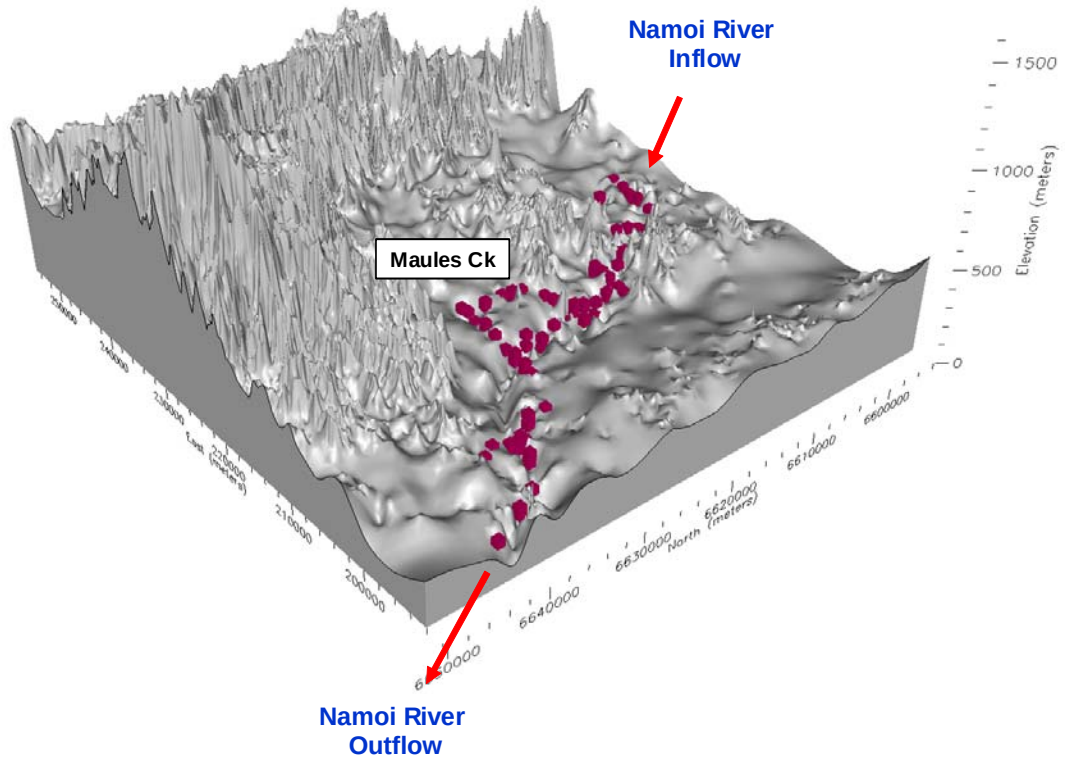

How to interpret the relative change in groundwater head

How to interpret the relative change in groundwater head

- The NSW State Government installed monitoring bores throughout the catchment in the 1970s.

How to interpret the relative change in groundwater head

- The NSW State Government installed monitoring bores throughout the catchment in the 1970s.
- The water level in the monitoring bores has been measured 4 or more times each year. This water level is the groundwater head.

How to interpret the relative change in groundwater head

- The NSW State Government installed monitoring bores throughout the catchment in the 1970s.
- The water level in the monitoring bores has been measured 4 or more times each year. This water level is the groundwater head.
- The recovered groundwater head is the value recorded just before the beginning of the groundwater extraction season (usually the reading recorded in June, July or August).

Monitoring Bore Hydrograph

Below is a groundwater monitoring bore hydrograph. The horizontal axis is time, and the vertical axis is the height of the water in the bore relative to the casing top.

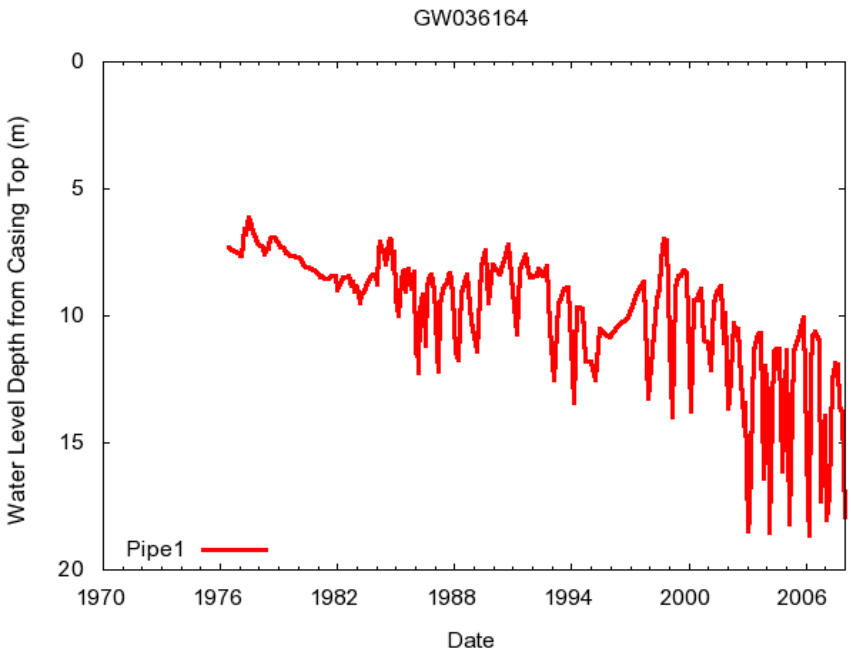

Reference Year

Recovered groundwater head measurements taken in 1980 are used as the base level.

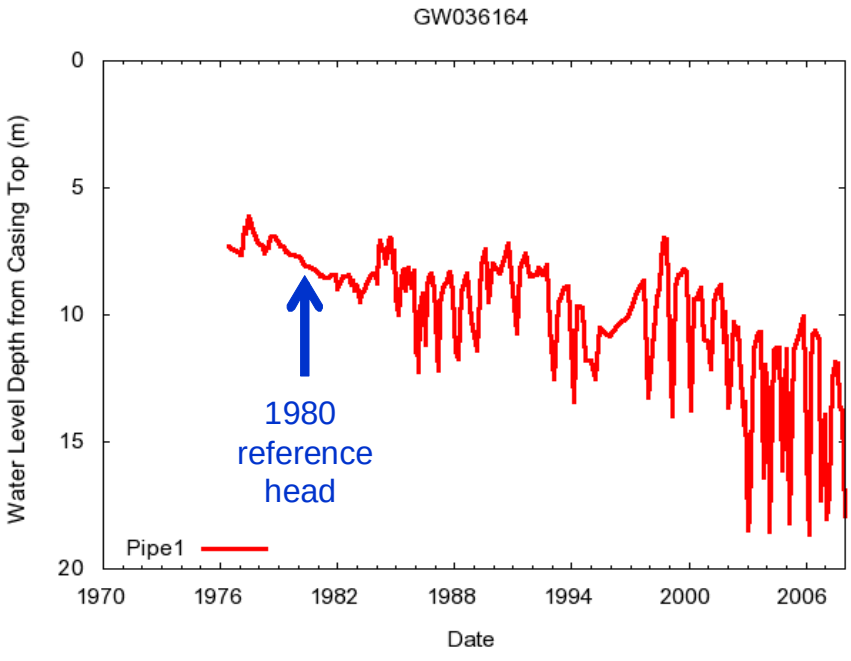

Pumping Drawdown

Each year the groundwater head falls when the pumps are turned on and rises when the pumps are turned off.

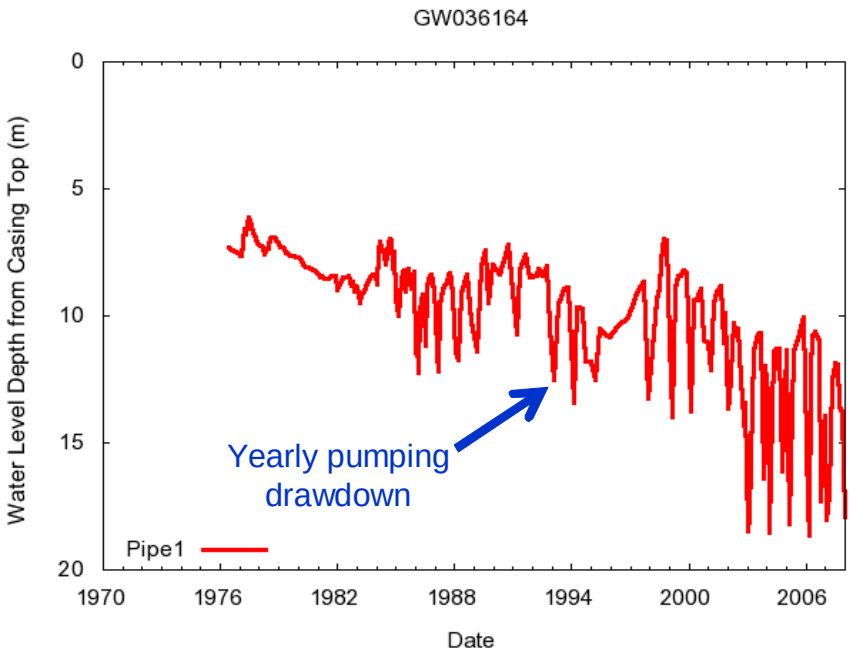

Recovered Head Reading

The recovered groundwater head is used to track the long term impact of groundwater extractions, and to monitor recharge from flood events.

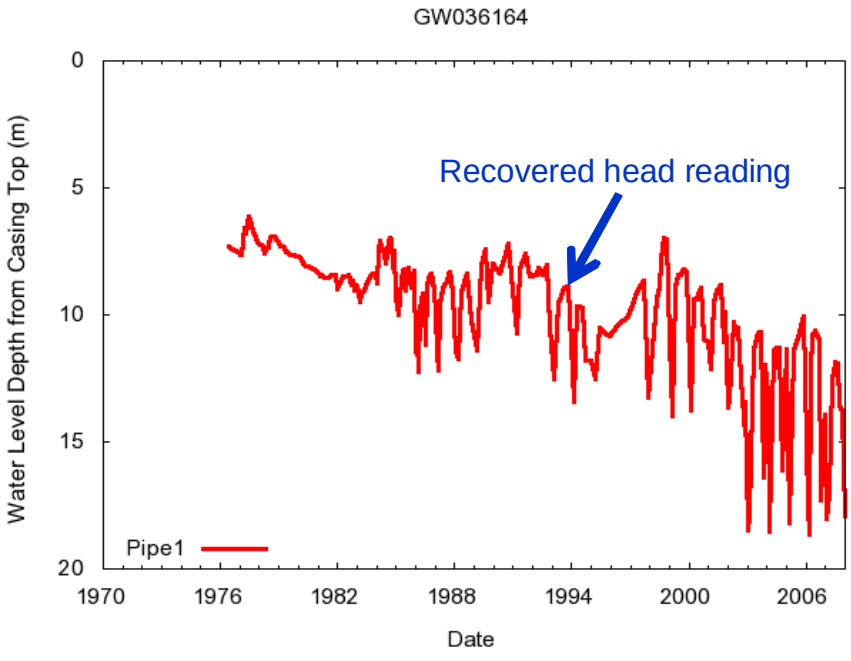

Relative Change in Head

The time-lapse video plots the relative change in head comparing the yearly recovered value to the head recorded in 1980.

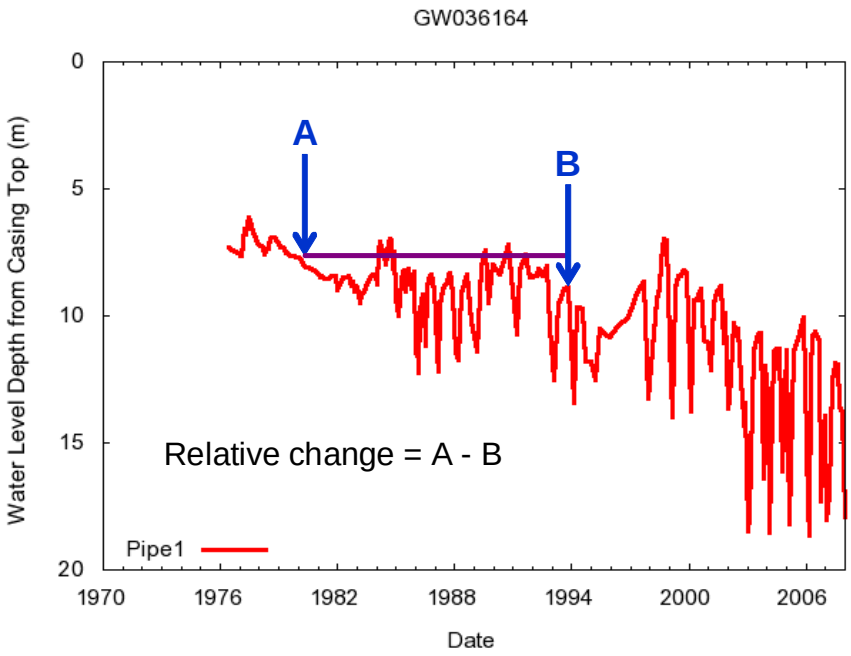

Plotting Position

The relative change in groundwater head is plotted in 3D at the mid-point of the slotted interval for each monitoring bore.

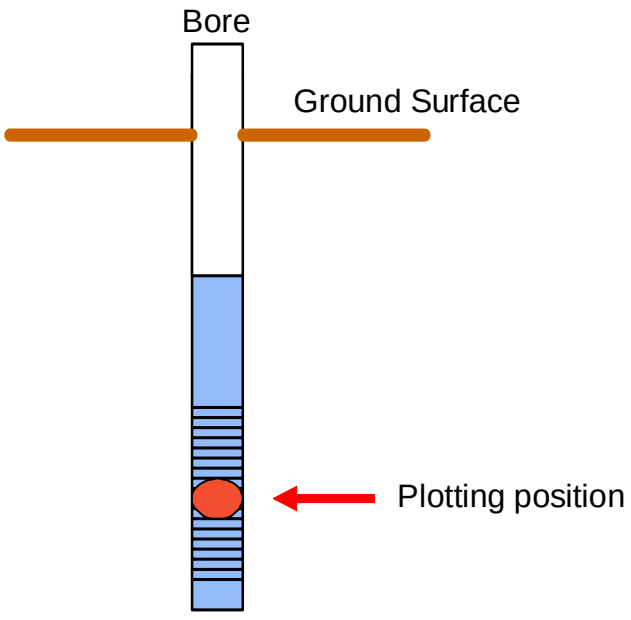

Head Colour Key

Relative change in groundwater head is represented as a coloured cube.

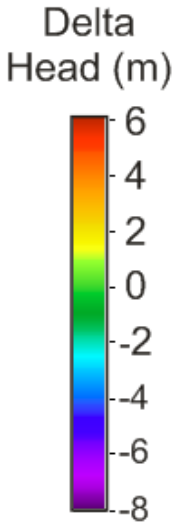

Green cubes indicate no change.

Head Colour Key

Relative change in groundwater head is represented as a coloured cube.

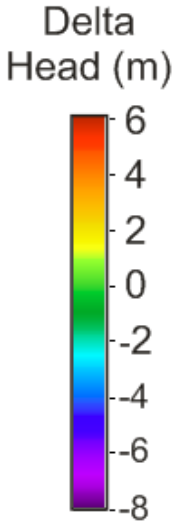

Yellow to red cubes indicate that there has been a rise in head, signifying that the aquifers are being recharged.

Head Colour Key

Relative change in groundwater head is represented as a coloured cube.

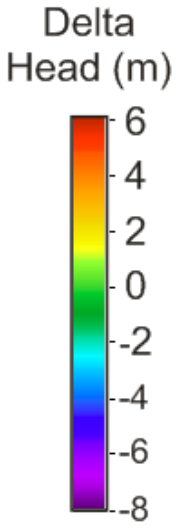

Blue to purple cubes indicate that there has been a decline in head, signifying that the aquifers are being mined.

How to interpret the histograms in the time-lapse presentation

How to interpret the histograms in the time-lapse presentation

- Rainfall at Boggabri
  - Orange bars: less than the median rainfall; 580.75mm per year
  - Blue bars: greater than the median rainfall; 580.75mm per year

How to interpret the histograms in the time-lapse presentation

- Rainfall at Boggabri
  - Orange bars: less than the median rainfall; 580.75mm per year
  - Blue bars: greater than the median rainfall; 580.75mm per year

- Streamflow at Boggabri
  - Red bars: less than the median streamflow; 343,537 ML per year
  - Blue bars: greater than the median streamflow; 343,537 ML per year

How to interpret the histograms in the time-lapse presentation

- Rainfall at Boggabri
  - Orange bars: less than the median rainfall; 580.75mm per year
  - Blue bars: greater than the median rainfall; 580.75mm per year
- Streamflow at Boggabri
  - Red bars: less than the median streamflow; 343,537 ML per year
  - Blue bars: greater than the median streamflow; 343,537 ML per year
- Groundwater Usage (Zones 5 and 11)
  - Red bars: less than 10,000 ML per year
  - Green bars: 10,000 to 20,000 ML per year
  - Blue bars: greater than 20,0000 ML per year

How to interpret the histograms in the time-lapse presentation

- Rainfall at Boggabri
  - Orange bars: less than the median rainfall; 580.75mm per year
  - Blue bars: greater than the median rainfall; 580.75mm per year
- Streamflow at Boggabri
  - Red bars: less than the median streamflow; 343,537 ML per year
  - Blue bars: greater than the median streamflow; 343,537 ML per year
- Groundwater Usage (Zones 5 and 11)
  - Red bars: less than 10,000 ML per year
  - Green bars: 10,000 to 20,000 ML per year
  - Blue bars: greater than 20,0000 ML per year
- Statistics calculated over the cotton growing year starting October 1st

Key Features in the Time-Lapse

The time-lapse of groundwater head change video is about to begin.

- Some features to observe are:

Key Features in the Time-Lapse

The time-lapse of groundwater head change video is about to begin.

- Some features to observe are:
- flood waters moved through the region in 1984,

Key Features in the Time-Lapse

The time-lapse of groundwater head change video is about to begin.

- Some features to observe are:
- flood waters moved through the region in 1984,
- from 1985 through 1992 there was little variation in groundwater head,

Key Features in the Time-Lapse

The time-lapse of groundwater head change video is about to begin.

- Some features to observe are:
- flood waters moved through the region in 1984,
- from 1985 through 1992 there was little variation in groundwater head,

- from 1993 through 1997 groundwater head declined in the sediments near the Namoi River,

Key Features in the Time-Lapse

The time-lapse of groundwater head change video is about to begin.

- Some features to observe are:
- flood waters moved through the region in 1984,
- from 1985 through 1992 there was little variation in groundwater head,
- from 1993 through 1997 groundwater head declined in the sediments near the Namoi River,
- flood waters moving through the catchment replenished the aquifers in 1998, and

Key Features in the Time-Lapse

The time-lapse of groundwater head change video is about to begin.

- Some features to observe are:
- flood waters moved through the region in 1984,
- from 1985 through 1992 there was little variation in groundwater head,
- from 1993 through 1997 groundwater head declined in the sediments near the Namoi River,
- flood waters moving through the catchment replenished the aquifers in 1998, and
- since 2000 there has been a gradual decline in head, which started in the sediments near the Namoi River and has migrated eastwards along Maules Creek road.

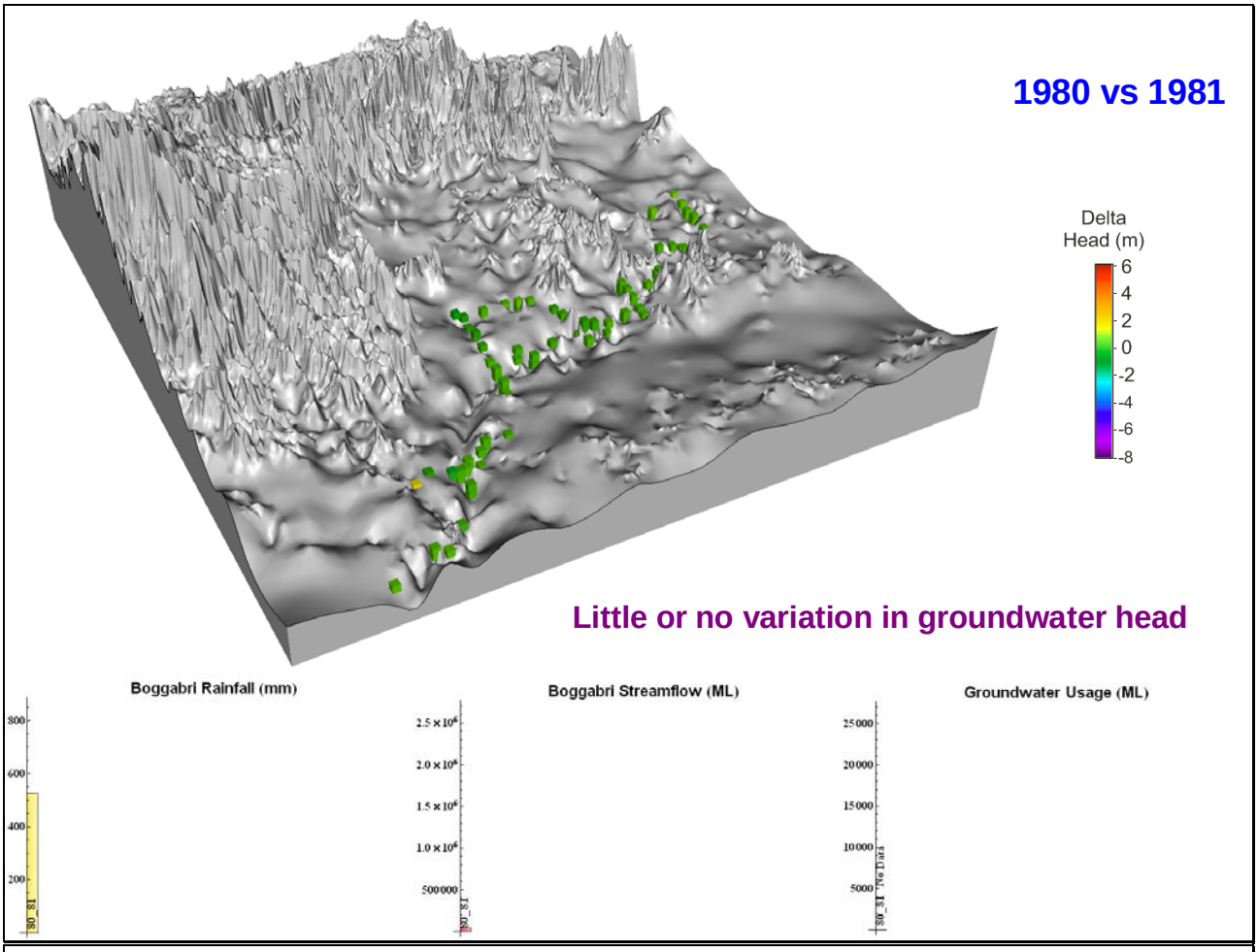
1980 vs 1981
Delta Head (m)
6
4
2
0
-2
-4
-6
-8
Little or no variation in groundwater head
Boggabri Rainfall (mm)
800
600
400
200
80_81
Boggabri Streamflow (ML)
2.5 x 10^6
2.0 x 10^6
1.5 x 10^6
1.0 x 10^6
500000
80_81
Groundwater Usage (ML)
25000
20000
15000
10000
5000
80_81 No Data

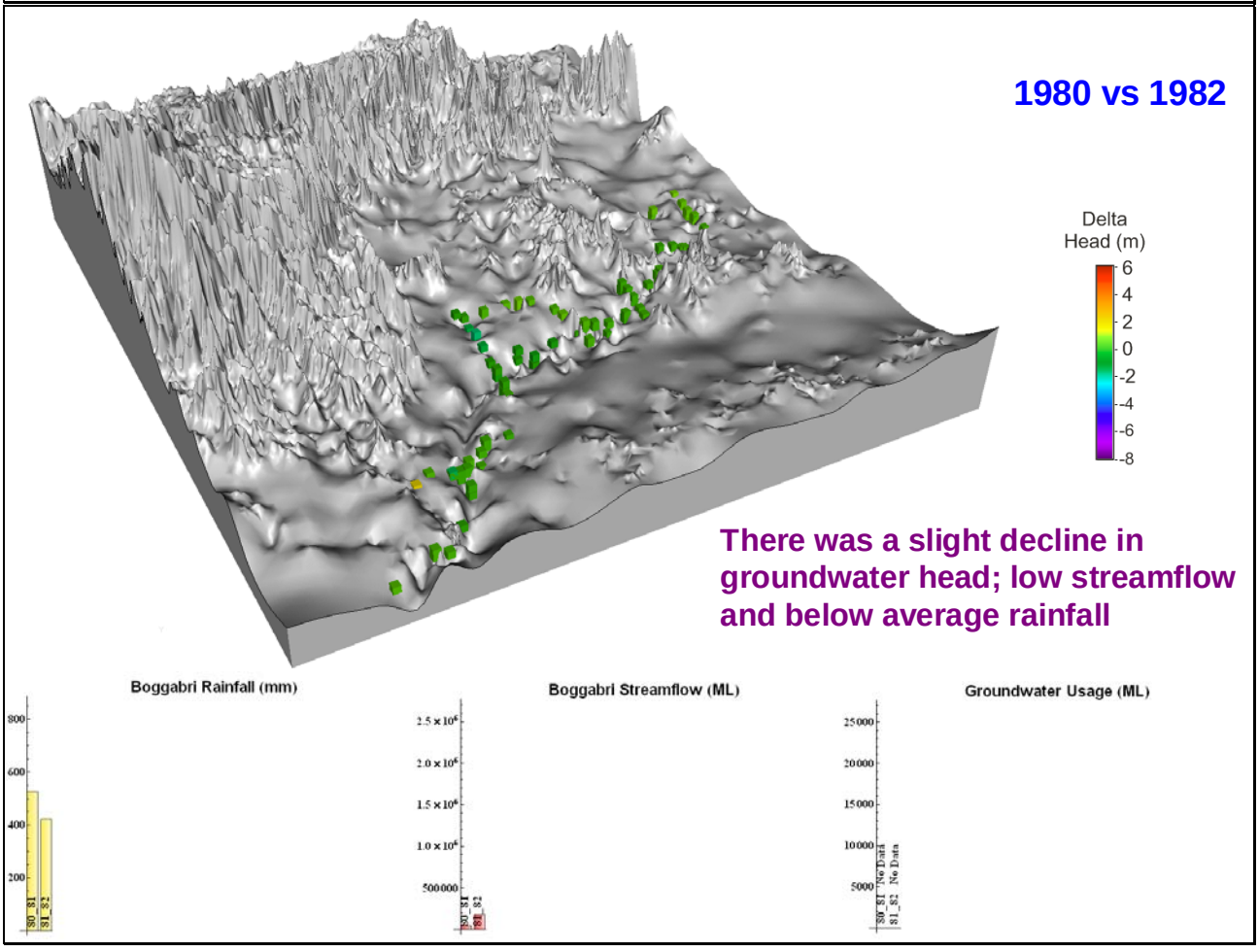
1980 vs 1982
Delta Head (m)
6
4
2
0
-2
-4
-6
-8
There was a slight decline in groundwater head; low streamflow and below average rainfall
Boggabri Rainfall (mm)
800
600
400
200
80_81
81_82
Boggabri Streamflow (ML)
2.5 x 10^6
2.0 x 10^6
1.5 x 10^6
1.0 x 10^6
500000
80_81
81_82
Groundwater Usage (ML)
25000
20000
15000
10000
5000
80_81 No Data
81_82 No Data

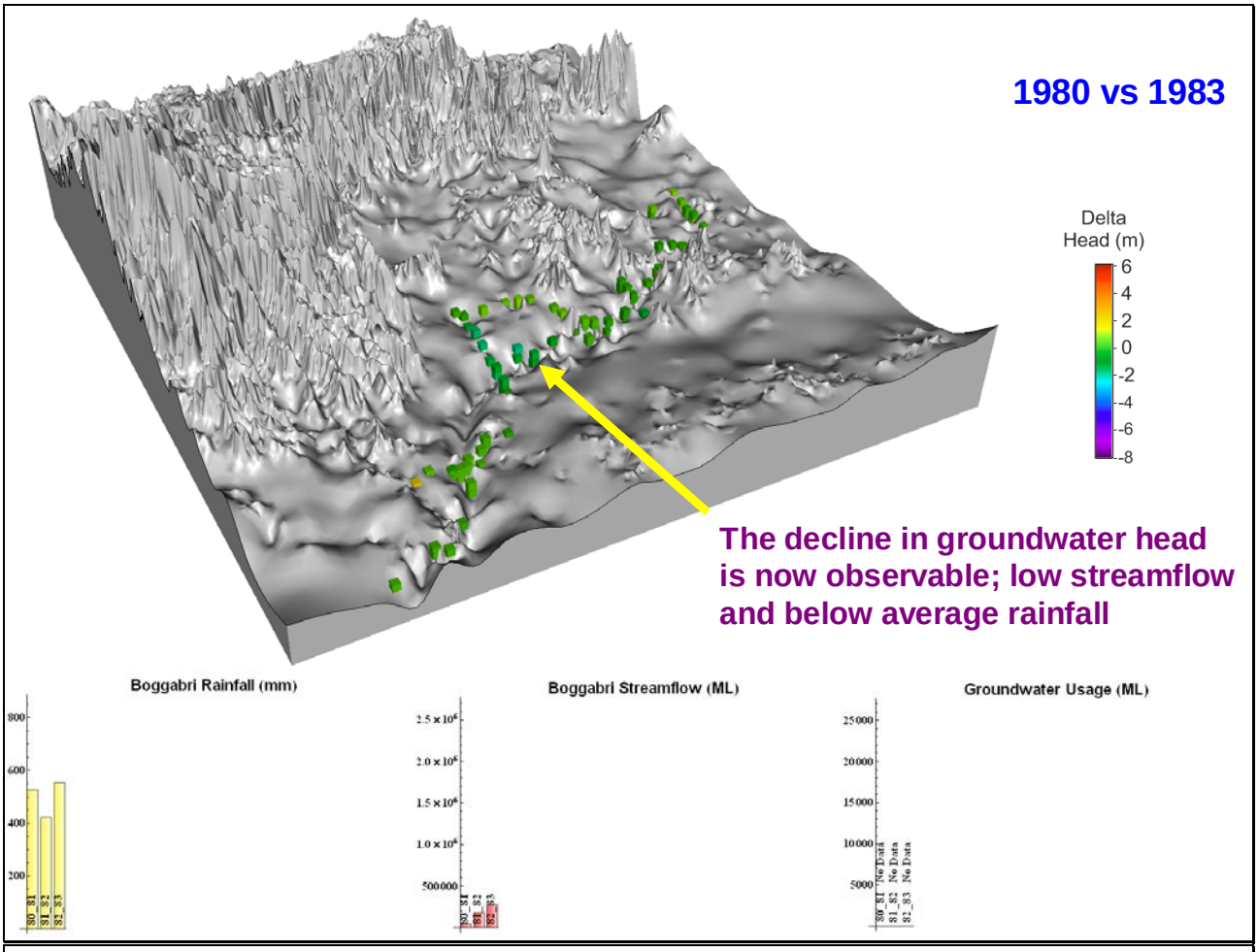
1980 vs 1983
Delta Head (m)
6
4
2
0
-2
-4
-6
-8
The decline in groundwater head is now observable; low streamflow and below average rainfall
Boggabri Rainfall (mm)
Boggabri Streamflow (ML)
Groundwater Usage (ML)

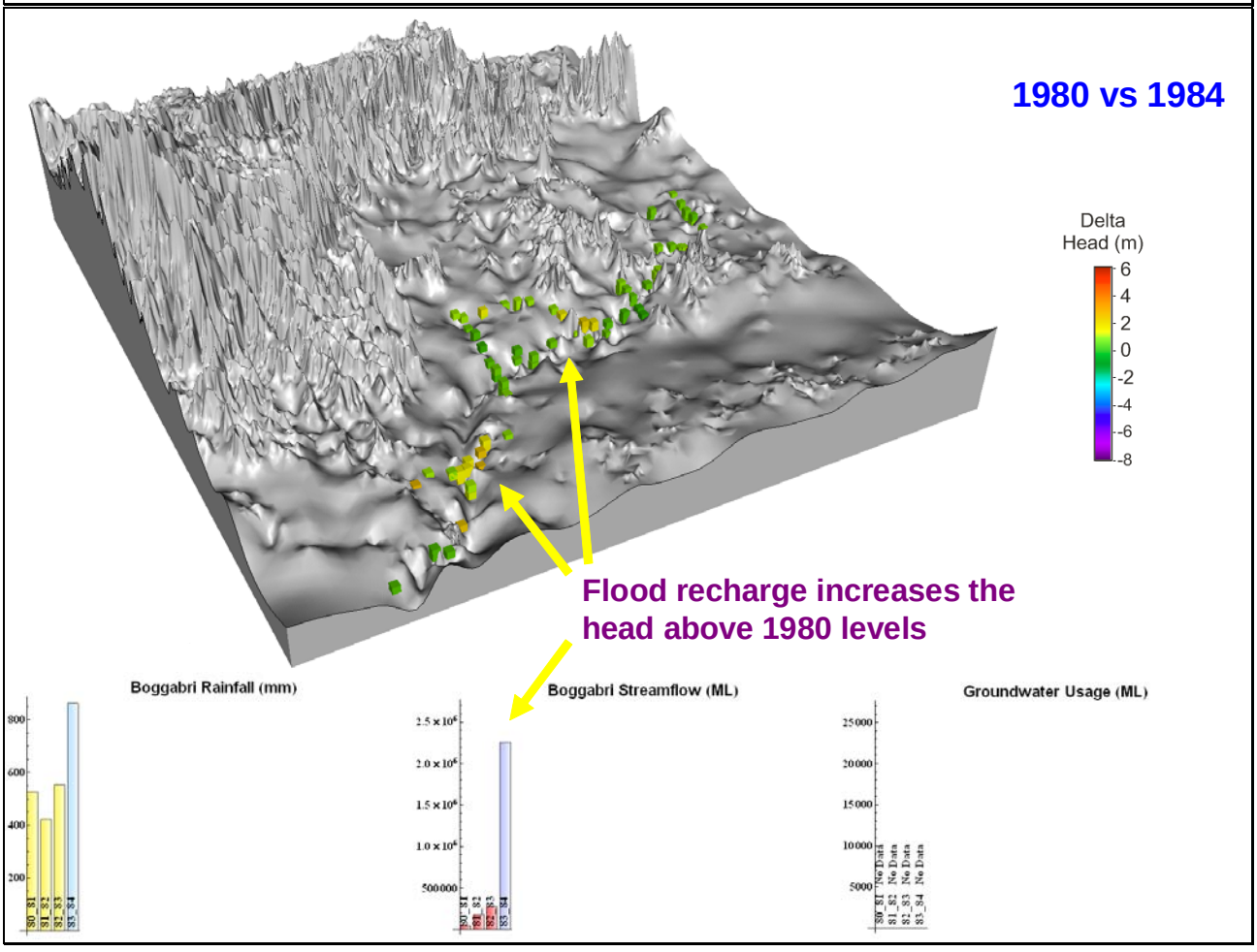
1980 vs 1984
Delta Head (m)
6
4
2
0
-2
-4
-6
-8
Flood recharge increases the head above 1980 levels
Boggabri Rainfall (mm)
Boggabri Streamflow (ML)
Groundwater Usage (ML)

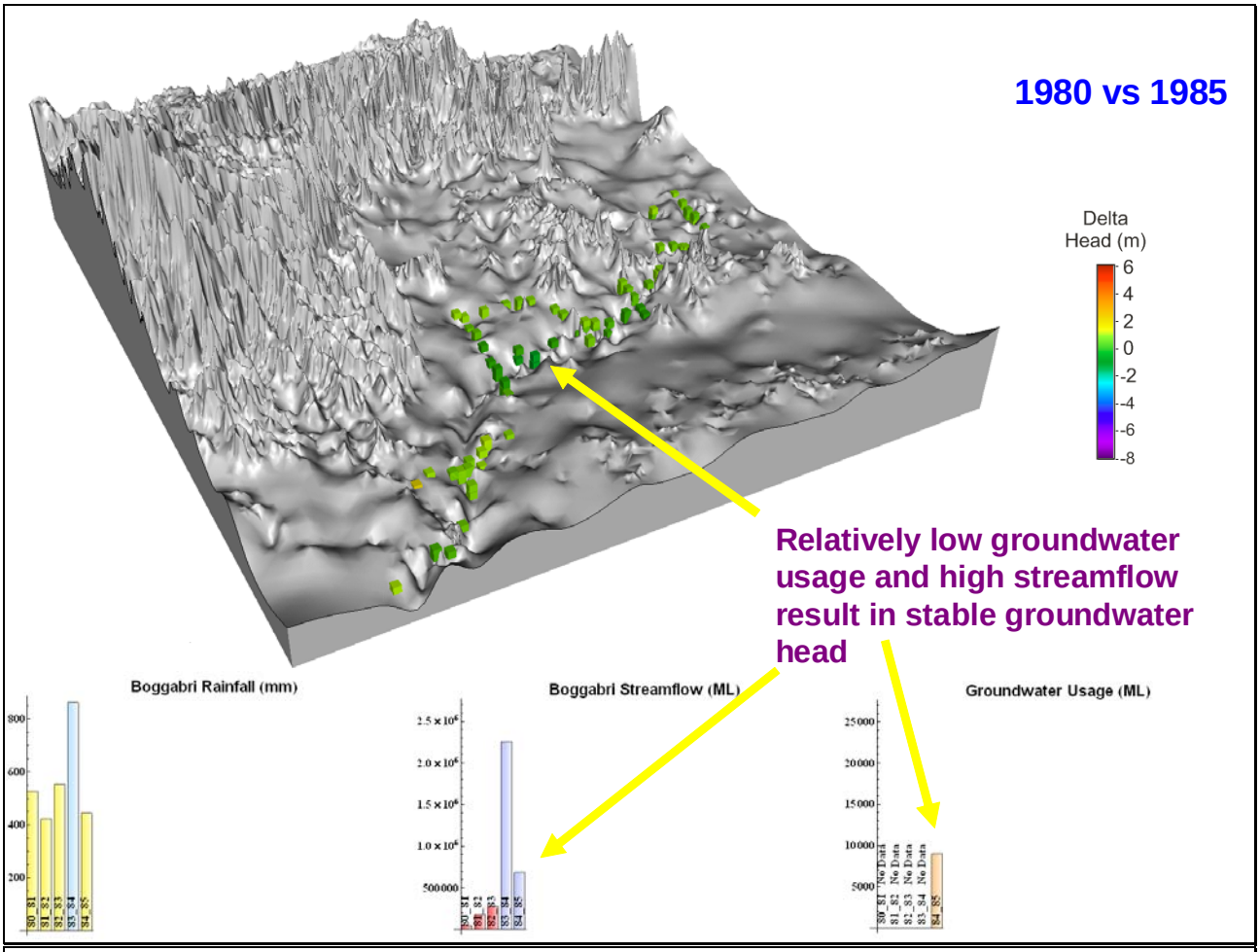
1980 vs 1985
Delta Head (m)
6
4
2
0
-2
-4
-6
-8
Relatively low groundwater usage and high streamflow result in stable groundwater head
Boggabri Rainfall (mm)
Boggabri Streamflow (ML)
Groundwater Usage (ML)

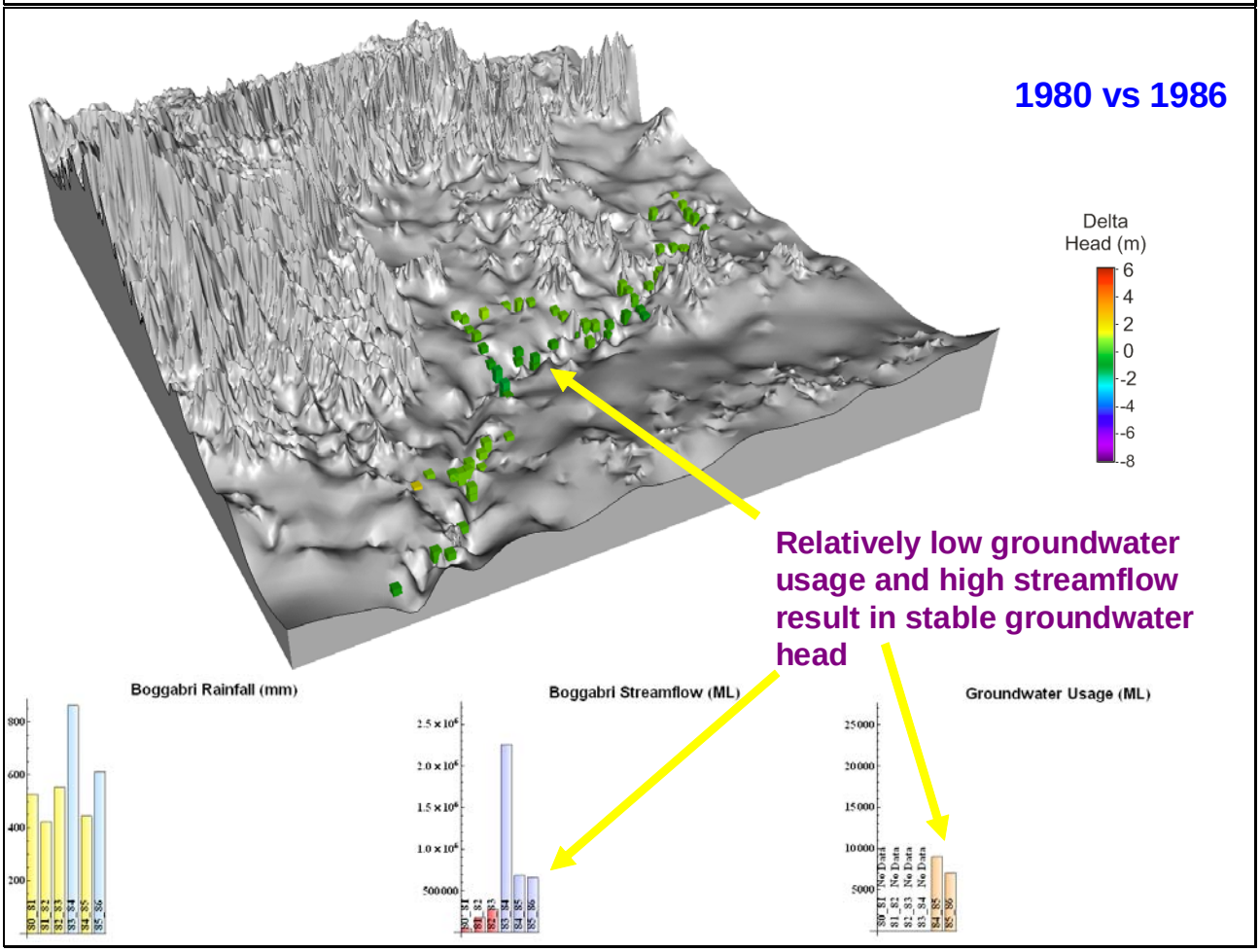
1980 vs 1986
Delta Head (m)
6
4
2
0
-2
-4
-6
-8
Relatively low groundwater usage and high streamflow result in stable groundwater head
Boggabri Rainfall (mm)
Boggabri Streamflow (ML)
Groundwater Usage (ML)

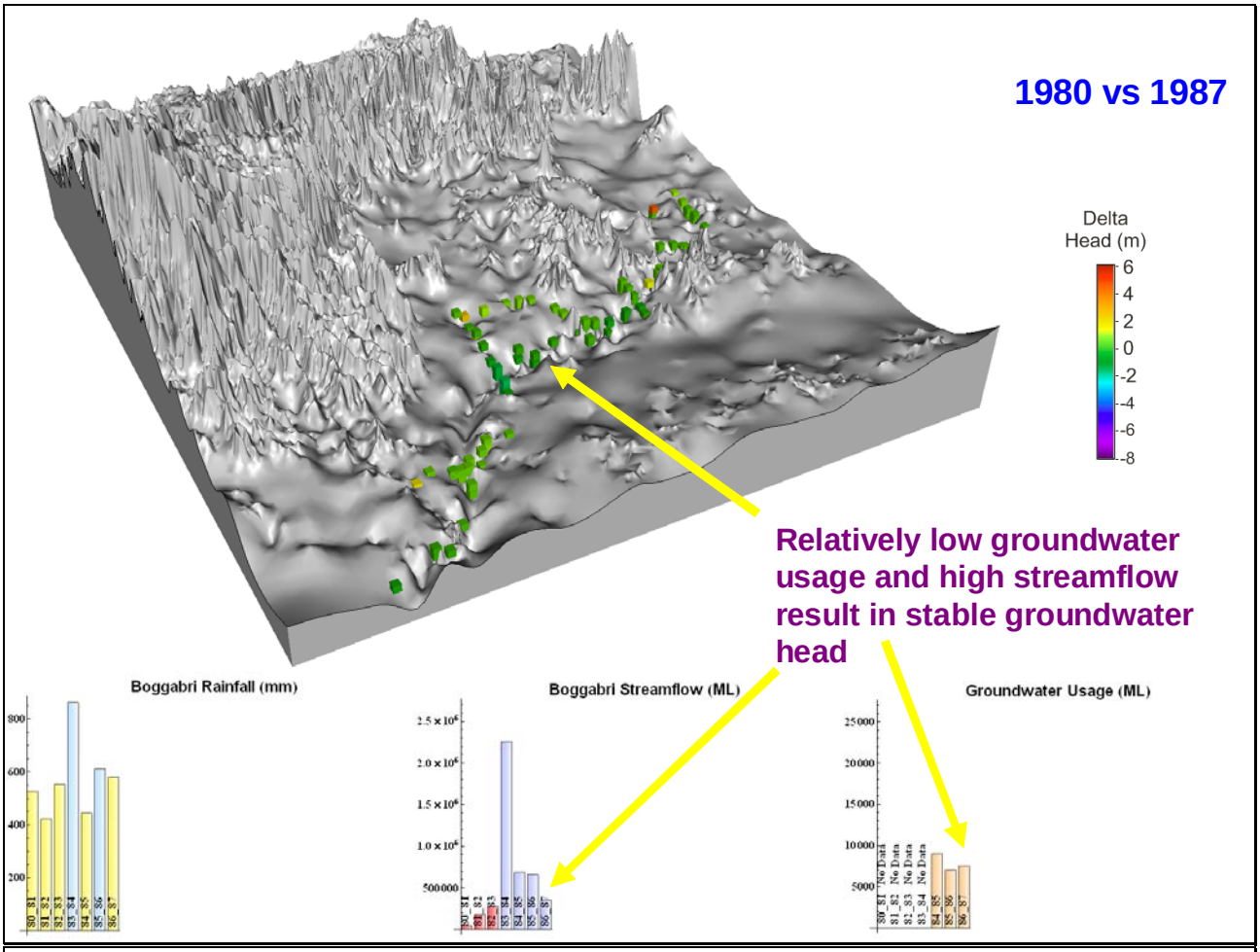
1980 vs 1987
Delta Head (m)
6
4
2
0
-2
-4
-6
-8
Relatively low groundwater usage and high streamflow result in stable groundwater head
Boggabri Rainfall (mm)
Boggabri Streamflow (ML)
Groundwater Usage (ML)

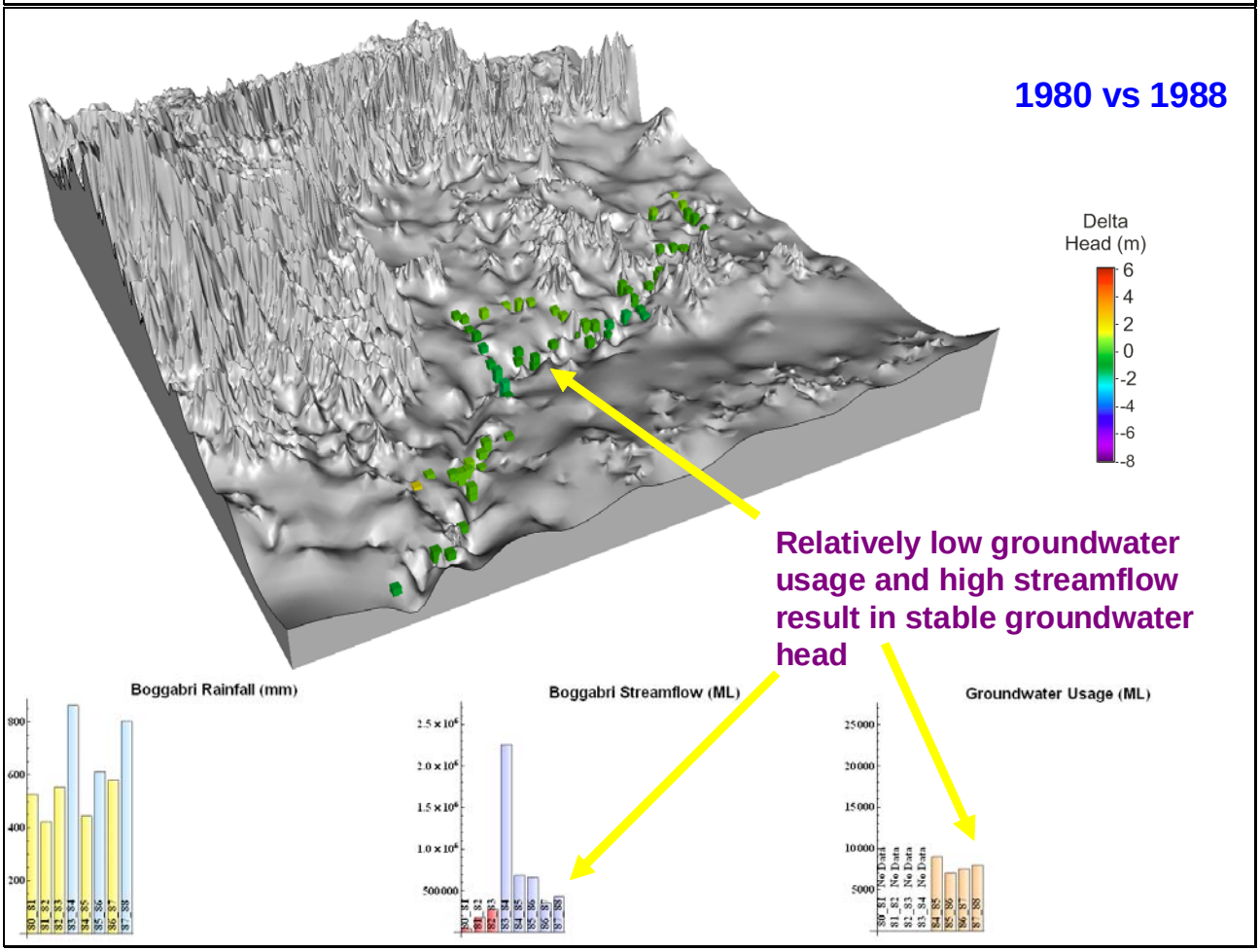
1980 vs 1988
Delta Head (m)
6
4
2
0
-2
-4
-6
-8
Relatively low groundwater usage and high streamflow result in stable groundwater head
Boggabri Rainfall (mm)
Boggabri Streamflow (ML)
Groundwater Usage (ML)

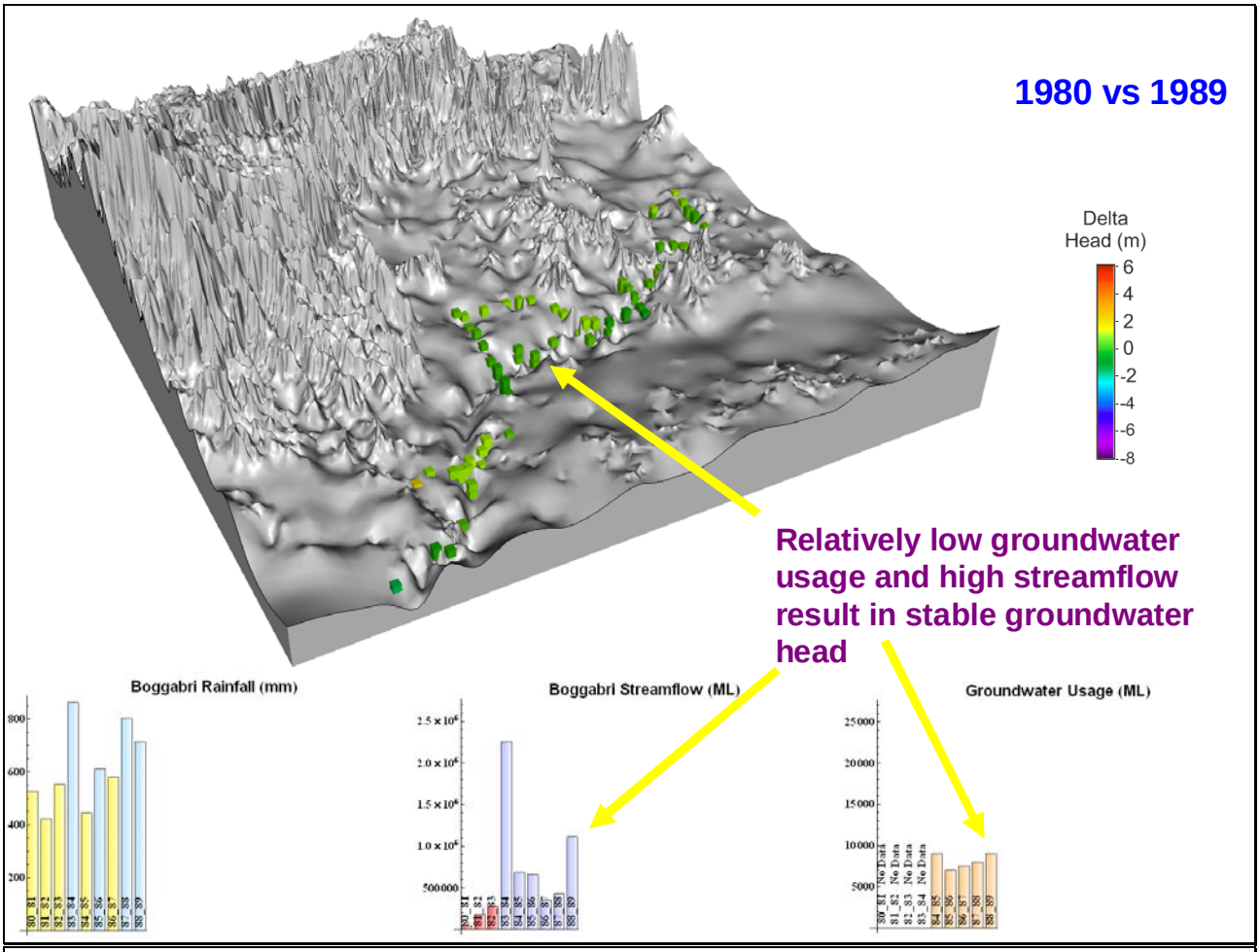
1980 vs 1989
Delta Head (m)
6
4
2
0
-2
-4
-6
-8
Relatively low groundwater usage and high streamflow result in stable groundwater head
Boggabri Rainfall (mm)
Boggabri Streamflow (ML)
Groundwater Usage (ML)

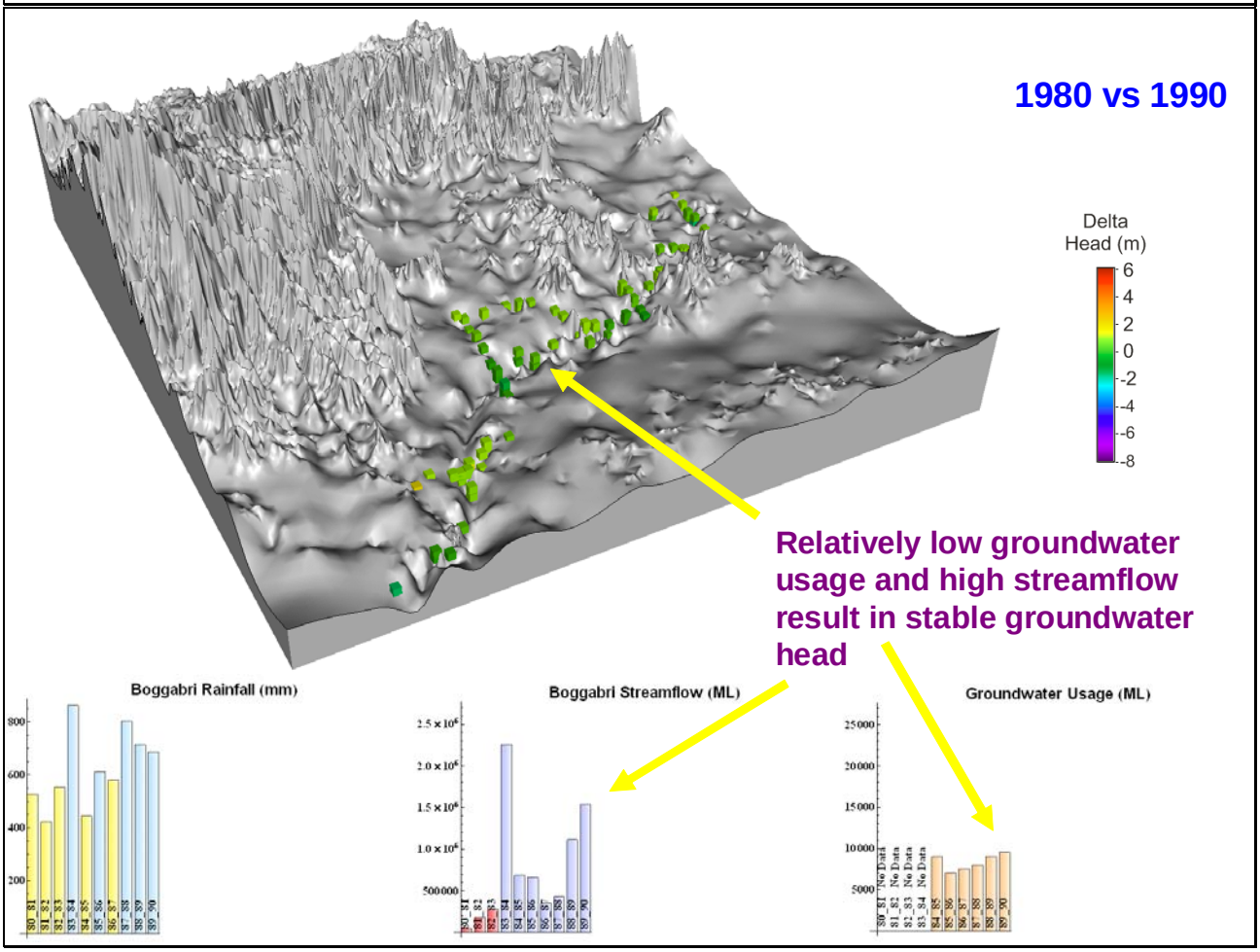
1980 vs 1990
Delta Head (m)
6
4
2
0
-2
-4
-6
-8
Relatively low groundwater usage and high streamflow result in stable groundwater head
Boggabri Rainfall (mm)
Boggabri Streamflow (ML)
Groundwater Usage (ML)

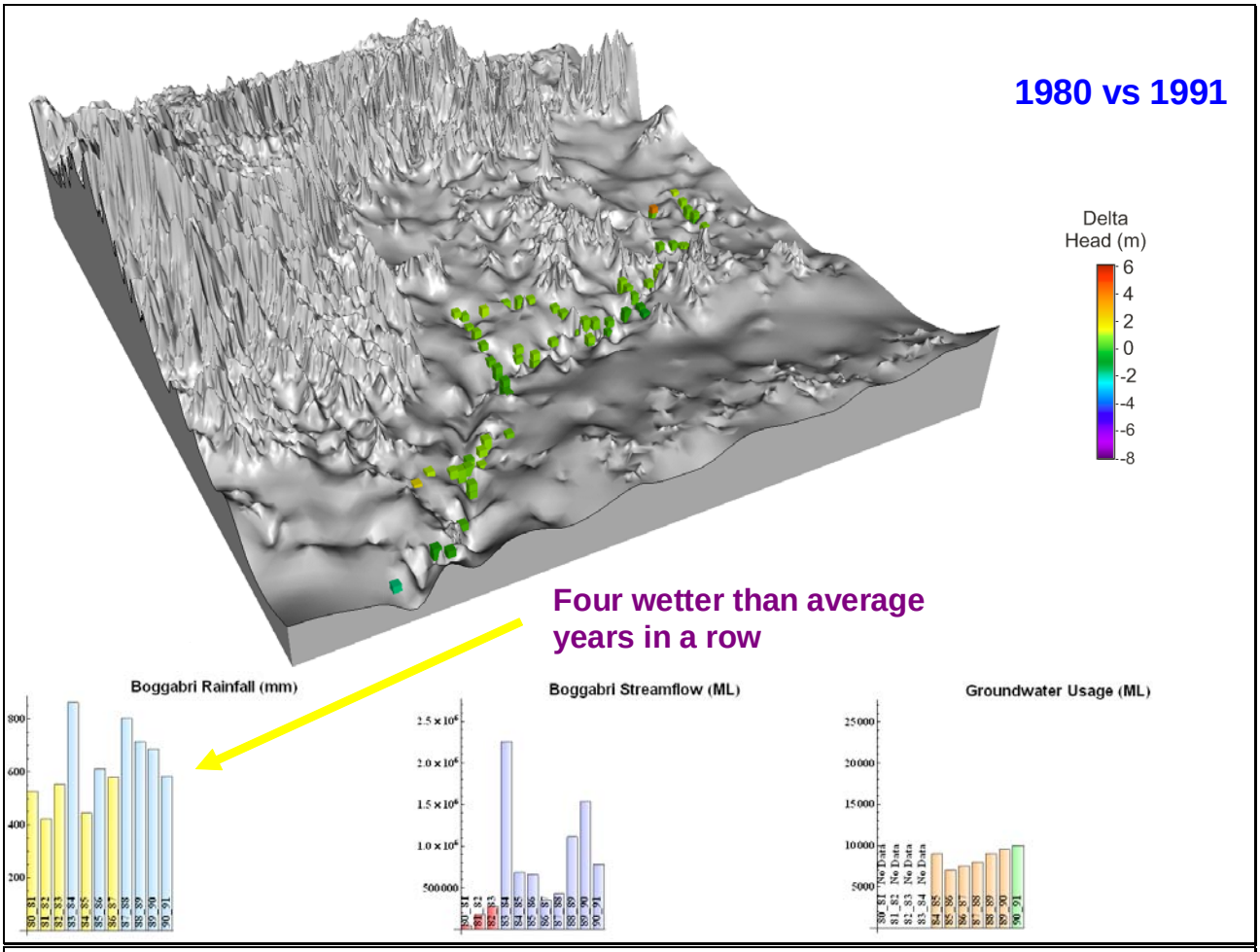
1980 vs 1991
Delta Head (m)
6
4
2
0
-2
-4
-6
-8
Four wetter than average years in a row
Boggabri Rainfall (mm)
Boggabri Streamflow (ML)
Groundwater Usage (ML)

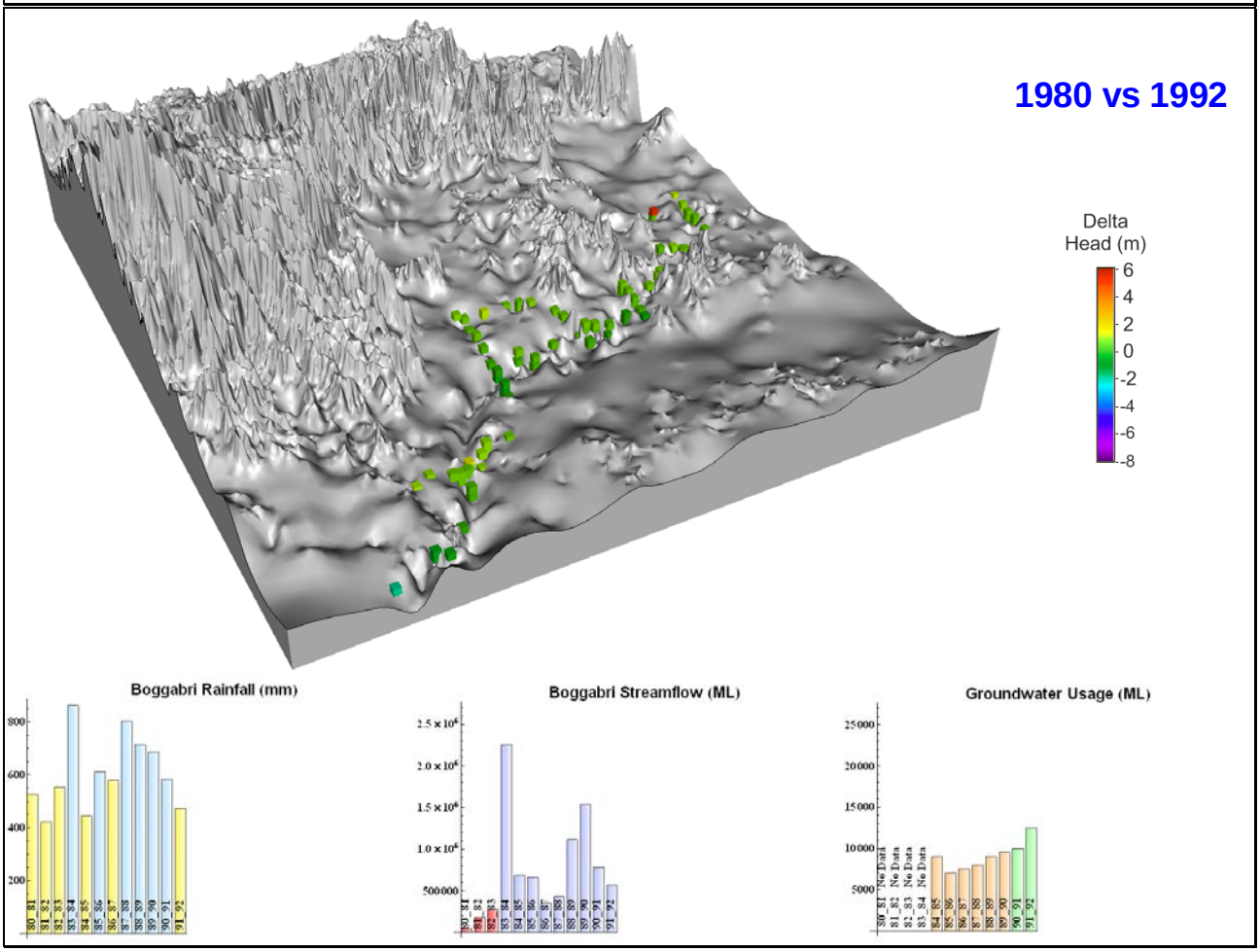
1980 vs 1992
Delta Head (m)
6
4
2
0
-2
-4
-6
-8
Boggabri Rainfall (mm)
Boggabri Streamflow (ML)
Groundwater Usage (ML)

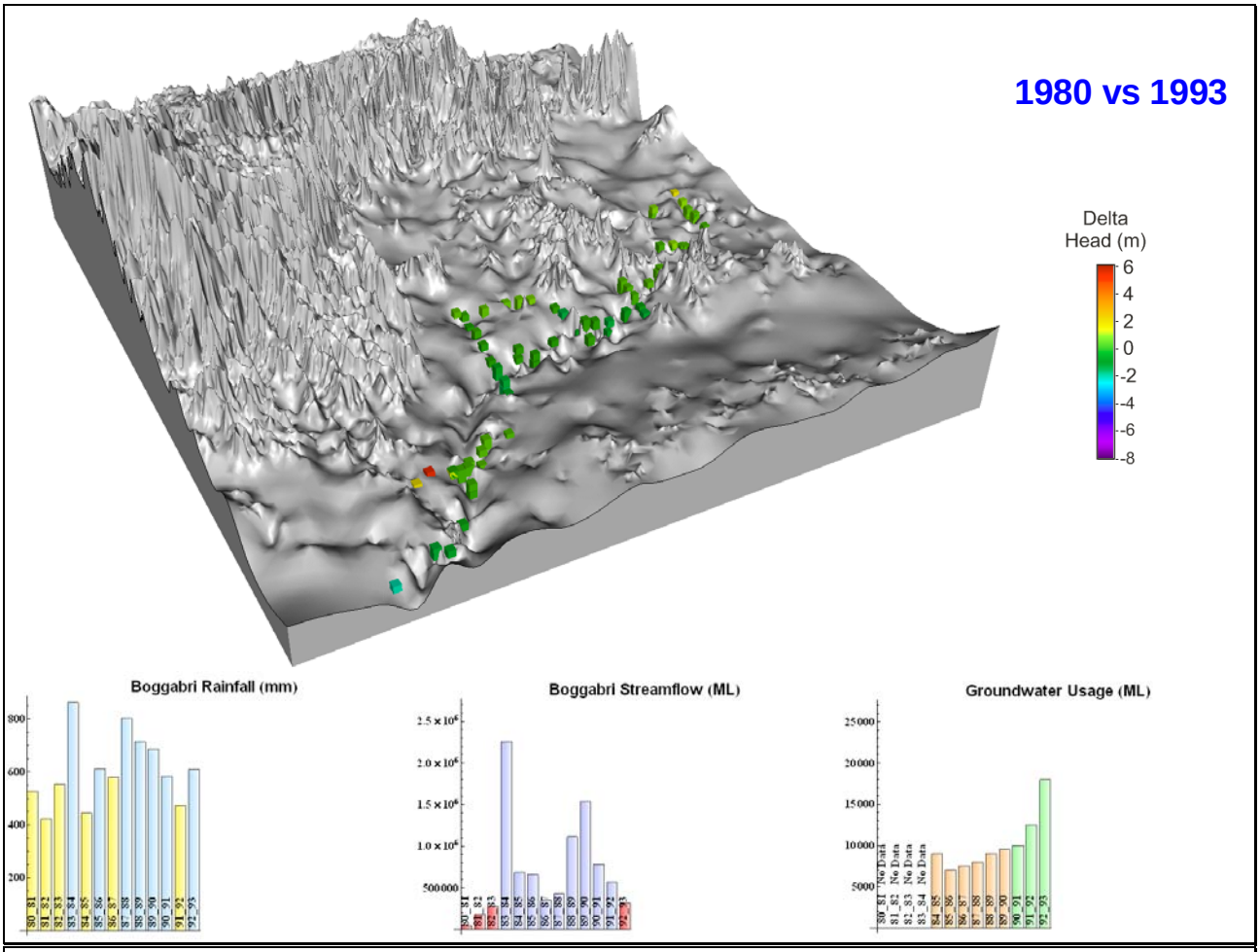
1980 vs 1993
Delta Head (m)
6
4
2
0
-2
-4
-6
-8
Boggabri Rainfall (mm)
Boggabri Streamflow (ML)
Groundwater Usage (ML)

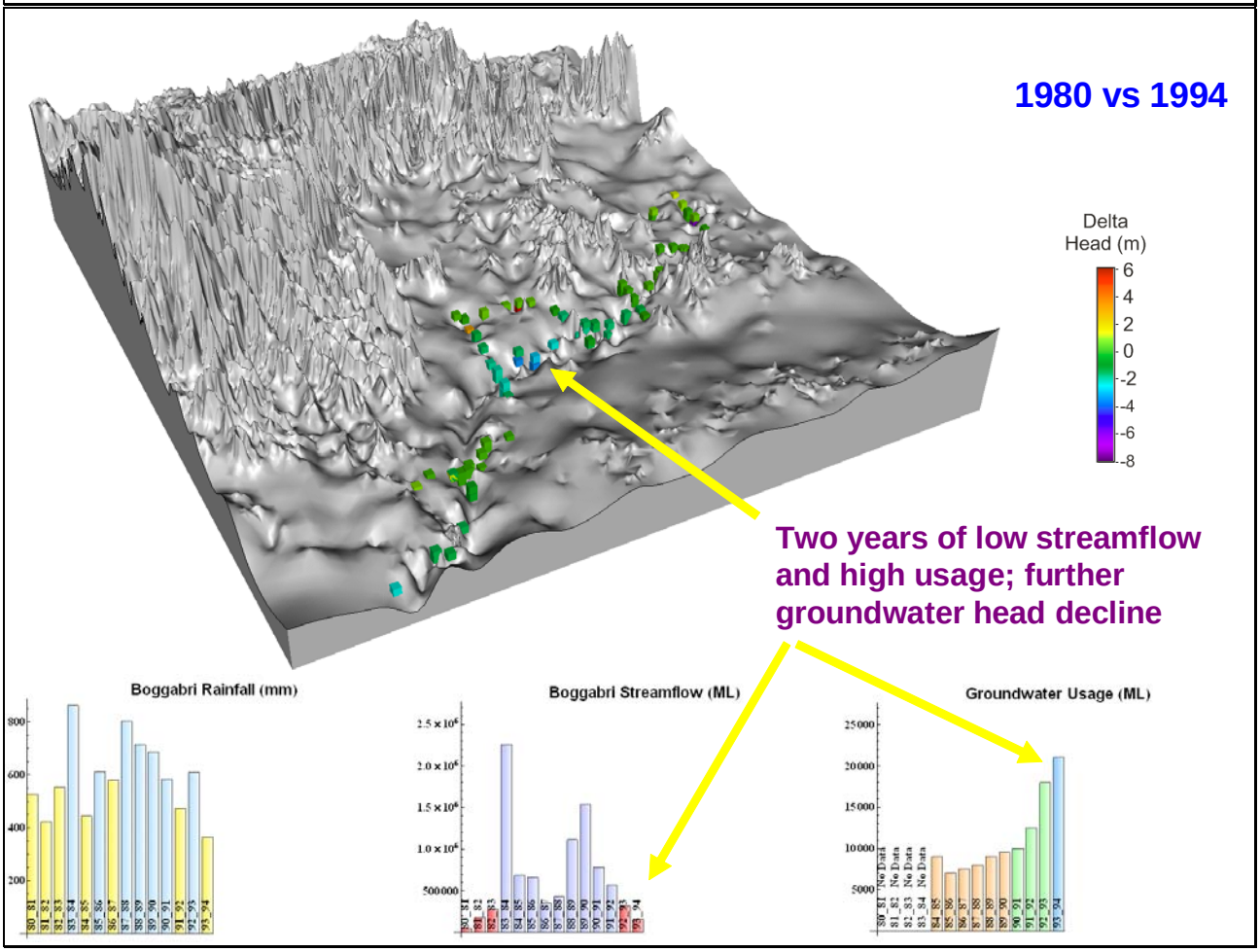
1980 vs 1994
Delta Head (m)
6
4
2
0
-2
-4
-6
-8
Two years of low streamflow and high usage; further groundwater head decline
Boggabri Rainfall (mm)
Boggabri Streamflow (ML)
Groundwater Usage (ML)

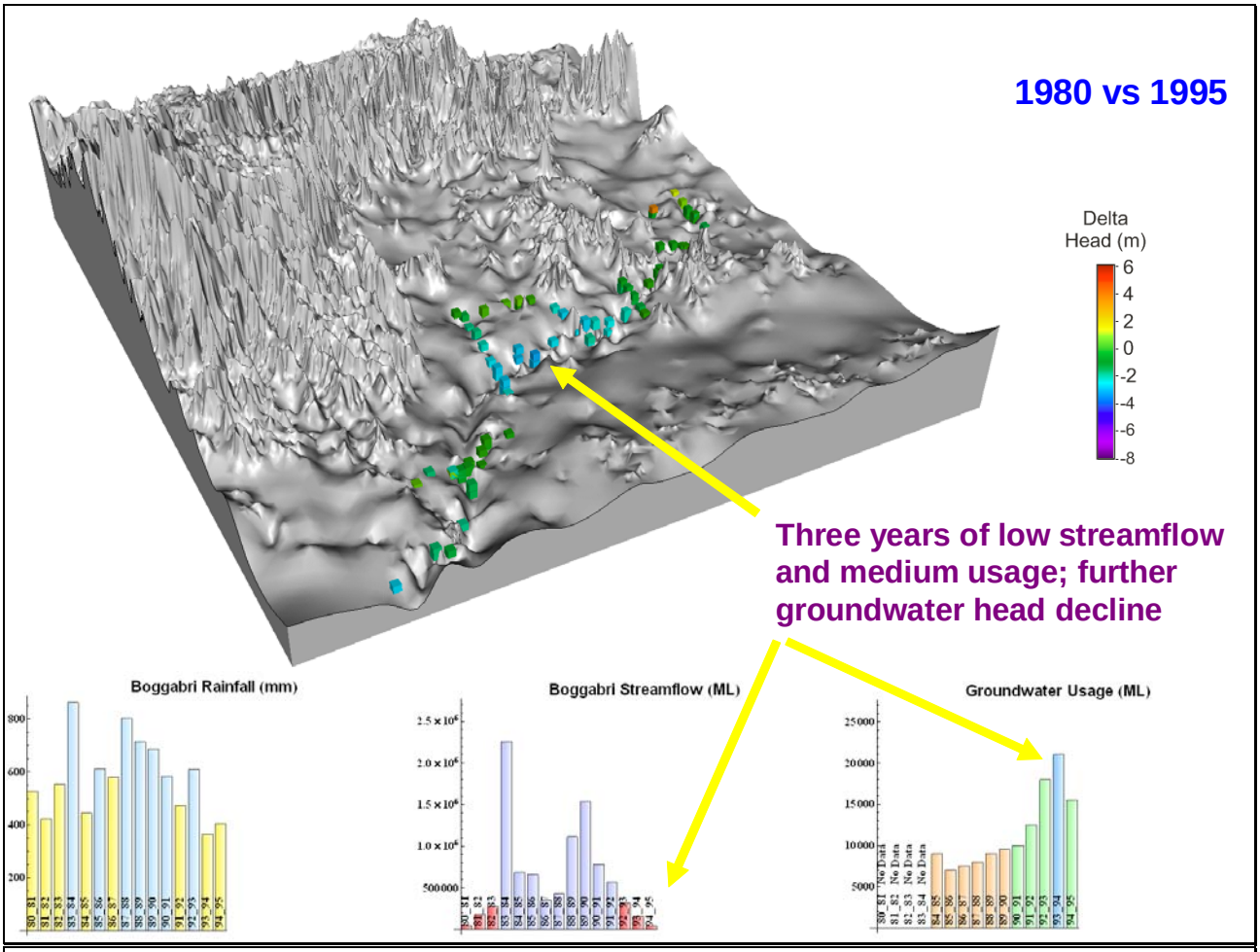
1980 vs 1995
Delta Head (m)
6
4
2
0
-2
-4
-6
-8
Three years of low streamflow and medium usage; further groundwater head decline
Boggabri Rainfall (mm)
Boggabri Streamflow (ML)
Groundwater Usage (ML)

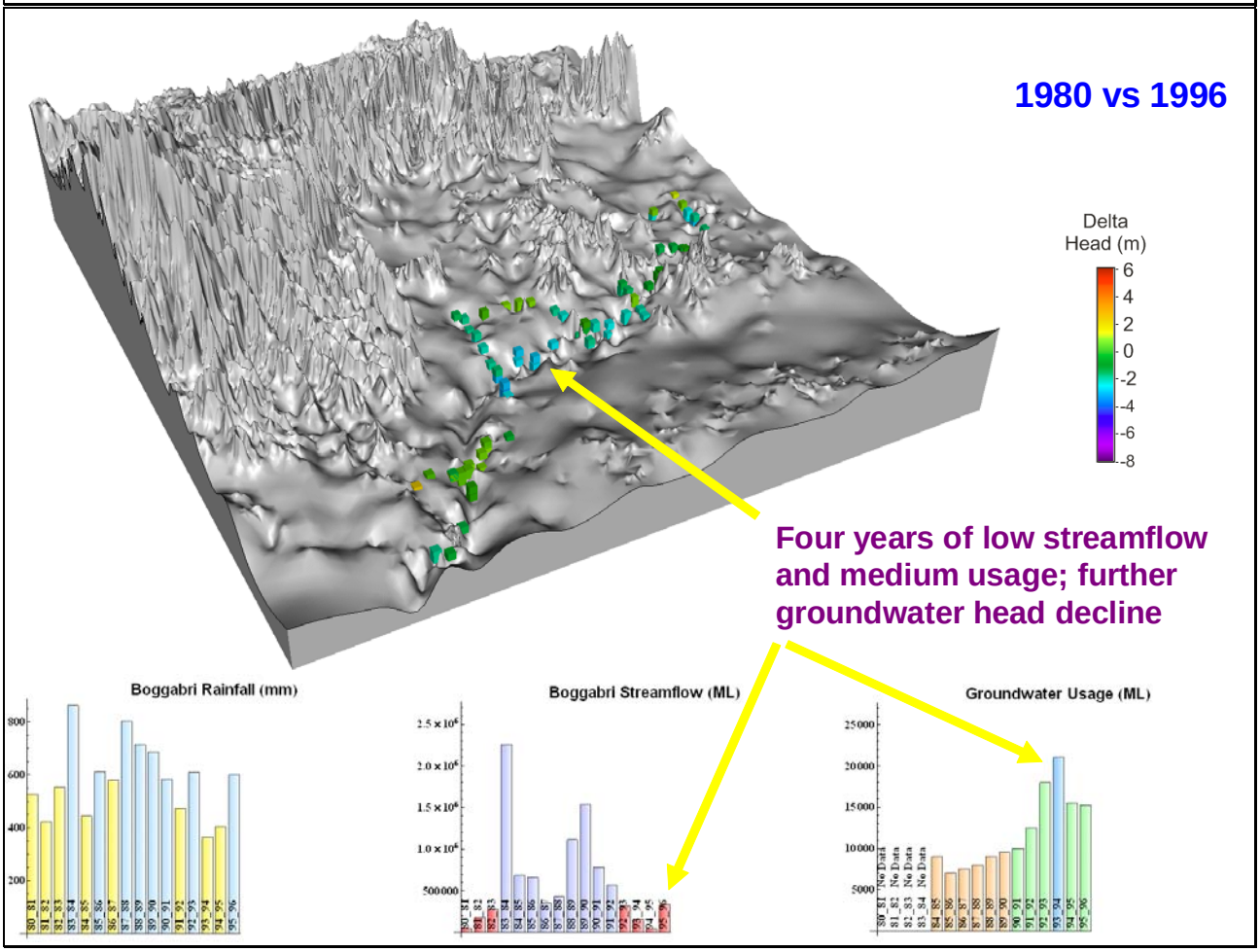
1980 vs 1996
Delta Head (m)
6
4
2
0
-2
-4
-6
-8
Four years of low streamflow and medium usage; further groundwater head decline
Boggabri Rainfall (mm)
Boggabri Streamflow (ML)
Groundwater Usage (ML)

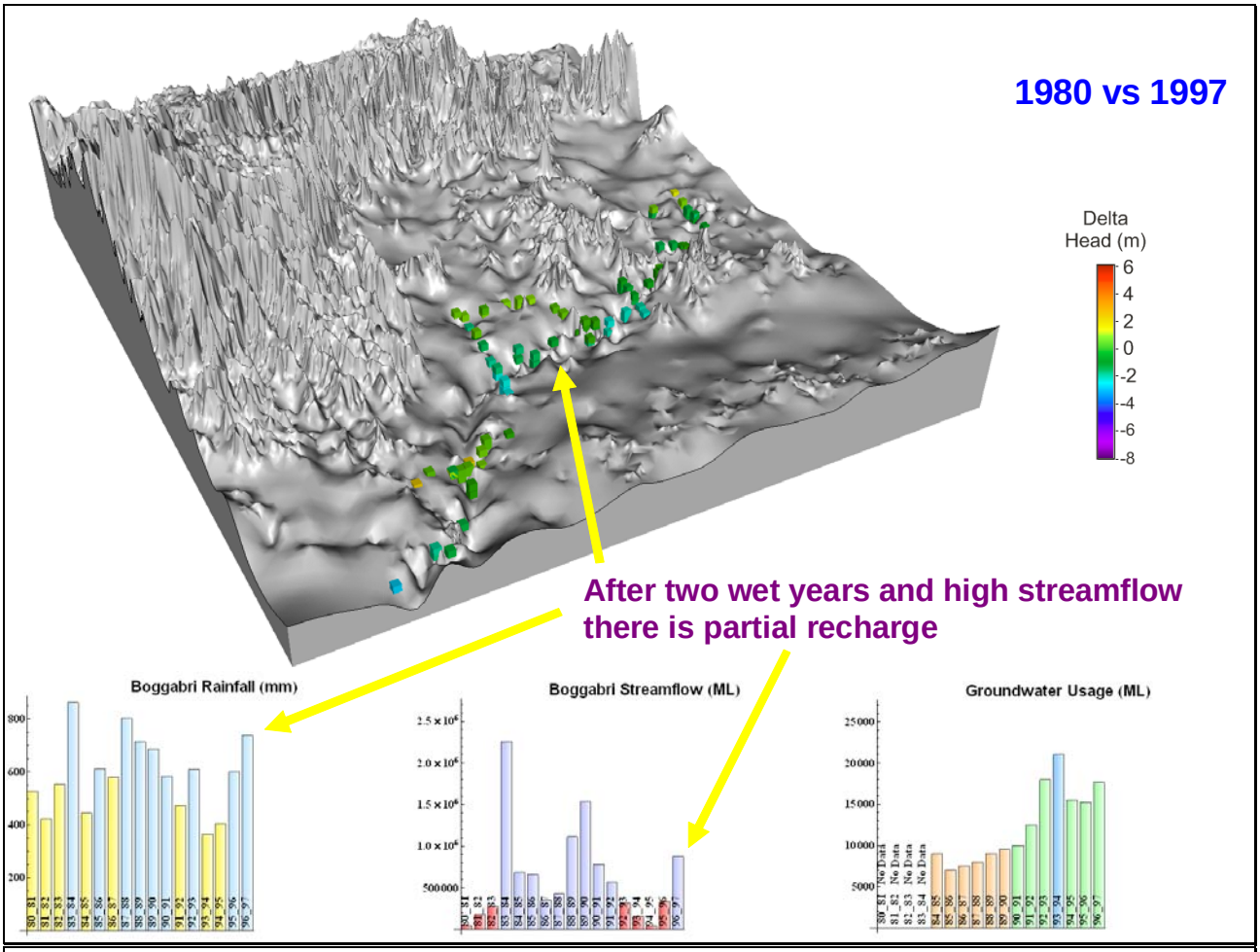
1980 vs 1997
Delta Head (m)
6
4
2
0
-2
-4
-6
-8
After two wet years and high streamflow there is partial recharge
Boggabri Rainfall (mm)
Boggabri Streamflow (ML)
Groundwater Usage (ML)

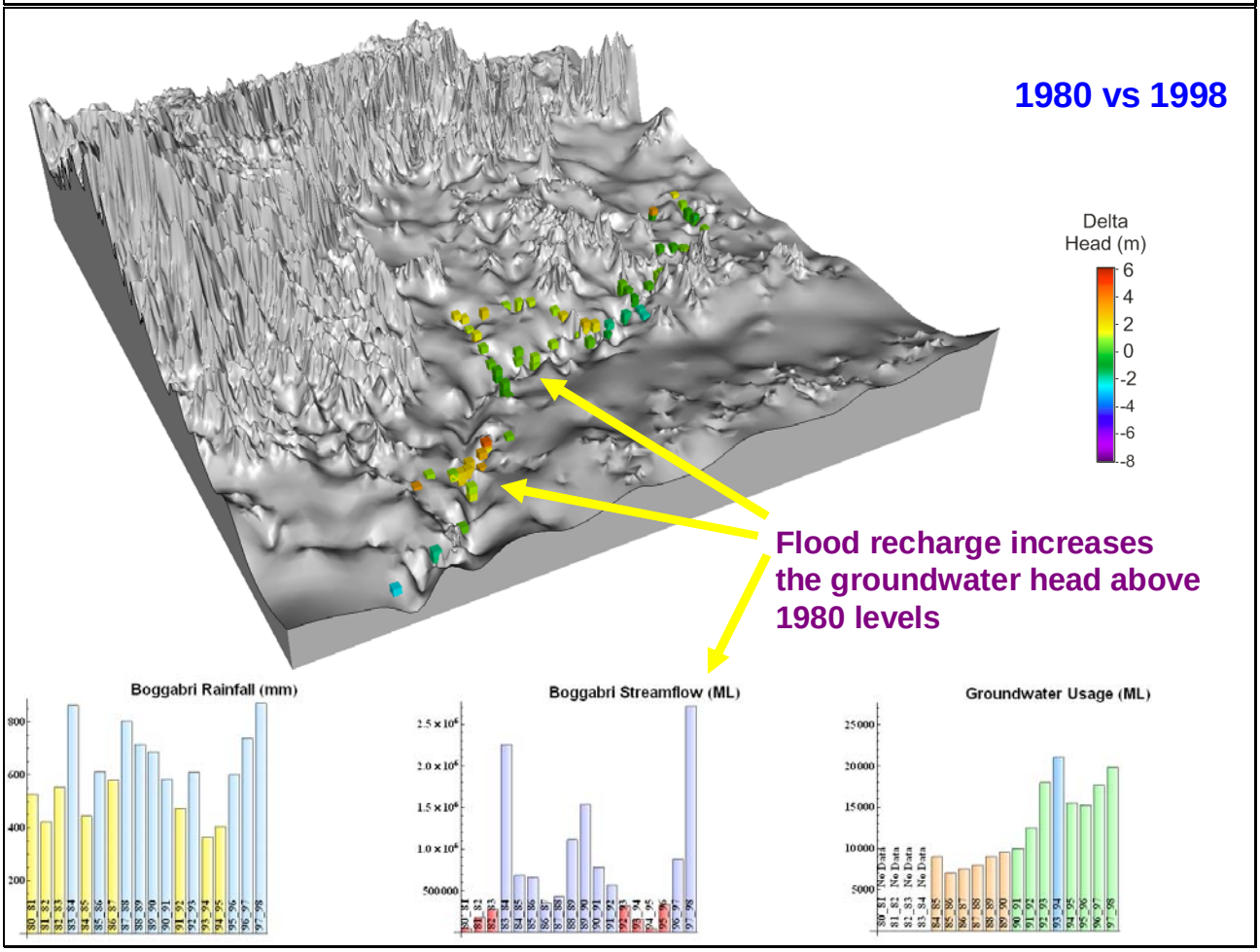
1980 vs 1998
Delta Head (m)
6
4
2
0
-2
-4
-6
-8
Flood recharge increases the groundwater head above 1980 levels
Boggabri Rainfall (mm)
Boggabri Streamflow (ML)
Groundwater Usage (ML)

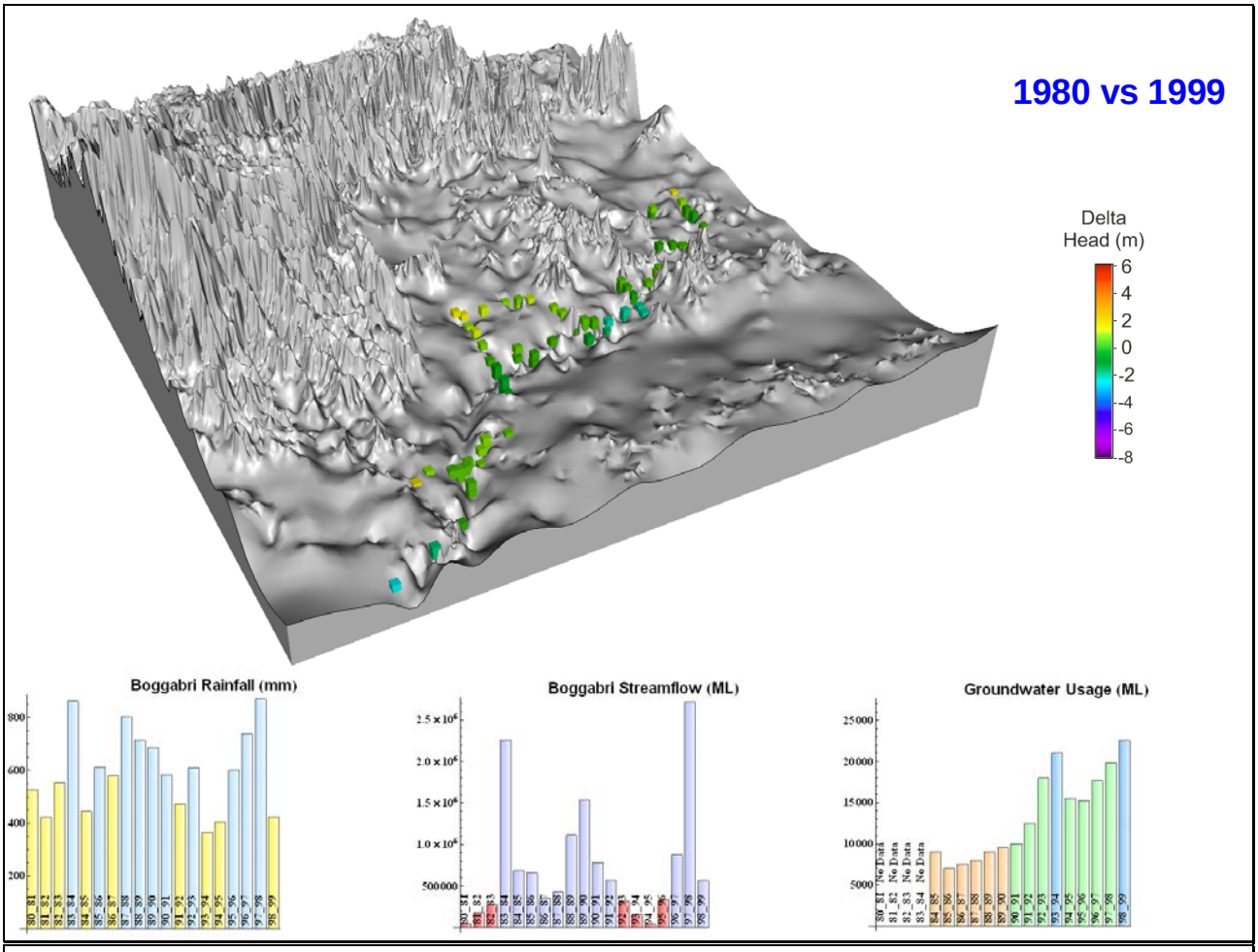
1980 vs 1999
Delta Head (m)
6
4
2
0
-2
-4
-6
-8
Boggabri Rainfall (mm)
Boggabri Streamflow (ML)
Groundwater Usage (ML)

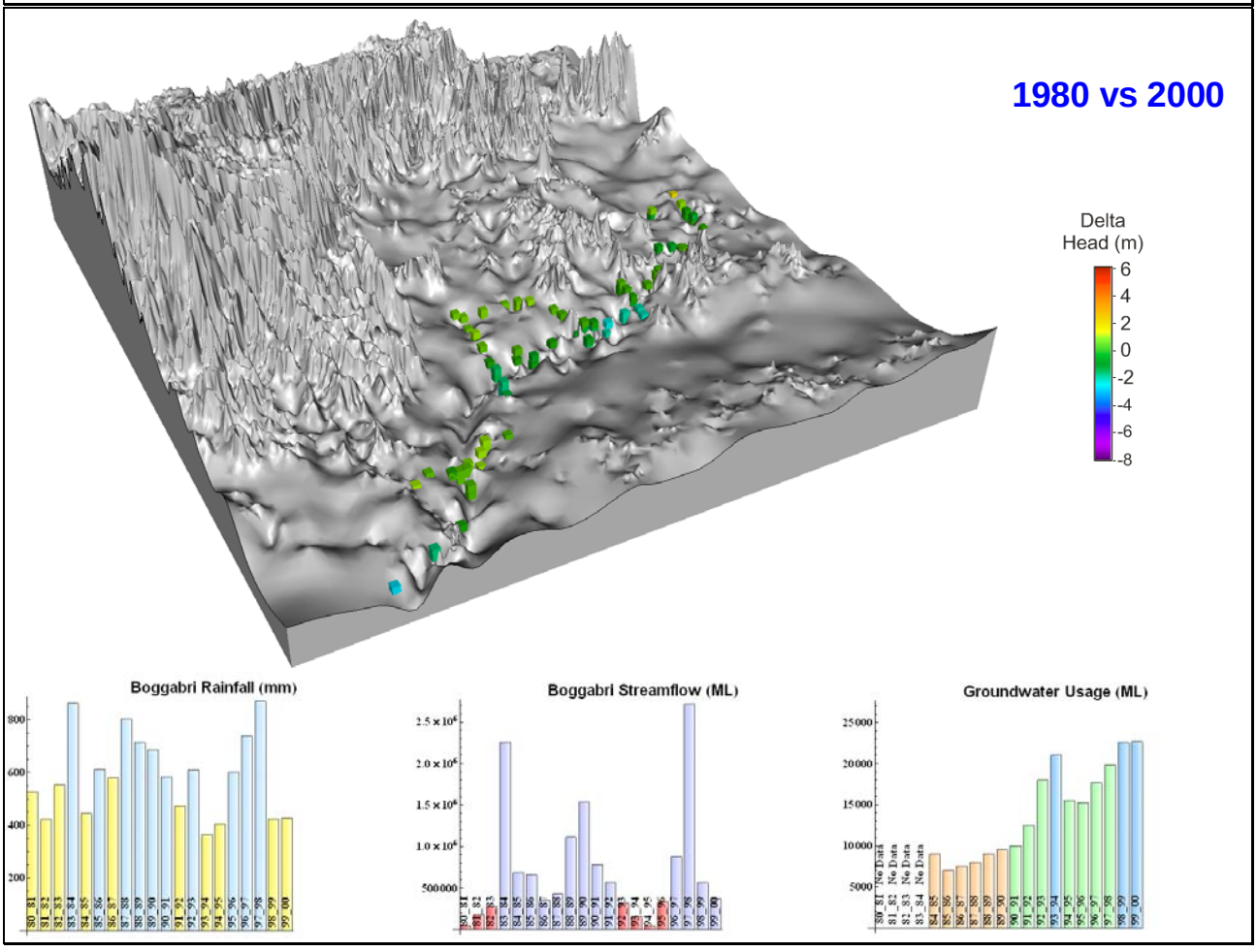
1980 vs 2000
Delta Head (m)
6
4
2
0
-2
-4
-6
-8
Boggabri Rainfall (mm)
Boggabri Streamflow (ML)
Groundwater Usage (ML)

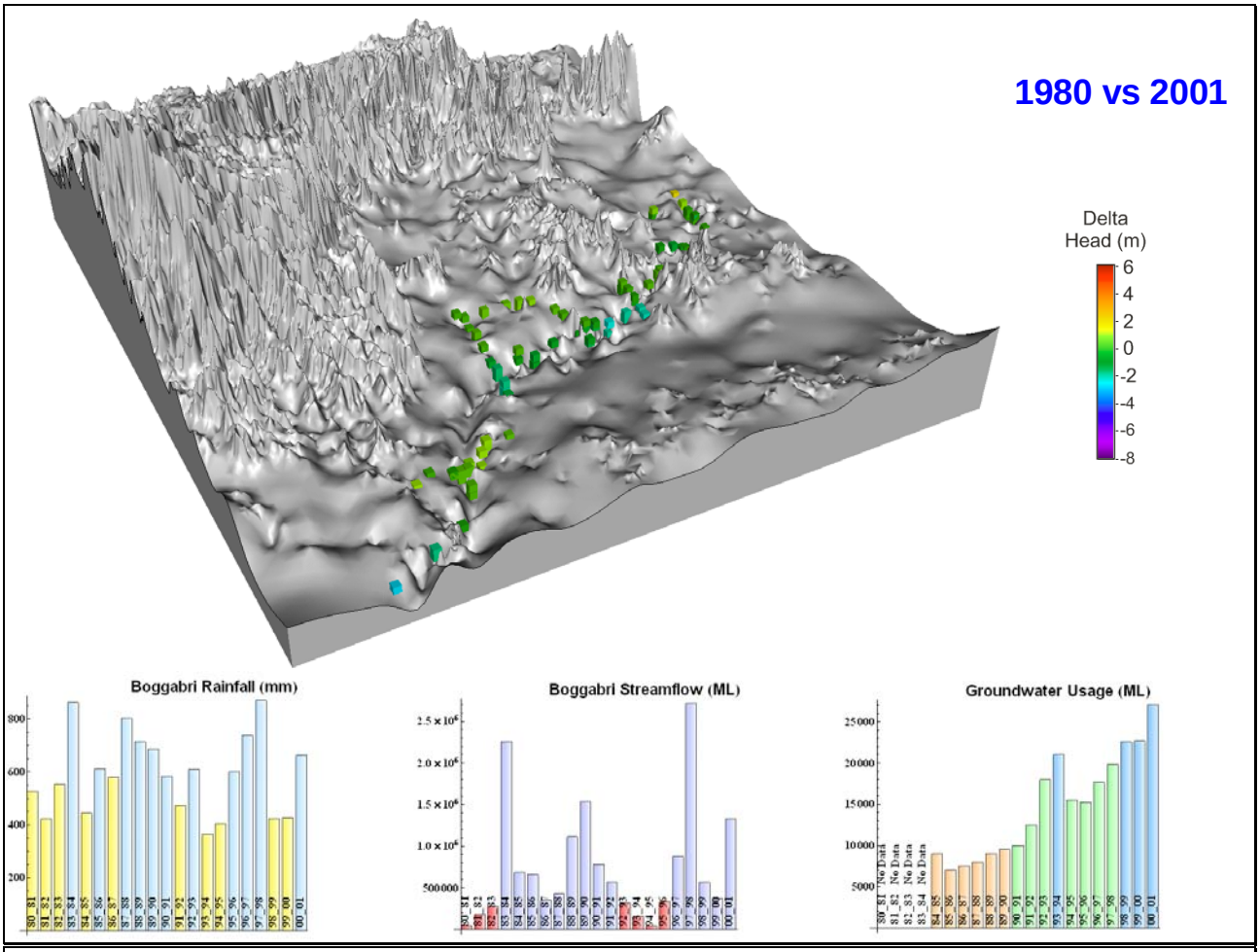
1980 vs 2001
Delta Head (m)
6
4
2
0
-2
-4
-6
-8
Boggabri Rainfall (mm)
Boggabri Streamflow (ML)
Groundwater Usage (ML)

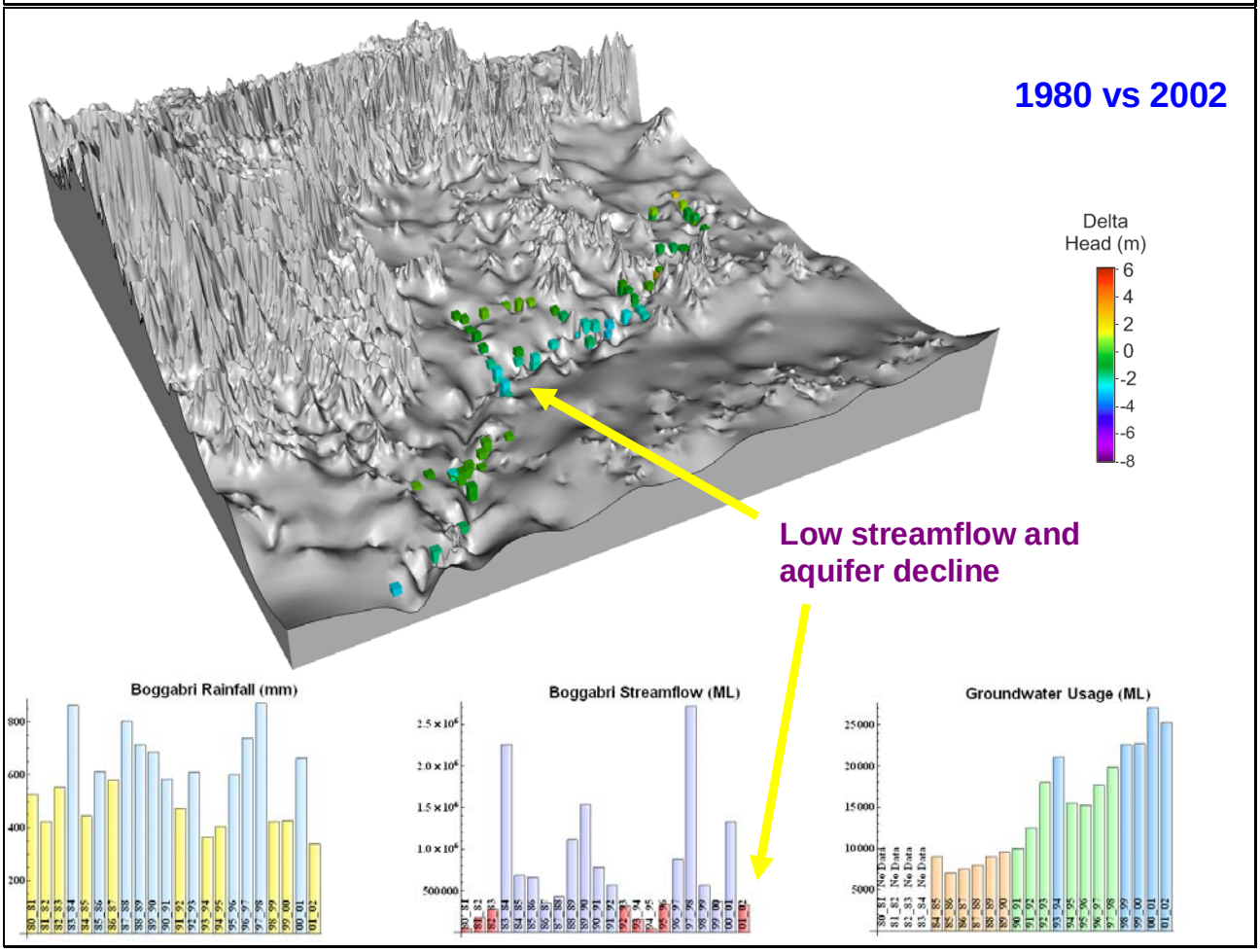
1980 vs 2002
Delta Head (m)
6
4
2
0
-2
-4
-6
-8
Low streamflow and aquifer decline
Boggabri Rainfall (mm)
Boggabri Streamflow (ML)
Groundwater Usage (ML)

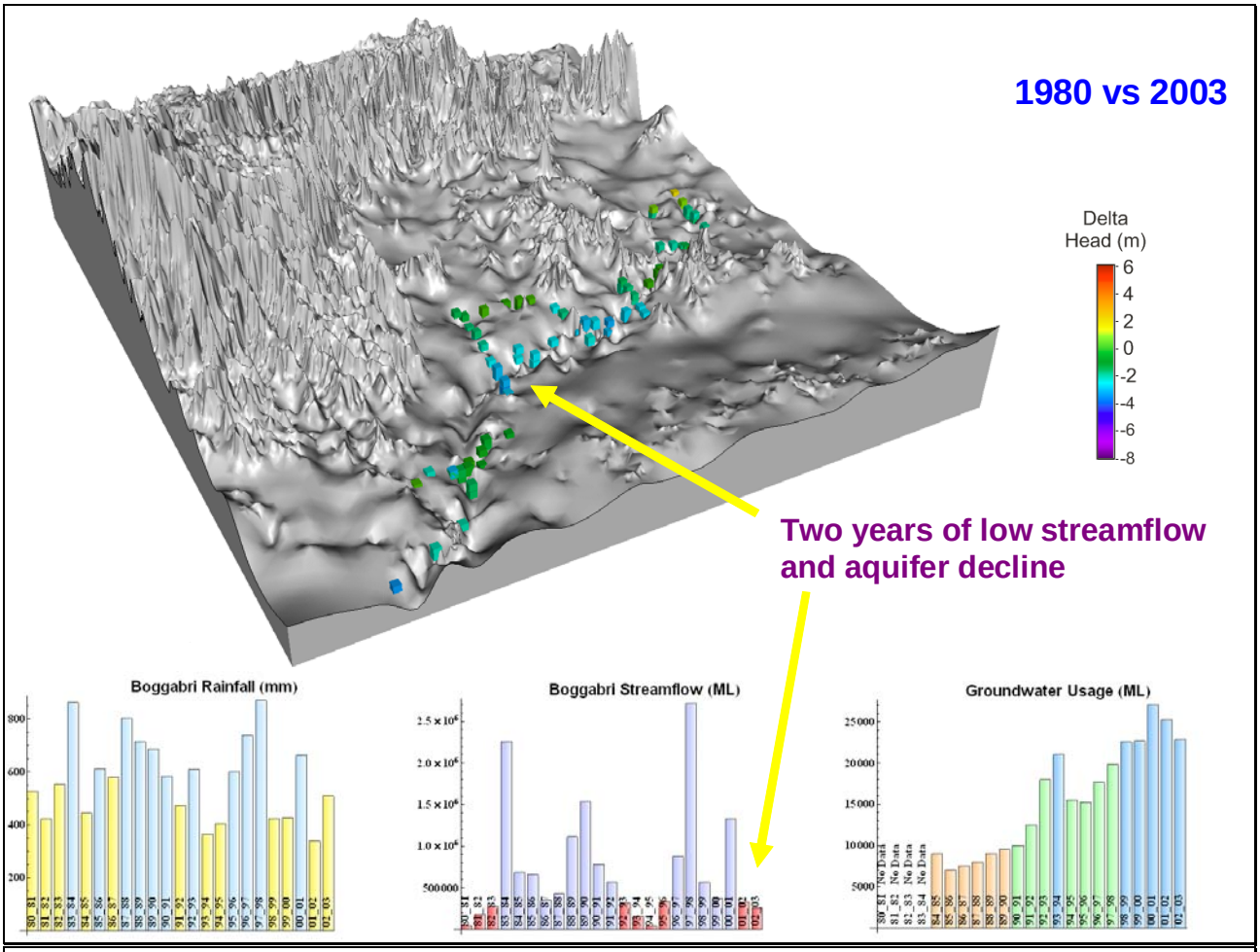
1980 vs 2003
Delta Head (m)
6
4
2
0
-2
-4
-6
-8
Two years of low streamflow and aquifer decline
Boggabri Rainfall (mm)
Boggabri Streamflow (ML)
Groundwater Usage (ML)

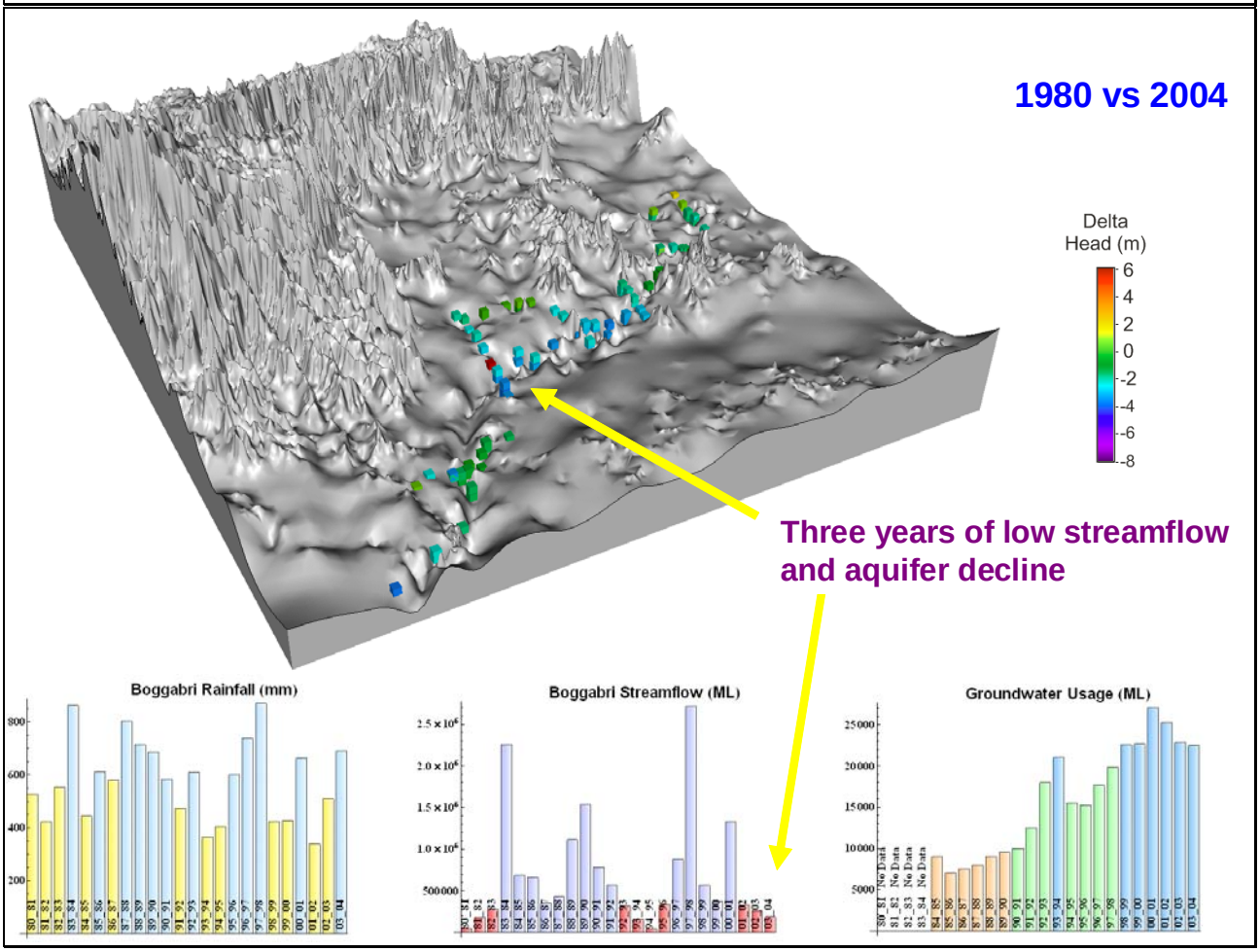
1980 vs 2004
Delta Head (m)
6
4
2
0
-2
-4
-6
-8
Three years of low streamflow and aquifer decline
Boggabri Rainfall (mm)
Boggabri Streamflow (ML)
Groundwater Usage (ML)

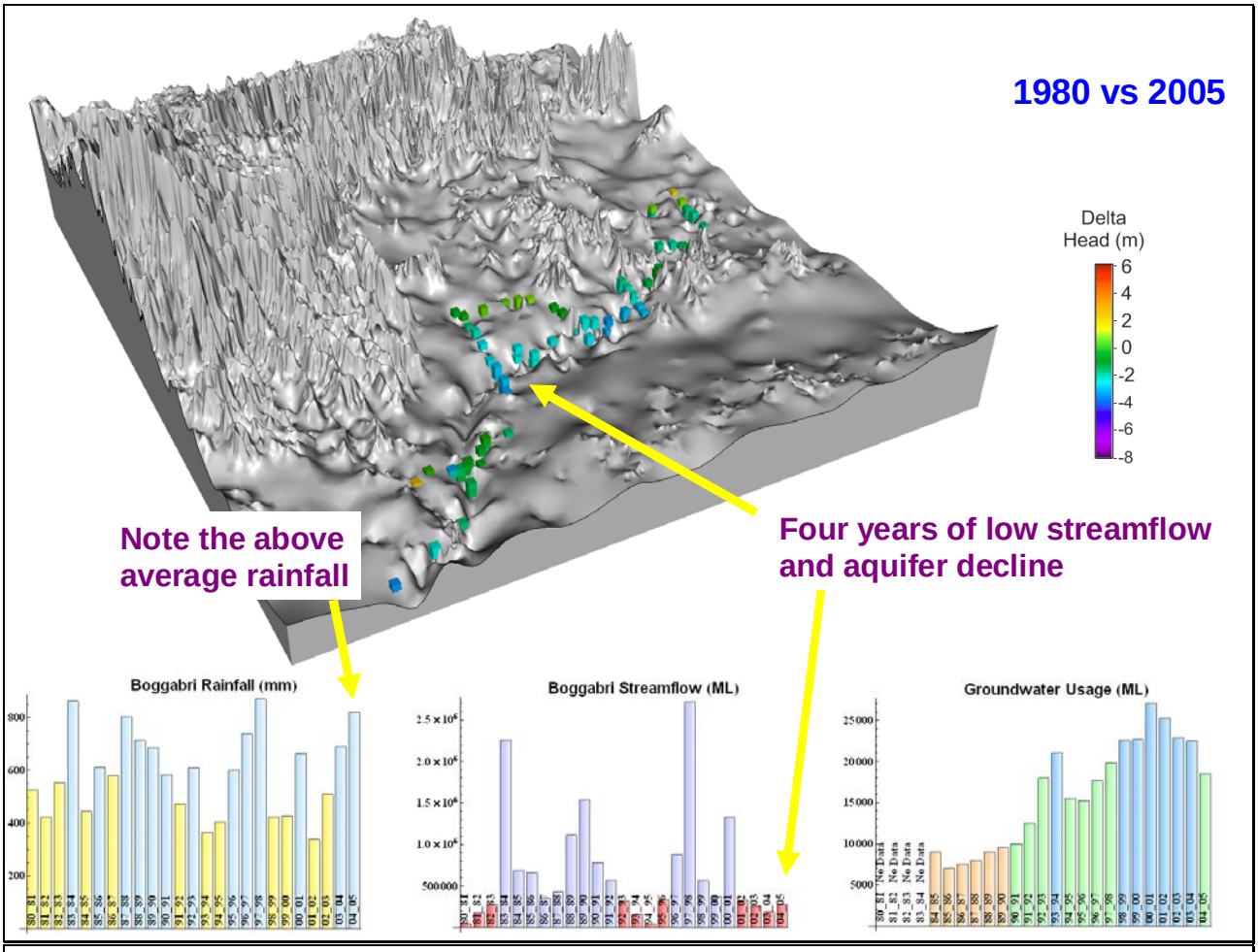
1980 vs 2005
Delta Head (m)
6
4
2
0
-2
-4
-6
-8
Note the above average rainfall
Four years of low streamflow and aquifer decline
Boggabri Rainfall (mm)
Boggabri Streamflow (ML)
Groundwater Usage (ML)

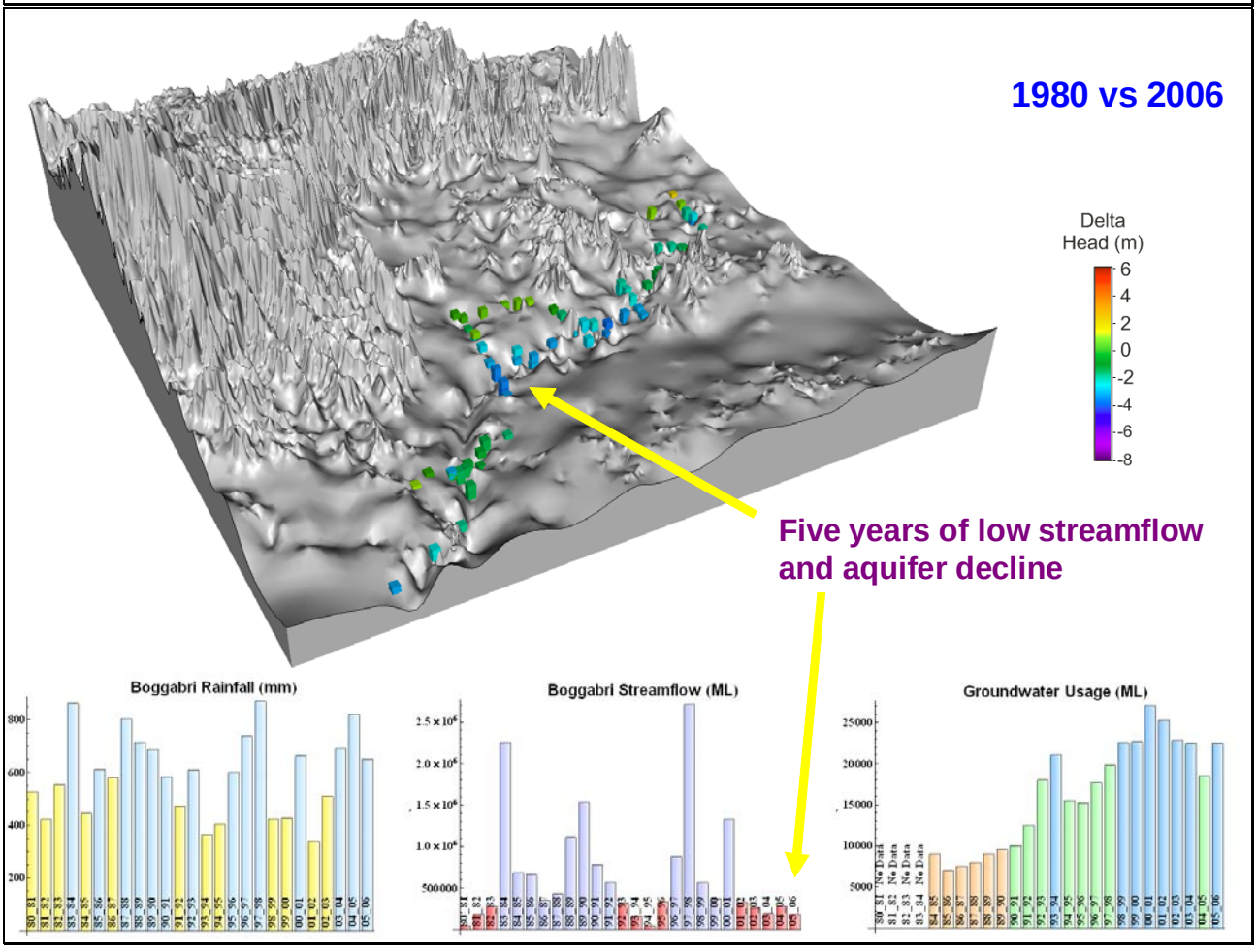
1980 vs 2006
Delta Head (m)
6
4
2
0
-2
-4
-6
-8
Five years of low streamflow and aquifer decline
Boggabri Rainfall (mm)
Boggabri Streamflow (ML)
Groundwater Usage (ML)

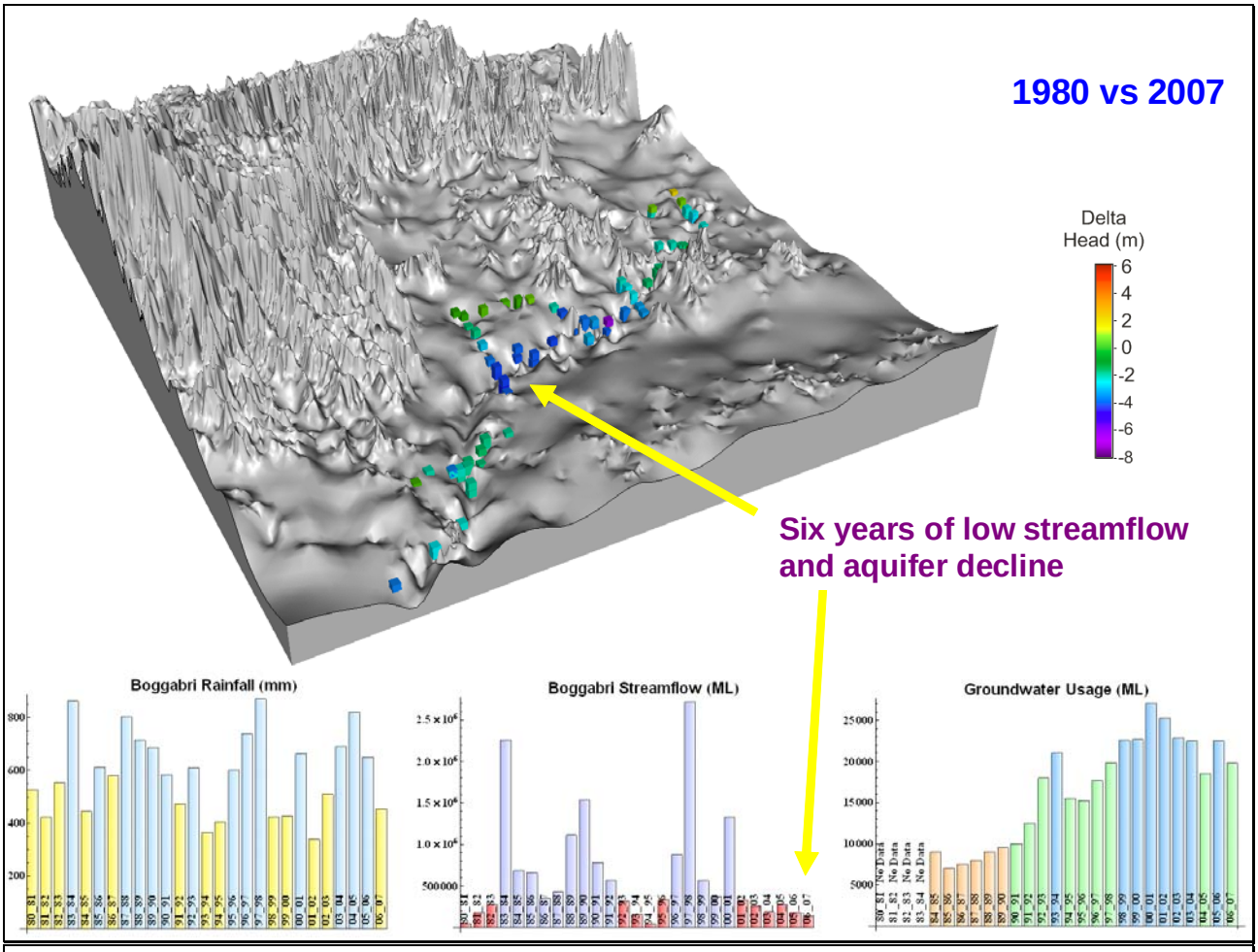
1980 vs 2007
Delta Head (m)
6
4
2
0
-2
-4
-6
-8
Six years of low streamflow and aquifer decline
Boggabri Rainfall (mm)
Boggabri Streamflow (ML)
Groundwater Usage (ML)

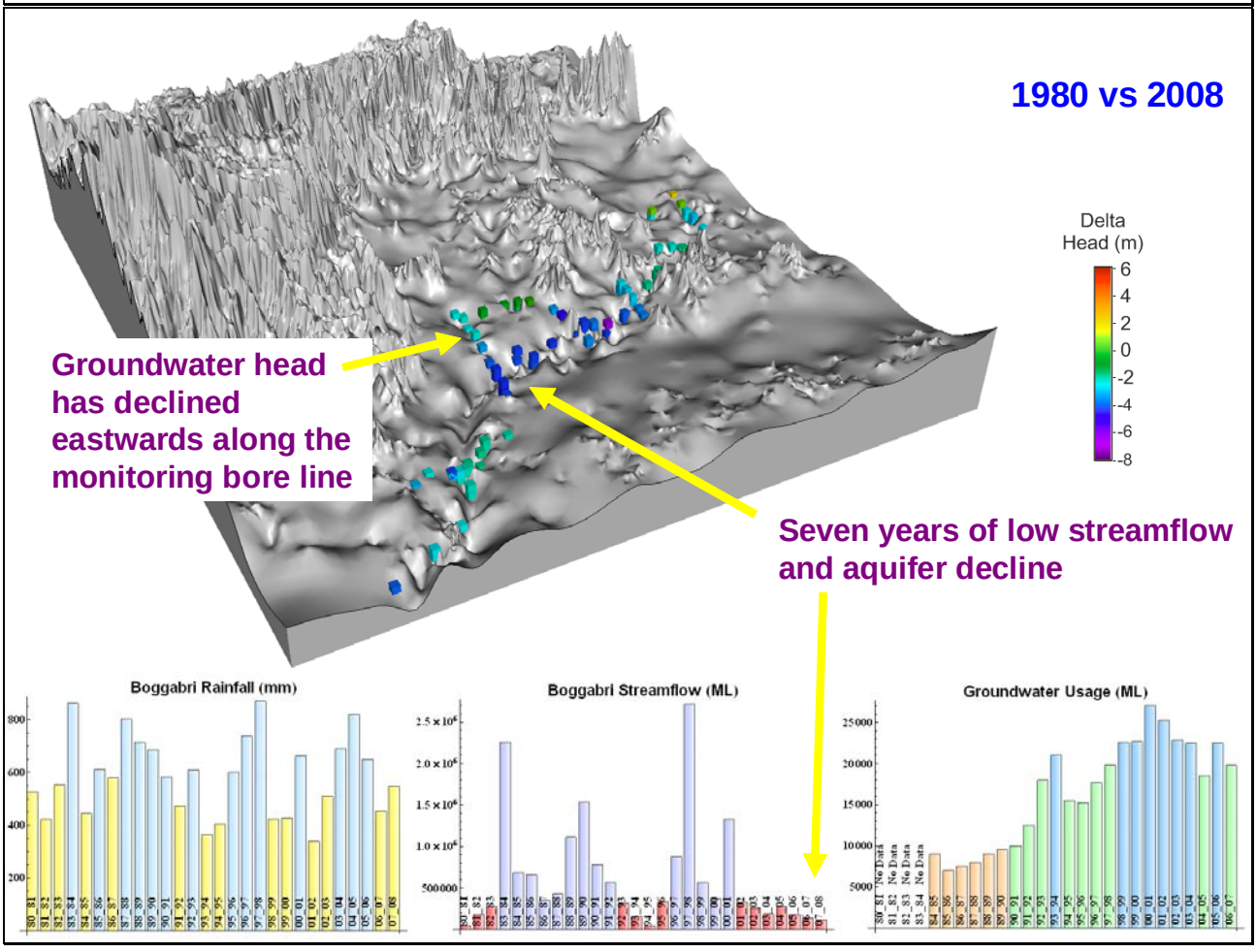
1980 vs 2008
Delta Head (m)
6
4
2
0
-2
-4
-6
-8
Groundwater head has declined eastwards along the monitoring bore line
Seven years of low streamflow and aquifer decline
Boggabri Rainfall (mm)
Boggabri Streamflow (ML)
Groundwater Usage (ML)

Data Sources

- Rainfall data
  - Australian Government Bureau of Meteorology
  - http://www.bom.gov.au/
- Streamflow data
  - NSW Government Historic data DVD "PINNEENA" for Continuous Monitoring
  - http://www.waterinfo.nsw.gov.au/pinneena/cm.shtml
- Groundwater head measurements:
  - NSW Government Historic data CD "PINNEENA" for Groundwater Works
  - http://www.waterinfo.nsw.gov.au/pinneena/gw.shtml
- Groundwater usage:
  - 1996 to 2008 data supplied by the NSW Department of Water and Energy
  - 1984 to 1995 data from:

    Upper Namoi Valley Groundwater Status Report 2004, Department of Infrastructure, Planning and Natural Resources, draft 22 June 2006.

Project Funding

- National Water Commission

  "Development of a 3D geological Mapping and Database Interface to Support Interconnected Groundwater and Surface Water Management (Upper Namoi Between Narrabri and Boggabri, and Maules Creek, Horsearm Creek and Namoi systems, NSW)"
- Namoi Catchment Management Authority
- Cotton Catchment Communities CRC

  "Surface Water Groundwater Interconnectivity Investigation"

Australian Government
National Water Commission

Namoi CMA Catchment Management Authority

Cotton Catchment Communities CRC

Connected Waters Initiative

A Research Centre at
The University of New South Wales

The CWI team working on Maules Creek

Professor Ian Acworth
A/Professor Bryce Kelly
Dr. Martin Andersen
Dr. Beatrice Giambastiani
Dr. Wendy Timms
Doug Anderson
Anna Greve
Andrew McCallum
Gabriel Rau
Hamish Studholme

UNSW THE UNIVERSITY OF NEW SOUTH WALES SYDNEY • AUSTRALIA

UNSW CONNECTED WATERS

Thank You

www.connectedwaters.unsw.edu.au

Updated almost weekly!

General news & articles
Fact sheets
Research updates
Poster downloads
Publications
Journal abstracts
Team & alumni

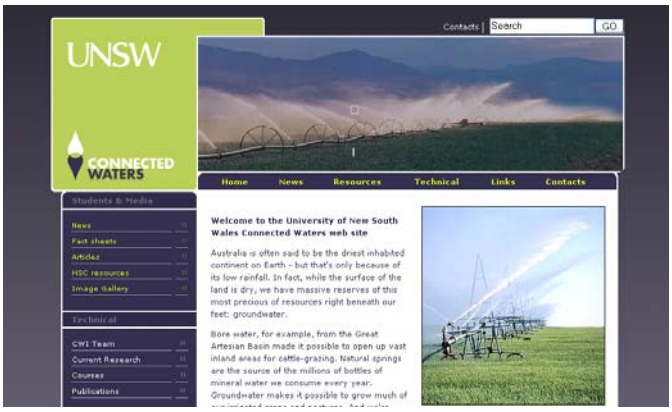

UNSW - School of Civil and Environmental Engineering
Water Research Laboratory

Appendix 10

Maules Creek Groundwater Chemistry

A10. 1 Introduction

In this appendix are four papers about the groundwater chemistry in the Maules Creek Catchment and adjacent reach of the Namoi River. These papers make use of the water chemistry data stored in the MS Access database.

A10. 2 Papers

Andersen M.S. & Acworth R.I. (2007): **Hydrochemical investigations of surface water groundwater interactions in a sub-catchment in the Namoi Valley, NSW, Australia.** *Proceedings of the XXXV IAH Congress "Groundwater and Ecosystems", Lisbon. September, 2007.*

Andersen M.S., Meredith K., Timms W. & Acworth R.I. (2008): **Investigation of δ18O and δ2H in the Namoi River catchment – elucidating recharge sources and the extent of surface water/groundwater interaction**. *XXXVI IAH Congress Toyama, Japan 26th of October - 1st of November 2008.*

Patterson J., Andersen M.S. & Acworth R.I. (2008): **Development of an integrated conceptual model of a connected surface water-groundwater system using a hydrochemical approach at Maules Creek, NSW, Australia.** *XXXVI IAH Congress Toyama, Japan 26th of October - 1st of November 2008.*

Andersen, M.S., and Acworth, I.R. (2009) **Stream-aquifer interactions in the Maules Creek catchment, Namoi Valley, New South Wales,** Australia Hydrogeology Journal, 17: 2005 - 2021. doi:10.1007/s10040-009-0500-9

Hydrochemical investigations of surface water groundwater interactions in a sub-catchment in the Namoi Valley, NSW, Australia

Martin S. ANDERSEN and R. Ian ACWORTH

Water Research Laboratory, School of Civil and Environmental Engineering, University of New South Wales, Australia m.andersen@wrl.unsw.edu.au; i.acworth@unsw.edu.au

Abstract Surface water and groundwater chemistry were studied in an alluvial catchment. Electrical conductivity (EC) was found to vary in a complex pattern in the catchment reflecting different sources of water as well as water rock interactions within the aquifer. Generally EC and major dissolved ions increased in the aquifer along the hydraulic gradient due to leaching of salts from clayey lithologies and weathering of minerals. A redox sequence was observed with anoxic conditions developing along the hydraulic gradient, and in particular near the Namoi River. The variations in EC; major dissolved ion composition; and redox sensitive species were used to identify possible zones of surface water groundwater interactions and flow directions. The results of this study show how natural hydrochemical tracers can be used to unravel surface water groundwater interactions. In addition understanding the hydrochemical processes may give important insight in the possible fate of various organic and inorganic pollutants linked to the infiltration of surface water or discharge of groundwater.

Keywords: Surface water groundwater interactions, hydrochemistry, water quality.

1. Introduction

Quantifying surface water and groundwater interactions over larger scales is often hampered by the lack of sufficiently detailed hydrogeological and stratigraphical data. In general, observed head gradients may indicate the potential for water flow between water bodies. However, hydraulic connectivity can not necessarily be inferred from such data within a heterogeneous geology (Cey et al 1998). Important clues about subsurface water flow and thus interconnectivity may be gained from studying the distribution of injected or natural tracers. Natural tracers have the advantage of being far simpler to utilize than tracer tests, which may be expensive, time consuming and often only applicable on a relatively limited scale (Kalbus et al. 2006). However, the use of natural tracers requires that there are natural contrasts in water chemistry between the water bodies of interest. In addition, a prerequisite for using reactive chemical species is that chemical reactions affecting these species can be understood and quantified. To test the use of natural hydrochemical tracers for studying connected surface water groundwater systems, groundwater and surface water samples were collected in the Maules Creek catchment of the Namoi Valley, NSW, Australia. The flow in Maules Creek appears to be dominantly controlled by surface water groundwater interactions, which makes it a well suited field site (see Andersen and Acworth this issue).

2. Method

Groundwater samples from monitoring piezometers (10-110 m deep) and surface water samples from Maules Creek and the Namoi River were collected at the beginning of August 2006.

2.1. Groundwater and surface water sampling

Generally piezometers were purged one well volume with a pump placed just below the standing water level in the well. Subsequently a groundwater sample was retrieved from the middle of the screened interval. Most groundwater samples were retrieved using a Bennett air driven sample pump (Model: 1800-8). For shallow wells (<30 m) the pump was lowered to the middle of the screened interval. For deeper wells (> 30 m) the pump intake was detached and extended downwards by adding tubes to the bottom of the pump. In this way samples could be retrieved from as deep as 80 m. Wells deeper than 80 m were sampled at this depth assuming that the water sampled represents fresh groundwater at the screen. Surface water samples were collected using a tube lowered to mid-water column. Luerlock syringes (60 mL) were used for collecting the samples.

2.2. Field Analysis

Redox-sensitive and volatile species (O_2, Fe^{2+}, H_2S and alkalinity) as well as pH, electrical conductivity (EC) and temperature were measured in the field. An inline flow-through cell (Sheffield-LFC, Waterra, SLF) prevented contact with the atmosphere and were used to obtain values of dissolved oxygen (DO), pH, EC and Eh and to monitor whether the piezometers were sufficiently purged for sampling. DO and pH were determined using a HACH portable meter (HQ40d) connected to a HACH luminescent (LDO101-03) oxygen probe and a HACH pH electrode (PHC301-03), respectively. A HACH SensION-156 EC-meter with a 4-pole conductivity probe was used to measure electrical conductivity (EC) and temperature. The redox potential (Eh) were measured by an Orion Platinum Redox electrode (model 96-78) connected to a TPS-meter (WP-80).

Water samples were collected directly from the sampling line without contact with the atmosphere using 60 ml Luerlock syringes (pre-rinsed 3-times in sample) and immediately filtered through Satorious minisart (Cellulose Acetate) 0.2 µm disposable filters. Sub-samples for major cations and minor trace elements were preserved in 20 ml PE-vials with 2% of 5 N HNO_3 and stored at 5°C for later analysis. The PE-vials for cations were pre-washed in a 10% HNO_3 solution. Sub-samples for anions were frozen in 10 ml PE-vials for later analysis. Samples for Dissolved Organic Carbon (DOC) were acidified with 1% concentrated H_2SO_4 and stored at 5°C in 40 ml amber glass vials for later analysis.

Alkalinity was measured in the field shortly after sample retrieval on a filtered 25 ml sub-sample by the Gran titration method (Stumm and Morgan 1981) using a HACH Digital Titrator Model 16900 and cartridges with 0.16 N H_2SO_4. The pH readings for the titration were measured by a TPS WP-81 pH and temperature meter and a TPS pH gel-electrode.

Ferrous iron (Fe^{2+}) and hydrogen sulfide (H_2S) were determined spectrophotometrically in the field on filtered sub-samples minutes within sample retrieval using a HACH spectrophotometer DR 2800. Fe^{2+} was determined by the Ferrozine method (Stookey 1970) and H_2S by the Methylene-blue method (Cline 1967).

2.3. Laboratory analysis.

Major cations (Na, Ca, Mg and K) and trace elements (Sr, Fe, Mn, Ba, Li and Si) were determined by ICP-OES using a Perkin Elmer, Optima 3000DV. Anions were determined by IC on a Waters 430 Conductivity detector (for Cl, PO_4^{3-} and SO_4^{2-}) and a Waters 484 Tunable Absorbance detector (for Br, NO_2^- and NO_3^-) connected to a Waters 510 HPLC Pump and a Waters U6K Injector. Dissolved Organic Carbon (DOC) was measured on a Shimadzu TOC-5000A (version 4.30) analyser with a 1 min. pre-purging step to remove inorganic carbon (CO_2).

3. Results

3.1 Electrical Conductivity

The electrical conductivity (EC), as a general measure for total dissolved solids, was found to vary in a complex pattern in the catchment reflecting different sources of water of varying quality as well as water rock interactions within the aquifer. In Maules Creek the surface water EC increased downstream from 295 to 457 µS/cm (blue numbers in Fig. 1) possibly indicating some interaction with groundwater of higher EC along its reach (see Andersen and Acworth, this issue). Only two surface water samples were collected from the Namoi River. They somewhat surprisingly showed a downstream decrease in EC from 640 to 542 µS/cm.

In the aquifer EC was generally found to increase along the hydraulic gradient from around 267-300 µS/cm in the northeast and east to 444-930 µS/cm in the west and southwest (Fig. 1). However, significant deviations from this trend were observed. Generally EC was found to be lowest at intermediate depths in the aquifer (from 30 to 60 m.b.s.) and increasing both toward the bottom and the surface of the aquifer (Fig. 2a). To the south of Maules Creek high groundwater EC (up to 1613 µS/cm) appears to be related to Permian volcanics and Triassic coal-measures located immediately to the south of the study site (Fig. 1). Figure 3 show a cross-section of the geology along Maules Creek with the EC distribution superimposed. In contrast to the surface water of Maules Creek, the EC of the groundwater below the creek increases much more rapidly down gradient up to 1613 µS/cm (Fig. 3). Downstream from this zone the EC again decreases to as low as 406 µS/cm (Fig. 3), which, interestingly, are EC values comparable with the surface water samples in the lower portion of Maules

Creek situated just above. Further westwards near the Namoi River the groundwater EC increases to a maximum of about 824 µS/cm. Low EC values in the western part of the transect seem to correlate with the location of a up to 120 m deep paleochannel (Fig. 3, see also Andersen and Acworth, this issue).

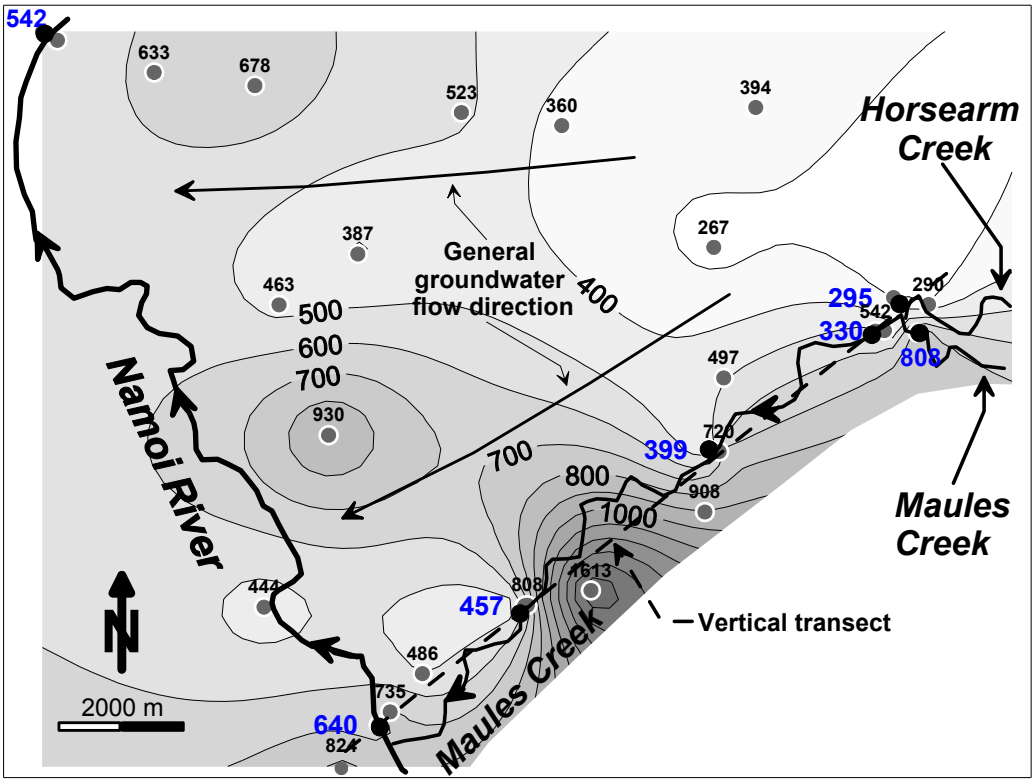

Fig. 1. Distribution of EC (µS/cm) in surface water samples and groundwater in piezometers shallower than 30 m in the lower part of the Maules Creek catchment. Surface water and groundwater sampling sites are indicated by large black and small grey circles, respectively.

3.2. Major ion chemistry

The water samples from the aquifer are generally of a Ca-HCO_3 composition but grading into a Na-HCO_3 and Na-Cl composition in the deeper and more down gradient parts of the system. The trend in EC described above is generally mimicked by most major dissolved ions. For example the concentration of Cl is highly correlated to EC: $r^2 = 0.89$ (Fig. 2b). The increase in Cl is believed to be related to a gradual leaching of salts from the more clayey lithologies (Lavitt 1999). Many dissolved ions exhibit a concomitant increase with Cl, which could well be related to the leaching of salts. In bi-variate plots with Cl, the following correlations coefficients (r^2) were found: Ca = 0.79, Sr = 0.78, SO_4^{2-} = 0.66, Mg = 0.65, Ba = 0.41, Na = 0.35 and alkalinity = 0.27 (n = 54). The alkalinity also shows a correlation with EC: $r^2 = 0.54$ (Fig. 2c) indicating that a significant part of the groundwater EC increase down gradient is related to alkalinity. In contrast this increase must be related to water rock interactions in the aquifer such as dissolution of carbonate minerals, silicate weathering or degradation of organic matter (Appelo and Postma 2005). The poorer correlations found between Cl and Na and alkalinity, respectively, was found to be mainly due to a lack of correlation in the deeper parts of the aquifer. This emphasizes that mineral weathering is contributing significantly to the water composition over time with higher residence times for the deeper parts. Such mineral weathering could partly explain the general down gradient increase in other dissolved ions. However, the extent to which the increase for individual ions are caused by weathering or leaching of salts are unknown, since the chemical composition of the salt is poorly known. The concentration of dissolved Si is surprisingly constant throughout the aquifer (averaging 17.8 mg/L) indicating that the precipitation of one or more secondary Si-phases is controlling the concentrations of dissolved Si released from weathering of primary silicate minerals. In Maules Creek the surface water concentration of Si is

comparable with the groundwater concentrations with 17.2 mg/L. In contrast the surface water concentration of Si is much lower in the Namoi River with 0.7 mg/L.

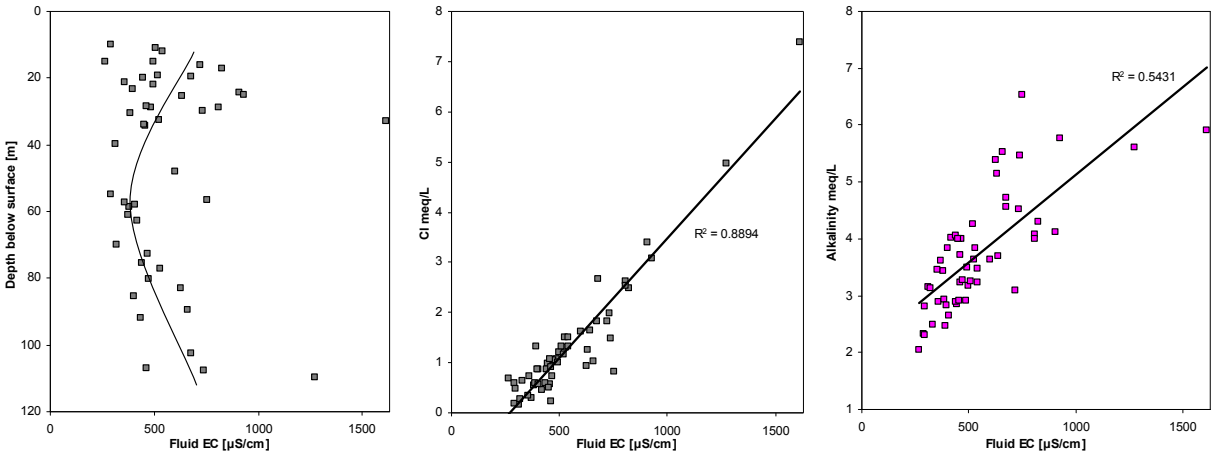

Fig. 2. a) Fluid EC as a function of depth below ground surface; b) Cl (mg/L) vs. fluid EC (µS/cm); c) alkalinity (meq/L) vs. fluid EC (µS/cm).

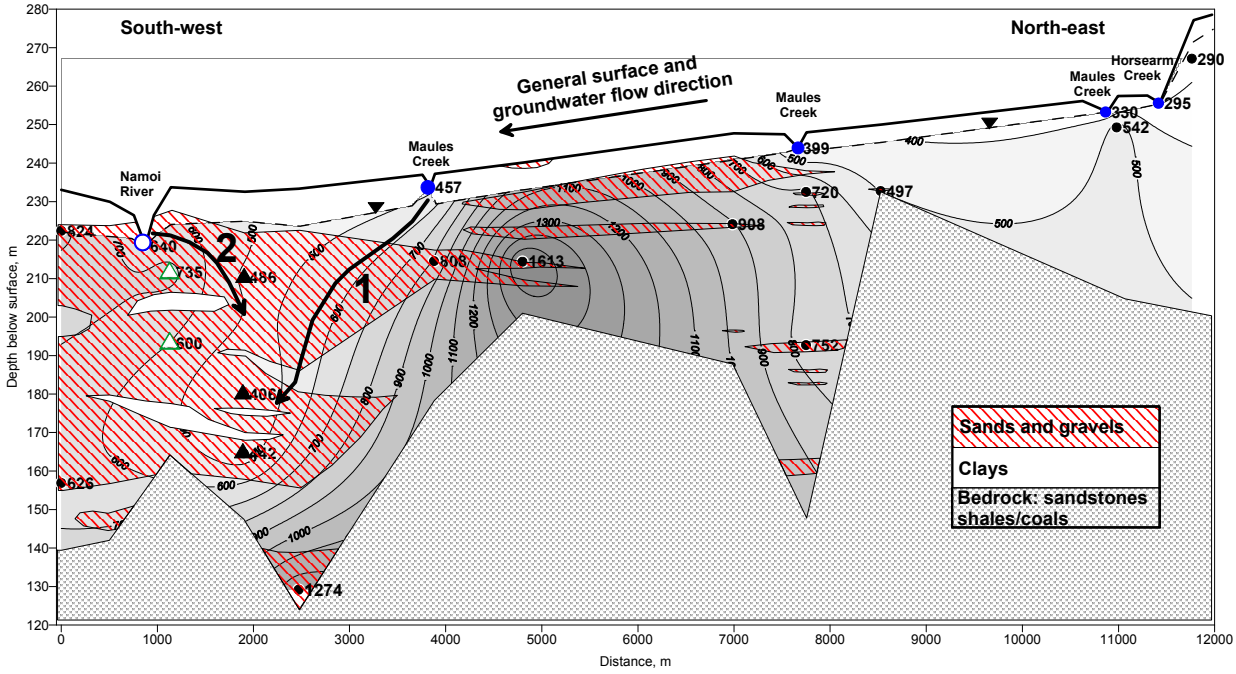

Fig. 3. Vertical transect of the geology (DNR 2006) and the EC distribution (µS/cm) along Maules Creek. The Namoi paleochannel is the large sand and gravel deposits found below the river. Arrows infer possible groundwater flow paths. Varying symbols for individual piezometer screens are referring to the symbols in the Piper diagram (Fig. 5).

3.3. Redox chemistry

In general the aquifer displays a classical redox sequence (Appelo and Postma 2005) going from oxic to anoxic along the hydraulic gradient. Dissolved oxygen (DO) is present in the eastern (up gradient) and upper part of the aquifer (Fig. 4c) in concentrations up to 8 mg/L. In the eastern part DO up to about 5 mg/L is found down to 70 m below ground surface. Nitrate (NO_3^-) is also present in the aquifer with concentrations up to 16 mg/L. The overall distribution of nitrate (Fig. 4d) is the same as for DO, but tends to have a more shallow distribution than oxygen: the aquifer is generally free of nitrate below 30 m.

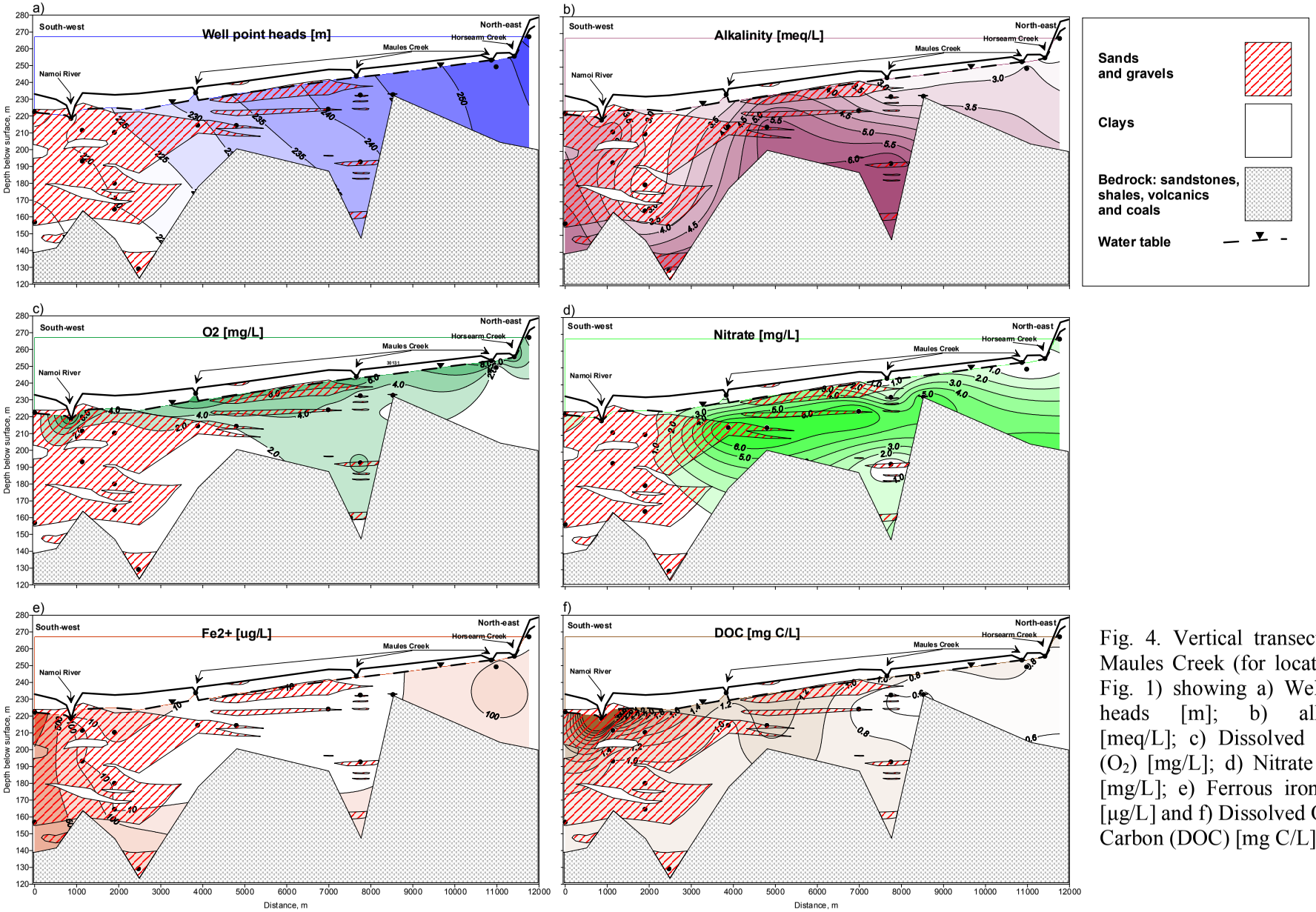

Fig. 4. Vertical transect along Maules Creek (for location see Fig. 1) showing a) Well point heads [m]; b) alkalinity [meq/L]; c) Dissolved oxygen (O_2) [mg/L]; d) Nitrate (NO_3^-) [mg/L]; e) Ferrous iron (Fe^{2+}) [µg/L] and f) Dissolved Organic Carbon (DOC) [mg C/L].

This discrepancy between oxygen and nitrate could indicate that the source of nitrate is recent and possibly related to farming activities in the last decades. Dissolved ferrous iron (Fe^{2+}) show an inverse correlation to DO and nitrate with increasing concentrations in the western (down gradient) and deeper parts of the aquifer (Fig. 4e). Between 0.1 and 1.5 mg/L of Fe^{2+} were measured in the vicinity of the Namoi River. Dissolved organic carbon (DOC) concentrations are generally low in the up gradient part of the aquifer ranging from 0.2 to 1.4 mg C/L with an average of 0.9 mg C/L (Fig. 4f). Elevated levels of DOC ranging from 0.8 to 3.7 mg C/L with an average of 1.4 mg C/L were measured in the groundwater in the vicinity of the river (~1-2 km). The levels of DOC in the Namoi River (4.9 mg C/L) were found to be about 5 times higher than in the aquifer in general, possibly reflecting a higher level of pollution with sewage effluent and nutrients in the Namoi River as well as soil erosion with an organic load. In contrast, Maules Creek had lower levels of DOC of 0.7-1.3 mg C/L (average of 1.0 mg C/L), indicating a less polluted state and possibly indicating a high proportion of surface water flow originating from low DOC groundwater.

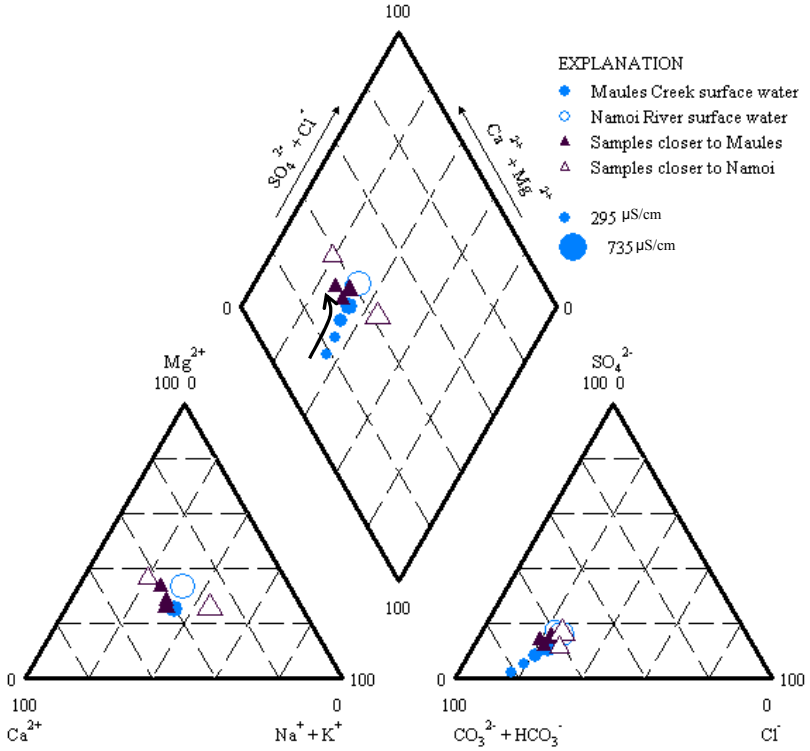

Fig. 5 Piper diagram showing the relative major ion composition of selected surface water and groundwater samples. The arrow indicates change in water composition down along Maules Creek and into the aquifer. For location of samples see symbols in Fig. 3.

4. Discussion

Implications for surface water groundwater interactions

The low groundwater EC (down to 406 µS/cm) near the confluence of Maules Creek and the Namoi River (Fig. 3) could possibly be explained by infiltration of relatively fresh low EC surface water from Maules Creek into the subsurface (see flow path 1 in Fig. 3). Downward hydraulic gradients were observed for this zone in August 2006 (Andersen and Acworth, this issue). Another plausible explanation could be infiltration of surface water from the Namoi River in the west (see flow path 2 in Fig. 3) at times with either high groundwater extraction from the Namoi paleochannel or high river stage and flow. However, this appears to be less likely based upon the available data as the EC of the Namoi River water was higher (640 µS/cm). Nevertheless lower EC levels are possible during floods, which would also be a condition with the highest likelihood of river water recharging the aquifer. Decreased levels of river water EC during floods have been observed for the Peel River, another tributary to the Namoi River system (Mawhinney 2005). Additional time series of river water quality is required to resolve this at the current field site. Plotting the major ion composition of selected surface water and groundwater samples in a Piper diagram (Fig. 5) gives additional, although not conclusive, clues about the source of the low EC groundwater. In the Piper diagram the surface water samples from Maules Creek plot on a trajectory (circles in Fig. 5) largely indicating an increase in chloride down along the creek. The surface water sample from the Namoi River is situated further

along this trend. The three groundwater samples from the low EC zone (solid triangles in Fig. 3 and Fig. 5) plot almost on the line in between the compositions of the Maules Creek and the Namoi River (arrow in Fig. 5). In contrast, the two groundwater samples from the zone between the Namoi River and the zone of low groundwater EC (open triangles in Fig. 3) are located further a field in terms of chemical composition, (curiously, in opposite directions). It therefore does seem less likely that the Namoi River is the source of the low EC groundwater (via flow path 2 in Fig. 3).

Hydrochemical data from the aquifer along the Namoi River indicate that there may also be interactions between the Namoi River and the aquifer in the proximity of the river. The two surface water samples taken from the Namoi River shows a downstream decrease in EC from 640 to 542 μS/cm over a distance of about 12 km. Such a decrease only seems possible with an influx of lower EC water to dilute the surface water EC. Groundwater of lower EC (~460 μS/cm) was found near the Namoi River between the two sampling sites. It is likely that the exchange between surface water and groundwater reverses direction depending on river stage, seasonal groundwater extraction and variations in the regional rain fed recharge of the aquifer. The DOC distribution and the redox chemistry (Fig. 4) do suggest that at times Namoi River water is in fact recharging the aquifer in some locations. Infiltration of river water with a relatively high organic carbon content and subsequent oxidation in the river bed sediments or in the aquifer could be a mechanism explaining such chemically reduced water quality. Other studies have found elevated groundwater DOC levels believed to be from infiltrating river water (Schwarzenbach et al. 1983; Dahm et al. 1998; Crandall et al 1999) and lakes (La Baugh 1986). As a consequence steep redox gradients are often found in aquifers near the surface water interface (Dahm et al. 1998).

The observed redox conditions in the aquifer could thus be explained by a sequence of reaction whereby organic carbon is firstly oxidized by electron acceptors dissolved in the infiltrating water (O_2 and NO_3^-) and subsequently by iron oxides ($Fe(OH)_3$) present in the sediment (Appelo and Postma 2005). However, at this stage it cannot be ruled out that sedimentary organic matter deposited together with the sands and gravels could be causing the reducing conditions. More detailed studies as well as age dating of the groundwater are necessary to provide more definite answers.

The results of this study show how natural hydrochemical tracers can be used to delineate areas of surface water groundwater exchange. In addition understanding how hydrochemical processes are linked to the infiltration of surface water or discharge of groundwater may give important insight in possible fate of various organic and inorganic pollutants exchanging with the water.

5. Conclusion

In summary, this study shows how hydrochemical analysis of surface water and groundwater samples may provide important evidence of surface water groundwater interactions by revealing connectivity and delineating flow paths. The variation in the EC distribution of both surface water and groundwater identified possible sites with surface water groundwater interactions, especially for a site on Maules Creek where there appears to be a significant recharge of the aquifer with surface water from the creek. The indications from the EC data were supported by the major ion chemistry, which showed that the groundwater composition below the suspected recharge site have similar composition as the surface water in the creek above.

Along the Namoi River EC data and redox chemistry points suggests both groundwater discharge into the river and surface water infiltration into the aquifer. Relatively high levels of dissolved organic carbon (DOC) in the river water appear to lead to slightly elevated DOC levels; anoxic conditions; and elevated dissolved Fe^{2+} in the aquifer in the vicinity of the river.

Acknowledgements We gratefully acknowledge the funding by the Cotton Catchment Community CRC (Project No. 2.02.03). In addition we would like to thank Rachel Gilmore for assisting with sampling and analysis in the field and Sue and Ken Crawford for providing accommodation and meals.

References

Appelo CAJ, Postma D (2005) Geochemistry, Groundwater, and Pollution. 2nd ed. A.A. Balkema, Rotterdam. 649 pp.

Cey EE, Rudolph DL, Parkin GW, Aravena R (1998) Quantifying groundwater discharge to a small perennial stream in southern Ontario, Canada. J. of Hydrol. 210, 21-37.

Cline JD (1967) Spectrophotometric determination of hydrogen sulfide in natural waters. Limnol. Oceanogr. 14, 454-458.
Crandall CA, Katz BG, Hirten JJ (1999) Hydrochemical evidence for mixing of river water and groundwater during high-flow conditions, lower Suwannee River basin, Florida, USA. Hydrogeology Journal 7: 454-467.
Dahm CN, Grimm NB, Marmonier P, Valett HM, Vervier P (1998) Nutrient dynamics at the interface between surface waters and groundwaters. Freshwater Biology 40: 427-451.
DNR (2006) Bore log data base. Department of Natural Resources, NSW, Australia.
Kalbus E, Reinstorf F, Schirmer M (2006) Measuring methods for groundwater surface water and their interactions: a review. Hydrol. Earth Syst. Sci. Discuss., 3, 1809-1850.
La Baugh JW (1986) limnological characteristics of selected lakes in the Nebraska sandhills, U.S.A., and their relation to chemical characteristics of adjacent ground water J. of Hydrol. 86, 279-298.
Lavitt N (1999) Integrated Approach to Geology, Hydrogeology and Hydrochemistry in the Lower Mooki River Catchment. PhD thesis, University of New South Wales. 388 pp.
Mawhinney W (2005) Water Quality in the Namoi Catchment 2003/2004. Department of Natural Resources, NSW, Australia. ISBN 0-7347-5619- 4.
Schwarzenbach RP, Giger W, Hoehn E, Schneider JK (1983) Behavior of organic compounds during infiltration of river water to groundwater. Field studies. Environ. Sci. Technol. 17: 472-479.
Stookey LL (1970) Ferrozine – A new spectrophotometric reagent for iron. Anal. Chem. 42, 7, 779-781.
Stumm W, Morgan JJ (1981) Aquatic chemistry. 2nd ed. Wiley & Sons, New York, 780 pp.

Investigation of $\delta^{18}O$ and $\delta^{2}H$ in the Namoi River catchment – elucidating recharge sources and the extent of surface water/groundwater interaction

Martin S ANDERSEN[1*], Karina MEREDITH[2], Wendy TIMMS[1], R Ian ACWORTH[1*]

[1] Water Research Laboratory, School of Civil and Environmental Engineering, University of New South Wales, Australia, m.andersen@wrl.unsw.edu.au, *Affiliated with the Cotton Catchment Communities CRC.
[2] ANSTO, Institute for Environmental Research, NSW, Australia

Abstract Stable isotopes ^{18}O and ^{2}H were analysed in water samples from rainfall, surface water and groundwater within the semi-arid Namoi River catchment in NSW, Australia. The isotopic composition of rainfall events and groundwater samples plot along the Local Meteoric Water Line (LMWL). In contrast, the surface water samples of the Namoi River clearly show signs of evaporative enrichment and plot on a Local Evaporation Line (LEL) constructed for the area based on $\delta^{18}O$ and $\delta^{2}H$ time-series for surface waters of the Namoi River. The river samples have a distinctly lower slope than the LMWL which is due to evaporation. Shallow groundwater near the Namoi River shows considerable enrichment compared to average groundwater signatures and plots in between the LMWL and the LEL on a $\delta^{2}H$ vs. $\delta^{18}O$ graph. These results clearly indicate that the Namoi River is recharging the shallow aquifer system. Conversely, the isotopic composition of surface water in the tributaries of Maules and Horsearm creeks are similar to groundwater indicating that these creeks are receiving groundwater discharge. This study reveals many complex hydrological processes occurring in the catchment. It would not have been possible to elucidate these processes without the use of stable isotope data.

Keywords: Stable isotopes, Hydrology, Groundwater, Surface water/groundwater interactions, Recharge

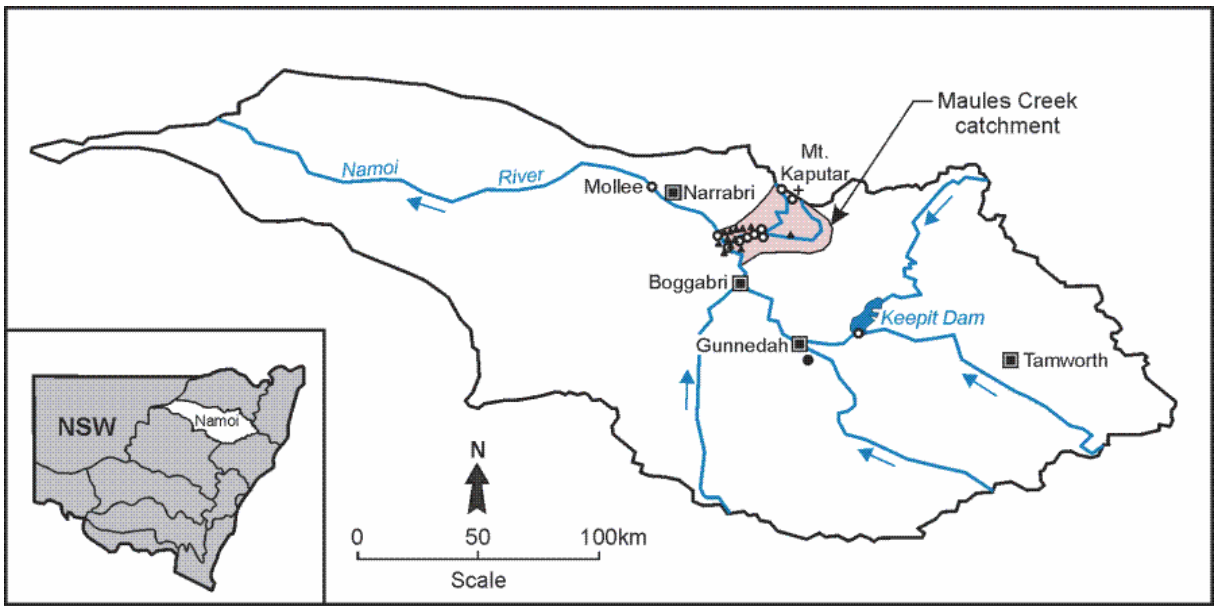

Fig. 1. The location of the Maules Creek catchment and sampling sites for rainfall (●), surface water (○) and groundwater (▲) in the Namoi catchment, NSW. The arrows refer to surface water flow direction.

1. Introduction

In arid and semi-arid regions where there is growing demand for irrigation, stock and domestic water uses, there is an increased need for science based decisions to implement sound water resource management planning. To date, this has largely been accomplished by numerical modelling of groundwater resources using a conceptual model based upon scarce available hydraulic head data (CSIRO 2007). However, it is increasingly realised that this approach may be insufficient to understand complex and dynamic hydrological processes such as recharge and surface

water/groundwater interaction. It is perhaps, particularly, insufficient for the assessment of resource sustainability.

This study demonstrates that the analysis of the stable isotopes of water (^{18}O and ^{2}H) can be extremely useful in providing further understanding of the hydrologeological processes occurring within a productive aquifer system and that these tools can then be used to further constrain the physical groundwater models developed for the area. Therefore, an interpretation of rainfall, surface water and groundwater samples, collected between 1998 and 2007, for the analysis of $\delta^{18}O$ and $\delta^{2}H$ at various sites in the semi-arid catchment of the Namoi River, NSW, Australia (Fig. 1) is presented.

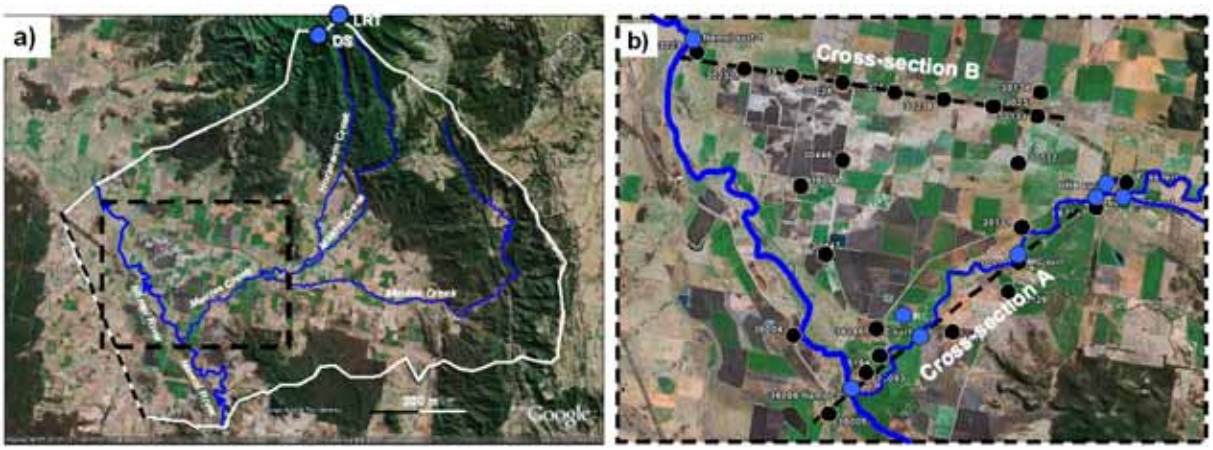

Fig. 2. a) The Maules Creek catchment showing major streams and the location of 2 surface water samples at Mt Kaputar (LRT and DS). Dashed line insert indicates the detailed field site area shown in b) with sampling sites and cross-sections. Black dots are groundwater sampling sites and blue dots are surface water sampling sites.

2. Methodology

Rainfall samples were collected near Gunnedah (Fig. 1) between March 1998 and January 2001 using a sampling system that prevented evaporative concentration of the captured rainfall sample (Timms and Acworth 2002). Surface water was sampled at several locations within the Namoi River catchment between 2002 and 2007. Surface water samples were collected from the Namoi River at: 1) Lake Keepit (a water supply dam), 2) Gunnedah, 3) between Boggabri and Narrabri and 4) Mollee Weir downstream of Narrabri (Fig. 1). In addition, surface water samples were collected between 2006 and 2007 from Maules and Horsearm creeks in the Maules Creek sub-catchment located between Boggabri and Narrabri (Fig. 1). Two surface water seeps were also collected from near the top of Mt Kaputar (1500 m) in the Nandewar Range (Fig. 2a). The two Mt Kaputar samples were collected in February 2007; one sample was taken from a surface seep on the basaltic plateau of Lindsay Rock Tops (LRT) and the other sample was taken from the collection pond at Dawson Springs (DS) downstream from a peat bog. Groundwater was sampled from 44 monitoring bores in the Maules Creek sub-catchment between August 2006 and September 2007 (Fig. 2b). The bores range in depth from 10 to 110 m bgs (below ground surface) and were purged for approximately 3 well volumes or until general parameters stabilised, prior to sample collection. All samples collected for $\delta^{18}O$ and $\delta^{2}H$ analysis were stored in 28 ml McCartney glass bottles. Samples were sent to CSIRO Land and Water in Adelaide, South Australia for analysis by Isotope Ratio Mass Spectrometry (IRMS). Reported precision was 0.15‰ for $\delta^{18}O$ and 1.0‰ for $\delta^{2}H$ and isotope ratios are expressed relative to Vienna Standard Mean Ocean Water (V-SMOW).

3. Results

3.1. Rainwater

The Local Meteoric Water Line (LMWL; $\delta^{2}H = 8.17 \cdot \delta^{18}O + 11.3$) for the area was based on 17 rain samples collected between March 1998 and January 2001 in the central part of the Namoi River catchment near Gunnedah (Fig. 1). The LMWL was calculated using individual rainfall events ranging from 3.6 to 57.6 mm. The rainfall data (Fig. 3) shows that there is a large degree of variability in results with $\delta^{18}O$ ranging from −11.4 to 1.5‰ and $\delta^{2}H$ ranging from −76.1 to 27.8‰. The LMWL is

parallel to, but slightly offset above the Global Meteoric Water Line (GMWL) shown in Fig. 3. The volume weighted isotopic average of the Gunnedah rain samples over the whole sampling period was calculated at $\delta^{18}O = -4.86‰$ and $\delta^{2}H = -24.67‰$ (see Fig. 3).

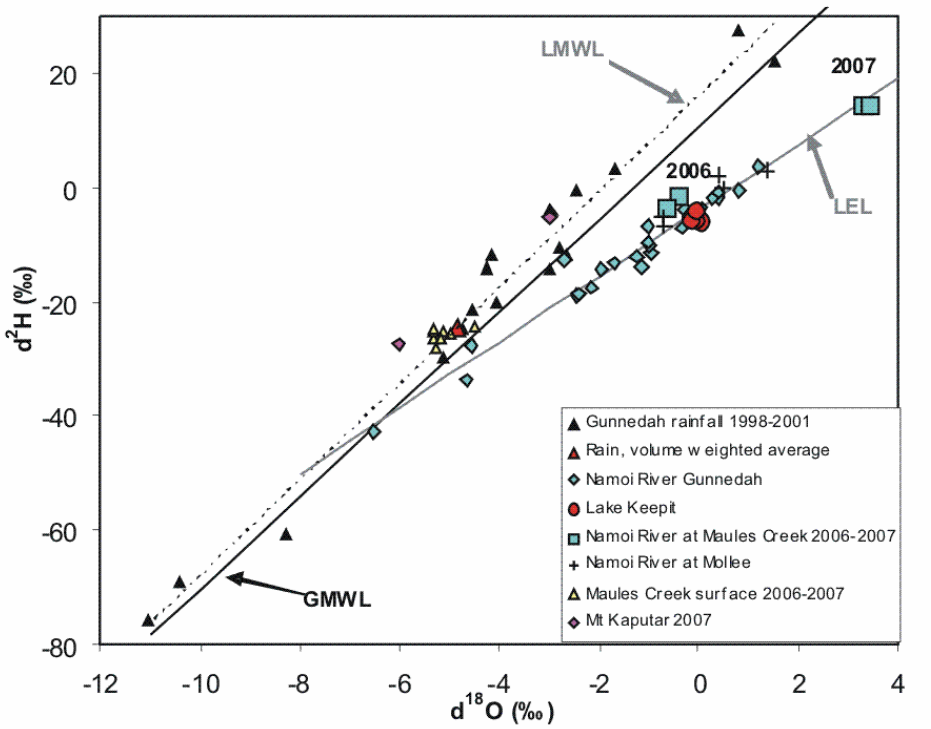

Fig. 3. Comparison of $\delta^{2}H$ (‰) and $\delta^{18}O$ (‰) (VSMOW) for rainfall and surface water. GMWL (Global Meteoric Water Line): $\delta^{2}H = 8.13 \cdot \delta^{18}O + 10.8$; LMWL (Local Meteoric Water Line): $\delta^{2}H = 8.17 \cdot \delta^{18}O + 11.3$ and LEL (Local Evaporation Line): $\delta^{2}H = 5.7 \cdot \delta^{18}O - 3.91$.

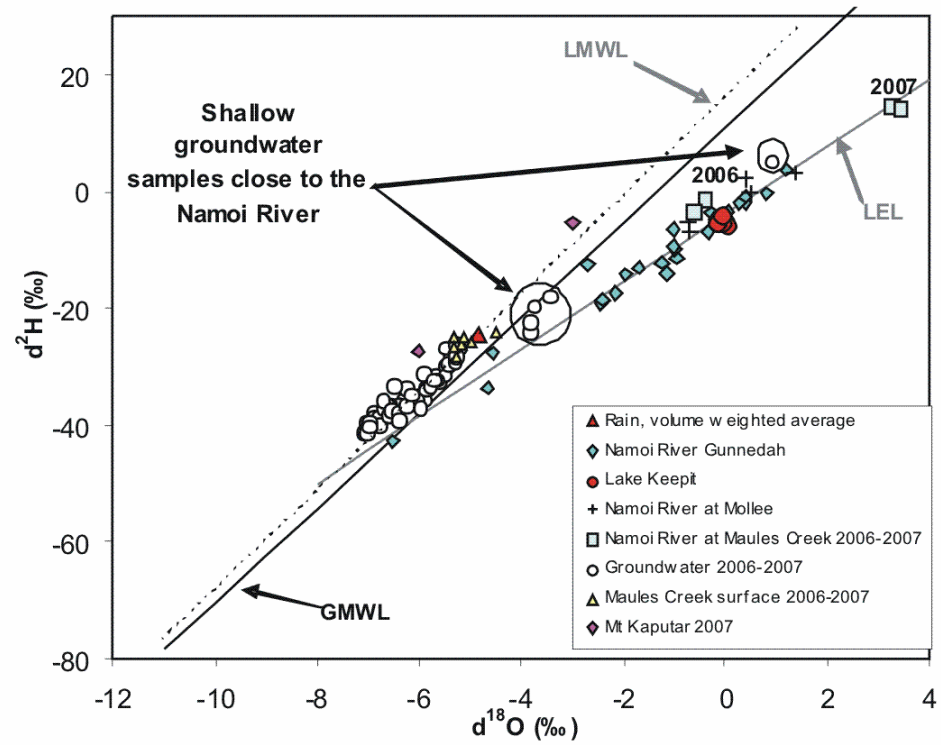

Fig. 4. Comparison of $\delta^{2}H$ (‰) and $\delta^{18}O$ (‰) (VSMOW) surface water and groundwater. GMWL (Global Meteoric Water Line): $\delta^{2}H = 8.13 \cdot \delta^{18}O + 10.8$; LMWL (Local Meteoric Water Line): $\delta^{2}H = 8.17 \cdot \delta^{18}O + 11.3$ and LEL (Local Evaporation Line): $\delta^{2}H = 5.7 \cdot \delta^{18}O - 3.91$.

3.2. Surface water

The majority of the surface water samples from various sections of the Namoi River plot below the LMWL, on a line which will be referred to as the Local Evaporation Line (LEL: $\delta^2H = 5.7 \cdot \delta^{18}O - 3.91$) for the area (Fig. 3). The LEL for this area was constructed by regression analysis of samples plotted in the δ^2H-$\delta^{18}O$ space. Samples that plot on this line are indicative of waters that have undergone isotopic enrichment due to evaporation. A similar evaporative pattern is also seen for surface water samples in the Darling River, NSW, Australia (Meredith et al. 2007). In contrast to the Namoi River samples, the surface water samples from the tributaries of Maules and Horsearm creeks plot in a narrow cluster ($\delta^{18}O$: −5.3‰ to −4.5‰ and δ^2H: −28.3‰ to −24.8‰) above the LEL, but close to the LMWL (Fig. 3). The two surface water samples from near the top of Mt Kaputar (in the Nandewar Range see Fig. 2a) plot considerably above the LMWL. The sample from the surface seep on the basaltic plateau of Lindsay Rock Tops (LRT: $\delta^{18}O$: −3.0‰ and δ^2H: −5.3‰) was significantly enriched compared to the other sample which was taken from the collection pond at Dawson Springs (DS: $\delta^{18}O$: −6.0‰ and δ^2H: −27.4‰) downstream from a peat bog. Both samples were collected after a prolonged dry period.

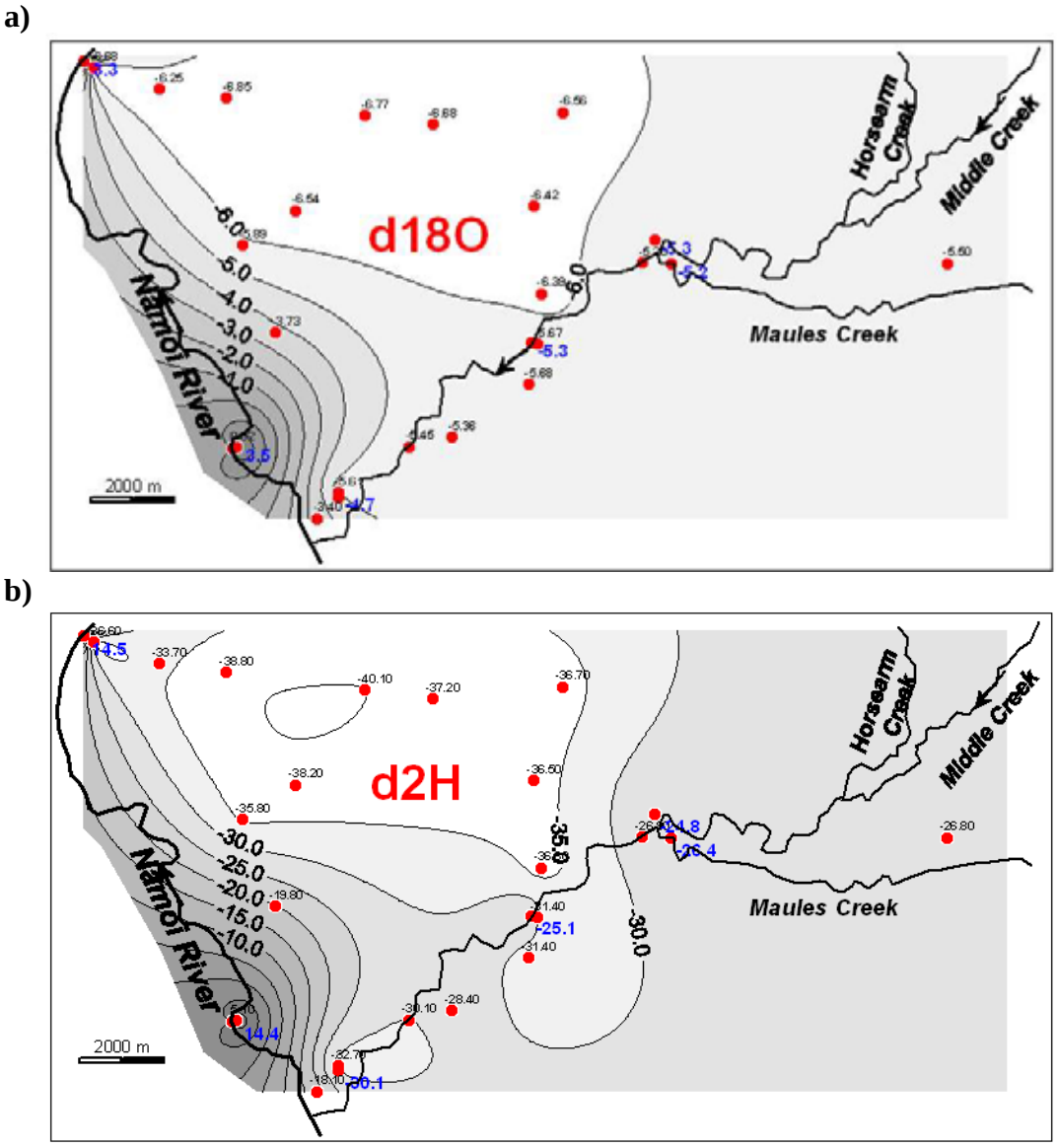

Fig. 5. Map plot of stable isotope signature in surface water and upper groundwater (< 30 m) for February 2007. a) δ^2H (‰) and b) $\delta^{18}O$ (‰). Blue numbers signify surface water samples.

3.3. Groundwater

Groundwater samples from the Maules Creek catchment (Fig. 2b) generally range from −7.1‰ to −5.2‰ for $\delta^{18}O$ and −41.5‰ to −26.6‰ for $\delta^{2}H$ with average values of $\delta^{18}O$ = −6.22‰ and $\delta^{2}H$ = −35.31‰ (Fig. 4). Most samples plot on or close to the LMWL (Fig. 4). However, a few groundwater samples show considerable enrichment compared to the bulk of the groundwater samples with $\delta^{18}O$ ranging between −3.8‰ and −0.9‰ and $\delta^{2}H$ ranging between −23.9‰ and 5.1‰. They plot in between the LMWL and the LEL (encircled in Fig. 4). These enriched groundwater samples were sampled from shallow wells (11.5 to 22.8 mbgs.) close to the Namoi River (< 1 km) as illustrated by the spatial distribution of groundwater isotope ratios (Fig. 5). In addition, Figure 5 shows that the most depleted groundwater samples were collected from wells located near the Nandewar Range in the north. In the southern part and below Maules Creek, shallow groundwater samples have isotopic signatures that are higher and range from −5.7‰ to −5.2‰ for $\delta^{18}O$ and −31.4‰ to −26.9‰ for $\delta^{2}H$. These groundwater samples are comparable to the surface water samples from Maules Creek ($\delta^{18}O$: −5.3‰ to −4.5‰ and $\delta^{2}H$: −28.3‰ to −24.8‰). Figures 6 and 7 show how $\delta^{18}O$ and $\delta^{2}H$ signatures vary along two cross-sections throughout the catchment (see Fig. 2b for location). The cross-sections are parallel to the overall hydraulic gradient in the aquifer as identified in Andersen and Acworth (2007a). In the cross-section along Maules Creek (Cross-section A) isotopic signatures of groundwater samples are slightly more depleted in the deeper parts of the aquifer with values ranging from −6.6‰ to −5.7‰ and −38.4‰ to −31.4‰ for $\delta^{18}O$ and $\delta^{2}H$, respectively (Fig. 6a and b).

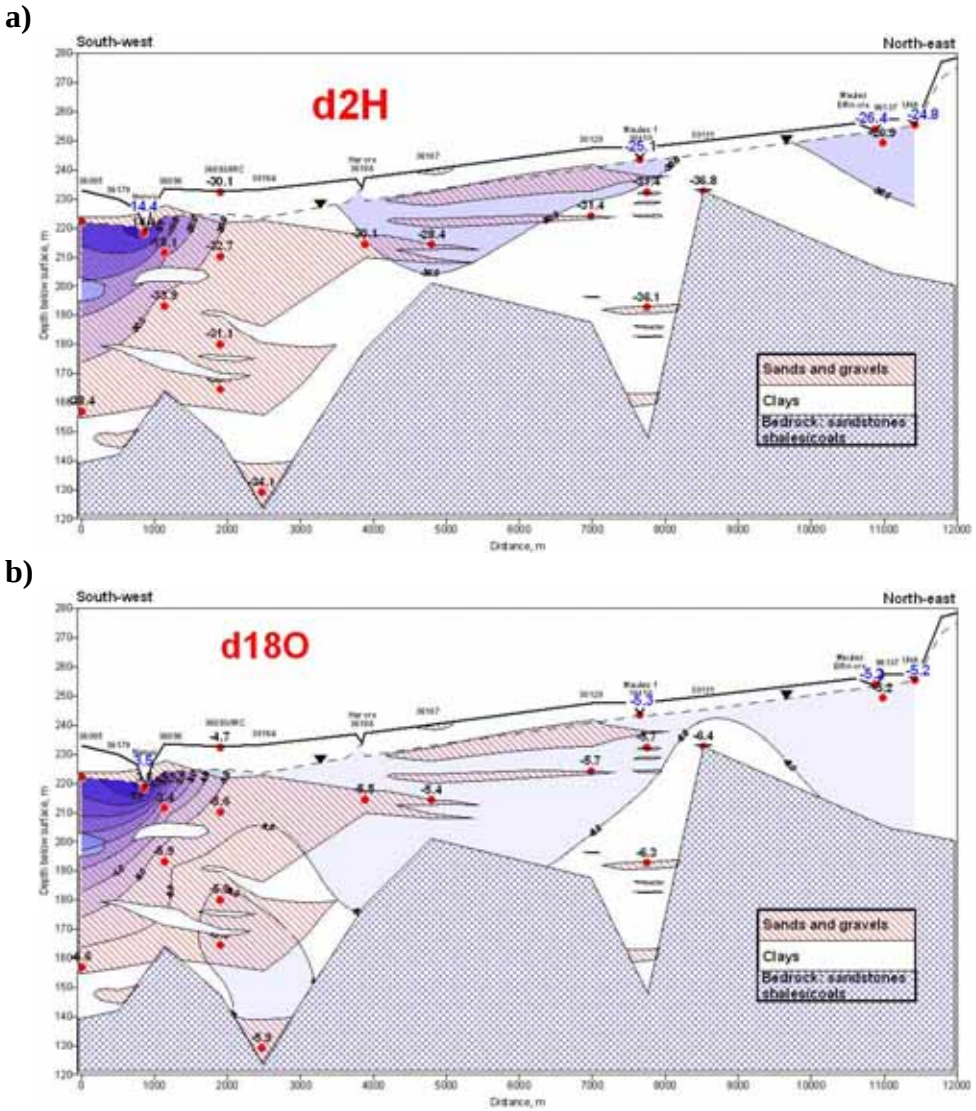

Fig. 6. Stable isotope data from February 2007 in a cross-section (A) along Maules Creek (for location see Fig. 2b) for a) $\delta^{2}H$ (‰) and b) $\delta^{18}O$ (‰). Blue numbers signify surface water samples.

To the north of Maules Creek in the northern cross-section (Cross-section B) groundwater isotopic signatures are more depleted than observed in the previous cross-section with $\delta^{18}O$: −6.0‰ to −7.1‰ and $\delta^{2}H$: −33.7‰ to −41.3‰ (Fig. 7a and b). In this part of the aquifer there also appears to be a decreasing isotopic signature with depth in the eastern and central part of Cross-section B. However, this is not the case for the deepest samples to the west near the Namoi River, where the more enriched samples are found at depth (Fig. 7).

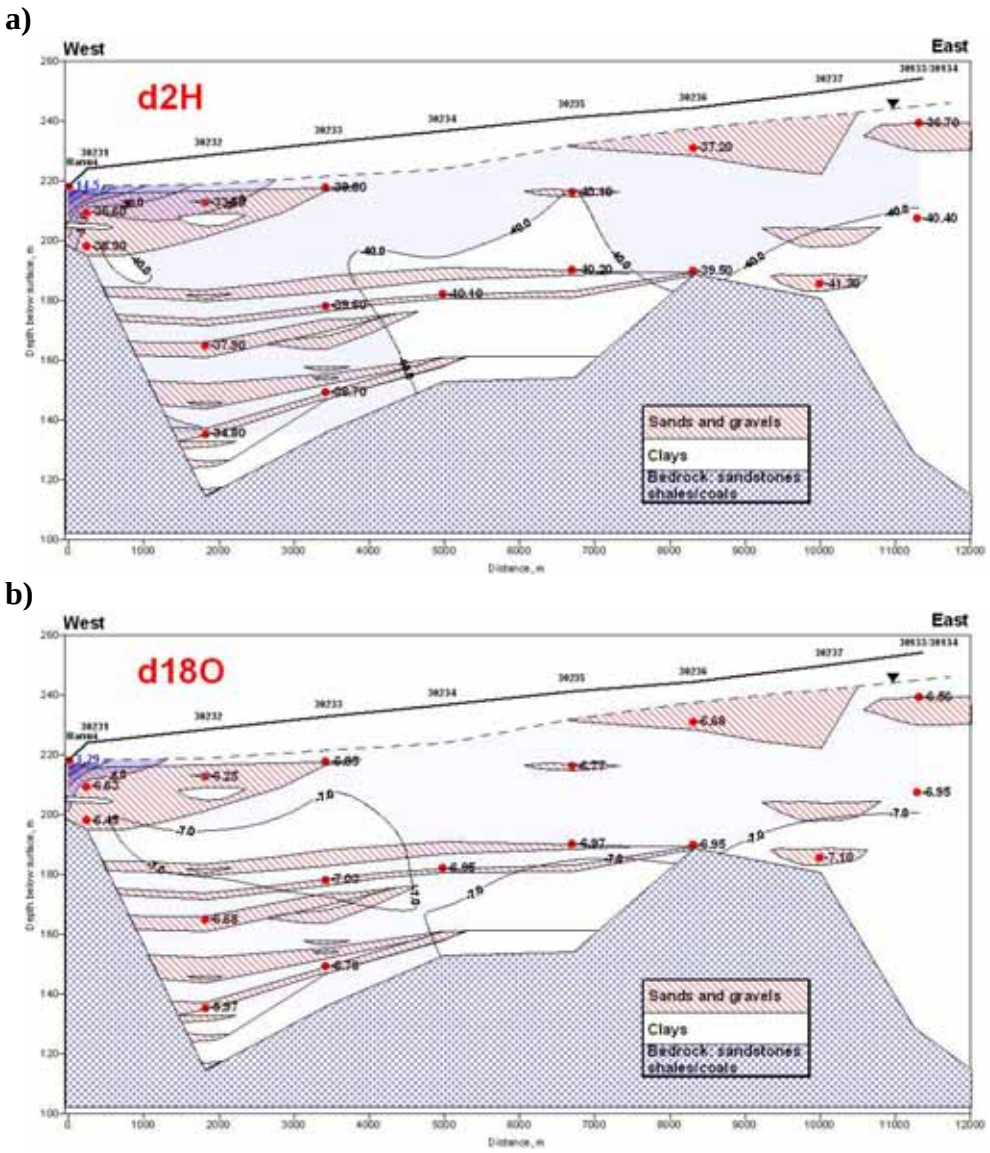

Fig. 7. Stable isotope data from February 2007 in the northern cross-section, B (for location see Fig. 2b) for a) $\delta^{2}H$ (‰) and b) $\delta^{18}O$ (‰). Blue numbers signify surface water samples (here of the Namoi River).

4. Discussion

Unravelling the sources of the observed isotopic signatures of the river water at this study site is complicated by the fact that there are numerous possible sources of inflow waters with different isotopic signatures (i.e. rainfall, dam release waters and groundwater base flow). In addition, surface water samples are susceptible to evaporative enrichment along the river system. The large degree of variability observed in the isotopic signatures of rain water for the area is due to the various types of rainfall events in the catchment i.e. large storm events would be likely to produce highly depleted rainfall signatures and small events would be expected to be more evaporative, particularly in this semi-arid environment. The variability in rainfall results is partly reflected in the Namoi River stable isotope signatures (Fig. 3). The surface water signatures also appear to be influenced by evaporative

enrichment as the water resides in the river channel or as storage in Lake Keepit. The large variability observed in the isotopic composition of rainwater and river water may appear to limit the use of these end-member waters for assessing aquifer recharge mechanisms. However, due to the high evaporation rates of this environment, most surface water samples from the Namoi River plot on the LEL imparting a distinct stable isotope signature. Furthermore, groundwater samples, at some distance from the river, plot in a relatively narrow cluster and have a fairly consistent signature close to the intersection of the LMWL and LEL (Fig. 4). Groundwaters that plot at the intersection of the LEL and the MWL often provide a useful empirical approximation of the weighted-mean isotopic composition of input waters to a catchment (Gibson et al. 2005). Therefore, groundwaters that plot near the intersection point of −6.5 for $\delta^{18}O$ and −43.0 for $\delta^{2}H$ are much more depleted than those of the amount weighted average rainfall values for the area ($\delta^{18}O = -4.86$ and $\delta^{2}H = -24.7$). These results indicate that the average recharge waters of this system are far more depleted than modern day rainfall recharge waters. In contrast, groundwaters sampled in close proximity to the river (<1 km distance) are much more enriched (Fig. 4). These results indicate that the proximal groundwaters have been recharged from the Namoi River, demonstrating that there is hydraulic connection between the groundwater and surface water system in this part of the study site. Thus, the isotopic enrichment of the Namoi River samples compared to the groundwater samples in the Maules Creek catchment indicate that there is a significant contrast in stable isotope signatures, enabling these stable isotope results to be used for studying surface water/groundwater interaction and in a qualitative manner to delineate river recharge to the groundwater system.

In stark contrast to the Namoi River samples, the surface water samples from Maules Creek have similar isotopic signatures to the underlying groundwater system (Fig. 4). This strongly indicates that the surface water in Maules Creek, at the time of sampling had a groundwater origin. Furthermore, the surface water in Maules Creek appears to have been subjected to very little subsequent evaporative enrichment in the creek. This is somewhat surprising considering that the surface waters sampled from Maules Creek in summer 2007 were taken more that 2 months after gauged surface water flow had ceased in the creek and they were obtained from what appeared to be stagnant pools of water. These results suggest that the pools are not stagnant and that water is flowing through the streambed sediments where evaporation is largely hindered. This was corroborated by surface water level measurements in the pools along the creek (Andersen and Acworth 2007a). Further to the west, there is a reversal in hydraulic gradient and this surface water appears to be recharging the aquifer as indicated by the slightly enriched signatures observed in the upper part of Cross-section A from 3000 to 7000 m in Fig. 6.

Closer inspection of the spatial distributions of $\delta^{18}O$ and $\delta^{2}H$ values in the Maules Creek aquifer shows several different hydrological trends. It is interesting to note that the groundwater samples in general are significantly more depleted than the volume weighted average stable isotope composition of rainfall from the Gunnedah site (Fig. 4). Therefore, recharge processes other than rapid piston flow infiltration of rainfall is suggested. The much depleted signatures in the northern part of the aquifer (Fig. 5 and 7) could indicate either rapid infiltration of large and more depleted rainfall through the more coarse grained lithology of that region thus minimising evaporative enrichment, or perhaps the recharge waters are derived from the isotopically depleted precipitation that has fallen on the slopes of the Nandewar Range, which drains into the Maules Creek catchment from the north. According to Dangaard (1964) every 100 m rise in surface altitude causes an additional depletion in rainfall of −0.15 to −0.5‰ for $\delta^{18}O$ and −1 to −4‰ for $\delta^{2}H$. Taking the maximum altitude difference between the valley bottom (310 m at the Gunnedah Research station) and Mt Kaputar (1500 m) would yield additional depletion of −1.8 to −6.0‰ for $\delta^{18}O$ and −11.9 to −47.6‰ for $\delta^{2}H$. This altitude effect could well explain the observed depleted isotopic signatures in groundwaters, highlighting the significance of precipitation on the mountain range as a significant recharge source for the aquifer. Alternatively, it is possible that this groundwater could represent palaeo-waters recharged during cooler climates. However, the lack of consistent spatial trends (along the flow path from east to west or with depth) in Cross-section B (Fig. 7) renders this explanation unlikely, since a modern and more enriched signature should be expected in an upstream direction. Furthermore, the presence of NO_3^-, presumably derived from agriculture, at considerable depth (in some cases up to 80 mbgs.) in the aquifer indicates that at least a significant portion of the groundwater has recharged recently (Andersen & Acworth 2007b). The somewhat more enriched groundwater isotope signatures to the

south along Maules Creek either represent: a) a higher component of evaporative enrichment prior to recharge, b) recharge of isotopically less depleted rainfall at a lower altitude, or c) substantial recharge from Maules Creek. However, since the slope of $\delta^{18}O$ and $\delta^{2}H$ values in all the groundwater data (Fig. 4) is parallel to the LMWL, it does not indicate any evaporative enrichment. The similarity in isotopic composition between groundwater and surface water in Maules Creek (Fig. 4 and 5) indicate a high degree of connectivity with discharge of groundwater into the creek in the upper reach and recharge back into the aquifer further downstream.

5. Conclusions

The results of this study show that $\delta^{18}O$ and $\delta^{2}H$ values of rainfall, surface waters and groundwaters provide an important tool for understanding hydrological processes such as recharge and surface water/groundwater interaction within semi-arid catchments. For the Maules Creek catchment in particular, it was found that the stable isotopes of water have two different relationships: one for Namoi River water and one for the regional groundwater of the catchment. The isotopic composition of the regional groundwater is relatively depleted and plots on the LMWL (Local Meteoric Water Line) of $\delta^{2}H = 8.17 \cdot \delta^{18}O + 11.3$. On the contrary, the surface water of the Namoi River generally plots to the right of the LMWL, clearly showing signs of evaporative enrichment. These surface waters plot on a LEL defined by: $\delta^{2}H = 5.7 \cdot \delta^{18}O - 3.91$. Shallow groundwater (< 22.8 m bgs) in the vicinity of the Namoi River (< 1 km) shows considerable isotopic enrichment compared to most groundwater samples in the region and plots in between the LMWL and the LEL. This clearly indicates the mixing of Namoi River water and regional groundwater and that, for the reach studied in this work, surface water from the Namoi River is recharging the aquifer. In contrast, the surface water collected from the tributary creeks of Maules and Horsearm do not show any noticeable effects of evaporation and plot on the LMWL with an isotopic composition similar to the groundwater situated upstream. This strongly suggests a groundwater origin for these surface waters. Groundwater discharge into the creek is further corroborated by temperature and geochemical data reported by Andersen and Acworth (2007a and b).

Spatial trends in isotopic composition were observed in the aquifer of the Maules Creek catchment with the most depleted groundwater isotopic values situated to the north, below the slopes of the Nandewar Range. The average isotopic composition of this groundwater was found to be considerably more depleted than the average composition of local modern rainfall collected in the valley. It is thus possible that the main source of recharge to the aquifer is from precipitation at higher altitude on the slopes of the Nandewar Range. The $\delta^{18}O$ and $\delta^{2}H$ data presented in this study reveal many complex hydrological processes occurring in the catchment that have not previously been observed. The stable isotope data has proved invaluable in determining an appropriate conceptual model for the area studied. The results of this study can now be used to constrain previously constructed physical groundwater models that are commonly used for water resource management on a catchment scale.

Acknowledgements We gratefully acknowledge the funding by the Cotton Catchment Community CRC (Project No. 2.02.03). We would also like to thank the Department of Water and Energy (DWE) for allowing us access to sampling their system of monitoring wells. Finally we like to thank Sue and Ken Crawford for providing accommodation and meals when in the field.

References

Andersen MS, Acworth RI (2007a) Surface water groundwater interactions in an ephemeral creek in the Namoi Valley, NSW, Australia – Controls by geology and groundwater abstraction. Proceedings of the XXXV IAH Congress "Groundwater and Ecosystems", Lisbon. September, 2007.

Andersen MS, Acworth RI (2007b) Hydrochemical investigations of surface water groundwater interactions in a sub-catchment in the Namoi Valley, NSW, Australia. Proceedings of the XXXV IAH Congress "Groundwater and Ecosystems", Lisbon. September, 2007.

CSIRO (2007) Water Availability in the Namoi: A report for the Australian Government from the CSIRO Murray-Darling Basin Sustainable Yields Project. CSIRO, Australia. 154pp

Dangaard W (1964) Stable isotopes in precipitation. Tellus XVI, 436-468.

Gibson JJ, Edwards TWD, Birks SJ, St Amour NA, Buhay WM, McEachern P, Wolfe BB, Peters DL (2005) Progress in isotope tracer hydrology in Canada. Hydrological Processes 19, 303-327.

Meredith K, Hollins S, Hughes C, Cendon D, Stone D (2007) Groundwater/surface water exchange and its influence on stable water isotopic signatures along the Darling River, NSW, Australia. Proceedings of the XXXV IAH Congress "Groundwater and Ecosystems", Lisbon. September, 2007

Timms W, Acworth RI (2002) Induced leakage due to groundwater pumping and flood irrigation at the Pullaming Agricultural Field Station, Liverpool Plains. UNSW Water Research Laboratory, Research Report No. 208. http://www.wrl.unsw.edu.au/publications

Development of an integrated conceptual model of a connected surface water-groundwater system using a hydrochemical approach at Maules Creek, NSW, Australia

[1]James PATTERSON, [2]Martin S. ANDERSEN, [2]R. Ian ACWORTH

[1]*Now at*: Institute for Sustainable Futures, University of Technology Sydney, Australia, James.Patterson@uts.edu.au
[2]Water Research Laboratory, School of Civil and Environmental Engineering, University of New South Wales, Australia & affiliated to the Cotton Catchment Communities CRC m.andersen@wrl.unsw.edu.au, i.acworth@unsw.edu.au

Abstract Hydrochemistry was studied in an alluvial aquifer to develop knowledge of important geochemical processes which could be related to surface water-groundwater interactions in the system. Hydrochemical data consisting of major ions (Na^+, Ca^{2+}, Mg^{2+}, K^+, Cl^-, HCO_3^-, SO_4^{2-}, H_4SiO_4) and water quality parameters (pH, PCO_2, O_2) were used as natural tracers and to characterise chemical processes in the aquifer system. Primary silicate weathering was found to be a key process, with leaching of salts from the clays also likely to play a role. Using this geochemical understanding and linking it to hydrogeological data and previous investigation of surface water-groundwater interactions, further deductions were made regarding hydrochemical and hydrogeological processes. This enabled development of a stream-reach scale conceptual hydrogeological model which integrates the hydrogeology and hydrochemistry of the aquifer system.

Keywords: hydrochemistry, hydrogeology, chemical weathering, conceptual model, surface water groundwater interactions

1. Introduction

Aquifer heterogeneity often complicates the estimation of water fluxes in sedimentary aquifer systems. This problem is often exacerbated at points of surface water-groundwater exchange (i.e. discharge and recharge processes), and may additionally be seasonally variable (e.g. Sophocleous 2002, Winter et al. 1998). To gain an improved understanding of hydrogeological processes, a hydrochemical approach using naturally occurring chemical species, such as major ions, can be useful. This approach was adopted to develop a process-based conceptual model of aquifer hydrogeology incorporating surface water-groundwater connectivity at Maules Creek, NSW, Australia. This paper focuses on major ion data to develop understanding of important geochemical processes controlling water quality. Subsequently the obtained geochemical knowledge was combined with basic hydrogeological data to deduce important hydrogeological processes and present an integrated conceptual model the aquifer system.

2. Site description

Maules Creek is located in the Namoi Valley, NSW, Australia (Fig. 1), and is situated within an economically-significant irrigated agricultural region. The climate is semi-arid with annual average rainfall approximately 700 mm in the flatter south-west part of the catchment, increasing to 1200 mm towards Mt Kaputar and the Nandewar Ranges in the North. Maules Creek runs from the slopes of Mt Kaputar (1500 m) in the North, across the alluvial catchment and joins the Namoi River in the south-west (Fig. 1). The catchment is underlain by a basement of Permian siltstones, sandstones, conglomerates, coal measures, basaltic and rhyolitic lavas, and tuffs with interbedded shale. These formations outcrop at catchment margins in the north, east and south (DMR 1998). The Nandewar ranges and Mt Kaputar, a 20 million year old Tertiary volcano, are situated in the North of the catchment. Quaternary alluvial sediments varying in thickness from 30 - 100 m unconformably overlie the Permian basement and are comprised of interspersed clay, sand and gravel sequences grading from thick clayey layers further upstream to more frequent sand and gravel layers towards the Namoi River (DNR 1996). In the vicinity of the Namoi River deep coarse gravel and sand deposits comprise the Namoi River paleochannel which is the principal aquifer in the catchment.

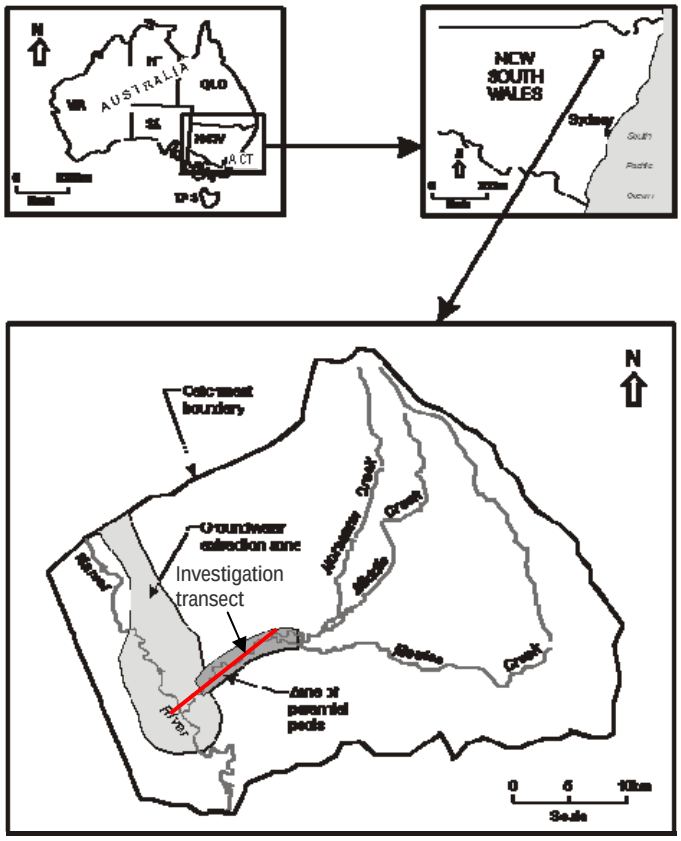

Fig. 1. Location of the Maules Creek catchment in New South Wales. Insert shows the location of the investigation transect along Maules Creek which consisted of both surface water and groundwater sampling locations.

The aquifer system can be divided into a lower-yielding clayey up-catchment region (max. 20-30 L/s) and the higher-yielding Namoi River paleochannel (~120 L/s) in the lower catchment (Sinclair et al. 2005). Groundwater flow is broadly towards the Namoi River driven by average horizontal head gradients of approximately 0.003 m/m (Fig. 2, 3). However, the flow pattern is complicated by varying drawdown magnitudes throughout the aquifer due to groundwater abstraction, which is occurring predominantly during spring and summer (October-February). The relatively intensive pumping regimes during these times can lower groundwater levels by up to 11 m, most significantly within the Namoi River paleochannel. These reduced aquifer pressures are often most pronounced in the Lower aquifer zone, and seem to be transmitted vertically through to overlying zones. This has ramifications for surface water groundwater (SW-GW) exchange processes in the vicinity of the Namoi River and in the lower reaches of Maules Creek. Upstream of Elfin Crossing near the top of the transect, groundwater appears to discharge into Maules Creek. Approximately 0.5-7.5 km further downstream of Elfin Crossing surface water is subsequently thought to infiltrate back into the aquifer (Andersen and Acworth 2007a). This seems to be in accordance with decreasing surface water flow in this reach of Maules Creek with the onset of the groundwater pumping season. In most years surface water flow seems to cease altogether with limited flow in the creek bed sediments between seemingly stagnant pools by the end of summer. In the vicinity of the Namoi River where seasonal groundwater pumping is most significant, surface water from the Namoi River appears to infiltrate the streambed during summer months due to aquifer drawdowns (Andersen et al. 2008). However, large gaps remain in the conceptual understanding of hydrogeological and geochemical processes within the aquifer, in the context of surface water-groundwater connectivity.

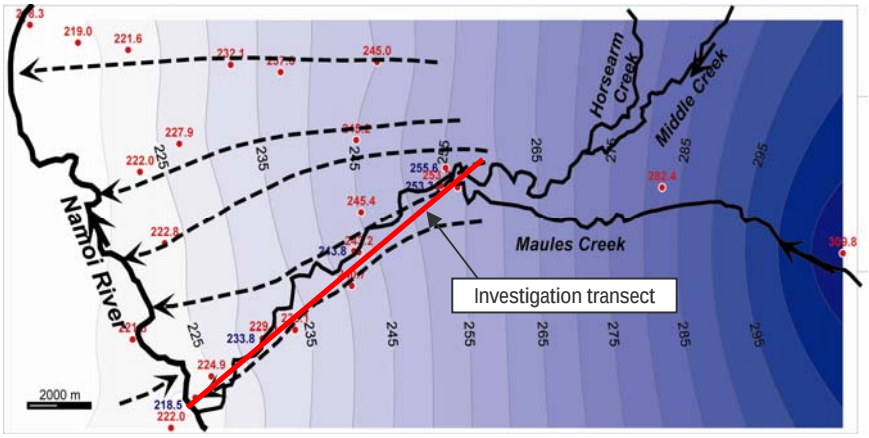

Fig. 2. Hydraulic head distribution (mAHD) and inferred flow directions in plan in the Upper aquifer (<30 m) in August 2006, also showing distribution of monitoring wells across the catchment.

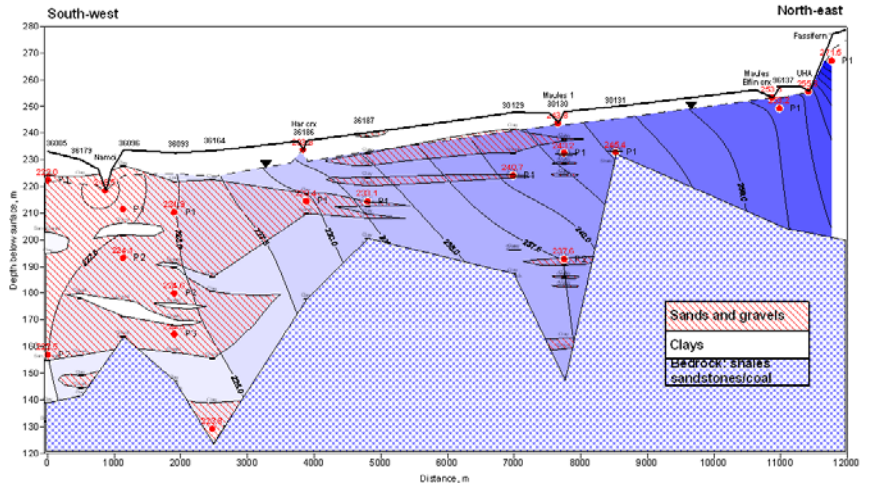

Fig. 3. Hydraulic head distribution (mAHD) in a cross-section parallel to Maules Creek in August 2006. Also included is the borehole locations, screened depths (red circles) and the basic geology based on drillers logs from monitoring wells installed c.1970-80 (DNR 2006).

3. Methodology

Groundwater samples were taken from a network of monitoring piezometers, 10-100 m deep, (DNR 2006) and from surface waters along an investigation transect along the lower reaches of Maules Creek (Fig. 1, 2) at the beginning of August 2006. Dissolved oxygen (DO) and pH were measured using a HACH portable meter (HQ40d) with a HACH luminescent oxygen probe and pH electrode arranged inline using a flow-through cell. Field analysis for alkalinity was conducted immediately after sample collection on a filtered 25 mL sub-sample using the Gran titration method (Stumm and Morgan 1981) with a HACH Digital Titrator (Model: 16900) and 0.16 N H_2SO_4 cartridges. Major cation samples were collected in 20 mL PE vials and acidified with 2% 5 N HNO_3 and stored at 5°C for preservation, prior to later analysis by ICP-OES using a Perkin Elmer, Optima 3000DV. Anion samples were collected in 10 mL PE vials and frozen for later analysis by IC using a Waters 430 Conductivity detector for chloride. Additional method description on groundwater sample retrieval and collection, and field and laboratory analysis protocols is given in Andersen and Acworth (2007b).

4. Results

4.1 CO_2, pH and dissolved oxygen

The Upper aquifer was characterised by high and relatively constant P_{CO2} (~$10^{-1.4}$atm) which is likely to be due to respiration processes in the overlying root zone (Appelo and Postma 2005). pH was correspondingly relatively constant ~6.8 (Fig. 4a, b). Deeper samples within the upstream clayey region of the transect, and deep within the Namoi River paleochannel (MW36164) showed lower CO_2 pressures and higher pH than observed for the Upper aquifer, which may reflect the consumption of acidity via weathering processes. However locations near the Namoi River showed uniform pH and P_{CO2} through vertical depth in the aquifer. P_{CO2} observed in surface waters were high upstream of Elfin Crossing (comparable to values in the Upper aquifer) and decreased towards atmospheric equilibrium in a downstream direction, with concurrent increase in pH. This appears to indicate degassing of CO_2-charged surface water originating from discharging groundwater upstream of Elfin Crossing. The

Upper aquifer was generally oxic within the upstream clayey region of the transect but anoxic close to the Namoi River (Fig. 4c) where higher dissolved organic carbon (DOC) levels produce a steep redox gradient between surface water and groundwater (Andersen and Acworth 2007b). Interestingly, relatively high DO levels (4.5 mg/L) were observed in the Middle aquifer at MW30130 (~60 m depth). Surface water upstream of Elfin Crossing showed DO levels comparable to Upper aquifer groundwater which then increased to atmospheric equilibrium downstream from Elfin Crossing.

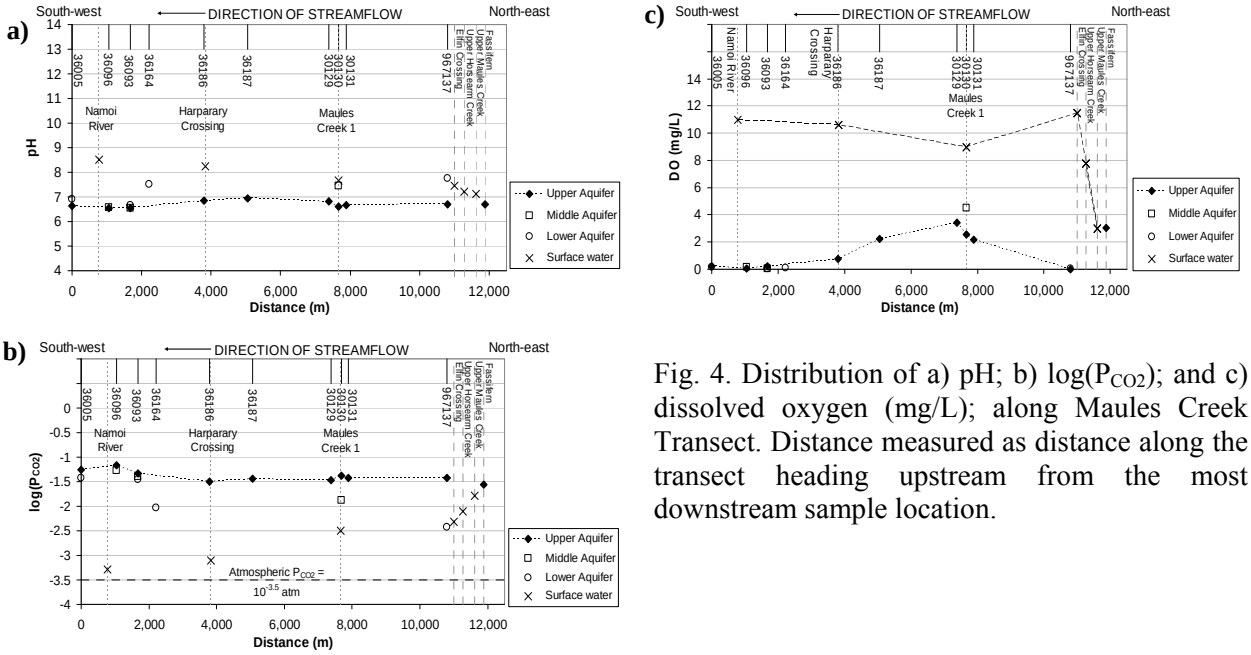

Fig. 4. Distribution of a) pH; b) log(P_{CO2}); and c) dissolved oxygen (mg/L); along Maules Creek Transect. Distance measured as distance along the transect heading upstream from the most downstream sample location.

4.2 Chloride and alkalinity

The distributions of chloride and alkalinity with depth were found to be relatively similar, showing approximately linear increase in concentration with depth through the Middle and Lower aquifer zones, however more variable and sometimes higher chloride and alkalinity levels were observed in the Upper aquifer (Fig. 5). Along the investigation transect the concentrations of both chloride and alkalinity were variable, and both species showed an elevated region in the Upper aquifer near MW36187 approximately halfway along the transect (Fig. 6). This area also showed elevated nitrate levels (NO_3^- ~7.5 mg/L) relative to immediate upstream and downstream regions (where NO_3^- ~0 mg/L) as well as concurrent elevations in other species including Na^+, Ca^{2+}, Mg^{2+}, Ba^+, Sr^{2+}, and SO_4^{2-}. In the Middle aquifer MW30130 showed relatively low chloride and relatively high alkalinity (Fig. 6). In the Lower aquifer, MW36164 showed relatively high chloride and alkalinity (Fig. 6). Other samples within the Namoi River paleochannel showed remarkably uniform chloride and alkalinity signatures through depth and in comparison to surface water (and similar patterns were observed for EC, Na^+, K^+, Ca^{2+}, Mg^{2+}, Sr^{2+}).

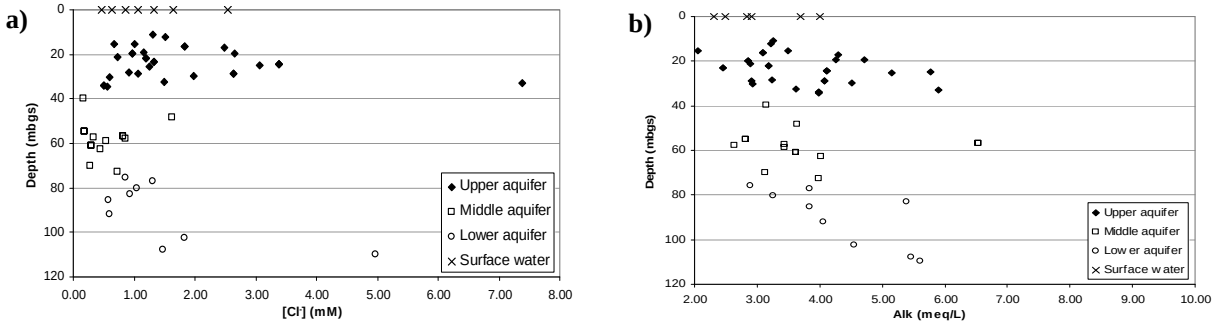

Fig. 5. Distribution of a) chloride (mM); and b) alkalinity (meq/L) against depth (m below ground surface) through the aquifer in the catchment

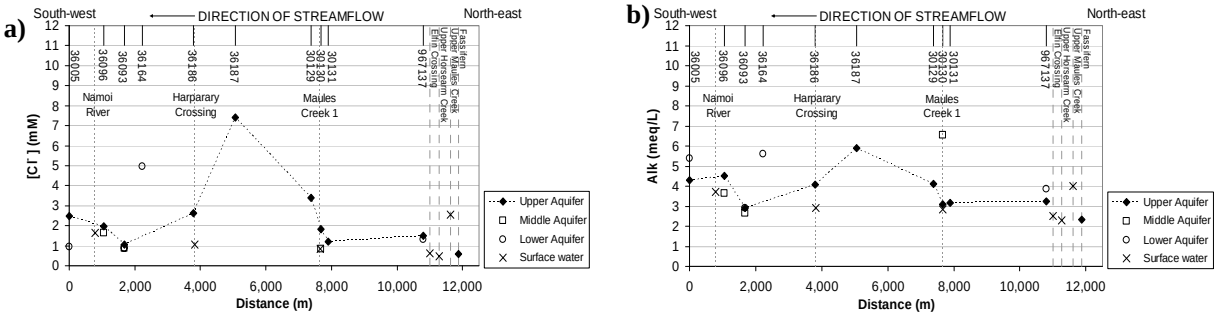

Fig. 6. Distribution of a) chloride (mM); and b) alkalinity (meq/L) along Maules Creek Transect. Distance measured as distance along transect from the most downstream sample location.

4.3 Major ions

Na^+, Ca^{2+} and Mg^{2+} increased approximately linearly with HCO_3^- (Fig. 7a, b, c) which seems to indicate mineral weathering processes releasing these species to solution and possibly also leaching of salts from sediments. The Lower aquifer samples from within the Namoi River paleochannel, as well as within suspected gravel beds deep beneath thick clay layers contained relatively low levels of Ca^{2+} and Mg^{2+} compared to the Upper aquifer. K^+ concentrations were relatively constant with HCO_3^- (Fig. 7d). Dissolved silica levels were high and relatively uniform in magnitude (average groundwater concentration 0.64 mM = 18 mg/L), and supersaturated with respect to some silica oxide phases (e.g. SI_{quartz} ~0.9, $SI_{chalcedony}$ ~0.5) (Fig. 7e). SO_4^{2-} showed an approximately linear trend for most samples except for some Lower aquifer samples which plotted relatively lower (Fig. 7f). Ratios of major ions to HCO_3^- were also examined, and the $(Ca^{2+}+Mg^{2+})/HCO_3^-$ ratio (meq/L) showed an approximately linear trend for most Upper aquifer, Middle aquifer and surface water samples, however some of the deeper samples showed relatively lower values (Fig. 7g). The Na^+/HCO_3^- ratio (meq/L) showed an approximately linear trend for most samples (Fig. 7h).

Alkalinity (as HCO_3) can be acquired through various water-rock interactions such as weathering of carbonate or silicate minerals, or by degradation of organic matter (Appelo and Postma 2005). However the aquifer does not seem to contain appreciable amounts of carbonate minerals (except where fluctuating water tables may cause precipitation and re-dissolution of carbonates from solution), and the groundwater is generally sub-saturated with respect to calcite ($SI_{calcite}$ ~ -1.2 to -0.4). There also does not seem to be appreciable degradation of organic carbon in most of the aquifer away from the Namoi River, indicated by the general presence of DO and NO_3^- and absence of Fe(II) and S^{2-}. Therefore it can be assumed that most of the acquired alkalinity is due to primary silicate weathering processes, which are known to be relatively slow and kinetically controlled processes (Appelo and Postma 2005). As a consequence alkalinity should increase with residence time and is therefore used as a progress variable in the plots in Fig. 7.

4.4 PHREEQC model results

A PHREEQC (Parkhurst and Appelo 1999a) batch-reaction model was developed to investigate the influence of primary silicate weathering on the aquifer hydrochemistry. The modelling approach consisted of dissolving increasing amounts of the Ca-plagioclase end-member anorthite into an upstream water composition in a stepwise batch fashion to simulate the geochemical evolution of groundwater along a flowpath subject to the dissolution of anorthite. Anorthite was used as a single idealised primary silicate phase due to the prevalence of Ca^{2+} observed in the groundwater (Fig. 7c), as well as the relatively high weathering rates of anorthite (Appelo and Postma 2005). The geochemical model dissolved 1 mM anorthite into an initial upstream water composition. P_{CO2} was held constant to represent the observed field data of almost constant P_{CO2} in the Upper aquifer (Fig. 6b), which could imply that the dominant weathering reactions occurring in the real system do not substantially consume protons, or that there is an additional source of CO_2 from within the aquifer. Observed Ca^{2+} and alkalinity were represented relatively well (Fig. 8a, c). The silica behaviour was also modelled well (Fig. 8b), because Si was conserved in the solid phase by allowing kaolinite precipitation (a secondary weathering product) when the solubility for kaolinite was

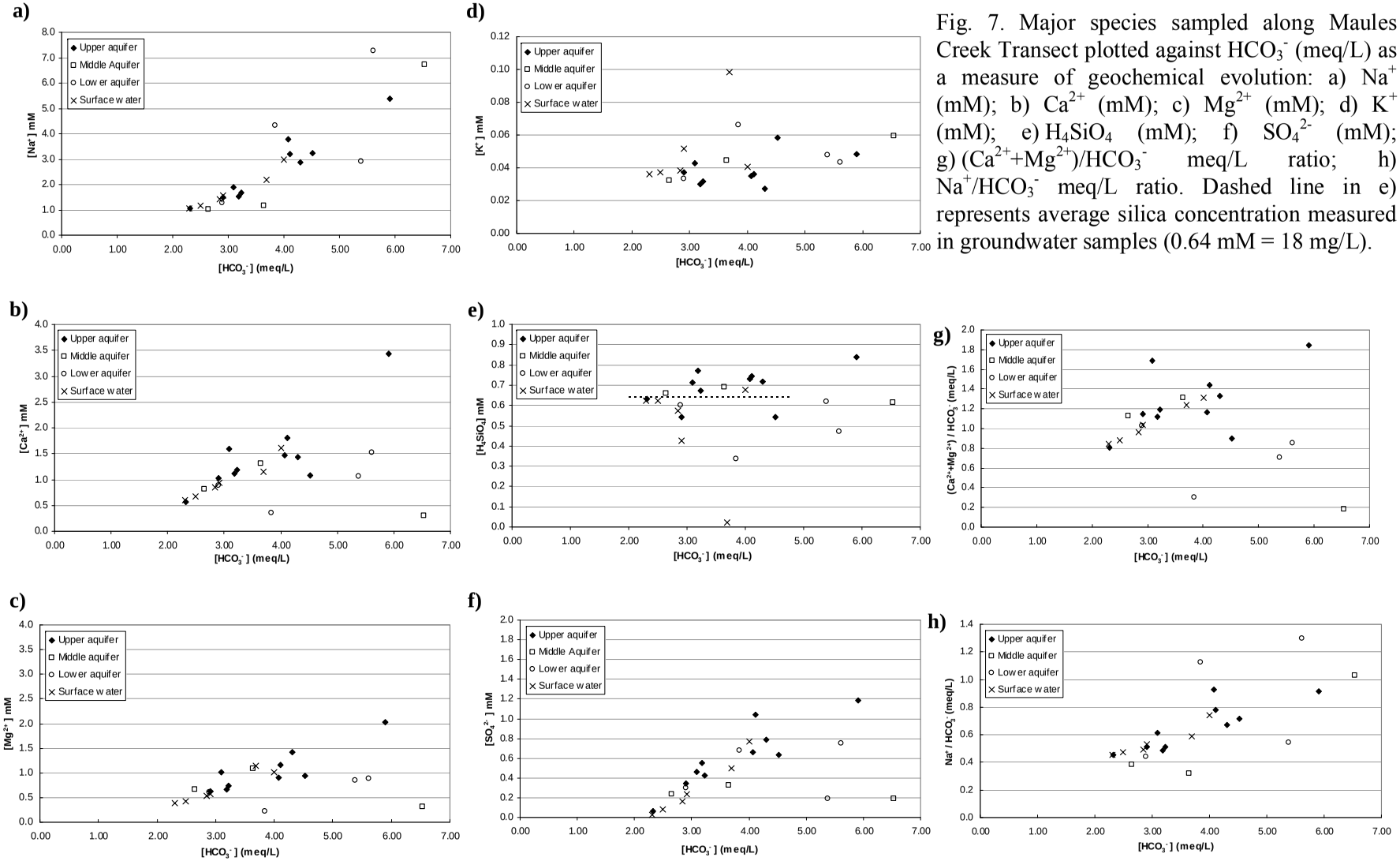

Fig. 7. Major species sampled along Maules Creek Transect plotted against HCO_3^- (meq/L) as a measure of geochemical evolution: a) Na^+ (mM); b) Ca^{2+} (mM); c) Mg^{2+} (mM); d) K^+ (mM); e) H_4SiO_4 (mM); f) SO_4^{2-} (mM); g) $(Ca^{2+}+Mg^{2+})/HCO_3^-$ meq/L ratio; h) Na^+/HCO_3^- meq/L ratio. Dashed line in e) represents average silica concentration measured in groundwater samples (0.64 mM = 18 mg/L).

exceeded. The modelling of the weathering reaction therefore did not liberate silica to the dissolved phase. pH was also modelled well (Fig. 8d). Based on the observed kaolinite precipitation in the model, this suggests that a weathering reaction such as Equation 1 (Appelo and Postma 2005) could be occurring in the aquifer system.

$$\underset{\text{anorthite}}{CaAl_2Si_2O_8} + 2H^+ + H_2O \rightarrow Ca^{2+} + \underset{\text{kaolinite}}{Al_2Si_2O_5(OH)_4} \quad (1)$$

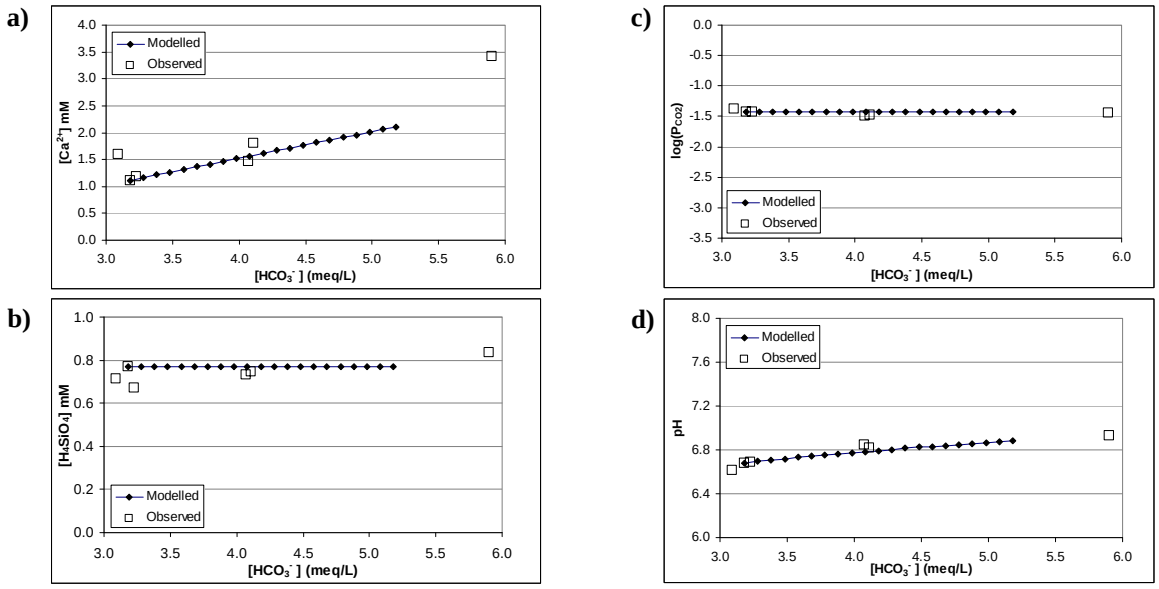

Fig. 8. Modelled evolution of Upper aquifer water compared to observed data for an anorthite weathering model for a) Ca^{2+}; b) dissolved silica (H_4SiO_4); c) PCO_2; and d) pH.

4.5 Stability diagrams

Stability diagrams were constructed to further investigate the sorts of secondary weathering products that may result from primary silicate weathering. The Ca-silicate stability diagram indicates that a Ca-rich montmorillonite phase may be a stable weathering product for a Ca-plagioclase (Fig. 9a), whereas the Na-silicate stability diagram indicates that kaolinite may be a stable weathering product for a Na-plagioclase (Fig. 9b). Based on the volcanic geology and semi-arid climate it may be reasonable to expect formation of montmorillonite (Appelo and Postma 2005) however the complex and heterogeneous geochemistry would mean that many different weathering products would be likely to co-exist. Based on the results of the PHREEQC modelling above combined with the stability diagrams montmorillonite and kaolinite weathering products seem to be likely.

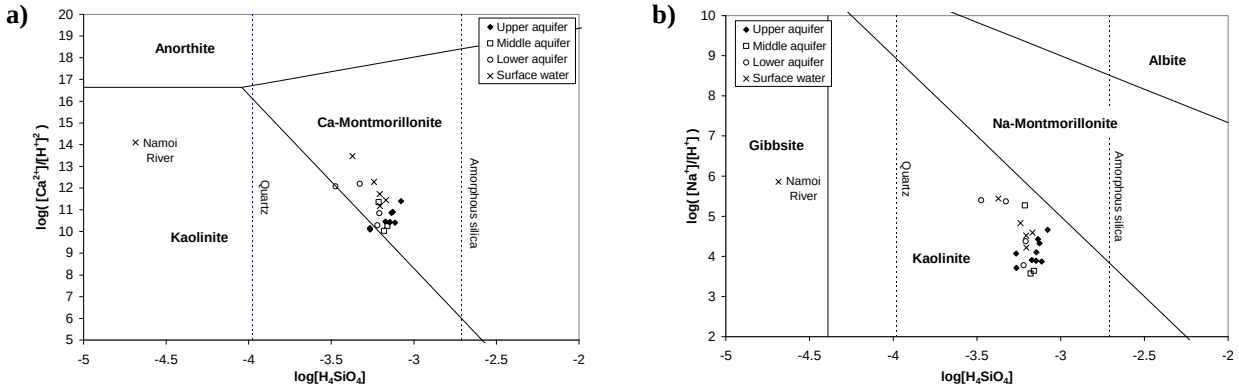

Fig. 9. Stability diagrams for idealised a) Ca-silicate system; and b) Na-silicate system, developed from thermodynamic data sourced from Parkhurst and Appelo (1999b) and Langmuir (1997).

5. Discussion

5.1 Geochemical processes

Increases in the major cations Na^+, Ca^{2+} and Mg^{2+} measured against HCO_3^-, and relatively high dissolved silica levels seem to indicate that primary silicate weathering is a key geochemical control on water composition. Leaching of salts from aquifer sediments is also likely to play a role in providing dissolved material. However, the relative contribution from salt leaching cannot be distinguished. Volcanic rocks such as basalt and rhyolite contain reactive primary silicate minerals which are susceptible to weathering (Appelo and Postma 2005), and both basalt and rhyolite formations are extensive in the up-catchment geology of the region and are likely to have provided much of the Quaternary material that comprises the aquifer. Fragments of primary silicate minerals abound within the sediments along Maules Creek and this sort of detrital material is likely to be ubiquitous within the aquifer matrix. Mineral weathering rates for weathering of relatively reactive primary silicate minerals such as plagioclase feldspars are likely to be comparable to the expected timescales of aquifer residence time. Furthermore, different primary silicate phases may have varying degrees of importance through different aquifer units as a result of varying groundwater residence times. More-reactive calcic plagioclases such as anorthite may play a more important role in the Upper aquifer, whereas in the Middle and Lower aquifer, where aquifer residence times are greater, the influence of less-reactive sodic-plagioclases such as albite may be more significant. This could explain the relatively greater increases in Na^+ compared to Ca^{2+} and Mg^{2+} in some Middle and Lower aquifer samples relative to the Upper aquifer in Fig. 7. Secondary silicate weathering products forming from primary silicate weathering are likely to be kaolinite and montmorillonite. The PHREEQC model suggested that anorthite would weather to kaolinite, with the solution sub-saturated ($SI_{Ca\text{-}mont.} \sim -1.5$) with respect to an idealised pure phase Ca-montmorillonite (Parkhurst and Appelo 1999a,b). However stability diagrams, although highly idealised, seem to indicate that the solution may be relatively close to stability with respect to a montmorillonite phase. Overall, there would be a large amount of heterogeneity both in terms of distribution and type of secondary weathering products throughout the aquifer with many different secondary products likely to co-exist. Idealised reactions for weathering of the Ca-plagioclase end member anorthite to montmorillonite, and the Na-plagioclase end member albite to kaolinite are given in Equations 2 and 3 to illustrate the sorts of primary silicate weathering reactions that could be important in the aquifer.

$$\underset{\text{anorthite}}{7CaAl_2Si_2O_8} + 12H^+ + 8H_4SiO_4 \rightarrow \underset{\text{Ca-montmorillonite}}{6Ca_{0.165}Al_{2.33}Si_{3.67}O_{10}(OH)_2} + 6Ca^{2+} + 16H_2O \quad (2)$$

$$\underset{\text{albite}}{2NaAlSi_3O_8} + 2H_2CO_3 + 9H_2O \rightarrow \underset{\text{kaolinite}}{Al_2Si_2O_5(OH)_4} + 2Na^+ + 2HCO_3^- + 4H_4SiO_4 \quad (3)$$

Primary silicate minerals in the aquifer are also likely to contain K^+. However, K^+ concentrations were observed to be relatively constant (Fig. 7) and this may be linked to formation of a secondary silicate mineral phase containing potassium acting to control K^+ concentrations in solution. However, the PHREEQC model indicated that the water composition was strongly subsaturated with respect to the K-containing secondary silicate mineral illite ($SI_{illite} \sim -3.2$). This may indicate that some other secondary silicate mineral phase is locking up K^+, or alternatively K^+ may be adsorbing to clay minerals (Petrides and Cartwright 2006). The possibility of ion exchange reactions was also considered by examining ion ratios as plotted in Fig. 7g,h. However, no clear trends of concurrent increase and decrease in the concentration of sets of cations could be discerned. Therefore there is little evidence for ion exchange processes providing Na^+ to solution, and increases in Na^+ observed in the deeper, down-gradient samples are more likely to be due to weathering of Na-containing primary silicate minerals. The relatively lower levels of Ca^{2+} and Mg^{2+} observed in these deep samples is likely to be related to different geochemical processes across these locations, with some samples located in the Namoi River paleochannel and others within suspected gravel beds beneath thick overlying clay layers.

5.2 Hydrogeology

Various hydrogeological processes can be inferred from the hydrochemical data. The variable and sometimes elevated chloride and alkalinity levels in the Upper aquifer compared to underlying groundwater (Fig. 5) could reflect return flows of irrigation water sourced from deeper aquifer units (Middle and Lower aquifer) recharging the Upper aquifer. Evaporative up-concentration of solutes prior to infiltration is unlikely based on the observed isotope signatures of this groundwater (Andersen et al. 2008). A specific zone of interest in the Upper aquifer was the region of elevated solute load approximately mid-way along the transect in the vicinity of MW36187 (Section 3.2). Solute material could have a geological source as these boreholes are located close to an outcrop of Permian volcanic deposits, however due to the elevated DO and nitrate signatures return flow of irrigation waters may also play a role. In the Middle aquifer at MW30130, high DO (~4 mg/L) and low Cl^- could reveal the presence of deep gravel beds connected to hillslopes at the foothills of Mt Kaputar beneath the thick overlying clay layers. Deep in the Namoi River paleochannel at MW36164, relatively high Cl^-, HCO_3^-, Ca^{2+}, Mg^{2+} and Na^+, $SI_{calcite}$ ~0 (compared to average $SI_{calcite}$ in the aquifer ~ -0.6), and the detection of sulphide, could indicate that this is geochemically 'old' water from within a sand-gravel aquifer which could be isolated from the main aquifer by the overlying clay layer (Fig. 3). In other samples within the Namoi River paleochannel, similarities in the major ion signature through vertical depth of the aquifer and compared to surface water supports the hypothesis that surface water is a source of recharge to the aquifer, which would be most significant during summer pumping. Furthermore, the hydrochemical data including P_{CO2}, DO, Cl^- and HCO_3^- have confirmed previous conclusions that groundwater discharge upstream of Elfin Crossing plays an important role in supplying baseflow to Maules Creek.

Fig. 10 summarises a conceptual model of the aquifer system and integrates the hydrochemical and hydrogeological process understanding developed in this investigation, with the surface water-groundwater interactions investigated previously (Andersen and Acworth 2007a,b).

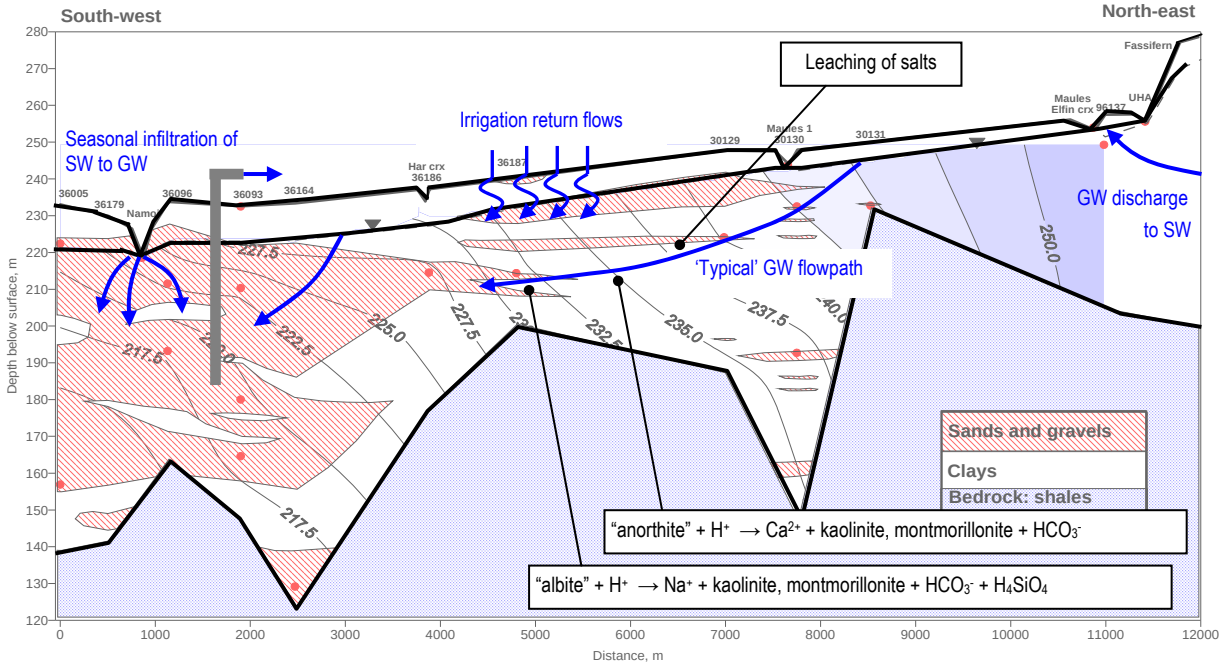

Fig. 10. Conceptual model of hydrogeology and hydrogeochemistry developed from the hydrochemical investigation, and from previous investigations by Andersen and Acworth (2007a,b).

6. Conclusion

This study shows how major ions can be used as natural tracers to characterise geochemical processes occurring in a connected surface water-groundwater alluvial aquifer system in a semi-arid environment. Weathering of primary silicates was found to be a significant process controlling aquifer hydrochemistry, in addition to leaching of salts. However by also considering the role of geochemical processes in relation to hydrogeological processes further insight into aquifer hydrogeology was gained. For example, similarity in the major ion signatures of groundwater compared to surface water in the vicinity of the Namoi River indicates that surface water recharges the aquifer. In addition hydrochemical data suggest that the hillslope regions may potentially contribute to aquifer recharge via deep gravel beds connected to the upper parts of the catchment. The hydrochemical data also indicate that groundwater deep within the paleochannel may be somewhat disconnected from the overlying aquifer. By combining this understanding with previous knowledge of surface water-groundwater interactions at the site, an integrated conceptual model of the aquifer system was developed. Overall this study demonstrates how concurrent hydrochemical and hydrogeological studies using major ion chemistry and basic hydrogeology in this case, can shed significant light on aquifer processes.

Acknowledgements We gratefully acknowledge the funding by the Cotton Catchment Community CRC (Project No. 2.02.03). We would also like to thank the Department of Water and Energy (DWE) for allowing us access to sampling their system of monitoring wells. In addition we would like to thank Rachel Gilmore for assisting with sampling and analysis in the field and Sue and Ken Crawford for providing accommodation and meals.

References

Andersen MS, Acworth RI (2007a) Surface water groundwater interactions in an ephemeral creek in the Namoi Valley, NSW, Australia – Controls by geology and groundwater abstraction. Paper presented at the 35th Congress of IAH, Universidade de Lisboa, Portugal, 17-21 September 2007.

Andersen MS, Acworth RI (2007b) Hydrochemical investigations of surface water groundwater interactions in a sub-catchment in the Namoi Valley, NSW, Australia. Paper presented at the 35th Congress of IAH, Universidade de Lisboa, Portugal, 17-21 September 2007.

Andersen MS, Meredith K, Timms W, Acworth RI (2008) Investigation of δ18O and δ2H in the Namoi River catchment – elucidating recharge sources and the extent of surface water/groundwater interaction. Paper presented at the 36th Congress of IAH, Toyama City, Japan, 26 October-1 November 2008.

Appelo CAJ, Postma D (2005) Geochemistry, Groundwater and Pollution. 2nd Ed. A.A. Balkema, Rotterdam. 649 pp.

DNR (2006) Bore log database. Department of Natural Resources, NSW, Australia.

Langmuir D (1997) Aqueous Environmental Geochemistry. Prentice Hall, New Jersey, 600 pp.

NSW Department of Mineral Resources (DMR) (1998) Gunnedah Coalfield (North) Regional Geology (1:100,000 map). Geological Survey of NSW, Department of Mineral Resources, Sydney, Australia.

Parkhurst DL, Appelo CAJ (1999a) PHREEQC (version 2), US Geological Survey, Available: http://wwwbrr.cr.usgs.gov/projects/GWC_coupled/phreeqc/.

Parkhurst DL, Appelo CAJ (1999b) User's Guide to PHREEQC (Version 2) - A Computer Program for Speciation, Batch-Reaction, One-Dimensional Transport, and Inverse Geochemical Calculations, US Geological Survey, Denver, Colorado.

Petrides B, Cartwright I (2006) The hydrogeology and hydrogeochemistry of the Barwon Downs Graben aquifer, southwestern Victoria, Australia. Hydrogeology Journal, 14(5): 809-826.

Sinclair P, Barrett C, Williams RM (2005) Impact of groundwater extraction on Maules Creek - Upper Namoi Valley, NSW, Australia. Paper presented at the NZHS-IAH-NZSSS 2005 Conference, Auckland, 29 November-1 December 2005.

Sophocleous M (2002) Interactions between groundwater and surface water: the state of the science. Hydrogeology Journal, 10: 52-67.

Stumm W, Morgan JJ (1981) Aquatic Chemistry: Chemical Equilibria and Rates in Natural Waters. 2nd Ed. John Wiley & Sons, New York, 780pp.

Winter TC, Harvey JW, Franke OL, Alley WM (1998) Ground Water and Surface Water: A Single Resource. USGS Cir.1139, 75p.

Stream-aquifer interactions in the Maules Creek catchment, Namoi Valley, New South Wales, Australia

Martin S. Andersen · R. I. Acworth

Abstract The interaction between surface-water streams and groundwater in the Maules Creek catchment of northern New South Wales, Australia has been investigated using a wide range of techniques. Zones of groundwater discharge were mapped by measuring the temperature and fluid electrical-conductivity distribution in bores and surface water. Zones where surface water appears to be recharging the aquifer were investigated by measuring the vertical head gradient between the stream and adjacent bores and by estimates of the decreasing surface flow. Geological heterogeneity appears to be the most significant factor in controlling exchange. Lithological information was assembled using geophysical logging of existing bores, supplemented by the results of electrical resistivity imaging. A preliminary water balance was assembled from the available State records of groundwater abstraction for irrigation, rainfall, evapotranspiration and flow gauging in Maules Creek and the adjacent Namoi River. The analysis has demonstrated the complexity of these coupled systems and gives an indication of the most efficient techniques to be deployed in the field to investigate these complex but important systems.

Keywords Groundwater/surface-water relations · General hydrogeology · Geophysical methods · Groundwater recharge/water budget · Australia

Introduction

The exchange of water between streams and aquifers has recently received increased attention as it has been recognized how important such processes are for the ecological health of streams and rivers (Findlay 1995; Winter 2001; Winter et al. 1998; Woessner 2000) and for groundwater ecosystems (Hancock et al. 2005; Humphreys 2009). Surface water and groundwater have in many cases in the past been managed as separate resources (Winter 2001; Braaten and Gates 2003). However, in areas where there is considerable connection between the two resources, such management practices cause conflict in resource allocations between users as well as potential water stress for groundwater dependent ecosystems (Winter et al. 1998; Fullagar et al. 2006). It is increasingly realized that understanding exchange processes is a necessity for proper water-resource management on the catchment scale (Brodie et al. 2007). This in turn necessitates extensive field mapping and monitoring of spatial and temporal changes in the exchange of water.

Stream–aquifer interactions are complex in space as well as in time (Morrice et al. 1997; Wroblicky et al. 1998; Cey et al. 1998; Fleckenstein et al. 2006). The type of interaction may vary as the scale changes from shallow hyporheic interactions such as in pool and riffle systems (Harvey and Bencala 1993); through meander necks (Peterson and Sickbert 2006); to exchange on a more regional scale (Hinkle et al. 2001). Extensive groundwater abstraction has been shown to result in changes in the regional exchange of water causing a general decrease in groundwater discharge (Winter et al. 1998; Sophocleous 2000; Winter 2007). On a smaller scale, the interactions are quite variable but often characterized by an in-flux of groundwater or hyporheic zone water at the upstream end of pools and an out-flux in the downstream end (Harvey and Bencala 1993). However, these general patterns are significantly perturbated by stream geometry (curvature), the permeability of the stream-bed sediments and temporal variations in stream water levels, each potentially making the exchange of water extremely variable (Lee and Hynes 1977; Cey et al. 1998; Duff et al. 2000; Fleckenstein et al. 2006). Understanding such systems thus requires detailed field investigation under variable hydrologic conditions, e.g. seasonal climatic variations (Morrice et al. 1997; Wroblicky et al. 1998), seasonal regulated surface water flows (e.g. dam releases) and groundwater pumping (Winter et al. 1998). For more regional scale studies, this becomes increasingly difficult thus prompting the need for extensive data collection (Fleckenstein et al. 2006) or methods that integrate over larger scales (Kalbus et al. 2006; Ivkovic 2009).

Received: 13 April 2008 / Accepted: 25 June 2009

M. S. Andersen (✉) · R. I. Acworth
Water Research Laboratory,
School of Civil and Environmental Engineering,
University of New South Wales,
NSW 2093, Sydney, Australia
e-mail: m.andersen@wrl.unsw.edu.au
Tel.: +61-299-494488
Fax: +61-299-494188

Hydrogeology Journal
Published online: 12 August 2009
DOI 10.1007/s10040-009-0500-9

The dynamics of stream–aquifer interactions are still relatively poorly understood (Winter et al. 1998; Sophocleous 2002; Kalbus et al. 2006). This is probably due to the fact that directly measuring water fluxes is notoriously difficult. Devices such as the Lee-type seepage meter (Lee 1977; Lee and Cherry 1978) are prone to artifacts, are time consuming and finally yield only point estimates of flux (Libelo and MacIntyre 1994; Cey et al. 1998; Shinn et al. 2002; Murdoch and Kelly, 2003; Andersen et al. 2007). Darcy-type flux calculations, by evaluating head and permeability variations, may, on the other hand, give larger scale (10s to several 100s of meters) estimates depending on piezometer locations. However, they rely on a detailed investigation of the geology and related permeability distribution (Cey et al. 1998). This is often not attainable on larger spatial scales, especially in complex alluvial deposits where the permeability may vary orders of magnitude on a scale of 10s of meters or less (Cey et al. 1998; Huggenberger et al. 1998; Fleckenstein et al. 2006). In addition, relatively thin layers of fine-grained low-permeable material (clay and organic matter) may line the streambed. This may cause the flux of water to be overestimated by orders of magnitude if bulk aquifer hydraulic conductivities are applied in the Darcy estimate. The problems outlined above indicate that a suite of methods should be employed when investigating exchange processes and constraining water fluxes.

Study site

The Maules Creek sub-catchment to the Namoi River has a surface area of approximately 1,100 km^2 (Fig. 1) and is located on the western slopes of the Great Dividing Range south-east of the township of Narrabri, NSW, Australia. It is bound to the east by the New England Fold Belt and the Great Dividing Range; to the north by the Nandewar Range and Mount Kaputar (altitude: 1,510 m); to the south by the Leard State Forest and Gins Leap Gap: and to the west by a low ridge of hills that represent the edge of the Great Artesian Basin sediments (Fig. 1). The Namoi River flows into the catchment from the south and drains an area of approximately 23,000 km^2 .The river is gauged at two locations at either end of the sub-catchment. The Boggabri gauge (Fig. 1) is located upstream of Gins Leap, a narrow (1,000 m) constriction in the valley. The downstream Turrawan gauge is at the northern end of the catchment (Fig. 1). The aquifer material comprises coarse alluvium comprising well-rounded cobbles and sand derived from weathering of a Tertiary volcano (Mount Kaputar) in the Nandewar Range (Fig. 1). Horse-arm Creek and Middle Creek directly drain the Mt Kaputar area in the Nandewar Range while Maules Creek follows a longer path over fractured and folded Palaeozoic sediments before turning west to enter the Quaternary alluvial plain of the Maules Creek catchment (Fig. 1). The Quaternary sediments comprise gravels and clays overlying Permian volcanics and coal measures. An early Tertiary channel has been cut into these deposits which the current Namoi River partially follows. Sands and gravels in this 120-m deep channel form an important groundwater resource. The climate is semi-arid and in the lower part of the catchment along the Namoi River, flood irrigation farming relies on extensive groundwater abstraction from a palaeochannel of the Namoi River to grow cotton, sorghum and wheat.

Maules Creek is a tributary to the Namoi River and is largely ephemeral, but has a perennial section in its middle reach. At low-flow conditions, the surface-water flow in Maules Creek at this middle reach (near Elfin Crossing (Fig. 1)) is exclusively controlled by surface-water/groundwater interactions (Sinclair et al. 2005), since the reaches above and below this reach dry out except when the creek is in flood. This makes it a very suitable site for studying stream–aquifer exchange processes and for testing techniques for measuring and mapping surface-water/groundwater interactions.

The objectives of this report are to: (1) describe surface water and groundwater exchange processes at a connected stream–aquifer system in the Maules Creek sub-catchment to the Namoi River located in northern New South Wales, Australia (Fig. 1); and (2) to evaluate the techniques that were applied to describe the exchange of water between the aquifer and streams.

Methodology

A series of deep monitoring bores installed to bedrock by the Department of Natural Resources since the 1970s were utilized in this study (Fig. 2). Frequently, separate piezometers were installed at each site, targeting the main aquifer horizons. Well completion data and lithological logs were obtained from the Department. These logs often contained ambivalent lithological descriptions such as: “sand coarse some clay” or “clay sandy” causing considerable uncertainty about the hydraulic properties of the layers in question. Furthermore these descriptions seem to vary between bores depending on the driller. This necessitated more objective measures of the hydraulic properties of the sediments. As a consequence, geophysical logs were generally run in the deepest piezometer at each bore location. A Geovista logging system (winch: GV 100 series, model 118) was used to run the logging tools. At each site the following logging tools were employed: caliper, natural gamma and EM39 (Geonics EM39 induction sonde). As part of this study the monitoring bores (Fig. 2) were dipped to obtain water levels and sampled for fluid EC and temperature.

Resistivity imaging of the subsurface was obtained at selected sites (Fig. 2) in the Maules Creek streambed by using multi-core cables with an array of steel electrodes spaced 2.5 or 5 m apart. The cables were connected to an ABEM LUND ES464 switching unit and to an ABEM SAS4000 Terrameter. Surface-water investigations were carried out along the flowing reach of Maules Creek in the beginning of August 2006 before

DOI 10.1007/s10040-009-0500-9

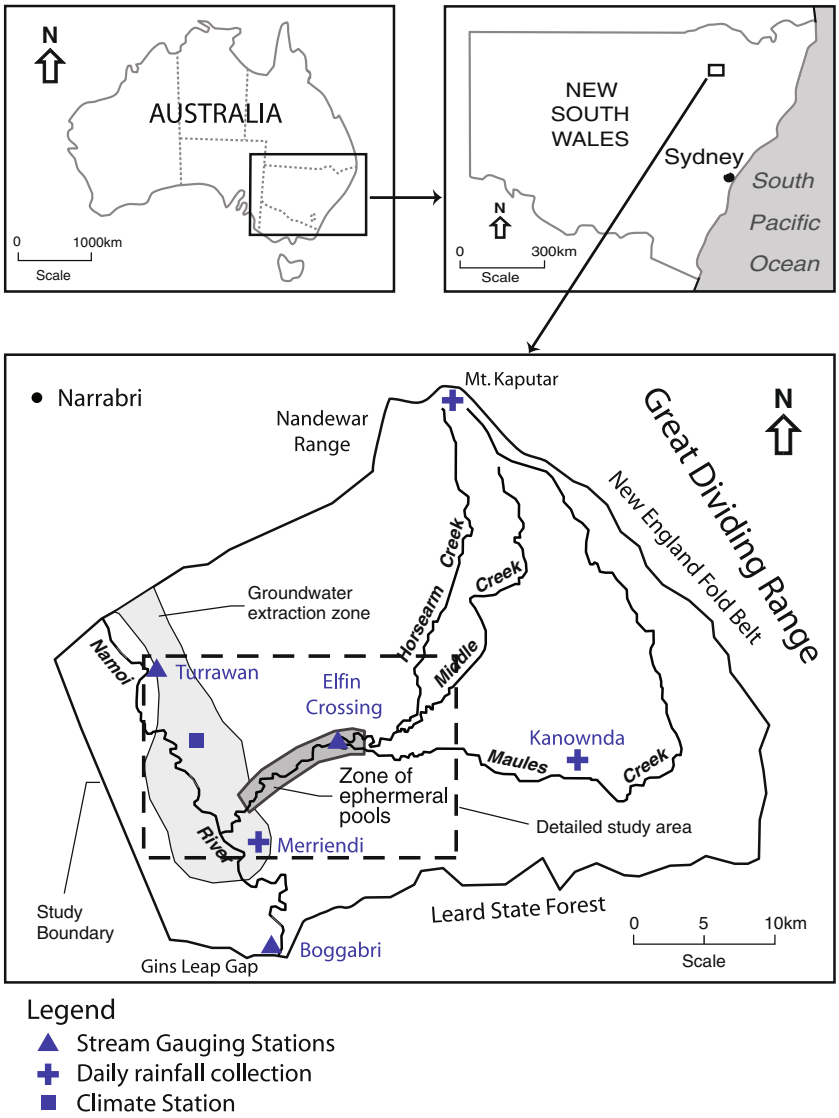

Fig. 1 Location of the Maules Creek study area in New South Wales (NSW), Australia. *Insert* shows the study area with the approximate location of the semi-permanent pools on Maules Creek and the zone of groundwater abstraction

the onset of the irrigation season and later at the end of October 2006, some time into the irrigation season. A HACH SensION-156 EC-meter with a 4-pole conductivity probe was used to measure groundwater and surface-water electrical conductivity (EC) and temperature. The positioning of piezometers and well levels and water levels along the creek was obtained by Real Time Kinematic (RTK) differential GPS using Trimble 5800 equipment. The RTK DGPS precision was generally better than 0.015 m in the horizontal plane and 0.02 m vertically. However, the precision below dense tree cover was considerably poorer with a precision probably in the order of meters. This was something of a problem along the stream channel which was frequently covered by trees. Daily rainfall data for the period 1966–2007 was obtained from the Australian Bureau of Meteorology (BOM) for two sites in the study area (Fig. 1). From October 2007, full daily climate data was measured using a Campbell Scientific climate station installed in the lower part of the catchment area (Fig. 1). The annual distributed groundwater abstractions for the study area were obtained from the Department of Water and Energy (NSW) and surface-water diversion data were obtained from Statewater (NSW).

Results

Geophysics

Well logging

A number of logging tools were run in most of the deeper monitoring bores throughout the catchment. Figure 3 shows gamma and bulk electrical conductivity logs in two bores. Figure 3a shows a log from bore 36164 in the western part of the study area (location see Fig. 2). Since the groundwater is generally fresh in this area with

DOI 10.1007/s10040-009-0500-9

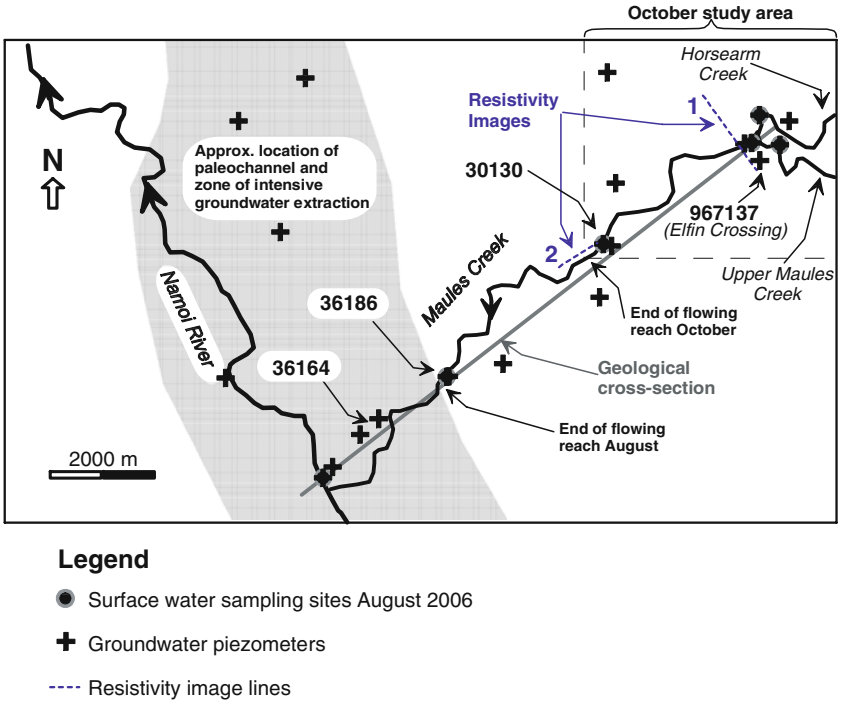

Fig. 2 The Maules Creek study site with location of surface-water sampling sites in August 2006. *Insert* shows area investigated during end of October 2006. The *grey line* shows the location of the geological cross-section and the *short dashed lines* (not to scale) show the location of resistivity images 1 and 2

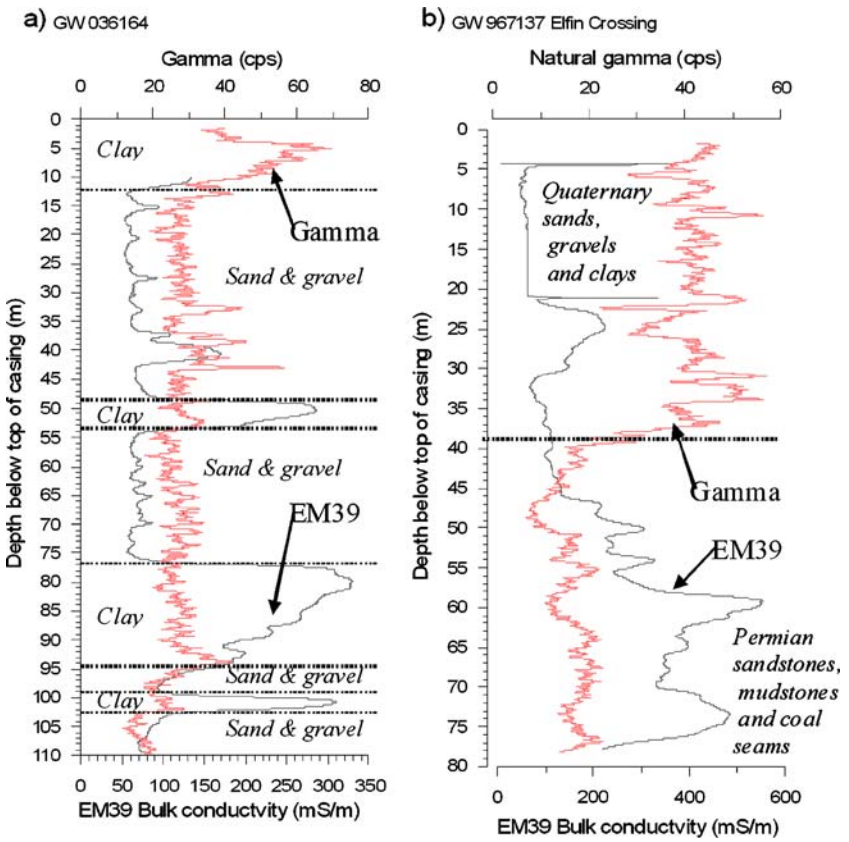

Fig. 3 Examples of geophysical bore logs and lithology from monitoring bores. *Black lines* denote EM39 logs (mS/m) and *red lines* denote natural gamma logs (counts per second). **a** bore 36164 and **b** 967137. For locations see Fig. 2

 DOI 10.1007/s10040-009-0500-9

measured fluid electrical conductivity not exceeding 1,600 μS/cm (Andersen and Acworth 2007), the peaks of high conductivity in the electromagnetic induction log (EM39) must be caused by clay layers, in this case at the surface, at 40, 50, 80 and 100 m (Fig. 3a). Distinct peaks in bulk electrical conductivity are thus interpreted as low-permeable clay layers.

It is surprising that the gamma-logs appear to have problems in distinguishing between the clay and the sand and gravel lithologies. An explanation could be that the Quaternary sands and gravels of the Maules Creek Catchment are derived from the volcanic Mt Kaputar complex having very high potassium (K) content (Department of Mineral Resources 2002). The total K content in the clay layers and the more coarse alluvium could therefore be comparable. The gamma-tool is therefore a poor tool for distinguishing between lithologies within the Quaternary alluvium. In contrast, the logs from bore 967137 (Fig. 3b) show a distinct decrease in the gamma signal at 39 m. In this case the decrease appears to correlate with the interface between the K-rich Quaternary deposits and the seemingly more potassium deprived Permian sediments of the Maules Creek Formation. The well-log results, EM39 in particular, were used to augment the lithology derived from the drillers-logs and to enable a hydrogeological interpretation of the stratigraphy.

Resistivity imaging

Resistivity imaging (Fig. 4a,b) at two sites along the creek (location see Fig. 2) gives a representation of the shallower (< 50 m) lithology below the creek bed. The image acquired across the streambed (Fig. 4a) shows an upper zone of 5–10 m with a resistivity ranging from 70–1,000 Ohm m. Below this zone, the resistivity drops to between 2 and 100 Ohm m. The automated image interpretation was compared to the lithological data from bore 967137 located at 685 m in the profile (Department of Natural Resources 2006). In the bore, the upper 5 m is described as loamy and unsaturated sand followed by gravel down to 11 m. The decrease in resistivity corresponds to a transition into a more clayey lithology from 11 to 31 m. A sequence of interlayered sands and claystones are found from 31 to 76 m and could perhaps explain the increasing resistivity below 30 m at the bore location. Weathered volcanic bedrock (Permian) is encountered at 76 m grading into solid bedrock at 78 m. The high resistivity in the upper part of the image (Fig. 4a) thus appears to represent variably saturated sands, gravels and cobbles deposited in the streambed of Maules Creek. The resistivity image traversing the creek (Fig. 4a) thus gives an impression of the width of the sands and gravels in the streambed, which at this site is less than 200 m. Further to the north, several high resistivity zones are seen at 10–20 m depth probably representing former stream channels filled with sand, gravel and cobbles. These deposits could serve as conduits for groundwater flow. Further north of the bore location, resistivities are considerably lower at depth (> 20 m) indicating the presence of thick clay layers perhaps with pore water of elevated salt content.

Figure 4b shows an image run along the bottom of the streambed in Maules Creek (for location see Fig. 2) and again reveals an upper zone (2–3 m) of higher resistivity (70–200 Ohm m) which could represent coarse streambed sediments. Below this the resistivity is generally quite low (8–20 Ohm m), possibly representing a more clayey lithology. However, several deeper zones of higher resistivity (up to 100 Ohm m) are present, e.g. at 100 and 160 m. It is possible that these zones represent a more sandy/gravely composition, which could be permeable conduits connecting the streambed to the aquifer below. Unfortunately, no bores with lithology were available in the immediate vicinity of this profile to verify the interpretation.

Geology

The geology of the catchment is rather complex. In the southern and central part, the bedrock geology of the catchment consists of Permian volcanic deposits of rhyolitic and dacitic composition which in the central and southern part form the Boggabri Ridge. To the west and southeast, the bedrock is overlain by a sequence of Permian sedimentary deposits (also known as the Maules Creek formation) consisting of claystones, siltstones, sandstones, conglomerates and coal measures (Department of Mineral Resources 1998). A major regional thrust (The Mooki Thrust) zone runs approximately north–south through the eastern part of the catchment and separates the Permian sediments and volcanic deposits from Carboniferous crystalline, meta-sediments and volcanic deposits (Department of Mineral Resources 1998) of the New England Fold Belt. To the north, the geology is dominated by the Middle Miocene (20–17 million years ago) basaltic and trachytic lava flows of the Nandewar Range (Young et al. 2002) that have been emplaced along the Mooki Thrust zone. In the central part of the catchment and at lower altitudes, the bedrock is overlain by Tertiary and Quaternary alluvial deposits that vary in total thickness from 20 to more than 120 m and consist of clays, sands and gravels. A large and more than 100 m deep north–south oriented palaeochannel, filled with Quaternary sands and gravels, is situated below and to the east of the Namoi River (Fig. 2). The approximate location of this channel was determined by examination of the existing borehole records.

Figure 5 shows a geological cross-section through the palaeochannel and up along Maules Creek, based on the drillers-logs from the monitoring bores (Department of Natural Resources 2006). The division between clay, and sands and gravels are aided by the geophysical well-logs. However, the bores are quite frequently several km apart and as a consequence, the interpolation of geology between bores is clearly subjective and contains considerable uncertainty. Nevertheless, the cross-section clearly shows the overall features with the more than 120 m deep and 4 km wide palaeochannel to the west and the

DOI 10.1007/s10040-009-0500-9

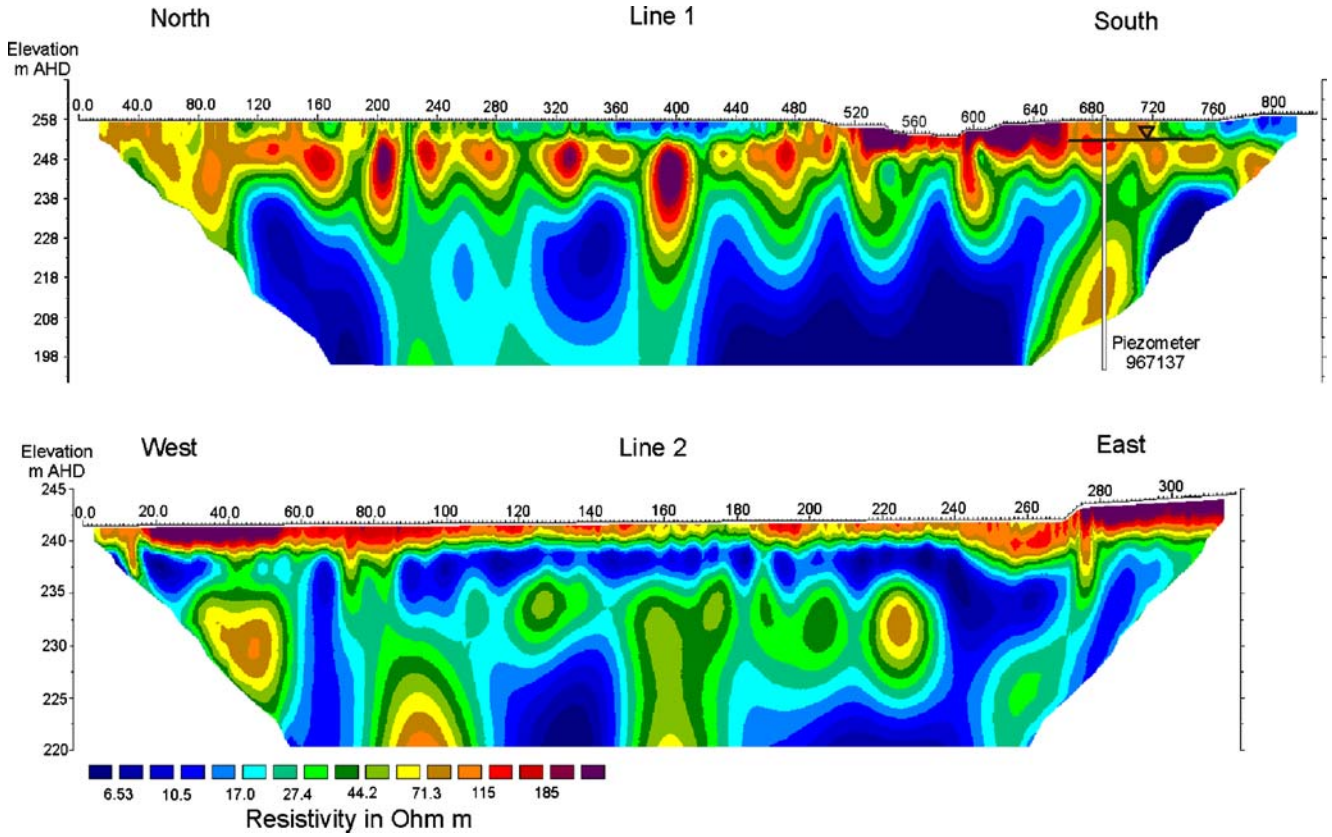

Fig. 4 Resistivity images: **a** *Line 1* across Maules Creek. Electrode spacing 2.5 m. Location of bore 967137 and the water table is indicated. **b** *Line 2* along the creek. Electrode spacing 1.25 m. (For location see Fig. 2)

gradually more clay dominated lithology to the east. The palaeochannel is cut into the underlying Permian Maules Creek Formation and was established by mid Tertiary times (Young et al. 2002). It is not clear exactly when the channel fill commenced and whether gravels derived from weathering the late Tertiary basalt from Mount Kaputar form the deepest gravels or whether these predate the volcanic emplacement. The sands and gravels in the

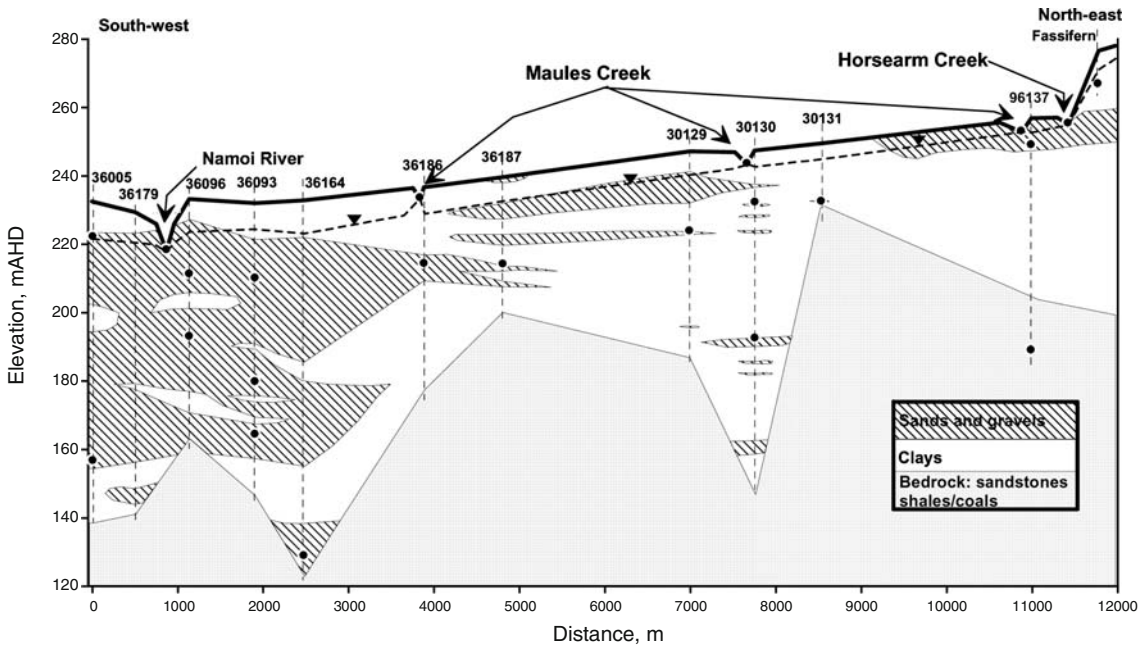

Fig. 5 Geological cross-section along Maules Creek based on bore-logs (Department of Natural Resources 2006) and geophysical results (see Fig. 2 for location). *Notches* in the surface topography indicate where the creek intersects the cross-section. *Dots* indicate location of screened piezometers in the aquifer. The water table is based on the water level in the shallowest piezometer at each site

 DOI 10.1007/s10040-009-0500-9

palaeochannel form a high yielding aquifer and an important source of groundwater for local irrigated farming.

Climate data

Rainfall is variable both across the catchment (spatially) and from year to year (temporally). The annual average in the lower parts of the catchment is 590 mm/year (1966–1997). Figure 6a shows the monthly rainfall of the lower catchment from 2005 to 2007. In the higher areas of the catchment to the north and east (as on Mt Kaputar) average rainfall is about 1,224 mm/year (1967–1987). As part of this research program, a climate station was installed in September 2007 in the central part of the study area. Data from this climate station highlights the variable rainfall which is dominated by storms (Fig. 6b) in summer. The cumulative rainfall at this station for the year 2007–2008 was 560 mm.

The average daily maximum and minimum air temperatures for the same site and period are 25.8 and 9.6°C, respectively, with a mean of 17.7°C (Fig. 6c). In the 2007 winter period (May to October), the climate station recorded average daily maximum and minimum air temperatures of 20.6 and 3.9°C, respectively, with a mean of 12.2°C. Potential annual evapotranspiration (ET_P) is high and has been estimated to 1,200 mm in the Nandewar Range, increasing to 1,800 mm in the lower altitudes of the catchment.

Stream flow

Stream flow patterns are quite diverse in the study area. The Namoi River flows into the study area from the south

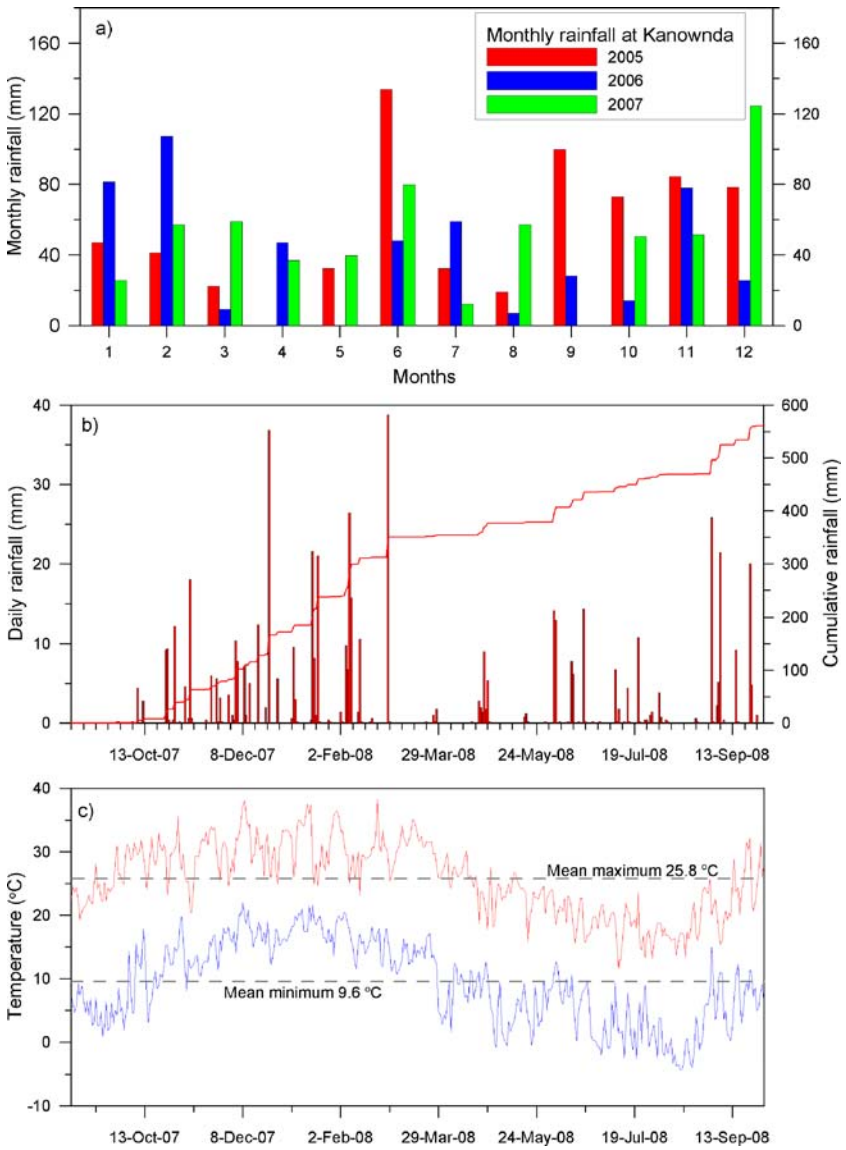

Fig. 6 **a** Monthly averages of daily rainfall from the Kanownda site for the years 2005–2007. **b** Daily and cumulative rainfall for the climate station for the water year 2007–2008. **c** Daily maximum and minimum air temperatures for the climate station for the water year 2007–2008

 DOI 10.1007/s10040-009-0500-9

and is dominated by regulated flow from dam releases higher in the Namoi Valley and storm derived flooding events. Flows in Maules Creek and its two main tributaries Horsearm and Middle Creek (Fig. 1) are unregulated. The upper reaches of Maules Creek and tributaries drain the basaltic slopes of the Nandewar Range (Fig. 1). However, only during severe storms and associated flooding do Maules Creek and its tributaries flow across the alluvial fan between the mountains and the confluence of Maules and Horsearm Creeks at Elfin Crossing. To the east of Elfin Crossing (a road crossing to the creek that forms a weir), the creek flows through a constriction in the Quaternary sediments (see Fig. 1). A gauging station in the weir pool monitors water levels and surface-water flow into the lower part of the Maules Creek catchment. It appears that the surface-water runoff from the upper reaches infiltrate the valley alluvium below the foot slopes, which is composed of basalt boulders, cobbles and gravel originating from Mount Kaputar. Further down in the catchment, very clean groundwater with a low content of dissolved solids (EC <300 μS/cm) discharges into a number of deep pools upstream of Elfin Crossing to form renewed surface-water flow near the confluence of Maules and Horsearm Creek. This surface flow continues through a 2-km stretch of semi-permanent pools (Fig. 1). The stretch from the last pools and downstream to the Namoi River (approximately 8–10 km) is usually dry. However, in August 2006 (winter) stream flow extended about 8 km downstream from the confluence of Maules and Horsearm Creek (Fig. 2) but still did not reach the Namoi River. By October 2006 (spring), stream flow only extended 4 km downstream from the confluence (see Fig. 2).

Figure 7a,b show 2 years of daily stream flow time series for Maules Creek at Elfin Crossing and the Namoi River at the upstream site of Boggabri and at the downstream site of Turrawan (locations shown in Fig. 1). The figures highlight the very different flow patterns and volumes of discharge in the two streams. It also shows distinct temporal variations between dry and wet periods. In the unregulated Maules Creek, the first part of the hydrograph (Fig. 7a) from May 2005 to March 2006 is dominated by flow events of short duration caused by rainfall. The later part of the hydrograph from March 2006 to April 2007 shows a gradual decrease in flow. This pattern is also recognizable in the Namoi River. However, the river flow in the period from March 2006 to April 2007 is largely dominated by dam releases. Maules Creek generally exhibits low, but prolonged flow at Elfin Crossing (Fig. 7a). Sharp drops and rapid recoveries in flow at Elfin Crossing during June 2006 are associated with local shallow groundwater abstraction at this time. During the period of zero flow shown between December 2006 and March 2007, surface water was restricted to localized deep pools in Maules Creek upstream of Elfin Crossing.

By calculating the difference in flow through the upstream (Boggabri) and downstream (Turrawan) gauging stations on the Namoi River overall losses or gains can be estimated (Fig. 7c). The data can be presented as either a continuous cumulative difference or as data for specific flow events. Both are presented in Fig. 7c revealing that early in the studied period (around July 2005) there was a significant gain in river flow for the reach. This seems to be linked to short term high flow events generated by rainfall runoff rather than base flow which would be of a more gradual and prolonged nature. This is also supported by the high and erratic surface-water flow in Maules Creek for the same period (Fig. 7a). Later in the study period, large losses are observed in relation to the dam releases. It is thus clear that significant volumes of water are lost between the gauges presumably by river water recharging into the aquifer. Table 1 summarizes the cumulative surface-water flows (and differences for the Namoi River) for the water years (October–September) 2005–2006 and 2006–2007. Based on the annual cumulated difference in flow, the loss is 38,000 and 30,000 ML (mega-liters) for the two water years. Out of these losses only 3.4 and 4.9%, respectively, is due to surface water being diverted for irrigation purposes. The table also demonstrates that surface-water flows as well as apparent losses are orders of magnitudes greater in the Namoi River than in Maules Creek. This is not surprising given the difference in catchment sizes.

Hydraulic gradients

The hydraulic head distribution in the aquifer was determined by measurements in the network of monitoring wells in the Maules Creek catchment shown in Fig. 2. The derived potentiometric surface (Fig. 8a) for August 2006 (winter) indicates a general flow of groundwater westwards towards the Namoi River with a gradient of 0.003. The inferred flow lines roughly parallel Maules Creek. The same general head distribution was observed a few months later in spring (October 2006) when groundwater abstraction for irrigation had started. However, a distinct zone of lowered hydraulic heads was observed in the irrigation area with drawdown of up to 8 m (Fig. 8b). The zone of drawdown approximately coincides with the Namoi palaeochannel (compare Figs. 2 and 8b).

Estimates of vertical-head differences between surface water and groundwater levels were derived at three sites along Maules Creek during August 2006 (Fig. 8a). As there are no nested piezometers available, the head differences do not represent true vertical head difference but have been compiled from the available stream profile and observation well data. The head difference, the horizontal distance and the overall horizontal gradient are shown in Table 2. Near the confluence of Horsearm Creek and upper Maules Creek at Elfin Crossing, there was almost no vertical gradient. However, a significant vertical head difference commences downstream and reached a maximum of −4.4 m at the location where the creek stopped flowing in August 2006 (Fig. 8a). This location appears to coincide with the eastern limit of the palaeochannel of the Namoi River (Fig. 5). Such a large vertical head difference combined with a horizontal head

DOI 10.1007/s10040-009-0500-9

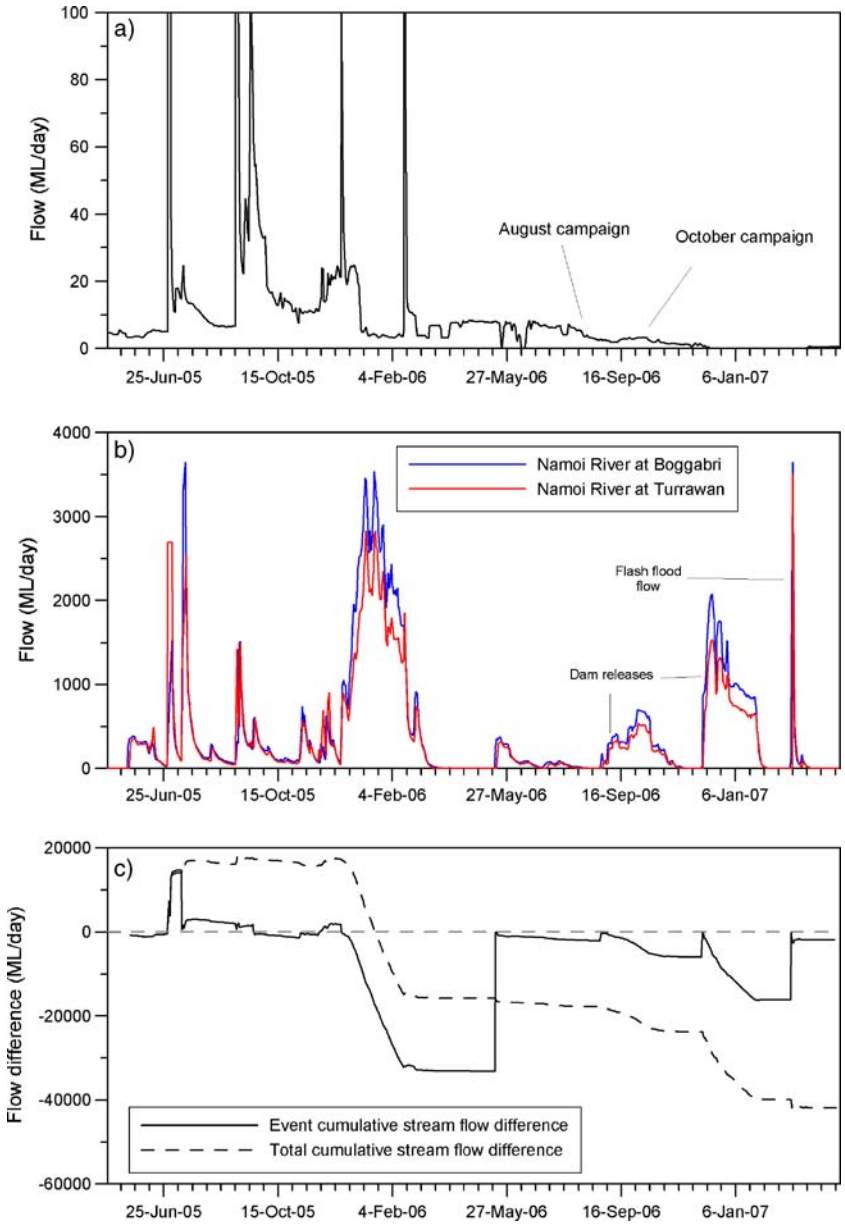

Fig. 7 Stream flow from 1 May 2005 to 18 April 2007 (ML/day) at **a** Elfin Crossing in Maules Creek, **b** Boggabri and Turrawan gauging stations in the Namoi River (Department of Natural Resources 2007), and **c** event specific as well as cumulative differences in stream flow between the Boggabri (upstream) and Turrawan (downstream) gauging stations (negative values indicate water lost from the river). Locations are shown on Fig. 1. Note difference in the scale of the y-axis between plots **a** and **b**

Table 1 Annual cumulative stream flow and surface-water usage for the Namoi River and Maules Creek. For locations see Fig. 1

		Water year[a]	
	Units	2005–2006	2006–2007
River flow upstream gauging station Boggabri	ML[b]	185,682	137,080
River flow downstream gauging station Turrawan	ML	147,675	106,875
Loss or gain between gauges[c]	ML	–38,007	–30,205
Surface-water usage Boggabri to Turrawan	ML	1,288	1,486
Surface-water usage in percent of total loss	%	3.4	4.9
Maules Creek flow at Elfin Crossing	ML	4,430	229
Surface-water usage Maules Creek	ML	0	0

[a] A water year is from October to September

[b] *ML* mega-liters

[c] Minus means the stream is losing to the aquifer

 DOI 10.1007/s10040-009-0500-9

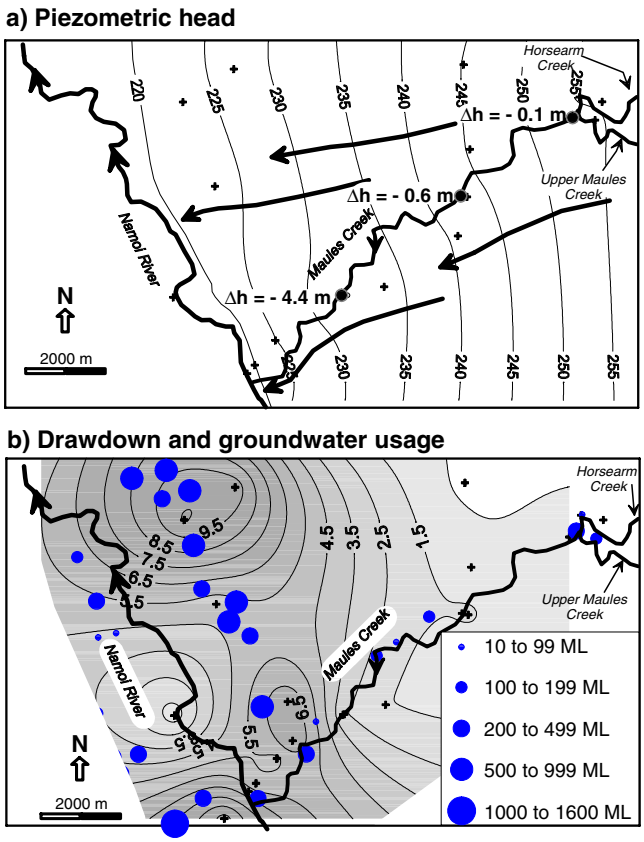

Fig. 8 **a** Hydraulic head distribution (m above Australian Height Datum) in the upper aquifer (< 30 m) August 2006. *Arrows* indicate the general groundwater flow. Vertical head differences (Δ*h*, m) between surface water and groundwater are also shown for three sites (negative for a downward gradient, see also Table 2). **b** Change in hydraulic heads (m) from August to October 2006 (*positive values* indicate drawdowns). Distributed groundwater abstraction volumes for the water year 2006–2007 are superimposed as *circles*

gradient of at least −0.29 m/m indicates a high potential for aquifer recharge, provided that there are favorable hydraulic conductivities of the sediments between the piezometer and the creek bed.

Figure 9 shows a time series of daily water levels from piezometer 36186 (Fig. 2) situated 15 m from the creek bed some 8 km downstream of Elfin Crossing. By comparing it to the flow in Maules Creek, it is apparent that the water level responds by an almost 3 m rise to the increased surface-water flow in the Creek during the later half of 2005. Of similar significance, is the sudden drop in water level after a period of fairly constant flow in the creek during the first 8 months of 2006. During field work, it was noted that the creek stopped flowing adjacent to piezometer 36186 on 16 August. This corresponds to a rapidly declining water level in the bore. These observations clearly demonstrate good hydraulic connectivity between the creek and the aquifer.

Diffuse recharge by infiltrating rainfall (see Fig. 9) may also explain a component of the water level rise at piezometer 36186 but is considered to be of secondary importance in explaining the groundwater hydrograph. An added complication here is that the creek flow also responds to the rainfall, making separation of these two factors extremely difficult.

By October 2006, the flowing reach of the creek had shrunk to a zone close to Elfin Crossing. Surface water was only found in seemingly disconnected pools that extended for a further 4 km downstream (insert Fig. 2). The October 2006 survey in Maules Creek was much more detailed than the survey carried out in August 2006. Measurements were made every 50–100 m and included surface-water level, fluid temperature and fluid EC. The surface-water levels determined by DGPS (Fig. 10a) fall on a very straight line (corresponding to a hydraulic gradient of 0.0025) and indicate that the pool water level represents the groundwater elevation. Contouring of the potentiometric surface (as in Fig. 8a) with and without the inclusion of surface-water levels gave an almost identical picture, further suggesting that there are hardly any gradients between the stream and the aquifer in the upper 4 km during October and that the system has reached a state of equilibrium.

Electrical conductivity and temperature

In August 2006 (winter) surface-water electrical conductivity (EC) and temperatures were measured at 5 sites along the creek (Fig. 11a,b black numbers) and within the aquifer in selected monitoring wells (Fig. 11a,b grey numbers). In the aquifer the groundwater temperatures (Fig. 11a, grey numbers) were very uniform averaging 21.1°C (SD=0.8, n=46), which is 3.4°C higher than the average annual air temperature of the region (Fig. 6c) at that time. In contrast, the measured surface-water temperatures in the study were generally lower, reflecting the cooler winter air temperatures, which for May–October 2007 averaged 12.2°C. In the upper section where the creek starts flowing, the surface-water temperatures were anomalously high: 16–18.1°C, reflecting the discharge of relatively warm groundwater. The surface-water temperatures dropped to around 11.5°C downstream due to cooling by the low winter air temperature and no inflow of warmer groundwater. In conjunction, measured surface

Table 2 Vertical head differences between Maules Creek and nearby wells in the aquifer. Location of wells are shown in Fig. 2 and vertical head differences are shown in Fig. 8a

Well no.	Screened interval [m below surface]	Distance to creek [m]	Vertical head difference [m]	Horizontal gradient[a]
30130	15–16	150	–0.6	–0.004
36186	23–26	15	–4.4	–0.293
967137	8–11	100	–0.1	–0.001

[a] A negative gradient denotes flow from the stream

DOI 10.1007/s10040-009-0500-9

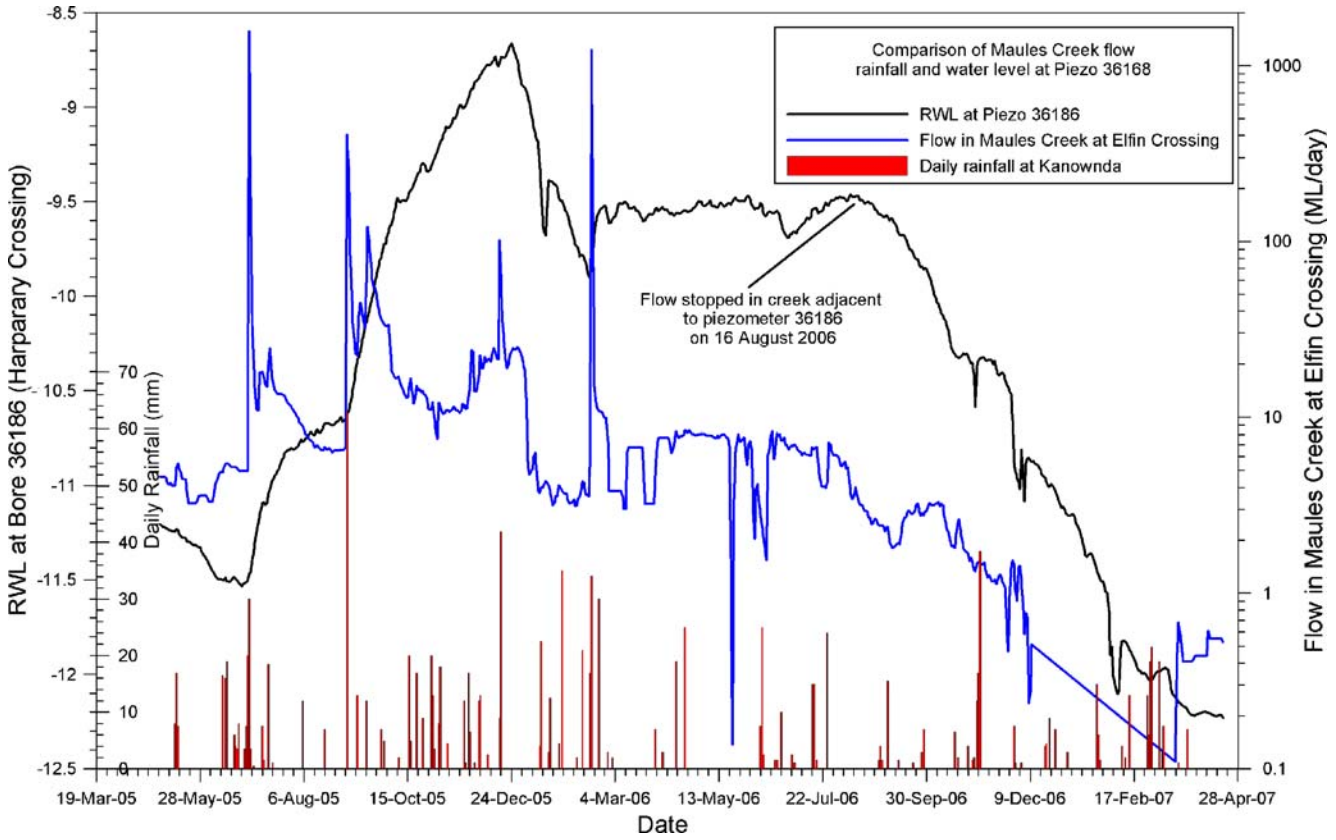

Fig. 9 Daily resting water levels (*RWL*) from piezometer 36186 (location see Fig. 2) situated on the bank of Maules Creek and approximately 8 km downstream of Elfin Crossing. Estimated creek daily flow (note log scale) from Elfin Crossing and daily rainfall are also shown

water and groundwater temperatures indicate that groundwater is actively discharging in the upper part of Maules Creek and its tributary Horsearm Creek. Later in the year (October) temperature measurements did not give any consistent clues about groundwater discharge since, surface-water temperatures were warmer (comparable to groundwater temperatures) and varied more erratically (20–35°C) due to the much warmer air temperatures and possibly also variations in the depth of the pools.

Fluid electrical conductivity, measured in the stream in August 2006 (Fig. 11b), shows low EC groundwater (~300 μS/cm) discharging into the Horsearm Creek and much higher EC groundwater (~800 μS/cm) discharging into the upper Maules Creek reflecting different sources of groundwater from the north and south, respectively (Fig. 11b, black numbers). This is supported by electrical conductivity measurements within the aquifer which range from 290 to 497 μS/cm north of the creek and 542 to 1,613 μS/cm south of the creek (Fig. 11b, grey numbers). In the surface water, EC increases from 330 μS/cm near the confluence of the Horsearm and upper Maules creek to 457 μS/cm at 8 km downstream where the flow disappears.

Later in October 2006, most of the flow was restricted to near the confluence of Maules and Horsearm creek and further downstream, surface water was only found in seemingly stagnant pools. The EC data (Fig. 10b) collected from the creek and the pools clearly shows that, in all probability, low EC groundwater (as low as 237 μS/cm) is still discharging to Horsearm creek from the north, whereas high EC water (830 μS/cm) is residing in Maules creek to the south. Downstream of the confluence there seems to be a rather steady increase in the EC from about 300 μS/cm to more than 600 μS/cm at 4 km downstream. However, there are also several locations where the EC decreases again indicating possible dilution by further influx of groundwater of lower EC. These variations also indicate that the system is rather complex with small-scale variation in hyporheic exchange.

Water balance considerations

To evaluate the relative significance of the river–aquifer exchange on a catchment scale, aspects of the water balance were computed. The aim here was not to obtain a detailed and all-inclusive spatiotemporal water balance, but rather to estimate orders of magnitude for comparison. The water balance calculations were carried out for the two water years (Oct.–Sept.) 2005–2006 and 2006–2007 (Table 3). The total groundwater abstractions for the area increased from 12,205 ML in 1996–1997 to 20,685 ML in 2006–2007. Abstractions for the two water years are shown in Table 3 and individual abstraction volumes for 2006–2007 are superimposed on the drawdown distribution in Fig. 8b. The major abstractions which are located in the palaeochannel (Fig. 2) largely coincide with the distribution of the drawdown (Fig. 8b). There are

DOI 10.1007/s10040-009-0500-9

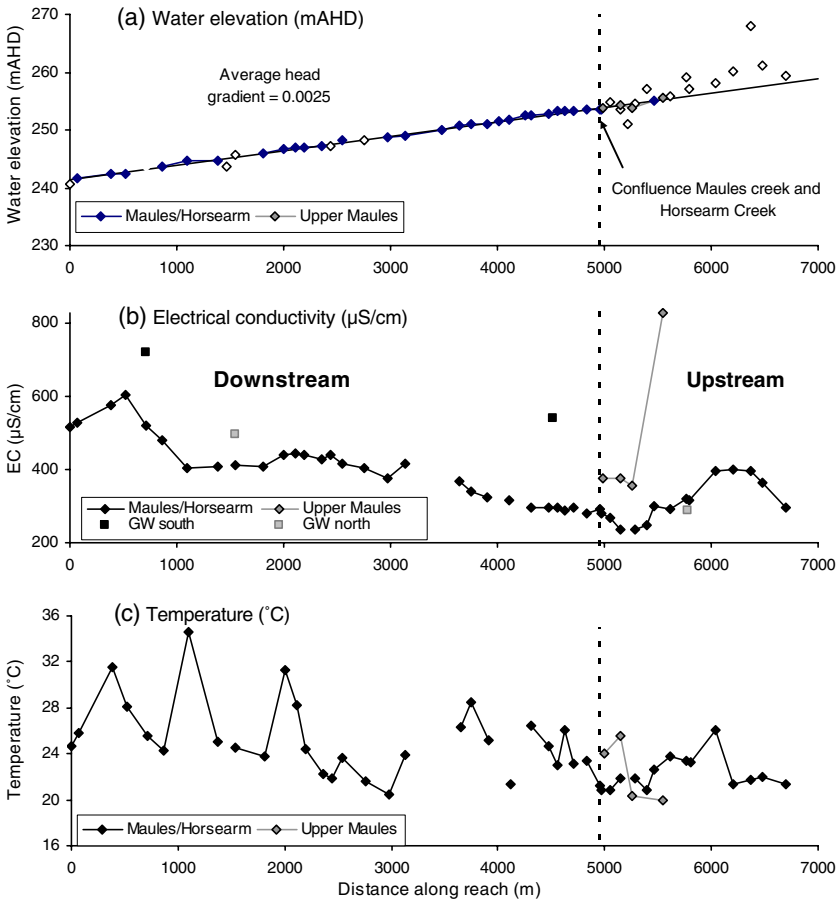

Fig. 10 Surface-water survey in Maules Creek during October 2006: **a** water elevation (m above Australian Height Datum). *Solid diamonds* indicate high precision positioning (h=0.015 m, v=0.02 m), whereas *open diamonds* are poor precision due to dense tree cover; **b** surface-water electrical conductivity (EC; µS/cm). Also included are four measurements of EC in the aquifer in piezometers less than 500 m to the north and south of the creek; and **c** surface-water temperature (°C). The survey commenced at the end of surface flow in Maules Creek (0 m) and extends upstream

discrepancies in the correlation between abstraction and drawdown mainly because abstraction wells and monitoring wells are often far apart (> 1 km) and because individual abstraction bores may not have been in operation at the time when the drawdown was recorded. The volume of surface water diverted for irrigation is small and comprises only about 7% of the total irrigation water use (Table 3).

Intensive flood irrigation of cotton is the main water-consuming agricultural activity in the catchment and it is therefore of interest to compare the water usage with the actual crop water demand. The total area of flood irrigation was estimated to 6,960 ha based on field visits and by analyzing Google Earth images. Seasonal crop evapotranspiration rates (ET_c) for cotton (being the main crop) was calculated by Tennakoon and Milroy (2003) from daily field water balances for several cotton farms in the Namoi region. They obtained 764 mm for 1996–1997 and 781 mm for 1997–1998. In a more recent study, Williams and Montgomery (2008) obtained a seasonal ET_c for cotton of 733 mm for 36 farms in the same region for the water year of 2006–2007. Using this estimate for both years and the calculated irrigated area, the total seasonal cotton crop water usage in the catchment was estimated to be approximately 50,000 ML per season (Table 3). The crop water demand is provided partly by in-field rainfall and partly by the application of surface-water and groundwater. Using the total irrigated area and rainfall records, the total in-field rainfall was 43,000 and 34,000 ML respectively for the 2 years.

If it is assumed that the total measured annual rainfall is all available for crop evapotranspiration (neglecting evaporation from fallow fields in winter and neglecting deep drainage and surface runoff from large rainfall events) then the irrigation loss (as surface-water and groundwater applied, but not utilized by the crop) can be estimated. Irrigation losses of 9,600 and 4,900 ML, respectively, (or 55 and 22%) where obtained (Table 3). These values are obviously subject to considerable uncertainty given the assumptions, but in all probability there appear to be significant losses of irrigation water as tail-water runoff and subsequent evaporation and/or as deep drainage (where an unknown quantity may return to the aquifer). In this water balance, the effects of rainfall, actual evapotranspiration

 DOI 10.1007/s10040-009-0500-9

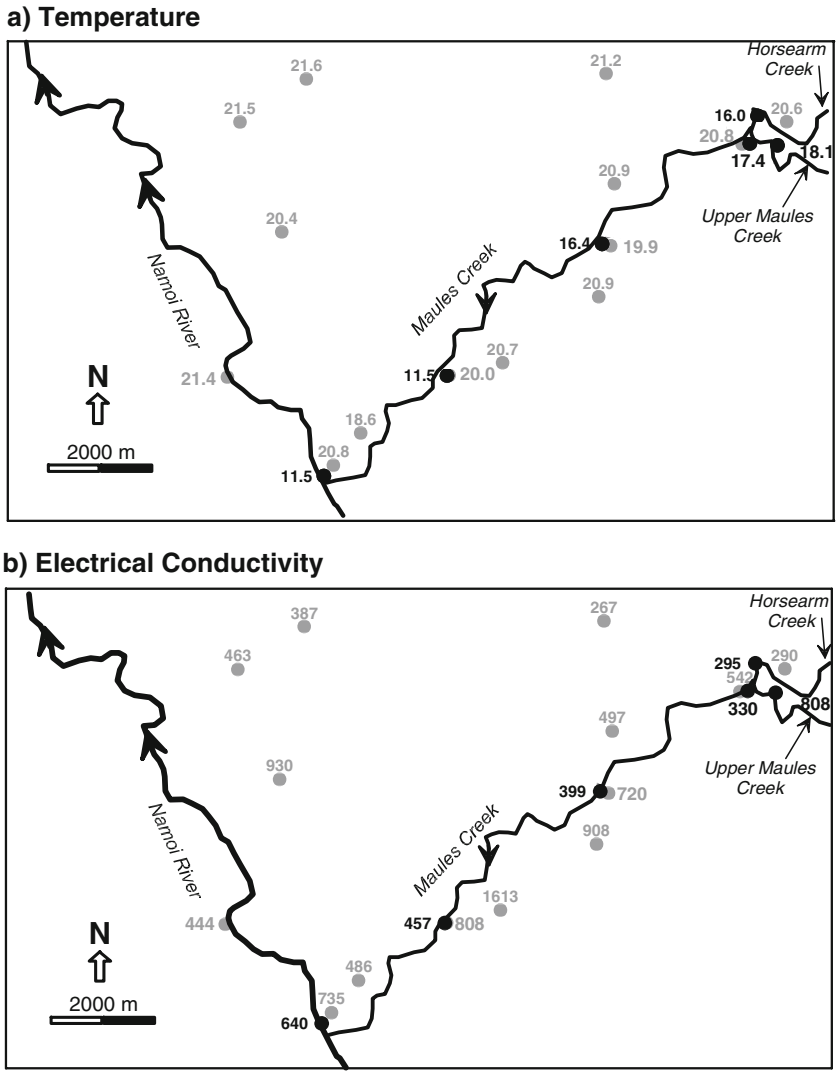

Fig. 11 **a** Temperature (°C) and **b** electrical conductivity (μS/cm). *Black numbers and symbols* are for surface-water measurements in Maules Creek whereas *grey numbers and symbols* are for shallow groundwater less than 30 m below the surface

from natural vegetation (including dry land cropping, woodlands and grasslands) in the remainder of the catchment and thus its possible contribution to recharge and groundwater flow have been neglected. In addition, crop evapotranspiration from crop rotation schemes (with corn, wheat and sorghum) where more than one crop is produced in a year, which would cause the field water use to be underestimated, is not accounted for.

Table 3 Water balance calculations for the Maules Creek study area

			Water year	
		Units	2005–2006	2006–2007
Total flood irrigated area in catchment[a]	A	ha	6,962	6,962
Seasonal cotton crop water use (ET_c)[b]	B	ML/ha	7.33[c]	7.33
Total crop water use in catchment	C = A × B	ML	51,031	51,031
Annual rainfall	D	mm	623	485
Estimated total in-field rainfall	E = A × D	ML	43,373	33,765
Groundwater abstraction	F	ML	15,921	20,685
Surface-water usage	G	ML	1,288	1,486
Adjusted crop water use	H = C − E	ML	7,658	17,266
Irrigation loss	I = F + G − H	ML	9,551	4,905
Irrigation loss	J = I/(F + G)	%	55	22

[a] Estimated using Google Earth

[b] Williams and Montgomery (2008)

[c] Estimate for 2006–2007

 DOI 10.1007/s10040-009-0500-9

Neither are fields left fallow which would tend to cause an overestimation of the overall field water usage. These two sources of error will tend to cancel each other out.

Discussion

By combining the various types of field data obtained in this study, it is possible to assemble a picture of the stream–aquifer exchange processes within the catchment. The use of multiple methods also allows for an assessment of method applicability; the identification of errors and for constraining the various fluxes of water.

It is tempting to resort to the use of seepage meters, since they appear to measure actual fluxes of water through the streambed at given locations. However, the literature abounds with reports of erroneous or biased fluxes due to instrumental factors and operational procedures (Brodie et al. 2009; Cey et al. 1998; Duff et al. 2000). In addition, they have proven exceptionally difficult to employ in coarse gravel or cobble-size materials (Lee and Hynes 1977; Brodie et al. 2009) of the type found in the creeks in this area. For this reason they were not employed in this study and instead use was made of indirect measures.

The analysis of sets of surface-water hydrographs, as carried out in this study, can give valuable information of net exchange of water between the stream and aquifer on the reach or catchment scale. To be valid, any contribution from tributaries and surface runoff has to be insignificant or at least quantified. The apparent gain observed in the early part of Fig. 7c testifies to this. In all probability, this gain is caused by surface-water runoff and not groundwater discharge as indicated by the high surface-water flow in Maules Creek in the same period (Fig 7a). An additional limitation to the use of sets of surface-water hydrographs is that they offer no information on the spatial variability of exchange between the gauging stations. Furthermore, for the method to be accurate, the relationship between the river stage and the flow at gauges needs to be regularly calibrated. This is especially the case in streams with high bed-loads and changing cross-sectional area due to events of scouring and re-sedimentation associated with flooding. So even though this approach appears to be useful for large-scale estimates of net exchange, it is susceptible to significant error.

The Darcy approach has been used extensively in the study of stream–aquifer interactions (Cey et al. 1998). In many studies where new methodologies have been employed or tested, head measurements and the derived gradients and fluxes have been used as a benchmark (Harvey et al. 1996; Morrice et al. 1997; Wroblicky et al. 1998). Head data will certainly indicate potential directions of flow, but without a good understanding of the permeability distribution it may not reveal the actual degree of connectivity, i.e. low permeability layers—e.g. in the streambed sediments (Huggenberger et al. 1998)—may impede flow, and thus not give correct fluxes of water. In this study, a general contouring of the piezometric surface in the aquifer (Fig. 8a) does not indicate that any significant stream recharge is occurring. Only a slight bulge in the 230 m head contour (Fig. 8a) at the eastern margin of the palaeochannel indicates that the stream might be recharging the aquifer. Contouring of the piezometric surface in the aquifer with the surface-water levels in Maules Creek during October also failed to reveal much potential for surface-water/groundwater exchange. This shows that when data is sparse, as in this case where general monitoring piezometers were used, a Darcian approach may be too insensitive to estimate surface-water/groundwater exchange. This appears to be particularly the case if the aquifer transmissivity is large relative to the surface-water flow. Furthermore the effect of stream recharge could be obscured by the much higher rate of groundwater abstraction (compare Tables 1 and 3). In such settings, gradient measurements are needed very close to the stream, as shown in Maules Creek (Fig. 8a). In addition, as pointed out by Sophocleous (2002), the exchange of water may not be linearly related to changes in the head gradient due to geometrical considerations. More importantly geological heterogeneity, as shown in many studies (Morrice et al. 1997; Cey et al. 1998; Huggenberger et al. 1998; Winter et al. 1998; Woessner 2000; Kalbus et al. 2006; Fleckenstein et al. 2006), appears to play a significant role in controlling the location and magnitude of surface-water/groundwater exchange. It is therefore paramount to develop a detailed knowledge of the geology and permeability of the streambed and the immediate vicinity in order to derive quantitative information from head data (Cey et al. 1998).

For a gaining stream (discharge of groundwater) measuring tracers, such as temperature and chemical solutes, in the stream can be very useful to qualitatively locate zones of discharge (Cook et al. 2003; Baskaran et al. 2009b). If groundwater tracer levels are well constrained, it becomes possible to quantify fluxes and to differentiate between hyporheic flows and more regional groundwater discharge. In-stream temperature measurements during winter successfully located zones of relatively warm groundwater discharging into Maules Creek (Fig. 11). This approach may be of limited applicability at times of the year when average stream and groundwater temperatures are comparable as indicated by the October surface-water temperature data (Fig. 10). The limited seasonal applicability of using surface-water temperatures may thus lead to significant bias in exchange estimates when steam aquifer interactions show seasonal variations. A promising approach, in particular for losing stream reaches, is the quantitative analysis of diurnal temperature fluctuations within the actual stream bed (Silliman et al. 1995; Stonestrom and Constanz 2003; Schmidt et al. 2007; Baskaran et al. 2009a). High-frequency streambed-temperature data has been collected during 2007 and will be reported at a later time (G. Rau, University of New South Wales, unpublished data, 2009).

Dissolved chemical tracers work best if they are non-reactive. Due to its relative ease of measurement, electrical

DOI 10.1007/s10040-009-0500-9

conductivity (EC) is very often used (Cey et al. 1998; Cook et al. 2003). The general increase in EC down along Maules Creek in both August (Fig. 11) and October (Fig. 10) could be interpreted as an influx of higher conductivity groundwater possibly mixing with the surface water in the hyporheic zone as suggested by the higher groundwater EC values measured along the reach (Figs. 10b and 11b). However, this is contradictory to the observed downward gradients (Table 2) and general downstream cessation of flow that implies losing conditions. Alternatively, dissolved salts in the surface water could be concentrated by evapotranspiration (and thus increase the EC) as water slowly flows through the pools down along the reach. However, if this were true, a simple mass balance on EC in October would imply that half of the surface water in the creek and the hyporheic zone has been lost to evapotranspiration. This is improbable, considering the low evapotranspiration during winter and spring. A more likely explanation could be that dissolved salts have concentrated and precipitated in the sediments during previous drying events. These salts may re-dissolve into events of renewed flow. The variable EC measured along the stream in October, as shown by Fig. 10b, shows a rather complex pattern and it is unclear to what degree this is caused by re-dissolution of salt; exchange and mixing of shallow water in the hyporheic zone or discharging groundwater of a more regional nature. This highlights the main disadvantage of using EC as a tracer in a dry environment with intermittent stream flow—that it may reflect chemical reactions especially precipitation and re-dissolution of salts rather than reveal flow conditions.

Truly non-reactive tracers or more age-specific dating techniques are required to determine the degree of hyporheic or more regional exchange of water in these environments. In the context of this study, EC and temperature are only qualitative indicators of the location and direction of surface-water/groundwater interactions. The groundwater and surface-water variability of these parameters needs to be much better constrained in order to use them quantitatively to determine actual fluxes of water. As pointed out by Kalbus et al. (2006) and Winter et al. (1998), quantifying flux is difficult. Either one has to resort to methods such as seepage-meters, that obtain point measurements and integrate the flux of many measurements, or use stream-flow or tracer methods that integrate over long reaches at the expense of detailed knowledge of specific zones of exchange (Cey et al. 1998; Duff et al. 2000).

Finally, water-balance considerations allow the various results to be compared to other easily measured or calculated fluxes in the catchment. In that light, it is puzzling that, compared to the Namoi River loss for the two water years (Table 1), the combined surface-water diversion and groundwater abstraction only account for 30 to 50% of the river loss in the two years. Furthermore, these two years represent relatively high usage compared to previous years and some delay between the groundwater usage and the induced recharge from the river could be expected (Sophocleous 2002). In addition, as pointed out above, part of the applied irrigation water probably returns to the aquifer as deep drainage. The irrigation losses corresponds to 140 to 70 mm, which are within the typical range of deep drainage estimates of 100 to 200 mm observed for irrigated cotton fields in the region (Silburn and Montgomery 2004). An explanation for the apparent imbalance could be that the annual balance presented here does not account for long-term effects and that the overall balance could be achieved over a longer timeframe. However, this does not seem likely since the groundwater usage has been almost continuously increasing over the last 10 years. It seems more likely that either the usage data is considerably underestimated or that the stage flow relationships for one or both of the river gauges are incorrect.

This results of this study, as well as other studies in the literature (Halford and Mayer 2000; Kalbus et al. 2006; Baskaran et al. 2009a), reveal that the employment of a single method is inadequate for understanding the temporal and spatial exchange processes and for estimating the exchange fluxes of water in most systems. The various methods used in this study have also lead to an increased understanding of the local system of interaction between the streams and the aquifer. Figure 12 conceptually summarizes this understanding.

Winter surface-water temperature data (and to some degree EC data) indicate that regional groundwater (as opposed to hyporheic exchange) is discharging slightly upstream of the confluence of Maules Creek and Horse-

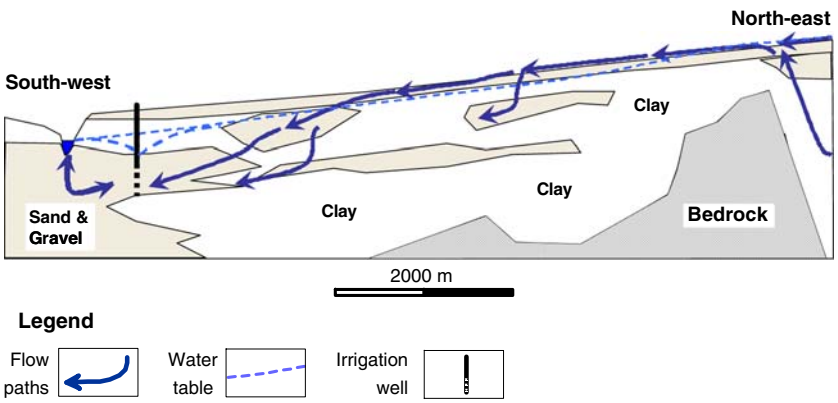

Fig. 12 Conceptual model of surface-water/groundwater interactions along Maules Creek

 DOI 10.1007/s10040-009-0500-9

arm Creek (Fig. 12). The exact reason for this groundwater discharge is presently unknown, but it is reasonable to suspect that lithological variation (such as a bedrock high) in the subsurface is the cause as suggested by Huggenberger et al. (1998). Downstream along Maules Creek, water seems to flow between pools and in a shallow unconfined sand and gravel aquifer limited to a few hundreds of meters on either side of the creek (Fig. 4a). Exchange with the aquifer below seems, despite the increasing downward gradients, to be largely prevented by the presence of thick clay layers (as indicated by the resistivity imaging, Fig. 4b). Eventually, flow in the creek bed ceases altogether when the creek bed sediments are intercepted by the highly permeable palaeochannel in the subsurface (Fig. 12). Integration of stream flow passing the gauge at Elfin Crossing gives an indication of the volumes of surface water recharging the aquifer. Compared to the annual groundwater abstraction (Table 3), this flux of surface water (Table 1), and thus the stream-induced aquifer recharge from Maules Creek, is rather insignificant. In contrast, the analysis of the annual flow difference between the two gauging stations on the Namoi River seems to indicate that the stream loss from the Namoi River is significantly larger than the combined surface-water diversion and groundwater abstraction. Stream fed aquifer recharge may well be a naturally occurring phenomenon during large surface-water flow events, but at this site it seems to be considerably enhanced by the extensive drawdown and increased downward gradients that have developed due to groundwater abstraction from the palaeochannel (Fig. 12).

This study clearly demonstrates how a combination of well-logging, resistivity, fluid EC, temperature, stream flow, hydraulic head and water-usage data can be used to map the spatial distribution of surface-water/groundwater exchange. The different types of data complement each other. The study also demonstrates the difficulty of building a representative conceptual model of process for an area unless diverse and extensive data sets are available.

Conclusion

The nature of surface water and groundwater exchange along a section of the Namoi River as well as beneath a zone of perennial pools at Maules Creek in northern New South Wales has been studied. The study comprised of the collection of geophysical well-logging data; electrical resistivity imaging; hydraulic head data; and fluid EC and temperature profiling along stretches of Maules Creek during winter and repeated in more detail during spring. In addition, existing geological data; stream flow data; climatic data; and surface and groundwater usage data was included in the analysis.

Based on temperature and EC data, zones of groundwater discharge were detected in the upper part of the perennial pools (the middle part of Maules Creek). Once water has discharged into the creek from the aquifer, it appears to be flowing for several kilometers between pools in a relatively thin (2–10 m) layer of sand and coarse gravel on top of more massive clayey layers as indicated by the resistivity imaging. Variations in the surface-water electrical conductivity downstream indicate possible exchange and mixing with groundwater or hyporheic zone water of varying EC. Re-dissolution of previously precipitated salts may also have some influence on the EC data. The EC data are consequently inconclusive in regards to surface-water/groundwater exchange. Further downstream, the stream is potentially recharging the regional aquifer as inferred by downward hydraulic gradients and variations in groundwater hydrographs. Inspection of the geological data revealed that the locations of high downward gradients correlated with a highly permeable palaeochannel. Seasonal drawdown in the groundwater level was observed in the palaeochannel due to groundwater abstraction. It therefore seems entirely likely that stream fed aquifer recharge is significantly enhanced by the regional abstraction of groundwater from the adjacent aquifer. This could be considered a good example of (unintended) conjunctive use of the river and aquifer systems.

Unraveling the dynamic nature of the water exchange is of importance for understanding the processes of aquifer recharge and in turn has implications for estimating the sustainable abstraction of groundwater from the palaeochannel. Equally important: the loss of surface-water flow due to groundwater abstraction, and subsequently more intermittent stream flow, may have important implications for aquatic and stygofaunal organisms associated with the stream environment.

Acknowledgements We gratefully acknowledge the funding by the Cotton Catchment Community CRC (Project No. 2.02.03). We would also like to thank the Department of Natural Resources (DNR) for allowing us access to their system of monitoring wells and their lithological borehole logs. We thank Dawit Berhane (DNR) for his help in the field. Also we thank Brad Morris and Mitch Harley for assistance with the DGPS equipment. We thank Sue and Ken Crawford for providing accommodation and meals when in the field. Finally we acknowledge the helpful reviews from two anonymous reviewers.

References

Andersen MS, Acworth RI (2007) Hydrochemical investigations of surface water groundwater interactions in a sub-catchment in the Namoi Valley, NSW, Australia. In: Ribeiro L, Chambel A, Condesso de Melo MT (eds) Groundwater and Ecosystems, Proceedings of the XXXV IAH Congress, Lisbon, September 2007

Andersen MS, Baron L, Gudbjerg J, Chapellier D, Jakobsen R, Gregersen J, Postma D (2007) Nitrate-rich groundwater discharging into a coastal marine environment. J Hydrol 336:98–114. doi:10.1016/j.jhydrol.2006.12.023

Baskaran S, Brodie RS, Ransley T, Baker P (2009a) Time-series measurements of stream and sediment temperature for understanding river-groundwater interactions: Border Rivers and Lower Richmond catchments, Australia. Aust J Earth Sci 56:21–30

 DOI 10.1007/s10040-009-0500-9

Baskaran S, Ransley T, Brodie RS, Baker P (2009b) Investigating groundwater-river interactions using environmental tracers. Aust J Earth Sci 56:13–19
Braaten R, Gates G (2003) Groundwater-surface water interactions in inland New South Wales: a scoping study. Water Sci Technol 48(7):215–224
Brodie RS, Sundaram B, Tottenham R, Hostetler S, Ransley T (2007) An adaptive management framework for connected groundwater-surface water resources in Australia. Bureau of Rural Sciences, Canberra, Australia
Brodie RS, Baskaran S, Ransley T, Spring J (2009) Seepage meter: progressing a simple method of directly measuring water flow between surface water and groundwater systems. Aust J Earth Sci 56(1):3–11
Cey E, Rudolph DL, Parkin GW, Aravena R (1998) Quantifying groundwater discharge to a small perennial stream in southern Ontario, Canada. J Hydrol 210:21–37
Cook PG, Favreau G, Dighton JC, Tickell S (2003) Determining natural groundwater influx to a tropical river using radon, chlorofluorocarbons and ionic environmental tracers. J Hydrol 277:74–88
Department of Mineral Resources (1998) Gunnedah coalfield north regional geology (1:100,000 map). Geological survey of NSW, Department of Mineral Resources, Sydney
Department of Mineral Resources (2002) Geology: integration and upgrade, NSW Western regional assessments Brigalow Belt South Bioregion (Stage 2). Geological Survey of NSW, Department of Mineral Resources, Sydney
Department of Natural Resources (2006) Bore log data base. Department of Natural Resources, NSW, Sydney
Department of Natural Resources (2007) Surface water hydrograph data base. Department of Natural Resources, NSW, Sydney
Duff JH, Toner B, Jackman AP, Avanzino RJ, Triska FJ (2000) Determination of groundwater discharge into a sand and gravel bottom river: a comparison of chloride dilution and seepage meter techniques. Verh Internat Verein Limnol 27:406–411
Findlay S (1995) Importance of surface-subsurface exchange in stream ecosystems: the hyporheic zone. Limnol Oceanogr 40:159–164
Fleckenstein JH, Niswonger RG, Fogg GE (2006) River-aquifer interactions, geologic heterogeneity, and low-flow management. Ground Water 44:837–852
Fullagar I, Brodie R, Sundaram B, Hostetler S, Baker P (2006) Managing connected surface water and groundwater resources. Bureau of Rural Sciences, Canberra, http://www.brs.gov.au. August 2008
Halford KJ, Mayer GC (2000) Problems associated with estimating ground water discharge and recharge from stream-discharge records. Ground Water 38:331–342
Hancock PJ, Boulton AJ, Humphreys WF (2005) Aquifers and hyporheic zones: towards an ecological understanding of groundwater. Hydrogeol J 13:98–111
Harvey JW, Bencala KE (1993) The effect of streambed topography on surface-subsurface water exchange in mountain catchments. Water Resour Res 29:89–98
Harvey JW, Wagner BJ, Bencala KE (1996) Evaluating the reliability of the stream tracer approach to characterize stream-subsurface water exchange. Water Resour Res 32:2441–2451
Hinkle SR, Duff JH, Triska FJ, Laenen A, Gates EB, Bencala KE, Wentz DA, Silva SR (2001) Linking hyporheic flow and nitrogen cycling near the Willamette River: a large river in Oregon, USA. J Hydrol 244:157–180
Huggenberger P, Hoehn E, Beschta R, Woessner W (1998) Abiotic aspects of channels and floodplains in riparian ecology. Freshw Biol 40:407–425
Humphreys WF (2009) Hydrogeology and groundwater ecology: Does each inform the other? Hydrogeol J 17:5–21
Ivkovic KM (2009) A top-down approach to characterize aquifer–river interaction processes. J Hydrol 365:145–155
Kalbus E, Reinstorf F, Schirmer M (2006) Measuring methods for groundwater surface water and their interactions: a review. Hydrol Earth Syst Sci Discuss 3:1809–1850
Lee DR (1977) A device for measuring seepage flux in lakes and estuaries. Limnol Oceanogr 22:140–147
Lee DR, Cherry JA (1978) A field exercise on groundwater flow using seepage meters and mini-piezometers. J Geol Education 25:6–10
Lee DR, Hynes HB (1977) Identification of groundwater discharge zones in a reach of Hillman Creek in southern Ontario. Water Pollut Res J Can 13:121–133
Libelo EL, MacIntyre WG (1994) Effects of surface-water movement on seepage meter measurements of flow through the sediment–water interface. Appl Hydrogeol 4:49–54
Morrice JA, Vallet HM, Dahm CN, Campana ME (1997) Alluvial characteristics, groundwater–surface water exchange and hydrological retention in headwater streams. Hydrol Proc 11:253–267
Murdoch LC, Kelly SE (2003) Factors affecting the performance of conventional seepage meters. Water Resour Res. 39(6): SWC2.1–SWC2.10. doi:10.1029/2002WR001347
Peterson EW, Sickbert TB (2006) Stream water bypass through a meander neck, laterally extending the hyporheic zone. Hydrogeol J 14:1443–1451
Schmidt C, Conant B Jr, Bayer-Raich M, Schirmer M (2007) Evaluation and field-scale application of an analytical method to quantify groundwater discharge using mapped streambed temperatures. J Hydrol 347:292–307
Shinn EA, Reich CD, Hickey TD (2002) Seepage meters and Bernoulli's revenge. Estuaries 25:126–132
Silburn DM, Montgomery J (2004) Deep drainage under irrigated cotton in Australia: a review. In: WATERpak a guide for irrigation management in cotton. Section2.4. Cotton Research and Development Corporation/Australian Cotton Cooperative Research Centre, Narrabri, Australia, pp 29–40
Silliman SE, Ramirez J, McCabe RL (1995) Quantifying downflow through creek sediments using temperature time series: one-dimensional solution incorporating measured surface temperature. J Hydrol 167:99–119
Sinclair P, Barrett C, Williams RM (2005) Impact of groundwater extraction on Maules Creek: Upper Namoi Valley, NSW, Australia. In: Acworth RI, Merrick N, Macky G (eds) Where waters meet. Proceedings of the NZHS-IAH-NZSSS 2005 Conference, Auckland, 29 November–1 December 2005
Sophocleous M (2000) From safe yield to sustainable development of water resources: the Kansas experience. J Hydrol 235:27–43
Sophocleous M (2002) Interactions between groundwater and surface water: the state of the science. Hydrogeol J 10:52–67
Stonestrom DA, Constanz J (2003) Heat as a tool for studying the movement of ground water near streams. USGS Circular 1260, US Geological Survey, Denver, CO
Tennakoon SB, Milroy SP (2003) Crop water use and water use efficiency on irrigated cotton farms in Australia. Agric Water Manage 61:179–194
Williams D, Montgomery J (2008) Bales per megalitre: an industry wide evaluation of the 2006/2007 season. In: Proceedings, Fourteenth Australian Cotton Research Conference, Brisbane, 12–14 August 2008
Winter TC (2001) Ground water and surface water: the linkage tightens, but challenges remain. Hydrol Proc 15:3605–3606. doi:10.1002/hyp.504
Winter TC (2007) The role of ground water in generating stream-flow in headwater areas and in maintaining base flow. J Am Water Resour Assoc 43:15–25
Winter TC, Harvey JW, Franke OL, Alley WM (1998) Ground water and surface water: a single resource. USGS Circular 1139, US Geological Survey, Denver, CO
Woessner WW (2000) Stream and fluvial plain ground water interactions: rescaling hydrogeologic thought. Ground Water 38:423–429
Wroblicky GJ, Campana ME, Valett HM, Dahm CN (1998) Seasonal variation in surface-subsurface water exchange and lateral hyporheic area of two stream-aquifer systems. Water Resour Res 43:317–328
Young RW, Young ARM, Price DM, Wray RAL (2002) Geomorphology of the Namoi alluvial Plain, northwestern New South Wales. Aust J Earth Sci 49:509–523